ASH VAPORIZATION UNDER SIMULATED PULVERIZED COAL COMBUSTION CONDITIONS

(Vol. I)

by

Richard John Quann

B.S.E., Princeton University
(1977)

SUBMITTED IN PARTIAL FULFILLMENT
OF THE REQUIREMENTS FOR THE
DEGREE OF

DOCTOR OF SCIENCE

at the

MASSACHUSETTS INSTITUTE OF TECHNOLOGY

January, 1982

Signature of Author_____
Department of Chemical Engineering

Certified by_____
Adel F. Sarofim, Thesis Advisor

Accepted by_____
Glenn C. Williams, Chairman
Departmental Committee on Graduate Theses

ASH VAPORIZATION UNDER SIMULATED PULVERIZED COAL COMBUSTION CONDITIONS

by

Richard J. Quann

ASH VAPORIZATION UNDER SIMULATED PULVERIZED COAL COMBUSTION CONDITIONS

by

Richard J. Quann

Submitted to the Department of Chemical Engineering in January, 1982 in partial fulfillment of the requirements for the degree of Doctor of Science from The Massachusetts Institute of Technology.

ABSTRACT

The objectives of this study were to elucidate the fundamental nature of mineral matter or ash volatilization processes during pulverized coal combustion. Vaporized ash results in the formation of submicron particulates which are undesirable from environmental and technical perspectives. A laboratory laminar flow combustion furnace having well defined and controlled combustion conditions was used for this experimental study.

The amount and composition of ash vaporized during combustion is strongly dependent on the temperature history of combustion and on coal type. The fractional vaporization rate of ash varied by over four orders of magnitude over the combustion temperature range of 1600-2750K. Twenty coals among three ranks were investigated at a moderate combustion temperature of 2000K. Typically 1-2 percent of the ash vaporized during combustion of bituminous coals and 5 percent of combustion of low rank coals at this condition. The submicron fumes produced were composed primarily of SiO_2 and FeO for bituminous coals and MgO and CaO for low rank coals. At lower temperatures (~ 1600K), however, the alkali oxides were the major components of the vaporized ash. The major difference between coals is that low rank coals contain high concentrations of the organically bound alkaline earth metals. This atomic dispersion in the raw coal significantly enhances volatilization.

A model developed to describe the volatilization process predicts with reasonable agreement the magnitude and temperature dependence of volatilization. The model considers that there are numerous micron sized oxide mineral inclusions in a coal particle. Each inclusion acts as a vapor source due to thermochemical reduction of refractory oxides (SiO_2, CaO, MgO) to more volatile forms by carbon monoxide. The reaction

is assumed to be locally at equilibrium. Internal and external diffusion processes control the rate of vaporization of the suboxide (SiO) or metal (Mg, Ca) from the burning char particle.

Thesis Supervisor: Adel F. Sarofim
Professor of Chemical Engineering

ACKNOWLEDGEMENTS

The author wishes to express his sincere gratitude to his advisor for his thoughtful guidance throughout the course of this thesis work. Professor Adel F. Sarofin's enthusiasim, approach and dedication to research and education has made a lasting impression on the author.

The author also wishes to extend his appreication to the members of his thesis committee, including Professors John F. Elliot, John P. Longwell, Glenn C. Williams and Jack B. Howard for their valuable discussions and suggestions and interest in the subject.

Special gratitude is also extended to Matthew Neville, Lyle Tymothy, Anthony J. Modestino, Charles A. Mims and Brian S. Haynes for their support, advise and assistance with the experimental and conceptual aspects of this study. The author is also grateful to Richard B. Frankel and Georgia C. Papaefthymiou for their assistance with the Mössbauer spectroscopy study, to Leneord Suddenfeld for his assistance with the Scanning Electron Microscope, and to Morteza Janghorbani for the Neutron Activation Analysis service.

Thanks are extended to Mary Kreuz for her superb and expedient typing of the manuscript.

This work was supported by the Electric Power Research Institute and N.I.E.H.S.

To all members of my family, and especially my parents who made this possible, the author cannot easily express

enough appreciation and respect for their encouragement and recognition of the importance of attaining this educational goal.

Finally, I wish to thank Paula, my wife and mother of our daughters Emily and Kathryn, for her continued support and encouragement, without which this could not have been possible. Although she endured countless weekends and nights alone, she has made the recent years a time of great joy for our growing family. In this I have been fortunate.

DEDICATION

TO THE MEMORY OF MY
BELOVED MOTHER

TABLE OF CONTENTS

Page

TITLE PAGE. i

AUTHORIZATION PAGE. ii

ABSTRACT. iii

ACKNOWLEDGEMENTS. v

DEDICATION. vi

TABLE OF CONTENTS vii

LIST OF FIGURES xii

LIST OF TABLES. xviii

CHAPTER ONE. SUMMARY. 1

1.1 Introduction. 1

1.2 Objectives and Approach 5

1.3 Experimental Methods. 6

1.4 Results 9

1.4.1 Coals Studies. 9

1.4.2 The Effect of Coal Type on Ash Vaporization. 16

1.4.3 The Effect of Combustion Conditions on the Vaporization of Ash. 25

1.4.4 Scanning Electron Microscopy of the Evolution of Ash During Combustion . . 37

1.5 Modelling 55

1.6 Discussion. 65

1.7 Conclusions 81

Page

CHAPTER TWO. BACKGROUND. 83

2.1 Introduction. 83

2.2 Occurance of Mineral Matter in Coal. 86

2.3 Fly-Ash Formation During Pulverized Coal Combustion 91

2.4 Thermochemical Considerations . . . 98

CHAPTER THREE. THESIS OBJECTIVES AND OUTLINE WORK . . . 103

CHAPTER FOUR. EXPERIMENTAL METHODS 107

4.1 Laboratory Combustion System. . . . 107

4.1.1 Combustion Furnace 108

4.1.2 Coal Feeding System. 110

4.1.3 Collection System. 110

4.1.4 Combustion Monitoring. . . . 113

4.2 Analytical Methods for Coal and Combustion Products 114

4.2.1 Coal Preparation and Sizing. 114

4.2.2 Proximate Analysis 115

4.2.3 Elemental Analysis 115

4.2.4 X-Ray Diffraction. 117

4.2.5 Mossbauer Spectroscopy . . . 118

4.2.6 Scanning Electron Microscopy 118

4.2.7 Density Fractionation of Coal 118

4.2.8 Ion-Exchanging Coals 119

CHAPTER FIVE. MINERAL MATTER OF CHARACTERISTICS OF COALS STUDIED. 121

5.1 Introduction. 121

5.2 Coals Studied and Proximate Analysis. 123

Page

5.3 Particle Size Distribution of Coals 125

5.4 Elemental Analysis of Coals. 127

5.5 Distribution of Elements by Density Fractionation. 127

5.6 Organically Held Metals in Low Rank Coals. 150

5.7 Mineralogical Characteristics of Coals. 153

CHAPTER SIX. COMBUSTION BEHAVIOR OF COALS IN LABORATORY FLOW FURNACE 176

6.1 Introduction 176

6.2 Modelling of Single Coal Particle Combustion . . . 177

6.3 Two-Color Optical Pyrometry Measurements of Coal Particle Combustion Temperatures. 185

CHAPTER SEVEN. ASH VAPORIZATION AND CONDENSATION PROCESSES IN LAMINAR FLOW FURNACE 194

7.1 Introduction 194

7.2 Size Distribution of Combustion Particulates 197

7.3 Submicron Particle Nucleation and Growth in Flow Furnace 208

7.4 Heterogeneous Condensation of Trace Metal Vapors 216

7.5 Elemental Material Balance on Laboratory Furnace 221

CHAPTER EIGHT. EXPERIMENTAL RESULTS - THE EFFECTS . . . 225

8.1 Introduction 225

8.2 The Effect of Coal Type on the Amount and Composition of Combustion Generated Submicron Ash 226

8.3 The Dependence of Ash Vaporization on the Combustion Conditions and on the Size of Pulverized Coal. 235

Page

8.4 Silicon Volatilization. 245

8.5 Iron Volatilization 251

8.6 Magnesium and Calcium Volatilization. 253

8.7 Alkali Volatilization 260

8.8 The Effect of CO_2 on Ash Vaporization. 267

8.9 Empirical Correlations of Ash Vaporization Kinetics 270

CHAPTER NINE. SCANNING ELECTRON MICROSCOPY OF THE CHEMICAL AND PHYSICAL EVOLUTION OF ASH DURING COMBUSTION. 275

9.1 Introduction. 275

9.2 Transformations of Ion-Exchangable Mineral Matter During Lignite Combustion 277

9.3 Microscopic Observations of the Physical Behavior of Bituminous Coals During Combustion 332

CHAPTER TEN. DISCUSSION AND MODELLING 336

10.1 Introduction. 336

10.2 Modelling of Vapor Transport Processes 340

10.3 Thermochemical Modelling and Discussion. 369

CHAPTER ELEVEN CONCLUSIONS AND RECOMMENDATIONS. 395

APPENDIX A. COAL DATA BASE 397

APPENDIX B. X-RAY DIFFRACTION SPECTRA OF COALS . . . 404

APPENDIX C. MOSSBAUER SPECTRA OF COALS 414

APPENDIX D. EQUILIBRIUM CONSTANTS FOR ASH CARBON REACTIONS. 427

REFERENCES. 429

LIST OF FIGURES

Figure No.		Page
1.1	Schematic of Ash Formation During Combustion. .	3
1.2	Laminar Flow Furnace.	7
1.3	Distribution of Mineral Matter in Coal Density Fractions	15
1.4	Comparison of Coal Ash and Submicron Fume Composition	24
1.5	The Effect of Silicon Concentration in Coal on Silicon Vaporization.	26
1.6	The Effect of Coal Type on Iron Vaporization. .	27
1.7	The Effect of Magnesium Concentration in Coal on Magnesium Vaporization	28
1.8	Time Resolved Measurement of Ash Vaporization .	30
1.9	Fractional Vaporization Rate of Ash	31
1.10	Elemental Fractional Vaporization Rates for Montana Lignite	33
1.11	The Effect of Coal Size on the Fractional Vaporization Rate of Silicon.	35
1.12	The Effect of Coal Size on the Fractional Vaporization Rate of Magnesium.	36
1.13	SEM of Partially Oxidized Lignite Char. 46% DAF Weight Loss	40
1.14	SEM of the Surface of a Lignite Char Particle 57% DAF Weight Loss	42
1.15	SEM of the Surface of a Lignite Char Particle, 57% DAF Weight Loss	46
1.16	SEM of the Surface of a Lignite Char Particle. 72% DAF Weight Loss	49
1.17	SEM of the Surface of a Lignite Char Particle. 85% DAF Weight Loss	52
1.18	Schematic of the Physical Distribution of Inclusion in a Char Particle.	57

Figure No.		Page
1.19	Comparison of Experimental and Predicted Partial Pressures of SiO at Char Surface	69
1.20	Comparison of Experimental and Predicted Partial Pressures of Fe at Char Surface.	73
1.21	Comparison of Experimental and Predicted Partial Pressures of Ca at Char Surface.	74
1.22	Comparison of Experimental and Predicted Partial Pressures of Mg at Char Surface.	75
4.1	Laminar Flow Furnace	109
4.2	Coal Feeding System.	111
4.3	Collection Probe	112
5.1	SEM of Raw Montana Lignite	126
5.2	Size Distribution of Montana Lignite	128
5.3	Size Distribution of Illinois No. 6.	129
5.4	Percentage of Coal Recovered in Float of Density Fractionated Floats.	137
5.5	Ash Content of Density Fractionated Floats . . .	138
5.6	Silicon Content of Density Fractionated Floats .	143
5.7	Aluminum Content of Density Fractionated Floats.	144
5.8	Iron Content of Density Fractionated Floats. . .	145
5.9	Calcium Content of Density Fractionated Floats .	146
5.10	Magnesium Content of Density Fractionated Floats	147
5.11	Sodium Content of Density Fractionated Floats. .	148
5.12	Potassium Content of Density Fractionated Floats	149
5.13	X-Ray Diffraction of Illinois No. 6.	155
5.14	X-Ray Diffraction of Alabama Rosa.	157
5.15	X-Ray Diffraction of West Virginia	158
5.16	X-Ray Diffraction of PSOC-3.	159

Figure No.		Page
5.17	X-Ray Diffraction of PSOC-26.	160
5.18	X-Ray Diffraction of PSOC-136	161
5.19	X-Ray Diffraction of PSOC-130	162
5.20	X-Ray Diffraction of Montana Lignite.	165
5.21	X-Ray-Difraction of Montana Lignite after Acid Treatment	166
5.22	Mossbauer Spectra of North Dakota Lignite . . .	169
5.23	Mossbauer Spectra of Illinois No. 6	170
5.24	Mossbauer Spectra of Western Kentucky	171
5.25	Mossbauer Spectra of Alabama Rosa	172
5.26	Mossbauer Spectra of PSOC-130	173
5.27	Mossbauer Spectra of PSOC-26.	174
6.1	Gas Temperature Profile in Furnace.	186
6.2	Coal Particle Burning Temperatures.	188
6.3	Coal Particle Burning Times	190
7.1	Schematic of Ash Formation During Combustoin. .	195
7.2	SEM of Ash Particles.	200
7.3	TEM of Submicron Ash Particles.	201
7.4	Distribution of Combustion Particulates on Impactor Stages. Illinois No. 6.	203
7.5	Distribution of Combustion Particulates on Impactor Stages. Alabama Rosa.	204
7.6	Distribution of Combustion Particulates on Impactor Stages. Montana Lignite	205
7.7	Ash Particulate Size Distributions.	207
7.8	Time Resolved Measurement of Ash Vaporization .	211
7.9	Predicted Condensation Behavior of Trace Metals	214
8.1	Correlation of Ash Vaporized with Ash Content of Bituminous Coals	236

Figure No.		Page
8.2	The Effect of Oxygen Pressure on Ash Vaporization. Illinois No. 6.	237
8.3	The Effect of Oxygen Pressure on Ash Vaporization. Alabama Rosa.	239
8.4	The Effect of Oxygen Pressure on Ash Vaporization. Montana Lignite	240
8.5	The Effect of Combustion Temperature on Submicron Ash Composition. Montana Lignite. . .	241
8.6	The Effect of Combustion Temperature on Submicron Ash Composition. Illinois No. 6 . . .	242
8.7	The Effect of Combustion Temperature on Submicron Ash Composition. Alabama Rosa	243
8.8	The Effect of Silicon Concentration in Coal on Silicon Vaporization.	246
8.9	The Effect of Oxygen Pressure on Silicon Vaporization. Bituminous Coals.	246
8.10	The Effect of Oxygen Pressure on Silicon Vaporization. Montana Lignite	250
8.11	The Effect of Coal Type on Iron Vaporization . .	252
8.12	The Effect of Oxygen Pressure on Iron Vaporization	254
8.13	The Effect of Magnesium Concentration in Coal on Magnesium Vaporization.	257
8.14	The Effect of Oxygen Pressure on Magnesium Vaporization	258
8.15	The Effect of Coal Type on Calcium Vaporization.	259
8.16	The Effect of Oxygen Pressure on Calcium Vaporization	261
8.17	The Effect of Coal Type on the Amount of Sodium Vaporized	263
8.18	The Effect of Oxygen Pressure on Sodium Vaporization	264
8.19	The Effect ofcoal Type on Potassium Vaporization	265

Figure No.		Page
8.20	The Effect of Oxygen Pressure on Potassium Vaporization.	266
8.21	Fractional Vaporization Rate of Ash	271
8.22	Elemental Fractional Vaporization Rates for Montana Lignite	272
8.23	Elemental Fractional Vaporization Rates for Illinois No. 6	273
9.1	SEM of Raw Montana Lignite Particles.	279
9.2	SEM of Devolatized Lignite Particles.	280
9.3	SEM of Partially Oxidized Lignite, 1750 K, 20% Oxygen.	284
9.4	SEM of Partially Oxidized Lignite, 1750 K, 20% Oxygen.	289
9.5	SEM of Partially Oxidized Lignite, 1750 K, 20% Oxygen.	291
9.6	SEM of Partially Oxidized Lignite, 1750 K, 20% Oxygen.	293
9.7	SEM Of Partially Oxidized Lignite, 1750 K, 20% Oxygen.	294
9.8	SEM of Partially Oxidized Lignite, 1750 K, 20% Oxygen.	296
9.9	SEM of Partially Oxidized Lignite, 1750 K, 20% Oxygen.	298
9.10	SEM of Partially Oxidized Lignite, 1750 K, 20% Oxygen.	300
9.11	SEM of Partially Oxidized Lignite, 1750 K, 20% Oxygen.	302
9.12	SEM of Partially Oxidized Lignite, 1750 K, 20% Oxygen.	304
9.13	SEM of Partially Oxidized Lignite, 1750 K, 20% Oxygen.	308
9.14	X-Ray Diffraction of Lignite Char	311
9.15	SEM of Partially Oxidized Lignite, 1750 K, 50% Oxygen.	313

Figure No.		Page
9.16	SEM of Partially Oxidized Lignite. 1750 K, 50% Oxygen.	318
9.17	SEM of Partially Oxidized Lignite. 1750 K, 50% Oxygen.	322
9.18	X-Ray Diffraction of Lignite Ash. 1750 K, 20% Oxygen.	325
9.19	X-Ray Diffraction of Lignite Ash. 1750 K, 20% Oxygen.	326
9.20	Phase Diagrams for CaO-MgO and CaO-Al_2O_3 Systems	329
9.21	Phase Diagram for SiO_2-Al_2O_3-CaO System	330
9.22	Phase Diagram for SiO_2-MgO-CaO System	331
9.23	SEM of Devolatilized Illinois No. 6 Particles	333
9.24	X-Ray Diffraction of Illinois No. 6 Combustion Ash. 1750 K, 20% Oxygen.	334
10.1	Schematic of Diffusion Controlled Vaporization.	339
10.2	Schematic of the Physical Distribution of Inclusions in a Char Particle	344
10.3	Schematic of Ash Droplet on Char Surface.	354
10.4	The Effect of the Modulus and Pore Size on the Partial Pressure of Metals at the Char Surface.	373
10.5	Comparison of Experimental and Predicted Partial Pressures of SiO at Char Surface.	376
10.6	The Effect of Coal Size on the Fractional Vaporization Rate of Silicon.	379
10.7	Comparison of Experimentally Determined Moduli for Different Coals	380
10.8	Comparison of Experimental and Predicted Partial Pressures of Fe at Char Surface	383
10.9	Comparison of Experimental and Predicted Partial Pressures of Ca at Char Surface	384
10.10	Comparison of Experimental and Predicted Partial Pressures of Mg at Char Surface	385
10.11	The Effect of Coal Size on the Fractional Vaporization Rate of Magnesium.	388

LIST OF TABLES

Table		Page
1.1	Selected Coals and Proximate Analysis.	10
1.2	Elemental Analysis of Bituminous Coals	11
1.3	Elemental Analysis of Low Rank Coals	12
1.4	Elemental Association with Extraneous Mineral Matter - Bituminous Coals.	17
1.5	Elemental Association with Extraneous Mineral Matter - Low Rank Coals.	17
1.6	Ash Vaporized for Combustion of Bituminous Coals at 1750K in 20% Oxygen	19
1.7	Ash Vaporized for Combustion of Low Rank Coals at 1750K in 20% Oxygen	20
1.8	Submicron Ash Composition for Combustion of Bituminous Coals in 20% Oxygen at 1750K.	21
1.9	Submicron Ash Composition for Combustion of Low Rank Coals in 20% Oxygen at 1750K.	23
1.10	The Effect of Combustion Temperature on the Composition of Submicron Ash	34
1.11	Effect of CO_2 on the Vaporization of Ash	38
2.1	Mean Elemental Composition for 101 Coals	89
2.2	Chemical Formulae of Some Common Minerals in Coal	90
2.3	Thermal Decomposition of Coal Minerals	93
2.4	Composition of Submicron Fly-Ash From Coal Fired Utilities.	98
5.1	Selected Coals, Rank and Proximate Analysis. . .	124
5.2	Comparison of the Ash Contents of Different Size Fractions of Coal	130
5.3	Multiple Elemental Analysis of Illinois No. 6 Coal	131
5.4	Multiple Elemental Analysis of Montana Lignite .	132

Table		Page
5.5	Elemental Analysis of Bituminous Coals.	133
5.6	Elemental Analysis of Low Rank Coals.	134
5.7	Inherent and Extraneous Mineral Matter Characteristics of Bituminous Coals	140
5.8	Inherent and Extraneous Mineral Matter Characteristics of Low Rank Coals	141
5.9	Elemental Association with Extraneous Mineral Matter - Bituminous Coals	151
5.10	Elemental Association with Extraneous Mineral Matter - Low Rank Coals	151
5.11	Proximate and Elemental Analysis of Low Rank Coals After Acid Treatment.	152
5.12	Percent Decrease in Ash and Elemental Content after Acid Treatment of Low Rank Coals.	152
5.13	Semi-quantitative Mineralogical Analysis of PSOC Coals.	163
6.1	Furnace Conditions.	179
7.1	Mass Distribution of Combustion Particulates on Cascade Impactor Stages	198
7.2	Elemental Material Balance on Furnace	222
8.1	Ash Vaporized for Combustion of Bituminous Coals at 1750K in 20% Oxygen.	228
8.2	Ash Vaporized for Combustion of Low Rank Coals at 1750K in 20% Oxygen.	229
8.3	Submicron Ash Composition for Combustion of Bituminous Coals at 1750K in 20% Oxygen	231
8.4	Submicron Ash Composition for Combustion of Low Rank Coals at 1750K in 20% Oxygen	232
8.5	Comparison of Metal and Metal Oxide Boiling Points.	234
8.6	Size Distribution of Products Obtained from Combustion of Pyrite in 20% Oxygen at 1750K . . .	255
8.7	The Effects of CO_2 on Elemental Volatilization During Combustion.	268

Table | Page

A.1 Composition of Bituminous Coal 1.8 Floats 398

A.2 Composition of Low Rank Coal 1.8 Floats. 399

A.3 Raw Coal Ash Composition - Bituminous Coals . . . 400

A.4 Composition of Inherent Ash for Bituminous Coals. 401

A.5 Raw Coal Ash Composition-Low Rank Coals 402

A.6 Composition of Inherent Ash - Low Rank Coals. . . 403

B.1 Minerals Identified by X-Ray Diffraction. 405

C.1 Iron-Bearing Coal Minerals Identified by Mössbauer Spectroscopy. 416

CHAPTER ONE

SUMMARY

1.1 Introduction

The combustion of pulverized coal for electric power generation is a major source of metal oxide and sulphate particulate emissions. Inorganic particulates arise from combustion because coal invariably contains significant amounts (2-20 percent) of non-combustible mineral matter. In recent years, concern over possible adverse environmental and health effects resulting from emissions has, accordingly, motivated a number of field investigators to examine the size distribution and chemical nature of coal combustion effluent particulates. The significant finding was that the combustion generated solids are bimodally distributed with respect to particle size (Ensor et. al., 1979; McCain et al., 1975). The primary mode of the particulate fly-ash size distribution occurs in the range of 10 to 20 microns and a secondary mode occurs in the submicron range at about 0.1 microns diameters. The submicron mode consists of only a few percent of the total mass of suspended solids, but is environmentally significant as downstream particulate control devices (i.e., electrostatic precipitators) are least effective in recovering the fine particles from effluent gases (Ensor et. al., 1979; Ondov et. al., 1979). Furthermore, the fine particles are enriched in the toxic trace metals that occur in coal and are within the respirable size range (Davison et. al., 1974; Ondov

et. al., 1979). The formation of the submicron particulates has been attributed to the vaporization of the ash or mineral matter during combustion and its subsequent condensation by homogeneous nucleation. The focus of this work was on the vaporization process which preceeds fine particle formation by condensation of the vapors evolved. With the aid of Figure 1.1, the general aspects of pulverized coal combustion, with regard to the current understanding of ash particle formation processes, is briefly reviewed.

Mineral matter in pulverized coal occurs primarily as mineral grains either embedded as inclusions in the carbonaceous matrix of pulverized coal particles, if sufficiently minute (1-10 microns), or as larger descrete mineral particles (~50 microns) free of association with the carbonaceous matter. The most common mineral forms, which incorporate the major inorganic elements in coal, include quartz [SiO_2], alumino-silicate clays, calcite [$CaCO_3$] and siderite [$FeCO_3$], and pyrite [FeS_2] (O'Gorman and Walker, 1972). At flame temperatures in combustors (1700-2500K), the minerals will decompose rapidly (or oxidize in the case of pyrite) and melt, yielding molten metal oxide droplets. As the char surface receeds during heterogeneous combustion, the molten inclusions will tend to adhere to the char's surface and, to a certain extent during the latter stages of char burnout, coalesce or contact to form larger ash droplets (Flagan and Friedlander, 1978; Padia, 1976). Particulates generated by this process will range in size from about one micron

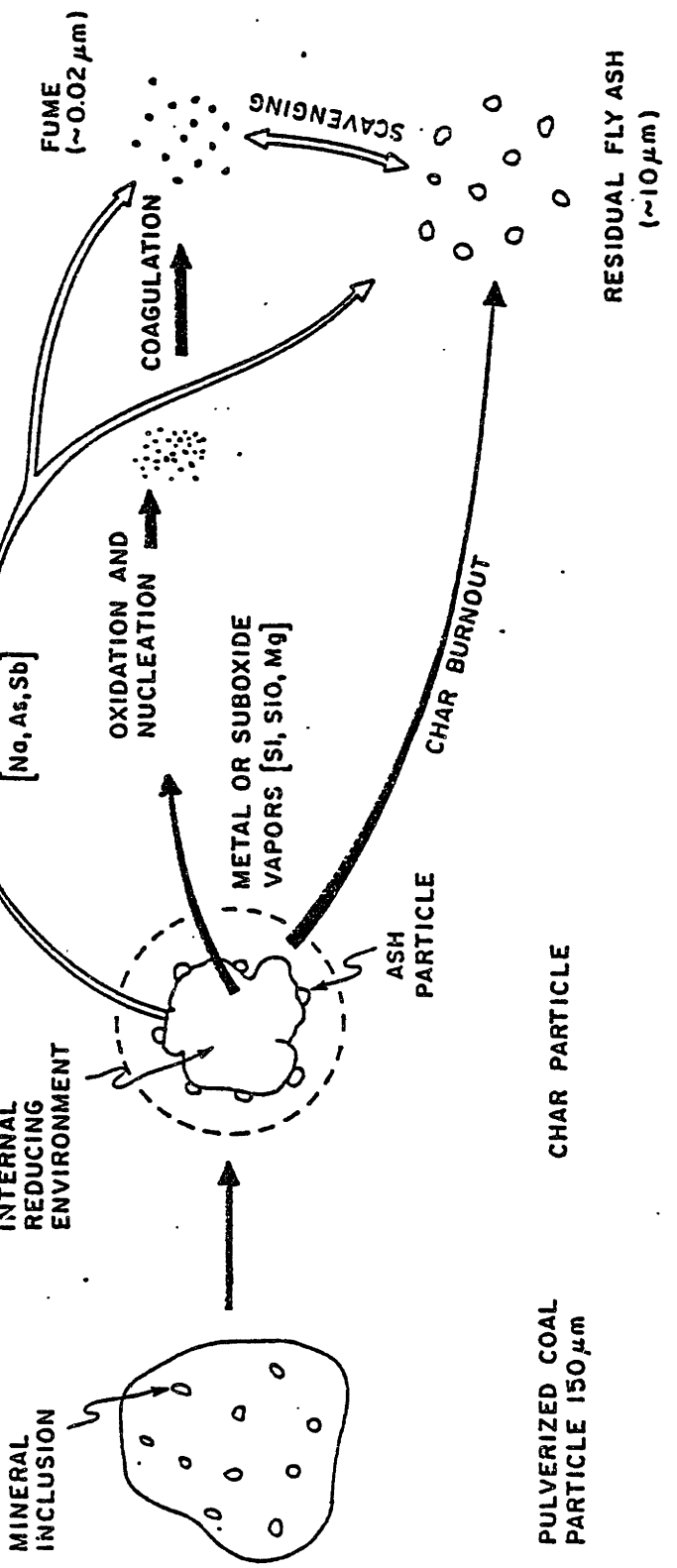

Fig. 1-1 : Schematic Diagram of Ash Formation and Behavior Mechanisms in Combustion.

corresponding to the characteristic size of the smallest inclusion - up to much larger sizes but typically averaging about 10 microns in diameter. Not all of the ash is necessarily released in this manner. At flame temperatures, it is expected that a number of relatively volatile trace metals in coal (As, Sb, and Na for example) will volatilize completely. The bulk of the ash is composed of refractory metal oxides (SiO_2, MgO, Al_2O_3, CaO and FeO) that have relatively low oxide vapor pressures and are, therefore, not expected to volatilize appreciably as oxides even at flame temperatures. However, when coal particles burn at high temperatures (above ~1800K), the carbon oxidation rate is sufficiently fast that oxygen partial pressures within the porous char are extremely low. Under these conditions, the locally reducing environment occurring within the burning char particle may facilitate the chemical reduction of refractory metal oxides to highly volatile suboxides (SiO) or metals (Mg, Ca). As metal vapors diffuse out of the char and through the chars external boundary layer, they encounter increasing oxygen potentials of the bulk gas. Reoxidation or combustion of metal vapors in the gas phase results in supersaturation with respect to the oxide vapors thus formed and subsequent condensation by homogeneous nucleation of extremely fine (~20Å) particles of metal oxides (Flagan, 1979; Desrosiers et. al., 1979). The fine particles of the metal oxide fume will then grow by collision and coagulation processes to mean diameters in the range of 0.02 to 0.1 microns. A bimodal size distribution of fly-ash is

consequence of the two particulate formation mechanisms.

1.2 Objectives and Approach

The objectives of this thesis were to study the volatilization behavior of mineral matter during pulverized coal combustion. An emphasis was placed on those refractory components of ash (SiO_2, CaO, FeO, and MgO) which may have enhanced volatilization rates brought about by chemical reduction of the oxides. The experimental basis of this investigation was the combustion of a dilute (continuous) stream of pulverized coal particles under the controlled conditions of a laboratory laminar flow furnace.

This investigation sought to determine by experimental measurement if:

a) the nature of the coal or mineral matter content, which vary considerably among coals, has an effect on the amount and chemical characteristics of vaporized ash. Twenty coals of three ranks were tested.

b) the combustion condition has a significant effect on the vaporization rate of mineral matter. Combustion conditions were systematically varied to simulate temperature histories encountered in typical PF boilers and extended to extremes (1600-3100K) to gain insight.

c) the mechanism by which refractory ash is volatilized is by chemical reduction within the locally reducing environment of a burning coal particle.

1.3 Experimental Methods

A schematic diagram of the laminar flow-drop tube furnace is presented in Figure 1.2. The furnace has electrically heated graphite elements, the temperature of which can be regulated with an automatic current controller. A central combustion zone is maintained within the core of the furnace by an alumina muffle tube of 50mm inside diameter. The maximum operating temperature of the furnace muffle tube is about 1800 K. The main gas, a pre-mixed oxygen-inert mixture, enters through the top of the furnace where it flows through an alumina honeycomb before entering the furnace combustion zone. The honeycomb serves as both a preheater and flow straightener to deliver the main gas at the specified furnace temperature with a uniform laminar velocity. The composition of the main gas is regualted by dual mass flow controllers. Coal particles entrained in $10^{-7} m^3/s$ of gas are injected axially into the furnace combustion zone via a water cooled feeder probe. Coal was fed at a rate of 0.03 gm/min. The main gas flow rate is maintained at $10^{-4} m^3/s$. On entering the furnace combustion zone, the particles are rapidly heated and ignited.

All gas and particulate combustion products are withdrawn from the combustion zone of the furnace by a water cooled collection probe which is inserted along the axis through the bottom of the furnace. The position of the probe is adjustable to allow time resolved combustion measurements. Combustion products are quenched to below 470 K as they enter the probe by a high volume

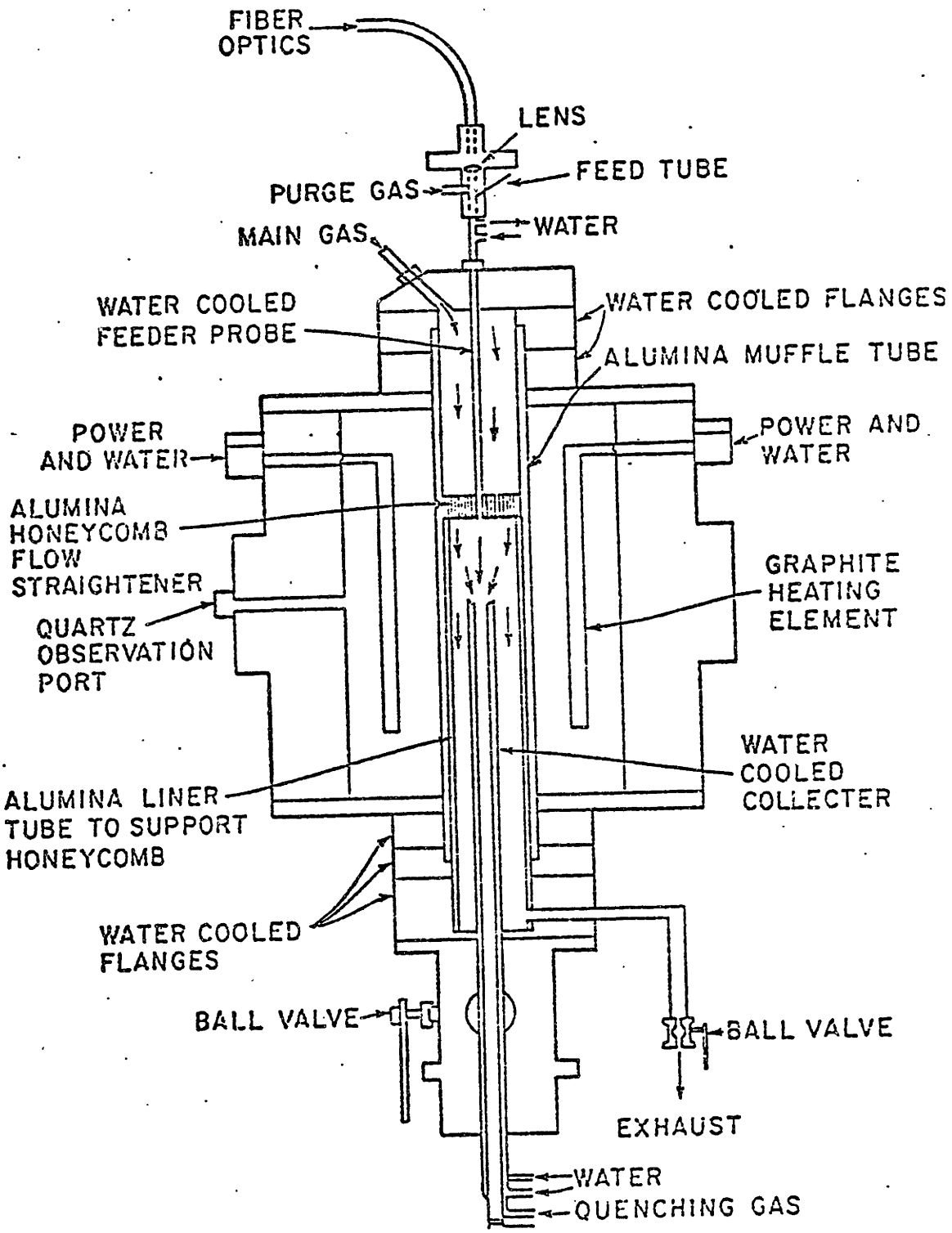

Figure 1.2 Laminar Flow Unit

flow rate of N_2. The inner core of the water cooled probe is fitted with a stainless steel porous tubing through which gas is transpired radially during the course of an experiment to prevent deposition and loss of particulates within the probe. From the collection probe, the gases and particulates enter directly into an Anderson 2000 cascade impactor for on-line aerodynamic size classification of the particulates. The impactor contains eight stages with theoretical effective cut-off diameters of 12.4, 7.9, 5.4, 3.7, 2.4, 1.2, 0.77, and 0.54 μm. The smaller submicron particulates pass completely through the impactor and are collected on a back-up Millipore membrane filter for weight determination and chemical analysis. Collection, isolation, and analysis of the submicron ash in this manner provided an accurate and reproducible method for determining the extent of ash vaporization at a specified combustion condition.

The combustion temperature and burning time of the coal particles was measured by two-color optical pyrometry (TCP). Optical access into the furnace combustion zone is obtained through the coal feeder probe. A more detailed description of this instrument is given by Tymothy (1981). Although the maximum furnace wall temperature is 1800 K, significantly higher particle temperatures were measured by TCP. This is due to the exothermicity of the char oxidation reaction. The combustion temperature of the coal particles was systematically varied by regulation of the oxygen partial pressure in the furnace and the furnace temperature.

The elemental content of the inorganics in the coal and particulate combustion products was obtained by instrumental neutron activation analysis, atomic absorption, plasma emission spectroscopy, and electron microprobe analysis. The principle mineralogical forms in the coals were determined by X-ray diffraction and Mössbauer spectroscopy (for iron-bearing minerals only). Scanning electron microscopy was employed to study the physical-chemical evolution of ash during char combustion. Char particles were obtained at successive stages of burnout by quenching the combustion process in the collection probe.

1.4 Results

1.4.1 Coals Studied

The twenty coals studied and their rank, proximate analysis and elemental analysis (for inorganics) are listed in Tables 1.1, 1.2, and 1.3. As evident by inspection, these coals are of varied mineral matter characteristics, having ash contents ranging from 2.3 to 28.4 weight percent, and variable elemental contents. The significant observation with respect to the relative abundance of the various metals is that the low rank coals are richer in calcium and magnesium than bituminous coals. The North Dakota lignite and the Montana Hardin subbituminous coal are unusual in that they contain uncharacteristically high levels of sodium. While the major elements occur primarily in the minerals, the alkaline earths and the alkalis occur primarily in organic form in low rank coals. Specifically, they are bound as cations on the carboxylic and phenolic groups of the organic matter and are, hence, atomically dispersed throughout the organic matrix

TABLE 1.1

Selected Coals, Rank and Proximate Analysis

Coal	Rank*	VM	FC	H_2O	Ash
Illinois No. 6	B	38.1	40.8	7.4	13.7
Western Kentucky	B	37.4	50.8	4.8	6.8
West Virginia	B	34.1	48.6	1.8	15.5
Pittsburgh No. 8	B	36.8	54.4	1.3	7.3
Alabama Rosa #18	B	21.9	63.4	8.1	6.6
Utah	B	38.7	46.9	6.4	8.0
Utah Price No. 1	B	38.5	46.9	6.3	8.3
PSOC-3, Kentucky Upper Elkhorn No. 3	B	35.7	59.0	1.8	3.5
PSOC-26, Illinois No. 6	B	36.0	42.9	12.2	8.9
PSOC-130, West Virginia Pocahontas No. 3	B	21.2	71.2	1.8	5.8
PSOC-136, Alabama Pratt Seam	B	24.1	73.0	0.6	2.3
PSOC-997, West Virginia, Pittsburgh Seam	B	37.9	54.4	1.5	5.2
Montana Rosebud	S	35.2	43.9	7.3	13.6
Montana Hardin No. 20	S	38.1	43.1	9.9	8.9
Montana, Powder River Region	S	----	----	8.8	12.5
Wyoming Commanche	S	----	----	10.2	6.2
Wyoming Rawhide	S	----	----	8.3	7.4
Montana Savage	L	37.0	44.2	10.0	8.8
North Dakota, Bevlah	L	38.5	41.7	12.3	7.5
Texas	L	33.3	28.9	9.4	28.4

B - Bituminous, S - Subbituninous, L - Lignite

TABLE 1.2

Elemental Analysis of Bituminous Coals (wT%)

Coal	Si	Al	Fe	Ca	Mg	K	Na	Ti	Cl	P	S
Illnois No. 6	2.86	1.20	1.75	0.80	0.10	0.18	0.047	0.056	-----	.011	4.35
Western Kentucky	1.41	0.79	1.60	0.59	0.038	0.13	0.011	0.048	0.024	.003	3.29
West Virginia	3.36	2.13	2.35	0.39	0.10	0.24	0.048	0.11	0.18	.055	2.85
Pittsburgh No. 8	1.31	0.90	0.81	0.56	0.077	0.081	0.063	0.042	0.10	.013	2.83
Alabama Rosa #18	1.65	0.70	0.56	0.70	0.060	0.17	0.033	0.022	0.049	.007	0.77
Utah	1.52	0.96	0.23	0.30	0.040	0.029	0.039	0.052	0.008	.031	1.00
Utal Price No. 1	2.45	1.00	0.17	0.15	0.032	0.039	0.040	0.049	0.030	----	0.62
PSOC-3	1.30	0.50	0.13	0.071	0.021	<0.005	0.017	0.067	0.170	----	0.61
PSOC-26	1.57	0.90	2.40	0.10	0.056	0.19	0.015	0.038	0.080	----	0.85
PSOC-130	0.92	0.72	0.46	0.67	0.13	0.026	0.032	0.038	0.022	----	0.51
PSOC-136	0.51	0.48	0.26	0.03	0.016	0.012	0.012	0.018	0.006	----	0.58
PSOC-997	1.27	0.82	0.56	0.17	0.046	0.050	0.033	0.03	0.10	----	1.57

TABLE 1.3

Elemental Analysis of Low Rank Coals (wT%)

Coal	Si	Al	Fe	Ca	Mg	K	Na	Ti	Cl	P	S
Lignites:											
Montana Savage	0.87	0.64	0.30	1.44	0.58	0.03	0.017	0.021	-----	0.031	0.55
North Dakota	0.55	0.39	0.62	1.10	0.52	0.03	0.66	0.023	-----	0.009	0.55
Texas	8.00	1.32	0.90	0.55	0.22	0.17	0.027	0.150	0.012	0.005	1.20
Subbituminous:											
Montana Rosebud	1.64	1.00	1.70	1.20	0.24	0.061	0.025	0.036	-----	0.012	1.33
Montana Hardin	1.16	0.75	0.50	1.20	0.18	0.031	0.26	0.035	0.011	-----	0.71
Montana Powder River	2.06	1.06	0.99	1.20	0.31	0.056	0.024	0.051	0.008	-----	1.16
Wyoming Commanche	0.63	0.51	0.34	0.99	0.27	0.014	0.064	0.038	-----	0.028	0.38
Wyoming Rawhide	1.36	0.62	0.37	1.10	0.25	0.015	0.048	0.038	0.004	-----	----

of lignite or subbituminous coal particles prior to combustion. In bituminous coals, calcium occurs primarily in the calcite [$CaCO_3$] mineral. Magnesium occurs in either dolomite [$CaMg(CO_3)_2$], which was rarely observed, or as a lattice substitution in the less ordered alumino-silicate clays such as illite. Other elements, including Na, K and Ca may also be substituted in clays. From XRD analysis, all of the coals were observed to contain quartz [SiO_2] and kaolinite [$Al_2Si_2O_5(OH)_4$]. Illite was not always observed. The mineral forms containing iron were found to vary from coal to coal. Nearly all coals contained pyrite [FeS_2], but certain bituminous coals were observed by the Mössbauer method to contain siderite [$FeCO_3$], iron sulfate minerals and iron-bearing illite clay.

The minerals are not distributed uniformly throughout the coal matrix. In a powdered sample of coal, some coal particles will contain numerous micron size mineral inclusions, others may contain very little inorganic matter, and still others may be composed almost entirely of mineral matter. Generally, mineral matter occurence in coal is classified in terms of geological factors related to the origin and evolution of coal (Mackowsky, 1956). For the present purpose of considering how the distribution of mineral matter in pulverized coal influences its fate during combustion, the classifications of O'Gorman and Walker (1972) are useful. Mineral matter which is intimately related to the organic matter of coal is classified as 'inherent'. In the present context, this category includes both the ion-exchang-

able or organically bound material and the finely disseminated micron-sized mineral grains or inclusions contained within carbonaceous coal particles. The second classifications is that of 'adventitious' mineral matter, which is less intimately associated with the coal material. In the present context this refers to the larger grains (20-50 microns) or 'extraneous' minerals essentially free of association with organic matter. This broad distinction between inherent and extraneous mineral matter is made because they have different temperature and chemical exposure histories during combustion. Specifically, it is only the inherent mineral matter that is exposed to the locally reducing environment within burning coal particles and the higher temperatures resulting from the exothermic oxidation of the coal.

Since the specific gravity of minerals (2.0-5.0) is greater than that of the carbonaceous matter (~1.3) of coal. coal particles containing significant quantities of mineral matter can be separated by float-sink from those containing lesser amounts of mineral matter. A series of density fractionations were performed on several coals and the results for only one coal are shown in Figure 1.3. The percent of the raw size classified (55μm) Illinois No. 6 coal recovered in each density fraction is shown in the first bar graph. The ash content of each density fraction was determined and these results are shown in the second bar graph. The 'coal' particles having a specific gravity of 1.8 or greater are seen to contain nearly 70% ash, indicating that this fraction is nearly all mineral matter in extraneous

ILLINOIS NO. 6

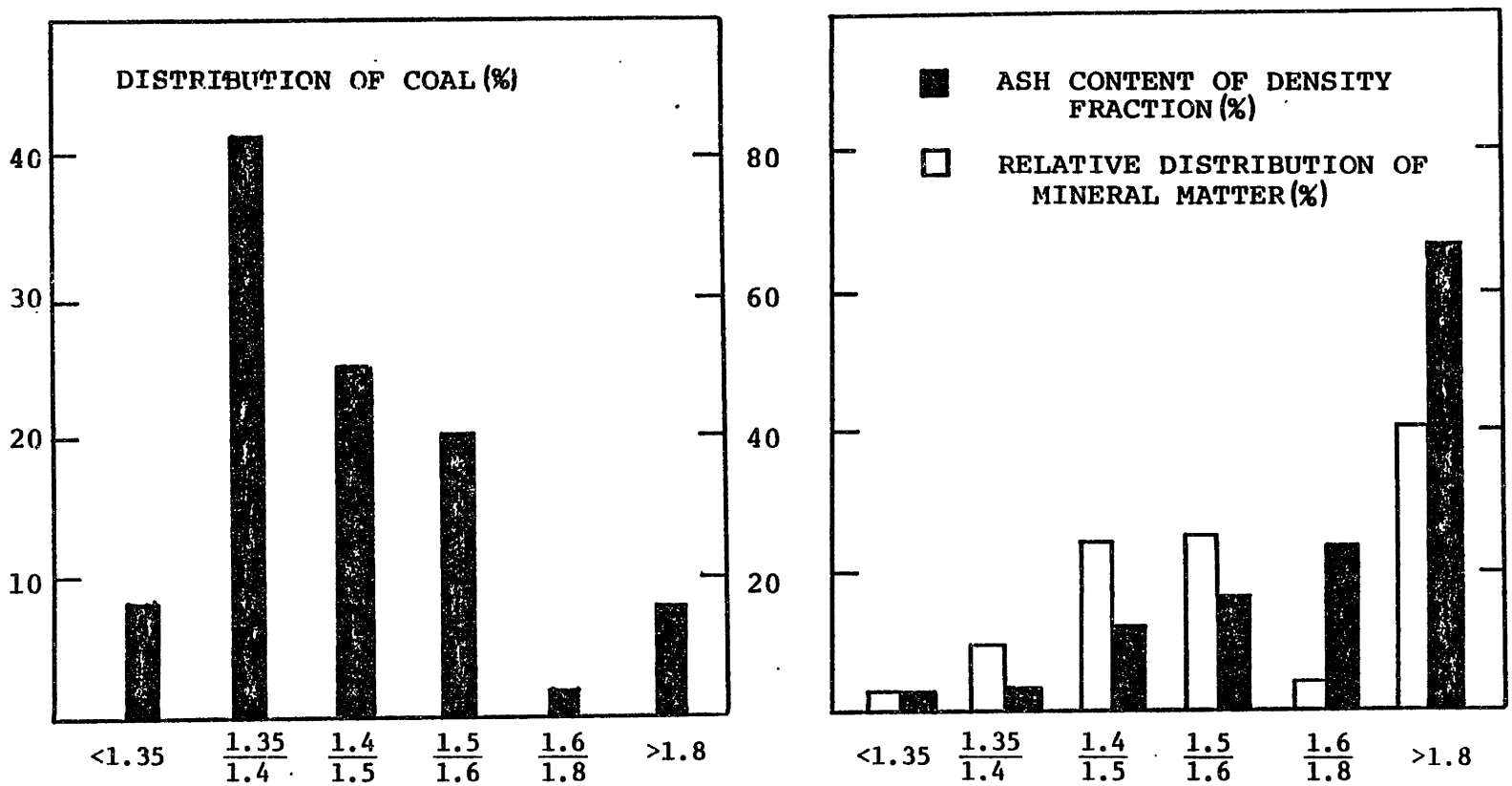

Figure 1.3 Density Fractionation of Coal

form. (Measured ash content is somewhat less than true mineral matter content from weight loss due to decomposition of minerals during the ashing procedure.) The relative distribution of the total ash among density fractions is also shown in the second bar graph of Figure 1.3. Nearly 40 percent of the mineral matter in the pulverized Illinois No. 6 is extraneous. At the other end of the density spectrum (<1.4), 50 percent of the coal is seen to contain less than 3 percent ash. It is to be recalled (Table 1.1) that the ash content of the raw Illinois No. 6 is 13.7 percent.

All of the coals were separated in a 1.8 specific gravity medium to determine the extent to which elements in the coal are associated with the extraneous minerals. The results shown in Tables 1.4 and 1.5 indicate that the extent to which an element is not associated with the combustible organic material (as finely disseminated minerals) is highly variable among pulverized coals but can be quite significant.

1.4.2 The Effect of Coal Type on Ash Vaporization

All of the coals, classified to nominal 50 to 60 microns in diameter, were burned to completion in the laminar flow furnace under an identical combustion condition - that of a furnace wall temperature of 1750 K, and a gas composition of 20 percent oxygen (80 percent nitrogen) to simulate air. The coal particle combustion (temperature) history simulates that which would occur in a flame of a typical utility boiler. The burning temperature of the coal particles are approximately 2000 K for lignites and

TABLE 1.4

Percent of Element in Raw Coal
Associated with Extraneous
Mineral Matter (1.8F) - Bituminous Coals

Coal	Si	Al	Fe	Ca	Mg	k	Na
Illinois #6	38	36	68	80	21	24	13
Western Kentucky	2.9	23	46	41	11	18	12
West Virginia	8.6	24	79	54	29	30	26
Pittsburgh #8	2.8	17	37	41	18	20	6
Alabama Rosa #18	56	42	44	93	51	68	39
Utah	15	33	62	60	29	21	17
Utah Price #1	45	30	41	30	10	39	16
PSOC-3	29	13	32	32	19	-	1
PSOC-26	9.2	26	72	26	5.6	39	12
PSOC-130	15	22	33	52	35	25	21
PSOC-136	3.9	17	55	3	33	3	0
PSOC-997	15	23	74	40	25	17	9.5

TABLE 1.5

Percent of Element in Raw Coal
Associated with Extraneous (1.8F)
Mineral Matter - Low Rank Coals

Coal	Si	Al	Fe	Ca	Mg	K	Na
Lignites:							
Montana Savage	38	25	72	7.3	8	45	0
North Dakota	12	15	45	4.4	15	9	4
Texas	54	18	34	36	34	62	19
Subbituminous:							
Montana Rosebud	55	60	83	33	23	58	20
Montana Hardin	39	31	79	19	0	20	7
Montana Powder River	21	24	83	23	1	38	10
Wyoming Commanche	19	33	35	13	0	18	7
Wyoming Rawhide	45	33	34	7	0	16	13

2100 K for bituminous coals at this specified furnace condition.

The amount of submicron ash generated during combustion (equivalent to the amount of ash vaporized), normalized on a basis of a gram of coal burned, are compared for the different bituminous coals and low rank coals in Tables 1.6 and 1.7, respectively. These results for the bituminous coals are in agreement with the few reported measurements of utility effluents where 1 to 2 percent of the fly-ash mass is within the submicron mode (McElroy and Carr, 1980). Calculation of the percent of ash vaporized in terms of the inherent metal oxide (SiO_2 + FeO + CaO + MgO + Na_2O + K_2O) content of the coal, rather than on an ASTM ash basis, may be a more appropriate comparison of coals as it is only the inherent ash that is exposed to the locally reducing environment and coal particle temperature overshoot during combustion. For most of the low rank coals, a greater amount and percent of ash vaporized during combustion than for the bituminous coals. The North Dakota lignite had a maximum with nearly nine percent of its ash vaporizing.

The type of coal burned also has an important impact on the composition of the submicron ash with the most pronounced differences again occurring with coal rank. As shown in Table 1.8, combustion of bituminous coals yields submicron ash composed mostly of SiO_2 and FeO with Na_2O occasionally present at comparable concentrations. In comparing the submicron ash with that of the bulk ash, relatively volatile species such as Na_2O and K_2O are mostly enriched as might be expected, whereas highly

TABLE 1.6

Ash Vaporized For Combustion of Bituminous Coals at a 1750K Furnace Temperature in 20% Oxygen

Coal	Grams of Ash Vaporized/ Gram of Coal Burned	Percent of ASTM Ash Vaporized	Percent of Inherent Metal Oxides Vaporized
Illinois No. 6	.00124	0.90	1.88
Western Kentucky	.00119	1.74	2.19
West Virginia	.00148	0.96	1.36
Pittsburgh No. 8	.00119	1.63	2.16
Alabama Rosa	.00103	1.56	3.62
Utah	.00090	1.12	2.04
Utah Price No. 1	.00072	0.87	1.57
PSOC-3	.00035	1.00	1.15
PSOC-26	.00104	1.17	1.89
PSOC-130	.00111	1.90	2.93
PSOC-136	.00036	1.56	1.71
PSOC-997	.00044	0.84	1.11

TABLE 1.7

Ash Vaporized For Combustion of Low-Rank
Coals at a 1750K Furnace Temperature in 20% Oxygen

Coal	Grams of Ash Vaporized/ Gram of Coal Burned	Percent of ASTM Ash Vaporized	Percent of Inherent Metal Oxides Vaporized
Lignites:			
Montana Savage	.00251	2.86	5.06
North Dakota	.00661	8.85	12.7
Texas	.00118	0.42	0.89
Subbituminous:			
Montana Rosebud	.00238	1.74	5.69
Montana Hardin	.00290	3.26	6.23
Montana Powder River	.00141	1.13	1.98
Wyoming Commanche	.00265	4.29	7.00
Wyoming Rawhide	.00252	3.40	5.42

TABLE 1.8

Submicron Ash Composition for Combustion of Bituminous Coals in 20% Oxygen at a Furnace Temperature of 1750K

Coal	SiO_2	FeO	MgO	CaO	Al_2O_3	K_2O	Na_2O	TiO_2	Cl	P_2O_5
Illinois No. 6	34.6	26.0	1.9	0.68	1.6	15.6	14.5	----	----	0.51
Western Kentucky	35.1	40.5	1.3	0.47	1.9	13.7	4.5	----	----	2.4
West Virginia	34.7	21.8	1.6	0.59	0.81	10.6	11.8	0.70	0.23	17.2
Pittsburgh No. 8	41.2	18.4	2.9	1.4	1.3	11.2	16.6	0.63	0.37	5.9
Alabama Rosa	19.6	47.4	3.7	1.1	1.9	4.6	14.7	0.47	2.9	2.3
Utah	26.0	15.8	6.1	0.56	1.6	5.8	30.0	0.24	0.44	13.3
Utah Price #1	24.0	23.0	3.5	0.53	2.4	4.0	24.9	----	1.4	16.4
PSOC-3	30.0	22.4	3.9	2.1	2.7	<1.0	35.1	3.1	----	0.57
PSOC-26	28.1	43.5	0.80	1.6	2.4	14.7	6.6	0.48	0.38	1.4
PSOC-130	35.8	39.3	6.8	4.2	1.7	1.5	6.9	----	1.6	2.0
PSOC-136	31.5	28.1	9.3	7.9	1.8	10.0	7.6	1.9	0.84	1.1
PSOC-997	33.8	15.7	2.8	1.1	4.1	13.3	25.3	1.9	0.68	1.5

refractory ash components such as CaO and Al_2O_3 are significantly depleted.

The composition of the submicron ash generated from combustion of low rank coals is quite different from that of the bituminous coals as shown in Table 1.9. With the exception of the Texas lignite, the combination of MgO and FeO dominate the refractory compounds present, with SiO_2 weight percents being significantly lower than the values for bituminous coal combustion fumes. For two of the low rank coals, the North Dakota lignite and the Montana Hardin, Na_2O, is observed to be the major component of the submicron ash. These coals contain the unusually high concentrations of sodium (see Table 1.3).

In Figure 1.4, a triangular diagram has been employed to compare the composition of the inherent ash (as oxides) of the coals with the composition of the submicron or vaporized ash generated during combustion. Only the major refractory ash components are considered. This figure illustrates that the composition of submicron ash generated during combustion can be roughly categorized by coal rank or coal ash composition. Low rank coals rich in alkaline earths have submicron ashes rich in the alkaline earths. Bituminous coal combustion fumes are rich in silica as are their coal ashes. In most cases, iron is observed to be enriched in the vaporized ash, compared to the bulk ash.

The submicron fume composition and its total mass reflect the volatilization properties of the individual elements (or oxides). The effect of inherent Si, Fe and Mg content of the

TABLE 1.9

Submicron Ash Compostion for Combustion of Low Rank Coals at a Furnace Temperature of 1750 K in 20% Oxygen

Coal	SiO_2	FeO	MgO	CaO	Al_2O_3	K_2O	Na_2O	TiO_2	Cl	P_2O_5
Lignites:										
Montana Savage	3.67	11.5	64.4	7.8	0.56	1.4	3.7	----	0.40	6.5
North Dakota	1.62	20.3	18.9	2.6	0.27	0.82	54.6	----	0.45	0.64
Texas	38.5	37.0	7.0	0.45	1.5	5.1	8.9	----	0.64	6.5
Subbituminous:										
Montana Rosebud	17.5	35.4	27.2	6.6	0.80	3.6	6.5	----	0.19	2.2
Montana Hardin	7.3	7.2	20.0	5.8	0.43	2.6	53.4	----	1.6	1.8
Montana Powder River	9.9	7.1	61.0	10.4	0.78	3.8	5.7	----	0.23	1.1
Wyoming Commanche	3.2	35.2	31.3	6.9	0.83	0.94	16.3	----	0.12	5.3
Wyoming Rawhide	6.5	38.9	30.5	8.1	0.54	0.52	9.6	----	1.1	4.3

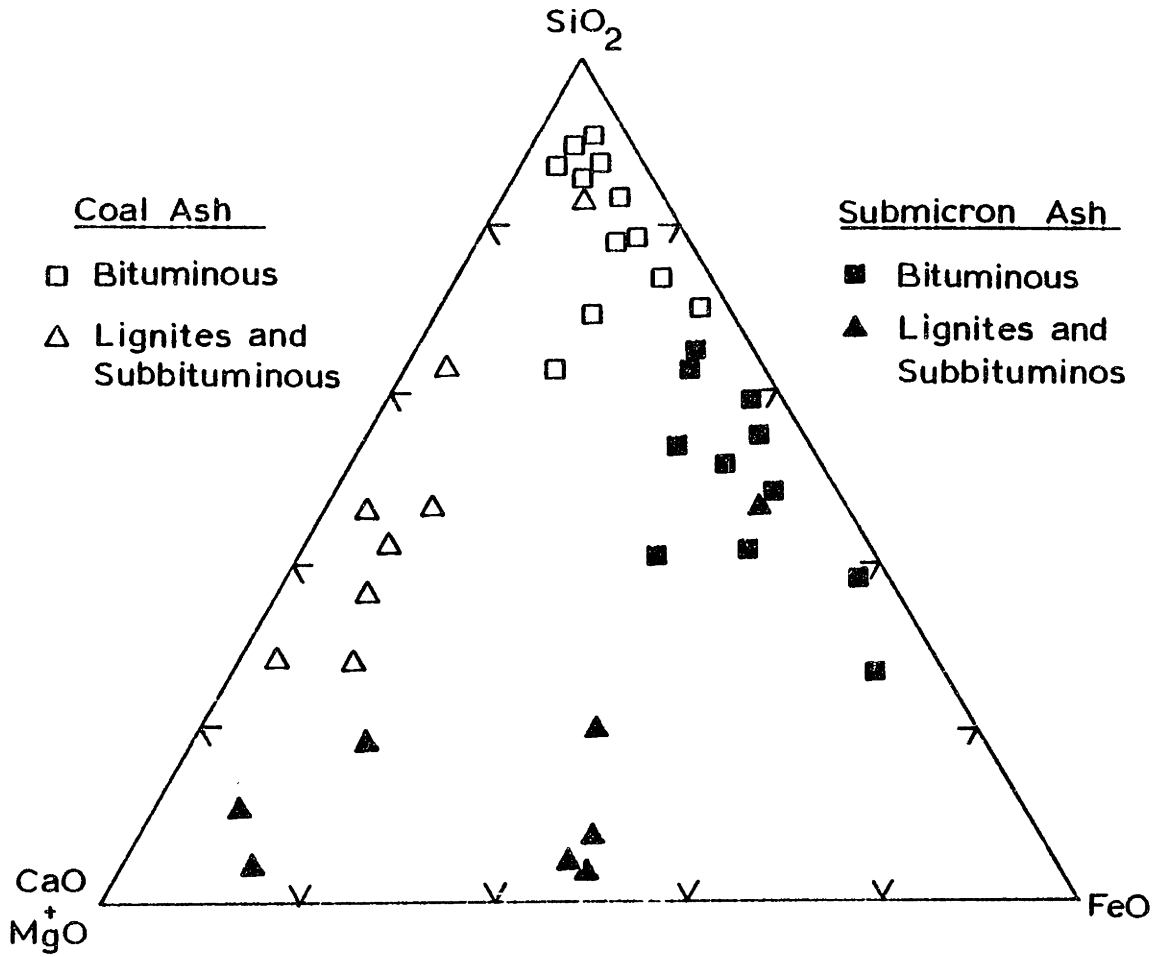

Figure 1.4 Comparison of Coal Ash and Submicron Fume Composition

coal on the absolute quantity of metal vaporized at this same combustion condition is shown in Figures 1.5, 1.6, and 1.7, respectively. Silicon vaporization is not well correlated with inherent silicon content of the coals. There is however, a general trend of increased amount of silicon vaporized with increased silicon content of the coal.

The effects of coal rank and original iron bearing mineral forms on the amount of iron vaporized during combustion is striking. All of the low rank coals contain iron only in the form of pyrite. The fraction of inherent iron vaporized during the combustion of most low rank coals was nearly .30 compared to .05 for bituminous coals containing only pyrite (+ iron sulphate minerals. Bituminous coals containing iron-bearing clays or siderite [$FeCO_3$] also vaporized a greater fraction of the iron during combustion than did bituminous coals containing only pyrite and iron sulfates minerals.

As shown in Figure 1.7 a linear correlation exists between the magnesium vaporized and the magnesium content of the low rank coals. At this combustion condition, the fraction of the magnesium vaporized was approximately .18 for low rank coals. Bituminous coals contain only minor amounts of inherent magnesium and consequently, little magnesium is vaporized during combustion.

1.4.3 The Effect of Combustion Condition on the Vaporization of Ash

The burning temperature and time of the coal particles in the laboratory furnace depend on the oxygen partial pressure in

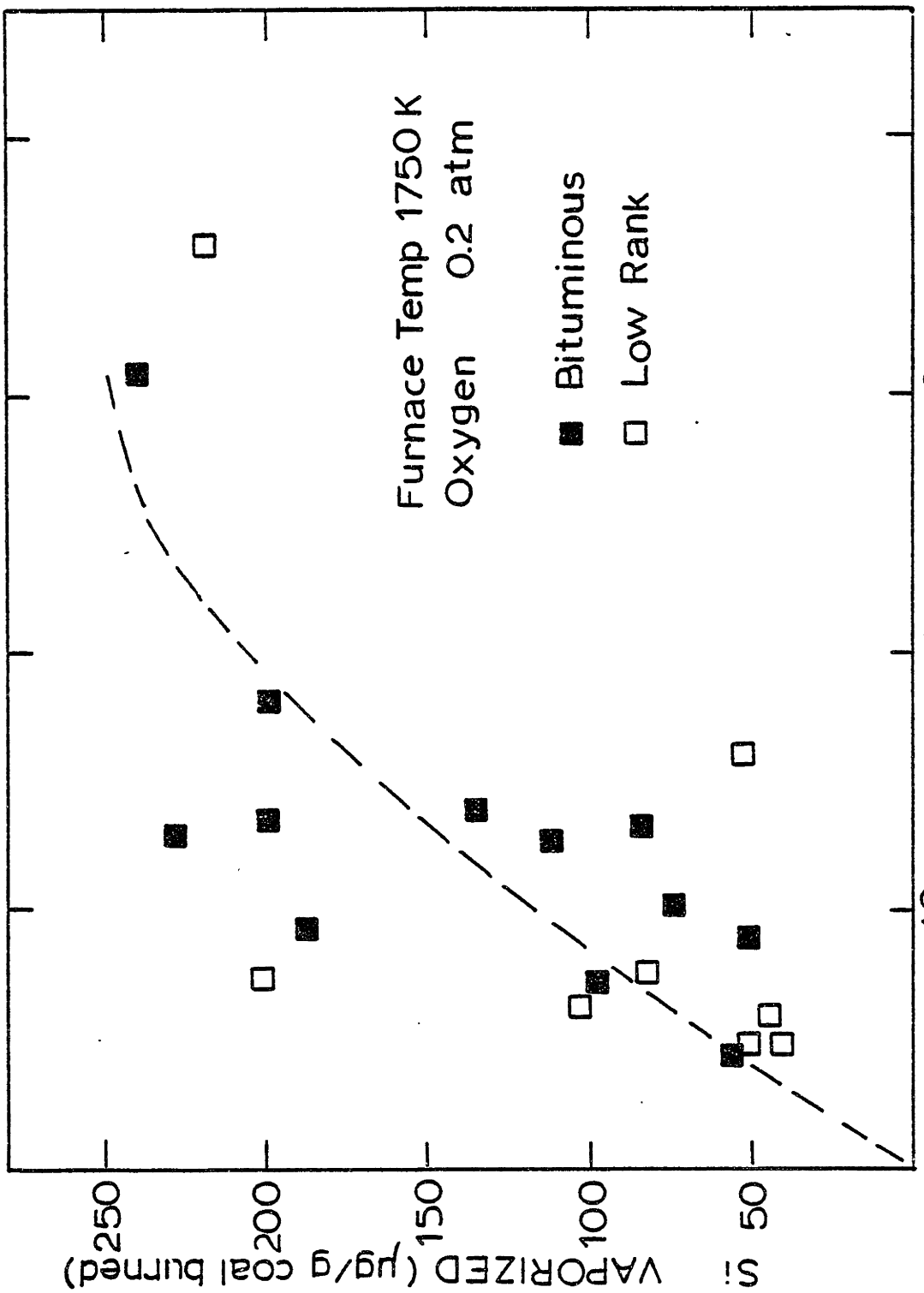

Figure 1.5 The Effect of Silicon Concentration in Coal on the Amount of Silicon Vaporized

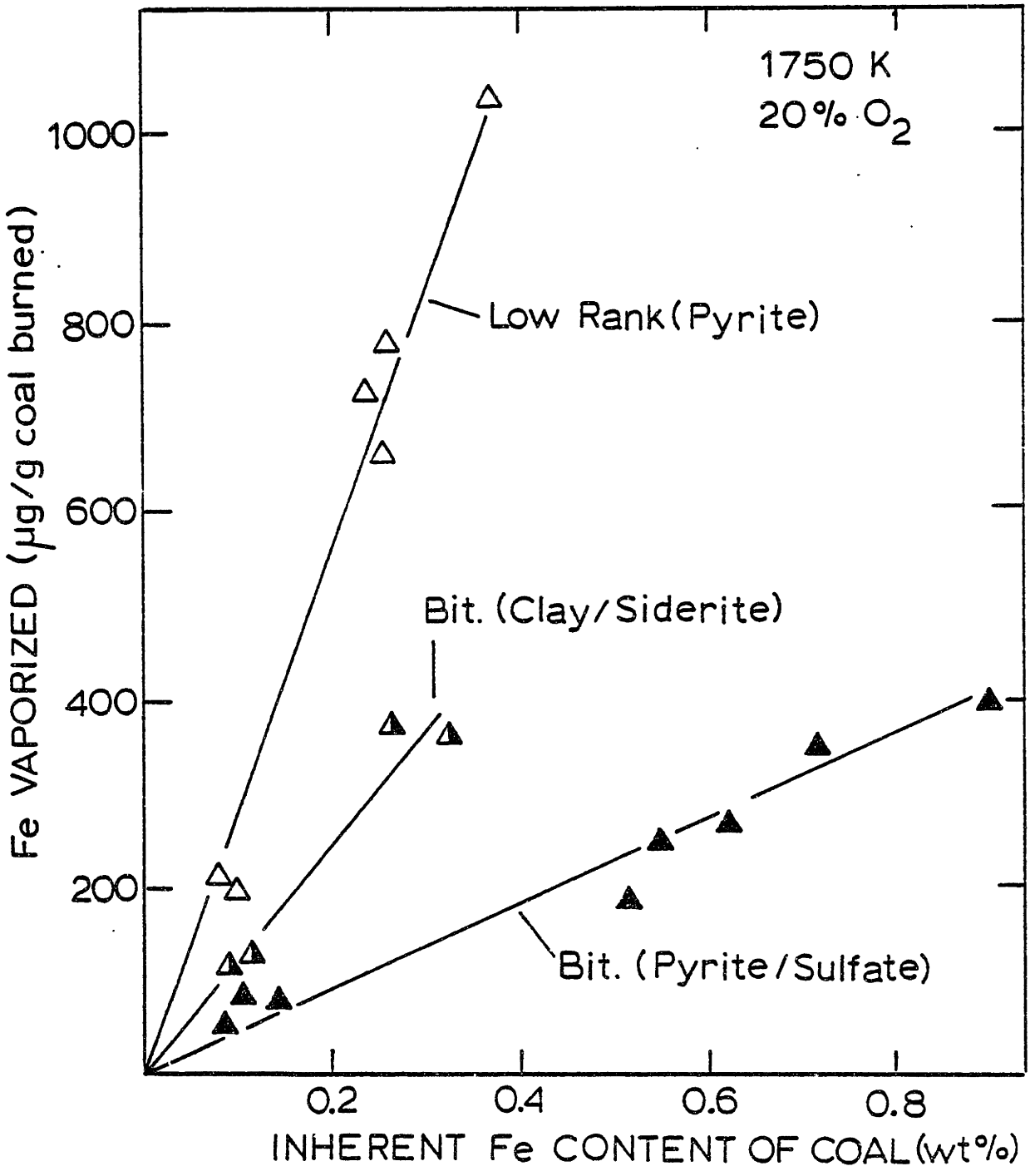

Figure 1.6 The Effect of Iron Concentration in Coal on the Amount of Iron Vaporized

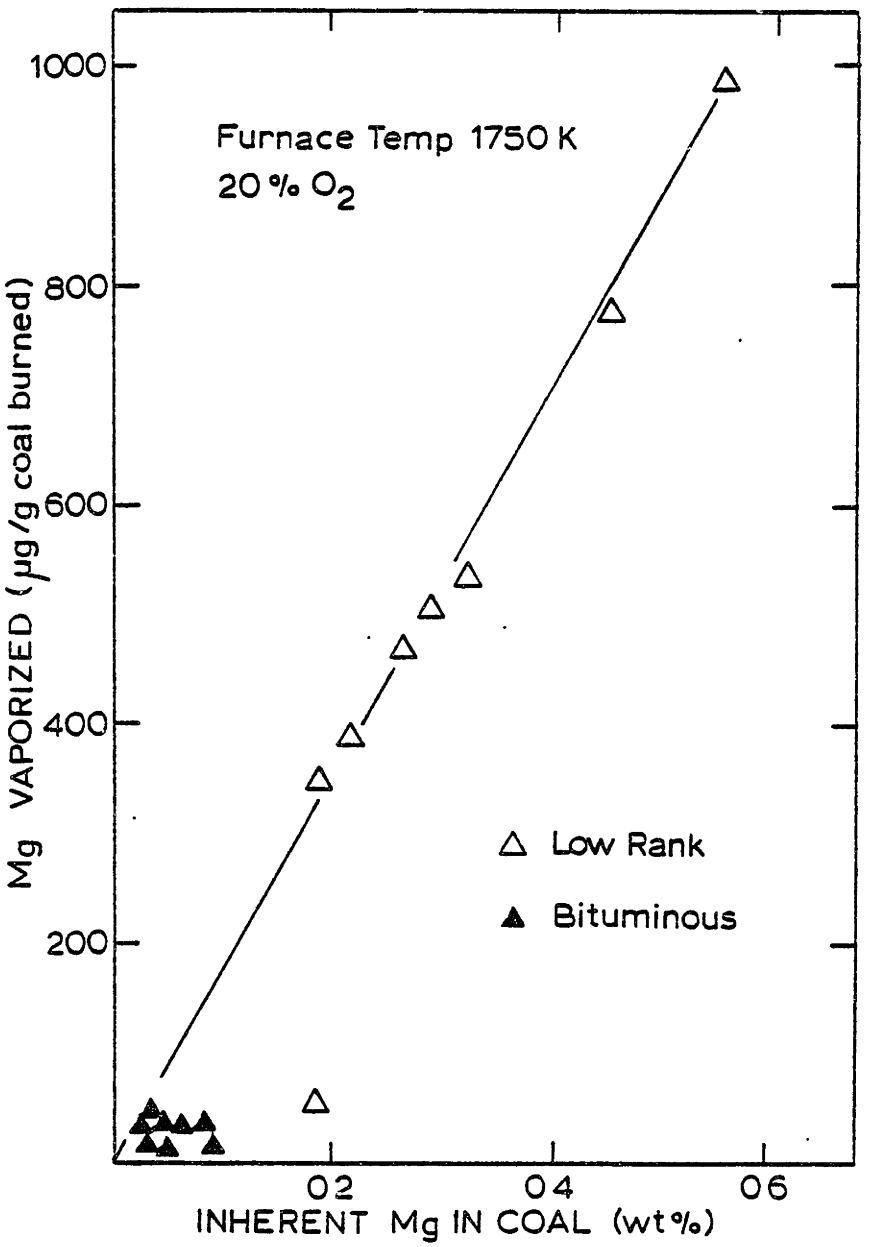

Figure 1.7 The Effect of Magnesium Concentration in Coal on the Amount of Magnesium Vaporized

the main gas and the furnace temperature. By systematic variation of combustion condition with the experimental variables, the kinetics of ash volatilization were studied over a temperature range of 1600 to 3100K. The variation of combustion condition in these experiments is a variation of the temperature history of the burning coal particles.

The significance of the temperature history of burning coal particles on the volatilization of ash is illustrated by the time resolve measurements shown in Figure 1.8. The products of partial combustion of the (140 μm) Montana Savage lignite were obtained at successive residence times in the furnace. In 30 percent oxygen, the lignite is burning at about 2150K with a furnace temperature of 1750K. These results indicate that the ash vaporizes only during the char combustion process. This is to be expected because it is only during this period that the ash experiences a locally reducing environment within the burning particles and the temperatures of combustion. There is no measurable change in the amount of vaporized ash in the post-combustion (0% DAF recovery) period. Thus the important parameters in determining kinetics of ash volatilization are the temperature and time of combustion of the particles, as will be further demonstrated below.

The results presented in Figure 1.9 demonstrate the effect of combustion temperature on the vaporization rate of ash for two coals. The fractional vaporization rate was obtained by dividing the fraction of inherent ash vaporized by the burning time of the coal particles. The maximum combustion temperature corresponds to burning the coals in 100 percent

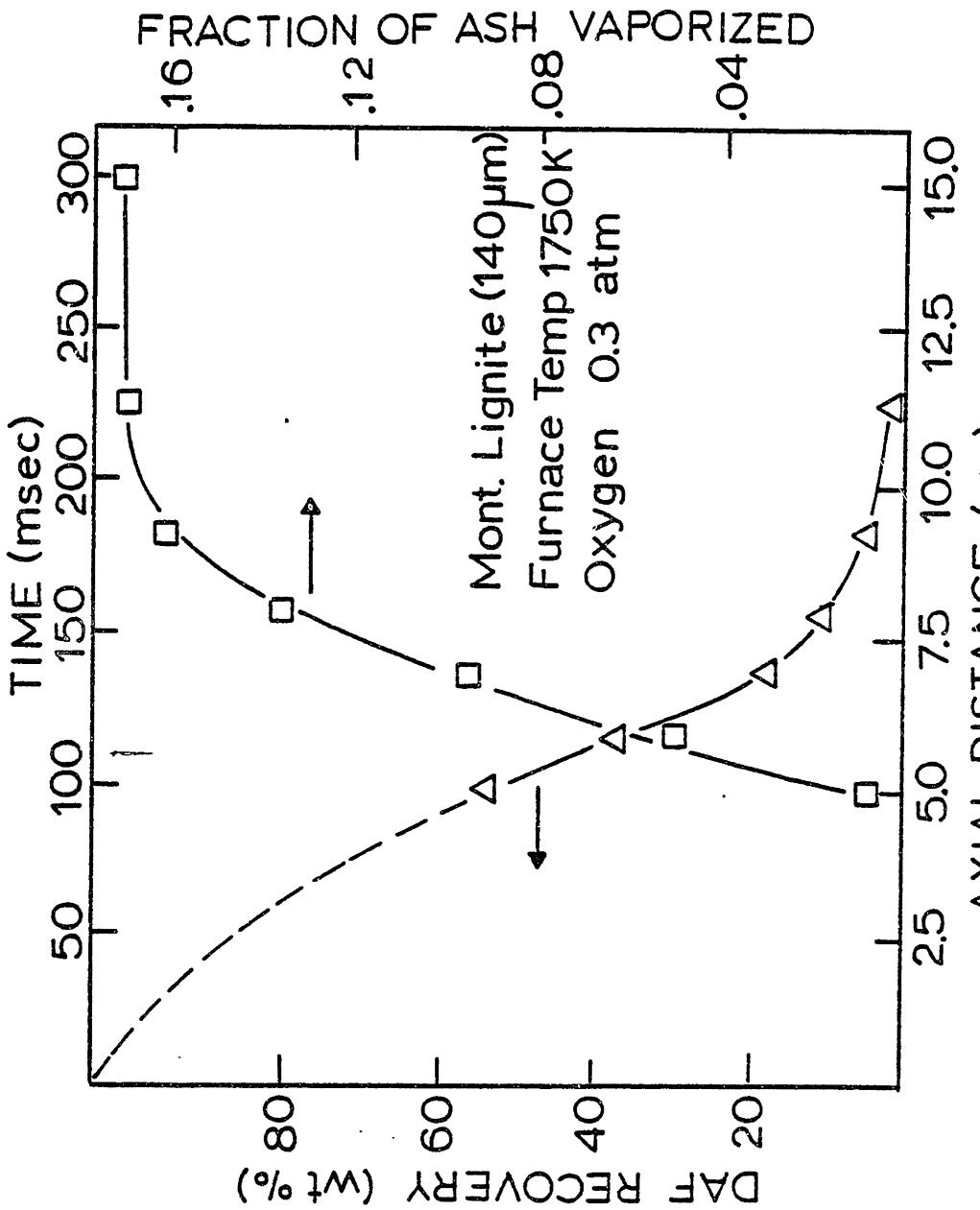

Figure 1.8 Time Resolved Measurement of Ash Vaporization

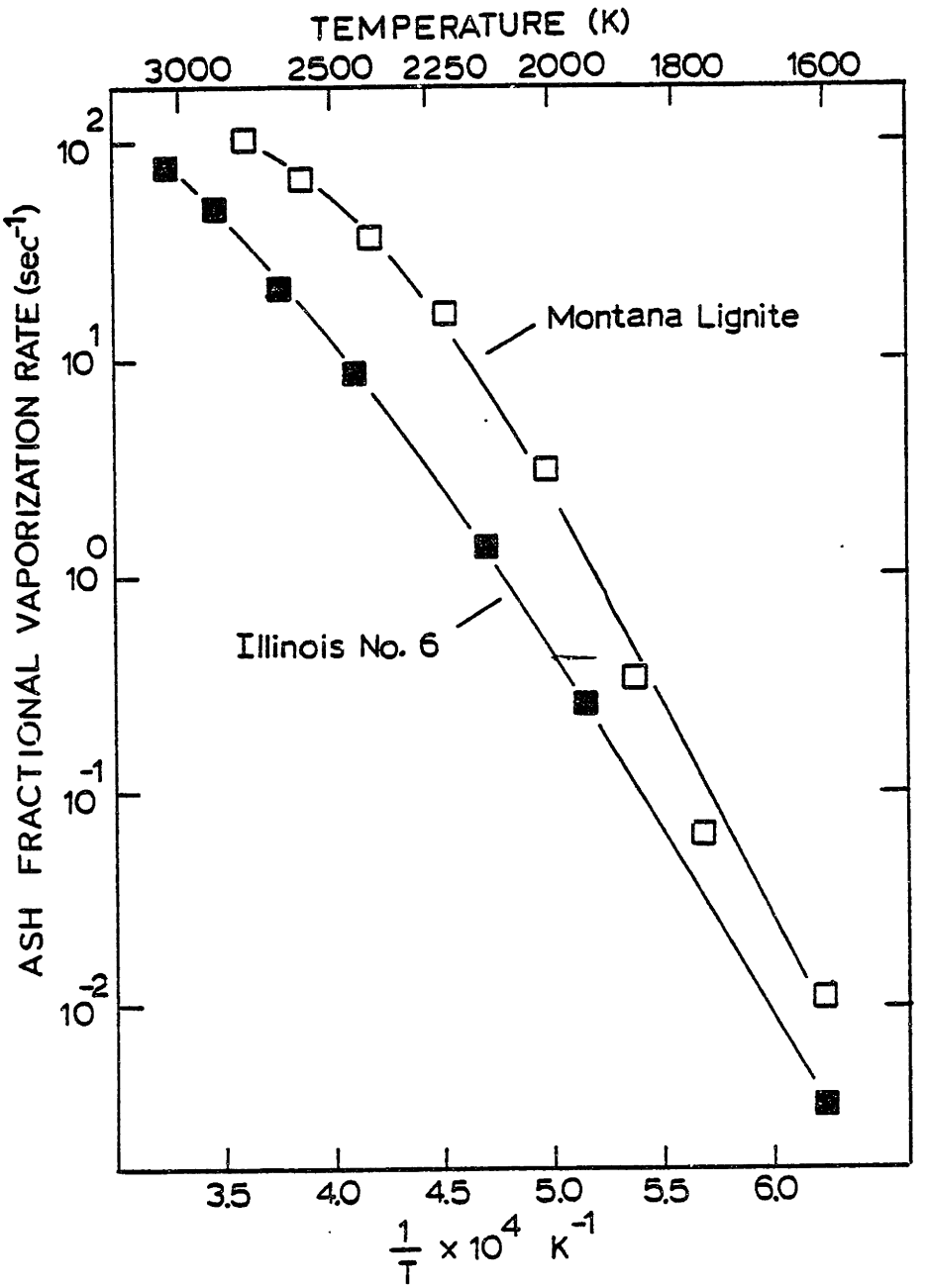

Figure 1.9 Fractional Vaporization Rate Correlation for Total Ash

oxygen at a furnace temperature of 1750K. This empirical correlation indicates that the volatilization rate of ash is a highly activated process, spanning four order of magnitude over the examined temperature range. Analysis of the submicron ash generated at each of these combustion conditions revealed that the elements have different volatilization rates. The results for the Montana lignite are shown in Figure 1.10 for selected elements. Of note is that sodium is considerably more volatile (less activated) having higher fractional volatilization rates than the other elements which are present in the coal ash as refractory oxide compounds. Similar results were obtained for the Illinois No. 6. Because the elements have different temperature dependences of volatilization rates, the composition of the submicron particulate matter varies greatly with combustion temperature as shown for selected conditions in Table 1.10. The volatile alkalis dominate the composition of submicron particulate at the lowest combustion condition. At higher combustion temperatures the vaporization rates of refractory oxides (SiO_2, CaO, MgO, FeO) become significant and hence the components dominate the submicron ash composition.

The effect of particle size on the vaporization rate of specific elements was also examined. These results are presented for selected elements (Si and Mg) in Figures 1.11 and 1.12. The silicon fractional volatilization rates are about a factor of 2 lower for the larger initial coal sizes for both coals. For magnesium, the volatilization rate of the larger lignite size is about a factor of 5 lower. It is a factor of 2 lower

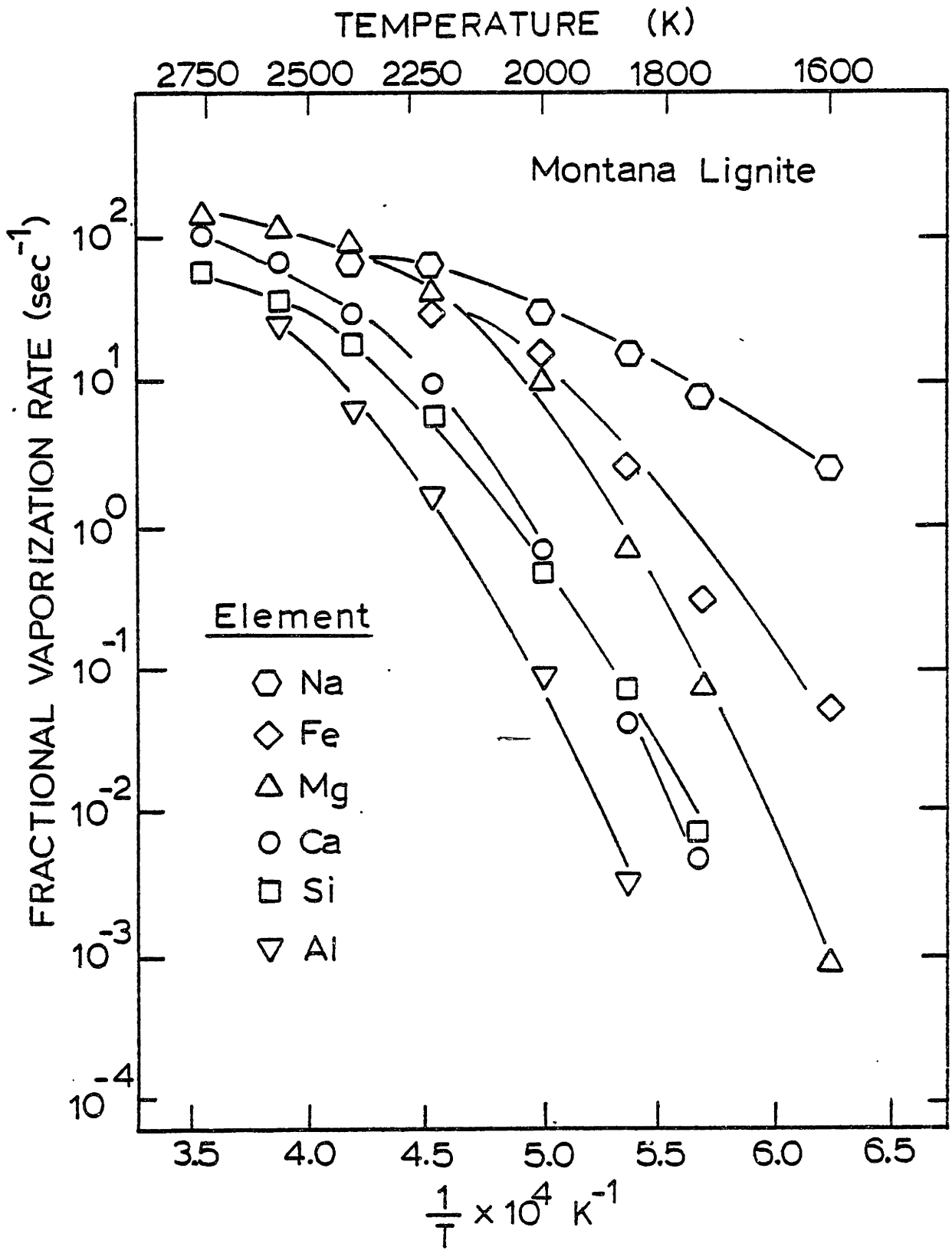

Figure 1.10 Elemental Fractional Vaporization Rate for Montana Lignite

TABLE 1.10

The Effect of Combsution Temperature on the Composition of Submicron Ash

Coal	Montana Lignite			Illinois No. 6		
Temp (K)	1600	2000	2550	1600	2130	2600
SiO_2	----	3.67	11.4	----	34.6	69.7
FeO	9.5	11.5	3.6	15.4	26.0	17.4
MgO	1.3	64.4	29.9	0.71	1.9	0.92
CaO	----	7.8	46.0	----	0.68	1.60
Al_2O_3	----	0.56	7.9	----	1.6	1.41
TiO_2	----	----	0.58	----	----	0.78
Na_2O	89.2	3.7	0.61	38.1	15.6	1.92
K_2O	----	----	----	45.8	14.5	5.50

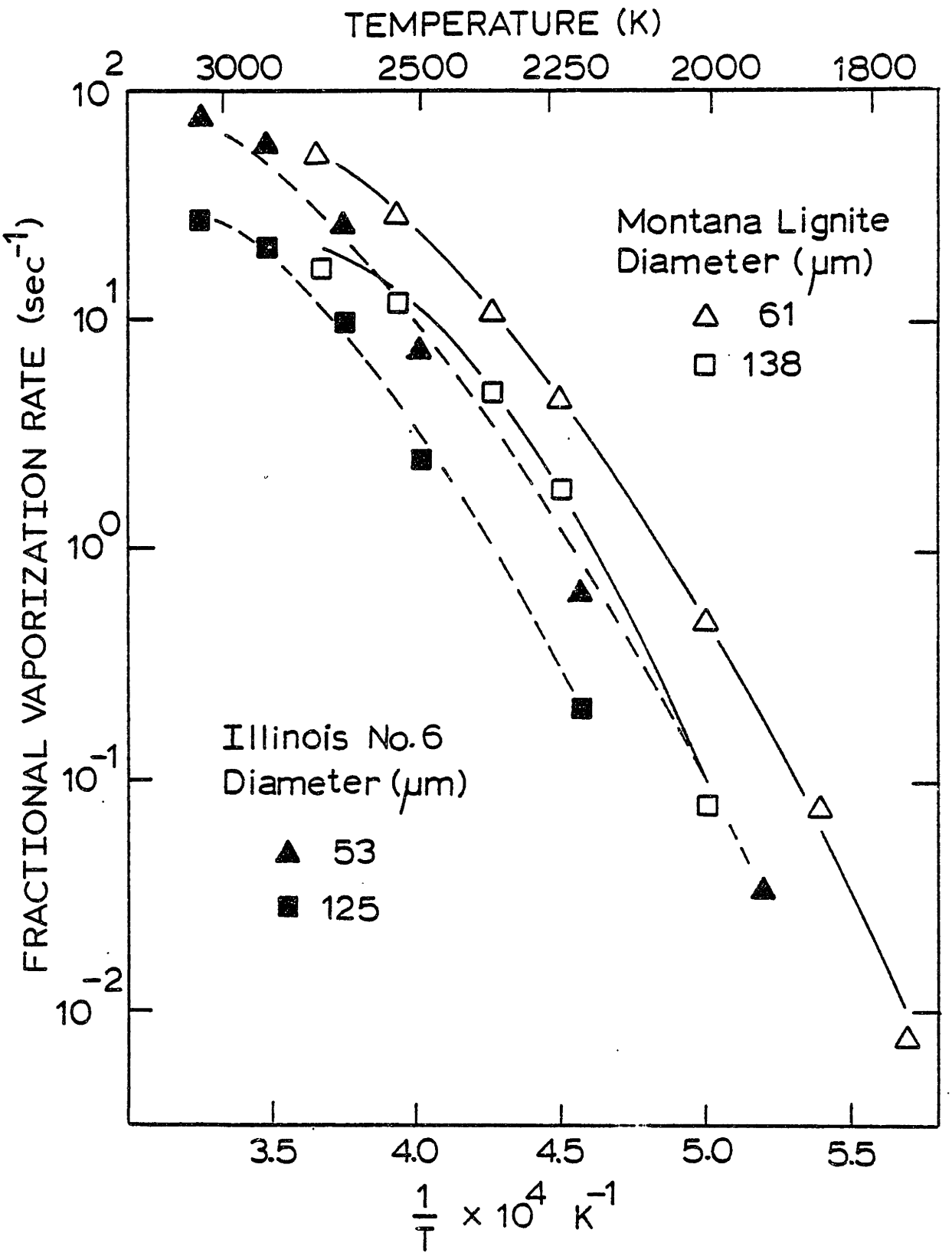

Figure 1.11 The Effect of Coal Size on the Fractional Vaporization Rate of Silicon

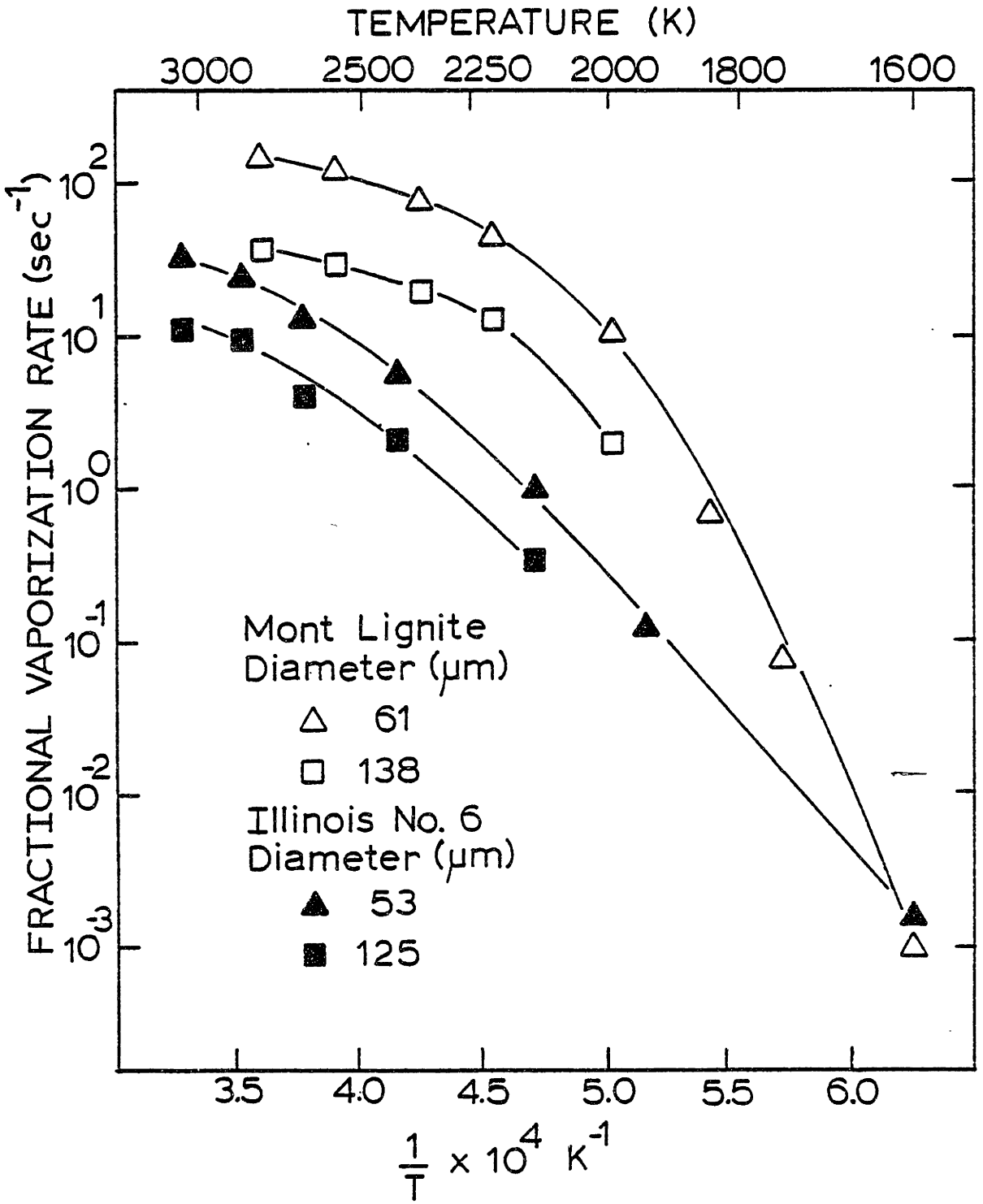

Figure 1.11 The Effect of Coal Size on the Fractional Vaporization Rate of Magnesium

for the larger bituminous Illinois No. 6. Other elements exhibited similar trends in that the larger coal size had consistantly lower fractional volatilization rates.

The effect of CO_2 on the extent of vaporization was also examined by metering .25 atmospheres of CO_2 in the main gas. Two-color optical pyrometry measurements indicated that it did not significantly effect the temperature history of combustion. Presumedly, the endothermic Bouduard reaction was not occurring at a sufficient rate. It did, however, reduce the amount of ash vaporized as shown in Table 1.11.

1.4.4 The Physical and Chemical Evolution of Ash During Combustion

The experimental results presented in the preceeding sections have focused on the vaporization behavior of ash during combustion. The bulk of the mineral matter, however, does not vaporize but is, rather, retained within the parent char particle or on the char's surface in the form of metal oxides ash droplets until the latter stages of char burnout. As will be demonstrated later, the distribution of mineral matter in coal and in burning char particles is an important factor governing the volatilization behavior of the metals. Previous experimental and theoretical studies (Padia, 1976; Flagan and Friedlander, 1979) have only considered the evolution of mineral inclusions during combustion with respect to mineral decompositions, fusion and coalescence of fused droplets on the char surface. Prior to this study, the detailed aspects of the physical and chemical evolution of the organically bound elements during combustion, with a specific reference to the alkaline

TABLE 1.11

The Effects of CO_2 in the Furnace Gas on Elemental Vaporization for Combustion of the Montana Savage Lignite (138 μm). Furnace Temp. 1750K

Furnace Gas Composition (O_2-N_2-CO_2)	Amount Vaporized (μg/g coal burned) Si	Fe	Ca	Mg	Al
20 - 80 - 0	37	254	180	910	17
20 - 55 - 25	10	53	18.5	90	2
35 - 65 - 0	467	346	1140	2882	114
35 - 40 - 25	79	262	327	1276	23
50 - 50 - 0	1100	454	3220	3220	593
50 - 25 - 25	335	298	1805	1832	84

earths held by ion-exchange on the carboxylic groups in low rank coals, were unknown. This phenomena was investigated by scanning electron microscopy (SEM), equipped with energy dispersive X-ray analysis (EDXA) for metal detection, and by X-ray diffraction, for compound identification, of partially oxidized lignite chars. Char particles were withdrawn from the furnace combustion zone and rapidly quenched with the collection probe at several stages of burnout. The samples were obtained at a condition corresponding to particle combustion temperatures of approxiamtely 2000K.

The char particle shown in Figure 1.13 is at approximately 57 percent DAF weight loss for combustion at 2000K. A region of its surface is shown at higher magnification in Figure 1.14A. Although the combustion rate of the char is expected to be controlled primarily by the external transport processes at this high temperature condition, it is evident from the lacy structure of the surface and the development of large holes (1-5 microns) and pores that oxygen is penetrating the chars outer layer to a certain extent. Also visible in Figure 1.14A are droples of ash. Close examination of the face of the organic material reveals that it is entirely covered by submicron 'grains'. The EDXA of the ash droplet marked by (a) and the carbonaceous area (b) in Figure 1.14A are compared in Figure 1.14B. The nearly identical spectra with respect to relative intensities of elements provides evidence for the transformation of the organically bound material into ash droples on the char surface as the organic matter is gasified. This process apparently first

Figure 1.13 Scanning Electron Micrograph of a Partially Oxidized Montana Lignite Particle at 57% DAF Weight Loss. Combustion Condition 1750 K in 20% Oxygen.

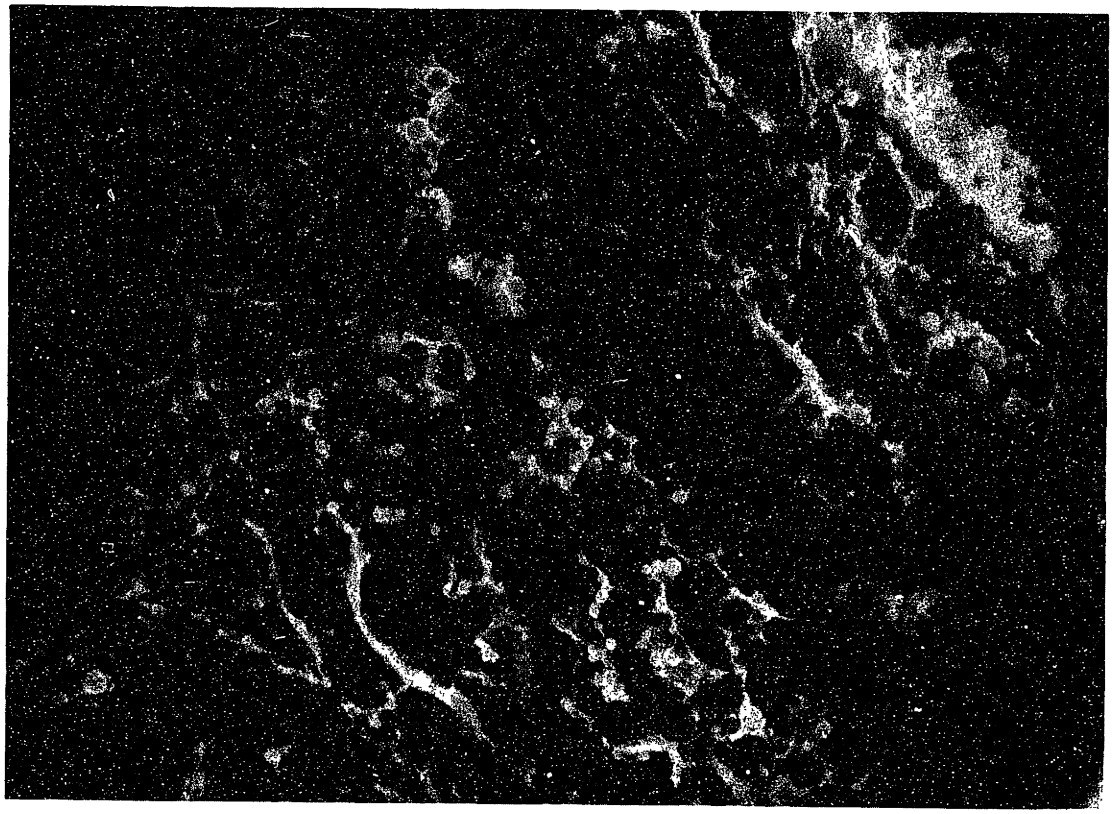
20 μm

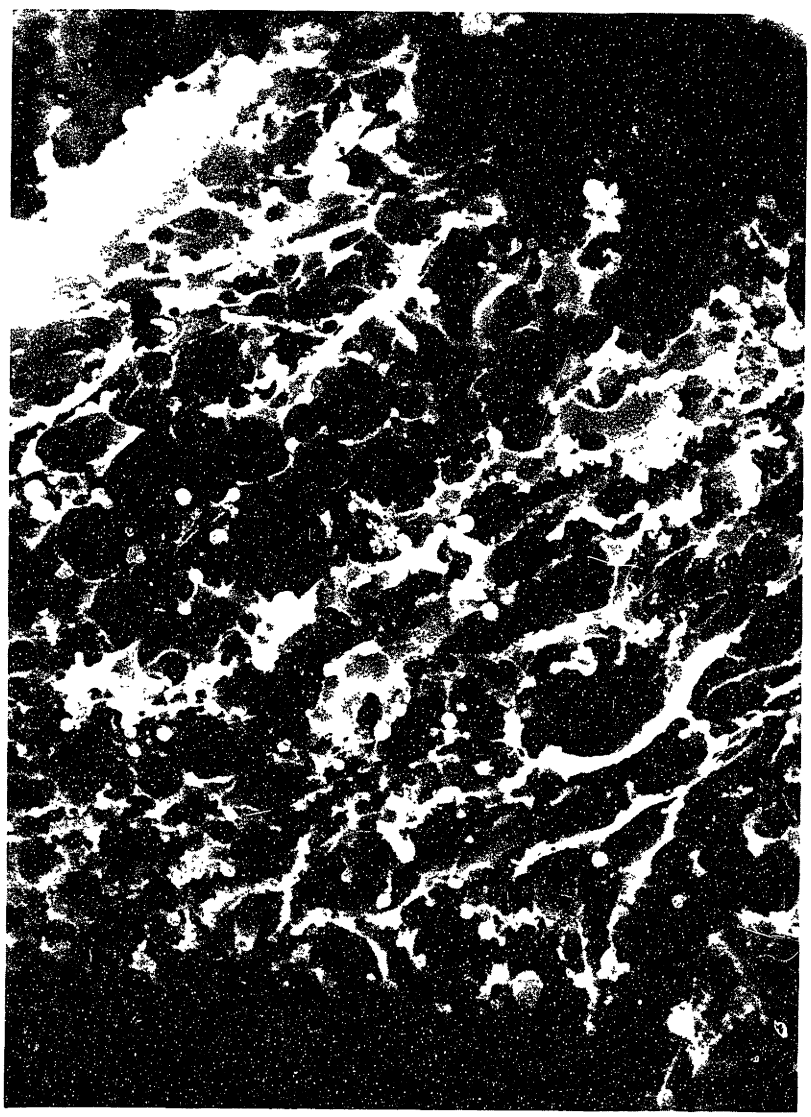

INTENTIONAL DUPLICATE EXPOSURE

Figure 1.14A Scanning Electron Micrograph of the Surface of a Montana Lignite Char Particle at 57% DAF Weight Loss. Combustion Condition at 1750K in 20% Oxygen.

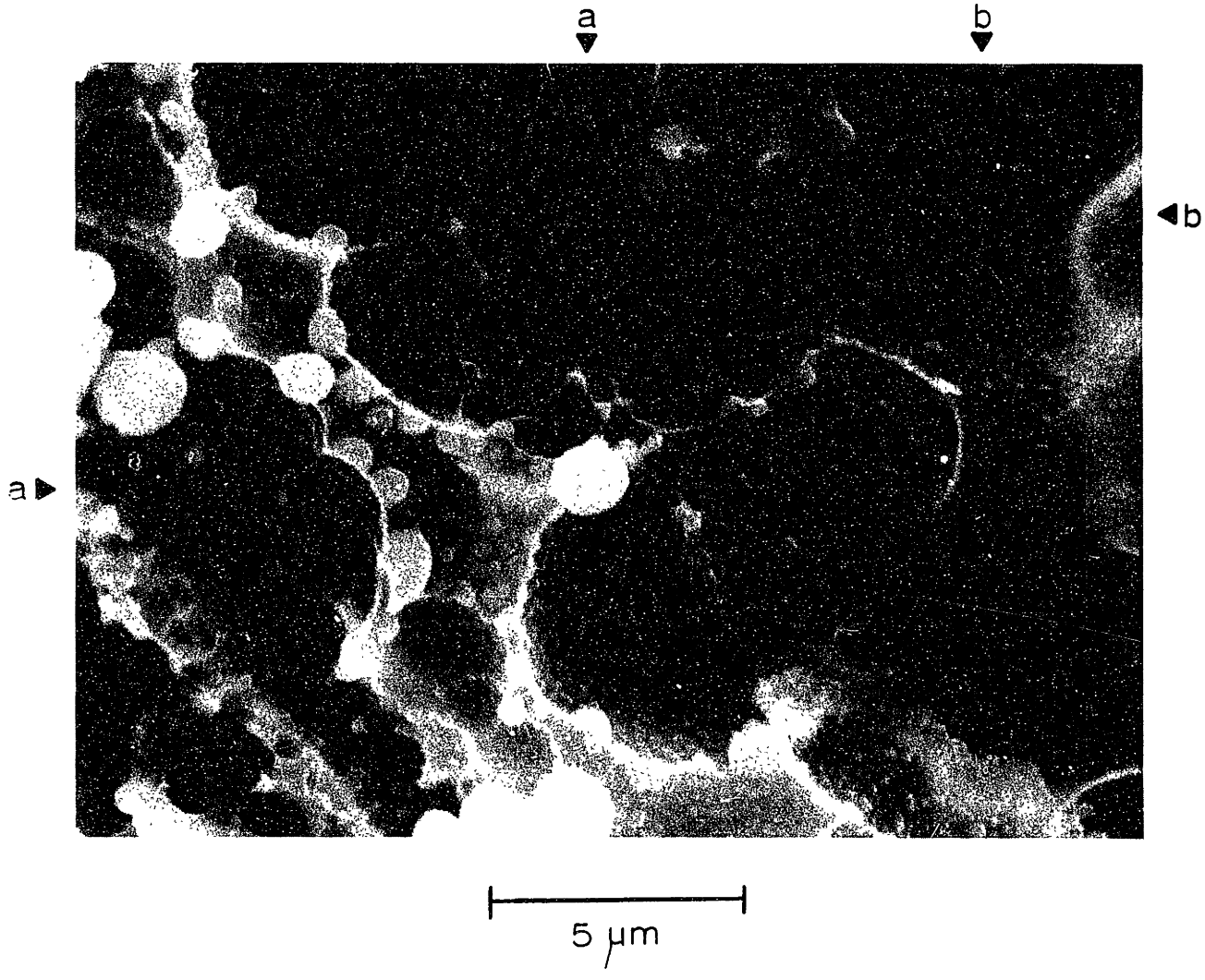
a
b
a
b
5 µm

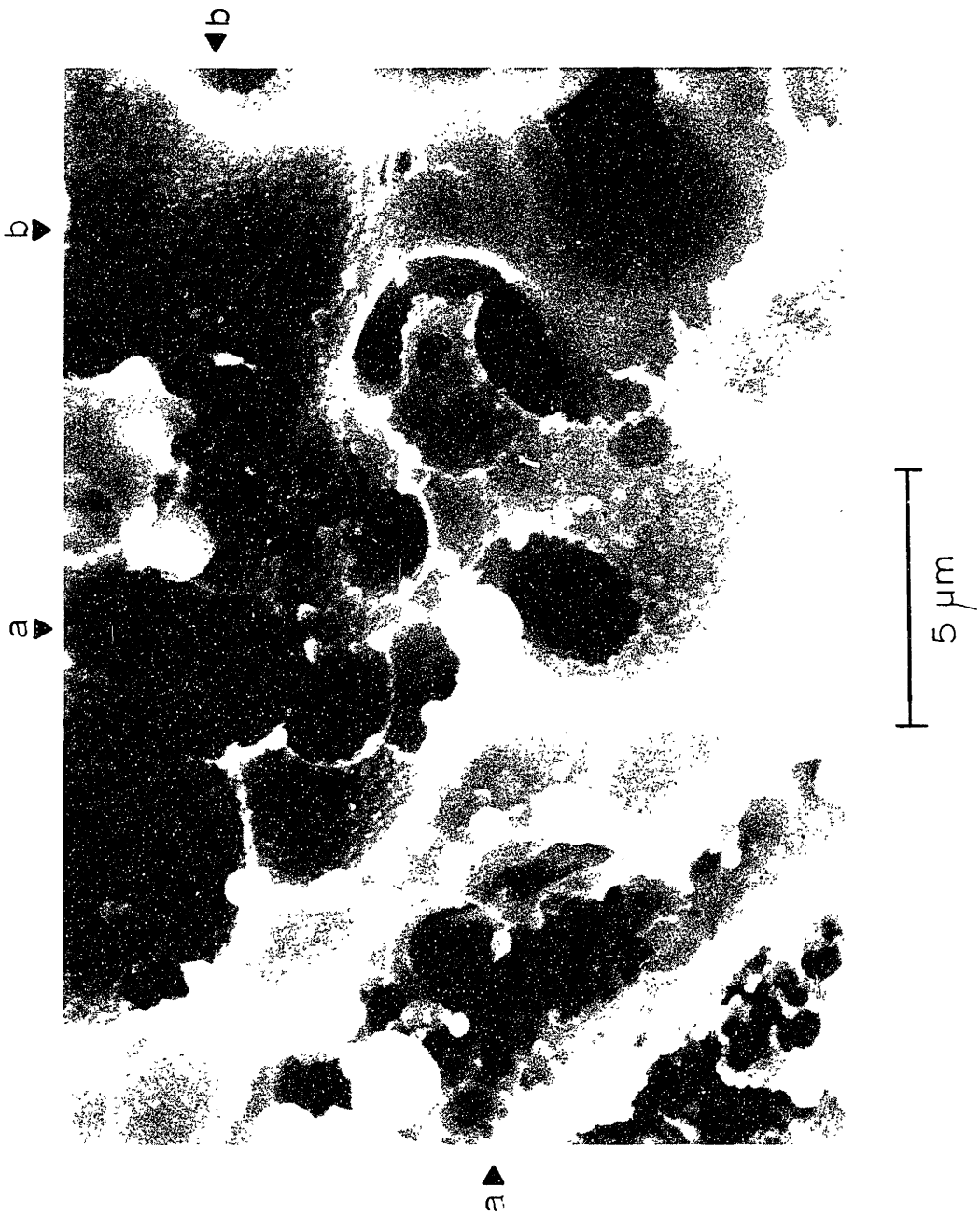

INTENTIONAL DUPLICATE EXPOSURE

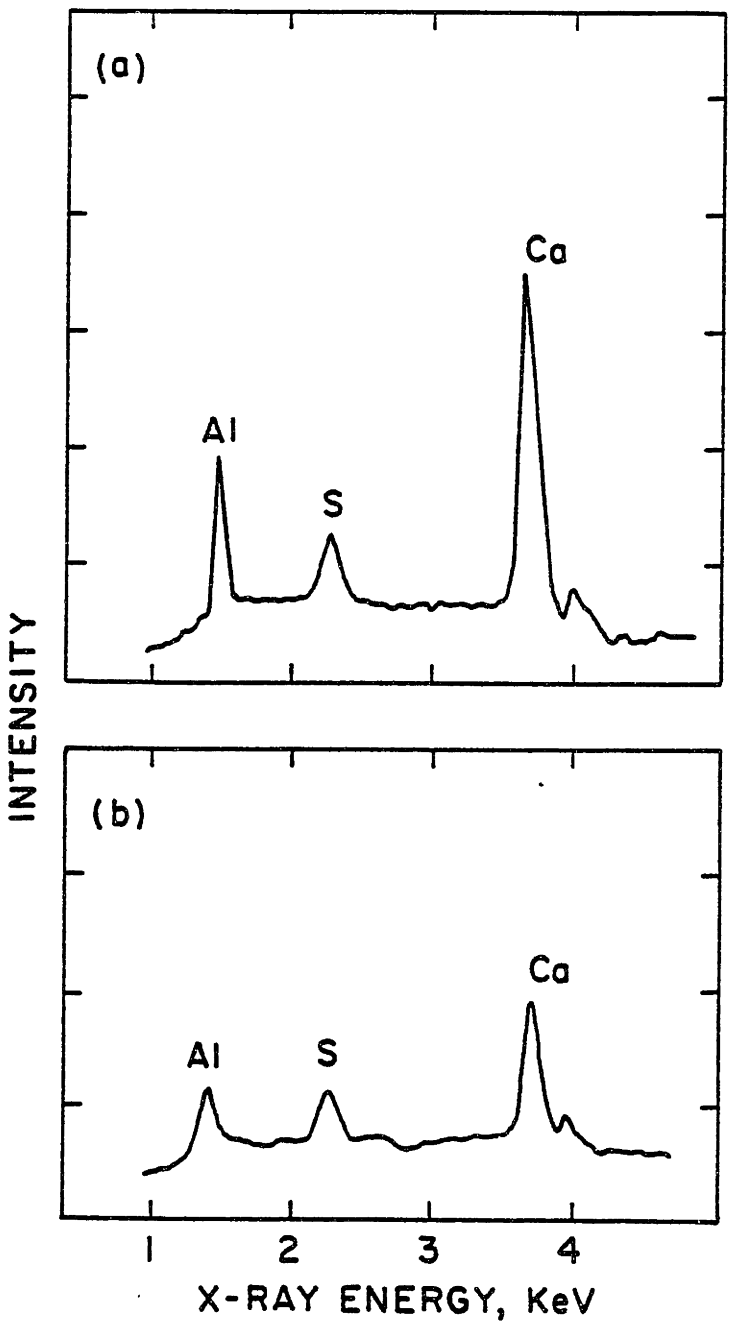

Figure 1.14B EDXA Spectra of Ash Droplet (a) and Organic Matter (b) in Figure 1.14A

proceeds by the formation of minute (submicron) grains of ash directly on the face of the carbonaceous material. The grains continue to grow to dimensions greater than 1 micron along the ridges created by the combustion process during the early stages of burnout. EDXA can only detect metals. It is assumed that the ash is in the form of metal oxide. At higher magnification (Figure 1.15A), the grains and their growth along carbon ridges are more clearly visible.

At a later stage of burnout (72% DAF wt. loss) as shown by the highly magnified view of the surface of another char particle in Figure 1.16A, the surface ash has undergone considerable growth and appears to be in a solid state. This material is composed primarily of the alkaline earth oxides. Heterogeneity is observed with respect to magnesium abundance as shown by the EDXA (Figure 1.16B) of the regions localized by the arrow. The alkaline earth oxide ash has apparently assimilated some of the silica in the char at this stage of burnout. At still later stages of burnout, the ash on the surface of the char has undergone still further growth as shown in Figure 1.17A. From EDXA (Figure 1.17B), the large molten ash inclusion marked by (a) was originally an alumino-silicate mineral embedded deep within the coal particle. The partially crystalline material (b) is the alkaline earth ash in its final stages of evolution. Solid MgO and CaO are stable as solid at 2000K (melting points of 3098 and 3200 K, respectively) but will form a eutectic at about 2550K. X-ray diffraction of chars obtained at the 2000K combustion condition did reveal the presence of both crystalline CaO and MgO.

Figure 1.15A Scanning Electron Micrograph of the Surface of a Lignite Char Particle (57% DAF Weight Loss) Illustrating the Presence of Ash Grains on the Organic Matter.

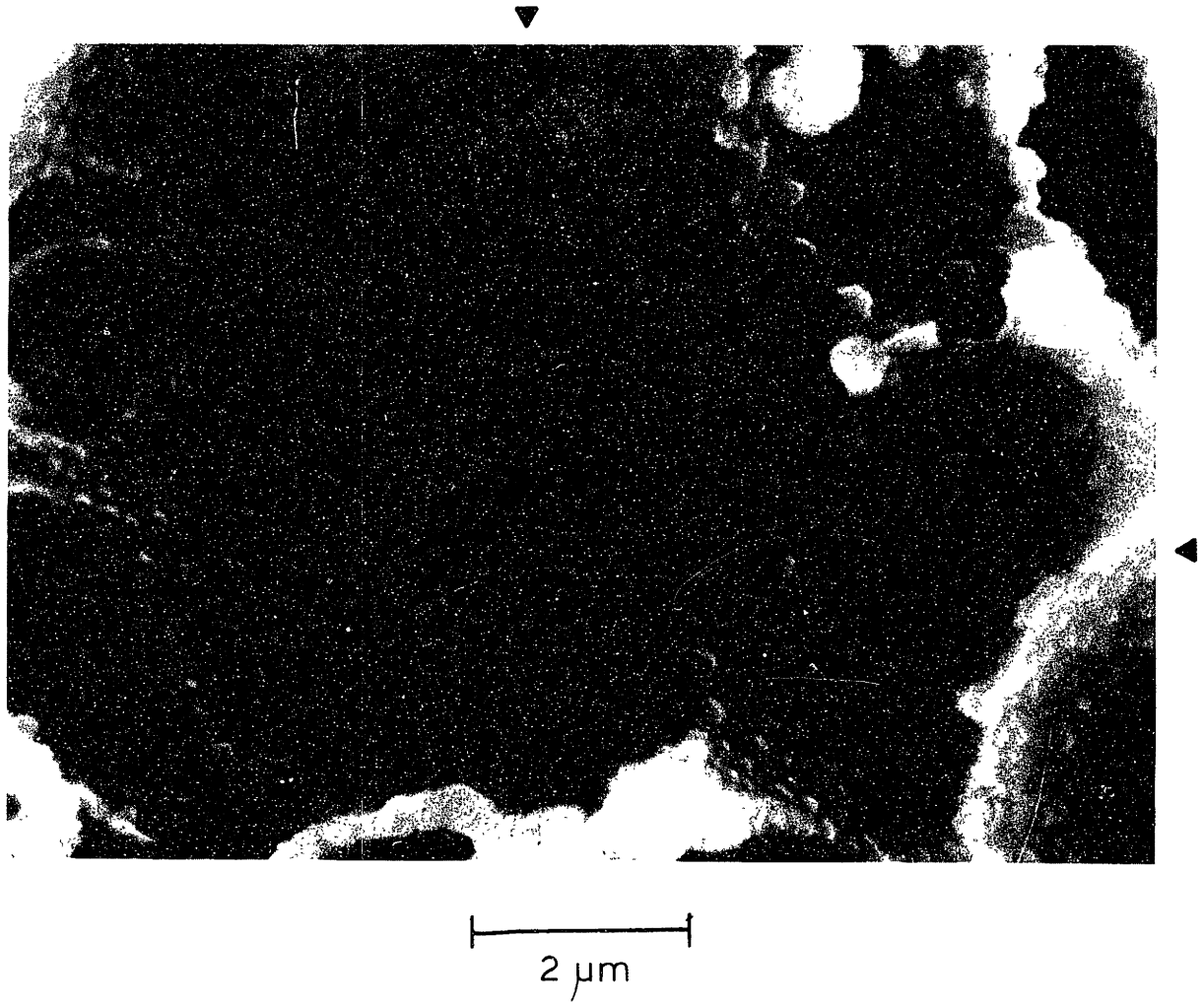
2 µm

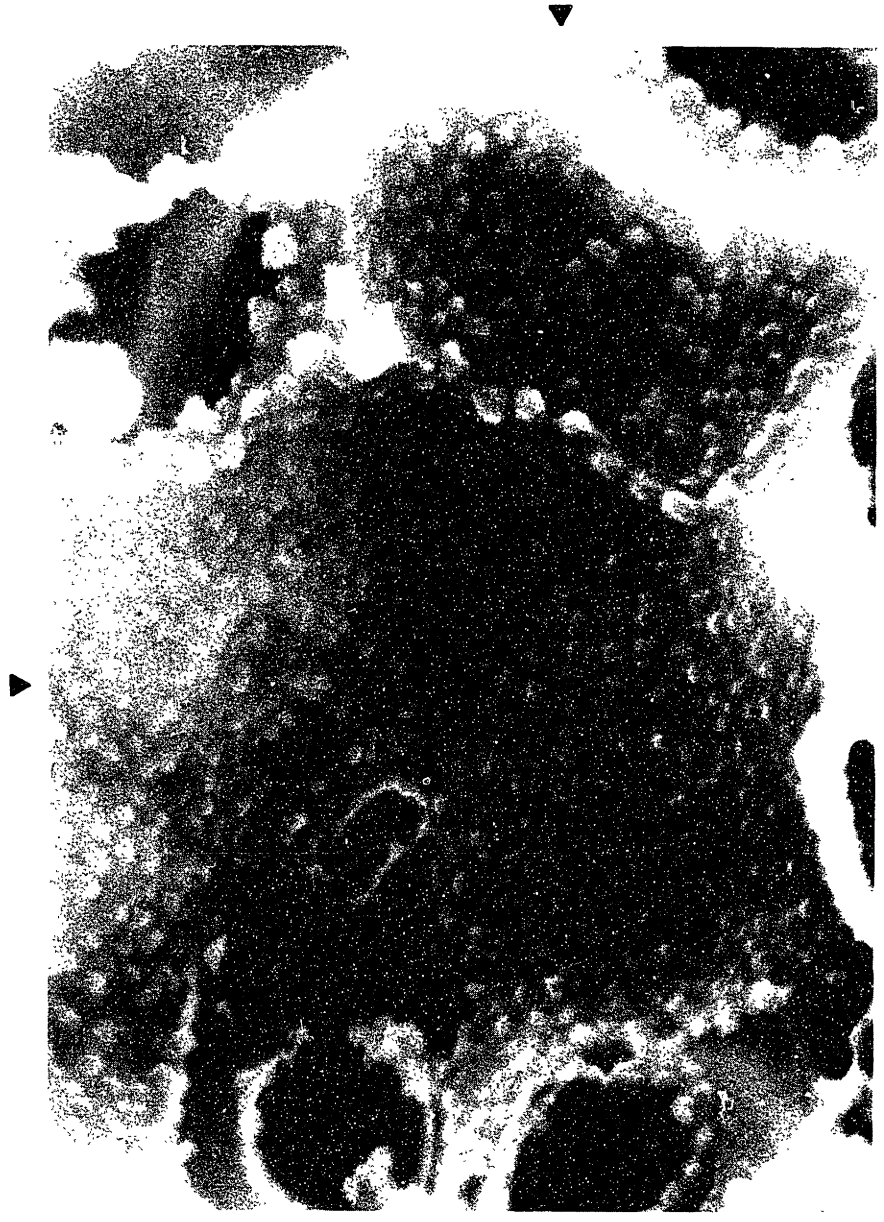

INTENTIONAL DUPLICATE EXPOSURE

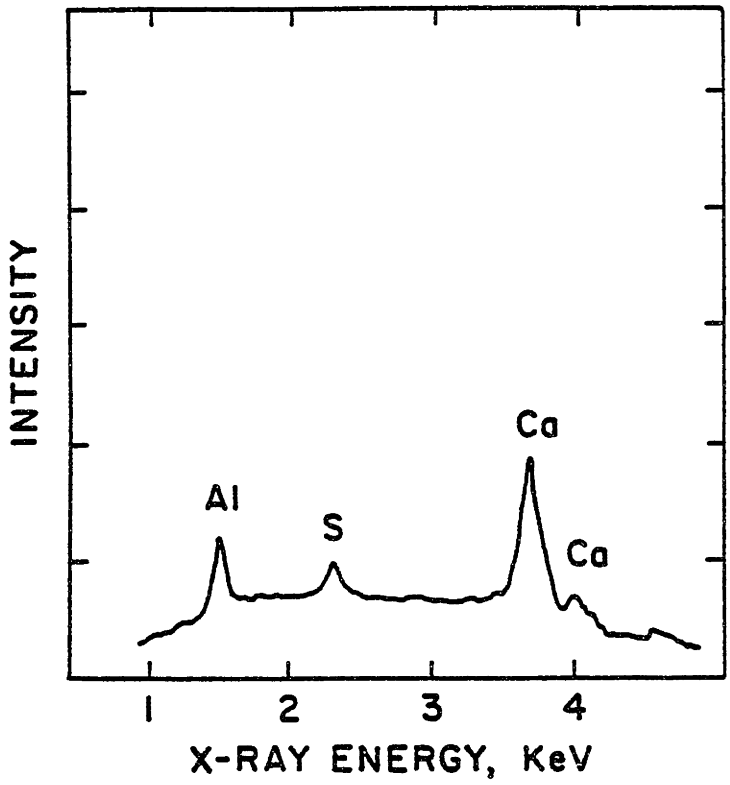

Figure 1.15B EDXA Spectra for Figure 1.15A

Figure 1.16A Scanning Electron Micrograph of the Surface of a Lignite Char Particle at 72% DAF Weight Loss. Combustion at 1750K in 20% Oxygen.

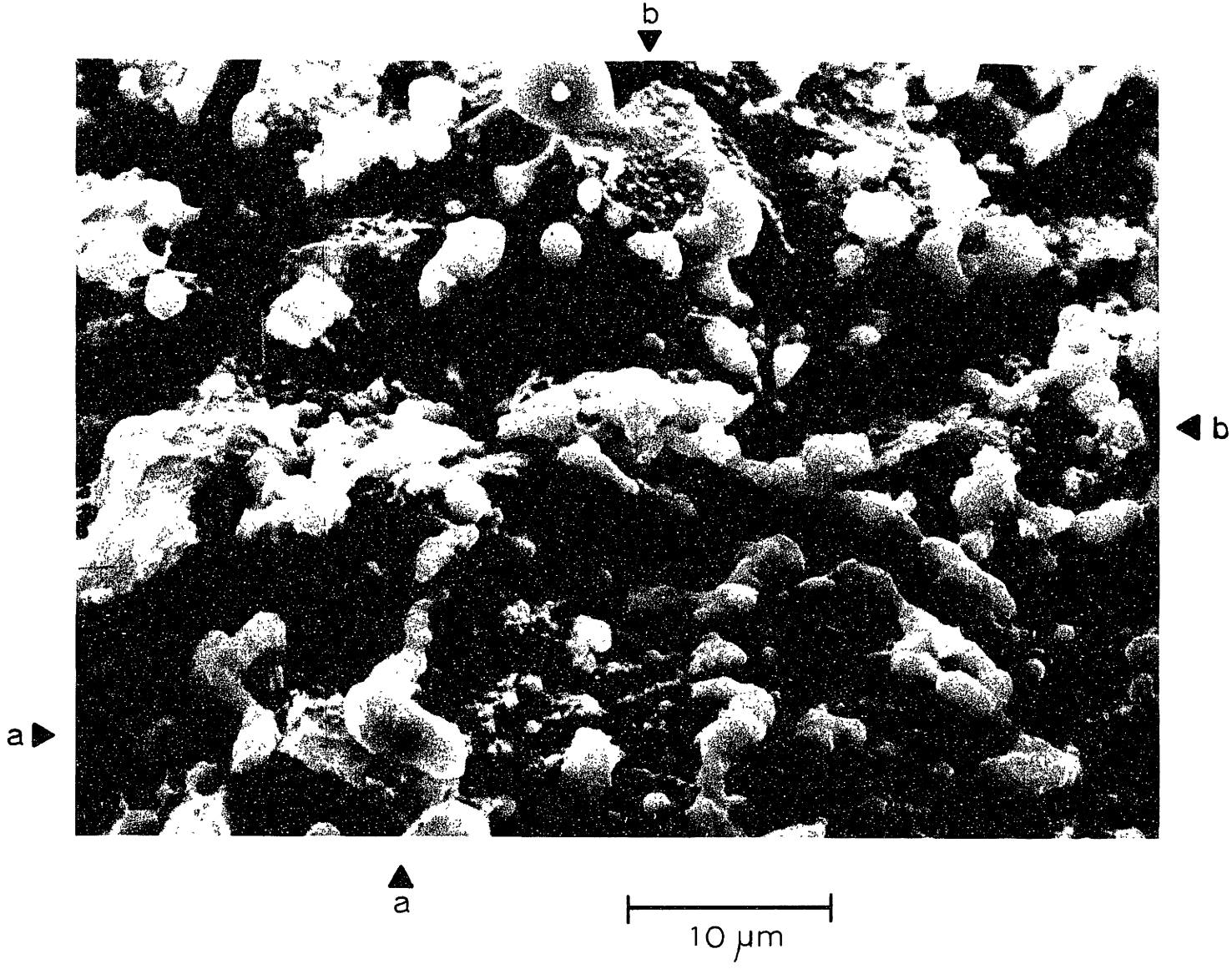
b
a
b
a
10 µm

INTENTIONAL DUPLICATE EXPOSURE

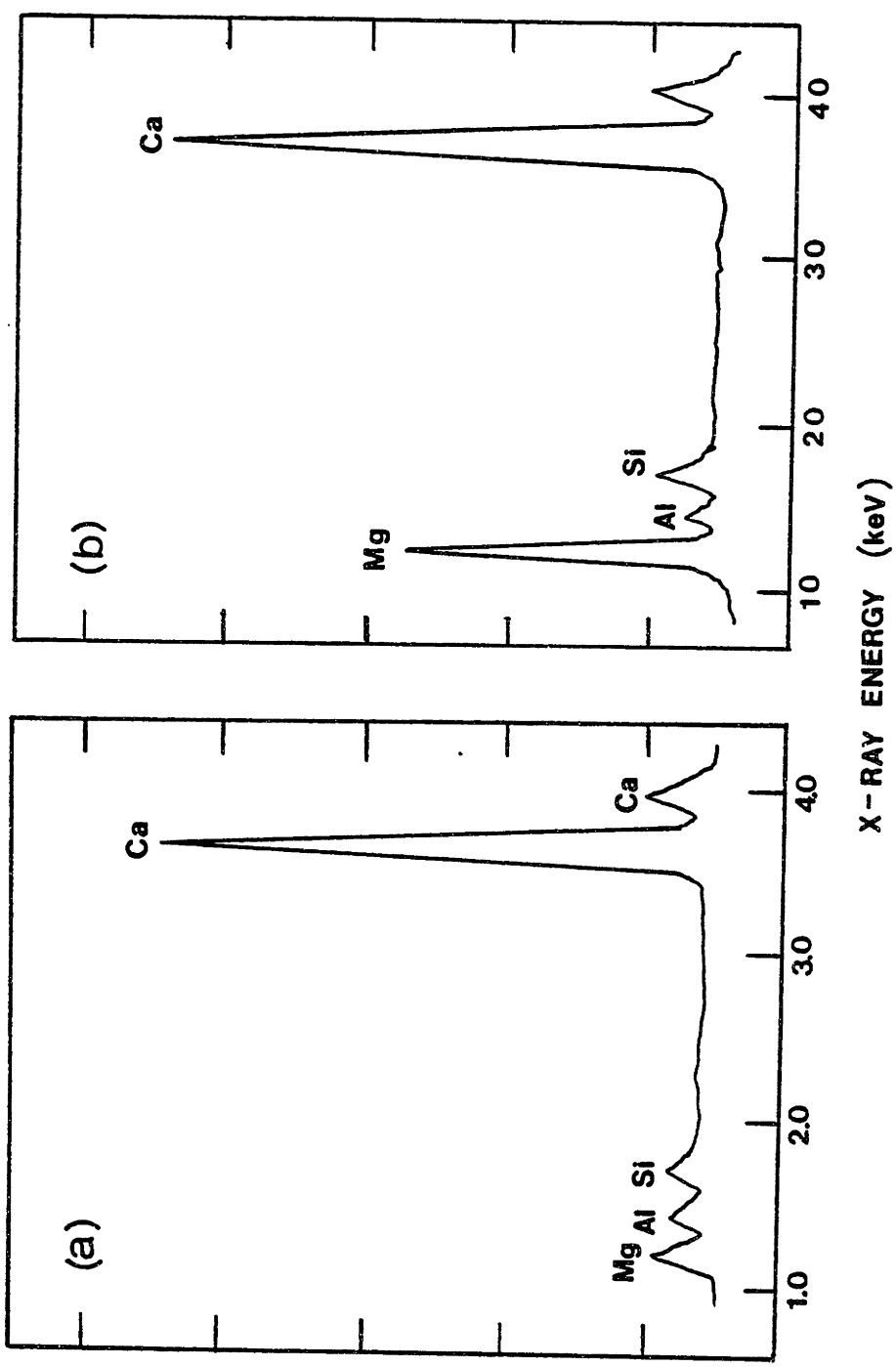

Figure 1.16B EDXA Spectra for Figure 1.16A

Figure 1.17A Scanning Electron Micrograph of the Surface of a Lignite Char Particle at 82% DAF Weight Loss. Combustion at 1750 K in 20% Oxygen.

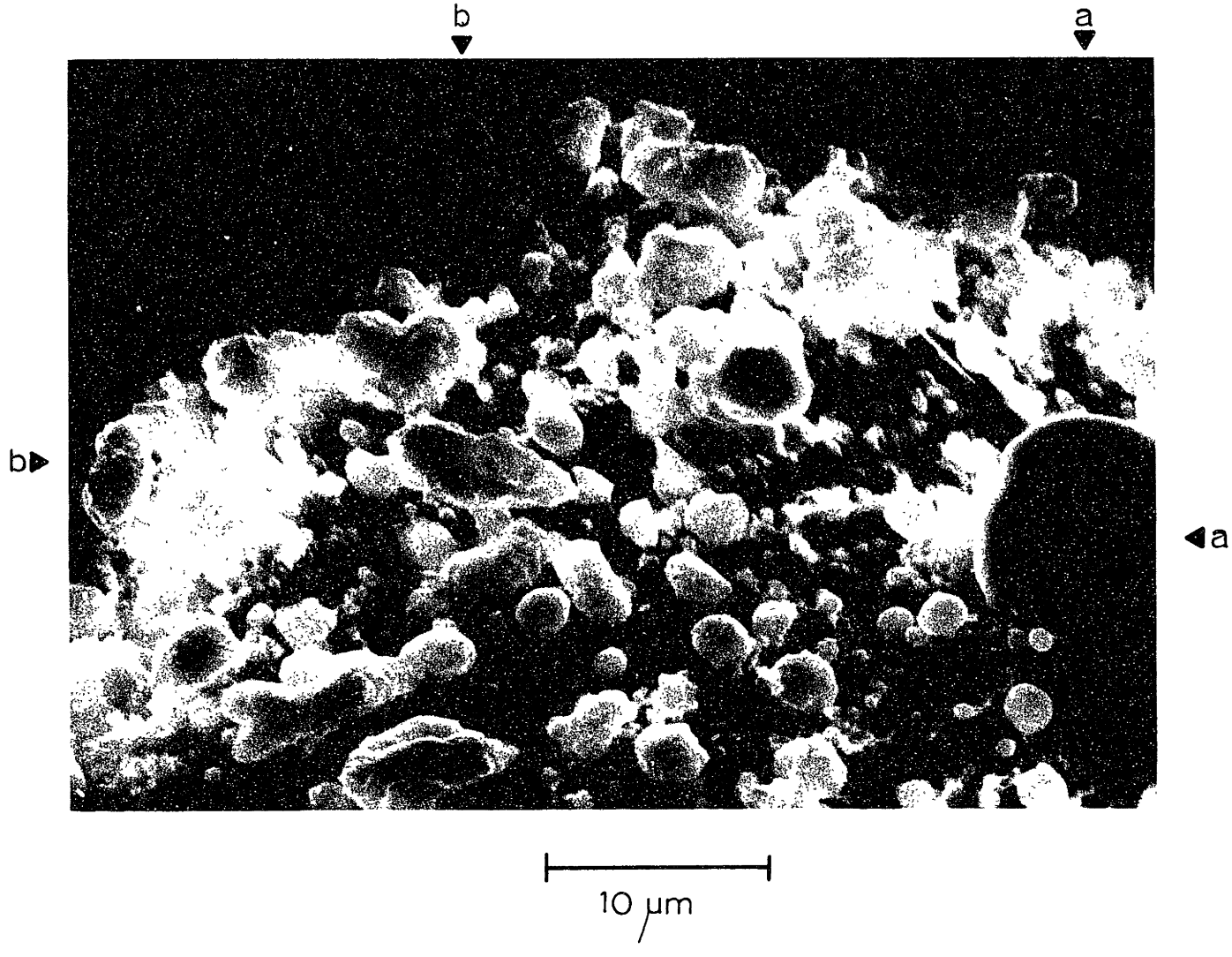
b
a
b
a
10 µm

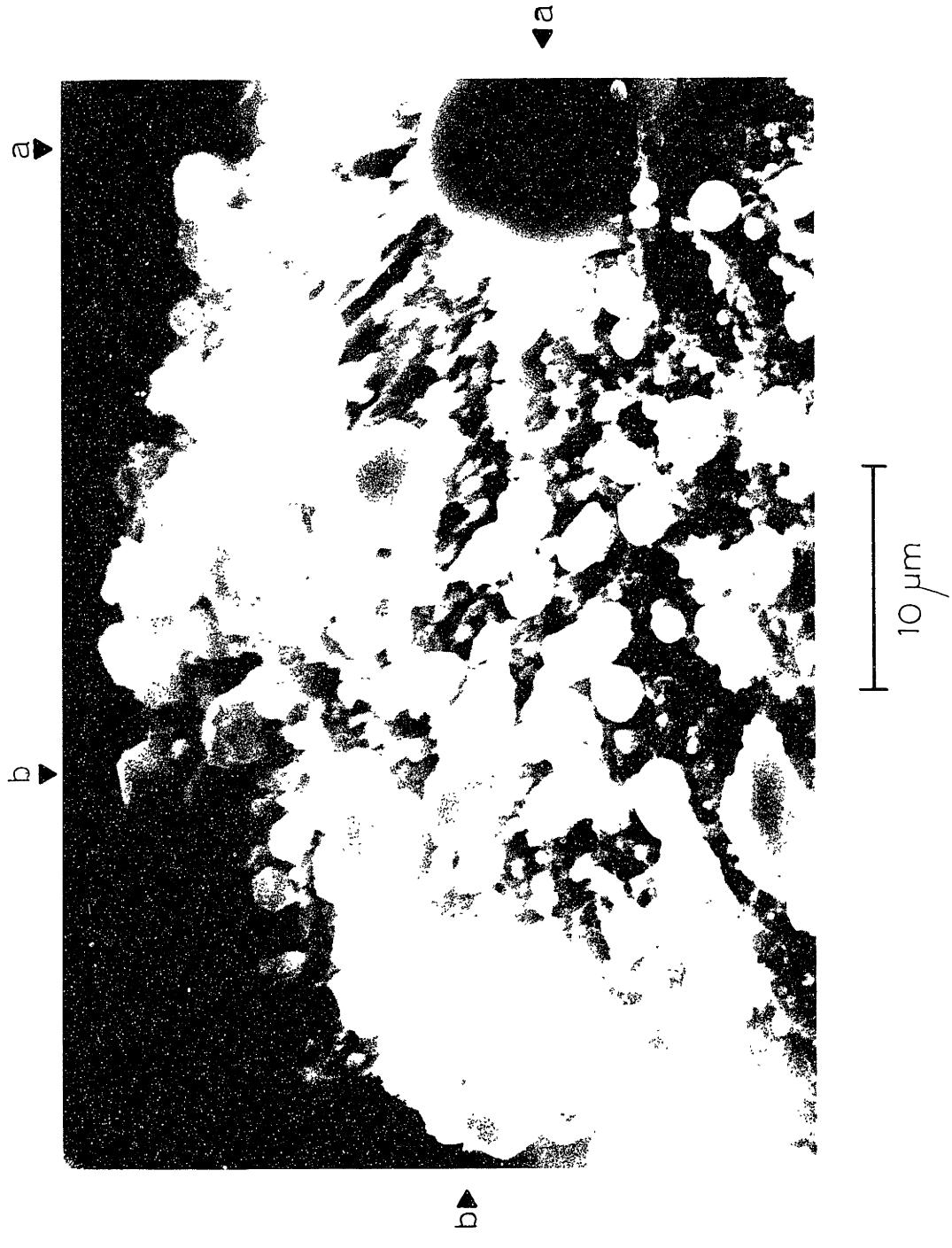

INTENTIONAL DUPLICATE EXPOSURE

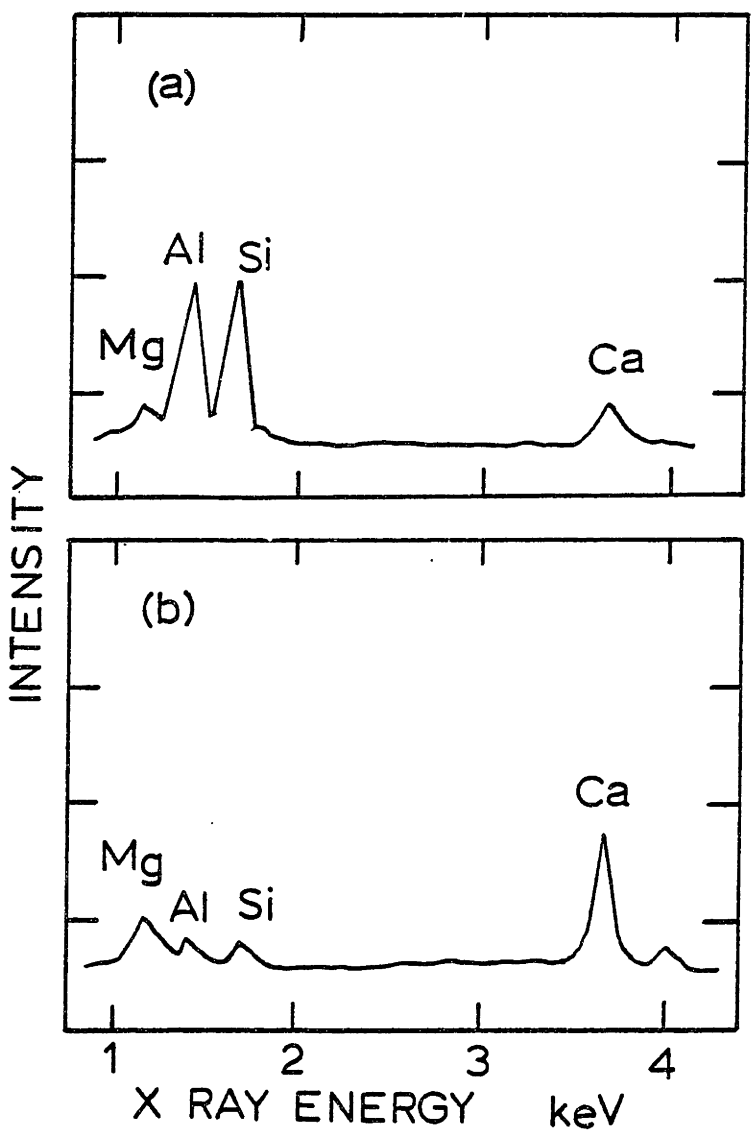

Figure 1.17B EDXA for Figure 1.17A

1.5 Modelling

The experimental results demonstrate that ash vaporization is dependent on combustion temperature and on coal type with respect to elemental concentration and also, in certain cases, with respect to the various forms of mineral matter in coal. Furthermore, the fractional vaporization rate correlations for specific elements (Figures 1.11 and 1.12) are not independent of the initial size of the coal or, for that matter, the coal type. An idealized model for a single burning coal particle was developed to examine and interpret the experimental results in terms of (a) physical processes, including the internal and external transport of inorganic vapors from the char particle, (b) thermochemical processes involving the generation of volatile inorganic vapors within char particles by the reduction of refractory metal oxides, and (c) the physical arrangement of mineral matter in pulverized coal particles.

Inherent mineral matter in coal occurs as either finely dissemenated crystallites or inclusions with typical characteristic dimensions of 2 μm or less (Padia 1976, Ward, 1977) embedded in the organic matrix of coal particles as in the case of silicon in quartz or clay minerals, or as elements organically bound and dispersed as in the principal occurance of calcium and magnesium in low rank coals. The general model considers the existance of a uniformly distributed array or assemblage of monodisperse discrete spherical mineral inclusions within each pulverized coal particle. As the coal ignites and the

temperature rises, each inclusion of the array within a single porous char particle acts as a vapor souce contributing to the overall volatilization rate of the inorganic species as shown schematically in Figure 1.18.

If θ_I is defined as the volume fraction of inclusions in the char particle for a specific mineral component, then the number of inclusions, N_I, inside a single char particle of radius r_p is given by

$$N_I = \theta_I \left(\frac{r_p}{r_i}\right)^3$$

For organically bound metals N_I tends to infinity. The radius of the char particle, and hence also N_I, is a function of time during combustion. For coals which burn as shrinking spheres, the char radius at time t is given by

$$r_p(t) = r_o \left(1 - \frac{t}{t_b}\right)^{1/2}$$

where t_b is the burning time of the coal particle and r_o is its initial radius. During the course of burnout, Θ_I remains constant because inclusions initially within the char appear on the char's receding surface.

The number of inclusions in a 50 micron diameter particle is on the order of a 1000 for typical concentrations of mineral matter in coal, assuming the inclusions are on the order of 1 micron in size.

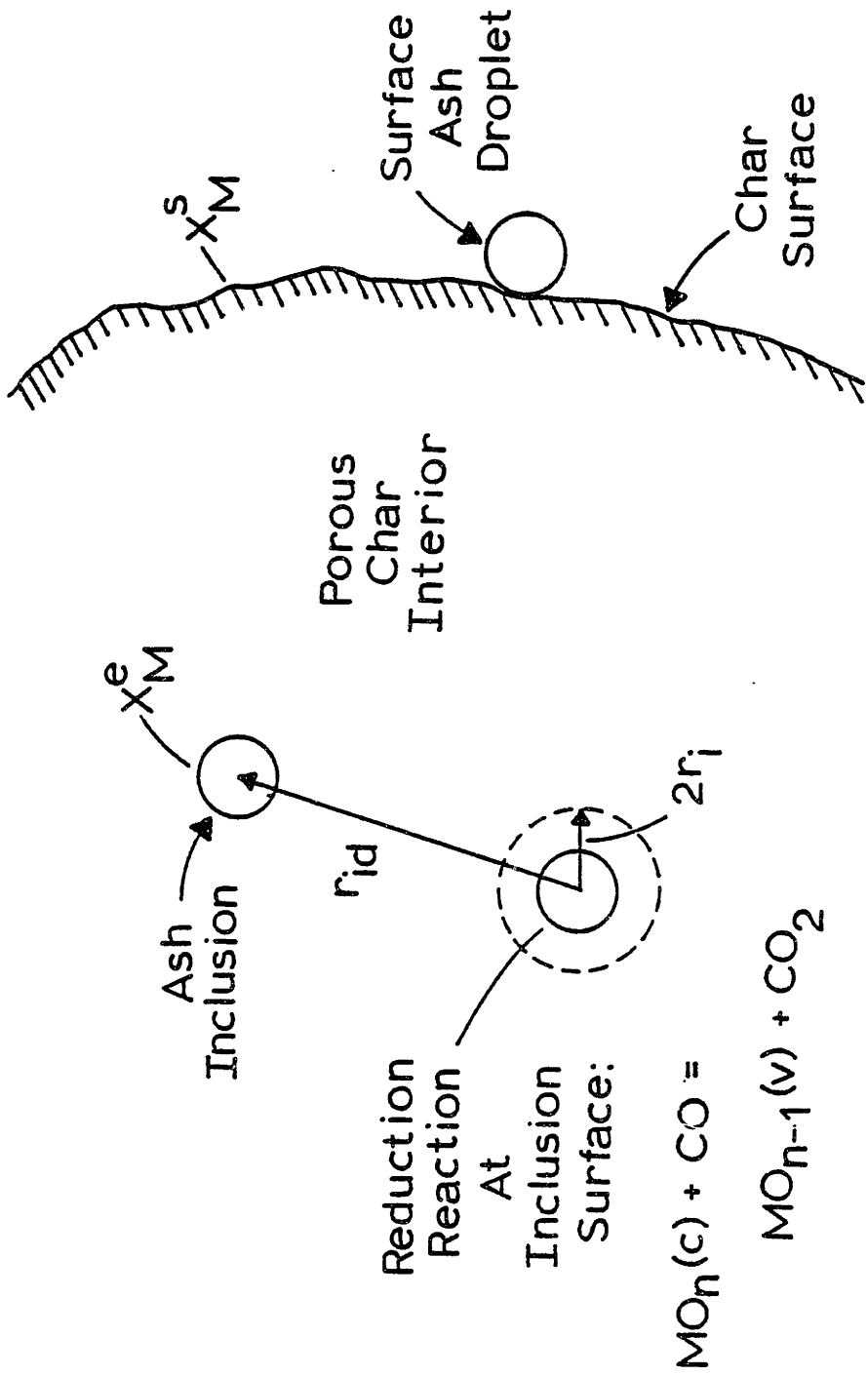

Figure 1.18 Schematic of the Physical Distributions of Inclusions in a Char Particle

Thermochemical Aspects

The key to the thermochemical aspect of ash volatilization is that, although the coal particles are burning in oxygen rich environments, the atmosphere experienced by the inherent mineral matter within the char particle is of low oxygen potential or reducing. Hence, as long as the char is burning, the refractory metal oxides of the inherent ash may undergo chemical reduction to more volatile forms. The overall reaction in the presence of excess carbon may be expressed as

$$MO_n(c) + C = MO_{n-1}(v) + CO \qquad (a)$$

where MO_n is the stable condensed metal oxide (i.e. SiO_2, MgO or CaO) and MO_{n-1} is the volatile suboxide (SiO) or metal vapor (Mg or Ca). Silicon monoxide (SiO) is only stable as a gas and the boiling points of Mg and Ca are below the combustion temperatures examined here. Reaction (a) as written in an inherently slow process requiring the contacting of three phases. Under the time scales of combustion (< 1 second) it is unlikely that reaction (a) reaches equilibrium. It is more likely that chemical reduction proceeds through gaseous intermediates (Szekely et al., 1976) via the heterogeneous reactions

$$MO_n(c) + CO = MO_{n-1}(v) + CO_2 \qquad (b)$$

$$CO_2 + C = 2CO \qquad (c)$$

Other gaseous species including H_2 and radicals may act as reducing agents. In the present analysis, these are neglected as they are expected to be at much lower concentrations in this experimental system. The assumption within the framework of

the model that reaction (b) is occuring and is at equilibrium at the surface of each inclusion within the char.

The equilibrium partial pressure of the metal or suboxide vapor, P_m^e, at the surface of each inclusion is then determined from the equilibrium constant K_e for reaction (b)

$$K_e = \frac{P_m^e P_{CO_2}}{a_{MO_n} P_{CO}}$$

The inclusions may be pure components such as molten silica from quartz or CaO (s) from decomposed calcite minerals, or as a multicomponent system resulting from, for example, the rapid high temperature decomposition of alumino-silicate clays. For the present, the coal is assumed to be a single component system with respect to a metal oxide. The presence of other ash components in the char or in solution may influence the volatilization of a specific component in several ways and a qualitiative consideration of these effects is reserved for the Discussion section. For a single component system, and assuming there is no other source of carbon dioxide to influence the equilibria at the surface of each inclusion, the partial pressure of the inorganic vapor at an inclusion surface is simply expressed as

$$P_m^e = P_{CO_2} = (K_e P_{CO})^{1/2}$$

The partial pressure of CO in the char particle is obtained by assuming that the oxygen diffusing to the surface of the char is completely consumed at the surface and that CO is the only product of combustion.

Vapor Transport Processes

Given that there is an equilibrium partial pressure of inorganic vapor at the surface of each inclusion within a char particle, the rate of vaporization from a single inclusion may be described by a local microscopic diffusion process centered about the inclusions. Provided that the inclusions are embedded in an isotropic porous medium where the characteristic dimensions of the pores are much less than the inclusion size, the rate of vaporization of a single isolated inclusion is given by

$$V_I^{ni} = 4\pi c D_e r_i X_m^e \qquad (1.1)$$

where X_m^e is the equilibrium mole fraction of the inorganic vapor at the inclusion surface and D_e is the effective diffusivity for Knudsen diffusion of the vapor in the porous char. The superscript ni designates that this rate is for an isolated non-interacting inclusion or droplet within the char. In actuality, a single char particle will contain a large number of inclusions. It is assumed that these inclusions are randomly distributed. As a result of pore diffusion processes, the inclusions are not isolated but, rather, are interacting through the inorganic vapor field within the char. An analogous problem on a larger scale is that of droplet interaction during the evaporation of sprays and 'group' combustion of fuel droplets (Samson et. al., 1978; Deutch et al., 1976; Labowsky and Rasner, 1978). Because of the low volume fraction of inclusions in coal (~.01), a "mean field approximation" (after Felderhof and Deutch, 1976)

can be employed to evaluate the 'macroscopic' mole fraction, X_m, profile of inorganic vapor in the porous char that results from the generation of ash vapor from a group of sources. If ρ_I is the number density of inclusions in a char particle, then the vapor mole fraction X_m with respect to the char's radial coordinate is determined by

$$cD_e \nabla^2 X_m + \rho_I V_I^i(r) = 0 \tag{1.2}$$

where V_I^i is the vaporization rate for a single inclusion and is, to a first order approxiamtion, given by

$$V_I^i = 4\pi r_i cD_e (X_m^e - X_m) \tag{1.3}$$

Thus the vaporization rate of an inclusion is, due to interaction among a large number of inclusions, dependent on its position in the char.

A quasi-steady profile within the char has been assumed here because the characteristic time for combustion is much greater than that for diffusion. The time dependence in this analysis only arises as a result of changes in the char particle radii during burnout and in the population balance of inclusions on the char's surface and within the char. The inclusion radius is assumed constant, a valid approximation at low vaporization rates. As shown in the schematic diagram (Figure 1.18) two types of inclusions or droplets were considered - those within the char and those continuously appearing on the char's external surface. The effect of external inclusions or droplets were also examined. Their consideration does not add significant insight into the nature of the volatilization process and so

are neglected here to avoid the mathematical complications. It is unlikely that they contribute significantly to the overall volatilization process because of the higher oxygen potential at the char surface than within the char.

The appropriate boundary conditions for the model are that

$$\text{at } r = 0: \qquad \frac{dX_m}{dr} = 0$$

and

$$\text{at } r = r_p: \; -4\pi r_p^2 c D_e \left.\frac{dX_m}{dr}\right|_{r=r_0} = 4\pi r_p c D_{o_2} \alpha_1 X_m^s$$

where

$$\alpha_1 = \frac{\ell n\left(1+X_{o_2}^b\right)}{\left[1 - e^{-\frac{D_{o_2}}{D_m}\ell n\left(1+X_{o_2}^b\right)}\right]}$$

where D_m and D_{o_2} are the gas diffusivities of the metal vapor and of oxygen, respectively, and $X_{o_2}^b$ is the mole fraction of O_2 in the bulk gas far away from the burning char particle. The second boundary condition is the equivalence of the internal and external (through the char's external boundary layer) rate of vapor transport with X_m^s defined as the mole fraction of the vapor at the char particle's external surface. It has been assumed that as r goes to infinity, X_m goes to zero. The factor α_1 accounts for the Stefan-flow effects brought about by diffusion controlled combustion.

Equation 1.2 can be cast into the form of the analagous problem of diffusion and reaction in a porous catalyst pellet (Satterfield, 1970):

$$\frac{1}{r^2}\frac{d}{dr}\left(r^2\frac{dX_m}{dr}\right) + \frac{\phi_I^2}{r_p^2}\left(X_m^e - X_m\right) = 0 \qquad (1.4)$$

where the Thiele modulus, defined as

$$\phi_I = \sqrt{3\theta_I}\frac{r_p}{r_i} \qquad (1.5)$$

is solely dependent on the physical distribution or occurance of mineral matter. The solution of this equation for the vapor mole fraction within the char particle is

$$X_m = X_m^e\left[1 - \left(1 - \left(\frac{X_m^s}{X_m^e}\right)\right)\frac{r_p \sinh\left(\phi_I \frac{r}{r_p}\right)}{r \sinh \phi_I}\right]$$

where X_M^s, the vapor mole fraction at the char surface ($r=r_p$) is given by:

$$X_m^s = \left[\frac{\frac{D_e}{\alpha_1 D_{o_2}}\left(\frac{\phi_I}{\tanh \phi_I} - 1\right)}{1 + \frac{D_e}{\alpha_1 D_{o_2}}\left(\frac{\phi_I}{\tanh \phi_I} - 1\right)}\right] X_m^e \qquad (1.7)$$

The total instantaneous rate of vaporization or loss of M from a char, V_c (moles/sec) of radius r_p is determined from

$$V_c = 4\pi r_p^2 c\, D_e \frac{dx_m}{dr}\bigg|_{r=r_p} = 4\pi r_p c D_{o_2} \alpha_1 X_m^s \qquad (1.8)$$

For non-interacting inclusions, the total vaporization rate from the char V_c^{ni} would be

$$V_c^{ni} = N_I\, 4\pi r_i c D_e X_m^e \qquad (1.9)$$

An effectiveness factor η,

$$\eta = \frac{3}{\phi_I}\left[\frac{1}{\tanh\ \phi_I} - \frac{1}{\phi_I}\right]\left[1 + \frac{D_e}{\alpha_1 D_{o_2}}\left(\frac{\phi_I}{\tanh\ \phi_I} - 1\right)\right]^{-1} \qquad (1.10)$$

gives the ratio of the total vaporization rate of M with particles interacting and with external diffusion control over that of the rate of N_I isolated and droplets in the char. Thus

$$V_c = \eta N_I\ V_I^{ni} \qquad (1.11)$$

The subtle aspect of this rate expression is that although the effectiveness factor becomes small due to interaction when ϕ_I is large, the total vaporization rate V_c from a single char particle increases with increasing ϕ_I because there is a greater number of inclusions (N_I) in the char particle. Equivalently, although a non-interacting inclusion will have a greater vaporization rate than an interacting inclusion, interaction is only significant (large ϕ_I) when N_I is large.

The expression for the pseudo-steady vaporization rate, V_c, can be re-cast in terms of the total fraction vaporization rate which was used for the empirical correlation of the experimental data (Figure 1.9, 1.10, 1.11 and 1.12). The total fractional vaporization rate is given by

$$\frac{f_v}{t_b} = \frac{N_v}{N_o t_b} \qquad (1.12)$$

where f_v is the fraction vaporized during combustion, t_b is the burning time of the coal particles, N_v is the moles vaporized per coal particle:

$$N_v = \int_o^{tb} V_c\ dt \qquad (1.13)$$

and N_o is the initial moles of metal in the char particle of initial radius r_o

$$N_o = \frac{\theta \rho_a 4\ r_o^3}{3w} \tag{1.14}$$

The terms ρ_a and w refer, respectively, to the density of the oxide inclusion and the molecular weight of the metal oxide.

1.6 Discussion of Results

The model described in the preceeding section is essentially a two parameter model, with the inclusion modulus ϕ_I (principally inclusion size, r_i) and the effective diffusivity D_e being adjustible, but with a temperature dependence of vaporization (accounting for the effects of temperature on effective and bulk diffusivities) primarily given by the thermochemical equilibria at the surface of each inclusion within the char particle. Values of ϕ_I and D_e, however, can be estimated within reason given the present knowledge of the occurance of mineral matter in coal and the structure of coal char. Rather than directly compare the experimental fractional vaporization rates with model predictions for assumed values of ϕ_I and D_e, the approach taken in this discussion is to compare predicted partial pressures (or mole fraction X_m^s) of inorganic vapor species at the char's surface with that calculated from the experimental vaporization rates. It will become apparent that this approach provides an easier comparison of the experimental data.

According to the model as evident in equation 1.7, the

partial pressures of metal containing vapors at the char surface will, in general, be less than the equilibrium value at the inclusion surface due to internal diffusion resistance and will vary during the course of char burnout for shrinking sphere combustion behavior. This time dependence arises as a result of the functional dependence of ϕ_I on char radius r_p. Since the experimental measurements are taken for complete combustion of the coal particles, a theoretical or model time average value of X_m^s is needed and can be calculated as

$$\bar{X}_m^s = \frac{1}{t_b} \int_o^{tb} X_m^s \, dt$$

using the time dependent modulus

$$\phi_I(t) = \phi_I^o \left[1 - \left(\frac{t}{t_b} \right)^{1/2} \right]$$

with ϕ_I^o defined as the initial modulus:

$$\phi_I^o = \sqrt{3\theta_I} \frac{r_o}{r_i}$$

Thus, a predicted value of $\bar{X}_m^s$ or average partial pressure of metal vapor at the char particle surface can be obtained from the thermochemical equilibria at the inclusion(s) surface and assumed values of ϕ_I^o and D_e.

The instantaneous vaporization rate of the metal from a single burning char particle is directly proportional to the partial pressure of the metal containing vapor at the char surface, as seen in equation 1.8, since internal and external diffusion resistances are in series. An experimentally determined (average) metal partial pressure may be unambiguously

calculated from the vaporization data using the external transport rate equation. In the following, experimentally determined partial pressures at the char particle surface are compared with model predictions for each element under consideration. Although the coal is a multicomponent system, the comparisons are made assuming a single component system for each metal. A final discussion will consider, in qualitative terms, multicomponent effects.

1.6.1 Silicon

Silicon is distributed as silica (SiO_2) in either quartz or finely diseminated micron sized clay minerals in the pulverized coal particles. For an inclusion diameters of about 0.5 to 2 microns, and an intitial coal size of 55 microns, the Thiele modulus ϕ_I^o is on the order of 5 to 20 for the coals examined in this study. Thus, if the effective diffusivity is small due to small pores such that

$$\frac{D_e \phi_I}{\alpha_1 D_{o_2}} << 1$$

then $\bar{X}_m^s$ is significantly less than X_m^e and is approximated by

$$\bar{X}_m^s = \frac{2D_e \phi_I^o}{3\alpha_1 D_{o_2}} X_m^e \qquad (1.15)$$

The term $D_e/\alpha_1 D_{o_2}$ is on the order of 10^{-3} for chars having an average pore radius of about 25Å and porosity of about 0.5. It is quite obvious that in this case the rate of vaporization is highly dependent on the structural characteristics of the char, which are likely to be changing during burnout, and the size of the

inclusions.

From the experimental vaporization rate data, average gas phase mole fractions of various species were calculated from the external diffusion rate. The results of these calculations for Si are shown by the data points in Figure 1.19 for several coals. For comparison, the equilibrium vapor pressure of SiO_2 and Si are also included. As evident, experimentally determined partial pressures of Si containing vapors at the char's surface far exceed the oxide vapor pressure at most combustion temperatures.

The solid lines corresponding to different values of ϕ_I in Figure 1.19 are the predicted partial pressures of SiO at the char's surface for the given value of ϕ_I, the equilibrium value of X_m^e at each inclusion's surface within the char, and a porosity of 0.5 and pore radius of 25Å for the calculation of D_e (Satterfield, 1970). The equilibrium mole fraction of SiO vapor at each inclusion's surface (X_m^e) is calculated for the reaction

$$SiO_2\ (c) + CO = SiO\ (v) + CO_2$$

assuming a pure component system, i.e.

$$X_m^e P = P_{SiO}^e = P_{CO_2}^e = (K_e P_{CO})^{1/2}$$

The solid line corresponding to $\phi_I = \infty$ is this calculated partial pressure of SiO vapor at an inclusion's surface. This notation is used because, according to the model, as the value of ϕ_I approaches infinity, the partial pressure of SiO at the char particles outer surface approaches that at each

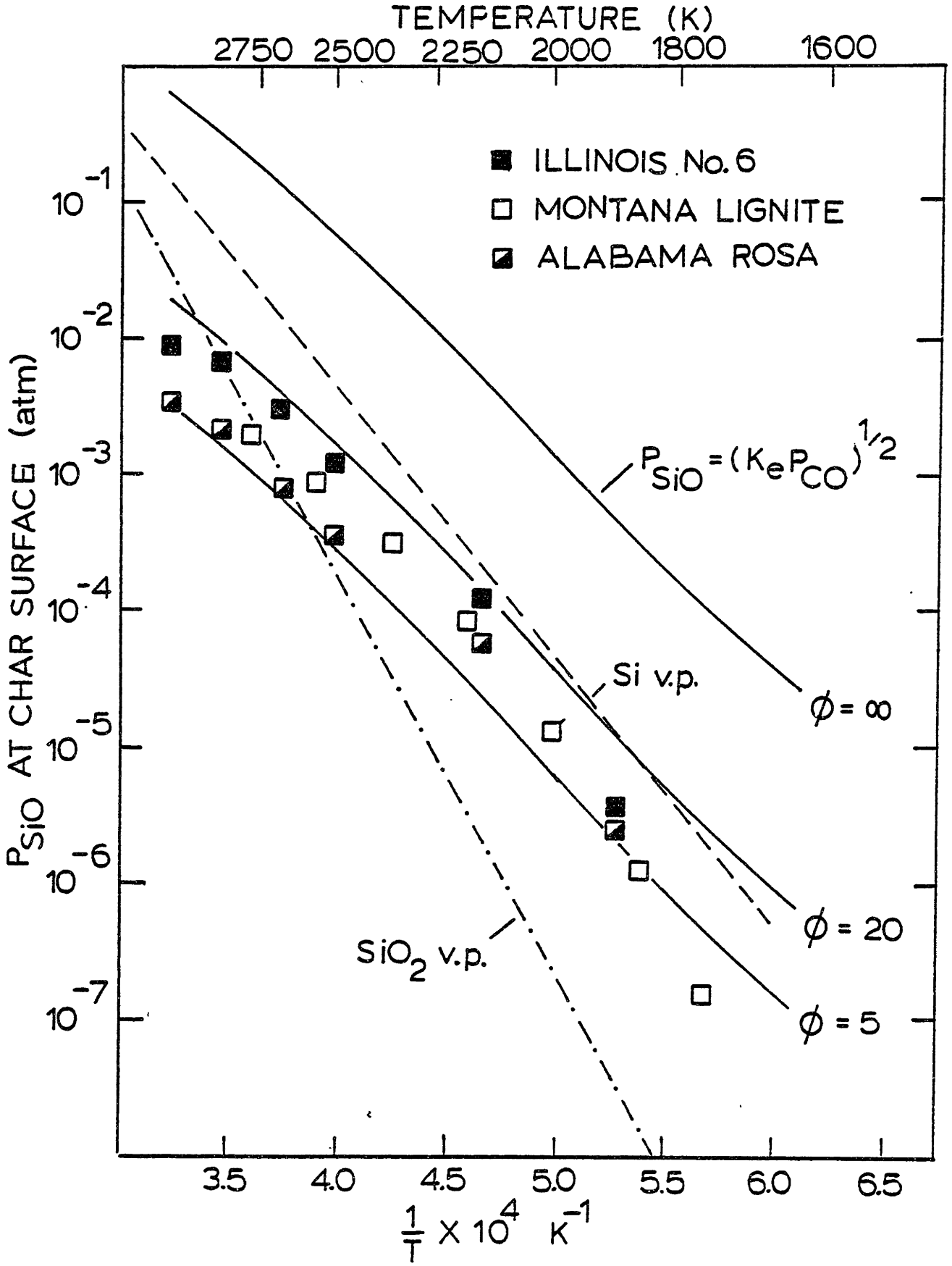

Figure 1.19 Comparison of Experimentally Determined Partial Pressures of SiO at Char Surface with Model Predictions

inclusion's surface. This is a special limiting case which will be re-examined in the discussion of the vaporization behavior of calcium and magnesium. The significant point here is that, for typical volume fractions of ash in the coal and characteristic mineral inclusion dimensions on the order of a micron, internal diffusion resistance significantly suppresses the SiO partial pressure at the char surface.

The transport model considering internal/external diffusion resistance in series and a thermochemical equilibria at the inclusion surfaces for reduction of SiO_2 by CO predicts with reasonable agreement the calculated average partial pressure of SiO at the char surface or, equivalently, the rate of vaporization and, quite accurately, its temperature dependence over nearly the entire range of combustion conditions. The observed suppression of the vaporization of Si by CO_2, and other elements as well (Table 1.11) qualitatively supports the proposed reduction mechanism.

The hypothesis that inclusions interact within a single char particle can be further examined in terms of the dependence of the fractional volatilization rate correlation (Figure 1.11) on the initial size of the coal. For values of ϕ_I expected for silica and with

$$\frac{D_e \phi_I}{\alpha_1 D_{O_2}} << 1$$

then the effectiveness factor is approxmated by

$$\eta \approx \frac{3}{\phi_I}$$

indicating strong interaction. The instantaneous vaporization rate from a single char particle is then

$$V_c = \sqrt{3\theta_I}\ \frac{r_p^2}{r_i}\ 4\pi_c D_e\ X_m^e \qquad (1.16)$$

Integrating over the burning time (equations 1.12 and 1.13), the fractional volatilization rate obtained is

$$\frac{f_v}{t_b} = \frac{54 w \rho_a c D_e X_m^e}{7\sqrt{3\theta_I}\ r_i\ r_o} \alpha \frac{1}{r_o} \qquad (1.17)$$

This inverse dependence on the initial coal particle radius is approximately observed for Si as shown in Figure 1.11. Had the vaporization been modelled assuming no interaction, the f_v/t_b predicted would have been independent of coal size, as is also predicted by a purely chemical kinetic model.

1.6.2 Iron

Iron is another element occuring as mineral inclusions in pulverized coal. However, its thermochemistry is significantly more difficult to deduce than for silica, as it occurs primarily in pyrite $[FeS_2]$. Under the rapid heating conditions and locally reducing environment characteristic of the combustion process, the decompostion of pyrite to FeS or a non stoichiometric FeS melt can be assumed instantaneous (Halstead and Raask, 1969) The FeS melt may undergo further but slower decomposition to liquid metallic iron or be oxidized by oxygen bearing gases (Halstead and Raask, 1969). The Fe-S-O system and its melt at these temperatures is complex and its composition or the activity

of Fe(ℓ) or FeO(ℓ) will depend strongly on the gaseous enviornment (Nagamori and Mitsuo, 1965) with respect to oxygen and sulfur bearing gases (O_2, CO_2, CO, H_2O, H_2, H_2S, SO_2, COS and S_2). The pronounced effect of coal type and iron-bearing mineral forms on the volatilization of Fe (Figure 1.6) may reflect the complicated nature of this system.

The experimentally determined partial pressures of Fe at the char's surface are compared in Figure 1.20 with predictions assuming a unit activity of Fe(ℓ) and the vapor pressure of Fe at the inclusion surface. Only fair agreement is obtained for values of ϕ_I between 1.0 and 100, corresponding to inclusion sizes on the order of 1.0 to 0.1 microns and a pore size of 25Å.

1.6.3 Calcium and Magnesium

Inherent calcium and magnesium in Bituminous coals are physically distributed in a manner similar to that of silicon. Calcium occurs primarily in the calcite mineral but may also occur in alumino-silicate clay minerals. The mineral dolomite was rarely observed so it is likely that magnesium occurs, for the most part, in the alumino-silicate clays of bituminous coals. Hence, the modulus ϕ_I is expected to be close to that for silicon and on the order of 10 for these elements. In the calculation of ϕ_I, the volume fraction θ for the clays bearing magnesium would be used rather than the metal oxide volume fraction in the coal.

The calculated partial pressures of Ca and Mg at the char's surface are shown for several coals in Figures 1.21 and 1.22.

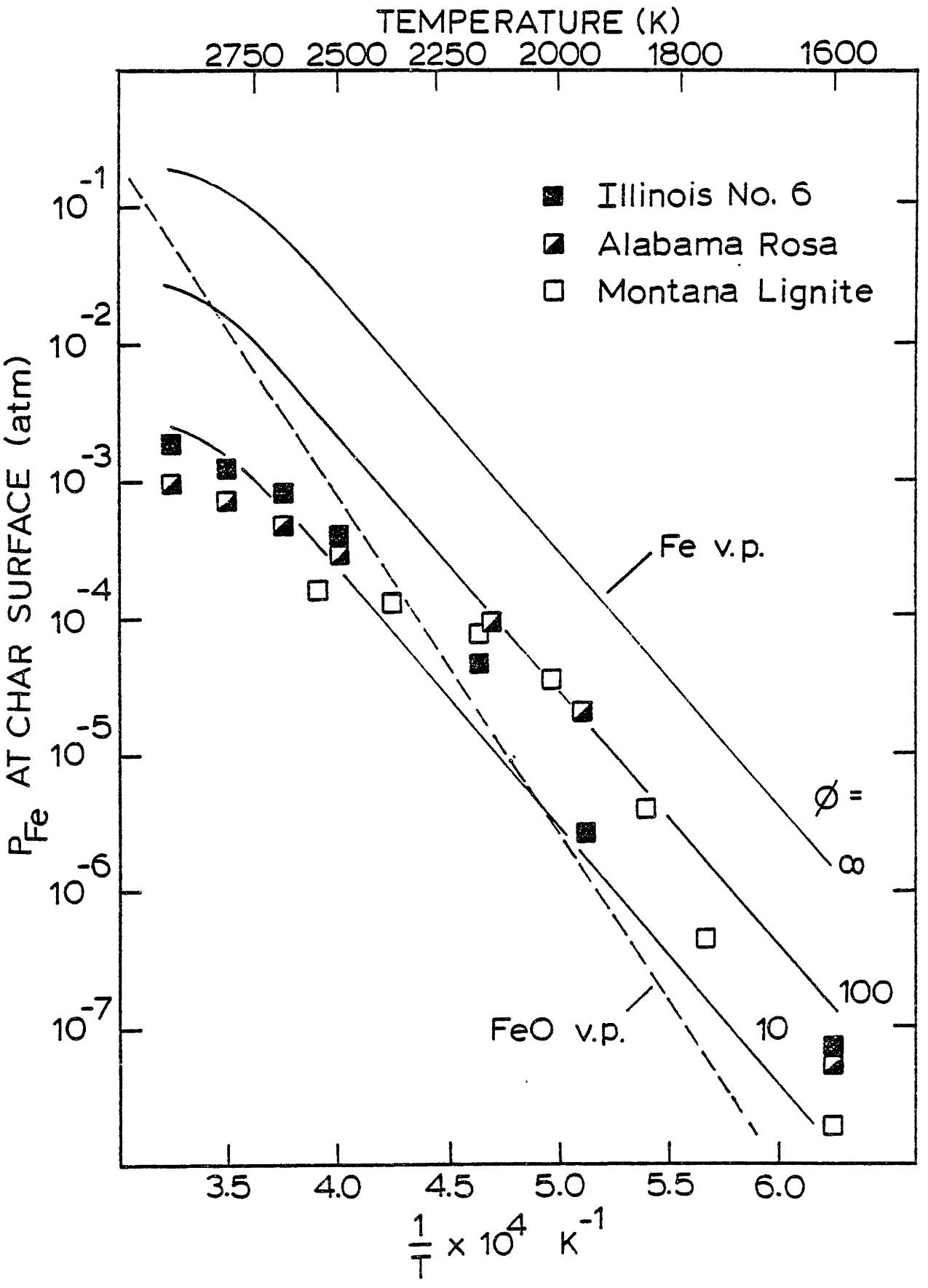

Figure 1.20 Comparison of Experimentally Determined Partial Pressures of Fe at Char Particle Surface with Model Predictions

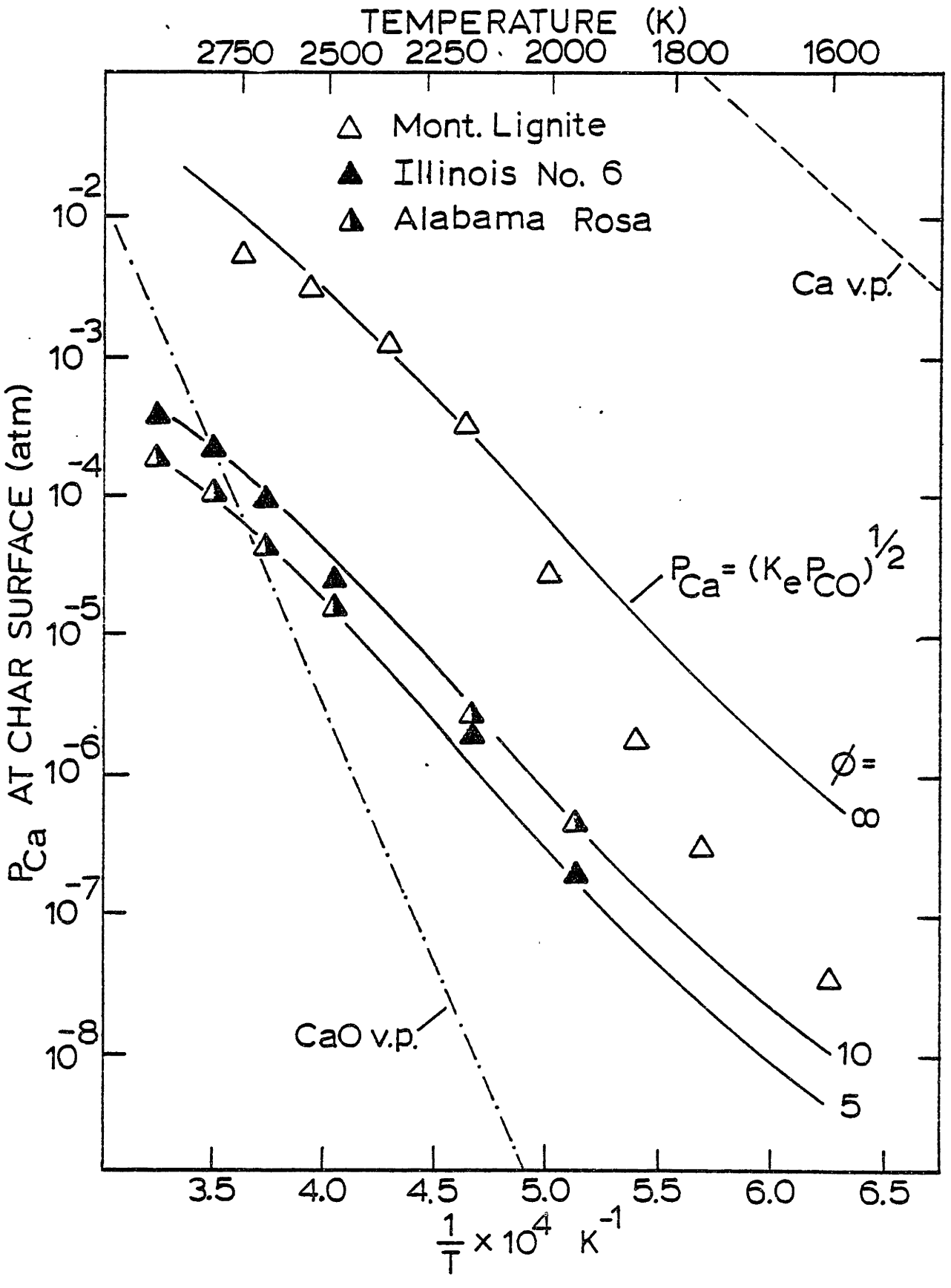

Figure 1.21 Comparison of Experimentally Determined Partial Pressures of Calcium at the Char Particle Surface with Model Predictions

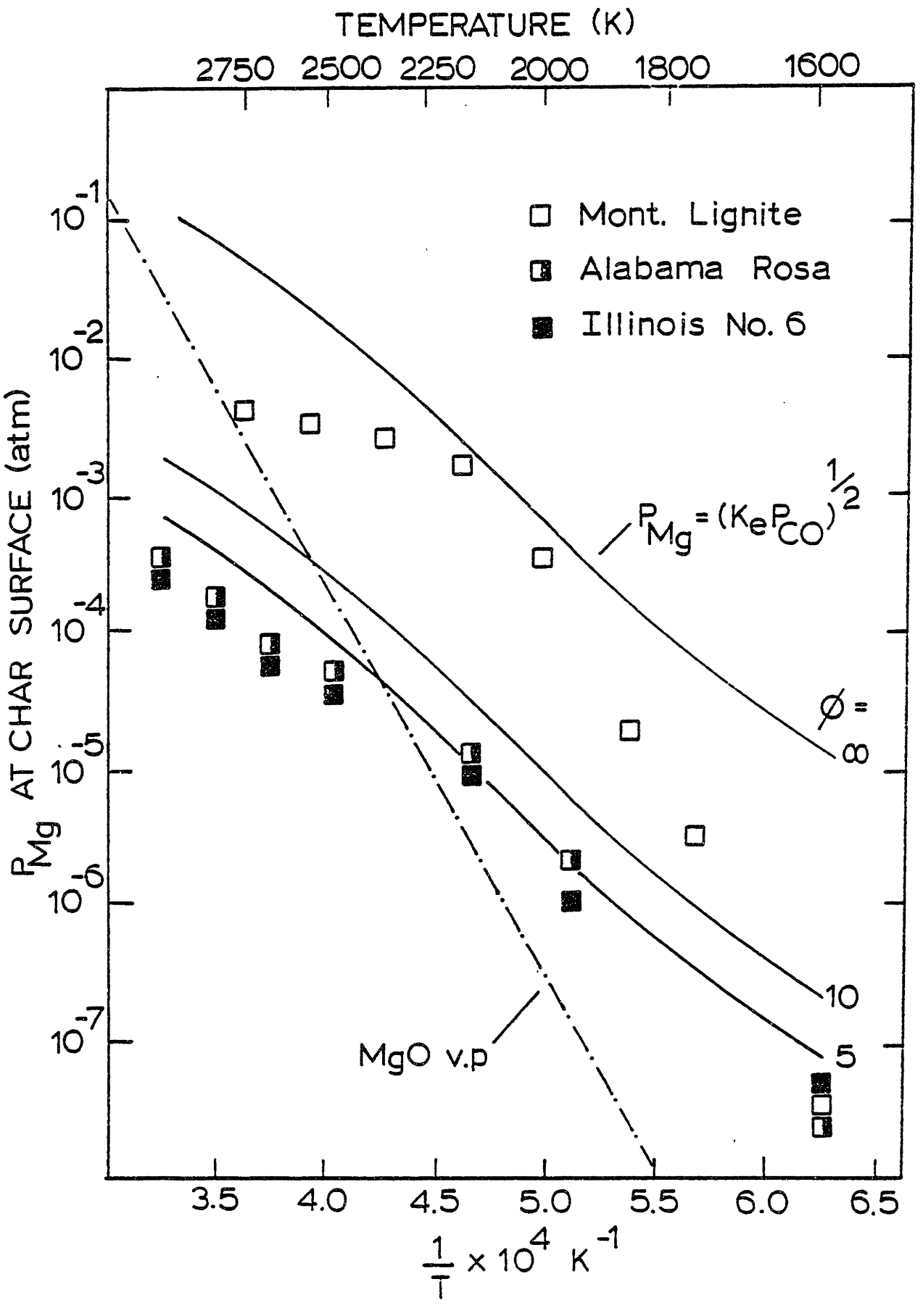

Figure 1.22 Comparison of Experimentally Determined Partial Pressures of Magnesium at the Char Particle Surface with Model Predictions

Again, the solid lines corresponding to different values of ϕ_I are predicted partial pressures at the char surface assuming the following reactions are at equilibrium at inclusion surfaces for pure component condensed phases:

$$CaO\ (s) + CO = Ca\ (g) + CO_2$$

$$MgO\ (s) + CO = Mg\ (g) + CO_2$$

For the bituminous (Illinois No. 6 and Alabama Rosa) coals it is observed that the temperature dependence and the magnitude of the surface partial pressure for reasonable values of ϕ_I are in close agreement with values calculated from experimental rate data. For the lignite, however, partial pressures of Mg and Ca calculated from the data approach predicted values for $\phi = \infty$. This is undoubtedly a consequence of the atomic dispersion of elements throughout the organic matter of the original coal. The scanning electron microscopy study (1.4) revealed that these metals form minute grains of ash on the char's surface during oxidation. Although it cannot be experimentally ascertained what their chemical or physical state is within the burning char, it appears that the parameter ϕ_I is exceedingly large due to this original atomic dispersion in the raw coal. With the formalism employed here, there is a limit to how large ϕ_I can become. It is assumed, of course, that the volume fraction of ash is realistically small. The value of ϕ_I in the present context then depends on r_i. For equation 10.14 to be valid, r_i must be significantly greater than the pore size. Rather if the size of the inclusion is on the order of the pore

size (25Å), then local Fickian diffusion controlled evaporation from an inclusion is not applicable. Intuitively, this is expected to be the case for the highly dispersed or atomically dispersed ion-exchangable calcium and magnesium in the lignite. If these molecules (assuming the carboxylic groups yield alkaline oxides upon pyrolysis) mobilize and collide by surface diffusion phenomena to form extremely small inclusions within the char in virtually oxygen free regions of the char, then the inclusions must be less than the characterisitc pore size. The theory of molecular vaporization would be more applicable. Thus,

$$V_I^i = \frac{\pi r_i^2 (X_m^e - X_m) P}{(2\pi mkT)^{1/2}}$$

The Thiele modulus for equation 10.20 would then be

$$\phi_I = r_p \left[\frac{3P\theta_I}{4cD_e r_i (2\pi mkT)^{1/2}} \right]^{1/2}$$

where P is total pressure and m is the mass of the metal vapor. The Thiele modulus would be exceedingly large and

$$\eta \to \frac{3\alpha_1 D_{o_2}}{D_e \phi_I^2}$$

The instantaneous rate of vaporization would, in this limit of ϕ_I approaching infinity as a result of extremely small inclusion size, be

$$V_c = 4\pi c\alpha_1 D_{o_2} r_p X_m^e$$

Thus the rate of vaporization is controlled by diffusion through the char's external boundary layer and it is not necessary to

specify the exact mechanism of local vaporization in the char. The surface gas phase mole fraction X_m^s of the metal is close to the equilibrium mole fraction X_m^e, as is observed experimentally for calcium and magnesium during lignite combustion.

The fractional vaporization rate f_v/t_b for calcium and magnesium in the case of the bituminous coals is given by the same expression (equation 1.17) obtained for silicon. As shown in Figure 1.12, an inverse dependence on coal size, as predicted was observed for the fractional rate of magnesium vaporization for combustion of the Illinois No. 6. For the lignite however, where the working limit is $\phi_I \to \infty$ for the organically bound metals, the fractional vaporization rate for external diffusion controlled vaporization is

$$\frac{f_v}{t_b} = \frac{2c\alpha_1 D_{o_2} w\rho_a X_m^e}{\theta r_o^2} \alpha \frac{1}{r_o^2}$$

An approximate inverse square dependence on the initial diameter of the coal was observed experimentally for the magnesium fractional vaporization rate in the case of lignite combustion as shown in Figure 1.12.

It is also observed that the partial pressure of Mg and Ca at the surface of the burning lignite particles drops off systematically from predicted values at lower temperatures. It is believed that this is a consequence of the increasing degree to which oxygen penetrates the char with decreasing combustion temperature, resulting in a suppression of the mole fraction of metal vapors near the surface of the char.

1.6.4 Multicomponent Effects

The preceding thermochemical analysis assumed that the metal oxides (SiO_2, MgO and CaO) exist within the char as pure and physically isolated phases. The only pure phases existing within the coal are quartz [SiO_2], calcite [$CaCO_3$] and pyrite [FeS_2] if it completely decomposes to iron metal. Silica, as well as Ca, Mg and Fe (for iron-bearing clay coals) may also occur in alumino-silicate metals arising from the high temperature decomposition of the clays. Furthermore, each coal particle may contain a suite of different mineral forms. There are several ways in which the multicomponent nature of mineral matter may influence the volatilization rates.

If an inclusion is a mixture of multicomponent oxides, then the simultaneous multicomponent reduction equilibria would be

$$P_{CO} \Sigma K_i a_i = P_{CO_2}^2$$

where K_i and a_i are the equilibrium constant and the activity of oxide i in the inclusion, and the partial pressure of the metal (Ca, Mg) or suboxide (SiO) at the inclusion's surface is:

$$P_i = K_i a_i \frac{P_{CO}}{P_{CO_2}}$$

In general, P_{CO_2} is not equivalent to P_i as in the pure component case. In addition, the carbon dioxide product of one inclusion may influence the local equilibria of another inclusion of different composition if the carbon dioxide does

not react sufficiently fast with the char. Given that there are a number of factors affecting the magnitude of the volatilization rate of specific metals from inclusions, the role of activity or multicomponent effects cannot be determined from a comparison of coals and their compositions. Furthermore, the equilibrium constants for reduction of SiO_2, MgO and CaO have nearly the same temperature dependence. The effect of condensed phase activity, however, may be reflected in the Mg vaporization data for low rank coals. As shown in Figure 1.6, the amount of magnesium vaporized is well correlated with the magnesium content of low rank coals. The model predicts that for the limiting case of $\phi_I \rightarrow \infty$, the amount (μg) of magnesium vaporized should have been independent of the magnesium content of the coal. It is likely that a CaO-MgO melt with additional impurities (e.g. Na_2O, Al_2O_3, P_2O_5) is formed from the ion-exchangable material in the coal during combustion (see Section 1.4.4). The data in Figure 1.6 may then reflect the non-unit activity of MgO in the melt.

It was initially suspected that the highly dispersed calcium and magnesium in the lignite would suppress the volatilization of silica by the reaction of SiO vapors diffusing through the char with the alkaline earth oxides resulting in the formation of low silica activity slags or stable orthosilicates compounds. This was investigated experimentally by measuring silicon vaporization during lignite combustion for lignite samples that had been acid washed to remove the ion-exchangable alkaline metals. There was no significant

difference in the amount of silicon vaporized between acid washed and raw lignite samples. It was concluded, therefore, that if such reactions between different components are occurring, their rates are not significant enough to influence the volatilization of silicon.

1.7 Conclusions

During the high temperature combustion of pulverized coal particles, the refractory metal oxide ash (SiO_2, CaO and MgO) in coal undergoes reduction by the carbon monoxide generated by the char oxidation reaction to form volatile inorganic vapors (SiO, Ca, and Mg) within the char particle. These vapors diffuse out and away from the burning char particles to form the submicron particulate ash.

A single coal particle contains numerous micron sized mineral inclusions and it appears that the reduction reaction is locally at equilibrium at the surface of each inclusion. The temperature dependence of the vaporization rate of the refractory oxides is determined primarily by the equilibrium constant for reduction. The magnitude of the vaporization rate is controlled by internal and external vapor transport processes.

The amount and composition of the vaporized ash is strongly dependent on the temperature history of combustion. At low combustion temperatures (~1600K), the vaporized ash is composed mostly of the relatively volatile alkali oxide material. At high combustion temperatures (~2500K), significant reduction occurs and the vaporized ash is composed

primarily of the refractory metal oxides. The amount and composition of the vaporized ash is also strongly dependent on coal type with respect to mineral matter forms. Coals with higher inherent ash contents yield greater amounts of combustion generated submicron ash. The major difference between coals is that the low rank subituminous coals and lignites contain high concentrations of organically bound alkaline earth metals. Volatilization is enhanced due to this original atomic dispersion in the coal.

CHAPTER TWO

BACKGROUND

2.1 Introduction

Mineral matter in coal undergoes various high temperature physical and chemical transformations that result in the formation of inorganic particulates during pulverized coal combustion. The effluent particulates generally range in size from about 100 microns down to the submicron and are composed primarily of oxides and sulfates of Si, Al, Fe, Ca, Mg, K, and Na. The larger particles, those greater than about 0.4 microns, correspond to the mineral matter residue of burned-out suspended coal particles and typically have a mass mean diameter of 10 to 20 microns. Not all the ash is necessarily released in this way. Flame temperatures in the radiant section of boilers (1700-2400K) are sufficiently high that significant partial pressures of inorganic vapors may evolve. As combustion products are cooled, these vapors must recondense either on the surfaces of pre-existing particles or by homogeneous nucleation, creating new submicron particles. Homogeneous nucleation would occur if the gas phase became critically supersaturated with respect to inorganic vapors. The importance of fine particle formation by this latter mechanism has been demonstrated both theoretically (Flagan, 1979; Desrosiers, et al., 1979) and in recent field studies of utility effluents that have shown the size distribution of fly-ash to be distinctly bimodal, with the additional mode occurring in the submicron range [Ensor et al., 1979;

McCain et al., 1975).

The total mass of particulate emissions from coal combustion sources has been abated for some time with high efficiency (99+ percent) gas cleaning devices such as electrostatic precipitators and scrubbers. There is, nevertheless, a growing concern regarding the preferential release and ensuing impact on health and on the environment of fine particulates in the submicron size range. Although, on a mass basis, submicron particles typically comprise less than a few percent of fly-ash, precipitators and scrubbers are inherently ineffective in trapping them out of utility effluent gases (Ensor et al., 1979; Ondov et al., 1979). To this end it has been extensively documented that certain volatile trace metals in coal, notably toxic As, Cd, Pb, Ni, Sb, Se, and Zn, are concentrated or enriched in the finer particulates and in the surface layers of the particulates (Davison et al., 1974; Coles et al., 1979). Furthermore, submicron particles are 'respirable'; as much as 60 percent are retained in the human lung upon inhalation. On emission, the finest particles also have the largest effect on visibility, and the longest atmospheric residence time.

The detrimental effects of mineral matter vaporization are not solely environmental. It has long been known that inorganic vapors, particularly the alkali vapor compounds, are partially responsible for fireside fouling and corrosion of water-tube boilers (Dunderdale and Durie, 1964; Jackson, 1979). It has also been suggested that submicron particles

play an important role in this respect because of their high mobility in thermal gradients, (Ulrich et al., 1977). Under the high temperature combustion conditions proposed for coal-fired MHD generators, significant amounts of ash vaporization are to be expected. Both the ash vapors and the submicron condensation nuclei may severely reduce the electron density and hence the combustion plasma conductivity and overall generator efficiency (Martinez-Sanchez et al., 1978).

Essentially all information that is available on ash volatilization has come from field sampling and analysis of coal-fired power plant fly-ash (Coles et al., 1979; Davison et al., 1974; Kaakinen et al., 1975). The emphasis of these numerous investigations has been to characterize the distribution of elements in particulates greater than about one micron. The significant finding was that the concentrations of volatile trace metals were systematically enriched with respect to decreasing ash particle size. The hypothesis is that they vaporize and later recondense or absorb on the surface of particles, with enrichment a consequence of greater surface to volume availability of smaller particles. In contrast, less is known about the properties of submicron ash and the vaporization and condensation processes that contribute to its formation during coal combustion. In any case, fundamental physicochemical mechanisms are not readily obtained from analysis of utility fly-ash because of the complex environments under which they were produced and because of difficulties in obtaining representative samples. Futhermore, in

most instances, the fundamental information on thermochemical and chemical kinetic behavior of complex inorganic slags in a highly reactive combustion enviornment is incompletely known.

The preceeding discussion underlines the need for conducting detailed laboratory studies on the volatilization behavior of mineral matter during pulverized coal combustion. The characteristics of coal and the coal combustion process related to ash formation are considered in more detail in the following.

2.2 The Occurrence of Mineral Matter in Coal

A considerable base of information has been developed on the geochemical occurrence of mineral matter in coal because of its negative impact on technical, environmental and economical aspects of coal utilization. The consensus of reviewers is that its occurrence is sufficiently complex and variable, especially between the ranks of coal, but also within a rank and even between seams of the same field, that few generalizations are applicable (Selvig and Gibson, 1956; Kemezys and Taylor 1964; Gluskoter, 1967). The specific mineral matter characteristic of coal is, in fact, an important constraint in the design and operation of a utility boiler. A major objective of this investigation will be to examine the importance of this variability in occurrence on its volatization behavior during high temeprature combustion.

Mineral matter in coal is frequently categorized as:

(a) Inherent: elements intimately or chemically bonded

to the carbonaceous or combustible matter of coal because of their association with the original plant material or as a result of ion-exchange processes with circulating ground waters during the coal formation period.

(b) Adventitious: Finely dessimenated micron sized mineral crystallytes in the carbonaceous material, arising from simultaneous deposition with the plant material and often classified as 'inherent' also.

(c) Extraneous: 'free dirt' from adjacent sedimentary bands without any appreciable association with the carbonaceous material.

The relative quantities and compositions of inherent, adventitious and extraneous modes, which depend on the history of the coal formation process and the geological location, vary significantly among coals. The inherent or elementally bonded material rarely exceeds 2 percent of the coal mass, but can be significantly higher in some low rank coals or lignites. Much of the extraneous mineral matter can be removed by flotation techniques prior to combustion. However, during the mechanical break up process of coal pulverization, some of the adventitious matter can be transferred to the extraneous phase, the extent of which increases with the degree of pulverization. When the coal is pulverized to about 10 to 100 microns extraneous mineral matter corresponds to about 20 percent of the total mineral matter in coal (Littlejohn, 1966).

The major, minor and trace element content in coals are listed in Table 1 as an average of 100 U.S. coals together with deviations. The major constituents, which include Si, Al, Fe, Ca and Mg, generally occur in common earth minerals, the most abundant being quartz, kaolinite, calcite and pyrite, and comprise both extraneous and adventitious phases. The relative and total concentrations of coal minerals varies considerably among coals. The only similarity is that all coals contain relatively significant amounts of silicates and aluminosilicates. Other accessory minerals that have been identified in coal are listed in Table 2.2.

In contrast to bituminous coals, lignites and, to a lesser extent, subbituminous coals, contain appreciable amounts of inherent or organically bound elements, predominantly Ca, Mg, K, Na and P. As much as 35 percent of the coal ash, computed as oxides, are originally present in some western lignites as Ca, Mg, Na, and K, ion-exchanged on carboxilic and phenolic groups in the organic substance of coal (O'Gorman and Walker, 1977).

Minor elements, which can include Na, K, P, and Ti, and trace elements (see Table 2.1) can occur in coals as rare accessory minerals, as impurities in the major minerals, or, as already described for Na and K, organically bound to the carbonaceous material. Some of the more important rare minerals are listed in Table 2.2. From geochemical considerations, trace elements in coal have been previously classified

TABLE 2.1

Mean Composition for 101 Coals

Constituent	Mean		Standard Deviation	Min	Max
As	14.02	PPM	17.70	0.50	93.00
B	102.21	PPM	54.65	5.00	244.00
Be	1.61	PPM	0.82	0.20	4.00
Br	15.42	PPM	5.92	4.00	52.00
Cd	2.52	PPM	7.60	0.10	65.00
Co	9.57	PPM	7.26	1.00	43.00
Cr	13.75	PPM	7.26	4.00	54.00
Cu	15.16	PPM	8.12	5.00	61.00
F	60.94	PPM	20.99	25.00	143.00
Ga	3.12	PPM	1.06	1.10	7.50
Ge	6.59	PPM	6.71	1.00	43.00
Hg	0.20	PPM	0.20	0.02	1.60
Mn	49.40	PPM	40.15	6.00	181.00
Mo	7.54	PPM	5.96	1.00	30.00
Ni	21.07	PPM	12.35	3.00	80.00
P	71.10	PPM	72.81	5.00	400.00
Pb	34.78	PPM	43.69	4.00	218.00
Sb	1.26	PPM	1.32	0.20	8.90
Se	2.08	PPM	1.10	0.45	7.70
Sn	4.79	PPM	6.15	1.00	51.00
V	32.71	PPM	12.03	11.00	78.00
Zn	272.29	PPM	694.23	6.00	5350.00
Zr	72.46	PPM	57.78	8.00	133.00
Al	1.29	%	0.45	0.43	3.04
Ca	0.77	%	0.55	0.05	2.67
Cl	0.14	%	0.14	0.01	0.54
Fe	1.92	%	0.79	0.34	4.32
K	0.16	%	0.06	0.02	0.43
Mg	0.05	%	0.04	0.01	0.25
Na	0.05	%	0.04	0.00	0.20
S	3.27	%	1.35	0.42	6.47
Si	2.49	%	0.80	0.58	6.09
Ti	0.08	%	0.02	0.02	0.15
Total Ash	11.41	%	2.95	3.28	25.85

Source: Ruch, R.R., Gluskoter, H.J., and Shimp, N.F., EPA Report No. EPA-650/2-74-054, July, 1974.

TABLE 2.2

Chemical Formulae of Some Common Mineral Groups in Coal

(Miller, 1978)

Clay group:	KAOLINITE $\left[Al_2(OH)_4 \mid Si_2O_5\right]$
	MONMORILLONITE $\left[(Al, Mg)_2(OH)_2 \mid Si_4O_{10}\right]\left[Na^+, Ca^{2+}\right] nH_2O$
	ILLITE $\left[(Al,Mg,Fe)_2(OH)_2\ (Si,Al)_4(O,OH)_{10}\right]\left[K^+, K, H_3O^+\right]$
Carbonate group:	CALCITE ($CaCO_3$); SIDERITE ($FeCO_3$);
	ANKERITE $CaFe(CO_3)_2$; DOLOMITE $CaMg(CO_3)_2$
Sulfide group:	PYRITE or MARCASITE (FeS_2)
	SPHALERITE (ZnS); GALENA (PbS);
	CHALCOPYRITE ($CuFeS_2$)
Sulphate group:	SULPHATES from weathering $\left[K, Na, Ca, Mg, Fe, Al\right]$ $\left[(OH, F, Cl)\ (SO_4)\right] nH_2O$
	GYPSUM ($CaSO_4$, $2H_2O$); BARITE ($BaSO_4$)
	THENARDITE (Na_2SO_4)
Associate group:	QUARTZ (SiO_2)
	RUTILE (TiO_2)

(Masson, 1966) as lithophilic (Cs, Hf, K, Mg, Mn, Na, Rb, Ti, Sc and rare earths) because of their association with alumino-silicate minerals, or as chalcophilic (As, Cd, Ga, Mo, Pb, Se, W, and Zn) because of their association with sulphide or pyritic minerals. In general, the level and nature of trace and minor element occurrence in coal is specific to the element and to the coal. Their occurrence, however, may have a profound effect on their behavior during combustion.

2.3 Fly-Ash Formation During Pulverized Coal Combustion

The behavior of mineral matter in a pulverized coal-fired power plant is a difficult problem to address despite existing knowledge of the thermal behaviro of its principle constituents, which have been studied at great length (Gluskoter and Mitchell, 1976, O'Gorman and Walker, 1976). These transformations are summarized in Table 2.3. It has been a traditional concern of utilities, causing technical and economic burdens such as waste disposal, slagging, fouling, corrosion and overall boiler efficiency reduction. The mineral matter characteristics of a specific coal, and the management of its ash, continues to be an important constraint in the design and operation of a pulverized coal-fired utility boiler. In this regard, most investigations in past (Watt and Fereday, 1969) have focused on determining the bulk properties of combustion ash, such as fusion temperatures, softening temperatures, viscosities and thermal conductivities, for engineering design criteria. It is now recognized (Boric and Narcisco, 1979; Bryers, 1979) that bulk properties are

not an accurate index of fouling and slagging behavior because, on the microscopic scale where interactions occur, mineral matter is not uniformly distributed. In recent years there has been a surge of interest in the details of fly-ash formation, not only from the standpoint of its deposition behavior in boilers, but from environmental perspectives as well. Some significant insights have been achieved in both field and laboratory studies.

In power plants, pulverized coal is burned as a suspension at flame temperatures ranging from 1500 to 2500K and for residense times of about 1 second (Field, 1967). After the initial evolution and combustion of the volatile organic matter of coal, the remaining char particles burn by heterogeneous oxidation. Temperatures are sufficiently high for the initial decomposition of the minerals evolving CO_2, H_2O and SO_2, followed by subsequent solid-solid and solid-liquid phase transitions.

The chemical transformations of individual coal minerals at high temperatures has been studied extensively Table 2.3, but under slow heating conditions which are not closely representative of time-temperature histories in combustors. Padia (1976) however, did study their transformation under the rapid heating conditions in simulated combustion experiments in a drop tube furnace with time scales of about one second. He observed that at the completion of combustion, essentially all minerals had dehydrated or decomposed to their respective oxide. Only calcium sulphate persisted up to combustion temperatures of about 1500K. Pyrite oxidized to hematite and

TABLE 2.3 Chemical Transformation of Mineral Matter During p.f. Combustion (Wibberley, 1980)

Quartz

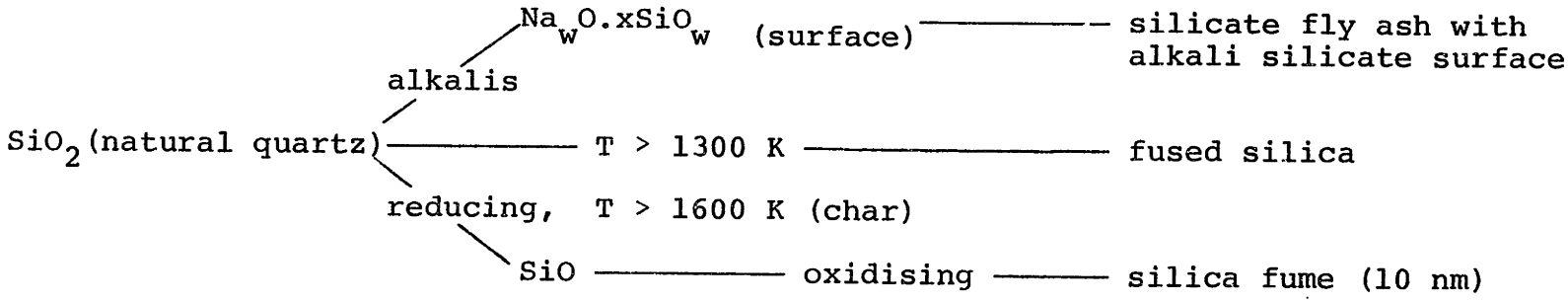

Kaolinite

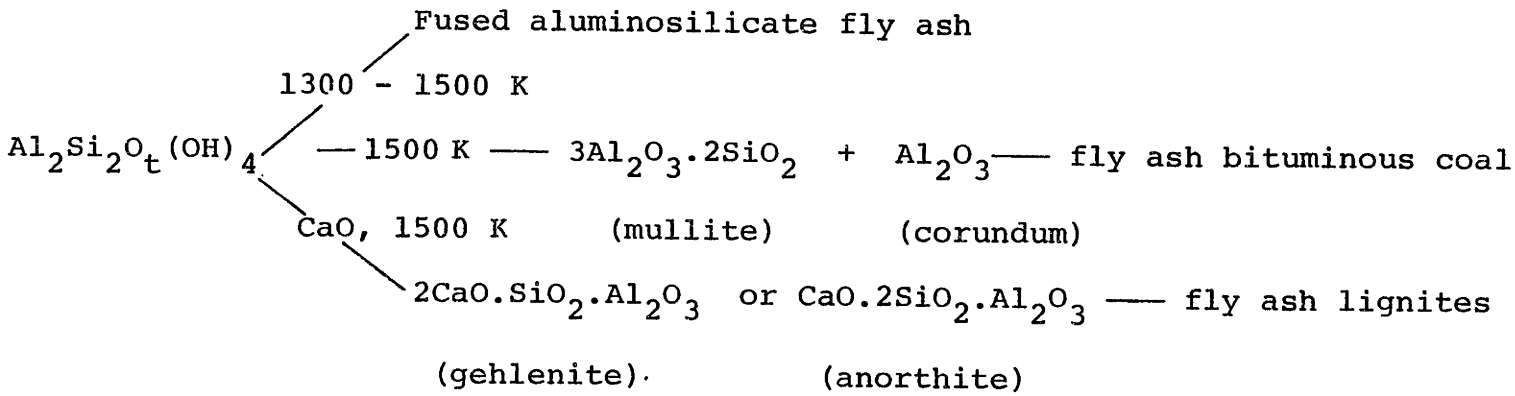

Pyrite

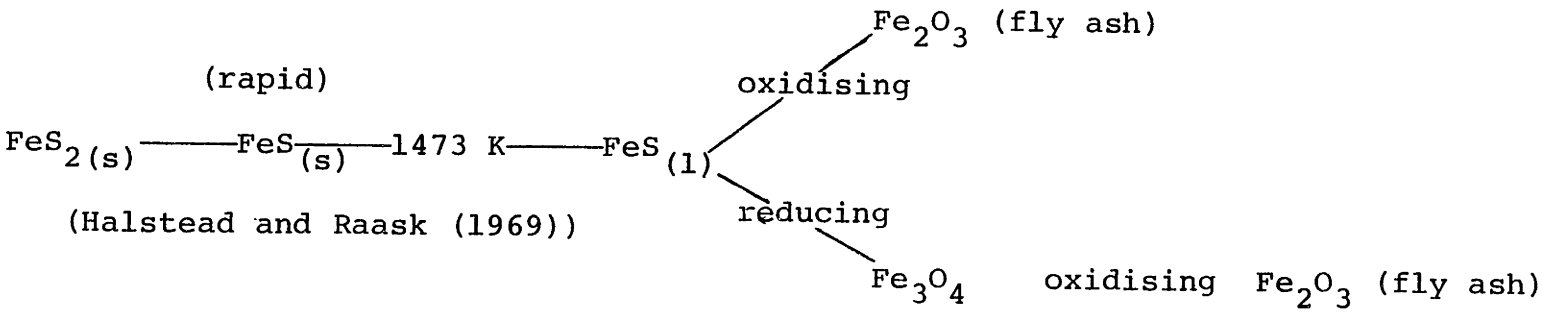

Carbonates

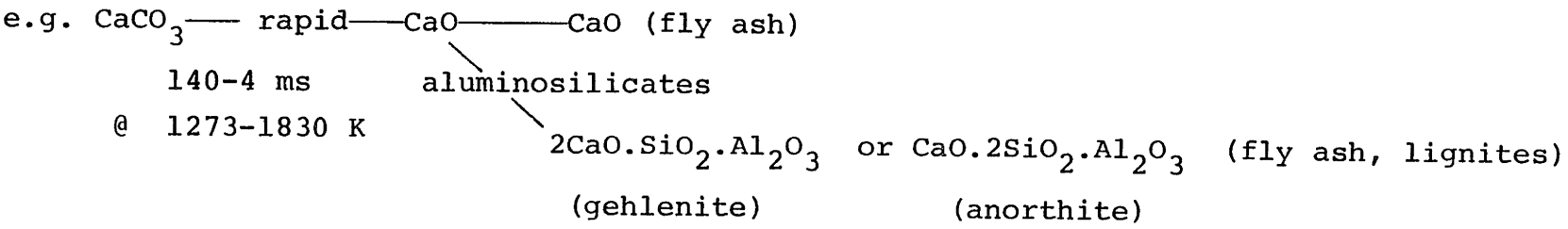

Gypsum

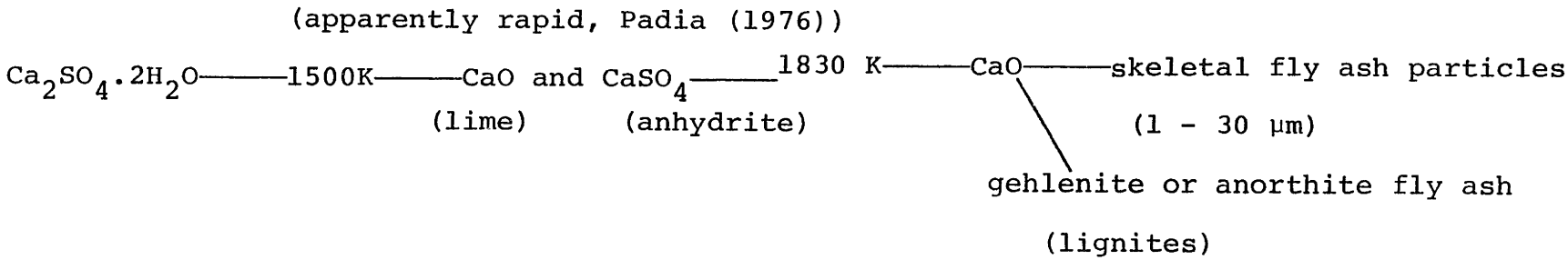
(apparently rapid, Padia (1976))
$Ca_2SO_4.2H_2O$
1500K
CaO and $CaSO_4$
(lime)
(anhydrite)
1830 K
CaO
skeletal fly ash particles
(1 - 30 μm)
gehlenite or anorthite fly ash
(lignites)

magnetite. Under reducing condition, it has been observed that $CaSO_4$ will decompose to the refractory sulphide CaS (Wriedt and Darken, 1972) and FeS_2 will decompose to FeS (Halstead and Raask, 1969). During combustion, reducing conditions may occur locally within burning char particles. No information has been reported on the chemical nature of mineral matter in a partially oxidized coal.

The larger or residual fly-ash particles ($\geq$ 0.5 μm) are formed by the coalescence on contact of molten mineral inclusions as the mass of the parent coal particle is gasified and as its surface receeds. Evidence for this mechanism has come from Padia's 1977 laboratory studies which have shown that the size distribution for ash particles was greater in mean diameter than that of the size distribution of the mineral inclusions originally present in the raw coal. This conclusion was further supported by microscopic examination of partially oxidized coal particles revealing the adherence and abundance of molten mineral droplets on the char surfaces (Ramsden, 1969). Morphological studies of sampled utility fly-ash confirm the hypothesis that they passed through a molten state by evidence of their spherical nature (Ramsden, 1969; Raulson and Ramsden, 1979). Additionally, the observed composition of individual particles (Fisher et al., 1978) indicate that coalescence and chemical interaction of unlike mineral species had occured. It is unknown to what extent the combustion conditions, the burning characteristics of the coal - for example; swelling behavior - and the mode of occurrence and composition of inorganic matter in the coal,

affect the overall phenomenology of formation and characteristics of residual fly-ash. Once formed, the supermicron particulates will either deposit on the internal structures of the utility or be efficiently recovered downstream by electrostatic precipitation.

In the high temperature radiant zone of furnaces (1500-2500K), significant partial pressures of inorganic vapors may evolve. Laboratory combustion studies (Padia, 1977) have shown that as much as four to eight percent of the coal ash may have been lost due to vaporization during combustion at about 1800K. As the hot combustion gases are cooled in the convective heat exchangers of boilers, exisiting particulates may provide surface sites for condensation of inorganic vapors. However, under certain conditions, the gas phase may become sufficiently saturated with respect to inorganic vapors, that homogeneous condensation may occur (Friedlander, 1977). In this case, nucleation of an inorganic fume would result in a large number density of new submicron particulates. Recent studies of utility effluents (Ensor et al., 1979), McCain et al. 1975) have, in fact, shown that the size distribution of inorganic particulates is bimodal, with a submicron mode occurring at about 0.1 micron. The physical process of nucleation and subsequent growth of nuclei by collision and coagulation in combustors have been previously investigated on a theoretical basis (Flagan, 1979; Flagan and Friedlander, 1979). It is unlikely that other proposed mechanisms, such as the burstiing of ash droplets that rapidly evolve H_2O or

CO_2 (Ramsden, 1969; Smith et al., 1979) would give a bimodal distribution or the characteristically sharp distribution of the submicron mode.

It is well expected that some of the trace elements in coal, such as As, Zn, Cr, Se and Sb, volatile in elemental or other chemical forms at conventional combustor conditions, will exhibit significant volatilization. Indirect evidence has come from field observation of enriched concentrations of these volatile elements in the finer size fractions or particulates. Presumably, this concentration effect is due to heterogeneous condensation or absorption and the greater surface to volume availability of finer particulates (Davison et al., 1974; Coles et al., 1979). It has also been observed that, in certain cases, these elements are located in the surface layers of particulates. Although submicron particulates contain the highest concentration of volatile toxic trace metals (Smith et al., 1979) they are primarily composed of the dominant retractory metal oxide consitituents of ash (Table 2.4); namely SiO_2, FeO, CaO, MgO and Al_2O_3.

2.4 Thermochemical Considerations

Since volatilization is an activated process, the temperature of combustion and the rate of combustion are likely to be important factors in the vaporization of metal oxides such as SiO_2, MgO, CaO, and FeO from condensed phases. In addition to the distillation of these oxides from the molten minerals, there exists the possibility of reduction to more

TABLE 2.4

Composition of Submicron Fly-Ash From
Commercial Coal-Fired Utilities (wt%)

SiO_2	49.2	47.0	48.0
Al_2O_3	24.6	20.8	10.0
FeO	7.2	4.5	8.0
CaO	6.6	8.4	10.0
MgO	3.0	3.8	1.7
Na_2O	1.5	2.7	2.4
K_2O	0.5	1.7	1.7

A,B from Smith et al., 1979

C from Desrosiers et al., 1979

volatile sub-oxides (SiO, AlO) or metals (Ca, Mg, Fe, Al). Reducing conditions may occur locally in fuel-rich regions of a combustor or within burning char particles. A number of agents could cause reduction reactions, including the carbon of the char, carbon monoxide, molecular hydrogen and sulphur. Reduction and straight decomposition of metal oxides become more thermodynamically favorable at higher temperatures. The reduction of condensed SiO_2 by carbon is thermodynamically favored above 2000 K (Raask and Wilkins, 1965). Also under reducing conditions, refractory compounds of silicon carbide and calcium sulphide may form and inhibit their volatization.

The reducing environment within burning char particles will depend primarily on combustion temperature. At lower combustion temperatures, around 1200 K, the gasification of char is controlled by the kinetics of oxidation. Hence, the char burns internally as well as externally and the oxygen partial pressure is more or less equivalent to the bulk. At higher temperatures, where the kinetics of oxidation are much faster that the transport of oxygen to the particle surface, virtually all oxygen is consumed at the surface of the char particle and the internal environment is highly reducing (Smith 1979). The relative rate of oxygen diffusion to the particles to the chemical reaction rate increases with decreasing coal particle size. The coal particle size is therefore also important in determining local oxygen partial pressures. Other important factors may include the porosity and specific surface area of chars and overall buring characteristics - some coals

swell under rapid combustion, forming large lacy cenospheric structures that burn internally (Street et al., 1969).

McNallen at al. (1981), in calculating an oxygen potential of the order of 10^{-15} atm in equilibrium with solid carbon at 2400 K and a corresponding equilibrium partial pressure of SiO of 4000 atm in the coal particle, concluded that, as this obviously does not occur, it is likely that chemical kinetics control the reduction of condensed SiO_2. Chemical kinetic information on the reduction of SiO_2 by carbon or carbon monoxide, or any other possible reactions involving other mineral components at high temperatures is limited.

Other factors which may obscure a thermochemical understanding of ash volatilization phenomena include the interaction of mineral matter with itself and the dependence of this on its composition and distribution in the coal. For example, silicates may form low melting point utectics or stable high temperature solids with iron and calcium oxides. Padia (1977) observed that under simulated combustion conditions up to 1800 K, ion-exchanged calcium formed the stable compounds of anorthite ($CaO \cdot 2SiO_2 \cdot Al_2O_3$) and gehlinite ($2CaO \cdot SiO_2 \cdot Al_2O_3$) for a lignite. He did not, however, observe this interaction of calcium with silicates in a bituminous coal. In molten solution, calcium oxide is known to significantly reduce the thermodynamic activitiy of SiO_2 (Darken and Gurry, 1946). In general, the high temperature thermochemical properties of complex multicomponent slags are very dependent on composition, non-ideal, and incompletely understood. It is, how-

ever, an active area of research because of its importance to other industries such as glass and steelmaking.

CHAPTER THREE

THESIS OBJECTIVES AND OUTLINE OF WORK

The broad objective of the research proposed here was to elucidate the fundamental physical and chemical processes of mineral matter volatilization during pulverized coal combustion. The experimental basis of this investigation was the combustion of well characterized pulverized coal in the defined and controlled environment of a laboratory laminar flow-drop tube furnace. The coal was fed at a constant rate and the combustion particulate products were collected. The approach was to examine the combustion products to determine, in effect, what physical, chemical and phase transformations have occurred. This included time resolve measurements at various stages of coal burnout. The quanitity and composition of submicron fume generated during combustion provided a direct measure of vaporization to be related to combustion conditions and coal type.

Specific experimental tasks undertaken in this study included:

1) Characterization of the elemental content, of the mineral forms and their adventitious or extraneous occurrence, and of the ion-exchangable tion content (of low rank coals) in selected coals.
2) Measurement of the extent of vaporization of specific elements during combustion by collection, isolation and subsequent analysis of the submicron fume. The objective was to determine how combustion parameters

and coal characteristics influence the degree of vaporization of specific elements.

3) Study of the high temperature evolution and interaction of mineral matter during combustion with regard to decomposition, solid-liquid phase transformations, chemical reactions and multicomponent slag formation processes that bear relevance to the volatility and relative volatility of specific elements/compounds. The objective was to determine if there is a significant dependence of overall high temperature behavior with coal characteristics and combustion parameters.

4) A parallel study of the combustion characteristics of the selected coals. This included measurement of the time temperature history of oxidizing coal particules using the two-color optical pyrometry technique, and the determination of the physical history or structural changes of oxidizing coal particles by microscopy. These experiments were essential to the evaluation of vaporization kinetics and the local reducing environment withing buring coal particles.

5) Integration of the results obtained from the above experimental tasks for the development of a model description of vaporization behavior.

The emphasis of this investigation was on Si, Al, Fe, Ca, Mg, K, and Na, as they are the major inorganic elements in coal, highly varied in their geochemical occurrence among coals,

and largely responsible for submicron particle formation. The thermodynamic properties of these elements or oxide, sub-oxide, sulfate, carbide and sulfide compounds as well as binary and tertiary are somewhat well established to permit evaluation of important of the thermochemistry.

The experimental combustion equipment and procedures and the techniques employed for analysis of the charcteristics of coals and of the nature of the ash combustion products are described in Chapter Four. Because of the large variability in coal characteristics, twenty coals from three ranks (lignites, subbituninous and bituminous) were examined to determine if any generalizations regarding mineral matter vaporization during combustion were applicable. A representative lignite and bituminous coal were used for detailed study. The coals were characterized for their mineral matter content with respect to elemental abundance and mineralogical forms. These results are presented in Chapter Five.

In the laboratory combustion furnace, the combustion rate and temperature of coal particles could be controlled by manipulation of the oxidant (O_2) concentration in the gas. Hence, the kinetic aspects of ash vaporization could be studied experimentally over a wide range of conditions. Chapter Six describes the results of the two-color optical pyrometer measurements of particle burning temperatures and rates. These results are compared with predicted behavior from a single particle combustion model.

The extent of ash vaporization during combustion under controlled and monitored conditions was determined by the

the amount of submicron particulates generated. The submicron particulates, isolated on-line by aerodynamic means, were further analyzed for their elemental content. An experimental and theoretical assessment of the method is given in Chapter Seven and the results of parametric investigations are reported in Chapter Eight.

In Chapter Nine, the results of a scanning electron microscopy investigation of the unusual transformations of organically bound mineral matter (ion-exchanged Ca and Mg) during lignite combustion are reported. Also shown are the physical characteristics of bituminous coals undergoing combustion.

Finally, in Chapter Ten, the results presented in the preceeding Chapters are integrated and a model is developed to interpret fundamental physical and thermochemical mechanism of ash vaporization processes during coal combustion. Conclusions and recommendations are discussed in Chapter Eleven.

CHAPTER FOUR

EXPERIMENTAL METHODS

4.1 Laboratory Combustion System

The central features of the laboratory scale combustion system are a laminar flow-drop tube furnace, into which pulverized coal is continuously injected, and a water cooled collection probe followed by an Anderson Impactor for the continous recovery, quenching and on-line size classification of particulate combustion products. The advantages of conducting combustion experiments on such an apparatus are that:

(1) The combustion conditions can be precisely defined, controlled and monitored to permit detailed investigations of a number of parameters affecting particulate formation.

(2) Small, homogeneous samples of well characterized coal are employed for the experiments.

(3) All particulate products leaving the furnace can be completely collected and size classified for subsequent analysis, thus eliminating questions inevitably present in field studies on the extent to which collected samples are representative.

(4) The laboratory system can simulate environments encountered in both conventional pulverized coal fired boilers and extreme conditions such as those proposed for advanced energy conversion systems such as MHD.

In this section, the combustion furnace, continuous coal

feeding system, collection system, monitoring capabilities and operating parameters are described in detail. In the next section of this chapter, the procedures for sample analysis are described.

4.1.1 Combustion Furnace - A schematic diagram of the laminar flow-drop tube furnace is presented in Figure 4.1. The furnace has electrically heated graphite elements, the temperature of which can be regulated with an automatic current controller. A central combustion zone is maintained within the core of the furnace by an alumina muffle tube of 50mm inside diameter. The maximum operating temperature of the furnace muffle tube is about 1800 K. The main gas, a pre-mixed oxygen-inert mixture, enters through the top of the furance where it flows through an alumina honeycomb before entering the furnace combustion zone. The honeycomb serves as both a preheater and flow straightener to deliver the main gas at the specified furnace temperature with a uniform laminar velocity. The composition of the main gas is regulated by dual mass flow controllers. Coal particles entrained in $10^{-7} m^3/s$ of gas are injected axially into the furnace combustion zone via a water cooled feeder probe. Coal is fed at rates that can be varied between 0.15 to 1.5 mg/s. The main gas flow rate is maintained at $10^{-4} m^3/s$. On entering the furnace combustion zone, the particles are rapidly heated and ignited.

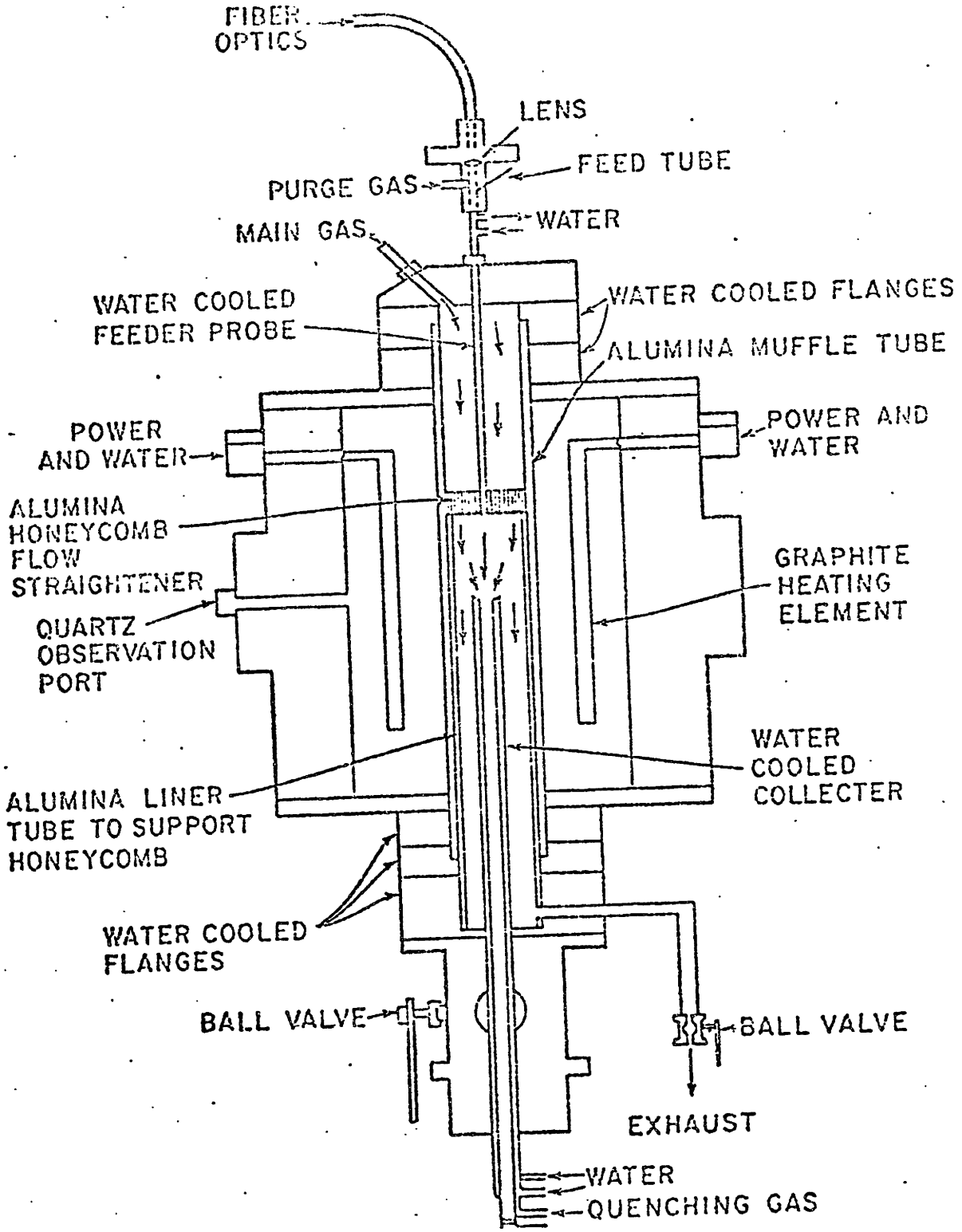

Figure 4.1 Laminar Flow Furnace

4.1.2 Coal Feeding System - A schematic diagram of the coal feeding system is presented in Figure 4.2. The coal particles are entrained by the carrier gas which flows over the surface of an agitated coal bed and into a stationary fine gauge tube. The gas velocity in the fine gauge tube is sufficient to keep the particles in suspension. The rate of entrainment is established by the rate at which the coal feed vial is driven towards the fine gauge tubing. After an initial transient, a fixed clearance is established between the top of the coal bed and the fine gauge tube. A range of feeding rates is obtainable by changing the speed of the syringe pump used to drive the coal vial towards the stationary tubing. One to five grams of coal are fed per experiment.

4.1.3 Collection System - All gas and particulate combustion products are withdrawn from the combustion zone of the furnace by a water cooled collection probe which is inserted along the axis through the bottom of the furnace. The position of the probe is adjustable to allow time resolved combustion measurements.

A schematic of the probe is presented in Figure 4.3. The inner core of the water cooled probe is fitted with a stainless steel porous tubing through which gas is transpired radially during the course of an experiment. In the first 25mm of the top section of the probe, gaseous and particulate products are quenched to below 470 K by $3 \times 10^{-4} m^3/s$ of N_2 gas. A minimal inward radial gas flow of $6 \times 10^{-8} m^3/s$ is maintained throughout the lower section of the probe to

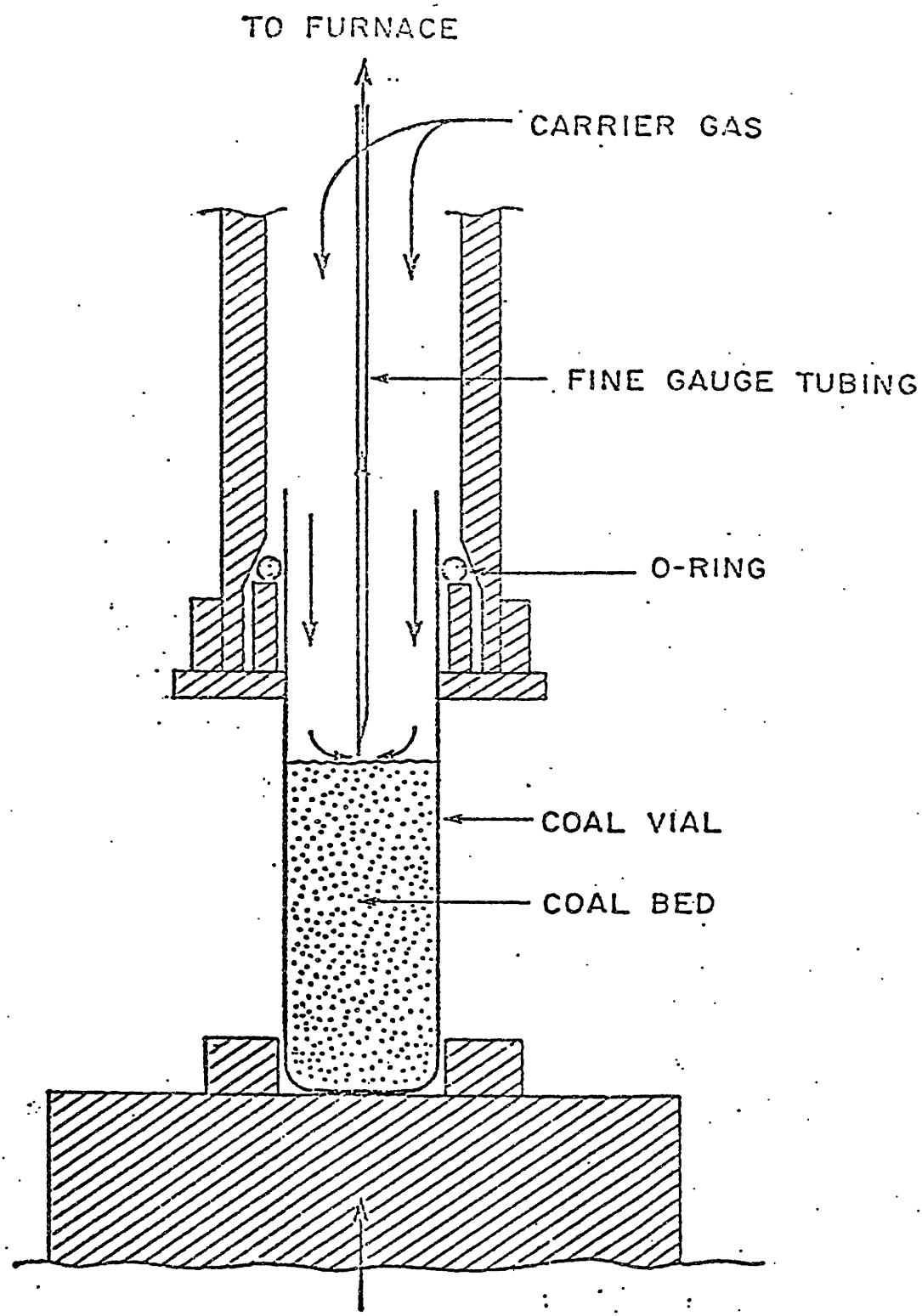

Fig. 4.2: Coal Feeding System.

COLLECTION PROBE SCHEMATIC

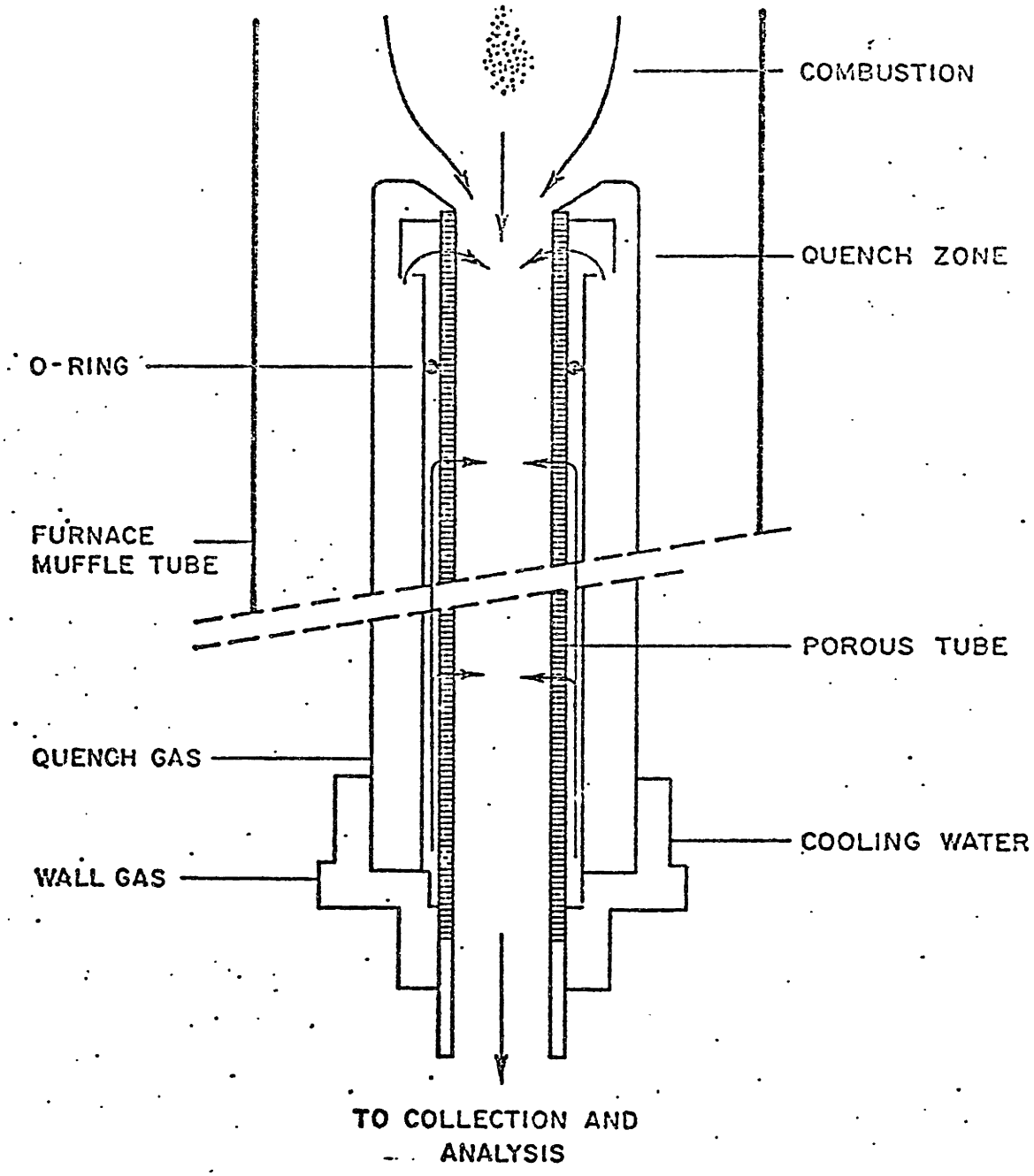

Fig. 4.3 : Collection Probe.

to prevent deposition and loss of particulates within the probe. From the collection probe, the gases and particulates enter directly into an Anderson 2000 cascade impactor for on-line aerodynamic size classification of the particulates. The impactor contains eight stages with theoretical effective cut-off diameters of 12.4, 7.9, 5.4, 3.7, 2.4, 1.2, 0.77, and 0.54 μm. The smaller submicron particulates pass completely through the impactor and are collected on a back-up Millipore membrane filter for weight determination and chemical analysis. For electron-microscopy of the fume, this filter is removed and a pulsed electrostatic aerosol sampler (TSI 3100) was used to deposit the submicron particles onto carbon coated transmission electron microscope grids.

It is known that the performance of the Anderson Impactor is limited by problems associated with wall loss, particle bounce and re-entrainment (Dzuby et al., 1976; Gordon et al., 1974). In the present study, re-entrainment and particle bounce were minimized by employing greased substrates on the impactor and a conical head was constructed with a porous carbon inner wall through which gas is transpired at a nominal rate to prevent deposition.

4.1.4 Combustion Monitoring - A two-color optical pyrometer is used to determine the buring temerpature history of ignited coal particles in the furnace combustion zone. For these measurements, a slightly modified feeding system is employed. The coal particle stream in the fine gauge tubing is passed through a dilution stage to reduce

particle number densities before entering the water cooled feeder probe in the furnace. This allows the measurement of the temperature of single coal particles from ignition to burn-out (Altrichter, 1980). Optical access into the furnace combustion zone is obtained through the coal feeder probe. A more detailed description of this instrument is given by Tymothy (1981). Thermocouple measurements of the centerline gas temperature were also performed. A Pt-Pt(10%Re) thermocouple was used. The thermocouple was mounted on the collection probe in the manner such that the position of the sheath holding the thermocouple was adjustible to allow measurement of the axial temperature profile at a fixed collection probe position.

4.2 Analytical Methods for Coal and Combustion Products

4.2.1 Coal Preparation and Sizing - Pulverized coal

samples were obtained by mechanically grinding in a rod-mill and then subsequently sized into narrow cuts by sieving in a ro-tap. The narrow size cuts were then spread over a fine (600) mesh screen to which a vacuum was applied. The purpose of this was to remove the fine (<10 micron) coal dust which was not removed by mechanically sieving. These samples were then retained for characterization of the mineral matter content and used directly in combustion experiments. Size distributions of the coal feed samples were obtained from photomicrographs.

4.2.2 Proximate Analysis - The total ash content and moisture content of the prepared pulverized coals were determined by the ASTM methods. The fixed carbon and volatile matter contents of the coals were obtained from Galbraith Analysis, Inc., Knoxville, Tennesse. In the case of coals obtained from the Pennsylvania State University Coal Bank, their reported values were used for fixed carbon and volatile matter content.

The low temperture ashing technique (LTA) was used to separate the mineral matter from coal in an essentially unaltered form. Samples obtained by this method could then be examined by the X-ray powder diffraction to determine the principle mineral forms in the coal. The principles and procedures of this technique have been described in greater detail in the coal literature (Gloskoter, 1965; O'Gorman and Walker, 1972). The basic principle is that atomic and excited oxygen, generated by a radio frequency oscillator, is used to 'burn' away the organic material of coal at low pressure (1mm Hg) and low temperature (100°C). The process takes approximately 2-3 days for a one gram sample of bituminous coal and somewhat longer (4-5 days) for lignites and sub-bituminous coals.

4.2.3 Elemental Analysis - Samples analyzed for their major, minor and trace metal content included the prepared pulverized coal, the filter collected submicron particulates generated during combustion, and, to a limited extent, the larger (>1 micron) combustion particulates that deposit on

the various impactor stages. The methods used included instramental neutron activation analysis (INAA), atomic absorption spectroscopy (AA), plasma emission spectroscopy (PES), and electron microprobe analysis (EMA).

INAA is the method of choice for major, minor, and trace elements because of its high sensitivity for small samples, minimum sample handling and contamination, and freedom from the tedium of wet chemical techniques. The INAA method for coal anf fly-ash samples has been used extensively and shown to produce accurate results (Ondov et al., 1975; Rancitelli et al., 1976). Samples are irradiated in the MIT Reactor and gamma ray counts are measured with a high resolution Ge(Li) detector. Elements analyzed by this method include:

Al, Ca, Mg, Na, K, Fe, Cl, As, Cr,
La, Mn, Sb, Sc, Sm, Ti, Th, V.

Approximately one tenth of a gram of coal is analyzed by this method. To determine the absolute amount of an element in the combrotion generated submicron material, the entire filter containing this collected material is irradiated and counted.

Elements determined by the PES method included Al, Fe, Mg, Ca, Na and K. Silicon was determined by AA. The AA and PES work was performed by Touchstone Environmental Consultants, Winchester, Massachusetts. For these methods, the coal samples were first ashed by the ASTM procedure prior to dissolution in acids. In the case of the filter collected material from combustion experiments, the material on the

filter was directly digested into solution without prior ashing.

The elctron microprobe (EMA) was also used to determine the composition of submicron material collected on the filters. The instrument was fully calibrated for oxides of Si, Al, Ca, Mg, K, Na, P and S. Repeated analysis was performed on several areas of the filter to ensure reproducibility.

Sulphur, silicon and phosphoru in the raw coals were also analyzed by Galbraith Analysis, Incorporated, Knoxville, Tennessee.

4.2.4 X-Ray Powder Diffraction (XRD) - This method was used primarily for the purpose of identifying the principle mineral forms in coal low temperature ash, which include quartz, kaolinite, illite, calcite and pyrite. The method is generally not quantitative unless considerable sample preparation and calibration is undertaken (Rao and Gloskoter, 1973). It has been used extensively in the analysis of coal minerals (O'Gorman and Walker, 1972; Rao and Gloskoter, 1973). In the present study, (TA powder samples were mounted on glass slides and scanned with CuKd radiation. XRD was also employed to determine the chemical nature of ash during combustion of the char. For example, it was used to determine the formation of high temperature crystalline phases of CaO MgO. Positive identification of such compounds requires that the material be in crystalline form.

4.2.5 Mössbauer Spectroscopy - This technique was used to identify the iron-bearing maineral forms in the various coals. The method has been applied extensively to coal (Huggins and Huffman, 1979) and the Mossbaver parameters for common iron-bearing minerals are fairly well known. A more detailed discussion of the principles of this technique is provided in Appendix C.

4.2.6 Scanning Electron Microscopy - The surface of partially oxidized chars obtained from time-resolved combustion experiments were examined in detail by scanning electron microscopy (SEM) and energy dispersive X-ray analysis (EDXA) for the purpose of providing direct evidence for the transformations of mineral matter during combustion and information on the burning characteristics of chars. The partially oxidized char samples were mounted on carbon discs and coated with copper for conduction. An AMR 1000 scope equipped with a KEVEX energy dispersive X-ray analyzer was used. The instrument has a point to point resolution of 50Å under optimum conditions (minimum sample charging). The resolution of elemental analysis by EDXA, however, is on the order of 1 micron because of electron scattering within the sample.

4.2.7 Density Fractionation of Coal - On a microscopic scale, the distribution of mineral matter in pulverized coal is quite heterogeneous. For example one coal particle may contain more minerals than another or minerals of different composition. Some coal particles may not contain any minerals or ash. One approach to determining the heterogeneity of coal with respect to mineral matter distribution

is by fractionating the pulverized coal in mediums of different specific gravity (Littlejohn, 1966). The specific gravity of the organic material of coal is about 1.3, whereas that of the minerals range from about 2 to 5. Coal particles containing a significant amount of mineral matter would have a specific gravity somewhat greater than 1.3. Particles which sink in a medium of s.g.1.8 would contain very little organic matter and would be so-called extraneous mineral. The significance of fractionating the coal is to determine the extent to which minerals and trace elements are associated with the combustible organic material and therefore exposed to the local combustion environment of coal particles.

A series of density fractionations were carried out on several coals in mediums ranging from 1.3 to 1.8 specific gravity. Mixtures of methylenechloride and ethylenebromide (reagent grade) were used to obtain the desired density of the separating medium. The fractionated coal was then analyzed for total ash distribution, elemental distributions and mineral distributions by the same methods previously described for the raw coal samples.

4.2.8 Ion-Exchanging Low Rank Coals - To determine the extent to which calcium, magnesium and sodium are bound organically to low rank coals on carboxylic groups, these elements were extracted from the coal by ion-exchanging with ammonium acetate. The procedures used in this study for the ion-exchange were those developed by Miller and Given (1978). The ion-exchanged coals were then analyzed

for total ash content and elemental (Ca, Mg, Na) content for comparison to the raw coal.

CHAPTER FIVE

MINERAL MATTER CHARACTERISTICS OF COALS STUDIED

5.1 Introduction

The non-combustible inorganic matter of coals occurs most frequently in the form of mineral grains of micron or greater size and, accordingly, is termed 'mineral matter'. As discussed previously in Chapter Two, the minerals commonly found in coals include Zhc clays such as Kaolinite and illite, quartz, pyrite, calcite, dolomite, and bassanite which, individually or collectively, contain the major inorganic elements Si, Al, Fe, Ca, Mg, Ma and K that derive the oxide ash residue obtained after burning the coal. There is significant variablility, however, in both the relative and total abundance of these minerals from coal to coal and even among different locations in a given seam. Hence, the concentration of a specific element in coal may vary among wals as might its form of occurance. For example, magnesium may occur in dolomite or in certain clay minerals (e.g. illite). Iron may occur in pyrite exclusively, or in additional mineral forms such as sulphastes and carbonates, or substituted in clay minerals. Nearly all coals contain both quartz and silicate clays, but the relative distribution of silicon between these phases may vary form coal to coal.

In addition to the presence of mineral forms, inorganic matter in coal may occur in organic combination. This is primarily a characteristic of low rank subbituminous coals and lignites where the greater protion of the calcium,

magnesium and sodium are bound to the organic matter of coal as cations ion-exchanged on carboxylic and phenolic functional groups. Such wals generally contain higher concentrations of calcium and magnesium than the bituminous coals.

The collective behavior of mineral matter during coal combustion may depend on several factors including the thermochemical behavior of the minerals, interactions between different minerals and with the carbonaceous matter, and the temperature history experienced by the minerals during combustion. This in turn will depend on how the minerals are distributed in as-fired pulverized coal. When coal is crushed to a fine powder of 50 microns, the charcteristic size of the mineral grains will range from less than a few microns to much greater sizes on the order of the size of the individual coal particles. The minerals with dimensions ranging from about 1 to 10 microns are, for the most part, included or embedded in the carbonaceous matter of coal particles. Those having much larger dimensions are necessarily free of appreciable association with the organic matter of coal particles. The former, along with the organically bound metals are often referred to as the 'inherent' ash of the coal, while the latter form is termed 'extraneous' mineral matter (O'Gorman and Wlaker, 1972). A distinction between inherent and extraneous occurance is important to understanding of mineral matter behavior during combustion. Minerals and elements distributed in the organic coal particles will be subjected to the temperature history and the locally reducing evnironment (which facillitates ash vaporization reactions) of

coal particles burining in a high temperature environment. Extraneous minerals would not experience a highly reducing gas environment nor the possible higher burning char particle tmeperatures over the gas temperature. Further heterogeneity in mineral matter distribution may occur on a coal particle to particle basis. Not necessarily all particles contain the same arrangement of minerals or elements that derive the ash upon combustion.

The focus of this chapter is to describe the characteristics of the minral matter in the coals studied.

5.2 Coals Studied and Their Proximate Analysis

Twenty coals, including twelve bituminous coals from Eastern, Interior and Gulf states, five subbituminous coals from the Northern Great Plains and Rocky Mountain States, and three Lignites from Montana, North Dakota and Texas, were used in the present study. Prior to proximate, elemental or mineralogical analysis, all coals were ground to a fine powder and mechanically sieved into narrow-sized fraction of nominal 50-60 microns in diameter. This same size fraction was also used in the compostion experiments described in later chapters. The selected coals, their origin, rank and proximate analysis are reported in Table 5.1. The coals used most extensively in the present investigation included the Illinois No. 6 and the Alabama Rosa No. 18, both of the bituminous rank, and a Montana Savage Lignite. A larger size fraction, of nominal 120 micron diameter was also prepared analyzed and used in the combustion experiments for these

TABLE 5.1

Selected Coals, Rank and Proximate Analysis

Coal	Rank*	VM	FC	H_2O	Ash
Illinois No. 6	B	38.1	40.8	7.4	13.7
Western Kentucky	B	37.4	50.8	4.8	6.8
West Virginia	B	34.1	48.6	1.8	15.5
Pittsburgh No. 8	B	36.8	54.4	1.3	7.3
Alabama Rosa #18	B	21.9	63.4	8.1	6.6
Utah	B	38.7	46.9	6.4	8.0
Utah Price No. 1	B	38.5	46.9	6.3	8.3
PSOC-3, Kentucky Upper Elkhorn No. 3	B	35.7	59.0	1.8	3.5
PSOC-26, Illinois No. 6	B	36.0	42.9	12.2	8.9
PSOC-130, West Virginia Pocahontas No. 3	B	21.2	71.2	1.8	5.8
PSOC-136, Alabama Pratt Seam	B	24.1	73.0	0.6	2.3
PSOC-997, West Virginia, Pittsburgh Seam	B	37.9	54.4	1.5	5.2
Montana Rosebud	S	35.2	43.9	7.3	13.6
Montana Hardin No. 20	S	38.1	43.1	9.9	8.9
Montana, Powder River Region	S	----	----	8.8	12.5
Wyoming Commanche	S	----	----	10.2	6.2
Wyoming Rawhide	S	----	----	8.3	7.4
Montana Savage	L	37.0	44.2	10.0	8.8
North Dakota, Bevlah	L	38.5	41.7	12.3	7.5
Texas	L	33.3	28.9	9.4	28.4

B - Bituminous, S - Subbituninous, L - Lignite

selected coals.

5.3 Particle Distribution of Classified Coals

Pulverization of coal prior to firing in utlitiy boilers produces a wide range of coal particles size with, in general, 90 percent of the coal by weight being smaller than 150 microns and larger than 20 microns (Littlejoh, 1966). Knowledge of the size distribution is of practical importance as it determines the residence time required for near complete combustion of the organic matter in boiturs. In so far as mineral matters behavior is concerned particularly that of its vaporization behavior, the size of the coal will determine, under a given combustion condition, the time of exposure to the locally reducing environment within the coal and the higher combustion temperatures of burning coal particles or that of the surrounding gas. The size of the coal is also a basic parameter in the calculation of the rate of ash vapor transport through particle external boundary layers during combustion. Hence, as a parameter it is essential to determining of kinetics and mechanisms involved in ash vaporization processes. Two coal sizes were prepared for the main coals to determine if this parameter influenced the extent of ash vaporization and submicron ash particulate formation during combustion.

The scanning electron micrographs shown in Figure 5.1 compares at the same magnification to two sizes of the Montana lignite and also provides a visualization of the nature of unreacted pulverized coal.

A

B

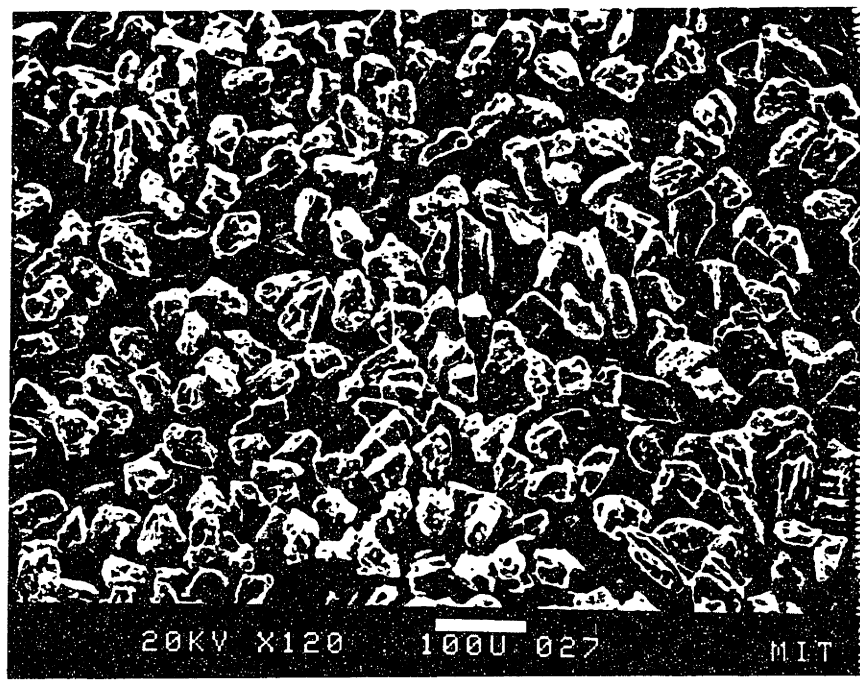

Figure 5.1 Scanning Electron Micrograph of Size Classified Lignite A-138 Microns, B-61 Microns

A

B

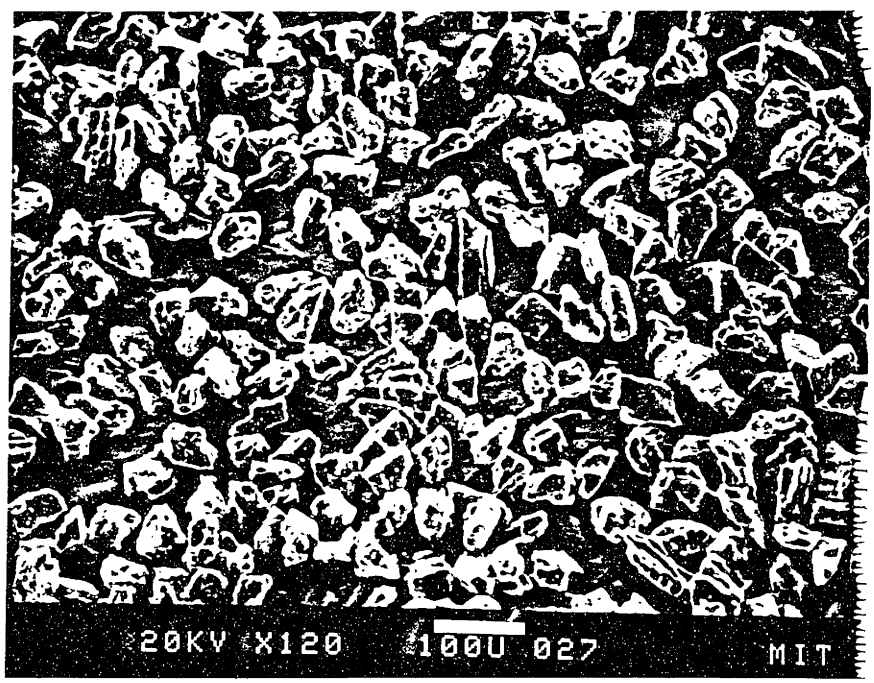

INTENTIONAL DUPLICATE EXPOSURE

Figure 5.1 Scanning Electron Micrograph of Size Classified Lignite A-138 Microns, B-61 Microns

The size distributions of the prepared coal samples were obtained directly with an automated image analyzer. These results are shown in Figures 5.2 and 5.3 for the Montana Savage lignite and the Illinois No. 6, respectively. The number of particles counted for each distribution is also given. The mean diameters were 61 and 138 microns, for the two Montana samples and 53 and 125 microns for the Illinois No. 6. For each coal, the size distribution of the two size classified coal samples are seen to bé effcetively separated.

The ash contents of the different size classified coal samples are compared in Table 5.2.

5.4 Elemental Analysis of Coals

To test the heterogeneity of coal samples and also the reproducibility of the analytical methods, multiple samples of the coals were analyzed for their elemental content. These results are given in Tables 5.3 and 5.4 for the Illinois No. 6 and the Montana Savage lignite. In general, the methods show reasonable agreeement and consistancy. The average elemental concentrations for these coals and the values obtained for the elemntal content of all other coals are given in Tables 5.5 and 5.6. The concentration of total sulphur and phosphorus were obtained form Galbraiths Analysis, Inc., Knoxville, Tennessee or from reported Penn. State values for PSOC coals.

5.5 Distribution of Elements By Density Fractionation

The major elements or their host minerals are not uniformly distirbuted throughout the carbonaceous matrix of

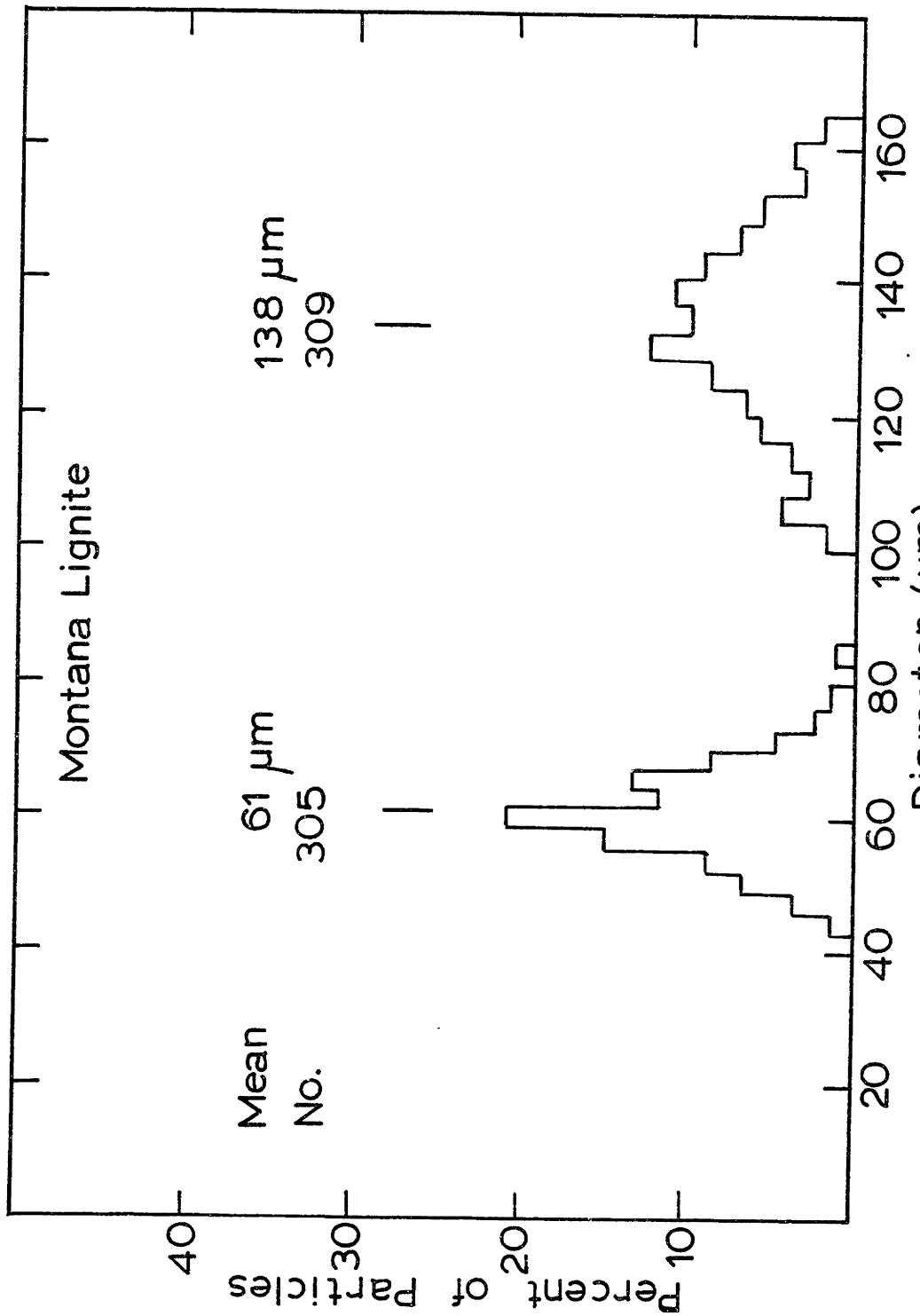

Figure 5.2 Particle Size Distribution for Montana Lignite Samples

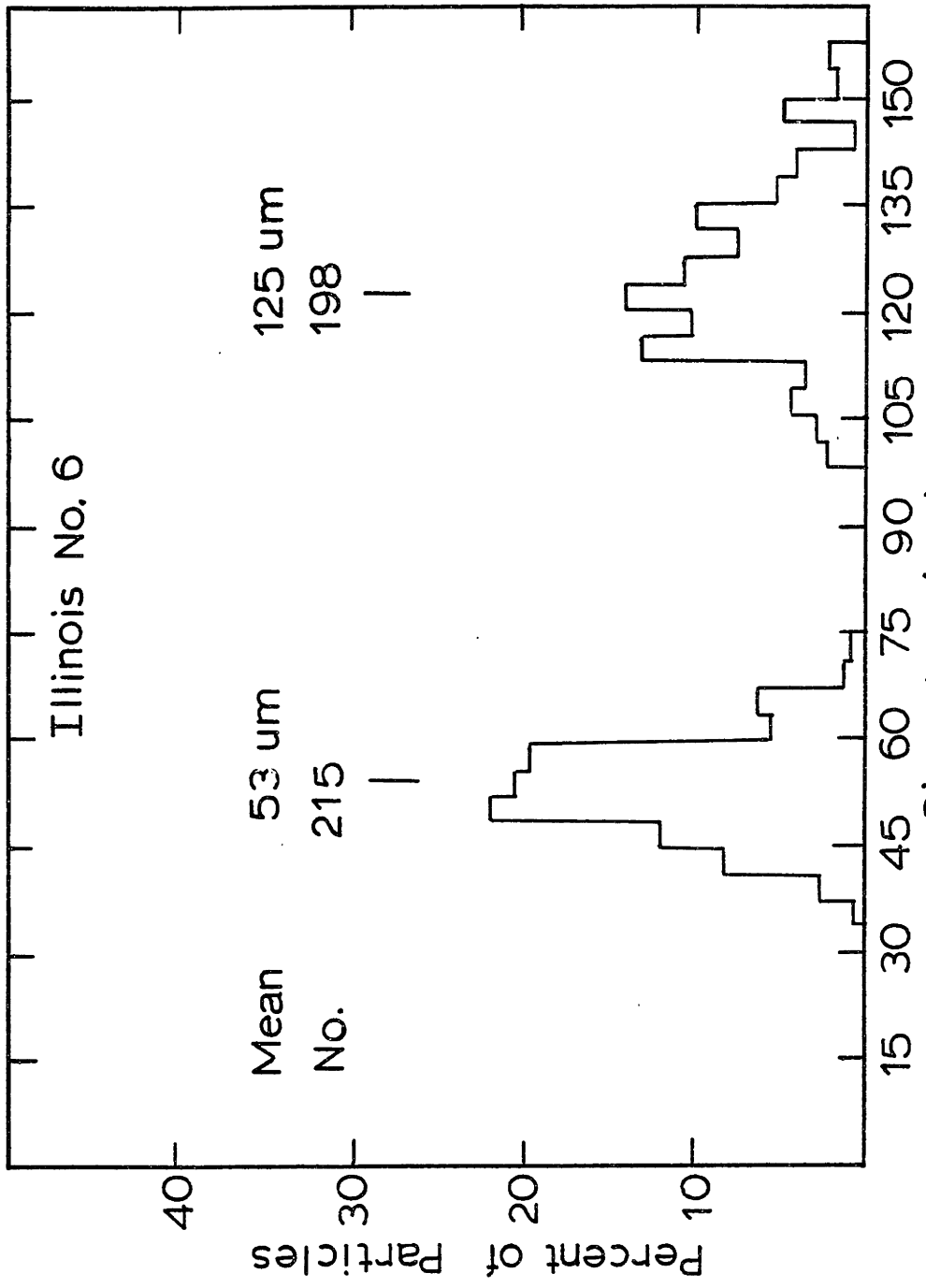

Figure 5.3 Particle Size Distribution for Illinois No. 6 Coal Samples

TABLE 5.2

Comparison of the Ash Content of
Different Size Fractions of Coal

Coal	Size (μm)	Ash Content (wT%)
Montana Savage	61	8.8
Montant Savage	138	8.6
Illinois No. 6	53	13.7
Illinois No. 6	125	12.1

TABLE 5.3

Multiple Elemental Analysis of Illinois No. 6 Coal (ppm of Coal)

Coal Size (m) Method	53 INAA	53 INAA	53 INAA	53 EMS	53 EMS	53 EMS	125 INAA	125 EMS
Si*	-----	-----	-----	294000	27700	28800	-----	20000
Al	12200	12100	11800	10300	12000	11000	11100	-----
Fe	17300	17400	17600	17800	17900	16700	16100	16300
Ca	10700	8700	8000	8000	8200	9000	8100	8100
Mg	----	----	----	1000	1010	1030	----	1010
Na	470	430	490	460	470	480	460	650
K	2000	1900	1800	1800	1900	1800	----	----
Ti	650	620	660	----	----	----	550	----
Cl	350	300	330	----	----	----	350	----

* Silicon analysis by AA

TABLE 5.4

Multiple Elemental Analysis of Montana Savage Lignite (ppm of Coal)

Coal Size (μm) Method	61 INAA	61 INAA	61 INAA	61 EMS	61 EMS	61 EMS	138 INAA	138 EMS
Si*	-----	-----	-----	9440	8640	9560	-----	9520
Al	6640	6640	6450	6120	6000	5800	7260	6710
Fe	3850	3370	3150	3150	3000	2800	3170	2960
Ca	13300	13200	13700	14300	13700	14700	14500	14500
Mg	-----	-----	-----	5900	5630	5700	-----	5790
Na	320	170	230	170	170	170	170	160
K	-----	-----	-----	270	270	270	-----	330
Ti	230	200	220	-----	-----	-----	-----	-----
Cl	170	120	100	-----	-----	-----	-----	-----

*Silicon analysis by AA

TABLE 5.5

Elemental Analysis of Bituminous Coals (wT%)

Coal	Si	Al	Fe	Ca	Mg	K	Na	Ti	Cl	P	S
Illnois No. 6	2.86	1.20	1.75	0.80	0.10	0.18	0.047	0.056	-----	.011	4.35
Western Kentucky	1.41	0.79	1.60	0.59	0.038	0.13	0.011	0.048	0.024	.003	3.29
West Virginia	3.36	2.13	2.35	0.39	0.10	0.24	0.048	0.11	0.18	.055	2.85
Pittsburgh No. 8	1.31	0.90	0.81	0.56	0.077	0.081	0.063	0.042	0.10	.013	2.83
Alabama Rosa #18	1.65	0.70	0.56	0.70	0.060	0.17	0.033	0.022	0.049	.007	0.77
Utah	1.52	0.96	0.23	0.30	0.040	0.029	0.039	0.052	0.008	.031	1.00
Utal Price No. 1	2.45	1.00	0.17	0.15	0.032	0.039	0.040	0.049	0.030	----	0.62
PSOC-3	1.30	0.50	0.13	0.071	0.021	<0.005	0.017	0.067	0.170	----	0.61
PSOC-26	1.57	0.90	2.40	0.10	0.056	0.19	0.015	0.038	0.080	----	0.85
PSOC-130	0.92	0.72	0.46	0.67	0.13	0.026	0.032	0.030	0.022	----	0.51
PSOC-136	0.51	0.48	0.26	0.03	0.016	0.012	0.012	0.018	0.006	----	0.58
PSOC-997	1.27	0.82	0.56	0.17	0.046	0.050	0.033	0.03	0.10	----	1.57

TABLE 5.6

Elemental Analysis of Low Rank Coals (wT%)

Coal	Si	Al	Fe	Ca	Mg	K	Na	Ti	Cl	P	S
Lignites:											
Montana Savage	0.87	0.64	0.30	1.44	0.58	0.03	0.017	0.021	-----	0.031	0.55
North Dakota	0.55	0.39	0.62	1.10	0.52	0.03	0.66	0.023	-----	0.009	0.55
Texas	8.00	1.32	0.90	0.55	0.22	0.17	0.027	0.150	0.012	0.005	1.20
Subbituminous:											
Montana Rosebud	1.64	1.00	1.70	1.20	0.24	0.061	0.025	0.036	-----	0.012	1.33
Montana Hardin	1.16	0.75	0.50	1.20	0.18	0.031	0.26	0.035	0.011	-----	0.71
Montana Powder River	2.06	1.06	0.99	1.20	0.31	0.056	0.024	0.051	0.008	-----	1.16
Wyoming Commanche	0.63	0.51	0.34	0.99	0.27	0.014	0.064	0.038	-----	0.028	0.38
Wyoming Rawhide	1.36	0.62	0.37	1.10	0.25	0.015	0.048	0.038	0.004	-----	----

coal. This is particularly true on a microscopic scale where the characteristic dimensions of coal particles are on the order of 50 or 100 microns and those of the mineral grains range from less than one micron to comparable sizes. The ultimate approach to characterization of mineral matter occurance, although impractical, would be to determine the concentrations of elements and minerals in a statistically significant number of individual coal particles. Routine analytical methods for this excercise do not as yet exist. The most frequent approach taken is to physically fractionate the powdered coal by means of specific gravity. This technique has been used extensively to determine whether certain trace elements in coal are associated with the organic matter (chelated) or with the inorganic matter or minerals in the coal (Gluskoter et al., 1977). The specific gravity of minerals range form 2.0 to 50.0 whereas that of the pure organic matter is around 1.3. Hence, coal particles containing numerous mineral inclusions would have higher a density than those contianing few or no mineral inclusions. Elements chemically bound to the organic matter would tend to concentrate in coal particles of low specific gravity where the organic matter predominates. Determining the distribution of pulverized coal particles with respect to specific gravity or density also provides information on the extent to which minerals such as quartz, calcite or pyrite are associated with the organic matter (inherent) within coal particles.

Separation of the coals was performed by centrifuging

in prepared mixtures of ethylene chloride and methylene bromide. In Figure 5.4, the percentage of coal particles recovered in the float after separation is plotted against the specific gravity of the separation medium for selected coals. The decreasing percentages of the coal float recovery with decreasing specific gravity is due to the decreasing mineral matter content. The overall density of the Alabama Rosa No. 18 is somewhat less than that of the Illinois No. 6, a result expected when comparing the ash contents of these bituminous coals (Table 5.1). The low rank Rosebud sub-bituminous coal and the Savage lignite arc of higher density for a given coal float recovery percentage than the bituminous coals.

The ASTM ash contents of the float fractions were determined. These results are shown in Figure 5.5, normalized against the float recovery rather than the specific gravity for the selected coals. Decreasing coal float recovery corresponds to decreasing mineral matter or ash content. The raw coal analysis corresponds to the 100% recovery point. The higher density of the low rank coals at low float recovery percentages is due to their higher ash contents at low float recoveries. For the savage lignite, it appears that the total ash is nearly evenly distributed throughout the coal.

All of the twenty coals used in the present study were examined by separation in 1.8 specific gravity. The purpose of this was to differentiate the occurance of inherent

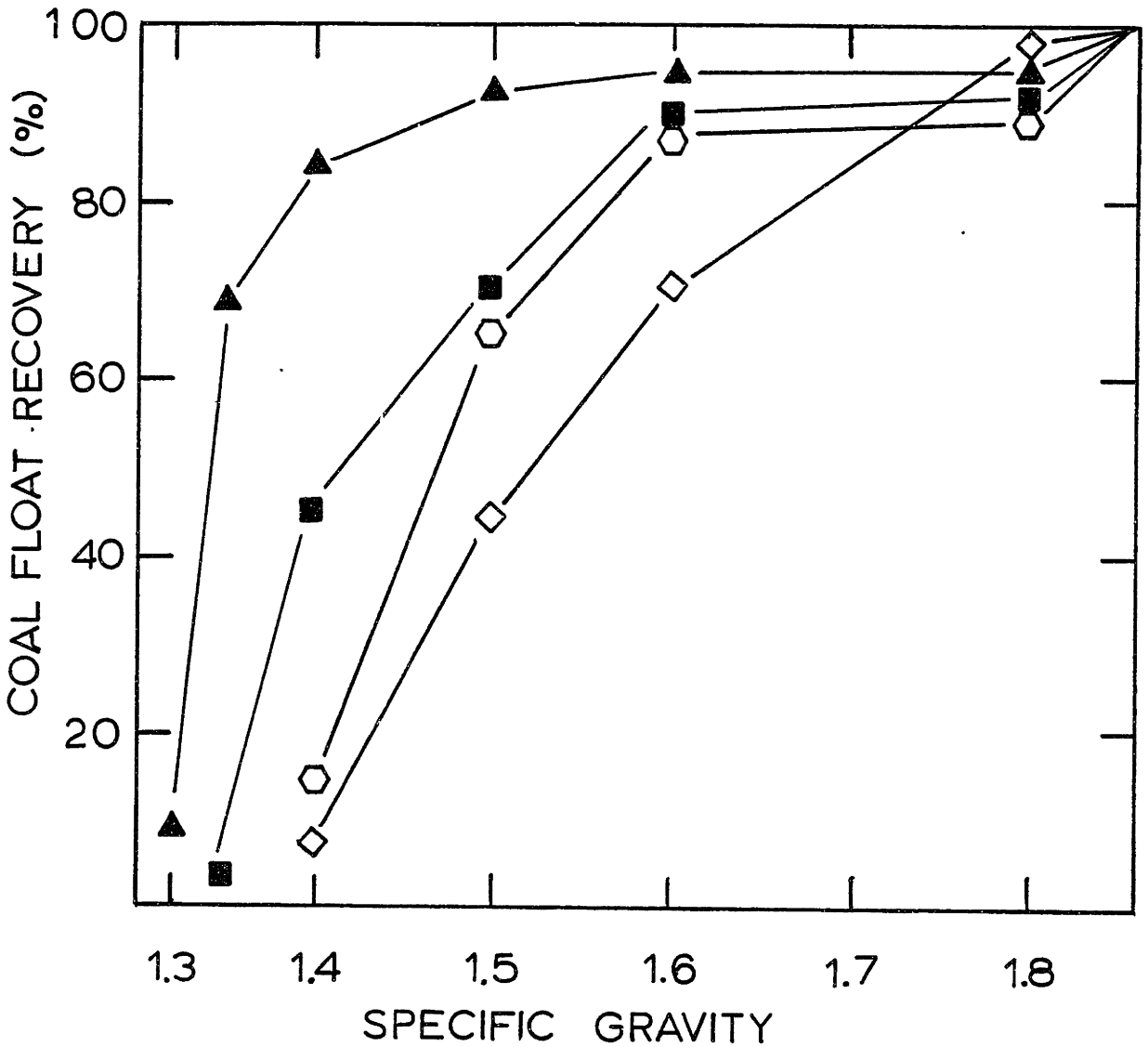

Figure 5.4 Percentage of Coal Recovered in Floats. Alabama Rosa: ▲, Illinois No. 6: ■, Montana Rosebud: ⬡, Montana Lignite: ◇,

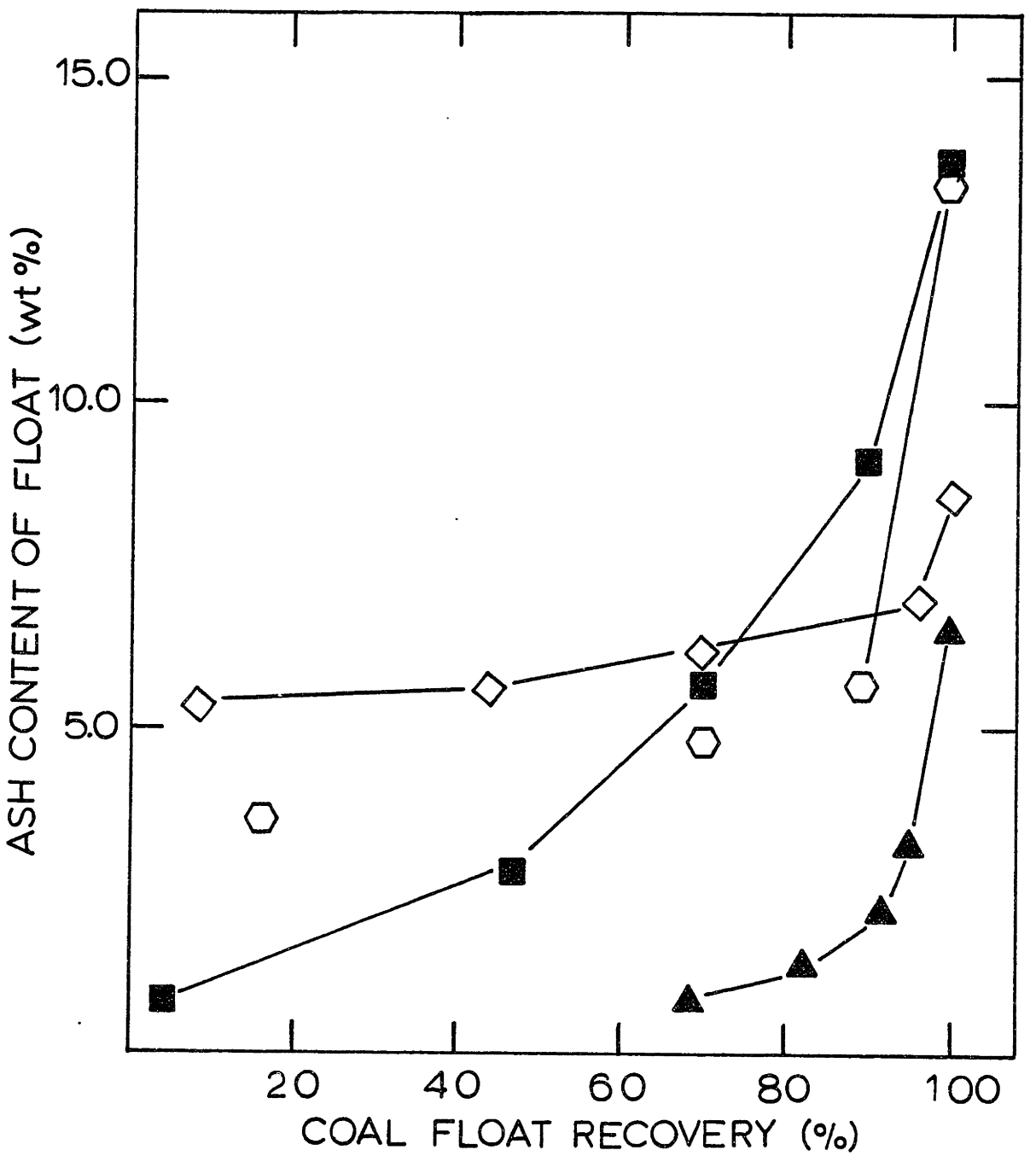

Figure 5.5 Ash Content of Coal Float Samples Obtained by Density Fractionation. Alabama Rosa: ▲, Illinois No. 6: ■, Montana Rosebud: ⬡, Montana Lignite: ◇,

mineral matter and extraneous mineral matter and the extent to which specific major elements are associated with the organic matter of coal. The ash contents of both the 1.8 float and the 1.8 sink were determined and the results are reported in Tables 4.7 and 5.8. Generally the ash content of the 1.8 sink fraction of the coals was quite high, averaging about 70 percent, indicating that it is essentially all mineral matter. The ASTM high temperature ashing procedure will decompose and dehydrate various minerals, yielding somewhat lower values than the true mineral matter content of the sample (Padia, 1976).

For the practical purpose of considering how mineral matter will behave during combustion, that which occurs in the coal 1.8 sink fraction is assumed to be extraneous mineral matter or ash. The inherent mineral matter which occurs within highly organic coal particles corresponds to that recovered with the 1.8 coal float. The ash contents of the 1.8 floats are somewhat and, occassionally, significantly lower than the ash content of the raw coals (see Table 5.1) due to the removal of the extraneous mineral matter. Although the amount of the raw coal sinking in a 1.8 specific gravity medium is typically a few percent, the amount of ash recovered with 1.8 sink ranged from under 10 to 60 percent of the ash in the raw coal as shown in Tables 5.7 and 5.8. The major conclusions that can be drawn from the results shown in Tables 5.7 and 5.8 is that the relative occurance or distribution of inherent and extraneous mineral matter is highly varied among coals and that for certain coals, a substantial

TABLE 5.7

Inherent and Extraneous Mineral Matter Characteristics of Bituminous Coals (wt%)

Coal	Percent of Raw Coal In 1.8 Sink	Ash Content of Coal in 1.8 Sink	Ash Content of Coal in 1.8 Float	Inherent Ash Content of Raw Coal	Percent of Total Ash That is Extraneous
Illinois No. 6	9.34	67.0	8.3	7.5	45.0
Western Kentucky	2.9	41.4	5.8	6.7	17.0
West Virginia	8.6	64.3	10.9	10.0	36.0
Pittsburgh No. 8	2.8	41.1	6.3	6.2	16.0
Alabama Rosa	4.5	81.5	3.1	2.9	56.0
Utah	4.7	70.0	4.9	4.7	41.0
Utah Price No.1	4.3	84.0	4.9	4.6	44.0
PSOC-3	1.0	31.0	3.2	3.1	9.2
PSOC-26	5.6	55.0	6.2	5.8	35.0
PSOC-130	3.0	53.0	4.4	4.3	27.0
PSOC-136	0.3	63.0	2.1	2.1	9.1
PSOC-997	3.7	31.1	4.3	4.1	21.0

TABLE 5.8

Inherent and Extraneous Mineral Matter Characteristics of Low Rank Coals (wt%)

Coal	Percent of Raw Coal in 1.8 Sink	Ash Content of Coal in 1.8 Sink	Ash Content of Coal in 1.8 Float	Inherent Ash Content of Raw Coal	Percent of Total Ash That is Extraneous
Montana Savage	3.2	72.0	6.6	6.4	27.0
North Dakota	2.6	41.0	6.6	6.4	14.0
Montana Hardin	4.2	71.0	6.2	5.9	34.0
Montana Powder River	6.6	66.0	8.8	8.2	35.0
Wyoming Commanche	4.1	28.0	5.2	5.0	19.0
Wyoming Rawhide	2.7	68.0	5.8	5.6	25.0
Montana Rosebud	13.0	69.0	5.6	4.9	64.0
Texas	19.0	85.0	14.8	12.0	58.0

amount of the mineral matter is not associated with the combustible organic matter.

It can be inferred from the results shown previously in Figure 5.5 that the inherent ash is not uniformly distributed throughout the coal particles, particularly for bituminous coals. This is indicated by the sloping nature of the recovery curves. For example, nearly 50 percent of the Illinois No. 6 coal has a cumulative ash content of less than 3.0 percent and nearly 70 percent of the Alabama Rosa No. 18 contains less than 0.8 percent compared to their raw coal values of 13.7 percent and 6.6 percent and 'inherent' or extraneous-free ash values of 7.5 and 2.9 percent, respectively.

The concentrations of the major and minor elements considered in this study, which include Si, Al, Fe, Ca, Mg, K and Na, were also determined for the density separated coal samples. These results are presented in Figures 5.6 through 5.12 in the same form, normalized on a coal float recovery percentage basis. Silicon, aluminum and iron concentrations in the bituminous Illinois No. 6 and Alabama Rosa coals drop off significantly with devreasing coal float recoveries due to their occurance in mineral forms. Magnesium and calcium also drop off somewhat with decreasing float recoveries for bituminous coals. In tnese coals the alkalines may occur as sulphate (bassanite) or carbonate minerals (calcite or dolomite) or in clay minerals (e.g. illite). The nearly flat profiles for calcium and magnesium concentation in the low rank subbituminous Montana Rosebud and particularly

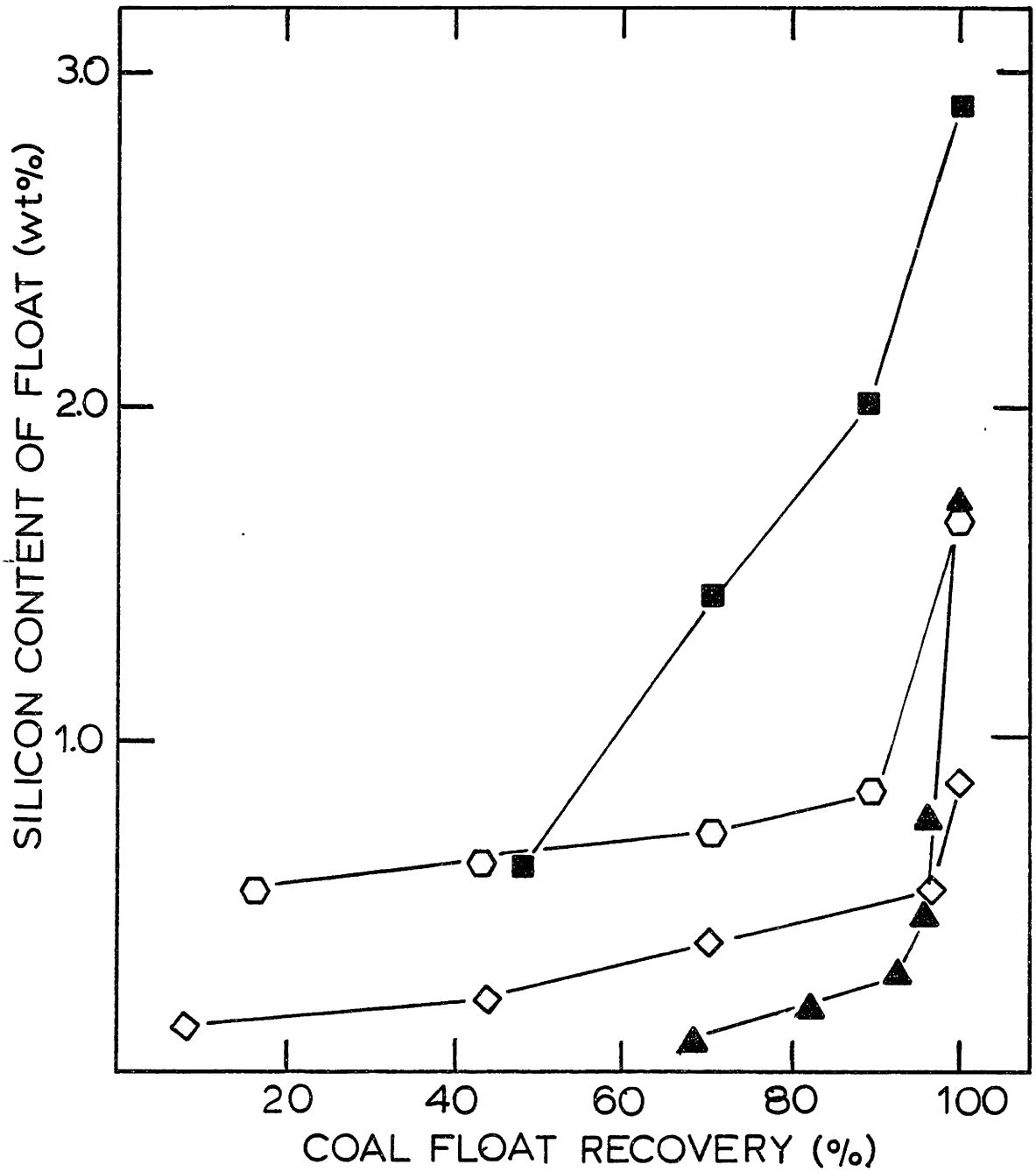

Figure 5.6 Silicon Content of Density Fractionated Coal. Alabama Rosa: ▲, Illinois No. 6: ■, Montana Rosebud: ⬡, Montana Lignite: ◇.

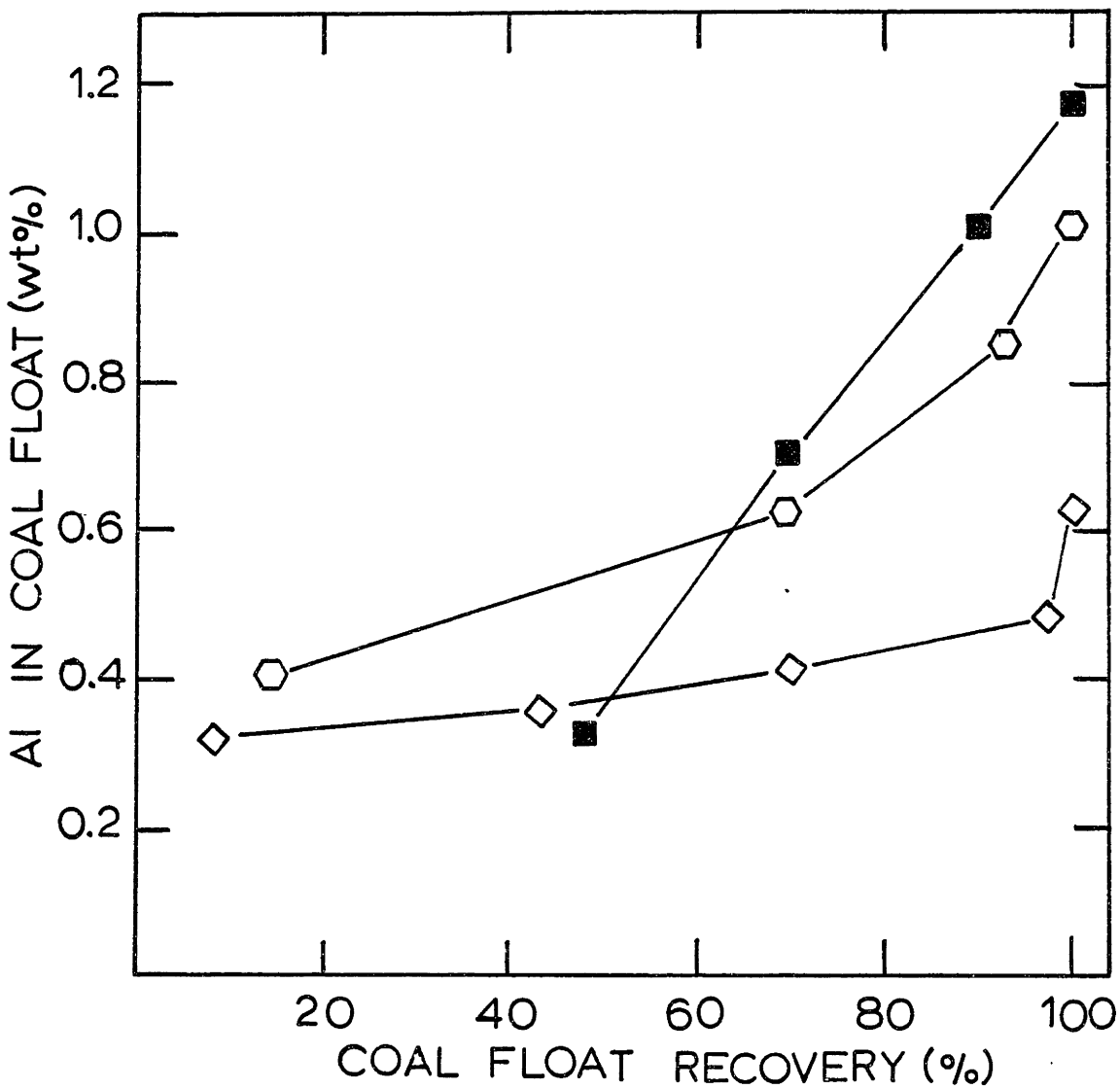

Figure 5.7 Aluminum Content of Density Fractionated Coal. Illinois No. 6: ■, Montana Rosebud: ⬡, Montana Lignite: ◇.

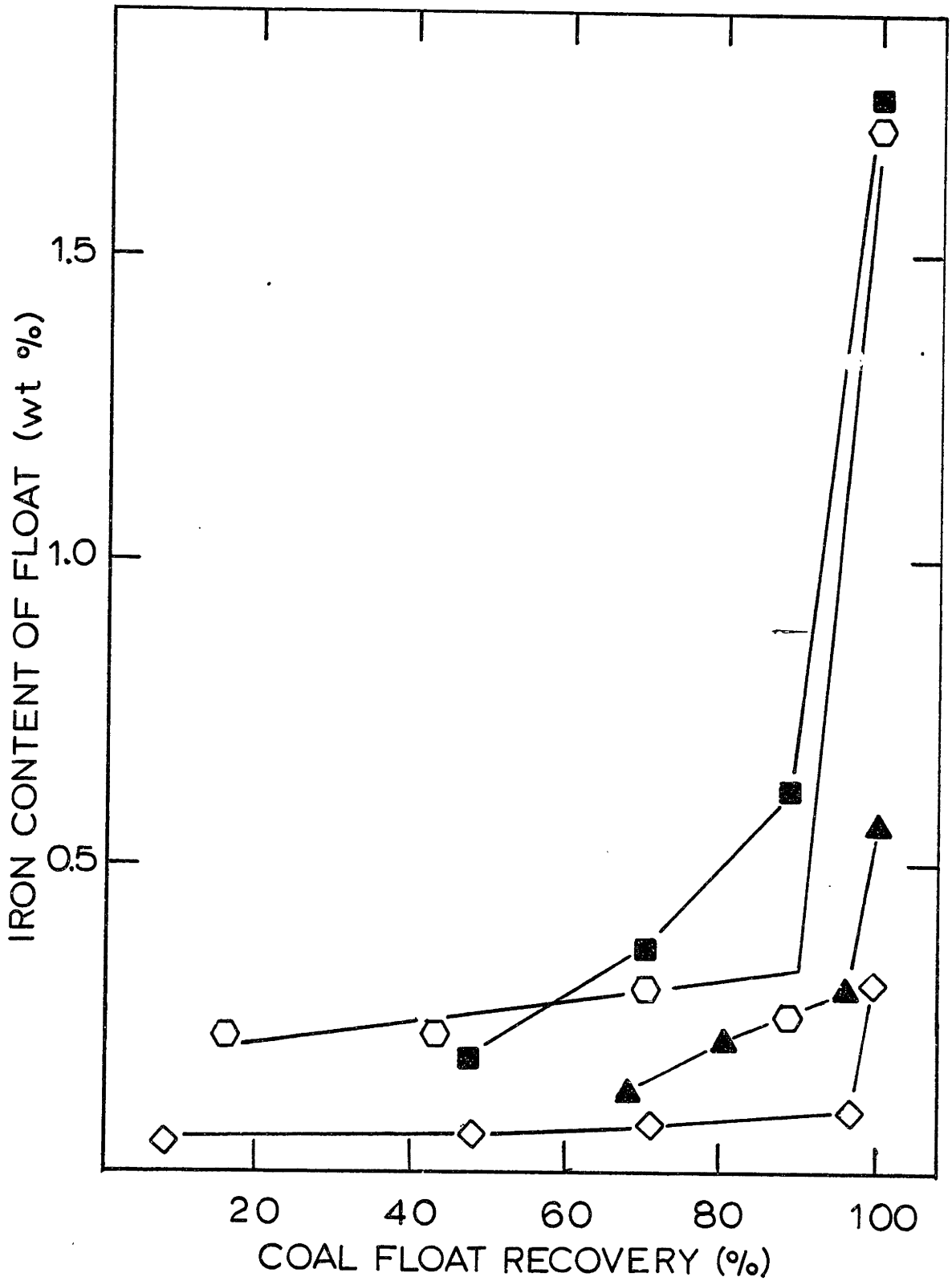

Figure 5.8 Iron Content of Density Fractionated Coal. Illinois No. 6: ■, Alabama Rosa: ▲, Montana Rosebud: ⬡, Montana Lignite: ◇.

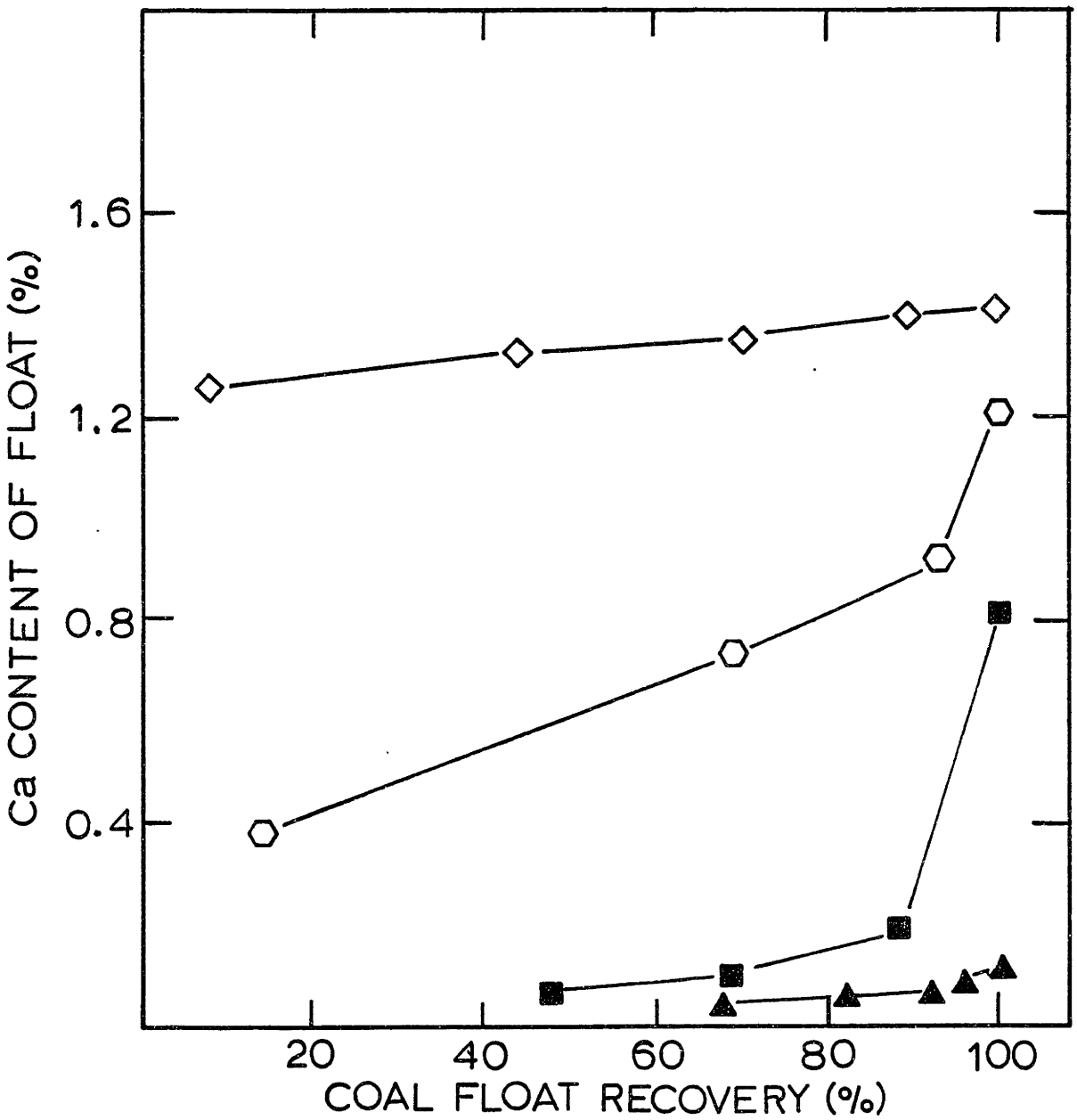

Figure 5.9 Calcium Content of Density Fractionated Coal. Illinois No. 6: ■, Alabama Rosa: ▲, Montana Rosebud: ⬡, Montana Lignite: ◇.

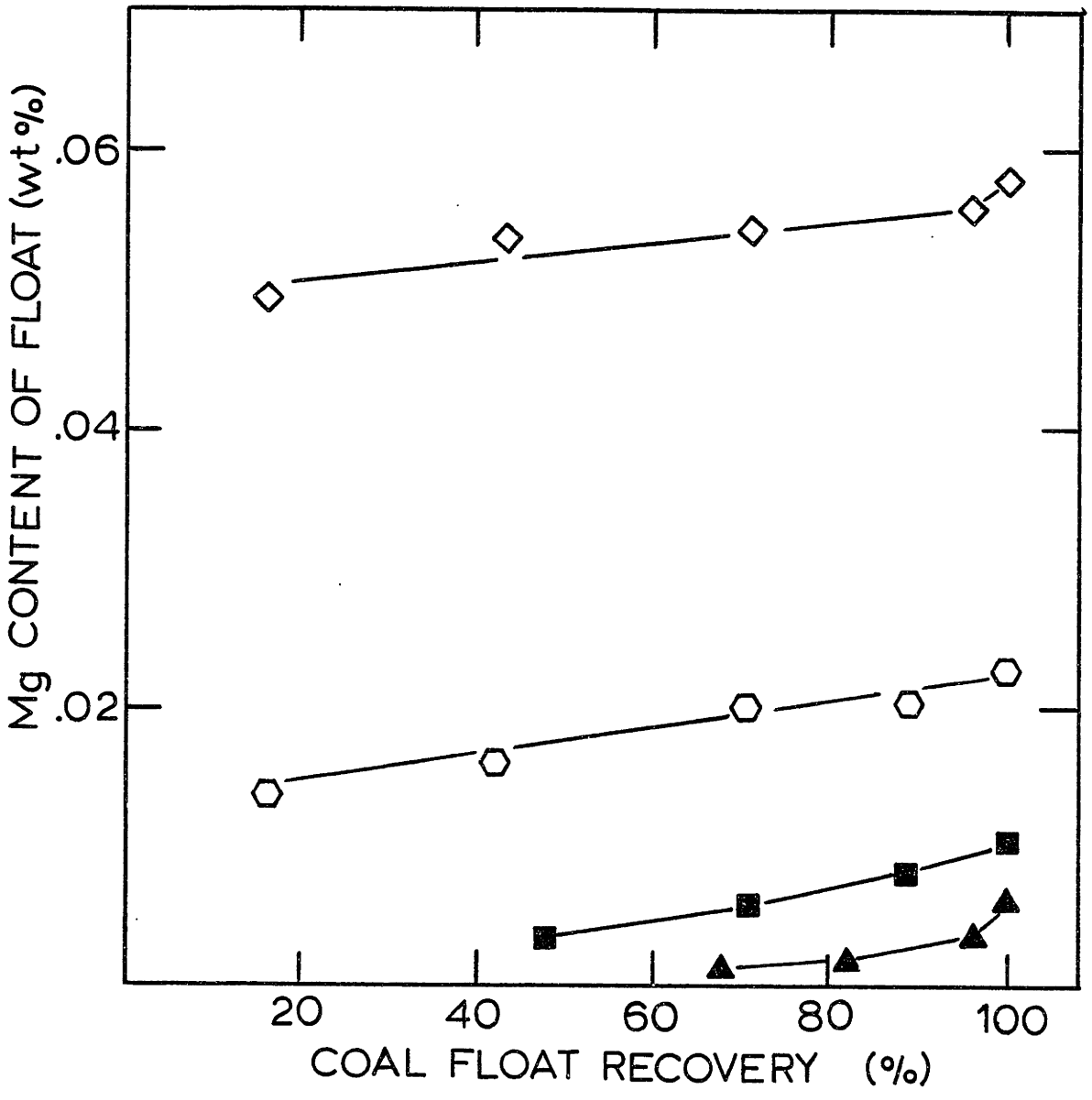

Figure 5.10 Magnesium Content of Density Fractionated Coal. Illinois No. 6: ■, Alabama Rosa: ▲, Montana Rosebud: ⬡, Montana Lignite: ◇.

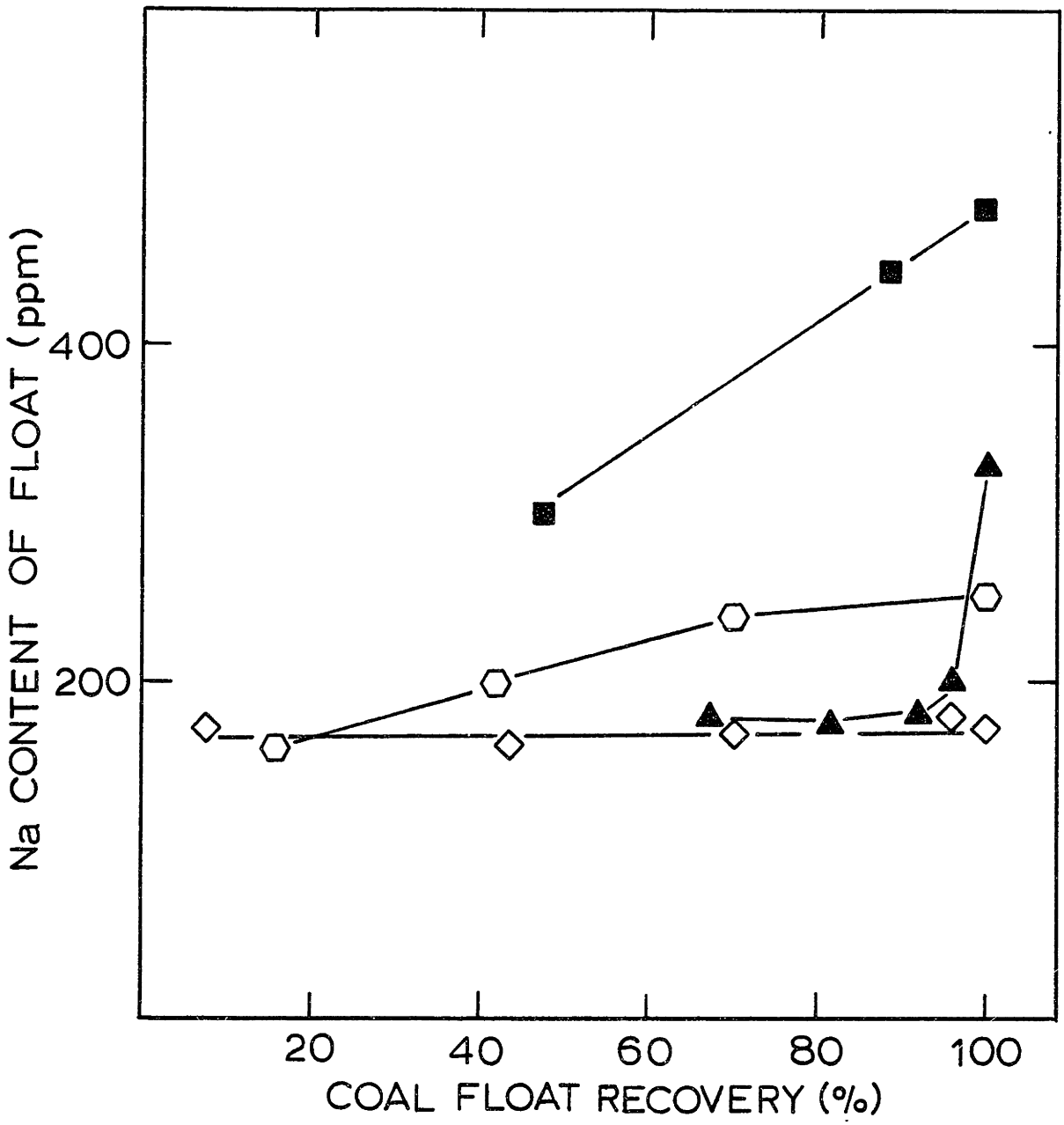

Figure 5.11 Sodium Content of Density Fractionated Coals. Illinois No. 6: ■, Alabama Rosa: ▲, Montana Rosebud: ⬡, Montana Lignite: ◇.

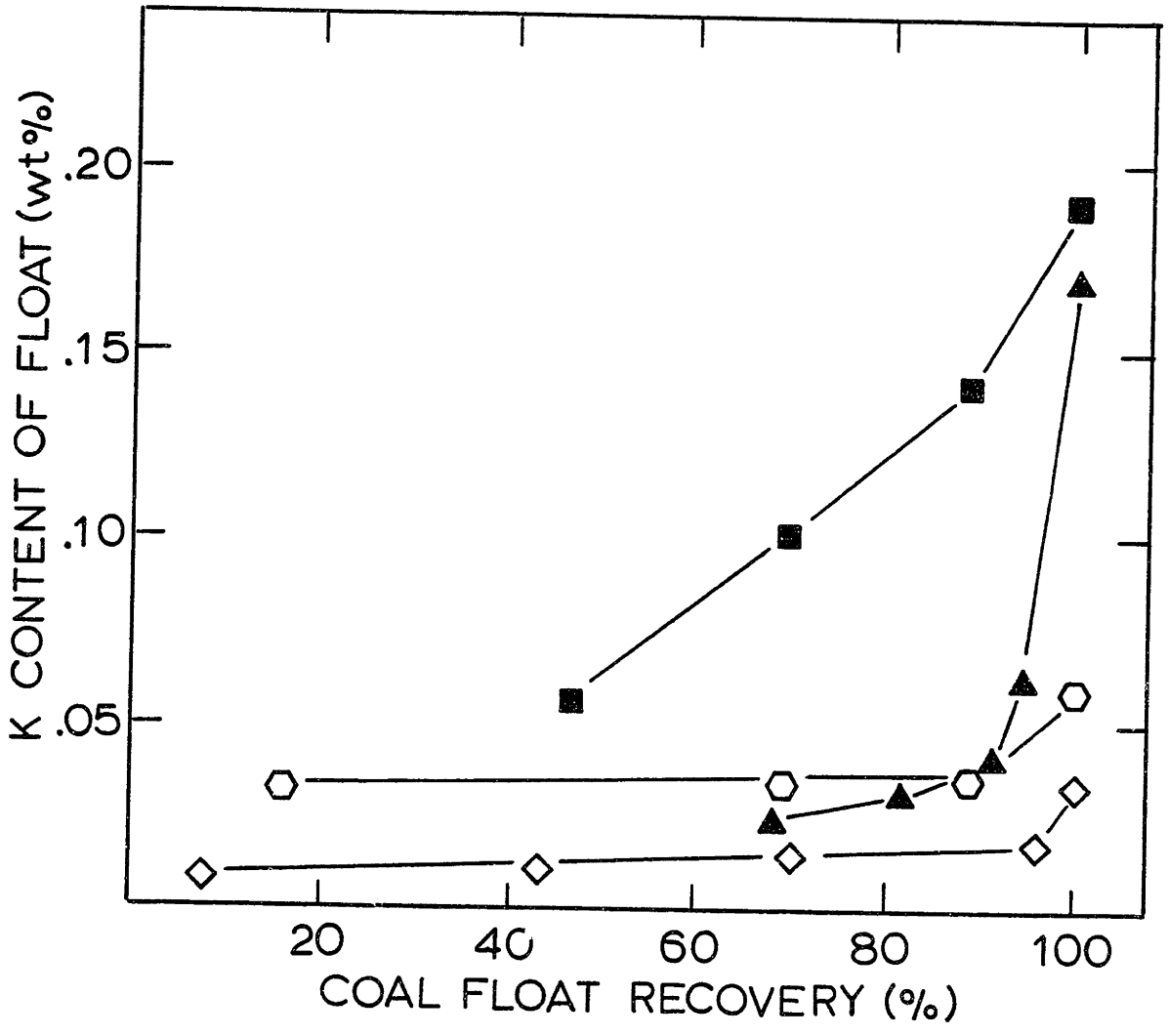

Figure 5.12 Potassium Content of Density Fractionated Coal Illinois No. 6: ■, Alabama Rosa: ▲, Montana Rosebud: ⬡, Montana Lignite: ◇.

the Montana Savage lignite is indicative of their occurance as metal cations ion-exchanged or carboxylic groups. Hence, they are distributed more uniformly throughout the coal.

Elemental analysis of the 1.8 coal floats was obtained for the other coals as well. These results are reported in Appendix A. The extent to which the element occured in the extraneous mineral matter phase (1.8 sink) or a raw coal basis was computed by difference. These results are presented in Tables 5.9 and 5.10.

5.6 Organically Held Metals in Low Rank Coals

The low rank lignites and subbituminous coals generally contain higher concentrations of calcium and magnesium than the bituminous coals. In addition to this difference, the calcium and magnesium occur in a more highly dispersed form in low rank coals, being bound organically to the carbonaccous matter ion-exchanged or carboxylic and phenolic functional groups.

A method of determing the extent of organic combination of these metals in low rank coals is that of extraction by ion-exchange in ammonium acetate as described in Chapter Four. The extraction was performed on all of the low rank coals and the coal residue obtained was then analyzed for moisture, ash and elemental content. The results are reported in Table 5.11. In comparing these results with that of the raw coal values in Table 5.1 and 5.6, significant decreases in both ash and elemental content are observed in all cases with the possible exception of the Texas lignite. The percent

TABLE 5.9

Percent of Element in Raw Coal
Associated with Extraneous
Mineral Matter (1.8F) - Bituminous Coals

Coal	Si	Al	Fe	Ca	Mg	k	Na
Illinois #6	38	36	68	80	21	24	13
Western Kentucky	2.9	23	46	41	11	18	12
West Virginia	8.6	24	79	54	29	30	26
Pittsburgh #8	2.8	17	37	41	18	20	6
Alabama Rosa #18	56	42	44	93	51	68	39
Utah	15	33	62	60	29	21	17
Utah Price #1	45	30	41	30	10	39	16
PSOC-3	29	13	32	32	19	-	1
PSOC-26	9.2	26	72	26	5.6	39	12
PSOC-130	15	22	33	52	35	25	21
PSOC-136	3.9	17	55	3	33	3	0
PSOC-997	15	23	74	40	25	17	9.5

TABLE 5.10

Percent of Element in Raw Coal
Associated with Extraneous (1.8F)
Mineral Matter - Low Rank Coals

Coal	Si	Al	Fe	Ca	Mg	K	Na
Lignites:							
Montana Savage	38	25	72	7.3	8	45	0
North Dakota	12	15	45	4.4	15	9	4
Texas	54	18	34	36	34	62	19
Subbituminous:							
Montana Rosebud	55	60	83	33	23	58	20
Montana Hardin	39	31	79	19	0	20	7
Montana Powder River	21	24	83	23	1	38	10
Wyoming Commanche	19	33	35	13	0	18	7
Wyoming Rawhide	45	33	34	7	0	16	13

TABLE 5.11

Proximate and Elemental Analysis of Low Rank Coals after Ammonium Acetate Treatment (wt%)

Coal	H_2O	Ash	Ca	Mg	Na	k
Lignites:						
Montana Savage	13.0	4.1	0.22	0.054	0.005	0.020
North Dakota	20.0	2.5	0.10	0.015	0.0060	0.005
Texas	7.3	27.5	0.077	0.030	0.015	0.180
Subbituminous:						
Montana Rosebud	7.2	10.0	0.13	0.030	0.016	0.048
Montana Hardin	8.3	4.7	0.17	0.017	0.0090	0.017
Montana Powder River	8.9	8.1	0.14	0.033	0.013	0.039
Wyoming Commanche	8.9	3.7	0.18	0.010	0.0030	0.007
Wyoming Rawhide	10.1	4.6	0.17	0.022	0.0044	0.012

TABLE 5.12

Percent Decrease in Coal of Total Ash and Elemental Content after Extraction with Ammonium Acetate

Coal	Ash	Ca	Mg	Na	k
Lignites:					
Montana Savage	53	85	91	68	33
North Dakota	68	91	97	99	83
Texas	3.3	86	86	44	0
Subbituminous:					
Montana Rosebud	26	89	81	36	21
Montana Hardin	48	86	91	96	45
Montana Powder River	35	88	89	46	30
Wyoming Commanche	40	82	94	96	50
Wyoming Rawhide	63	85	91	91	20

of the total and element extracted were computed and these results are given in Table 5.21. From eighty to over 90 percent of the calcium and magnesium in these coals were removed by extraction because of their association with the carboxylic groups. The remainder is presumedly in the form of dolomite or bassanite minerals or tightly bound in clay minerals. Virtually all of the sodium in the high sodium containing North Dakota lignite and Montana Hardin subbituminous coal was extracted. Generally lower percentages of the potassium were extracted due to its alternate occurance in clay minerals.

5.7 Mineralogical Characteristics of the Coals

With the exception of the alkalis and alkaline earths in low rank coals, the major and minor elements in coals occur in mineral forms, predominantly quartz, clays, pyrite and calcite and lesser amounts of rutile and dolomite. The coals used in the present study were examined by the x-ray diffraction (XRD) method to determine the occurance of these minerals. The forms of iron in various coals were also examined by the Mössbauer spectroscopy method. Pyrite [FeS_2] is the most common form of iron in coals, but certain coals may contain significant amounts of iron in carbonate, sulphate or clay minerals (Huffman and Huggins, 1978). The results of mineralogical analysis by these two methods are described in this section.

The minerals which contain the major elements occur to a certain extent as micron-sized inclusions embedded

within the carbonaceous matrix of coal particles. To identify these minerals by the X-ray diffraction method, the carbonaceous matter must first be removed without signficantly alterning mineral forms. This is achieved by the low temperature ashing method whereby the carbonaceous material of the coal is slowly oxidized at low temperature (100°C) and low pressure (1mm Hg) with atomic and ionic oxygen (Gluskoter, 1965). The activated oxygen is generated by a radio frequency osciallation. An LFE model LTA 104 asher was used. The procedure takes approximately two days for bituminous coals and up to one week for low rank coals. Because of the low temperature, the minerals are left in an essentially unaltered form, with the possible exception of slight pyrite oxidation (Miller and Given, 1978). The low temperature ash (LTA) powder was mounted on glass slides for scanning with Cu K_2 radiation. The X-ray line positions for all possible mineral forms in coals have been identified and tabulated previously (Padia, 1976; O'Gorman and Walker, 1972).

X-ray diffraction patterns of the LTA with line identification are given in Figures 5.13 through 5.20 for selected coals and in Appendix B for all other coals analyzed.

The XRD pattern of the Illinois No. 6 LTA is given in Figure 5.13. Both kaolinite and illite clay minerals exist in this coal in detectable amounts. Other identified mineral constitutents include calcite, pyrite, quartz and illite. Although quartz appears to have the largest intensity, this does not necessarily refelct that it is the major mineral component in the coal or the principle form of silicon. XRD

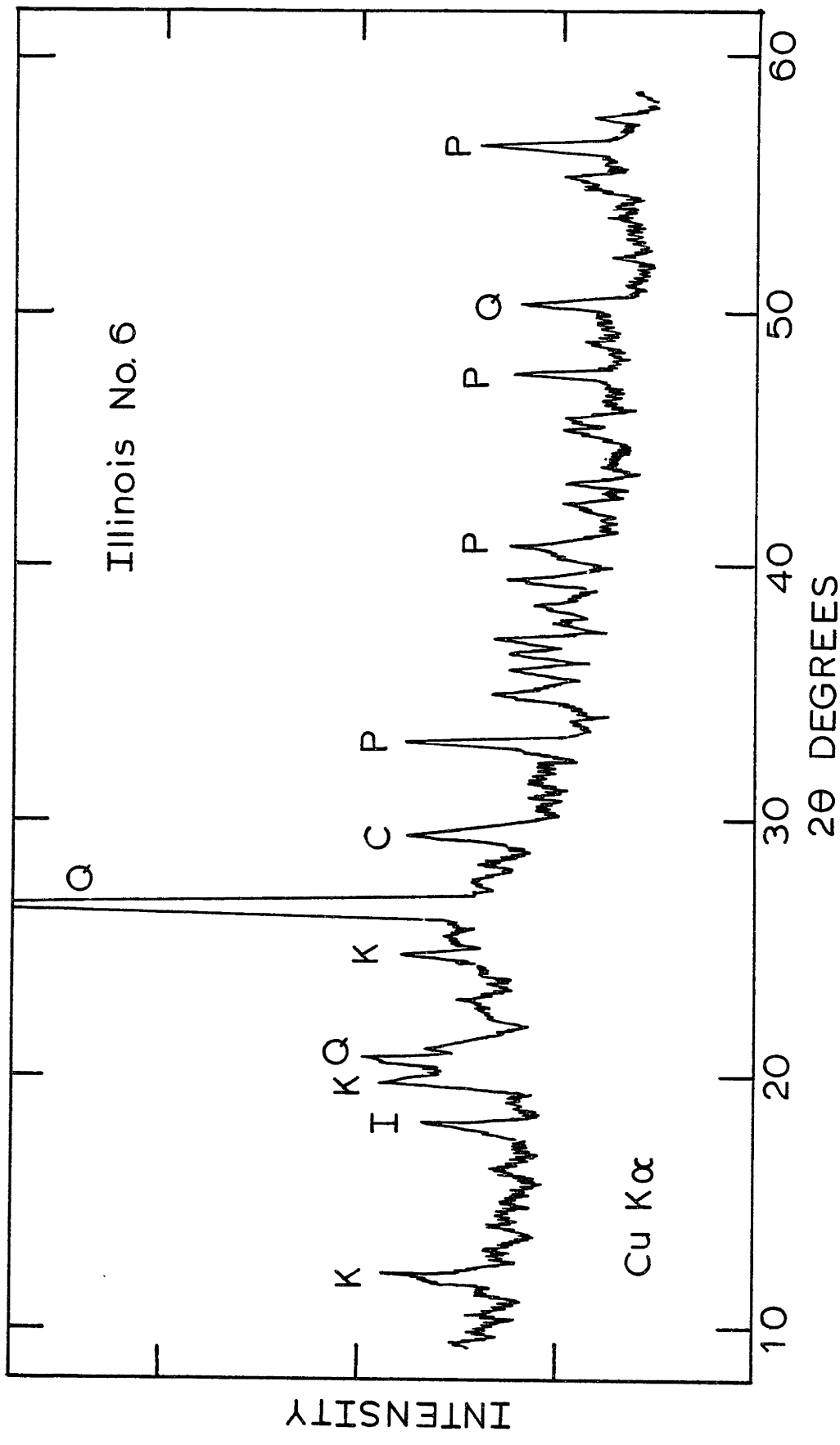

Figure 5.12 XRD Pattern of Illinois No. 6 LTA.
Q - Quartz, K - Kaolinite, P - Pyrite,
C - Calcite, I - Illite.

intensities of quartz lines are characteristically greater than that of the clay minerals due to the more ordered nature of the crystal. The diffraction pattern of the Alabama Rosa No. 18 LTA is shown in Figure 5.14. It is evident that, in this bituminous coal, pyrite and kaolinite are not present in significant amounts. Illite appears to be the major clay mineral in this coal. The XRD pattern of the LTA obtained from the West Virginia coal is shown in Figure 5.15. Evidently, this bituminous coal has significantly more kaolinite relative to quartz than the Illinois No. 6 or the Alabama Rosa. Illite clay was also identified in the XRD pattern of the West Virginia coal.

The XRD patters of the PSCO-3, PSOC-26 and PSOC-136 coal LTA are shown in Figures 5.16, 5.17 and 5.18, respectively. O'Gormoan and Walker (1972) performed semi-quantitative mineralogical analysis of these PSOC coals using infrared spectroscopy methods. Their results, given in Table 5.13, are in semi-quantitative agreement with the relative intensities of the XRD patterns. PSOC-3 contains a significant amount of quartz. By comparison, kaolinite is the major form of silicon in the PSOC-136 coal. Pyrite is a major mineral form in the PSOC-26. In PSOC-136, siderite appears to be the major iron-bearing mineral.

The XRD pattern of the PSOC-130 coal LTA is given in Figure 5.19. This particular coal appears to be high in carbonate minerals including calcite dolomite and siderite,

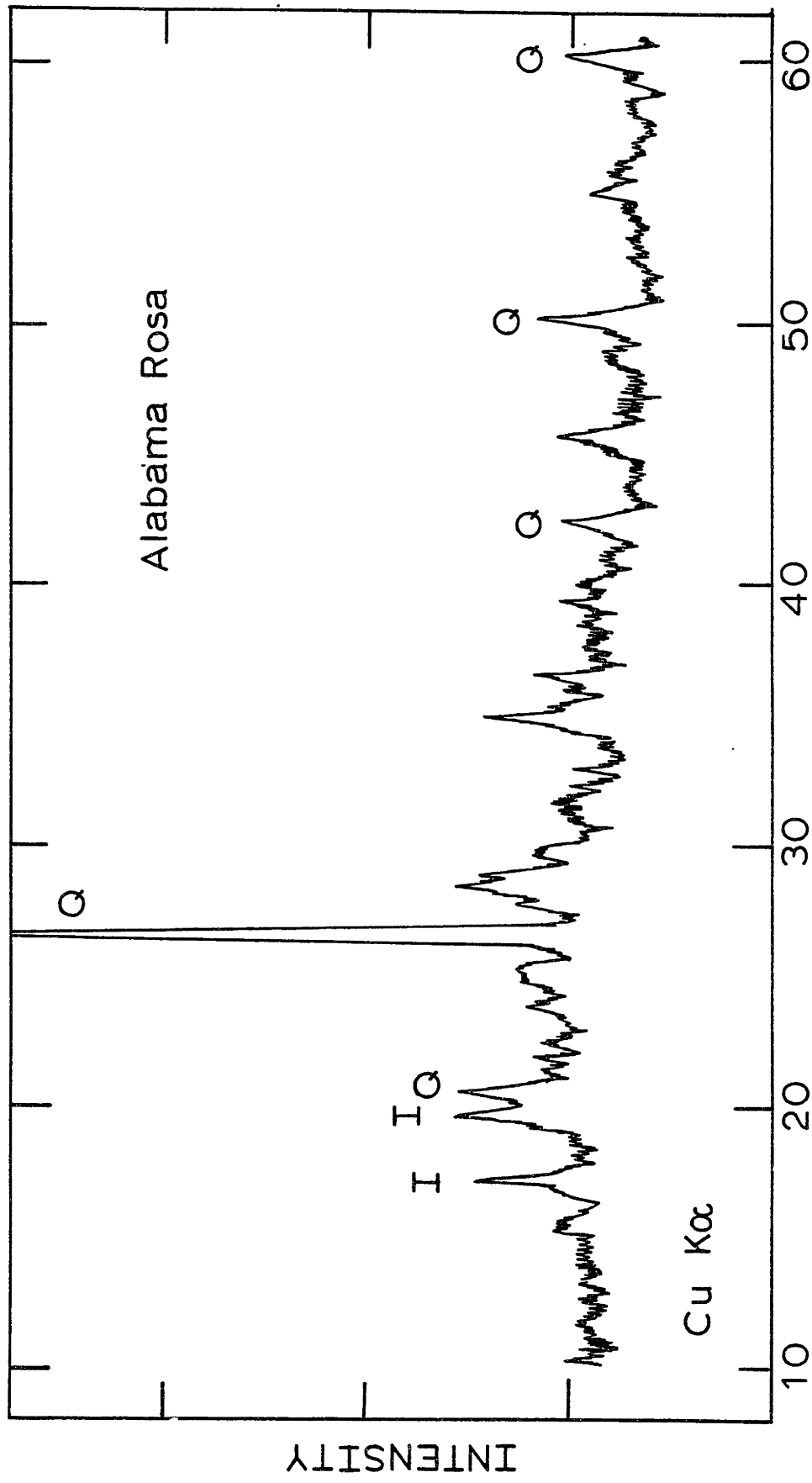

Figure 5.14 XRD Pattern of Alabama Rosa LTA.
Q - Quartz, I - Illite.

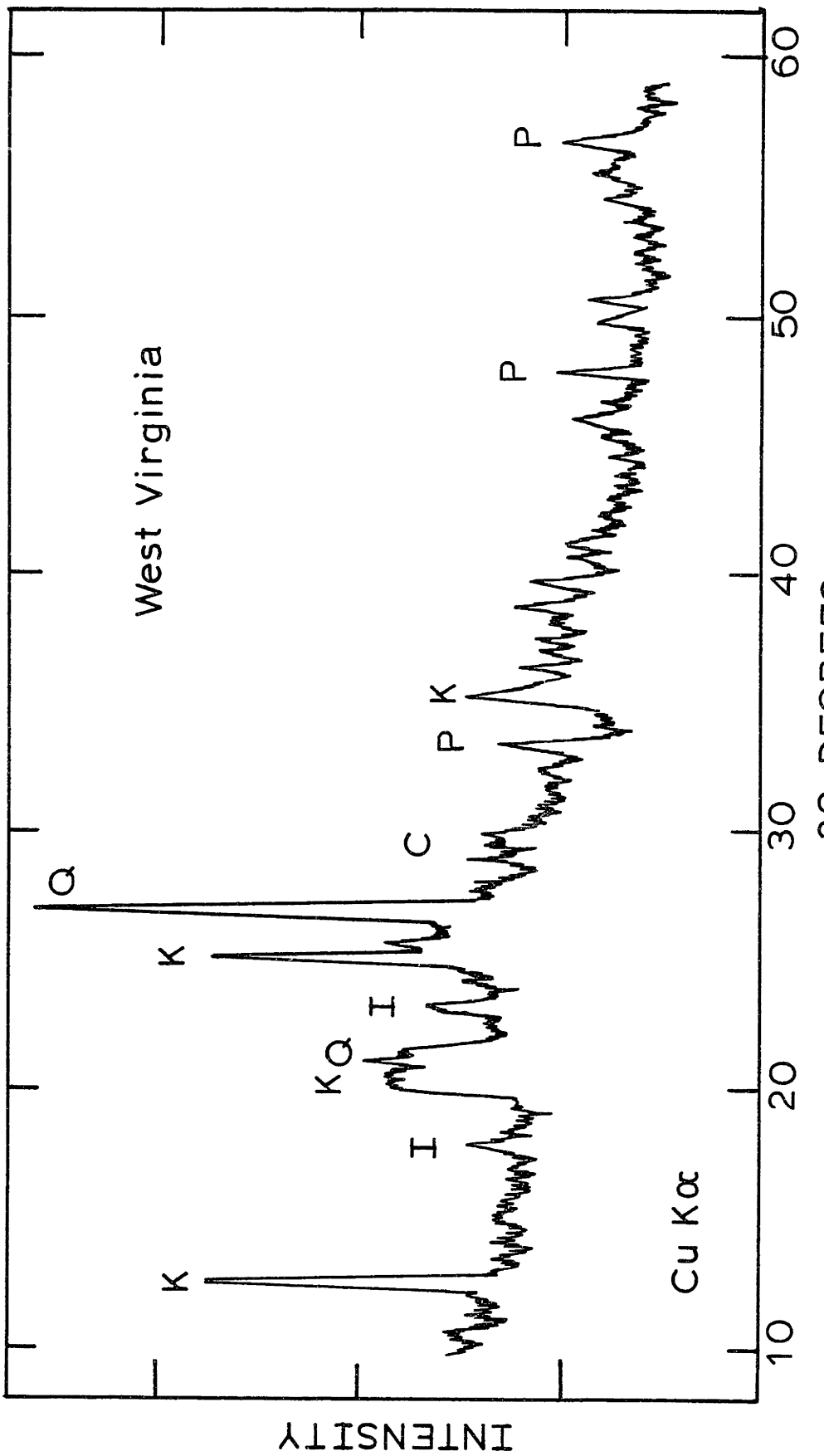

Figure 5.15 XRD Pattern of West Virginia Coal LTA.
Q - Quartz, K - Kaolinite, I - Illite,
C - Calcite, P - Purite.

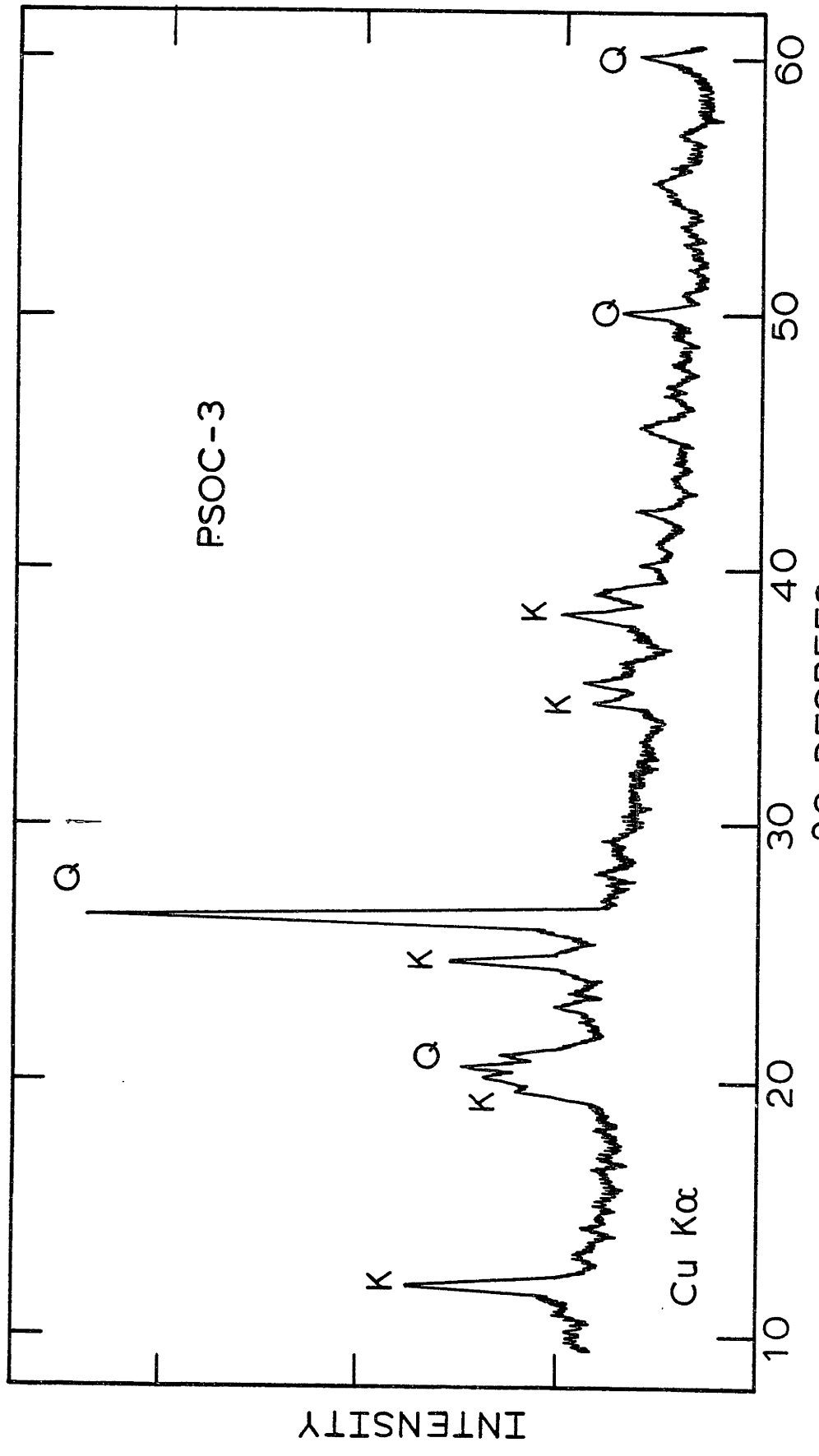

Figure 5.16 XRD Pattern of PSOC-3 LTA.
Q - Quartz, K - Kaolinite

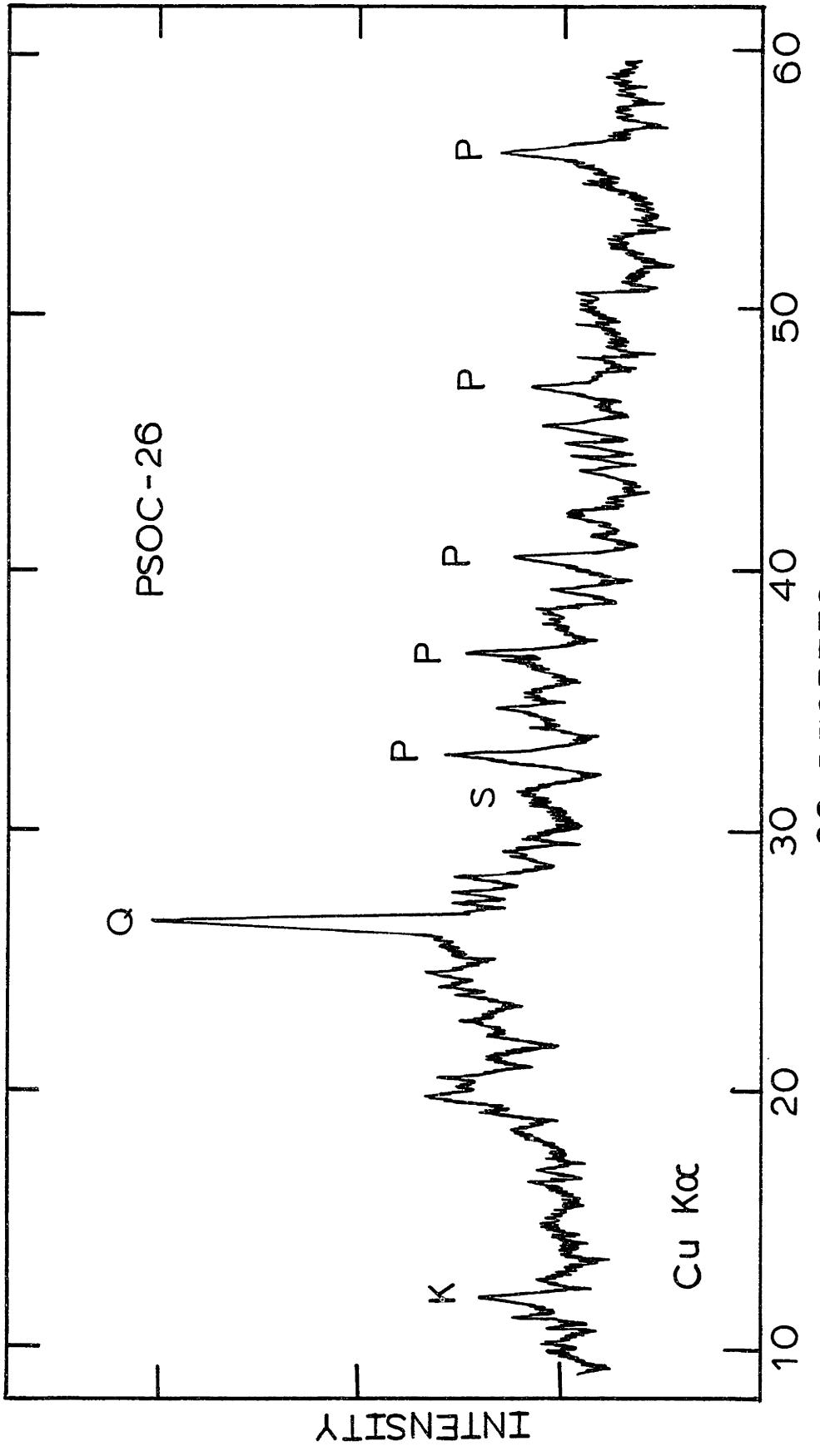

Figure 5.17 XRD Pattern of PSOC-26 LTA.
Q - Quartz, P - Pyrite,
K - Kaolinite, S - Siderite

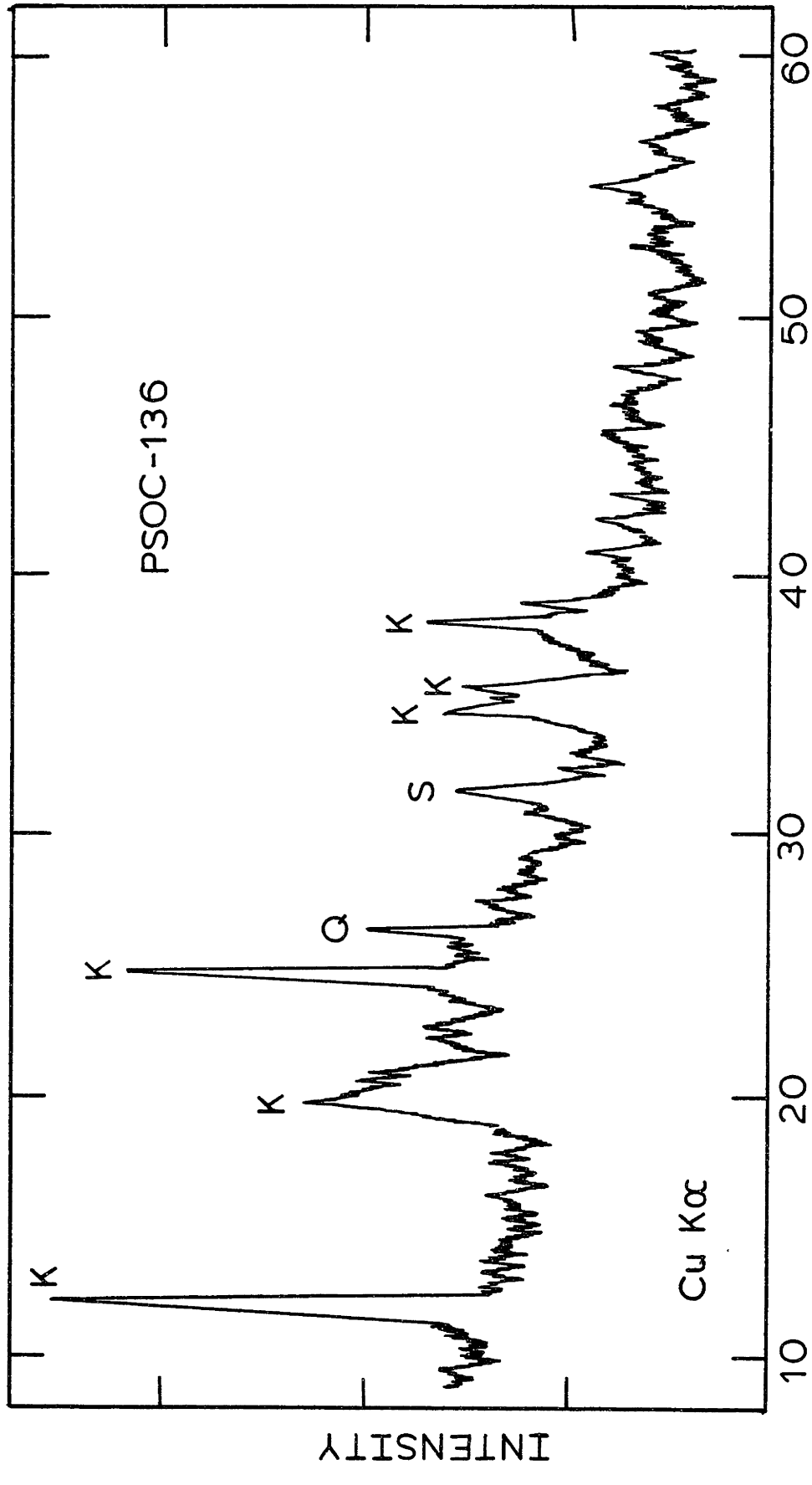

Figure 5.18 XRD Pattern of PSOC-136 LTA.
Q - Quartz, K - Kaolinite,
S - Siderite

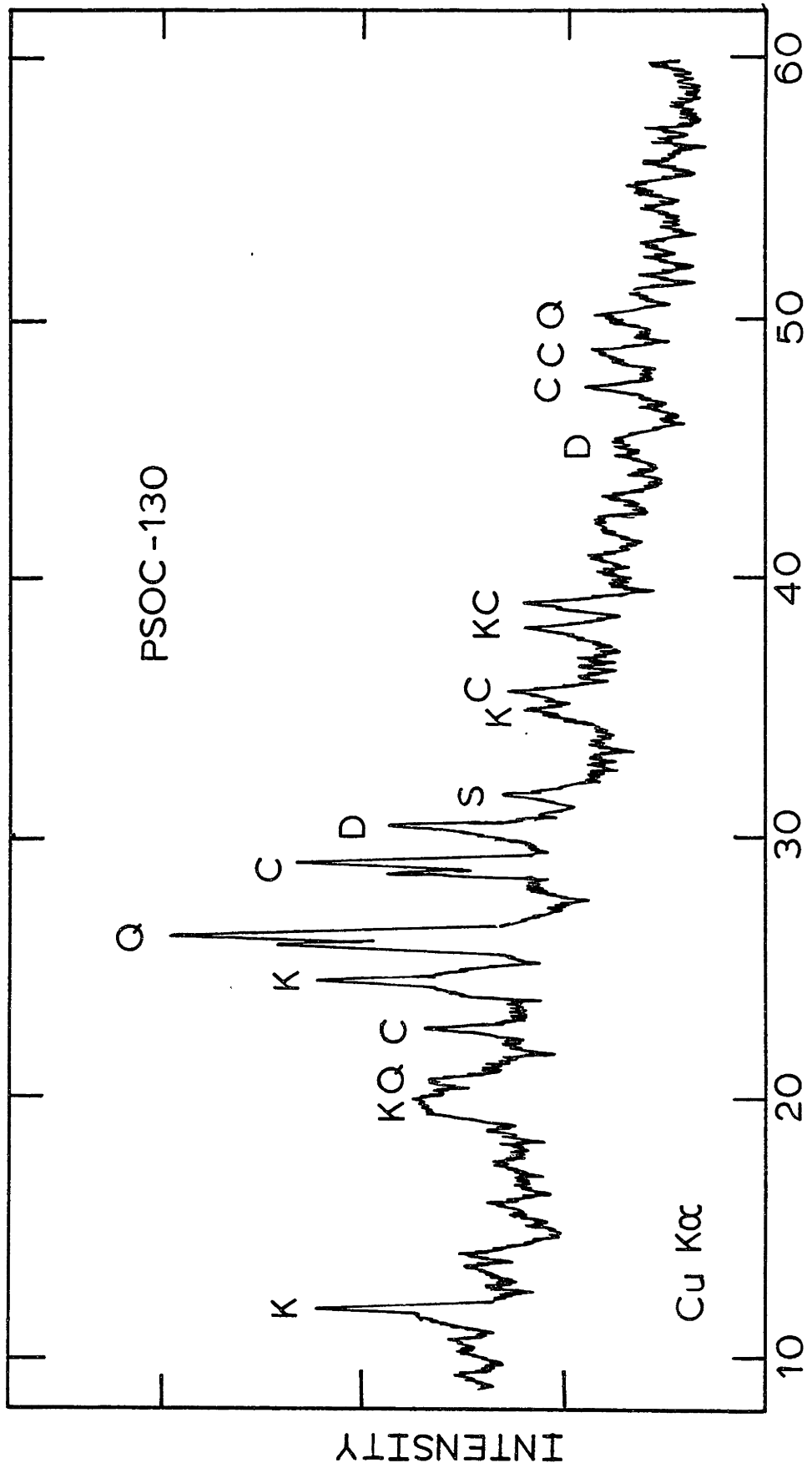

Figure 5.19 XRD Pattern of PSOC-130 LTA.
Q - Quartz, K - Kaolinite,
C - Calcite, D - Dolomite,
S - Siderite.

TABLE 5.13

Semi-quantitative Mineralogical Analysis of PSOC Coals (O'Gorman and Walker, 1972) - wt% of Mineral Matter

Mineral	PSOC-3	PSOC-26	PSOC-136
Quartz	40-50	1-10	1-10
Kaolinite	30-40	trace	60-70
Illite	trace	1-10	1-10
Chlorite	-	1-10	-
Muscovite	-	-	1-10
Mixed Layer Clays	trace	1-10	-
Calcite	-	-	-
Gypsum	1-10	1-10	1-10
Pyrite	1-10	60-70	1-10
Jarosite	-	1-10	10-20
Siderite	-	1-10	-
Rutile	-	1-10	-

and relatively low in quartz. Of the bituminous coals, PSOC-130 contains the highest elemental concentrations of calcium and magnesium.

Diffraction patterns of the LTA from low rank coals or lignites are somewhat different from bituminous coals in that significant backgrounds are observed along with pronounced and broad bassanite [$C_aSO_4 \cdot \frac{1}{2}H_2O$] peaks. The XRD pattern of the LTA obtained form the Montana Savage lignite shown in Figure 5.20, illustrates these features. The bassanite is believed to be formed, for the most part, during the low temperature ashing process by the fixation of the sulphur with the organically bound calcium (Miller and Given, 1978). Poor crystal ordering may result in large backgrounds or broadened lines. The Montant Savage lignite LTA was also examined by XRD after the coal had been treated with ammonium acetate to extract the ion-exchangable calcium. The diffraction pattern is shown in Figure 5.21. A reduction in background and bassanite peaks relative to other mineral forms is observed. Also present in this lignite is the mineral dolomite [$CaMg(CO_3)_2$].

All of the coals examined by XRD in the present study were found to contain quartz, but in varying amounts relative to the clay minerals. For coals containing primarily quartz and kaolinite, the relative distribution of silicon between these minerals can be estimated from the stoichiometric requirements of the minerals. The mineral formualae have been

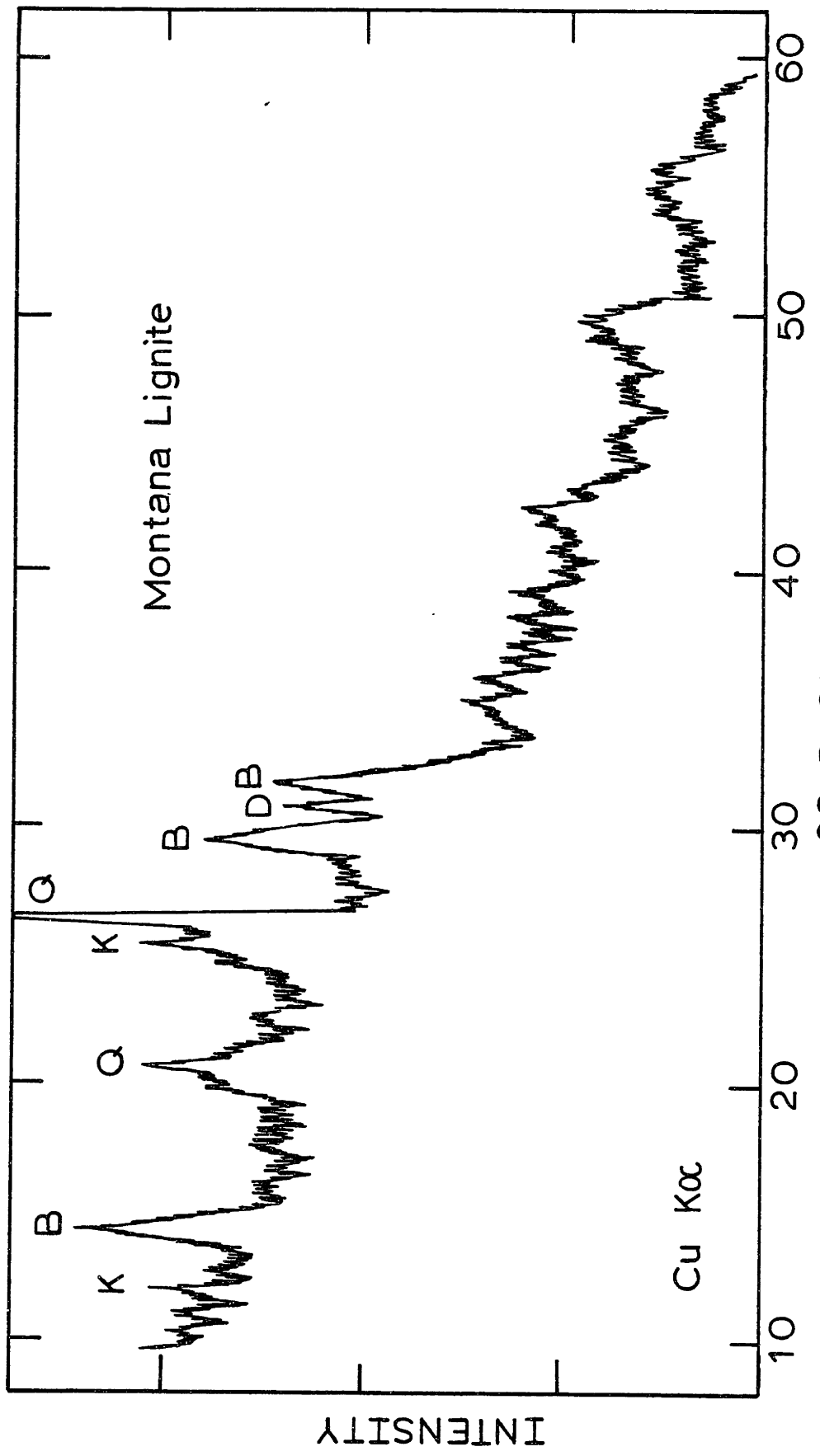

Figure 5.20 XRD Pattern of Montana Lignite LTA.
Q - Quartz, K - Kaolinite, B - Bassinate,
D - Dolomite

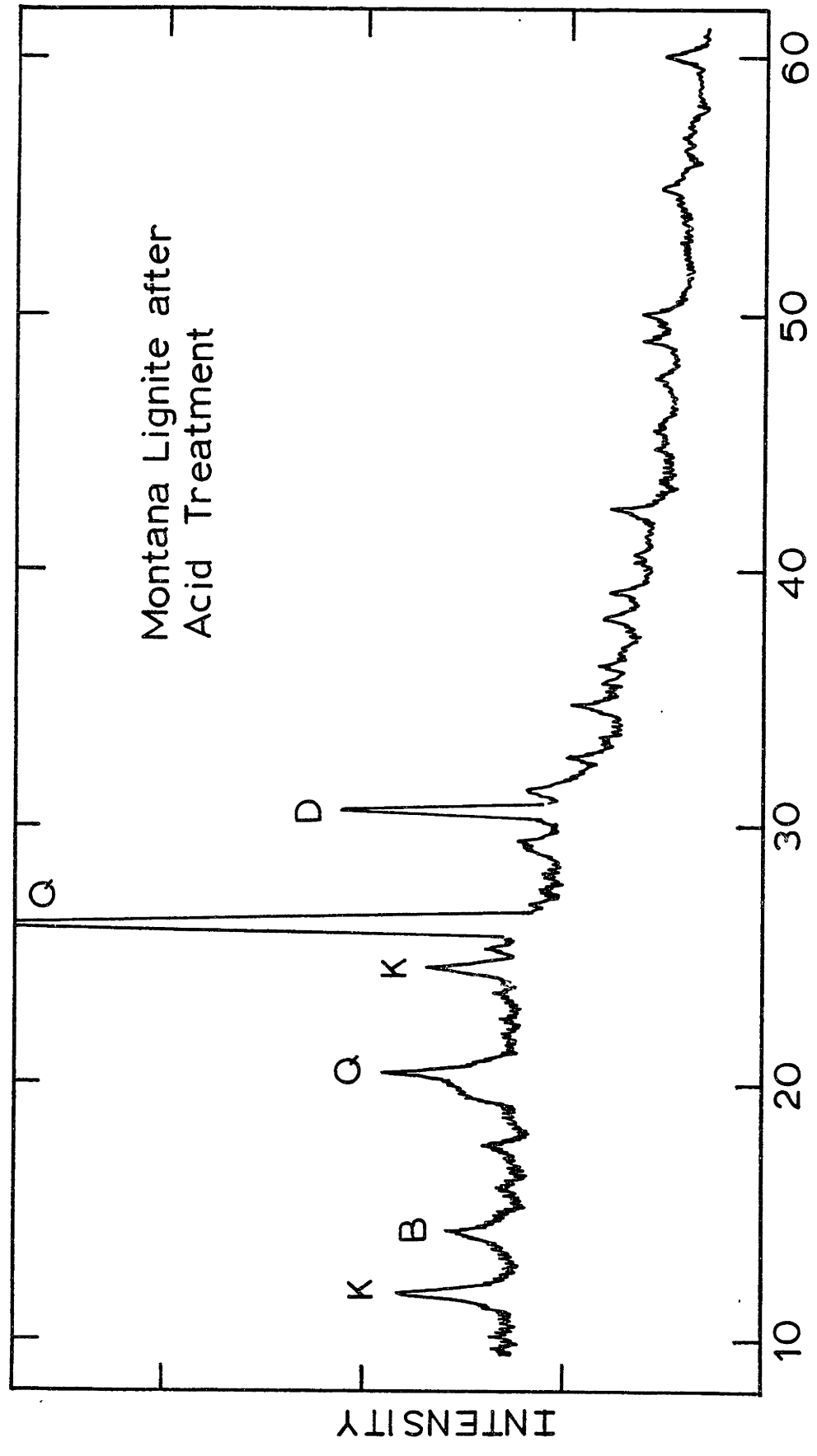

Figure 5.21 XRD Pattern of Acid Washed Montana Lignite LTA.
Q - Quartz, K - Kaolinite, B - Bassanite,
D - Dolomite

have been given in Table 2.2 of Chapter Two and, accordingly are not reproduced here. For coals that contain significant amounts of illites or other shales (e.g. montmorillinite), Si/Al ratios may vary because of lattice substitutions of Si and Al by H, K, Na, Ca, Fe or Mg. For example, the bituminous coals containing observable illite by XRD (Illinois No. 6, Alabama Rosa #18, West Virginia, Western Kentucky and PSOC-26) also contain the highest concentrations of potassium. Generally, however, the illite content of most coals is low relative to kaolinite. The excess silicon in quartz may therefore be approximated by the Si/Al ratio in the coal. Those coals which, on the basis of Si/Al ratios appear to be relatively low in quartz include the West Virginia, Pittsburgh No. 8, Utah, PSOC-130, PsOC-136, PSOC-997, Montana Savage, Montana Hardin and the Wyoming Commanche. On the basis fo the results presented in Table 5.8, there is no apparent trend among coals regarding the inherent vrs. extraneous occurance of clays relative to quartz.

In the bituminous coals, magnesium was not well correlated with illite or potassium content as it may also occur in carbonates, primarily dolomite.

Iron-bearing mineral forms in the coals were studied by the Mössbauer spectroscopy method. Spectra were obtained directly on the coal samples without prior treatment of low temperature ashing. A detailed discussion of the principles and application of this method of mineralogical analysis for coal, as well as a tabulation of the literature values for

the Mössba er parameters of various iron-bearing minerls, is provided in Appendix C. Only the results in the form of Mössba er spectra are presented and discussed here.

The Mössbaver spectra for selected coals, including the North Dakota lignite, Illinois No. 6, Western Kentucky, Alabama Rosa, PSOC-130 and PSOC-26, and the identification of iron-bearing minerals giving rise to the gamma-ray absorption lines of these coals, are shown in Figures 5.22 through 5.27.The identified iron-bearing mineral forms included pyrite.(P), szomolnokite (Sz), and jarosite (J), illite (I), and siderite (S). The Mossbauer spectra of additional coals are given in Appendix C.

In almost all of the low rank coals, pyrite was observed to be the only iron mineral form present. The exception was the Montant Rosebud, in which magnetic splittings corresponding to iron oxides were observed. Of the bituminous coals analyzed, the Illinois No. 6, Western Kentucky, West Virginia, Pittsburgh No. 8 and the PSOC-997 contained only pyrite and varying amounts of iron sulphate as szomolnokite [$FeSO_r \cdot H_2O$] or jarosite [$(x)Fe_3(SO_4)_3(OH)_6$]. The presence of iron sulphates (or oxides) in coals is an indication of severe weathering of the coal resulting in oxidation of some of the pyrite. For minerals having only quadrapole splittings (two equal absorption lines), the relative abundance of different mineral forms is roughly proportional to peak areas. The Alabama Rosa and the PSOC-130 bituminous coals were found to contain significant amounts of iron in illite clay as shown

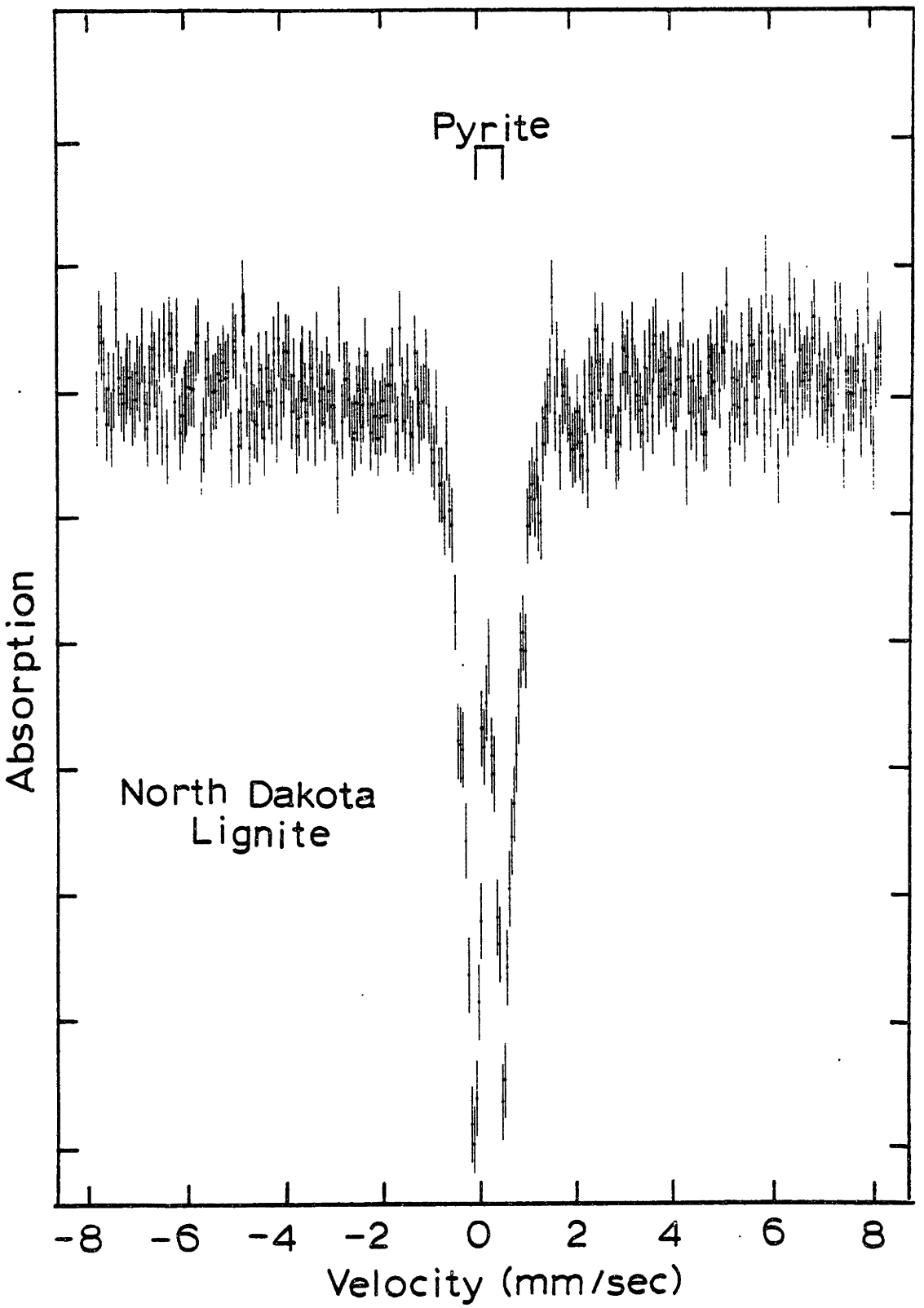

Figure 5.22 Mössbauer Spectra of
North Dakota Lignite

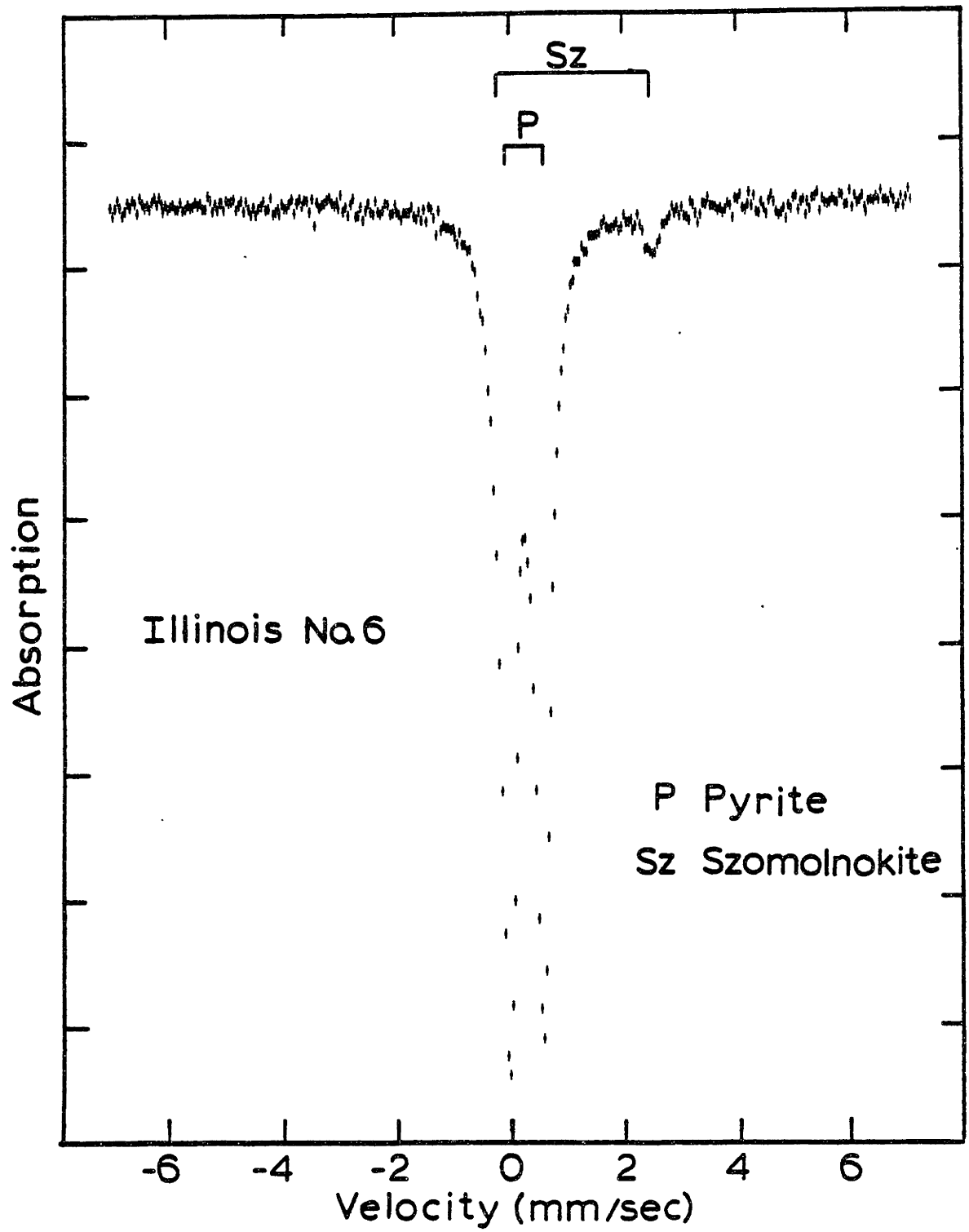

Figure 5.23 Mössbauer Spectra of Illinois No. 6

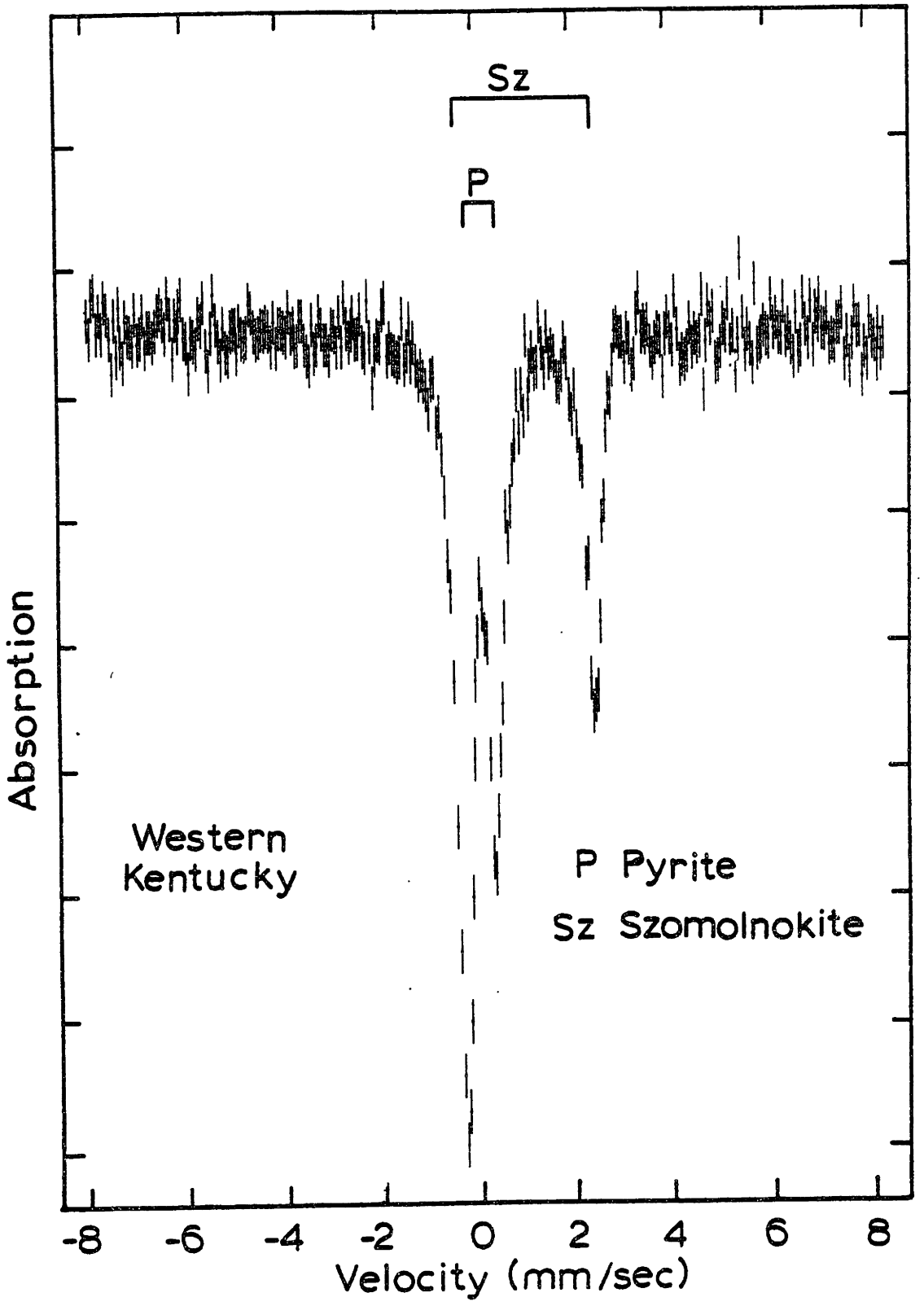

Figure 5.24 Mössbauer Spectra of Western Kentucky

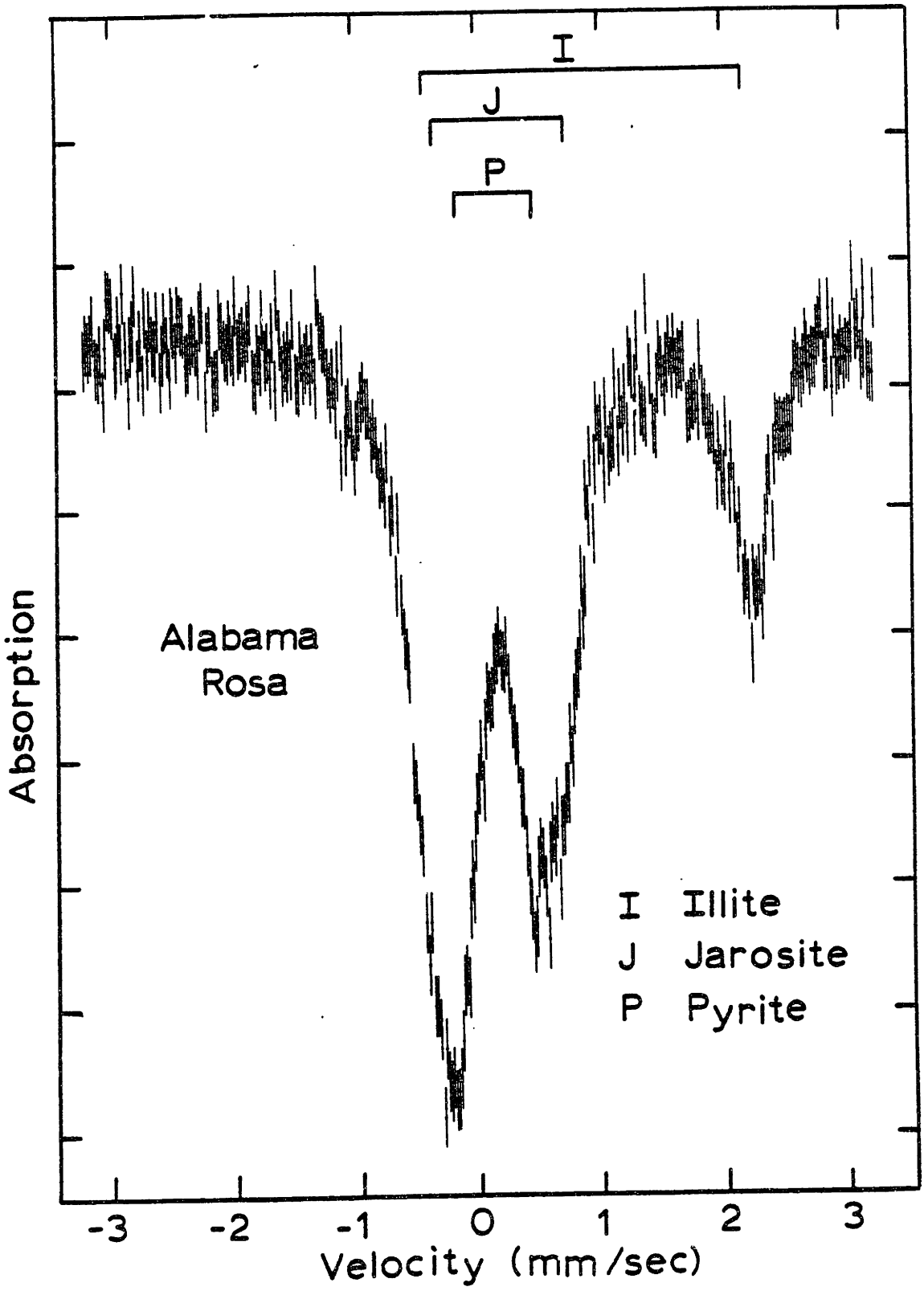

Figure 5.25 Mössbauer Spectra of Alabama Rosa

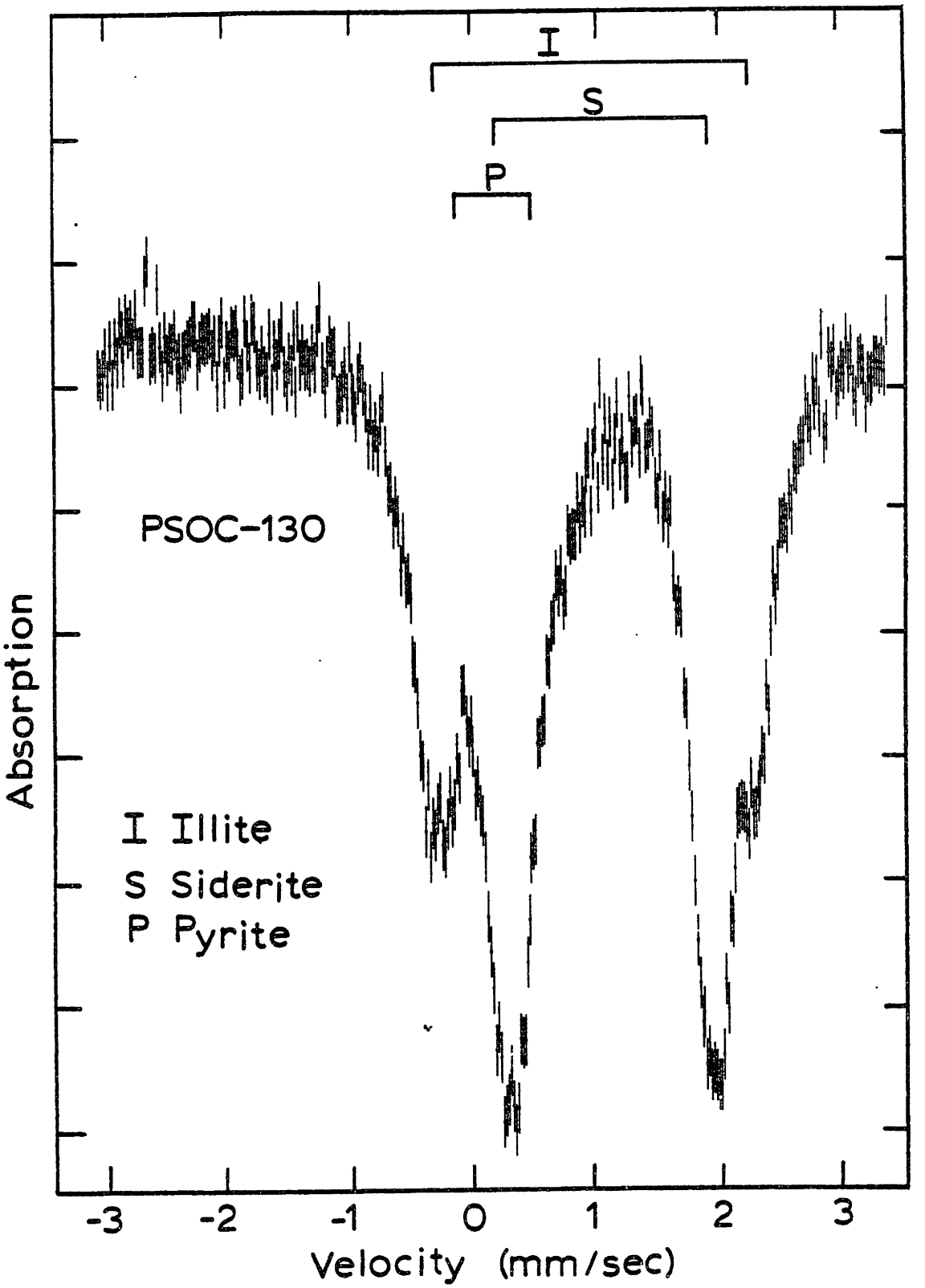

Figure 5.26 Mössbauer Spectra of PSOC-130

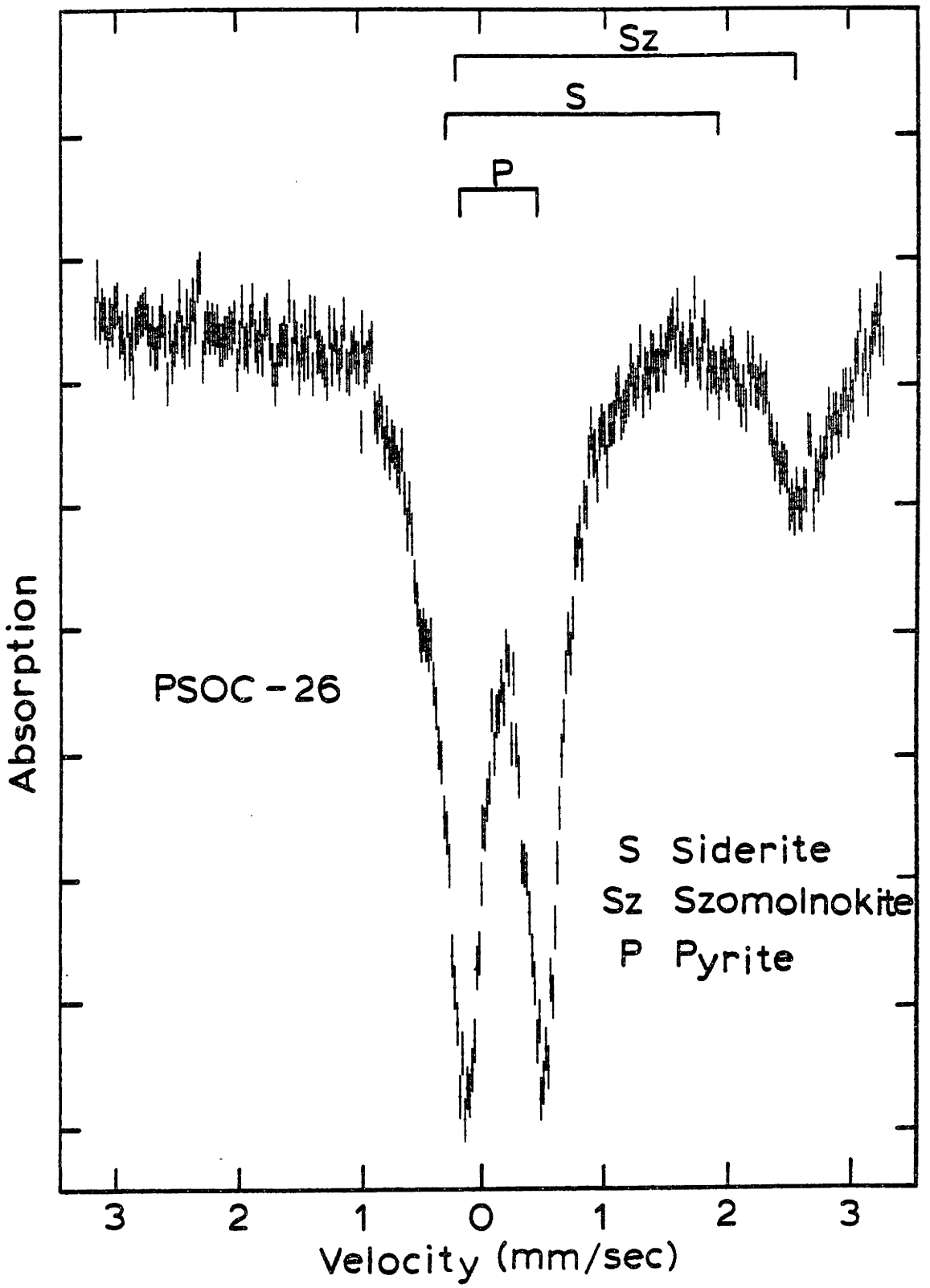

Figure 5.27 Mössbauer Spectra of PSOC-26

in Figures 5.25 and 5.26 respectively. The major form of iron in the PSOC-130 coal, however, is siderite. This is in agreement with the results obtained by XRD. Siderite was also observed in the PSOC-136 and the Utah Price No. 1 coals by XRD. It is interesting to note that although illite was observed in a number of coals by XRD including the Illinois No. 6, Alabama Rosa, West Virginia and Western Kentucky coals, only the Alabama Rosa illite contained measureable iron.

As discussed previously, a major portion of the iron in the coals is extraneous (see Table 5.9). The results of Mössbauer on raw coals then reflect both inherent and extraneous iron minerals. The 1.8 float fraction of coals having multiple iron forms were also analyzed by the Mössbauer method to determine if the inherent iron-bearing minerals were different than the extraneous iron bearing minerals. There was essentially no difference between the Mössbauer spectra of the raw coal and the coal 1.8 float fraction. These results are reported in Appendix C.

CHAPTER SIX

COMBUSTION BEHAVIOR OF COALS IN LABORATORY FLOW FURNACE

6.1 Introduction

The experimental basis of this investigation was the combustion of a dilute stream of pulverized coal particles under the controlled conditions of a drop tube-laminar flow furnace. Under carefully controlled combustion conditions, the amount of ash vaporized during combustion could be accurately determined. The experimental procedures employed for measuring ash vaporization were described in Chapter Four. An assessment of the method is given in Chapter Seven and the results of parametric investigations are reported in Chapter Eight. The aim of the present chapter is to consider in some detail the nature of the high temperature coal combustion process. More specifically, in the present investigation the temperature history of combustion was controlled by regulation of the oxygen partial pressure in the main furnace gas. In order to determine the kinetics of ash vaporization processes, it is necessary to determine the temperature history of combustion of coal particles for a specified set of furnace conditions. For the most part the temperature history of combustion was measured by two-color optical pyrometry. The principles and application of this technique to the combustion furnace used in this investigation is discussed elsewhere in greater detail (Tymothy, 1981, Altricher, 1981). Only the results obtained by the two-color method are presented here.

Before discussing these results, the theoretical aspects of the combustion of pulverized coal particles are considered.

6.2 Modelling of Single Coal Particle Combustion

The combustion of pulverized coal particles has been the subject of extensive theoretical and experimental efforts (e.g. Smith, 1967; Mulcahy and Smith, 1969; Simons, 1979a and 1979b). The combustion of small char particles at high temperatures is at least phenomenologically well understood. In the temperature range of approximately 900 to 1600K, the rate of combustion of the char (25-150 micron diameters) is controlled by the simultaneous diffusion and heterogeneous reaction of oxygen with the carbon in the porous char (Mulcahy, 1978). At temperatures above approximately 1600K, the chemical reaction rate becomes sufficiently fast at the surface of the char, and external diffusion resistance exerts a major influence on the combustion rate of the char. The combustion of coal particles is a more difficult problem to address because of the influence of the evolution of the combustible volatile matter. The release and combustion of the volatile matter may proceed or occur simultaneously with the heterogeneous combustion of the char or fixed carbon material depending upon temperature, heating rates, particle size and possibly other factors (Howard and Essenhigh, 1967; Altricher, 1981). In the following analysis, only the heterogeneous combustion of a char particle is considered. The analysis is then compared with the two-color optical pyrometry experimental data. The effects of volatile

evolution and combustion will then be discussed in qualitative terms.

The experimental furnace conditions used in the present investigation are listed in Table 6.1. Under most of these conditions, the combustion temperature of the coal particles was sufficiently high the major rate controlling step is the resistance to oxygen diffusion through the external boundary layer of the char. Under these conditions, the flux of oxygen to the external surface of the char particle No_2 (moles/cm^2 sec) is given by

$$N_{o_2} = -cD_{o_2} \frac{X_{o_2}}{dr} + X_{o_2} \sum N_i \qquad (6.1)$$

where c is the gas concentration, D_{o_2} is the diffusivity of oxygen, X_{o_2} is the mole fraction of oxygen and r is the radial coordinate. The term $\sum Ni$ is the net molor flux and is given by

$$\sum N_i = N_{o_2} + N_{N_2} + N_{co} \qquad (6.2)$$

to take into account the Stefan flow which arises from the reaction:

$$C + O_2 = 2CO$$

The molar flux of CO is then

$$N_{co} = -2N_{o_2} \qquad (6.3)$$

at that of nitrogen is

$$N_{N_2} = 0$$

By substitution of equations 6.2 and 6.3, equation 6.1 becomes

$$No_2 = \frac{-cD_{o_2}}{1+X_{o_2}} \frac{dX_{o_2}}{dr} \qquad (6.4)$$

TABLE 6.1

Furnace Conditions Used
In Present Investigations

Furnace Wall Temperature	Gas Composition (atm) O_2	N_2	CO_2
1500	.10	.90(He)	---
1750	.05	.95	---
1750	.10	.90	---
1750	.20	.80	---
	.20	.55	.25
1750	.35	.65	---
	.35	.40	.25
1750	.50	.50	---
	.50	.25	.25
1750	.75	.25	---
1750	1.00	---	---

The gasification rate R_d $(\frac{gm}{sec})$ is given by

$$R_d = -8\pi r^2 w N_{O_2} = -8\pi r_p^2 N_{O_2}\Big|_{r_p} \tag{6.5}$$

where r_p denotes the particle radius and w is the molecular weight of carbon. The appropriate boundary conditions for diffusion controlled combustion are:

$$\text{at } r = r_p \qquad X_{O_2} = 0$$

$$\text{at } r \to \infty \qquad X_{O_2} = X^b_{O_2}$$

where $X^b_{O_2}$ refers to the mole fraction of oxygen in the bulk gas or far away from the particle. By substitution of equation 6.4 into equation 6.5 and intergrating over r and Xo_2, the steady-state diffusion controlled combustion rate of the char is obtained as:

$$R_d = 8\pi w c D_{O_2} r_p \ln\left(1 + X^b_{O_2}\right) \tag{6.6}$$

For solid particles burning under external diffusion controlled conditions, the size of the char shrinks and the density remains more or less constant. The radius of the particle at time t is then

$$r_p(t) = r_o \left[1 - \left(\frac{t}{t_b}\right)^{1/2}\right] \tag{6.7}$$

with r_o being the initial radius and t_b being the time required for complete gasification of the solid particle. The burning time of the particle t_b can be obtained from the integration of the burning rate over time:

$$V_p \rho_p = \int_o^{t_b} R_d \, dt \tag{6.8}$$

with V_p being the particle volume and ρ_p the particle density with respect to carbon content. The result obtained by integration is the:

$$t_b = \frac{\rho_p d_o^2}{16 c w D_{o_2} \ln\left(1+X^b_{o_2}\right)} \tag{6.9}$$

This model is well suited for chars formed from non-swelling coals, e.g. lignite chars. Swelling bituminous coals, upon devolitilization, are observed to form spherical char particles with large scale internal voids. Under microscopic examination, these particles often appear as thin walled conospheres in which the mass of the char is located primarily on this outer wall. (Field, 1979; Ramsden and Smith, 1968). In Chapter Nine, microscopy of the Illinois No. 6 used in this investigation showed this to be case under the present experimental conditions. The combustion of a cenospheric char particle would proceed until the outer wall essentially disintegrates. The model adopted for the combustion of the bituminous Illinois No. 6 was that of a conosphere burning at constant size. The error introduced by a constant size approximation is not too great. For example, if 50 percent of the coal mass is lost by devolitilization, then, for a 125 micron diameter particle that did not swell, the inner radius of the cenosphere would be 100 microns. The burnout

time of the char cenosphere is then obtained by integrating equation 6.8 over time with the fixed diameter approximation. The burning time is then given by

$$t_b = \frac{\rho_p d_o^2}{24 w c D_{O_2} \ell n\left(1+X^b_{O_2}\right)} \tag{6.10}$$

A cenospheric char particle of equivalent carbon density and size would burn in 2/3 the time of a shrinking sphere char particle. The density ρ_p is that of the carbon contained within the total chenosphere volume.

At temperatures below about 1800K, pore diffusion and reaction within the char become significant as rate-controlling steps in the combustion of the char particles. It is necessary to consider these processes not only because of their effect on the temperature history of combustion, but also from the standpoint that the oxygen potential within the cahr will influence the vaporization reactions which proceed through the reduction of refractory metal oxides to more volatile forms. This aspect of the combustion process will be reconsidered in Chapter Ten.

At temperatures below about 1800K, the rate of combustion R_c of a gram (gm/sec) particle under conditions in which external diffusion exerts only partial control is given by

$$R_c = \frac{4}{3}\pi r_p^3 \eta \rho_p R_i P^s_{O_2} \tag{6.11}$$

where A is the specific surface area of the char (cm^2/gm), R_i is the intrinsic reaciton rate coefficient $\left(\frac{gm}{cm^2 sec \cdot atm \cdot O_2}\right)$

$P^s_{O_2}$ is the oxygen partial pressure at the surface of the char and η is the effectiveness factor. The effectiveness factor is related to the Thiele modulus ϕ by

$$\eta = \frac{3}{\phi}\left[\frac{1}{\tanh\ \phi} - \frac{1}{\phi}\right] \tag{6.12}$$

and the Thiele modulus is given by

$$\phi = r_p\left[\frac{RiA}{D_e}\right]^{1/2} \tag{6.13}$$

(Satterfield, 1970). The effective diffusivity D_e of a molecule in a porous char for knudson diffusion is determined from the pore diffusivity D_p, the toruosity θ, and the porosity by (Satterfield, 1970)

$$D_e = \frac{D_p\theta}{\tau} \tag{6.14}$$

and the pore diffusivity is given by (Satterfield, 1970)

$$D_p = 9700\ r_e\sqrt{\frac{T}{M}}$$

with M being the molecular weight of the diffusing molecule and r_e the pore radius. The mean pore radius is given by (Satterfield, 1970)

$$r_e = \frac{2\theta}{A\rho_p}$$

The oxygen partial pressure at the char's surface may be evaluated from equation 6.6 and 6.11;

$$R_d = R_c \tag{6.17}$$

or

$$8\pi wcD_{O_2}\, r_p\, n\left[\frac{1+Xo_2{}^b}{1+Xo_2{}^s}\right] = \frac{4}{3}\pi r_p{}^3\eta\rho_p R_i A P^s_{O_2} \tag{6.18}$$

The oxygen partial pressure within the char at any position can be calculated from (Satterfield, 1970):

$$P_{O_2} = P^s_{O_2} \frac{r_p}{r} \frac{r_p \sinh\left(\phi \frac{r}{r_p}\right)}{\sinh \phi} \tag{6.19}$$

with knowledge of the structural properties of the char (e.g. specific surface area, porosity, density and pore size) and of the intrinsic reaction rate coefficient, R_i, the combustion rate surface oxygen partial pressure and internal oxygen partial pressures can be calculated at a given temperature.

In order to evaluate the combustion rate R_c (or R_d), the temperature at which the particles burn must be determined. Assuming that the particles are at thermal steady state (Field, 1967), the heat balance around a single particle is

$$R\ \Delta H = Q + C \tag{6.20}$$

where ΔH is the heat of combustion (cal/gram) for the reaction $C + \frac{1}{2} O_2 = CO$ and Q is the radtiation loss (cal/sec):

$$Q = \varepsilon 4\pi r_p^2 \sigma \left(T_p^4 - T_\infty^4\right) \tag{6.21}$$

and C is the heat loss due to conduction (cal/sec):

$$C_{sf} = 4\pi c D_{O_2} r_p C_p (T_p - T_b) \ln\left(1 + Xo_2{}^b\right) \left[\frac{e^{-Le \ln\left(1+Xo_2{}^b\right)}}{1-e^{-Le \ln\left(1+Xo_2{}^b\right)}}\right] \tag{6.22}$$

or at lower oxygen partial pressures (neglecting Stefan flow):

$$C_{nsf} = 4\pi r_p k \left(T_p - T_\infty\right) \qquad (6.23)$$

The terms C_p, k and Le are the heat capacity of the gas, thermal conductivity of the gas and the Lewin number (=1), respectively. The heat capacity and the thermal conductivity of the gases are dependent on temperature. In the present analysis, average values were assumed in the integration of heat flux equations over the non-isothermal boundary layer (Field, 1967). Particle temperatures Tp can be calculated by reiterative solution of equation (9.17). In the next section, the results of two-color optical pyrometry of the burning temperatures and times of single coal particles are presented and compared with the theoretical predictions.

6.3 Two-Color Optical Pyrometry Measurements of Coal Particle Combustion Temperatures

Axial temperature profiles of the gas in the furnace combustion zone were determined by thermocouple measurements as described in Chapter Four. These measurements were preformed under flow conditions (6 liters/min main gas) identical to those used in combustion experiments. In addition, the water cooled collection probe was set as 15 cm from the honeycomb flow straightener as it was for the combustion experiments. Coal was not fed, however, for the gas temperature measurements. The measured axial gas temperature profiles at two furnace wall settings are shown in Figure 6.1. At a furnace wall temperature of 1750K, the average gas temperature is about 1700K. At a furnace wall temperature of 1500K, the average temperature is only about 1400K.

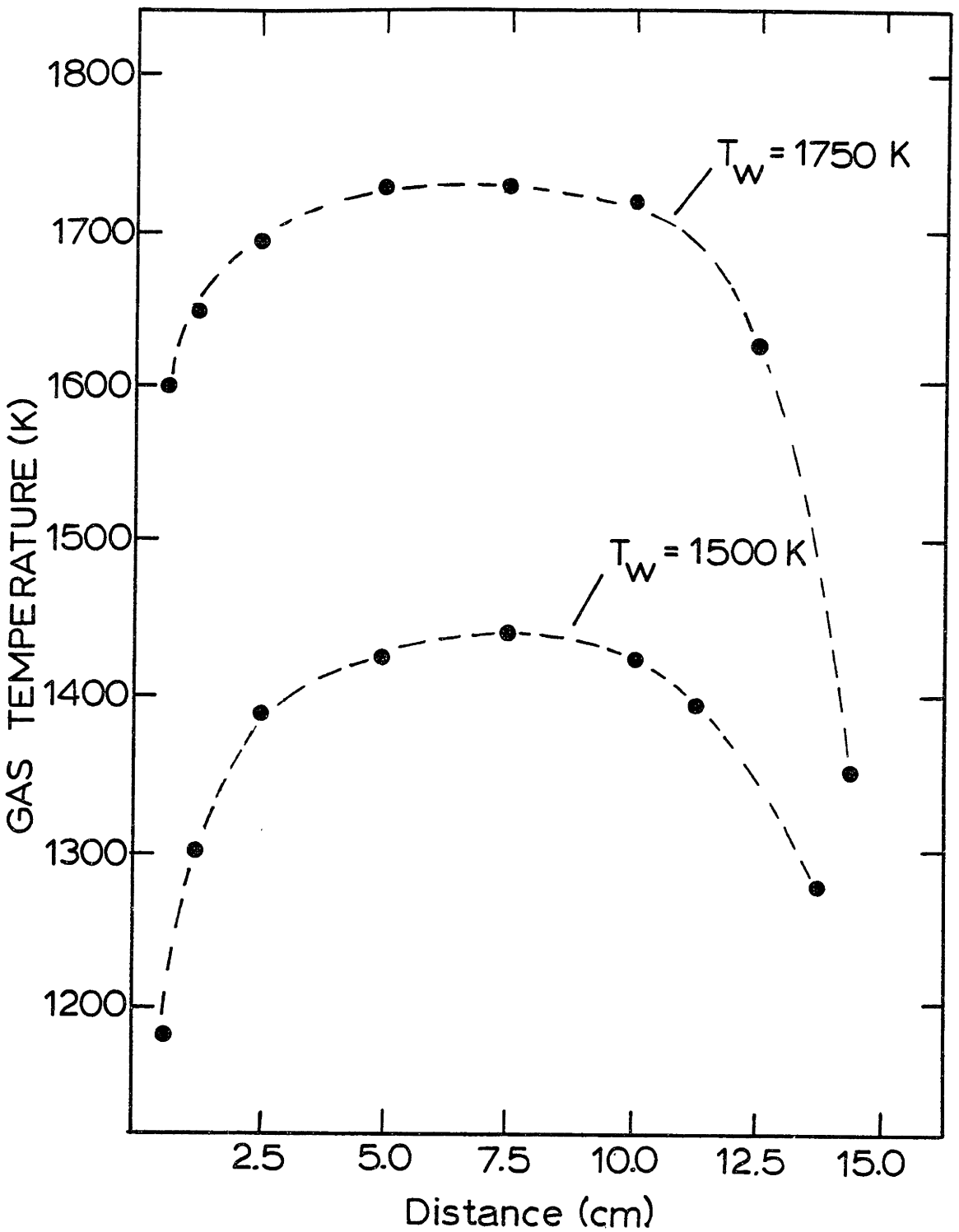

Figure 6.1 Axial Gas Temperature Profile with Collection Probe at 15 cm.

The combustion experiments studying ash vaporization behavior conducted at a furnace wall temperature 1750K with main gas oxygen partial pressures of .05, .10, .20, .35, .50, .75, and 1.0 atmospheres, and at a furnace wall temperature of 1500K with an oxygen partial pressure of .10 atmospheres. Particle temperature measurements by the two-color pyrometry method could only be obtained at a furnace temperatures of 1750K with the oxygen partial pressures of 0.35 or greater. At lower oxygen partial pressures, the light emitted from the burning particles was of insufficient intensity for photo-multiplier detection. The results of two-color optical pyrometry temperature measurements are shown in Figure 6.2 for those conditions under which measurements were possible. The data points correspond to an average particle combustion temperature of over 20 independent measurements of single particles. As evident, increasing the oxygen partial pressure in the furnace main gas results in an increase in the combustion temperature of the coal. The Illinois No. 6 bituminous coal shows consistantly higher particle burning temperatures than the Montana Savage lignite. This may be due to the higher heating value of the coal or to the nature of the coals volatile matter. The volatile matter of bituminous coals contain significantaly more combustible hydrocarbon material. Release of the volatile matter from a coal particle and its subsequent combustion in the gas phase may result in a local rise in the gas temperature and, consequently, the particle temperature. Also shown in Figure 6.2 is the theoretical prediction for the combustion

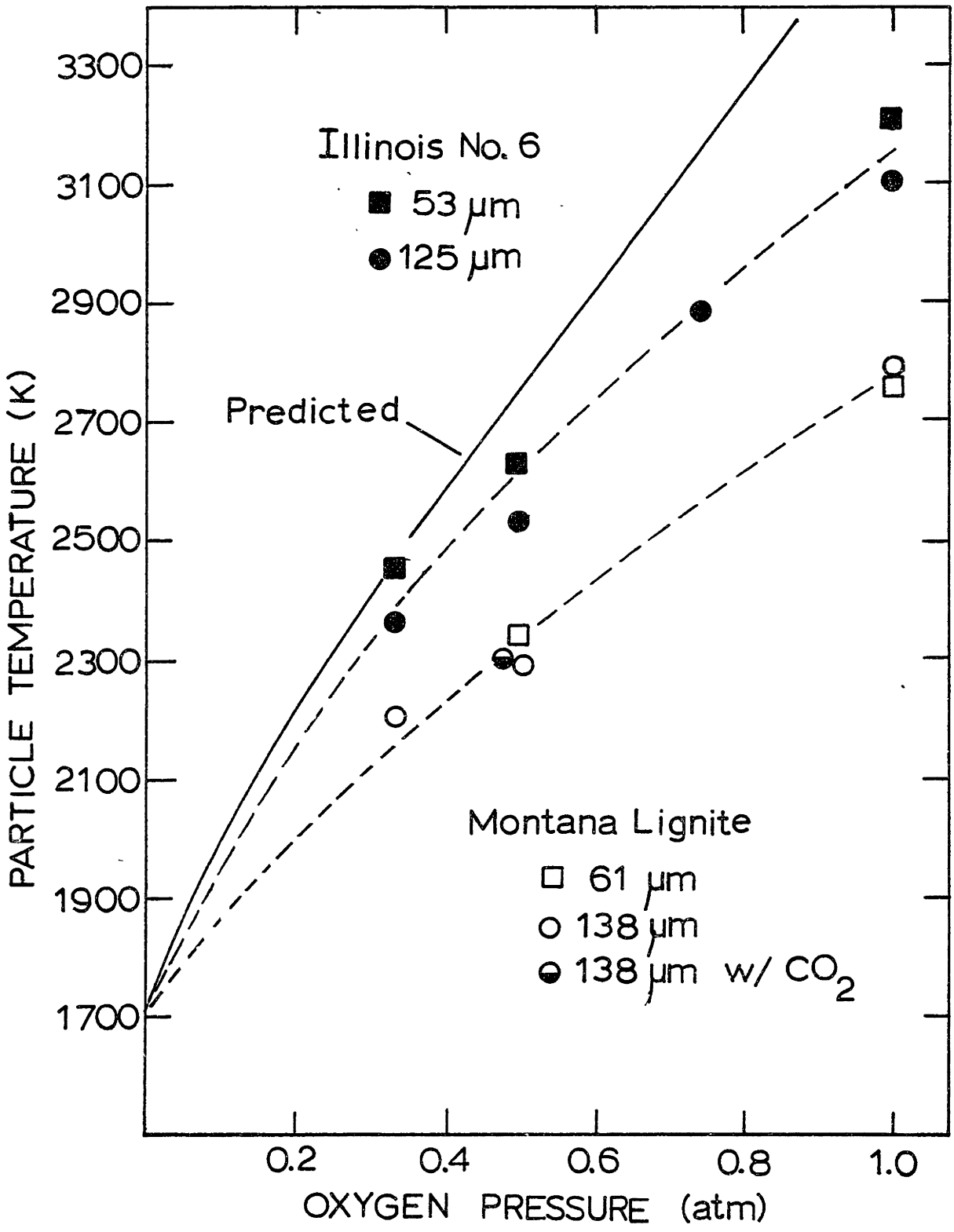

Figure 6.2 Two Color Pyrometry Measurement of Coal Particle Burning Temperatures

temperature of a char particle as determined by solution of the heat balance (equation 6.20) for external diffusion controlled combustion. At higher oxygen partial pressures, predicted combustion temperatures are significantly higher than measured combustion temperatures. This discrepancy may be due to unaccounted radiation losses to the cold furnace probe and furnace bottom or to increased thermal conductivity from high temperature dissociation of the gases in the particles boundary layer. A detailed consideration of these effects in predicting particle combustion temperatures is beyond the scope of this thesis. For the purpose of evaluating ash vaporization behavior with respect to temperature dependence, the measured values were used. At lower oxygen partial pressures (at a furnace temperature of 1750K), particle temperatures were obtained by extrapolation of experimental results for each coal type back to the gas temperature.

The average combustion temperature of the lignite in 50 percent oxygen was not significantly affected by the presence of 25% CO_2 in the main gas, as shown in Figure 6.2. Reliable measurements with 25% CO_2 present could not be obtained at the lower oxygen partial pressure conditions.

Particle burning times were obtained simultaneously with the temperature measurements for single coal particles. The measured burning time for a single particle was taken as the duration of the signals obtained by the photomultipliers. The results of these measurements are shown in Figure 6.3. Data points again correspond to the average of independent measurements of over 20 particles. Equation 6.9 has been used to

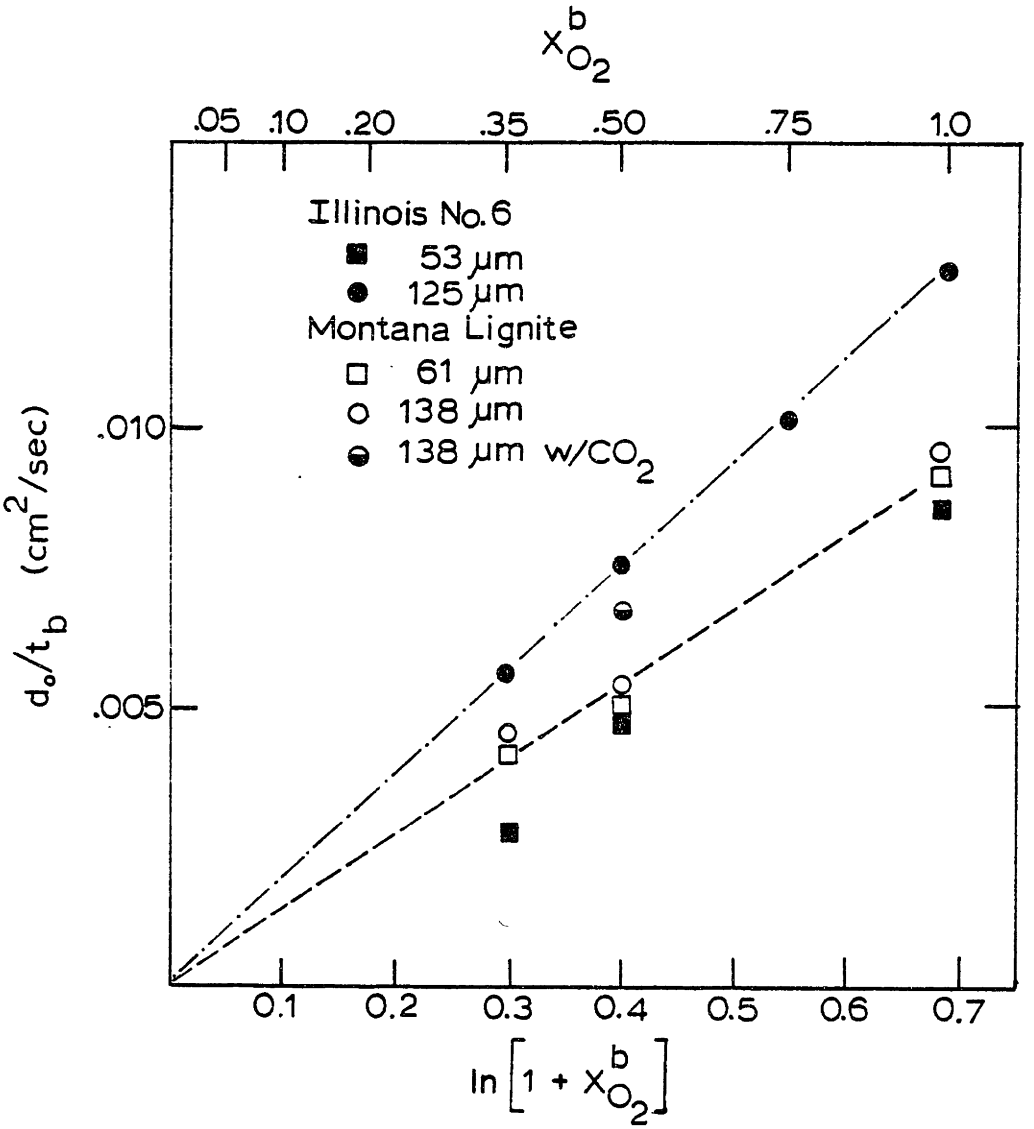

Figure 6.3 Two Color Pyrometry Measurement of Coal Particle Burnout Times

normalize the data with respect to the different size cuts of the coal feed. As evident a linear correlation of d_o^2/t_b with $\ell n\left(1+Xo_2^{b}\right)$ is obtained, indicating diffusion controlled combustion. Furthermore, d_o^2/t_b for the lignite is independent of initial coal size as predicted by equation 6.9. For the lignite, therefore, the burning time at a given oxygen partial pressure is proportional to the square of the initial particle diameter. The line down through the lignite data points corresponds to that predicted by equation 6.9 for a carbon density of 0.5 $\frac{gm}{cm^3}$ in the particles. However, as shown for the Illinois No. 6 bituminous coal, the term d_o^2/t_b is not independent of the initial size of the coal. The 125 micron diameter Illinois No. 6 apparently burns at an overall faster rate than predicted for the shrinking sphere model. Electron microscopy of the Illinois No. 6 chars obtained at these furnace conditions (reported in Chapter Nine) revealed that many of the particles have sphereical shapes with large internal voids and many appearing to be cenospheric. The line drawn through the Illinois No. 6 (125 micron diameter) corresponds to that predicted by equation 6.10 for a char burning as a cenosphere of approximately constant size (125 microns) for external diffusion controlled combustion and a carbon density of 0.5 gm/cm^3 within the total particle volume. For the Illinois No. 6 coal however, it is evident that burning time is not proportional to the square of the initial diameter as predicted by equation 6.10. It appears that the burnout time for the smaller bituminous coal particles is somewhat longer (about a factor of 1.5) than predicted for the cenospheric model

(equation 6.10). Further experimentation, beyond the scope of this thesis, is needed to elucidate these experimental findings. Howard and Essenhigh (1967) have predicted that for particles less than 65 microns, the oxygen diffusion rate is fast enough to result in simultaneous combustion of fixed carbon and volatile matter. For larger particles, a detached volatile flame is predicted to preceed the heterogeneous combustion of the char because of the slower oxygen diffusion rates. Hence, the burning times for the 53 micron bituminous coal may reflect the time required for diffusion controlled combustion of both volatile matter and fixed carbon, while that observed for the 125 micron bituminous coal reflects only the time required for combustion of the fixed carbon.

For the comparison of experimental and predicted combustion temperatures and burning times, gas diffusivities and thermal conductivities were estimated using the Chapman-Enskog kinetic theory of gases as outlined by Bird, Steward and Lightfoot (1960).

The combustion rate and temperature for the (61 micron) Montana Savage lignite in 10 percent oxygen in helium at a 1500K furnace temperature was estimated by reiterative solution of the heat balance (equation 6.20) and equation 6.18. Smith's (1978) intrinsic kinetics were used assuming a first order reaction rate with respect to oxygen concentration. A specific surface area of 500 m^2/g was assumed which is typical of low rank coal chars (Guerin et al., 1970). A porosity of 0.5 and a char density 0f 0.75 g/cm^3 were also assumed (the higher

value of density used here incorporates the presence of ash as well as carbon). Using equation 6.16, a pore radius of 27A is calculated. This is in agreement with the measurements obtained by Song (1978) for the same lignite. Reiteritive solution of equations 6.20 and 6.18 yielded a combustion temperature of 1600K and an oxygen partial pressure of 0.051 (atm) at the char surface. A time average diameter of 40 microns was assumed. Thus it appears that at this condition, external diffusion exerts only partial control of the combustion rate. The burning time was calculated to be approximately 50 milliseconds.

CHAPTER SEVEN

ASH VAPORIZATION AND CONDENSATION PROCESSES IN LAMINAR FLOW FURNACE

7.1 Introduction

This research was carried out in parallel with a complementary study by M. Neville. The focus of his work was to determine the physico-chemical characteristics of coal combustion generated inorganic submicron aerosols. The focus of the present work is on the mechanisms of ash vaporization that lead to the formation of the aerosol. In this study, the amount of ash vaporized during combustion was related to the material collected as submicron particulates. For this reason, it is necessary to consider the behavior of this aerosol by briefly summarizing the theory of submicron particulate formation drawing on the results obtained by Neville (1981).

Studies of pulverized coal combustion effluents have revealed that the mass or volume distribution of fly-ash is bimodal with respect to size. The smaller submicron mode arises from the homogeneous condensation of supersaturated inorganic vapors. However, not necessarily all inorganic vapors that evolve during combustion will condense via nucleation of new fine particles. Extensive field studies have shown that a number of trace metals are systematically enriched with respect to decreasing particle size for particles in the size range of 0.5 to 100 microns. Particles in this size range are the remains of molten mineral inclusion in the coal. Enrichment of trace metals has been attributed to a hetergeneous

condensation mechanism (Davison et al., 1974). Certain inorganic vapors, either because of their thermochemical properties or because of their presence in only dilute or trace amounts in the combustion gases, will not supersaturate but rather condence heterogeneously on the surface of pre-existing particulates as the combustion gases are cooled.

The speculated processes of ash particle formation are summarized in Figure 7.1. When pulverized coal particles are burned at high temperature (1700-2500K), virtually all of the oxygen is consumed at or near the surface of the porous char and the combustion rate of the char is essentially limited by the transport of oxygen to the char from the ambient. The temperature of the char may rise significantly above the surrounding gas due to the exothermicity of the carbon oxidation reaction. The details of this have been discussed in the preceeding chapter for the experimental conditions used in the present investigation. As the char burns and shrinks, the molten mineral inclusions will adhere to the char surface under the action of surface tension forces (Raask, 1966) and may agglomerate (Padia, 1976) upon contacting each other. At the completion of combustion, these ash droplets are liberated, thus forming the so-called residual fly-ash (Desrosiers et al., 1979). Particles produced by this mechanism will range from about 0.5 microns in diameter, corresponding to the smallest size of the mineral inclusions (Padia, 1976) to much larger sizes but typically averaging 10 to 20 microns in diameter. In Chapter Nine of this thesis, the

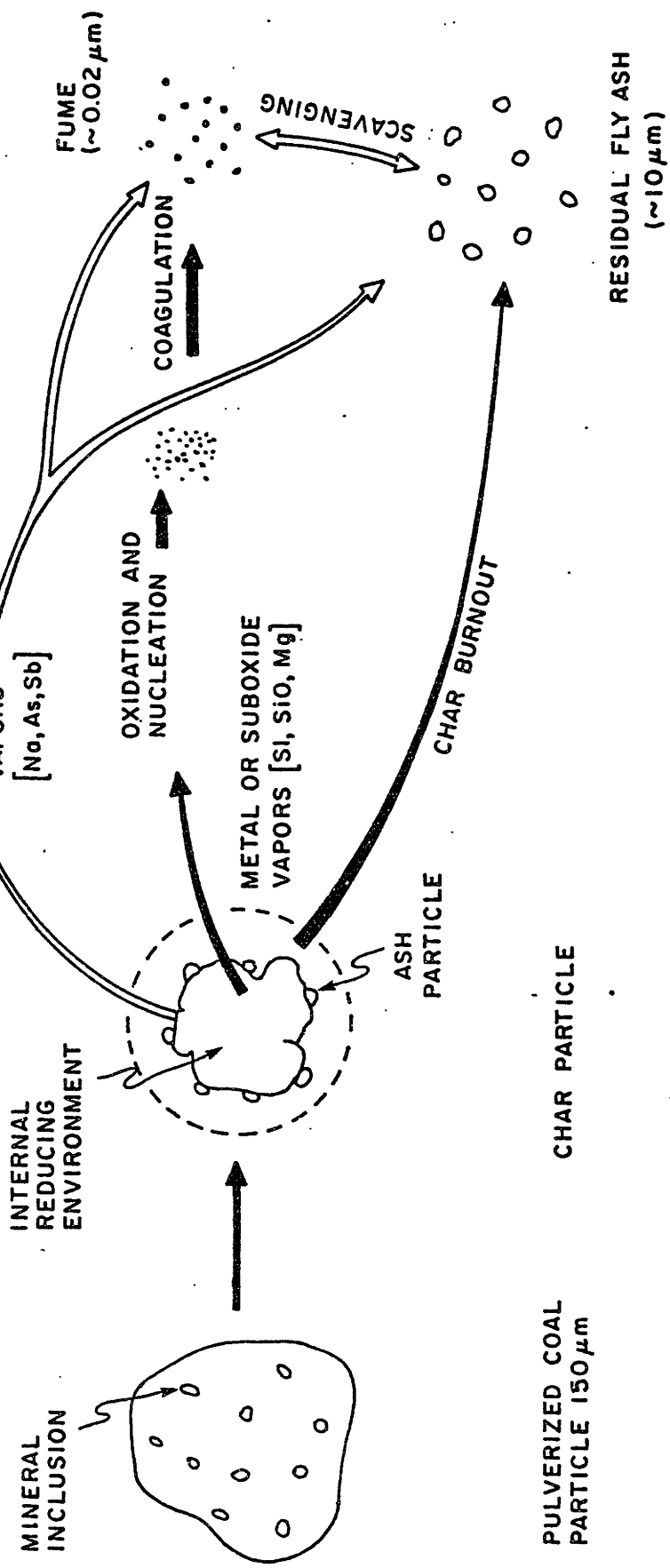

Figure 7.1 Schematic of Ash Formation and Behavior Mechanisms in Combustion

results of a detailed microscopic investigation of the chemical and morphological nature of ash on the surface of partially oxidized char particles is presented.

Under the high temperature, locally reducing environment of the char, a fraction of the oxide ash (SiO_2, CaO, MgO, FeO) may be reduced to suboxide forms (e.g. SiO, Mg, Ca, Fe) which are considerably more volatile. As the metal or suboxide vapors diffuse out and away from the char, they simultaneously encounter increasing oxygen potentials and decreasing temperatures. It is largely these two effects that lead to the reoxidation of suboxide vapors, causing supersaturation and rapid condensation by nucleation of submicron particles of refractory metal oxides in the combustion furnace.

The overall objective of this research was to obtain information on the mechanisms of ash vaporization processes during coal combustion. The measurement of ash vaporization was obtained by collection, isolation and analysis of the submicron particulates generated during combustion of coals under specified conditions. The procedures have been described in Chapter Four. It is the aim of this Chapter to assess the experimental method by considering in detail the behavior of ash vapors and the submicron aerosol in the present experimental system.

7.2 Size Distribution of Combustion Particulates

The mass distribution of combustion particulates on the cascade impactor stages and on the back-up final filter (FF) are reported in Table 7.1 for combustion of three

TABLE 7.1

Mass Distribution of Combustion Particulated for Combustion of Three Coals at 1750 K in 20% Oxygen (g/g Coal Burned)

Stage	Diameter	Montana Lignite	Illinois No. 6	Alabama Rosa
0	12μm	.0324	.0782	.0335
1	7.9	.0034	.0118	.0106
2	5.4	.0044	.0020	.0012
3	3.7	.0035	.0010	.0009
4	2.4	.0012	.0006	.0009
5	1.2	.0003	.0004	.0005
6	.77	.0001	.0001	.0001
7	.54	.00005	<.00005	<.00005
FF	.005 - .05	.0025	.0012	.0010

different coals at the same condition in the laboratory flow furnace. The distributions were obtained by weight analysis of the various impactor stages and calculated on a normalized basis of gram of coal burned. It is evident that the mass majority of the ash combustion products are collected on the preseparator (stage o) and are thus somewhat greater than 12 microns in size. The overall trend for all coals of decreasing mass with decreasing ash particle diameter is also evident. Relatively little material is collected on Stage 7 of the impactor, corresponding to particles of diameter on the order of 0.54 microns. There is, however, a significant increase in the amount of material collected by the back-up final filter. These are the very fine submicron particles generated by the condensation of ash vapors in the furnace. They have passed entirely through the cascade impactor because of their small size. The significant increase in the mass from stage 7 to the final filter reflections the bimodal nature of coal combustion particulates.

In Figure 7.2, a scanning electron micrograph illustrates the narrow size distribution of particles impacted on stage 5. The spherical morphology reflects the molten state of the ash at high temperature prior to quenching and collection of the combustion products. The transmission electrom (TEM) micrograph shown in Figure 7.3 illustrates the nature of the submicron particulates collected on the final filter and their agglomerate morphology in the fume. The samples were obtained by electrostatic precipitation onto TEM grids of the particles

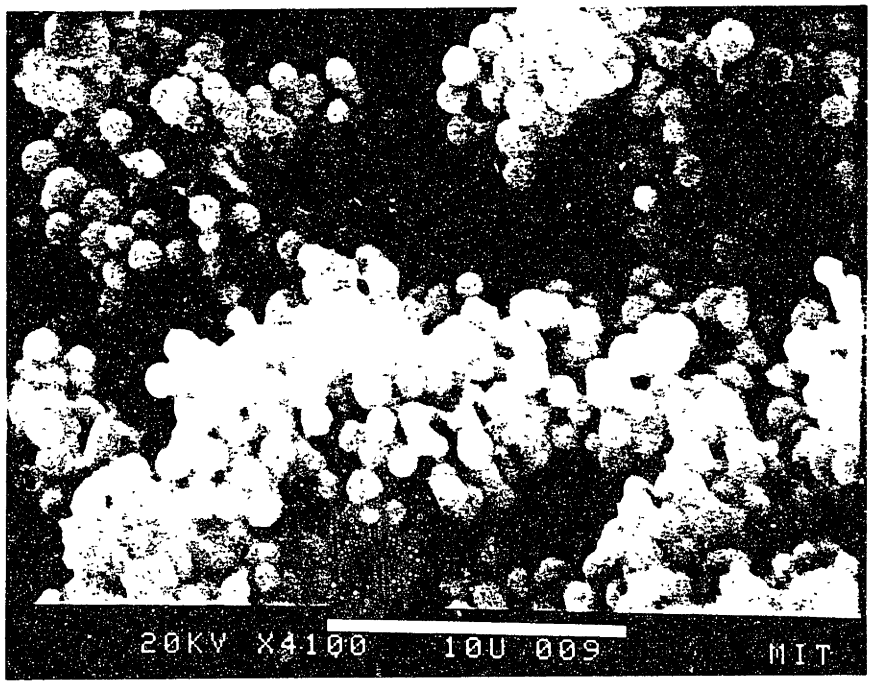

Figure 7.2 SEM Micrograph of Ash Particles Collected on Stage 5 of Impactor

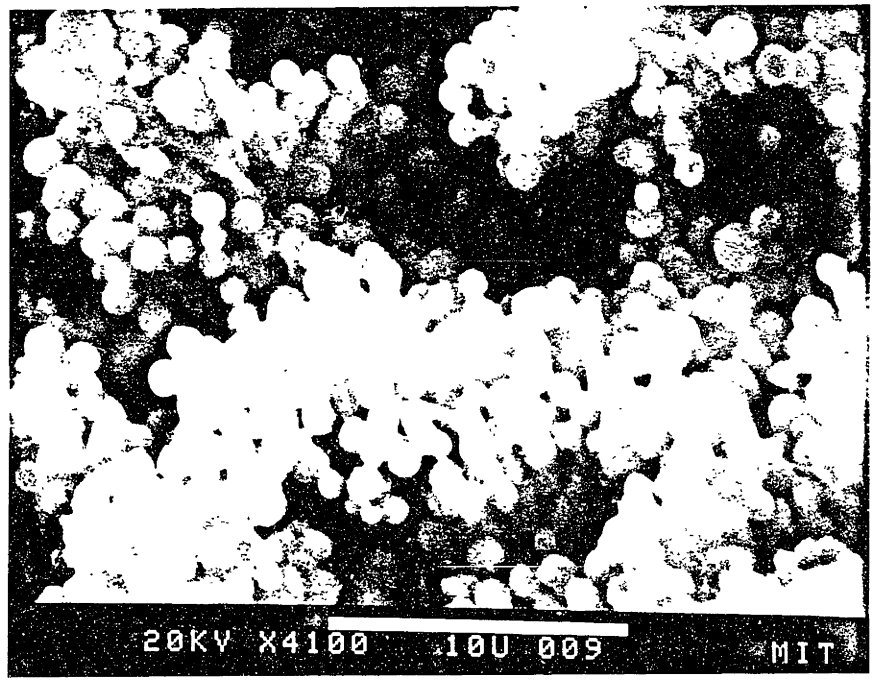

Figure 7.2 SEM Micrograph of Ash Particles Collected on Stage 5 of Impactor

INTENTIONAL DUPLICATE EXPOSURE

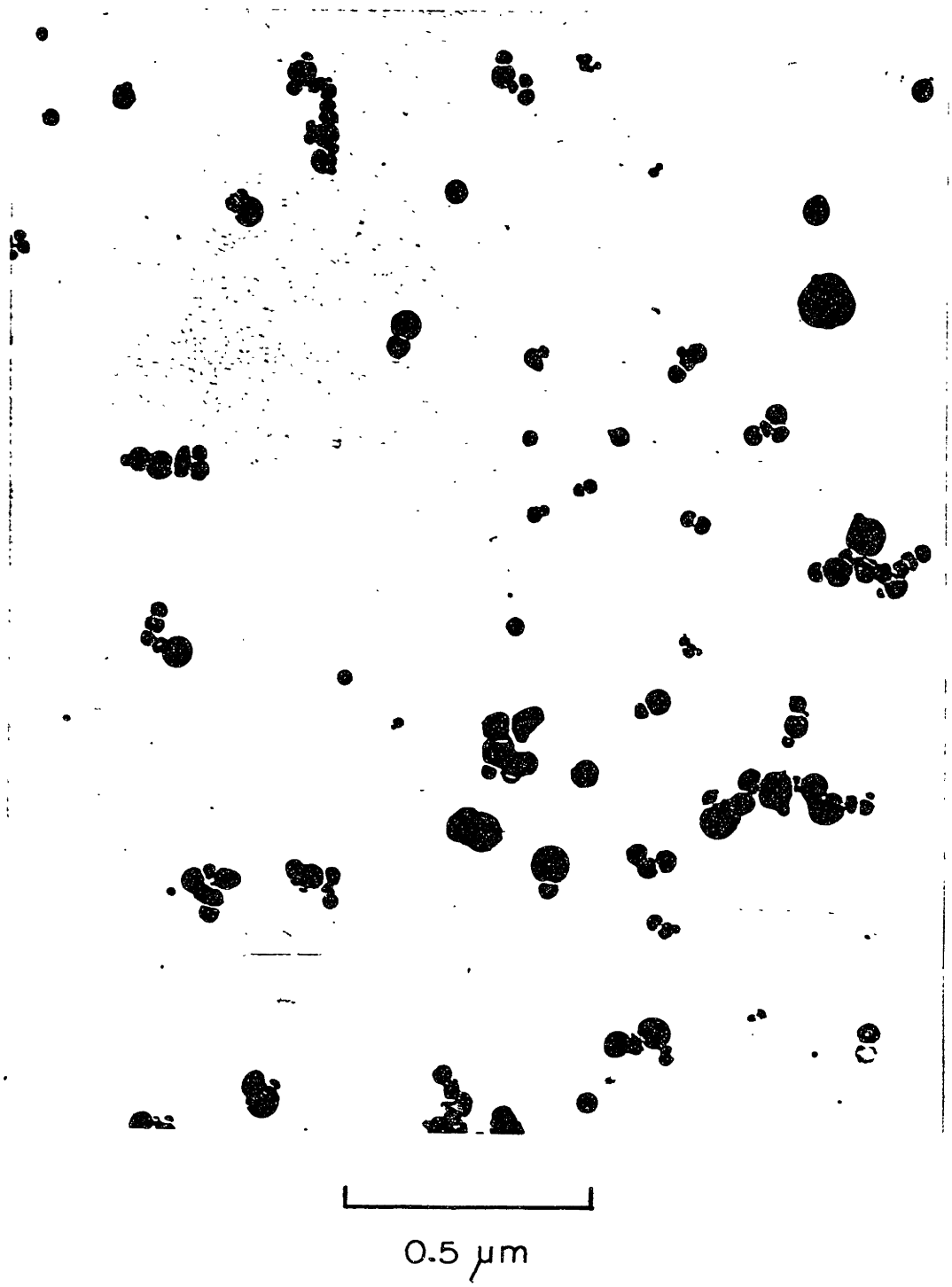

Figure 7.3 TEM Micrograph of Submicron Fume Generated During Combustion of Montana Lignite

passing completely through the cascade impactor with the combustion gases. For this run, a Montana Savage lignite was burned in 20 percent oxygen with the furnace wall temperature maintained at 1750 k.

The fact that the submicron material is formed by the condensation of vaporized ash is further supported by examining the size distribution of particulate matter as a function of combustion conditions. Although the effects of combustion conditions on the vaporization of ash is the subject of later chapters, it is necessary to this discussion to present some of the results on how combustion temperature influences the overall yield of submicron inorganic particulate matter. As described in Chapter Six, increasing the oxygen partial pressure in the main gas results in a corresponding increase in the combustion rate and temperature of burning coal particles. The temperature history of the (inherent) mineral matter contained within coal particles is then governed by the combustion conditions. The results of how increasing the combustion temperature by increasing the oxygen partial pressure in the furnace influences the mass distribution of ash particulates among the impactor stages are presented in Figures 7.4, 7.5 and 7.6 for the Illinois No. 6, Alabama Rosa and Montana Savage lignite, respectively. The furnace wall temperature in all cases was maintained at 1750 K and only the oxygen partial pressure in the furnace was systematically varied. The mass of submicron particulate matter, measured by the amount of material collected on the

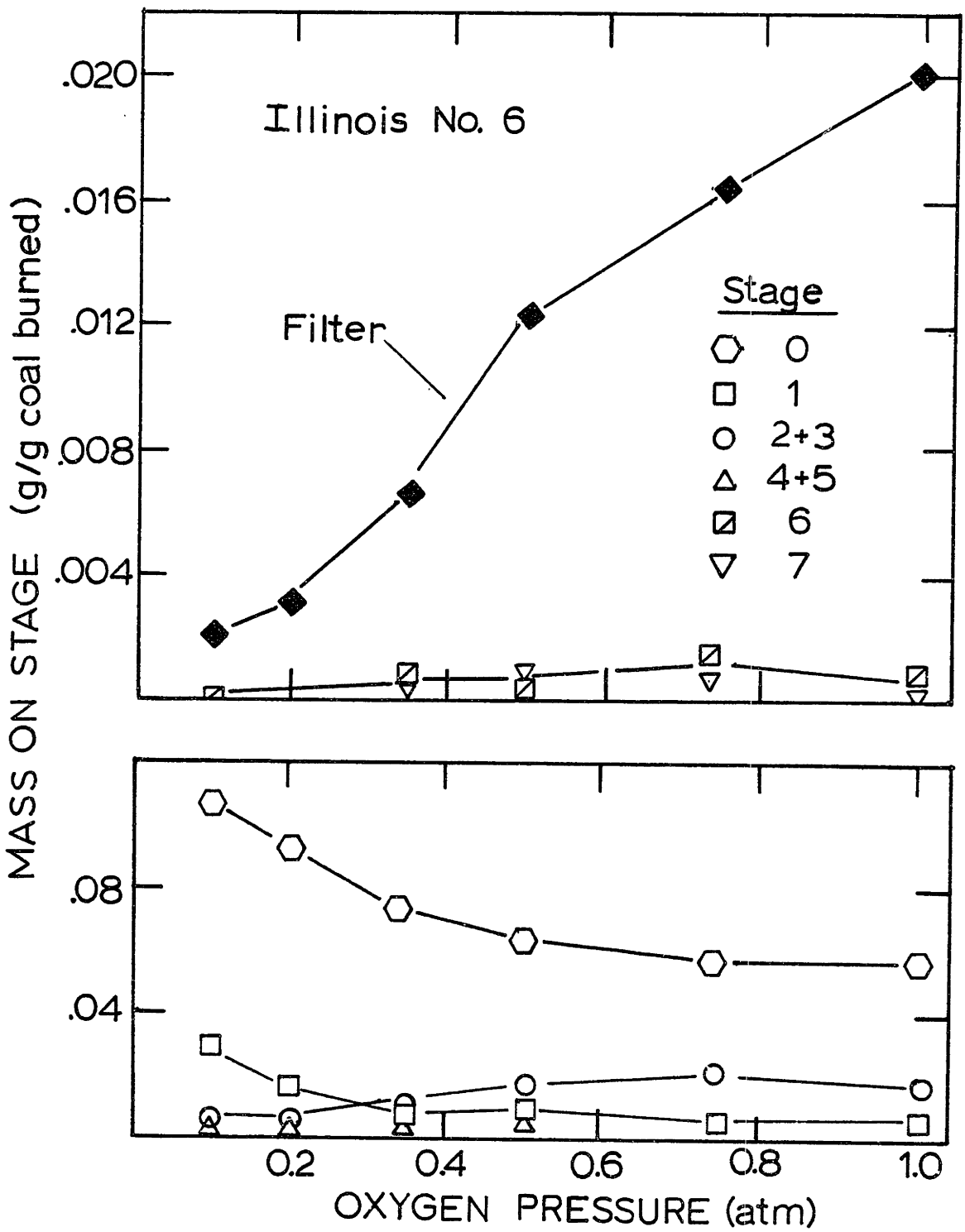

Figure 7.4 The Effect of Combustion Condition on the Distribution of Ash Particulate Mass on Impactor Stages for Illinois No. 6. Furnace Temperature 1750 K

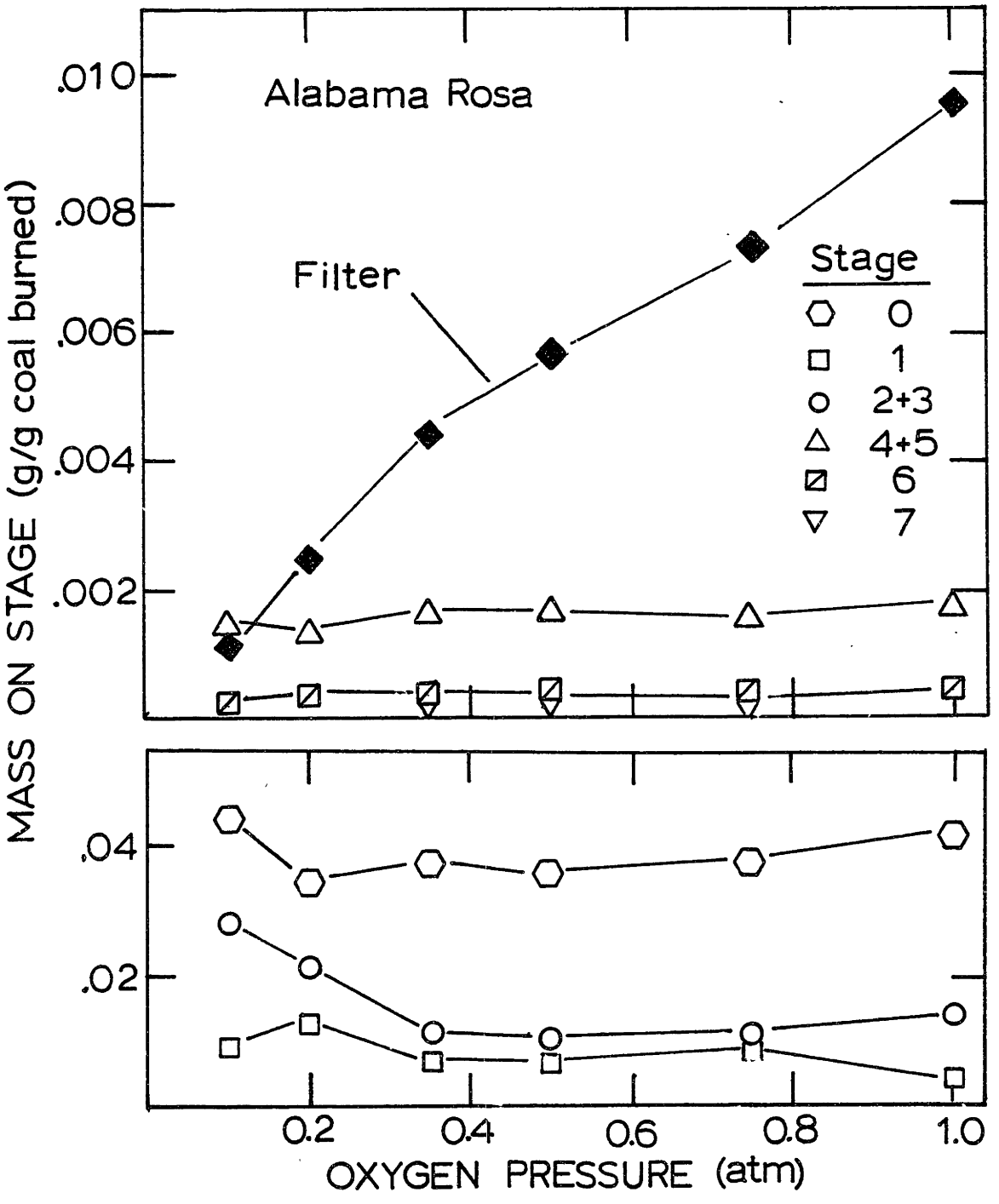

Figure 7.5 The Effect of Combustion Condition on the Distribution of Ash Particulate Mass on Impactor Stages for Alabama Rosa. Furnace Temperature 1750 K

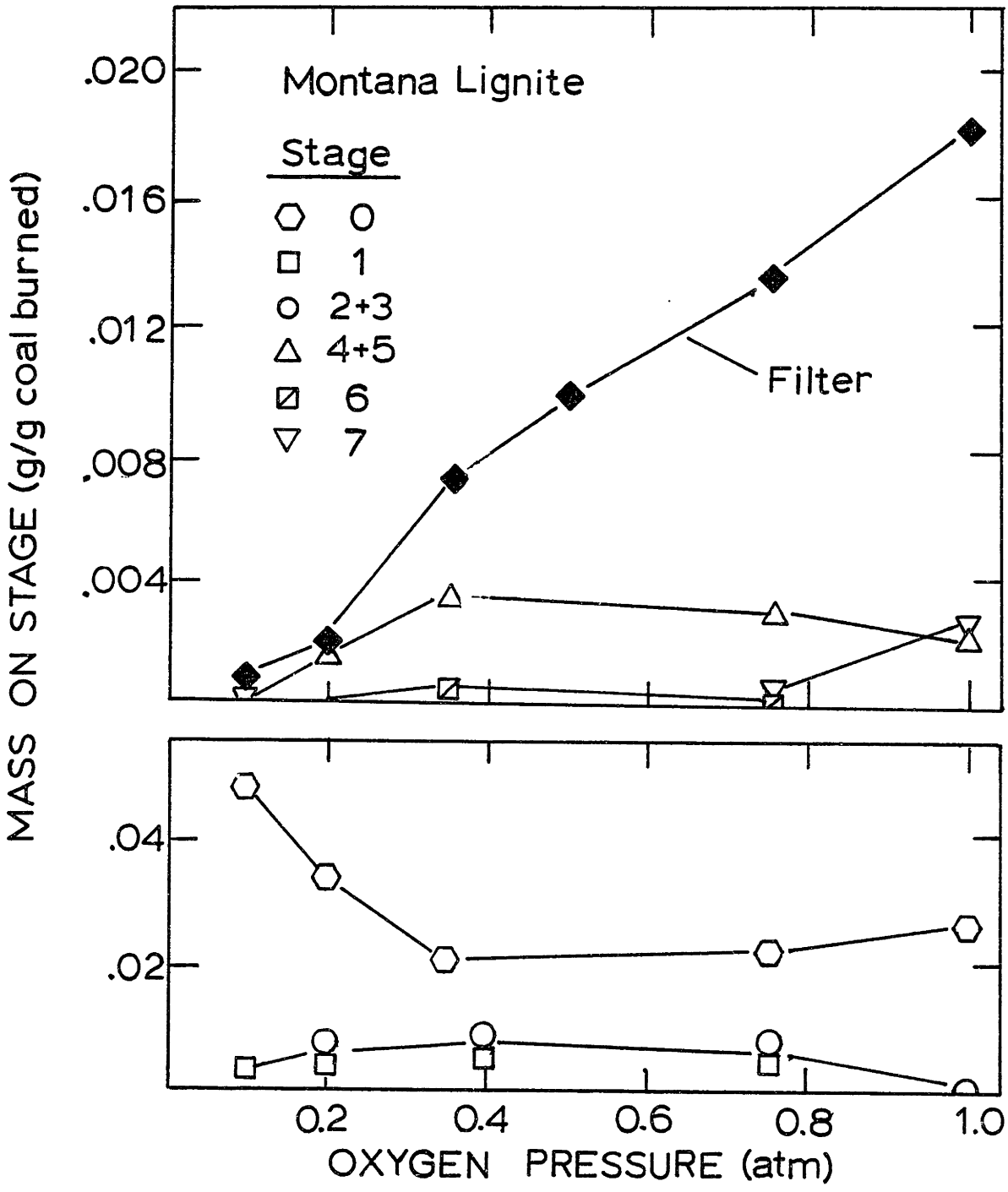

Figure 7.6 The Effect of Combustion Condition on the Distribution of Particulate Mass on Impactor Stages for Montana Lignite. Furnace Temp. 1750 K

back-up membrane filter (FF), increases significantly and systematically as the oxygen partial pressure (and combustion temperature) is increased. This is a trend expected for activated vaporization reactions. In comparison, the distribution of the larger sized particles (> 0.5 μm) collected on the impactor stages does not vary significantly with combustion conditions. These particles are formed primarily by physical mechanism not likely to be too sensitive to combustion conditions. It will be demonstrated in Chapter Eight that the composition of the vaporized ash (collected as the sumbicron particulate matter) is strongly dependent on the combustion conditions and on the particular characteristics of the mineral matter in different coals. The major components of the submicron material, in most cases, were found to be SiO_2, FeO or MgO, depending upon the coal type. These compounds are refractory but have volatile forms under reducing conditions (e.g. SiO(g), Mg(g) and Fe(g)).

The volume distribution with respect to size of the post-combustion ash particulates in the furnace at the point of collection (15 cm from the coal injector probe) of both submicron and impactor deposits of residual ash are shown in Figure 7.7 for the combustion of the Montana Savage lignite in 15 and 40 percent oxygen at a furnace wall temperature of 1750 K. The size distribution of the submicron particles shown in this Figure are the results obtained by Neville (1981) using the same experimental system.

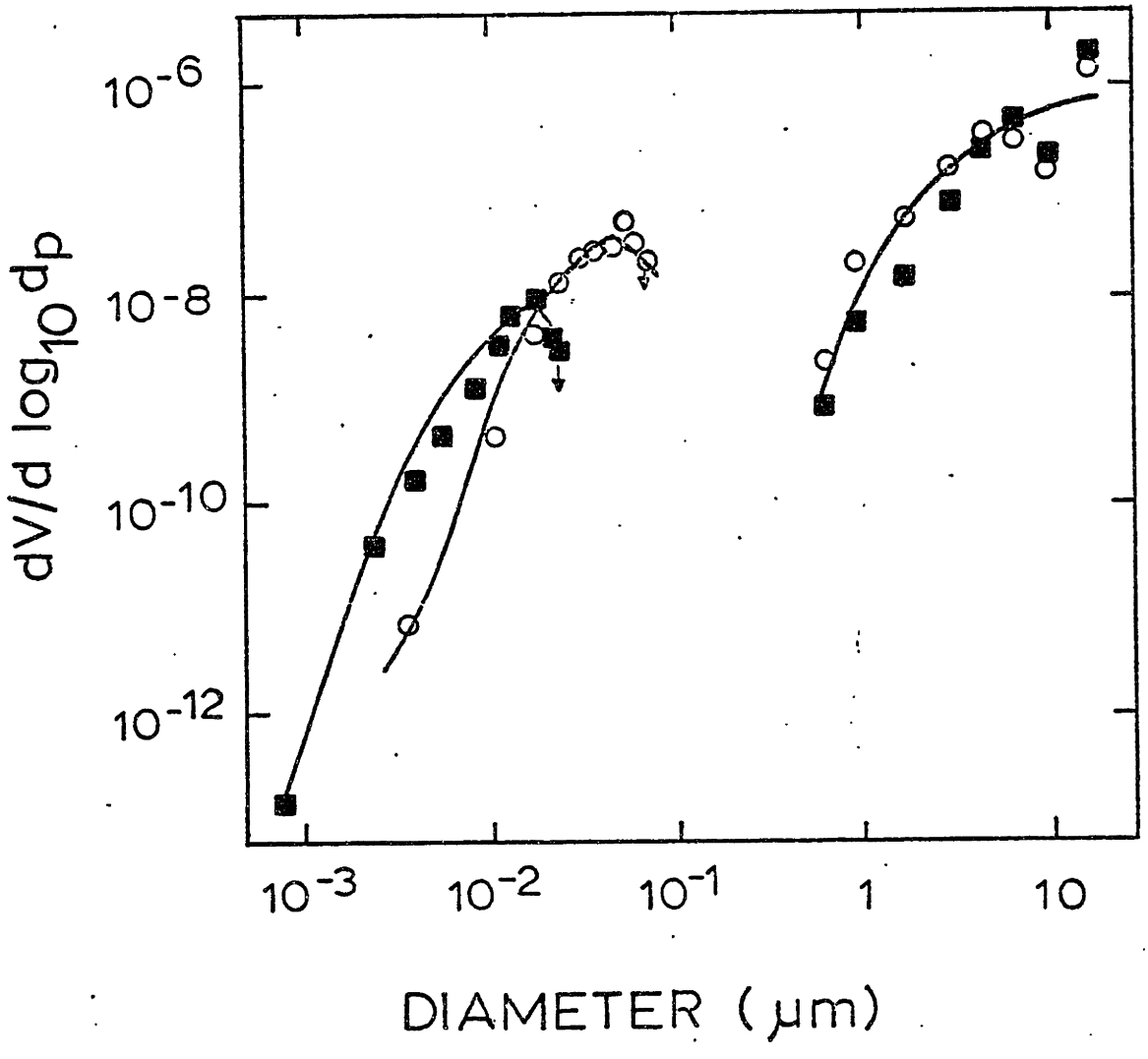

Fig. 7.7 : Aerosol Size Distributions Produced by Combustion of μm Lignite Particles in ■ 15% and ○ 40% Oxygen in Nitrogen at 1750K.

An automated image analyzer was used to count particle diameters from TEM micrographs of the fume. The distribution is of the primary particles in the fume and not of the aggregate of flow size. The characteristic bimodal size distribution that is prevalent in utility effluents (Ensor et al., 1979; McCain et al., 1975) is also clearly present in the laboratory combustion generated particulates. It is also evident from the data the the average size of the submicron particles is dependent on the amount of ash vaporized.

7.3 Submicron Particle Nucleation and Growth in Flow Furnace

Nucleation of submicron ash particles is initiated by the diffusion of metal and sub-oxide vapors (e.g. SiO, Fe, Mg) away from the high temperature-locally reducing atmosphere of a burning char partilce into the lower temperature, oxidizing environment of the surrounding gas. The composition of the surrounding medium is not significantly affected by the combustion process in the present experiments because of the low coal particle number density ($<20\ cm^{-3}$). From classical nucleation theory, a critical cluster radius of less thatn 15Å is predicted for homogeneous nucleation of oxides (e.g. SiO_2, MgO, FeO, CaO) in this system (Neville, 1981). Once these extremely fine particles have formed during the initial stages of combustion, further supersaturation by additional vaporization of ash from the char particles would be relieved by heterogeneous condensation or reaction on this high surface area material. Only the hotter burning char particles and the condensation nuclei in the cooler gas

are present at this early stage of combustion. The residual ash droplets are not formed until the char is nearly burned to completion. Hence, the submicron aerosol will grow by collision and coagulation processes resulting from their Brownian motion in the furnace combustion zone and by further condensation of vaporized ash. There is also the possibility that, during the post-combustion and sampling period, the fine particle numbers may be reduced by collisions with the larger residual ash droplets. These processes involving the submicron ash behavior are considered in this section.

The submicron ash generated by the nucleation of ash vapors in the furnace is considered a free-molecule aerosol, having diameters less than 0.1 micron and Knudsen nubers greater than 10. For a free-molecule aerosol undergoing particle collisions as a result of Brownian motion in a uniform flow field, the decrease in total number density N of the particles is given by (Lai et al., 1972):

$$\frac{dN}{dt} = \frac{1}{2}\int_0^\infty\int_0^\infty \beta(v,v')n(v,t)n(v',t)dv'dv$$

where $n(v,t)$ is the particle volume distribution function and $\beta(v,v')$ is the collision frequency between particles of volume v and v'. For the free-molecule regime, $\beta(v,v')$ is (Hidy and Brock, 1970):

$$\beta(v,v') = \left(\frac{3}{4\pi}\right)^{1/6}\left(\frac{6kT}{\rho}\right)^{1/2}\left[\frac{1}{v}+\frac{1}{v'}\right]^{1/2} \times\left[v^{1/3}+v'^{1/3}\right]^2$$

The terms k, ρ and T are the Boltzmann constant, gas density and temperature, respectively. The collision parameter β in

this case is for neutral particles with negligible intermolecular forces. Colliding particles are assumed to stick and coalesce instantaneously.

An aerosol evolving by this coagulation dominated growth process can, after a sufficiently long period of time (~ 1 msec), be described by a self-preserving size distribution function $\psi(\eta)$, using the relationship

$$n(v,t) = \frac{N^2}{V} \psi(\eta)$$

where η is the dimensionless particle volume given by

$$\eta = \frac{Nv}{V}$$

and where V is the volume fraction of the aerosol (Lai et al., 1972). The particle number density decay rate (Eqn. 7.1) then becomes:

$$\frac{dN}{dt} = -\frac{1}{2}\left[\frac{3}{4\pi}\right]^{1/16}\left(\frac{6kT}{\rho}\right)^{1/2} \alpha_c V^{1/6} N^{11/6}$$

where with α_c being the dimensionless collision intergral for the self-preserving distribution and having a value of 6.67 (Lai et al., 1972).

The total volume fraction of submicron particles, V, is directly proportional to the fraction of ash that vaporizes during combustion. At a specified combustion condition, the fraction of ash vaporized varies with residence time in the furnace as long as the char particles are burning. This is demonstrated by the time-resolved measurements shown in Figure 7.8. In these experiments, the Montant Savage lignite (nominal 140 micron diameter) was burned in 30 percent

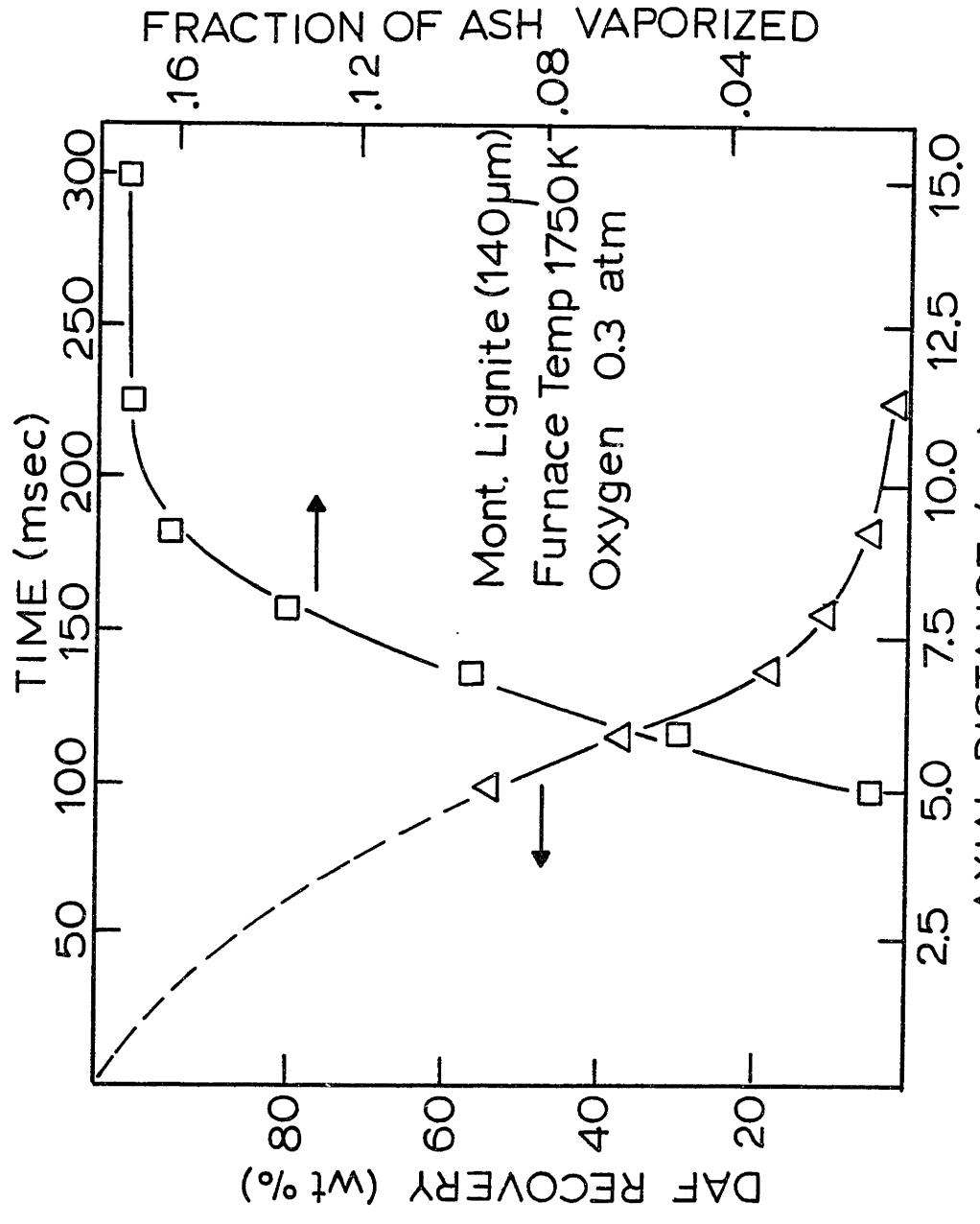

Figure 7.8 Time Resolve Measurement of Ash Vaporization

O_2 - N_2 mixture. The position of the collection probe was adjusted to quench the char particle combustion process at successive stages of burnout. Weight loss measurements were used to determine the extent of burnout at each position. The fraction of ash vaporized was determined by collection and isolation of the submicron fume on the final filter of the cascade impactor at each residence time. During the first 100 milliseconds, the coal is heated to the furnace temperature with concurrent devolatization. After this initial period, the char paticles ignite and burn to completion at about 12.5 cm. The data demonstrate that the ash vaporizes only during the char combustion process. This is to be expected because it is during this period that the ash experiences the locally reducing atmosphere within the char and the temperature overshoot caused by the exothermic char combustion reaction. It is of note that in the post-combustion period, their is no measurable change in the mass of submicron material.

At long coagulation times, the number density of submicron particles approaches (Flagan and Friedlander, 1978):

$$N = \left[\frac{5}{12}\left(\frac{3}{4\pi}\right)^{1/6}\left(\frac{6kT}{\rho}\right)^{1/2}\alpha_c V^{1/6} t\right]^{-6/5}$$

and the volume average diameter is

$$d = \left(\frac{\pi}{6}\right)^{-1/3}\left[\frac{5}{12}\left(\frac{3}{4\pi}\right)^{1/6}\left(\frac{6kT}{\rho}\right)^{1/2}\alpha V t\right]^{2/5}$$

The volume average diameter should increase with the fraction of ash vaporized ($d \sim V^{2/5}$). This is qualitatively

confirmed by the results shown in Figure 7.7.

A comparison of the theoretical self-preserving size distribution and the experimentally determined size distribution of the submicron particles is shown in Figure 7.9 for combustion of the Montana savage lignite in 20 percent oxygen at a furnace wall temperature of 1750 K. The experimental data was obtained by Neville (1981). For the theoretical calculation, the volume fraction of submicron particles was calculated from the fraction of ash that vaporized (0.039 of the metal oxides). The particles were assumed to remain within a 0.7 cm radius core in the furance on the basis of visual observation of burning char particles. Particle transport by radial diffusion is insignificant for the time scales of the combustion experiments. The tables of Lai et al., (1972) were used for the dimensionless distribution function.

The interaction of submicron particles with the larger residual ash droplets in the post burnout period has previously been given theoretical consideration. Using the Fuchs-Sutugin interpolation formula, Flagan and Friedlander (1978) modelled the loss of submicron particles to the larger droplets as

$$F = \frac{2\pi D(1+Kn)n(d)d(d)}{1+1.71Kn+1.333Kn^2}$$

where F is the number of particles diffusing to the surface of larger particles per unit time and n(d) is the number distribution of submicron particles. Under the comparitively

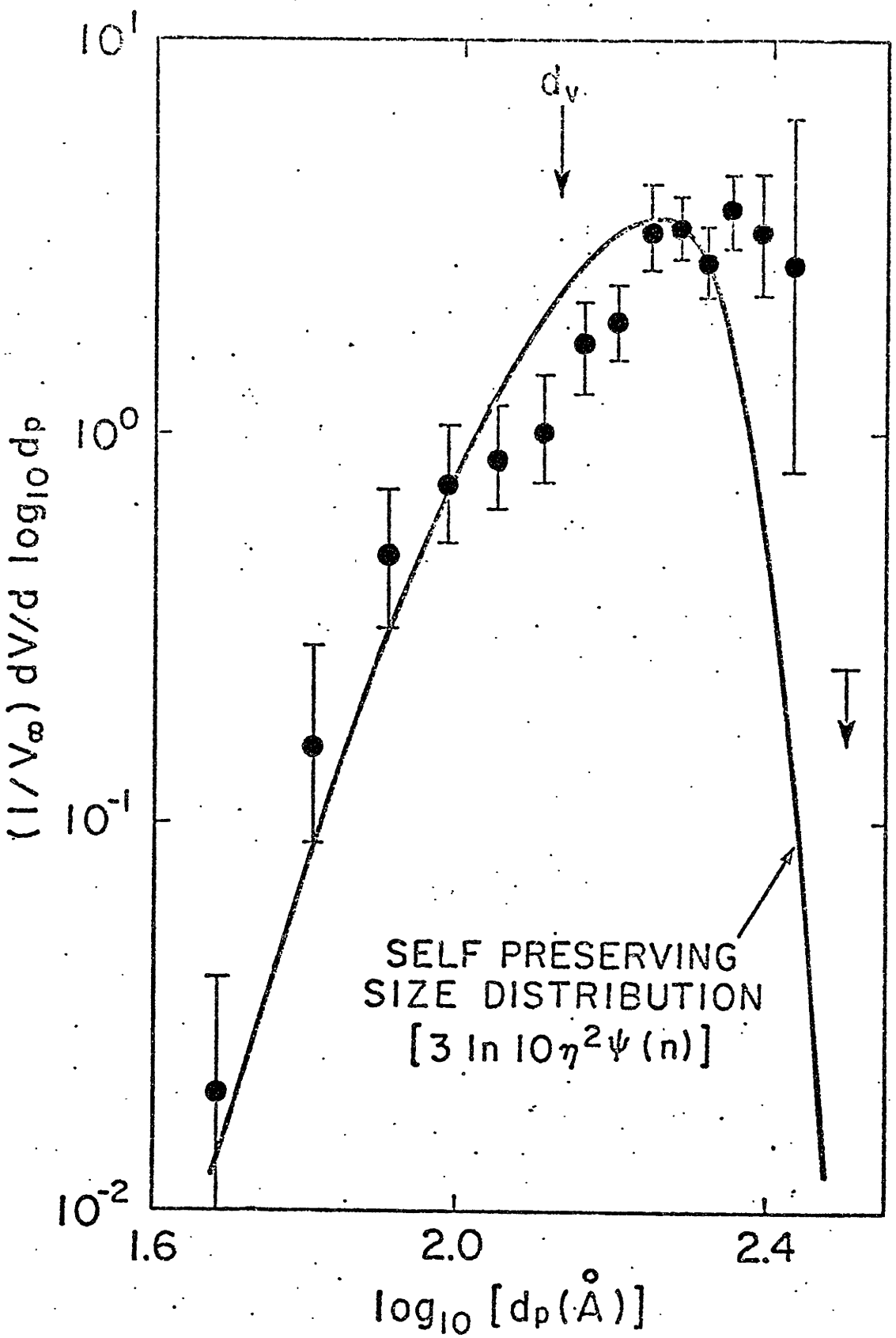

Figure 7.9 Comaprison of Self-Preserving Size Distribution with Experimental Data

long residence times experienced in utility boilders (~3 seconds), they concluded that as much as 30 percent of the submicron material may be lost to the larger particles. Neville (1981), however, concluded that under the experimental conditions of this laboratory flow furnace, less than 2 percent of the submicron material is lost to the layer ash droplets. He used an aerosol simulation code (Gelbard and Sienfeld, 1980) for his calculation. This is consistant with the experimental results (Figure 7.9) inasmuch as the self preserving size distribution approximation would not be valid if significant interaction occured (Flagan and Friedlander, 1978). Furthermore, as shown in Figure 7.8, post-combustion residence time does not affect submicron particulate yield. On the basis of these arguements, it is concluded that the amount of collected submicron particulate is an adequate measurement of the extent of ash vaporization for those compounds which must condense by particle nucleation in the hot furnace combustion zone because of supersaturation brought about by changes in the oxidation state of vapors (e.g. SiO, Mg, Ca and Fe).

7.4 Heterogeneous Condensation of Trace Metal Vapors

As mentioned previously, certain inorganic vapors that evolve during the combustion process will not supersaturate and condense by nucleation of submicron particles at the high temperatures. Rather, because of their thermochemical properties or because of their dilute concentration in the gas phase, condensation will occur heterogeneously on existing particulates as combustion gases are cooled in, for example, the convective heat exchangers of utility boilers. Particulates present at this stage of the combustion process include both the larger residual ash droplets and the submicron particulates. Vapor species which fall into the volatile category may indodsodium, as an oxide, chloride, metal or hydroxide vapor, and all possible compounds of, for example, the trace metals As, Sb, Pb, Se and others. Field studies have shown that these elements are systematically enriched in concentration with respect to decreasing ash particle size in the residual ash size range (>0.5 μm) Natusch et al. (1974) have proposed an absorption controlled pathway, by which the concentration of an element varies inversely with ash particle diameter from a simple geometric effect of surface to volume ratio. Flagan and Friedlander (1978) have proposed, alternativley, that condensation is controlled by diffusion to particle surfaces for particles in the residual size range. This leads to an inverse diameter squared proportionality of trace species concentration.

Neville (1981), using the same laboratory combustion

system of this investigation, has observed that the concentration of nearly all trace elements that vaporize to any significant extent (V, Mn, Na, As, Sb and K) are enriched with decreasing ash particle size in the residual mode of the size distribution. Condensation of these volatile vapors is likely to occur in the collection probe as combustion gases are quenched to a few hundred degrees centigrade. These results demonstrate that some condensation of trace volatile vapors occurs heterogeneously on the larger residual ash droplets. It is expected, however, that the submicron particulates, being of high surface area, would dominate as vapor sinks. As several of these volatile components are of interest to this study, an attempt will be made to provide a quantitative basis for determining the effectiveness of using the submicron fume as a measure of trace metal vaporization.

If the condensation of trace metal vapors is controlled by surface chemical kinetics or by absorption, then the relative distribution of condensed trace metal vapors is determined by the relative surface areas of the two modes of the particulate size distribution. The total area (A) of either mode is given by

$$A = \int n(v)\pi d^2 dV$$

where n(v) is the size distribution of the mode and the integration is carried out over the limits of the mode. For the sumbicron mode, the area is:

$$A = (36\pi)^{1/3} N^{1/3} V^{2/3} \int_0^\infty \eta^{2/3} \psi(\eta)\, d\eta$$

The integral is the 2/3 moment of the self-preserving size distribution and has a value of 0.90 (Lai et al., 1972). The total area of the residual ash mode can be evaluated from the impactor data.

If the condensation of the trace metals is controlled by diffusion, than the relative distribution of the trace metal vapors is determined by the flux integrals:

$$\int n(v)\ F_i\ dv$$

where the flux to particles in the submicron (free-molecule) mode is given by:

$$F_i = \frac{\pi d^2 (P_i - P_i^e)}{(2\pi mkT)^{1/2}}$$

and that to particles in the larger (continuum) made is given by:

$$F_i = \frac{2\pi dD(P_i - P_i^e)}{RT}$$

The partial pressures Pi and Pi^e refer to species i in the bulk gas and at the particulate surface, respectively.

These integrals were evaluated for the Montana Savage lignite assuming that the larger mode size distribution does not change except for a decrease in its total mass with increased total ash vaporization. The results of the calculations are shown in Figure 7.10 as a function of the fraction of ash vaporized. The fraction of ash vaporized corresponds

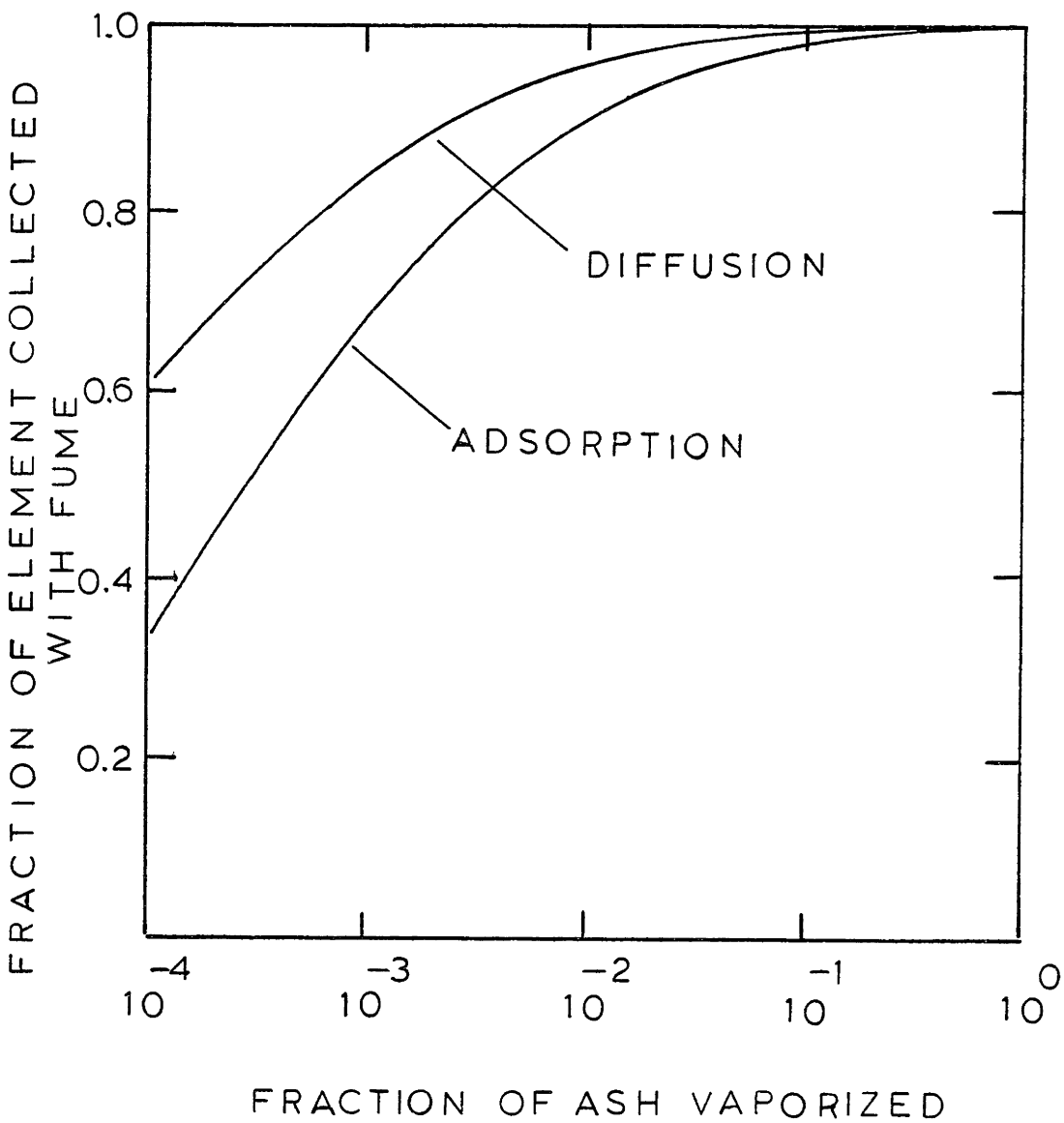

Figure 7.10 Predicted Condensation Behavior of Volatile Trace Metals

to the fraction of refractory metal oxides (e.g. SiO_2, MgO CaO and FeO) which vaporize and form a self-preserving submicron aerosol in the furnace. Most of the trace element vapors will be collected by the submicron particulate fraction unless extremely low percentages of the ash vaporize. This analysis, of course, assumes that chemistry is not a factor. Further experimentation on the condensation behavior of trace elements is required before this can be included in the analysis.

7.5 Elemental Material Balance on Laboratory Furnace

In order to test experimentally the effectiveness of using the amount of combustion generated submicron aerosol as a technique of the measure of ash vaporization and, as well, the sampling system, the Montana Savage lignite was burned at a relatively high combustion temperature in 50 percent oxygen. The purpose was to obtain an elemental material balance and to determine the extent to which specific elements appeared in the submicron fume at a condition where significant amounts of the ash are expected to vaporize. Two combustion experiments were performed; one measure the elemental content of the fume, and the other measuring the total recovery in all particulates.

The percentage of selected elements in the coal feed ultimately recovered after combustion in all particulate products is presented in the second column in Table 7.2. Generally, more than 90 percent of an element in the coal feed was recovered

TABLE 7.2

Elemental Material Balance on Furnace for Combustion of Montana Savage Lignite in 50% Oxygen at 1750k

Element	Concentration in Coal (ppm)	Recovered with all Particulates (%)	Recovered in Submicron Fume (%)	INAA Precision (%)
Al	6400	77.3	2.1	1
As	4.0	99.6	76.9	10
Ca	14400	96.0	19.4	5
Cr	7.5	100.5	25.0	10
Fe	3000	91.7	20.7	5
K	300	85.0	15.4	10
La	5.7	100.4	6.0	5
Mg	5800	80.7	50.0	10
Mn	71	90.0	13.3	4
Na	170	89.0	38.6	10
Sb	0.54	100.0	77.0	20
Sc	0.83	103.4	5.3	2
Sm	0.50	91.3	10.0	1
Ti	210	94.0	12.1	14
Th	1.5	103.5	14.5	10
V	9.0	71.3	14.0	6

in the particulate product, indicating no significant loss of particulate or inogranic vapor material within the furnace, collection probe, or modified impactor head. The fraction of the different elements recovered in the submicron fume is presented in the third column of Table 7.2. Regardless of the extent to which an element appeared in the fume, i.e. the extent of vaporization during combustion, good material closure was obtained.

The mineral matter that vaporizes can either condense on the larger ash particles or condense homogeneously as a submicron fume. For the conditions of the results presented in Table 7.2, the greater fraction of the ash vaporized is found in the submicron fume. The major elements in the fume for the Montana lignite are the alkaline earth metals. The refractory oxides of these elements condense to form aerosols in the high temperature zone of the furnace. The submicron aerosol provides a much higher surface area than the bulk ash for the subsequent condensation of the more volatile vapors, of, for example, Na, As and Sb or their respective compounds. The direct determination of the elements in the fume is therefore a sensitive measure of the extent of vaporization during combustion. Possible loss of material due to condensation on the larger particulates would appear to be small--for example, close to 80 percent of the As and Sb in the coal feed was found in the submicron fume at this combustion condition. Furthermore, the percentages of As and Sb collected with the fume on the back-up filter, in comparison with low values of,

for example, Al, Sc and La, clearly demonstrate an effective aerodynamic separation of the fume from the larger ash particulates by the impactor.

CHAPTER EIGHT

EXPERIMENTAL RESULTS - THE EFFECTS OF COAL TYPE AND COMBUSTION CONDITIONS ON THE VAPORIZATION OF ASH

8.1 Introduction

In the preceeding chapter, it was shown that a mode in the submicron range of the ash particle size distribution is formed as a result of ash vaporization and condensation phenomena. Specifically, inorganic vapors evolving from high temperature burning char particles will condense by homogeneous nucleation of very fine submicron particles. Furthermore, it was demonstrated in the preceeding chapters that the submicron fume generated during the combustion of pulverized coal under the well defined conditions of the laboratory furnace could be effectively collected and isolated. Recovery and analysis of the submicron ash affords the possibility of obtaining practical information on how a number of experimental variables affect its characteristics. The properties of combustion generated submicron ash, including composition, loading and size, are determined by the thermochemical or volitilization properties of specific elements (or compounds) occuring in the coal, how these elements are distributed in the coal and the conditions under which the coal is burned. Results presented in a preliminary manner in the preceeding chapter (Figures 7.4, 7.5 and 7.6) demonstrated the sensitivity of ash vaporization to combustion temperature. In this present chapter, the experimental results on how coal type, coal feed size, and combustion temperature influence the degree of ash vaporization, the

composition of the submicron ash and the vaporization behavior of specific elements, are reported.

8.2 The Effect of Coal Type on the Amount and Composition of Combustion Generated Submicron Ash

A major consideration in the design and operation of a utility boiler is the nature of the mineral matter in the pulverized coal and the properties of its ash up to and at combustion temperatures. For example, only coals having ash exhibiting certain properties (e.g. fusion temperature, viscosity) governed by their composition may be used in a specific boiler because of excessive fouling or corrossion problems that may otherwise develop, or because of the design (e.g. slag tap vrs. dry ash) employed for ash management. These considerations along with thermal efficiency place constraints on the combustion conditions or firing conditions. Hence, fuel variability should also be of major importance with regard to the submicron ash generated in and emitted from coal-fired utilities. The present investigation sought to determine if a meaningful relationship exists between the original coal properties and resulting properties of the submicron ash generated from combustion of the coals.

The twenty coals used in the present study are of varied mineral matter characteristics as described in Chapter Five. These coals, all size classified to nominal 50 to 60 microns in diameter, were burned to completion in the laminar flow furnace under an identical combustion condition-that of a furnace wall temperture of 1750K, and a gas composition of

20 percent oxygen-80 percent nitrogen to simulate air. The coal particle combustion (temperature) history closely simulated that which would occur in a flame of a typical utility boiler. The burning temperature of the coal particles is approximately 2000K (Chapter Six) at this specified furnace condition.

The products of combustion were collected and the submicron ash was isolated, using the cascade impactor, and analyzed for its chemical content for combustion of each coal. The results are reported in Tables 8.1 through 8.4. A discussion of results on the vaporization behavior of specific elements is reserved for later sections of this chapter. Only bulk properties of the submicron ash are discussed presently.

The amount of submicron ash generated during combustion (equivalent to the amount of ash vaporized), normalized on a basis of gram of coal burned, are compared for the different bituminous coals and low rank coals in Tables 8.1 and 8.2, respectively. These results for the bituminous coals are in agreement with the few reported measurements of utility effluents were 1 to 2 percent of the fly-ash mass is within the submicron mode (McElroy and Carr, 1980). Calculation of the precent of ash vaporized in terms of the inherent metal oxide (SiO_2 + FeO + CaO + MgO + Na_2O + K_2O) content of the coal, rather than on an ASTM ash vasis, may be a more appropriate comparison of coals as it is only the inherent ash (see Chapter Five) that is exposed to the locally reducing environment and coal particle temperature overshoot during

TABLE 8.1

Ash Vaporized For Combustion of Bituminous
Coals at a 1750K Furnace Temperature in 20% Oxygen

Coal	Grams of Ash Vaporized/ Gram of Coal Burned	Percent of ASTM Ash Vaporized	Percent of Inherent Metal Oxides Vaporized
Illinois No. 6	.00124	0.90	1.88
Western Kentucky	.00119	1.74	2.19
West Virginia	.00148	0.96	1.36
Pittsburgh No. 8	.00119	1.63	2.16
Alabama Rosa	.00103	1.56	3.62
Utah	.00090	1.12	2.04
Utah Price No. 1	.00072	0.87	1.57
PSOC-3	.00035	1.00	1.15
PSOC-26	.00104	1.17	1.89
PSOC-130	.00111	1.90	2.93
PSOC-136	.00036	1.56	1.71
PSOC-997	.00044	0.84	1.11

TABLE 8.2

Ash Vaporized For Combustion of Low-Rank Coals at a 1750K Furnace Temperature in 20% Oxygen

Coal	Grams of Ash Vaporized/ Gram of Coal Burned	Percent of ASTM Ash Vaporized	Percent of Inherent Metal Oxides Vaporized
Lignites:			
Montana Savage	.00251	2.86	5.06
North Dakota	.00661	8.85	12.7
Texas	.00118	0.42	0.89
Subbituminous:			
Montana Rosebud	.00238	1.74	5.69
Montana Hardin	.00290	3.26	6.23
Montana Powder River	.00141	1.13	1.98
Wyoming Commanche	.00265	4.29	7.00
Wyoming Rawhide	.00252	3.40	5.42

combustion. For most of the low rank coals, a greater amount and percent of ash vaporized during combustion than for the bituminous coals. The North Dakota lignite had a maximum with nearly nine percent of its ash vaporizing. The amount of ash vaporized as reported in Tables 8.1 and 8.2 was determined from chemical analysis of the collected submicron material.

The selection of a coal also has an important impact on the composition of the submicron ash with the most pronounced differences again occuring with coal rank. As shown in Table 8.3, combustion of bituminous coals yields submicron ash composed mostly of SiO_2 and FeO with Na_2O occassionally present at comparable concentrations. In comparing the submicron ash with that of the bulk ash (Appendix A), relatively volatile species such as Na_2O and K_2O are mostly enriched as might be expected, whereas highly refractory ash components such as CaO and Al_2O_3 are significantly depleted. As oxides, SiO_2 and FeO are not likely to vaporize appreciably. However, their abundance in the submicron ash suggest that reduction to more volatile forms such as SiO and iron metal has occured under the locally reducing enviornment within burning char particles.

The composition of the submicron ash generated from combustion of low rank coals is quite different from that of the bituminous coals as shown in Table 5.4. With the exception of the Texas lignite, the combination of MgO and FeO dominate the refractory compounds present, with SiO_2 weight percents

TABLE 8.3

Submicron Ash Composition for Combustion of Bituminous Coals in 20% Oxygen at a Furnace Temperature of 1750K

Coal	SiO_2	FeO	MgO	CaO	Al_2O_3	K_2O	Na_2O	TiO_2	Cl	P_2O_5
Illinois No. 6	34.6	26.0	1.9	0.68	1.6	15.6	14.5	----	----	0.51
Western Kentucky	35.1	40.5	1.3	0.47	1.9	13.7	4.5	----	----	2.4
West Virginia	34.7	21.8	1.6	0.59	0.81	10.6	11.8	0.70	0.23	17.2
Pittsburgh No. 8	41.2	18.4	2.9	1.4	1.3	11.2	16.6	0.63	0.37	5.9
Alabama Rosa	19.6	47.4	3.7	1.1	1.9	4.6	14.7	0.47	2.9	2.3
Utah	26.0	15.8	6.1	0.56	1.6	5.8	30.0	0.24	0.44	13.3
Utah Price #1	24.0	23.0	3.5	0.53	2.4	4.0	24.9	----	1.4	16.4
PSOC-3	30.0	22.4	3.9	2.1	2.7	<1.0	35.1	3.1	----	0.57
PSOC-26	28.1	43.5	0.80	1.6	2.4	14.7	6.6	0.48	0.38	1.4
PSOC-130	35.8	39.3	6.8	4.2	1.7	1.5	6.9	----	1.6	2.0
PSOC-136	31.5	28.1	9.3	7.9	1.8	10.0	7.6	1.9	0.84	1.1
PSOC-997	33.8	15.7	2.8	1.1	4.1	13.3	25.3	1.9	0.68	1.5

TABLE 8.4

Submicron Ash Compostion for Combustion of Low Rank Coals at a Furnace Temperature of 1750 K in 20% Oxygen

Coal	SiO_2	FeO	MgO	CaO	Al_2O_3	K_2O	Na_2O	TiO_2	Cl	P_2O_5
Lignites:										
Montana Savage	3.67	11.5	64.4	7.8	0.56	1.4	3.7	----	0.40	6.5
North Dakota	1.62	20.3	18.9	2.6	0.27	0.82	54.6	----	0.45	0.64
Texas	38.5	37.0	7.0	0.45	1.5	5.1	8.9	----	0.64	6.5
Subbituminous:										
Montana Rosebud	17.5	35.4	27.2	6.6	0.80	3.6	6.5	----	0.19	2.2
Montana Hardin	7.3	7.2	20.0	5.8	0.43	2.6	53.4	----	1.6	1.8
Montana Powder River	9.9	7.1	61.0	10.4	0.78	3.8	5.7	----	0.23	1.1
Wyoming Commanche	3.2	35.2	31.3	6.9	0.83	0.94	16.3	----	0.12	5.3
Wyoming Rawhide	6.5	38.9	30.5	8.1	0.54	0.52	9.6	----	1.1	4.3

being significantly lower than the values for bituminous coal combustion fumes. For two of the low rank coals, the North Dakota lignite and the Montana Harlin Na_2O is observed to be the major component of the submicron ash. These coals contain the highest concentration of sodium, the values of which are reported in Table 5.5. Sodium in oxide, chloride, metal or sulphate form is the most volatile of the metals listed in these Tables. Magnesium in oxide form is one of the more refractory compounds present in coal ash. However, under the locally reducing conditions within burning coal particles, magnesium metal vapor may evolve as a result of reduction of the oxide. Magnesium metal boils at a temperature well below the combustion temperature of the experiments described here. The low rank coals contain higher concentrations of magnesium, much of which is bound organically, than the bituminous coals as seen in Tables 5.4 and 5.5 in Chapter Five.

Although a detailed discussion of thermochemical vaporization mechanisms is reserved for Chapter Ten, the importance of a locally reducing environment on the relative volatilization behavior of these elements can be seen in the comparison of metal and metal oxide boiling points as shown in Table 8.5.

The composition and total amount of submicron ash generated during coal combustion depends on the relative vaporization rates of individual mineral matter components present in the coal. This in turn depends upon their distribution and concentration in the coal as well as other factors, primarily combustion condition as will be shown. The relationships

Table 8.5

Comparison of Metal
and Metal Oxide Boiling Points (K)

Element	Metal B.P.	Oxide B.P.
Mg	1379	3533
Ca	1757	3123
Fe	3145	3687 (decomposes)
K	1037	1154 (decomposes)
Na	1156	2223 (decomposes)
Al	2740	>3500

Source: JANAF Thermochemical Tables, 1971.

between the vaporization behavior of elements and the mineral matter characteristics is discussed at length later in this Chapter for specific elements. For the present, it is observed that for bituminous coals, which have in general similar mineral matter characteristics and compositions, a rough correlation exists between inherent ash content and ash vaporized as shown in Figure 8.1.

8.3 The Dependence of Ash Vaporization on the Combustion Condition and on the Size of the Pulverized Coal

By systematic variation of the oxygen partial pressure in the furnace main gas, the temperature history of combustion of the coal could be varied. As described in Chapter Six, increasing the oxygen partial pressure in the system results in an increase in the combustion rate of the coal particles and particle temperatures that significantly overshoot the gas temperature. The Illinois No. 6, the Alabama Rosa and the Montana Savage lignite were burned in a range of oxygen partial pressures at a furnace wall temperature of 1750K. The submicron ash, corresponding to the vaporized ash, was collected and retained for elemental analysis. In addition, the effects of initial coal size on the extent of ash vaporization was investigated. The results of these experiments are reported in this section.

The variation in the fraction of ash vaporized with oxygen partial pressure in the furnace for combustion of the Illinois No. 6 bituminous coal is shown in Figure 8.2. The furnace wall temperature was maintained at 1750K for all

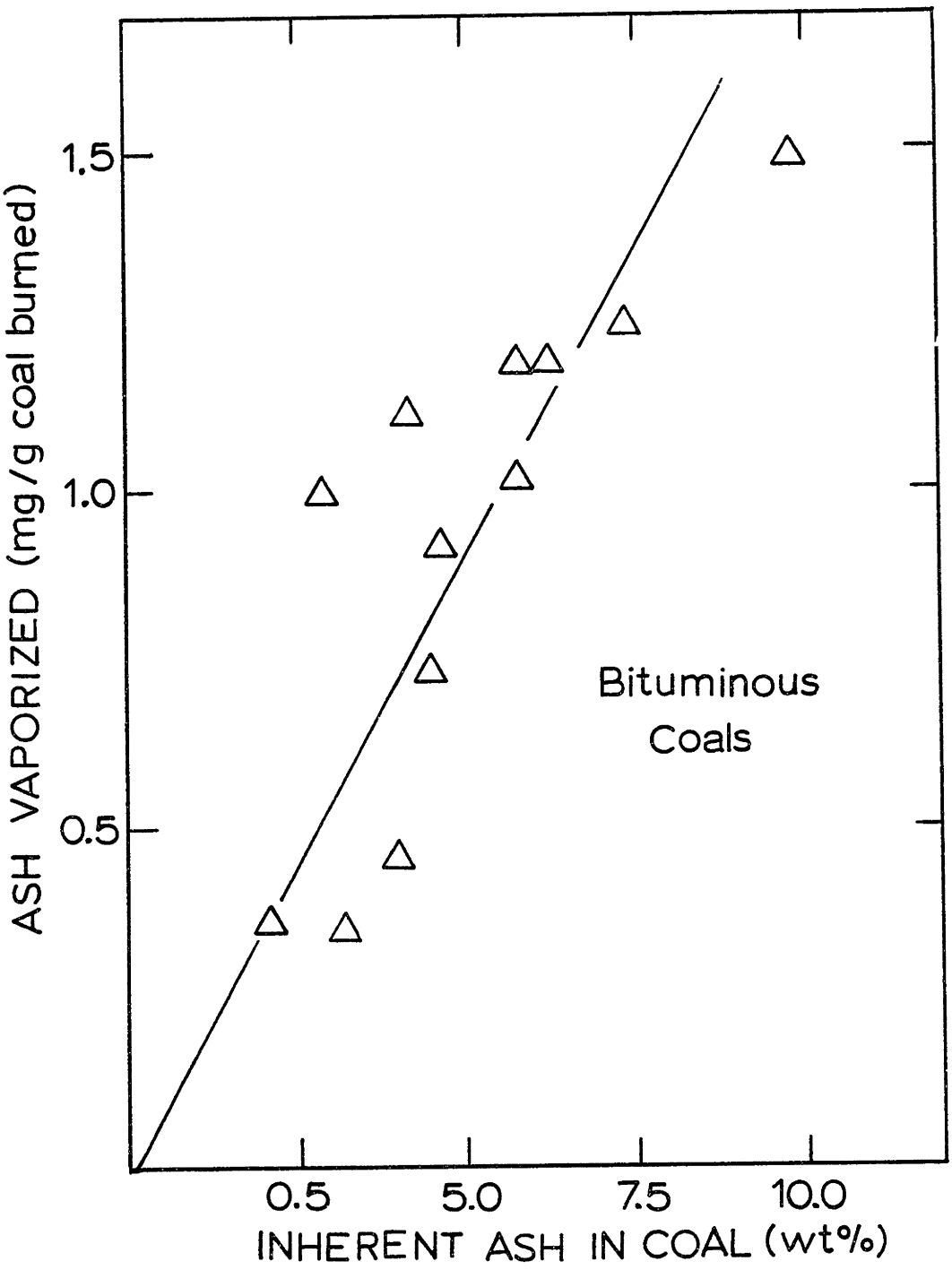

Figure 8.1 Correlation of Ash Vaporized at 1750K in 20% Oxygen with Inherent Ash Content of Bituminous Coals

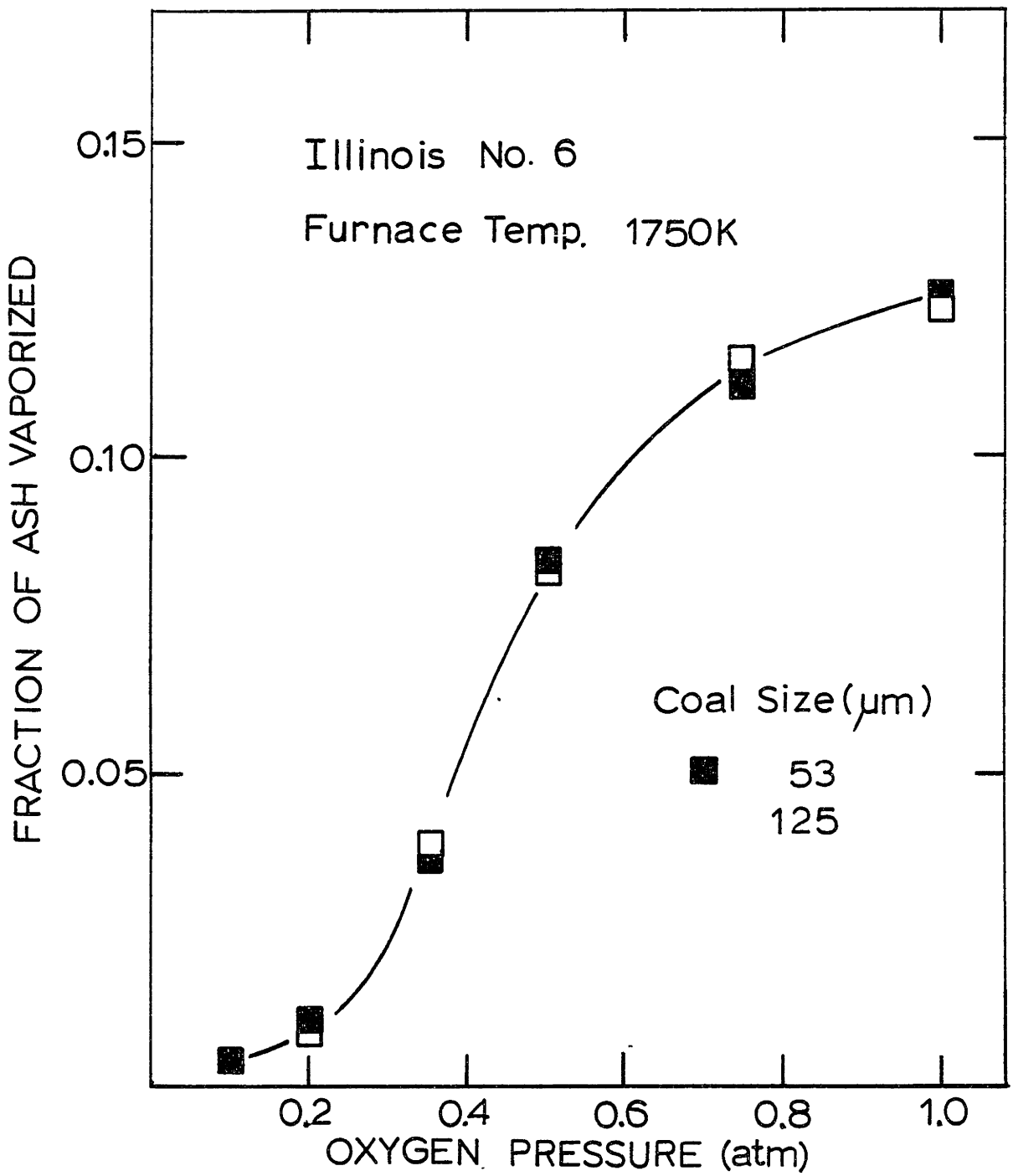

Figure 8.2 The Effect of Oxygen Partial Pressure and Coal Size on the Vaporization of Ash. Illinois No. 6

experiments. As it might be expected, increasing the particle combustion temperature significantly and systematically results in an increase in the amount of ash vaporized. For this coal however, there is no significant dependence on the initial size of the coal particles. The maximum amount of ash vaporized in 100 percent oxygen, was 12.5 percent of the total ash in the coal. A similar result was obtained for the Alabama Rosa No. 18 bituminous coal, as shown in Figure 8.3.

The effect of temperature and initial particle size on the ash vaporized during combustion of the Savage lignite is shown in Figure 8.4. A greater fraction of the lignite ash vaporized during combustion compared to the bituminous coals. Furthermore, the fraction of lignite ash vaporized is slightly dependent on the initial size of the lignite particles, with the effect increasing with combustion temperature.

The composition of the submicron ash samples obtained in the above described experiments were determined by the elemental methods described in Chapter Four. These results are presented in Figures 8.5, 8.6 and 8.7. Because of the highly oxidizing bulk gas pahse in the furnace, metal oxides was the assumed chemical form of the submicron ash. It is likely that the alkalis and, possibly the alkaline earths, are actually in sulphate form (Neville, 1981) und the present experimental conditions.

As shown in Figure 8.5, the composition of the submicron ash generated during the combustion of the Montana Savage lignite is sensitive to the combustion temperature. At the

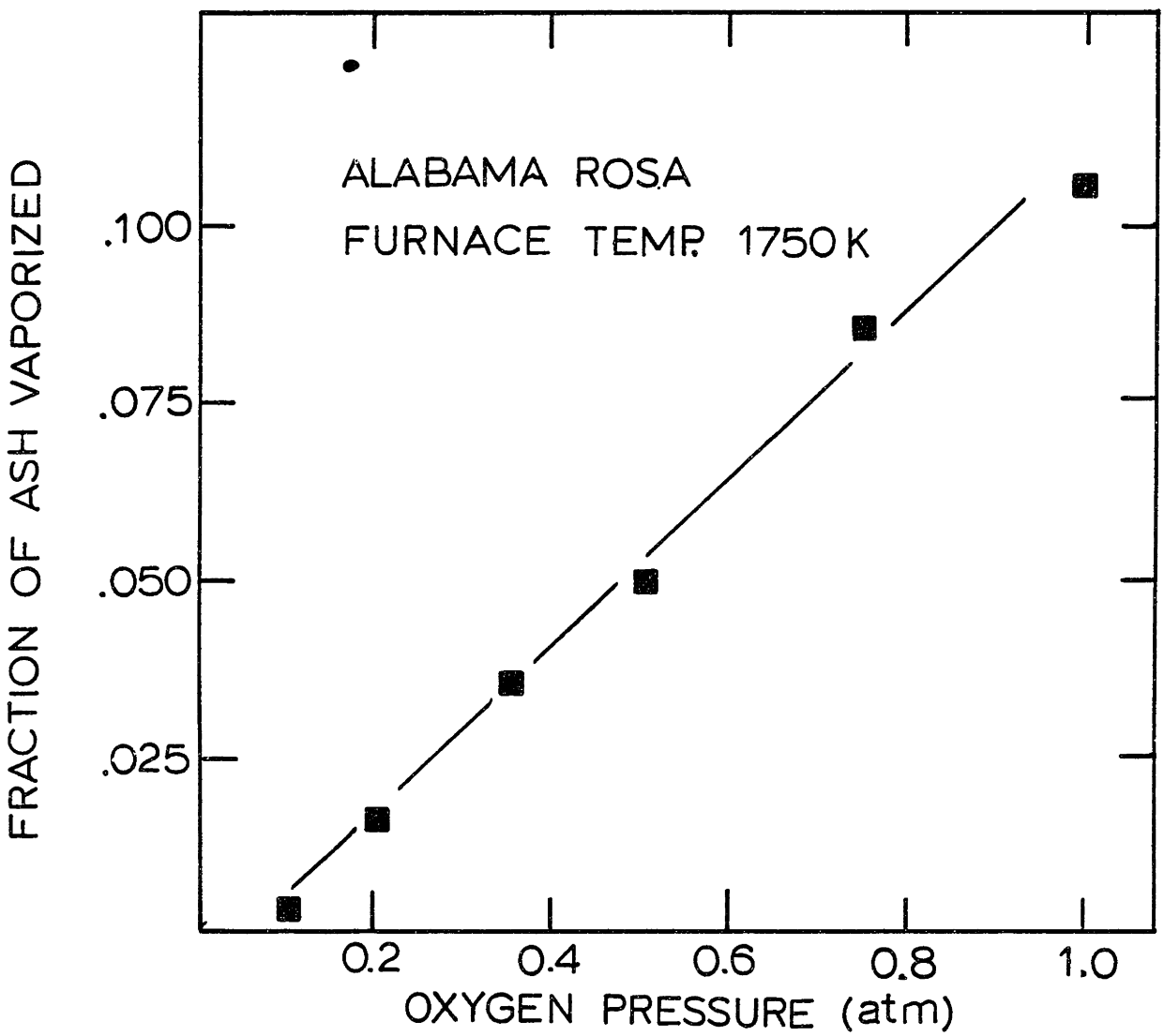

Figure 8.3 The Effect of Oxygen Pressure on the Vaporization of Ash. Alabama Rosa

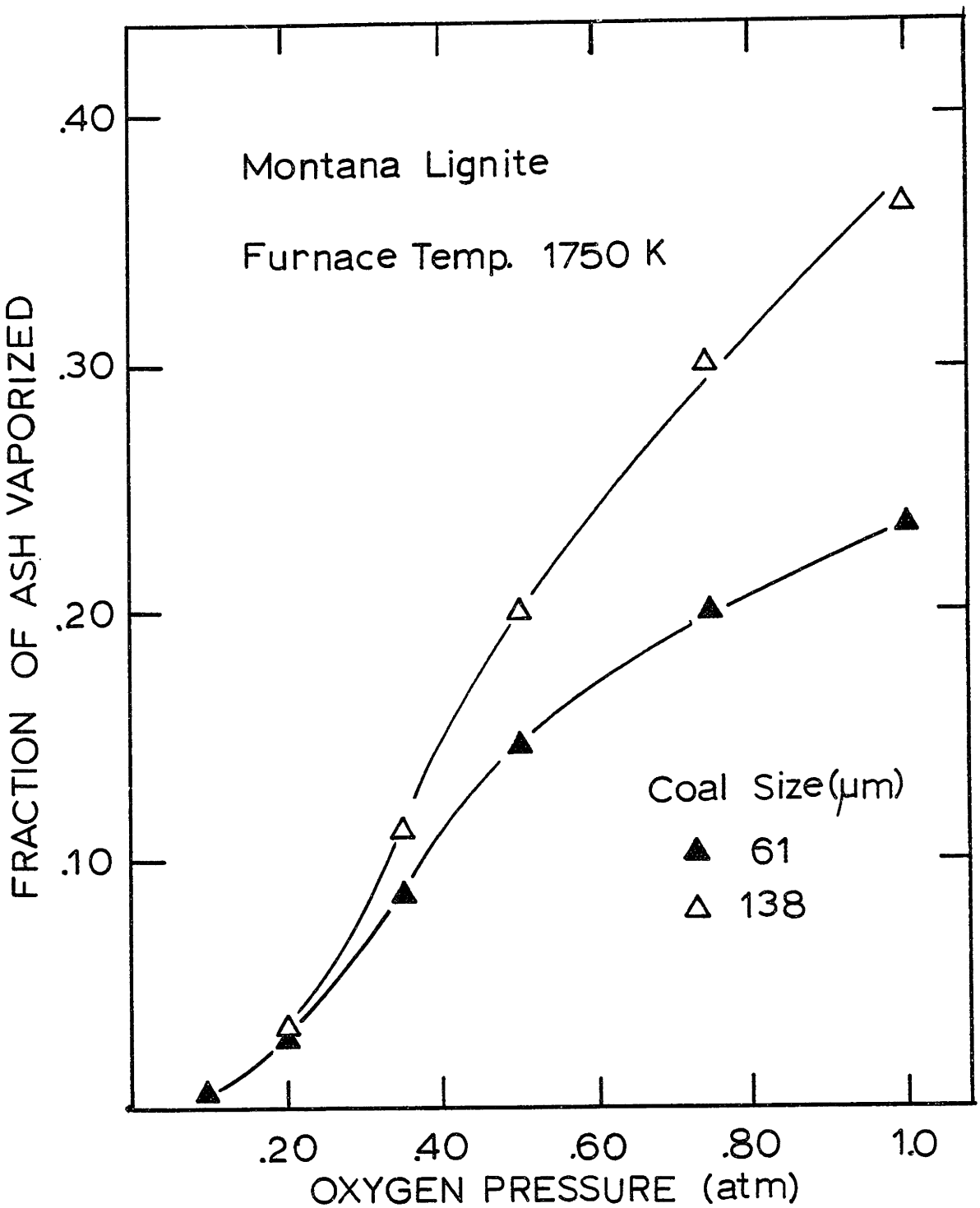

Figure 8.4 The Effect of Oxygen Partial Pressure and Coal Size on the Vaporization of Ash. Montana Lignite

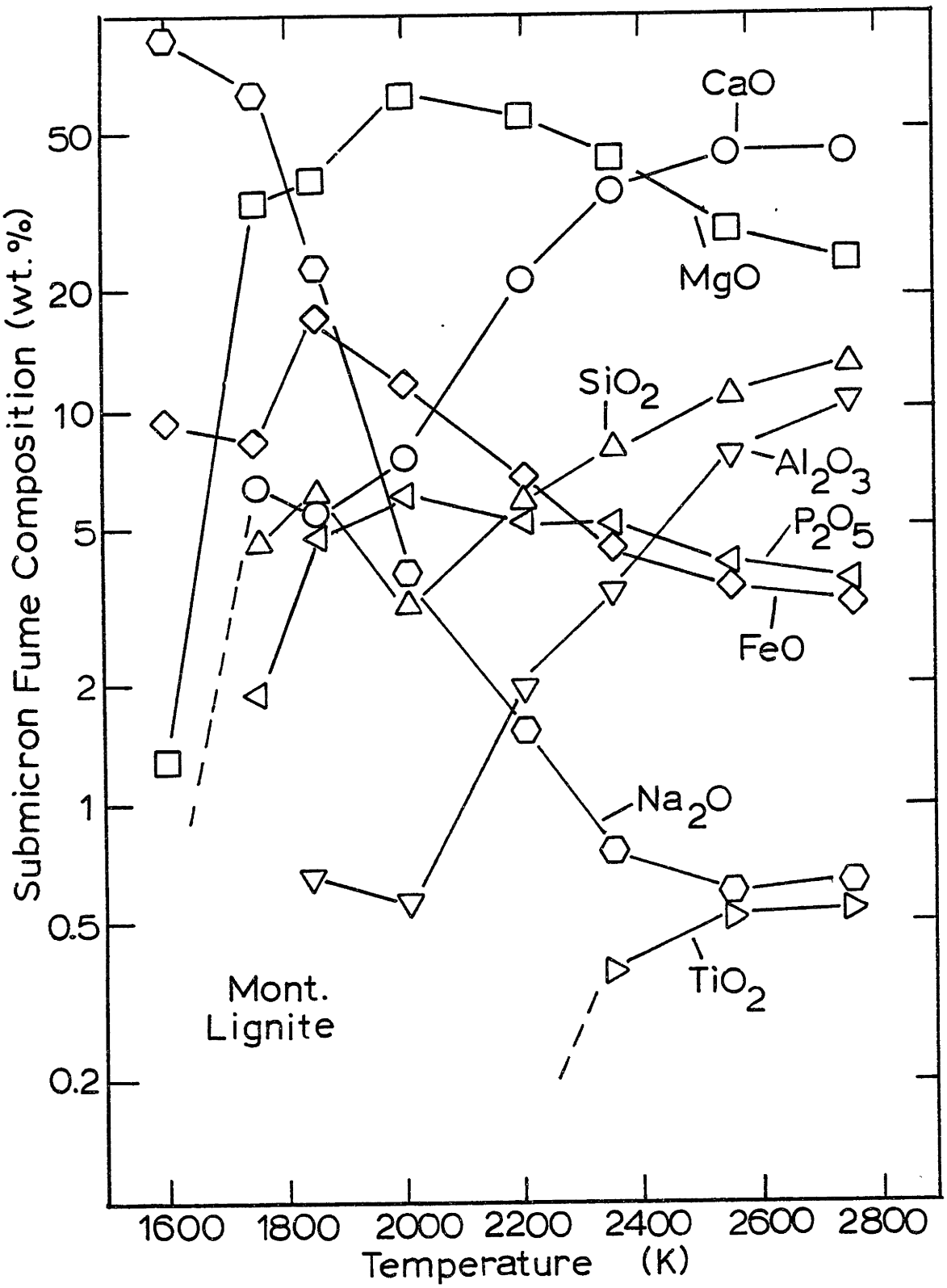

Figure 8.5 The Effect of Combustion Temperature on the Submicron Fume. Montana Lignite

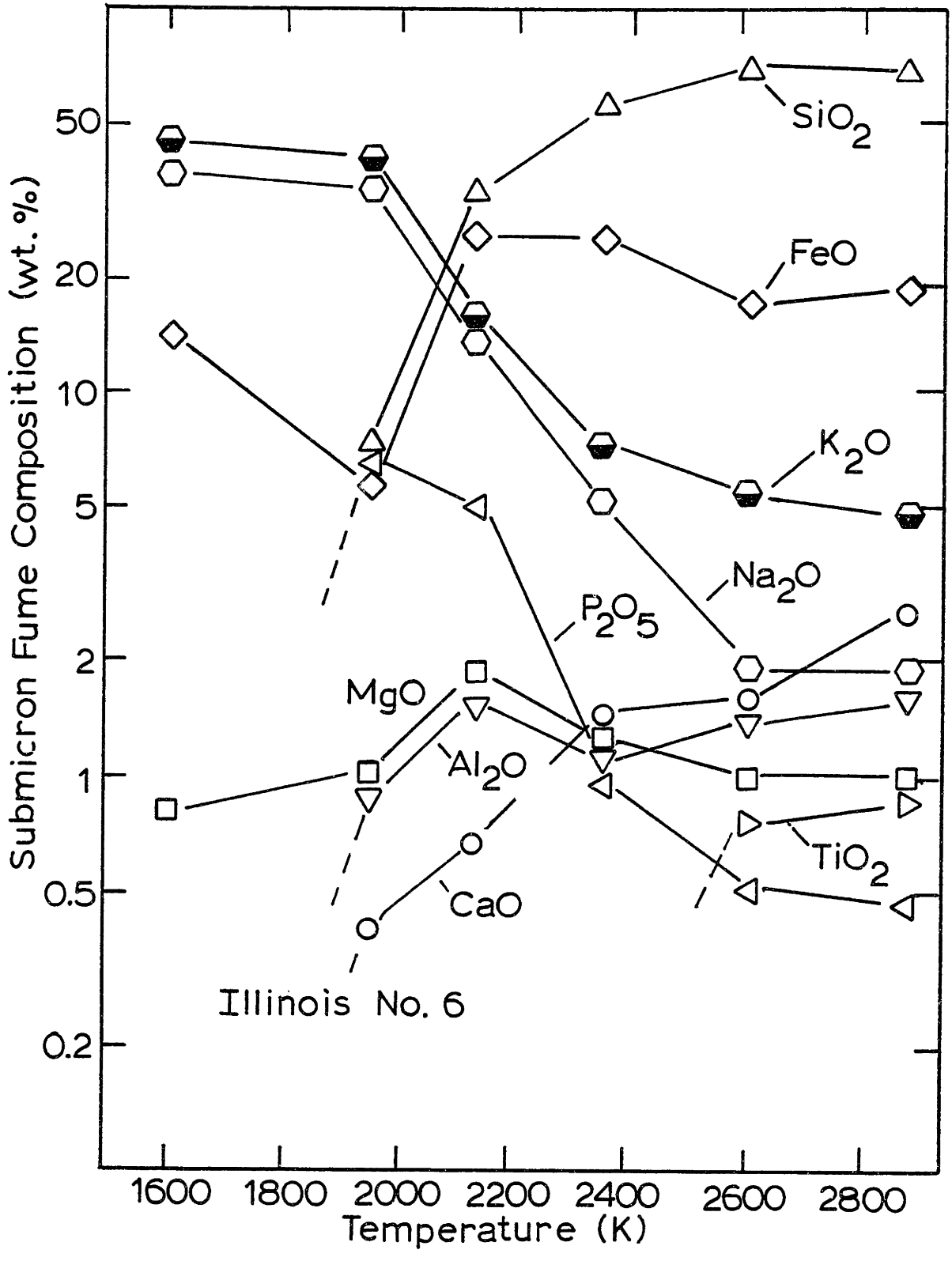

Figure 8.6 The Effect of Combustion Temperature on the Composition of Submicron Ash. Illinois No. 6

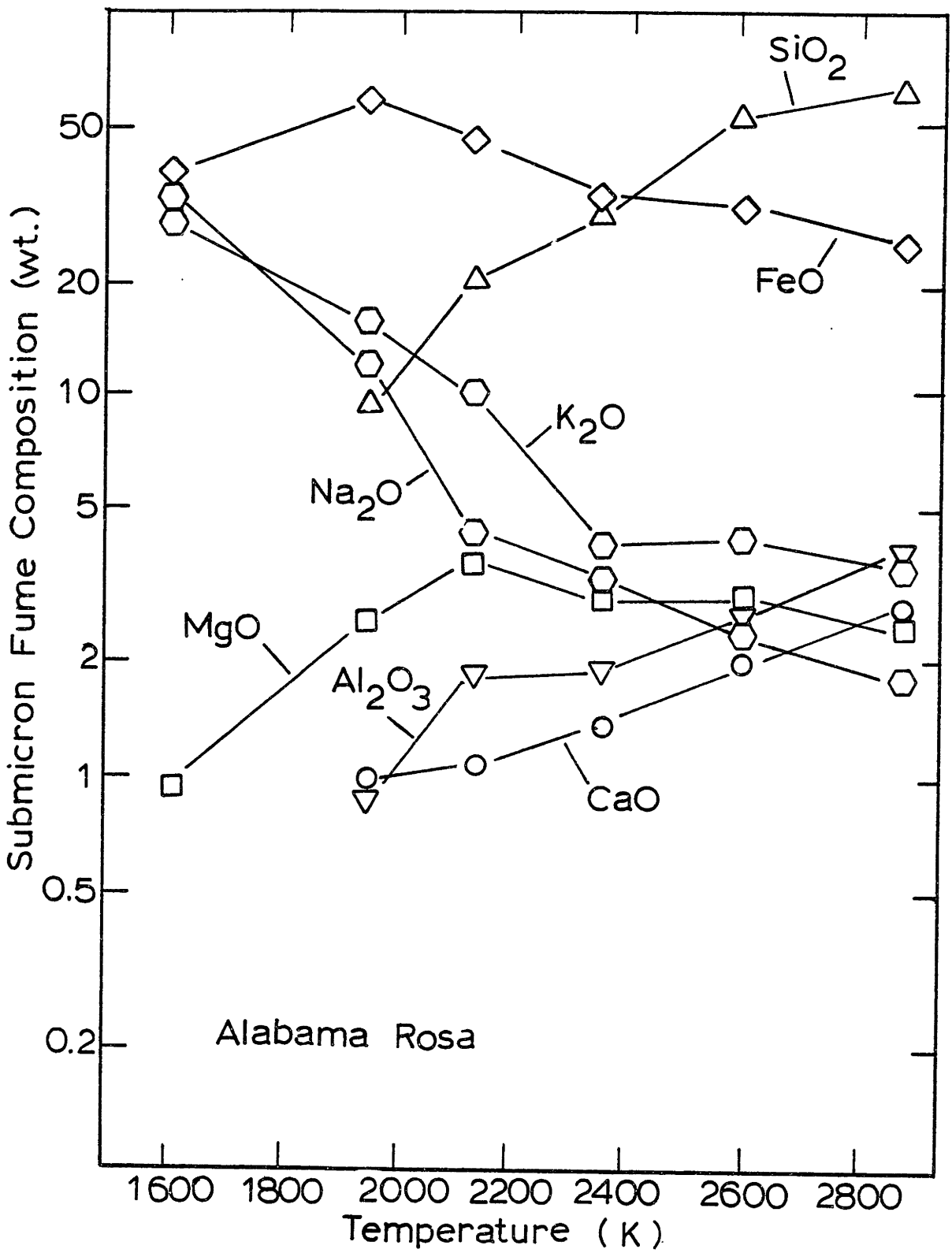

Figure 8.7 The Effect of Combustion Temperature on the Composition of Submicron Ash. Alabama Rosa

lowest combustion temperature (1600K), Na_2O is the major metal oxide component. With increasing combustion temperature, the refractory MgO begins to dominate the fume composition and at still higher combustion tmeperatures CaO is the major component. With increasing combustion temperature, the fume composition approaches that of the coal ash composition. The dependence of fume composition or combustion temperature is a reflection of the activated nature of the volatilization process. For example, although sodium is only present at trace levels in the coal (170 ppm), it is considerably more volatile in oxide or elemental form than MgO or CaO. It will be shown in Chapter Ten that magnesium and calcium vaporize by reduction of the oxide to the volatile metal vapors. Thermodynamically, reduction of these refractcry oxides becomes less unfavorable with increasing temperature. Furthermore, the nature of the combustion processes is such that the reducibility of the local environment within a char particle burning in a highly (external) oxidizing environment increases with increasing combustion temperature.

The variation in the composition of the combustion generated submicron material with the temperature of combustion for the Illinois No. 6 bituminous coal is shown in Figure 8.6. With increasing combustion temperature, the dominant refractory oxide component of the fume becomes SiO_2. In contrast to the lignite, the alkaline oxides MgO and CaO in this case are of minor importance. However, a similar trend for the alkali oxide content of the fume with combustion temperature is observed.

Specifically, the alkalis dominate the composition of the submicron fume.

In Figure 8.7, the variation in the composition of the submicron ash with combustion temperature is shown for the Alabama Rosa bituminous coal. At the lowest combustion temperatue examined (~ 1950K), the iron oxide was found to be the major submicron ash component. At higher temperatures, SiO_2 is the major component.

8.4 Silicon Volatilization

The elemental silicon contents of the raw coals examined in this study range from about 0.5 percent up to 8.0 percent. As it occurs in the form of quartz and clay mineral grains, silicon is heterogeneously distributed throughout the organic matter of coal particles. On the average for the twenty coals, nearly 30 percent of the silicon was found to be associated with the extraneous minerals. In comparing individual coals, however, the percent of silicon in the raw coal occurring with the extraneous minerals ranged from less than 3 to over 50 (Tables 5.8 and 5.9). Thus only a fraction of the silicon in the coal is exposed to the temperature of particle combustion and the locally reducing environment within the burning particles. In Chapter Ten, the effects of a locally reducing environment on the vaporization of silicon are discussed in detail. To provide a basis for comparison of the vaporization of silicon for the combution of different coals, only the inherent silicon in the coal is considered. The results presented in Figure 8.8 compare the amount of silicon vaporized per unit mass of coal

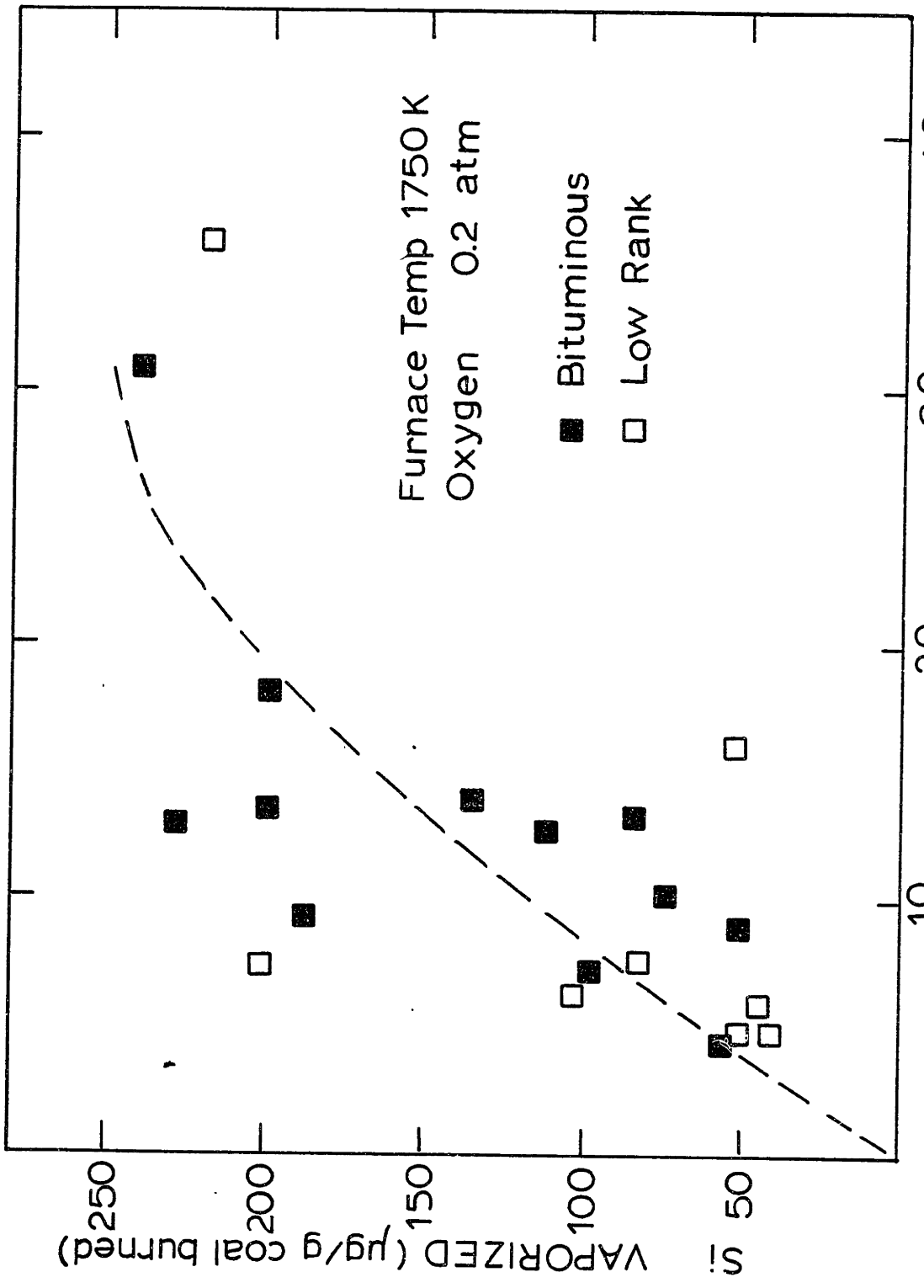

Figure 8.8 Correlation of Silicon Vaporized During Combustion with Inherent Silicon Content of Coals

burned with the inherent silicon content of the coal. The combustion condition in all cases was that of 1750K furnace wall temperature and a 20 percent oxygen - 80 percent nitrogen gas mixture. These results indicate that there is no obvious correlation between the amount of silicon vaporized and the inherent silicon content of the coal or, for that matter, with the rank of coal. In the inherent silicon content range of 0.5 to 1.5 percent there is great variability in the amount of silicon vaporized. Possible reasons behind the variability may include the activity of silica (SiO_2) in the char and the frequency of the occurance of silica containing minerals in the coal particle population. For example, increasing silicon content may be associated with increasing frequency of occurance of silica containing coal particles. In Chapter Nine, it will be shown by microscopic examination that not all of the char particles contain silica or the same ash composition.

The dependence of silicon vaporization with combustion condition will now be considered for selected coals. The amount of silicon vaporized (per unit mass of coal burned) at various oxygen partial pressures in the furnace is shown in Figure 8.9 for combustion of the Illinois No. 6 and the Alabama Rosa bituminous coals. Increasing the oxygen partial pressure in the furnace increases the combustion temperature of the coal particles and, as a result, the amount of silicon vaporized is also increased. For the Illinois No. 6, the size of the coal feed does not affect the amount of silicon vaporized per unit mass of coal burned at any of the examined combustion

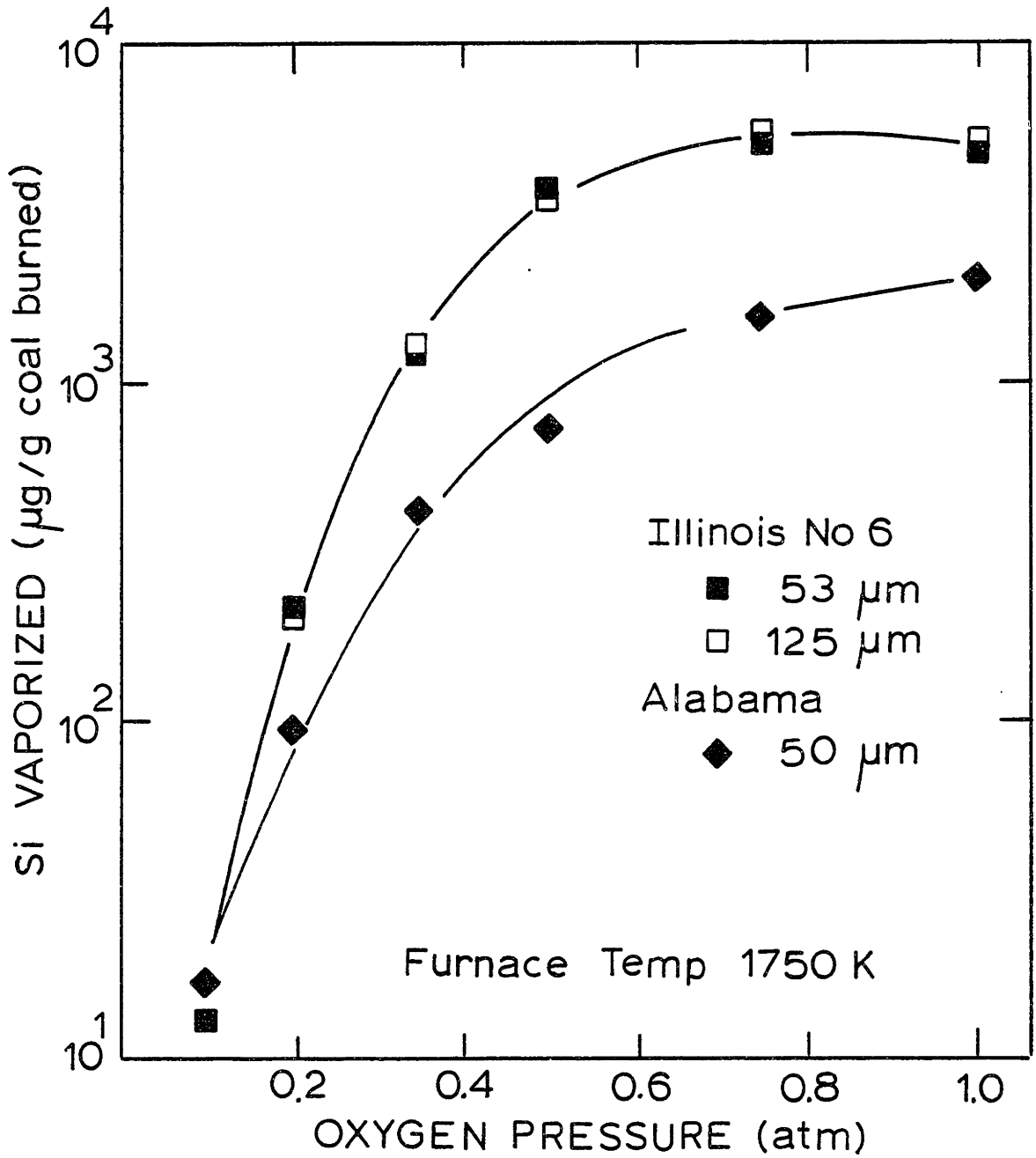

Figure 8.9 The Effect of Oxygen Partial Pressure on Silicon Vaporization. Illinois No. 6 and Alabama Rosa

conditions. At the higher oxygen partial pressures, considerably less silicon vaporized during combustion of the Alabama coal than for the Illinois No. 6. This finding is to be considered in light of the density fraction studies reported in Chapter Five. Nearly 82 percent of the Alabama coal (1.4 float fraction) had a silica content of about 2000 ppm (Figure 5.6). For combustion in 100 percent oxygen, this corresponds to nearly complete vaporization of the silicon for the 1.4 float fraction of the Alabama coal. Under similar reasoning, from Figure 5.6 it can be seen that for 82 percent of the Illinois No. 6 recovered in a coal float fraction (specific gravity less than 1.62) has a silicon content of about 18,000 ppm.

The effect of conditions on the vaporization of silicon for combustion of the Montana Savage lignite was also investigated. In addition to burning the raw lignite at various conditions, samples of the lignite after removal of the ion-exchangable calcium, magnesium and alkalis by ammonium acetate extraction were burned. Silica and the alkaline oxides (CaO + MgO) are strongly interacting compounds at high temperatures. Stable high melting point silicate compounds or melts of low silica activity may form at combustion temperatures. The raw lignite contains high concentration of calcium, much of which is organically bound. The purpose of burning samples of acid-treated lignite was to determine if these basic (MgO + CaO) components affect the volitilization of silica. The results are presented in Figure 8.10. As is evident, there is no significant difference in the amount of silicon vaporized per gram of coal burned between the cases of raw lignite and acid treated lignite. Increasing

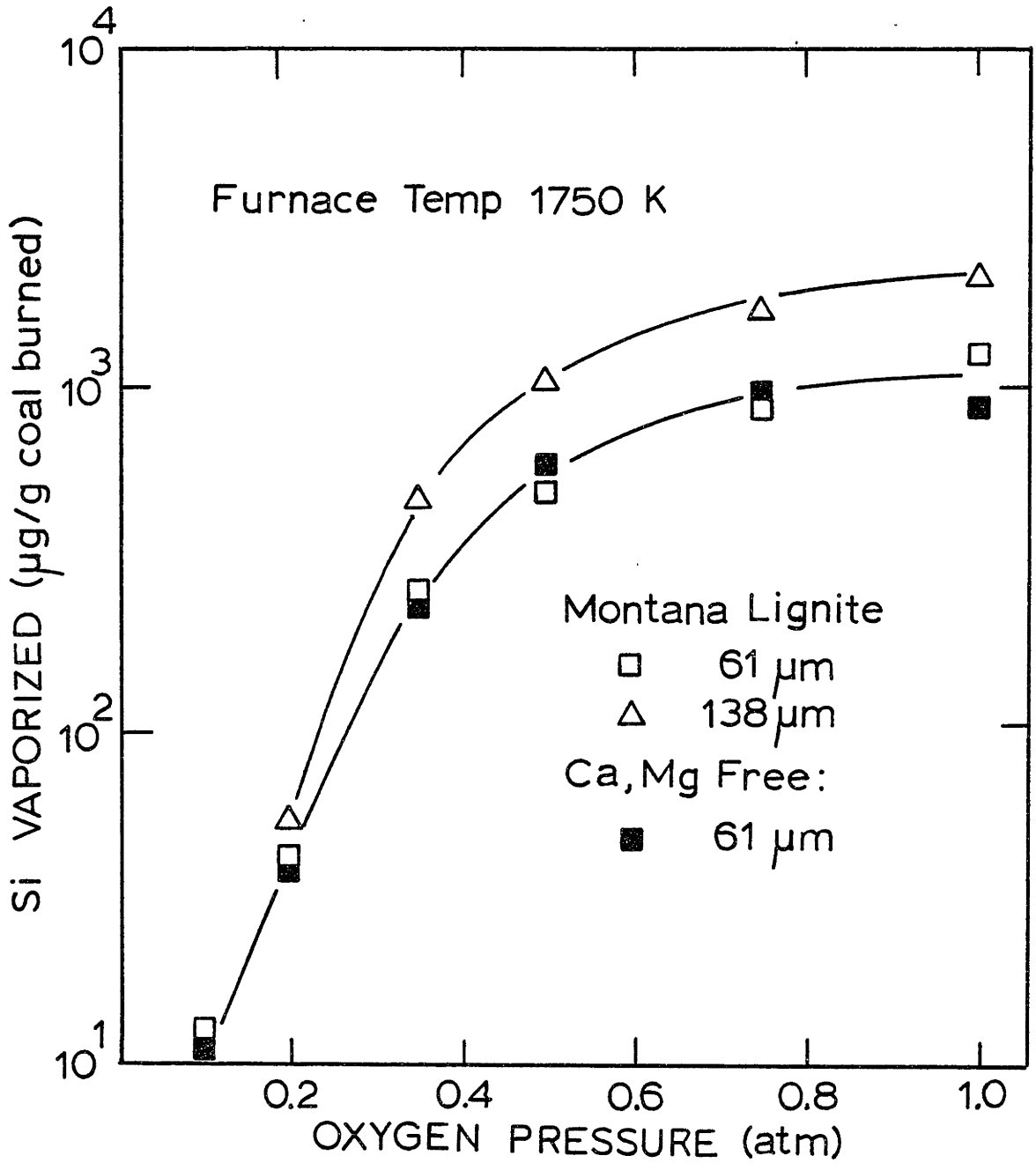

Figure 8.10 The Effect of Oxygen Partial Pressure on Silicon Vaporization. Raw Montana Lignite and Acid Washed Lignite

the oxygen partial pressure of the combustion temperature does result in significant increases in the vaporization of silicon, particularly at the lower temperature conditions. There is also a slight dependence of silica vaporization on the particle size of the lignite. Although this dependence is not significantly above experimental error (20%), it is constant over a range of combustion conditions.

8.5 Iron Volatilization During Combustion

The effect of the inherent iron content of the coal on the amount of iron vaporized per gram of coal burned at 1750K in 20 percent oxygen is shown in Figure 8.11. The effects of coal rank and iron-bearing mineral forms on the volitilization of iron are striking. The iron-bearing mineral forms in the raw coal were determined by the Mössbaver method as described in Chapter Five and Appendix C. Pyrite was the only form of iron present in the low rank coals. The fraction of iron vaporized during combustion of the lignites and subbituminous coals is seen to be significantly greater than that for bituminous coals. Furthermore, bituminous coals which were observed to contain iron-bearing clays (illite) and carbonates (siderite) vaporized a greater fraction of the iron during combustion than bituminous coals containing only pyrite or sulphate forms of iron. Linear correlations between inherent iron content and the amount of iron vaporized are obtained for the three discussed classes of behavior. A notable exception is the Texas lignite which appeared to correlate with the bituminous coals. Explanations for these observations are proposed in

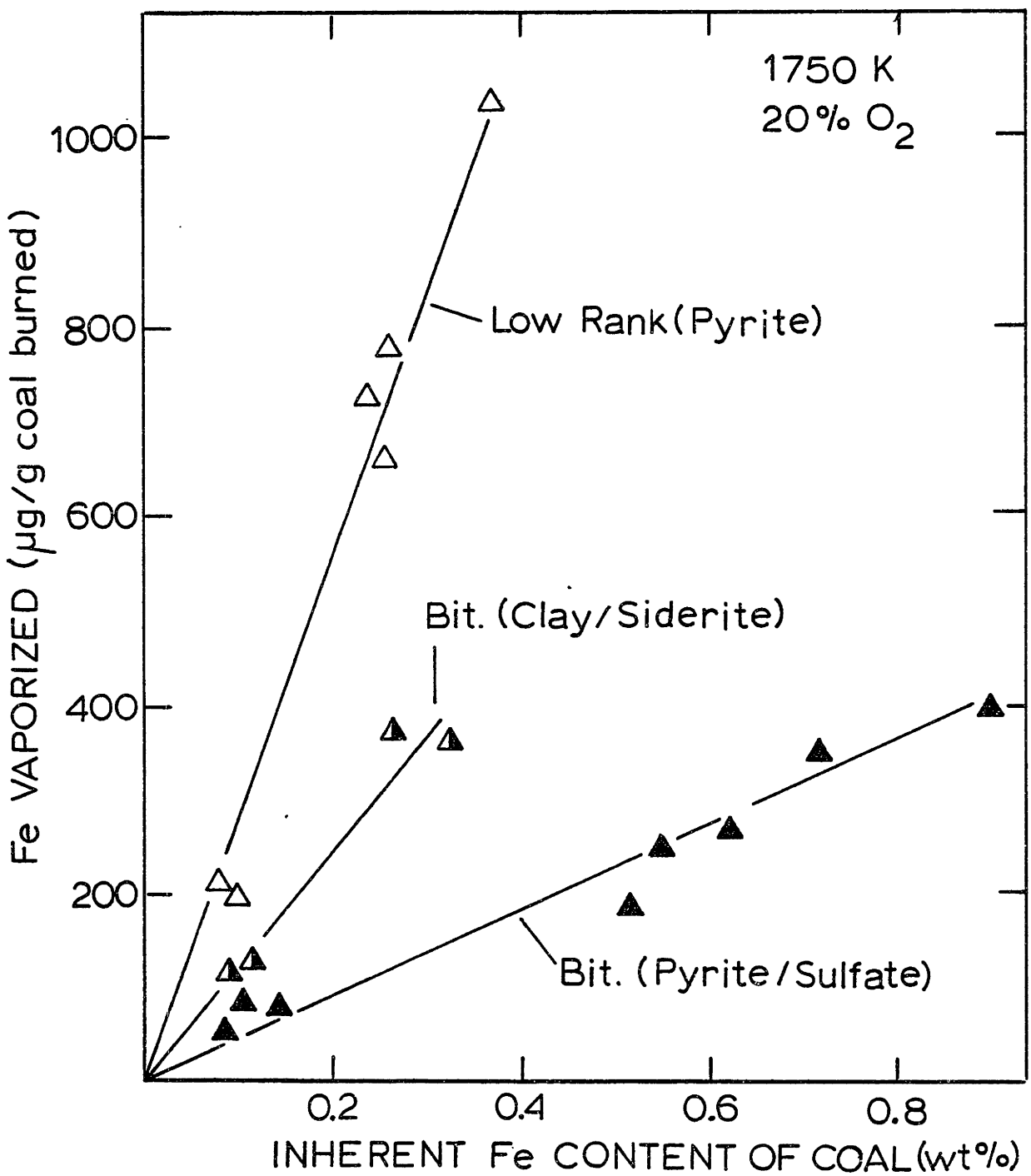

Figure 8.11 The Effect of Coal Type and Iron Bearing Mineral Forms on the Vaporization of Iron

Chapter 10.

The dependence of iron vaporization on oxygen partial pressure is shown in Figure 8.12 for the Illinois No.6, the Alabama Rosa and the Montana Savage lignite. The amount of iron vaporized per gram of coal burned is strongly dependent on oxygen partial pressure or combustion temperature in the range of .05 to .40 oxygen partial pressure but weakly dependent at higher oxygen partial pressures.

In Chapter Five it was shown that a major portion of the pyrite present in coals is extraneous. Extranseous pyrite would not be exposed to the reducing environment within coals, but rather, would undergo rapid oxidation or combustion in the oxidizing main gas. In a separate experiment, pyrite particles (<100 μm) were injected into the furnace to determine if pyrite combustion by itself results in significant iron volitilization and formation of an iron oxide (or sulphate) submicron fume. The impactor was again used to size classify the products (particulates) of pyrite combustion. These results are reported in Table 8.6. No chemical or elemental analysis was performed. Weight analysis, however, does indicate a bimodal size distribution, indicating iron vaporization and fume formation. If it is assumed that all of the material on the final filter is in the form of FeO, then these results would indicate that extraneous pyrite in coals contributes negligibly to iron vaporization under these oxidizing furnace conditions.

8.6 Magnesium and Calcium Volitilization During Combustion

The distribution of magnesium in the raw coals is strongly dependent on coal rank. In lignites and subbituminous coals,

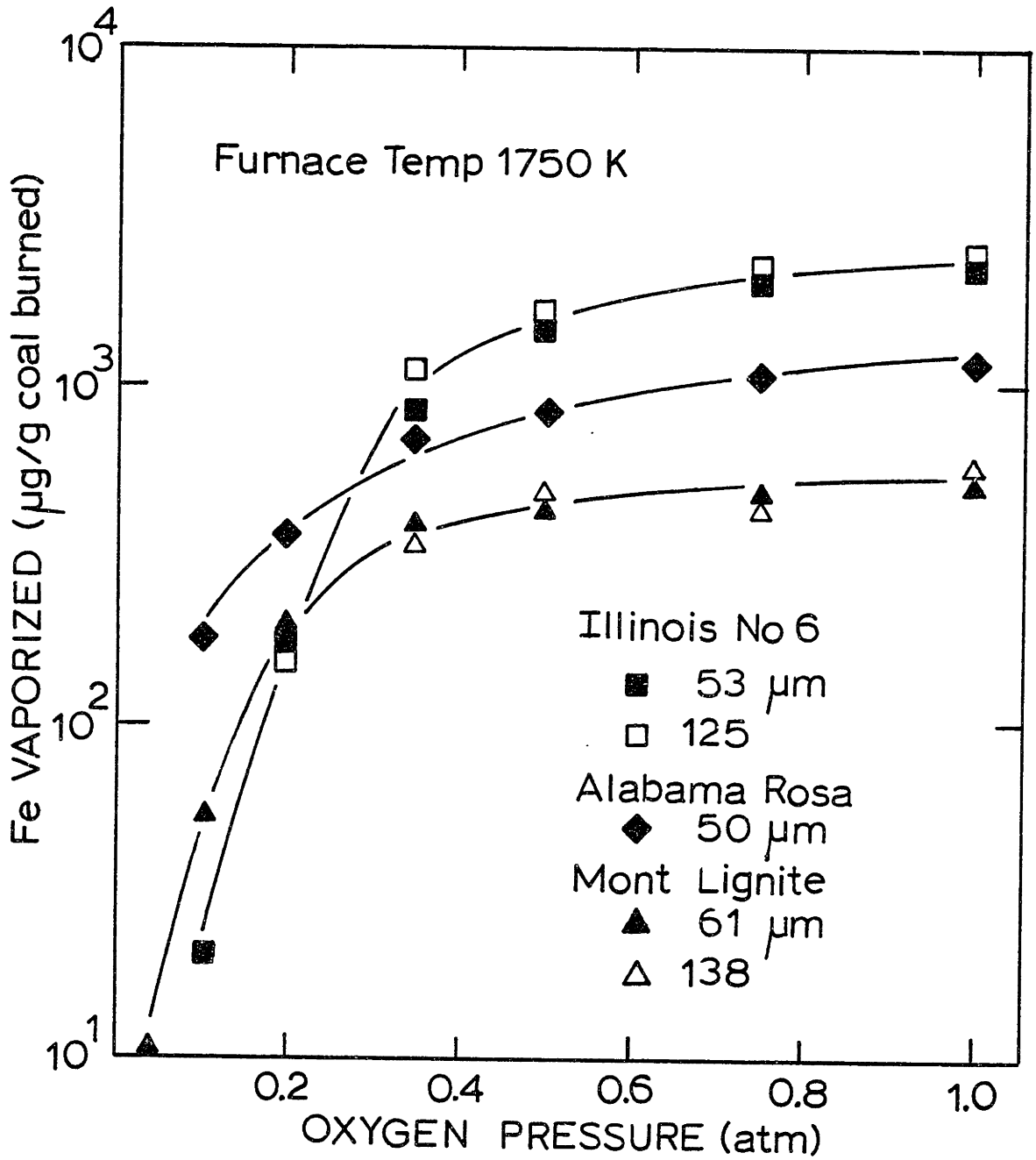

Figure 8.12 The Effect of Oxygen Pressure on the Vaporization of Iron

TABLE 8.6

Size Distribution of Particulate Products
Obtained From Combustion of Pyrite in 20% Oxygen
at 1750K (gram/gram pyrite burned)

Cascade Impactor Stage	Grams Collected
0	.4093
1	.0536
2	.0090
3	.0131
4	.0068
5	.0018
6	.0002
7	.0001
Final Filter	.0010

much of the magnesium is automatically distributed throughout the organic matter of the coal ion-exchanged on carboxylic groups. In bituminous coals, the magnesium is associated with carbonate minerals (dolomite) or in clay minerals as a minor component and, as described in Chapter Five, only a fraction of these minerals are included in the carbonaceous matrix or pulverized coal particles.

The variation in the amount of magnesium vaporization with the inherent magnesium content per gram of coal burned at 1750K in 20 percent oxygen is shown in Figure 8.13. The results indicate that for low rank coals the amount of magnesium vaporized is proportional to the concentration of magnesium vaporizing at this combustion condition. There is considerable less inherent magnesium in the bituminous coals and, as a consequence, signficantly less magnesium is volatilized during combustion.

The variation of the amount of magnesium vaporized with oxygen partial pressure in the furnace, or, equivalently with particle combustion temperature, is shown in Figure 8.14 for selected coals. The vaporization of magnesium increases sharply with increasing oxygen partial pressure in the range of 0.05 to 0.40 atmosphere and then levels off at the higher oxygen partial pressures.

The distribution of calcium in coals is similar to that of magnesium. Much of the calcium in low rank coals is organically bound. Hence, these coals contain high concentrations of inherent calcium. In bituminous coals, calcium is in the mineral forms of calcite, domite or bassanite and these

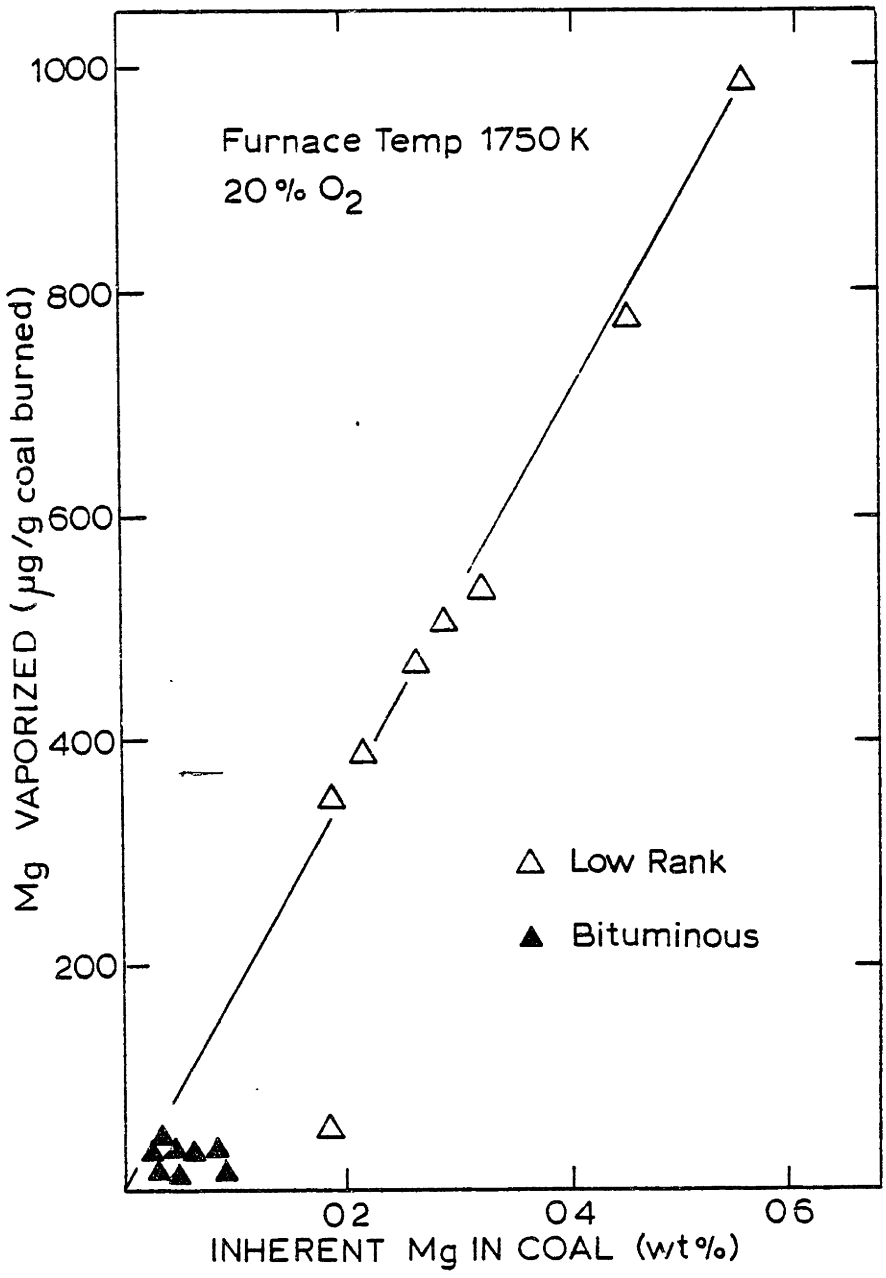

Figure 8.13 The Effect of Magnesium Content of Coal on Magnesium Vaporization

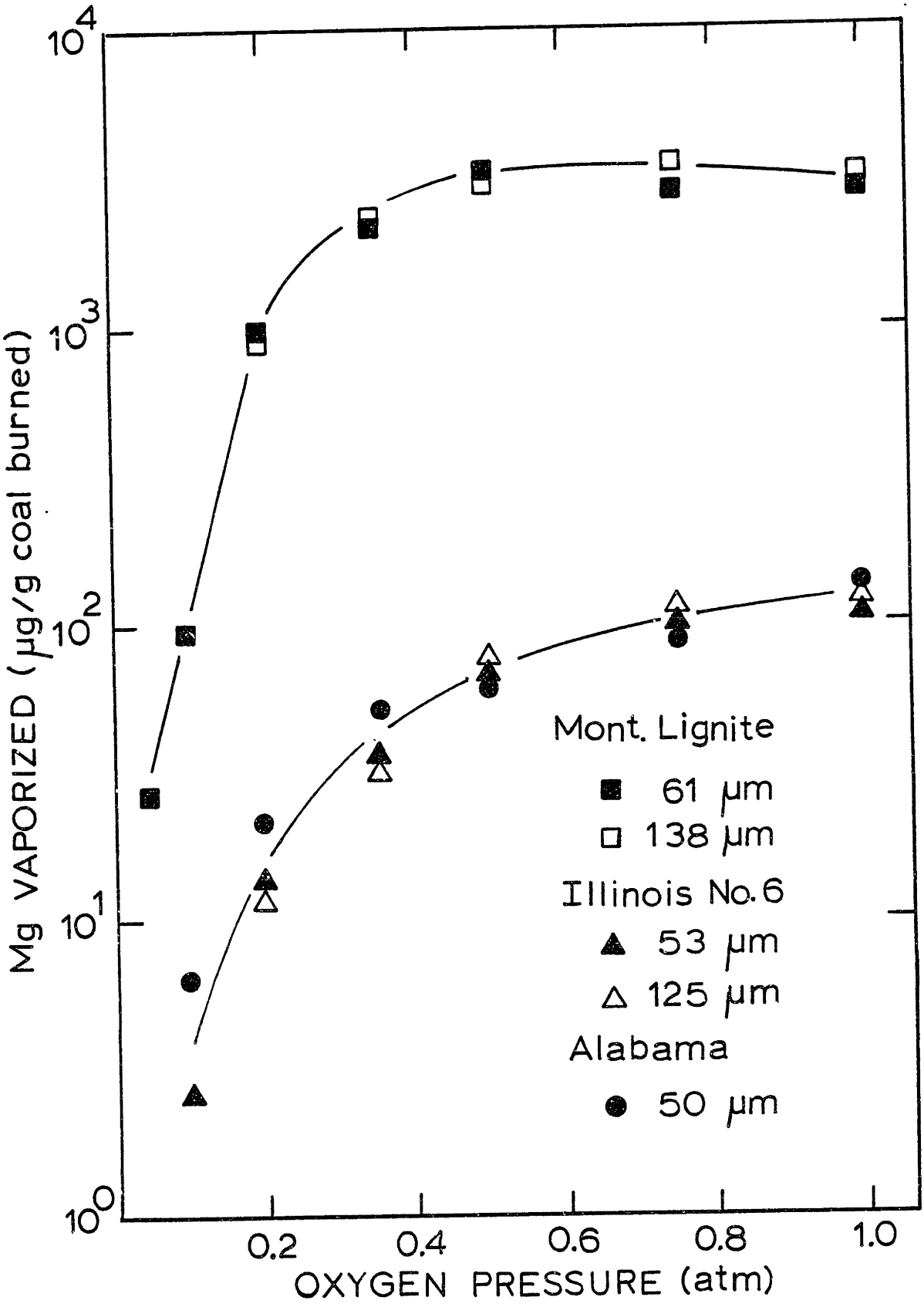

Figure 8.14 The Effect of Oxygen Pressure on Magnesium Vaporization. Furnace Temperature 1750K

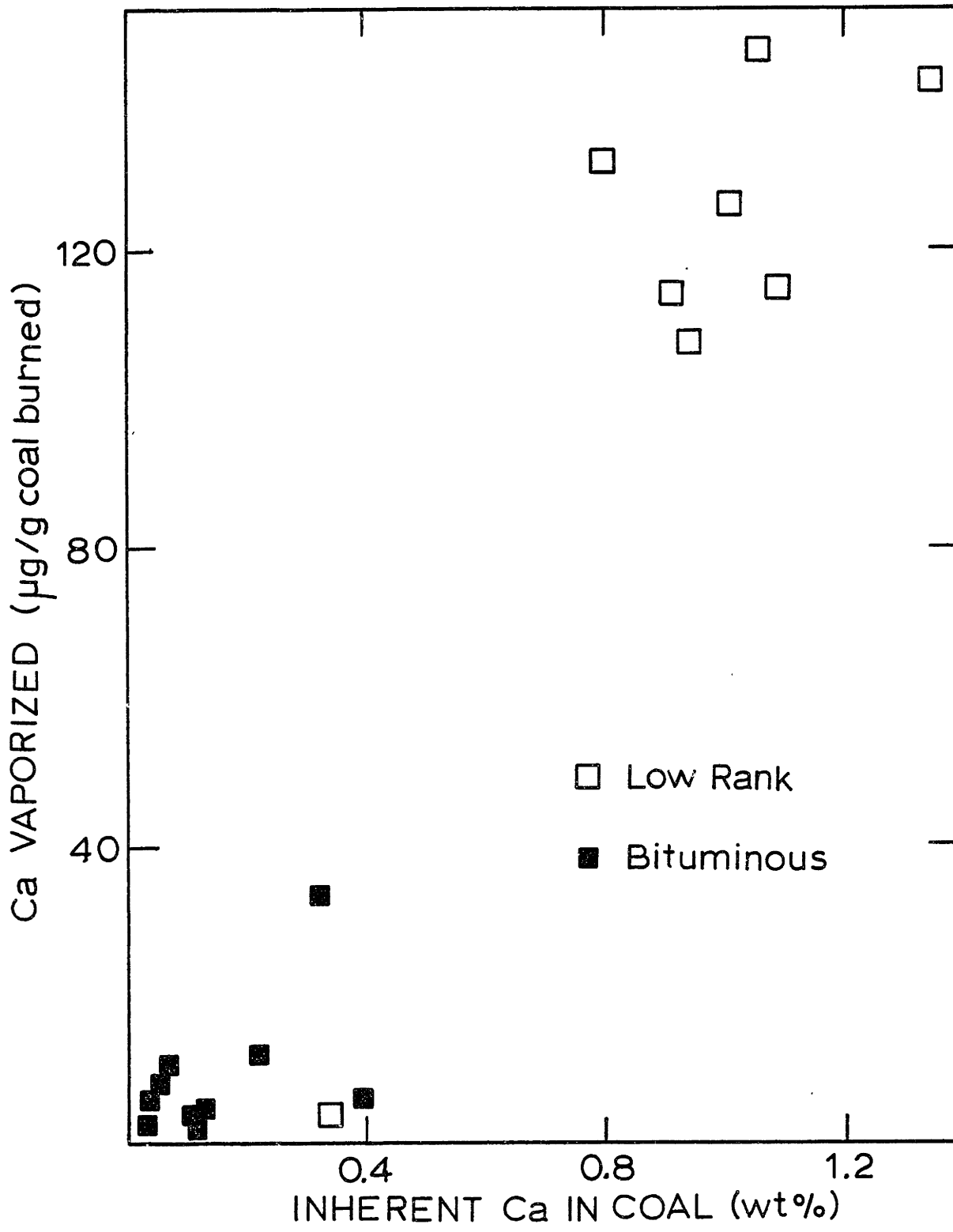

Figure 8.15 The Effect of Calcium Content of Coals on Calcium Vaporization. Furnace Temp. 1750K, 20% Oxygen

minerals are often extraneous. For example, in the Illinois No. 6 and the Alabama Rosa, 80 and 93 percent (Table 5.8) of the calcium in the raw coal was found to be associated with the extraneous mineral matter respectively. The variation in the amount of calcium vaporized per unit mass of coal burned with the inherent calcium content of the coal is shown in Figure 8.15. These results are similar to that of magnesium with the exception that there is no clear trend for the low rank coals. Low rank coals, however, did produce considerably more calcium vapor for combustion at 1750K in 20 percent oxygen.

The effects of combustion conditions and initial coal particle size on the amount of calcium vaporized per gram of coal burned is shown in Figure 8.16. For the raw Montana Savage lignite, there is a slight dependence on the size of the lignite particles with the larger size (138 micron) yielding about a factor of 1.3 greater calcium vaporization than the smaller (61 micron) sized lignite.

8.7 Alkali Vaporization During Combustion

Sodium and potassium as metals or oxides are considerably more volatile than the refractory oxides of magnesium, calcium, silicon and iron. In the low rank coals, much of the sodium, as described in Chapter Five, is distribured throughout the organic matter ion-exchanged on carboxylic groups. In the bituminous coals, sodium occurs predominantly in clay minerals or as the chloride salt. The concentrations of sodium in the coals examined here varied (Tables 5.4 and 5.5) by tow

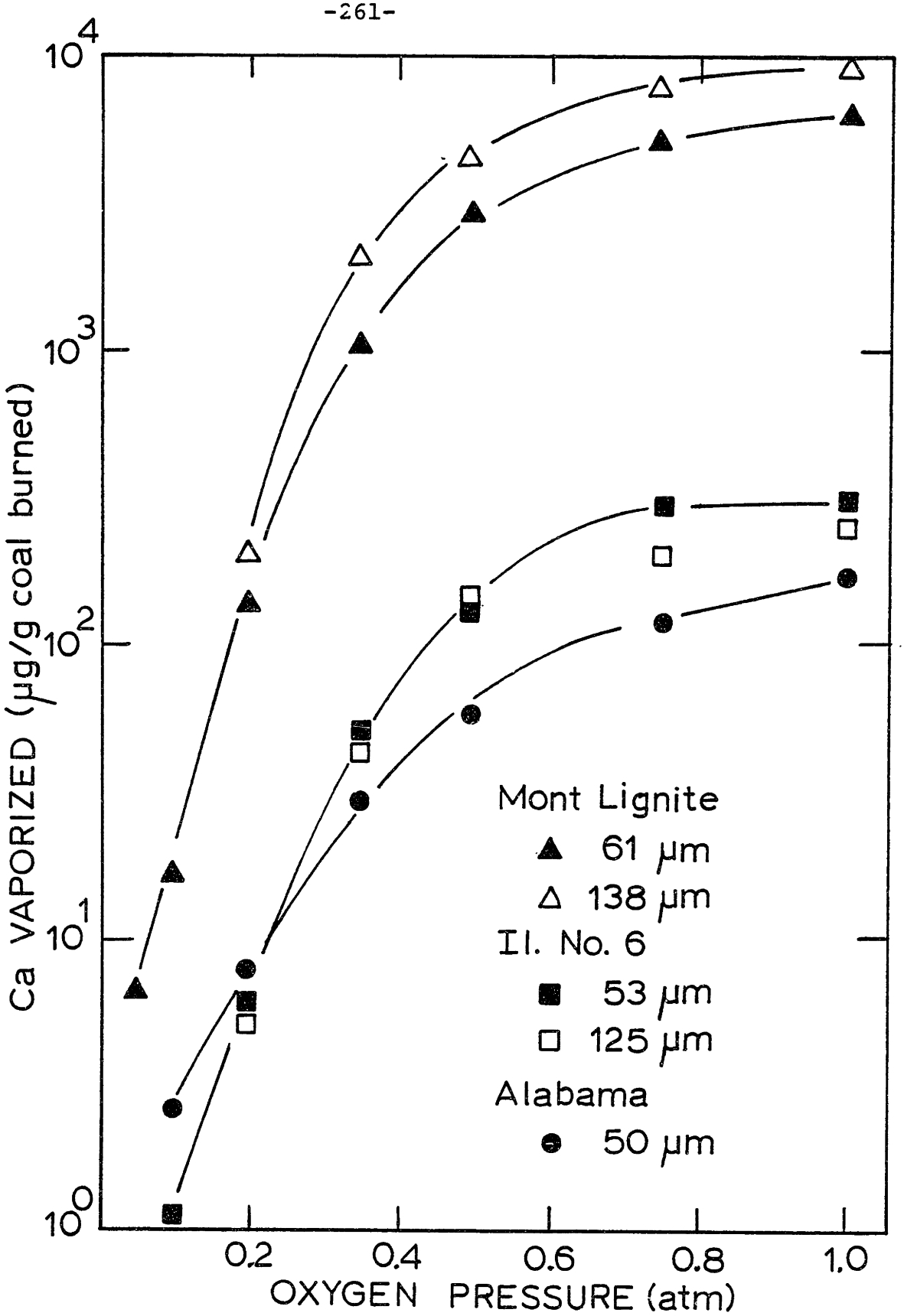

Figure 8.16 The Effect of Oxygen Pressure on Calcium Vaporization. Furnace Temperature 1750 K

orders of magnitude. The amount of sodium collected with the submicron ash per gram of coal burned correlated closely with the concentration of sodium in the coal, as shown in Figure 8.17. Typically, at a combustion condition of 1750K in 20 percent oxygen, 40 percent of the sodium in the coal was found in the submicron ash. For the coals containing unusually high sodium contents (North Dakota lignite and Montana Hardin), sodium (lxide or sulfate) was the major component of the submicron ash generated at this combustion condition. In comparison with the vaporization behavior of Si, Fe, Ca, and Mg, the vaporizatoin of sodium is relatively insensitive to combustion temperature under the high temperature conditions of this study. The data shown in Figures 8.17 and 8.18 correspond to the amount of sodium collected with the submicron ash generated during combustion. For the reasons discussed in some detail in Chapter Seven, only a fraction of the sodium that actually vaporized during combustion is collected with the submicron ash. More specifically, sodium containing vapors may also condense on the larger residual particulates. The data presented here, therefore, indicate the minimum amount of sodium vaporized. A more detail consideration of the condensation behavior of sodium and other volatile trace metals is given by Neville (1981).

The amount of potassium collected with the submicron ash is dependent on the potassium concentration in the coal as shown in Figure 8.19. The dependence of the fraction of potassium collected with the submicron ash on combustion conditions for selected coals is shown in Figure 8.20. The

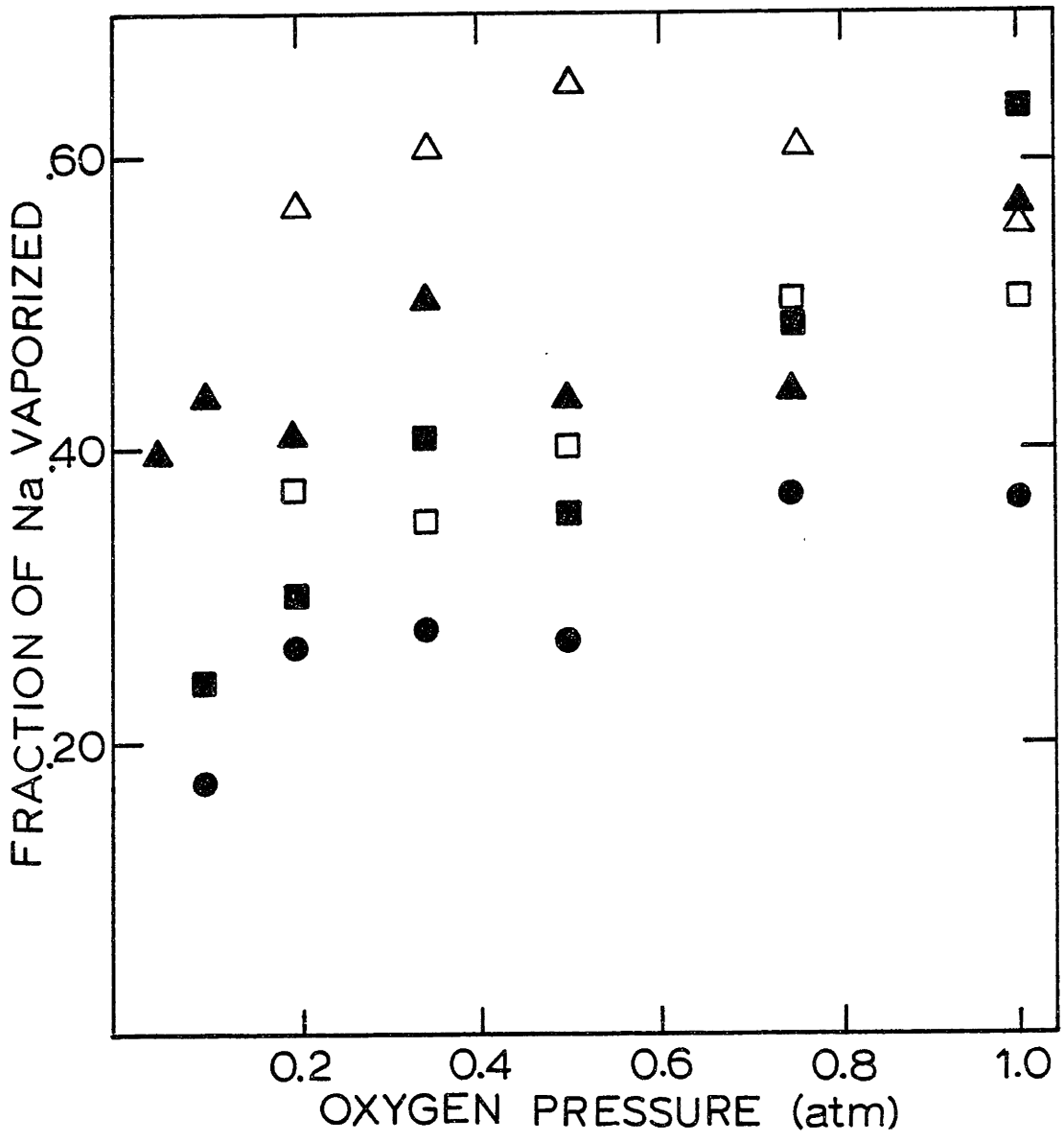

Figure 8.18 The Effect of Oxygen Pressure on the Vaporization of Sodium. Illinois No. 6 55 μm (■), 125 μm (▲); Montana Lignite 61 μm (□), 138 μm (△); Alabama Rosa (●).

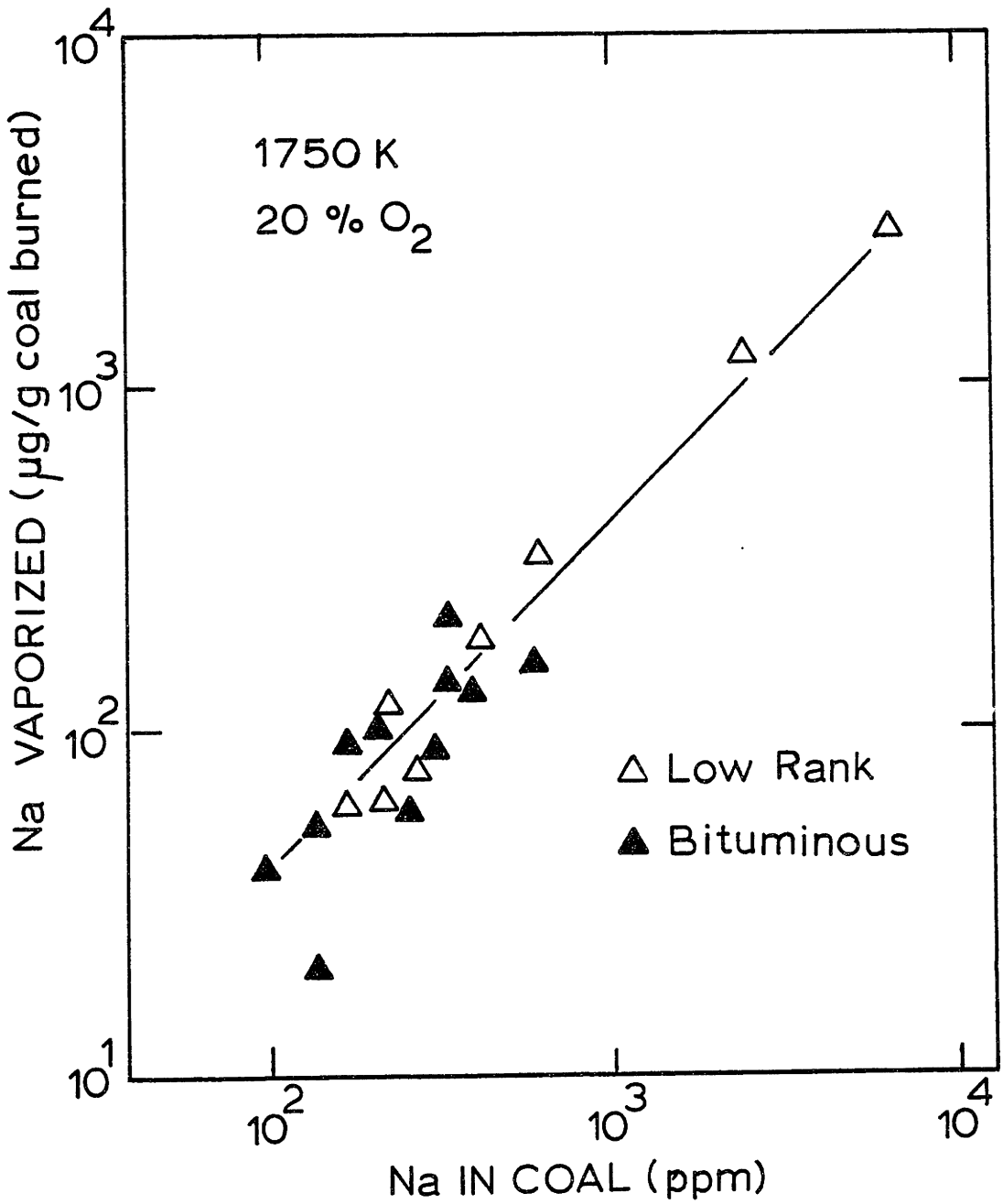

Figure 8.17 Correlation of Sodium Vaporized with Sodium Content of Coals

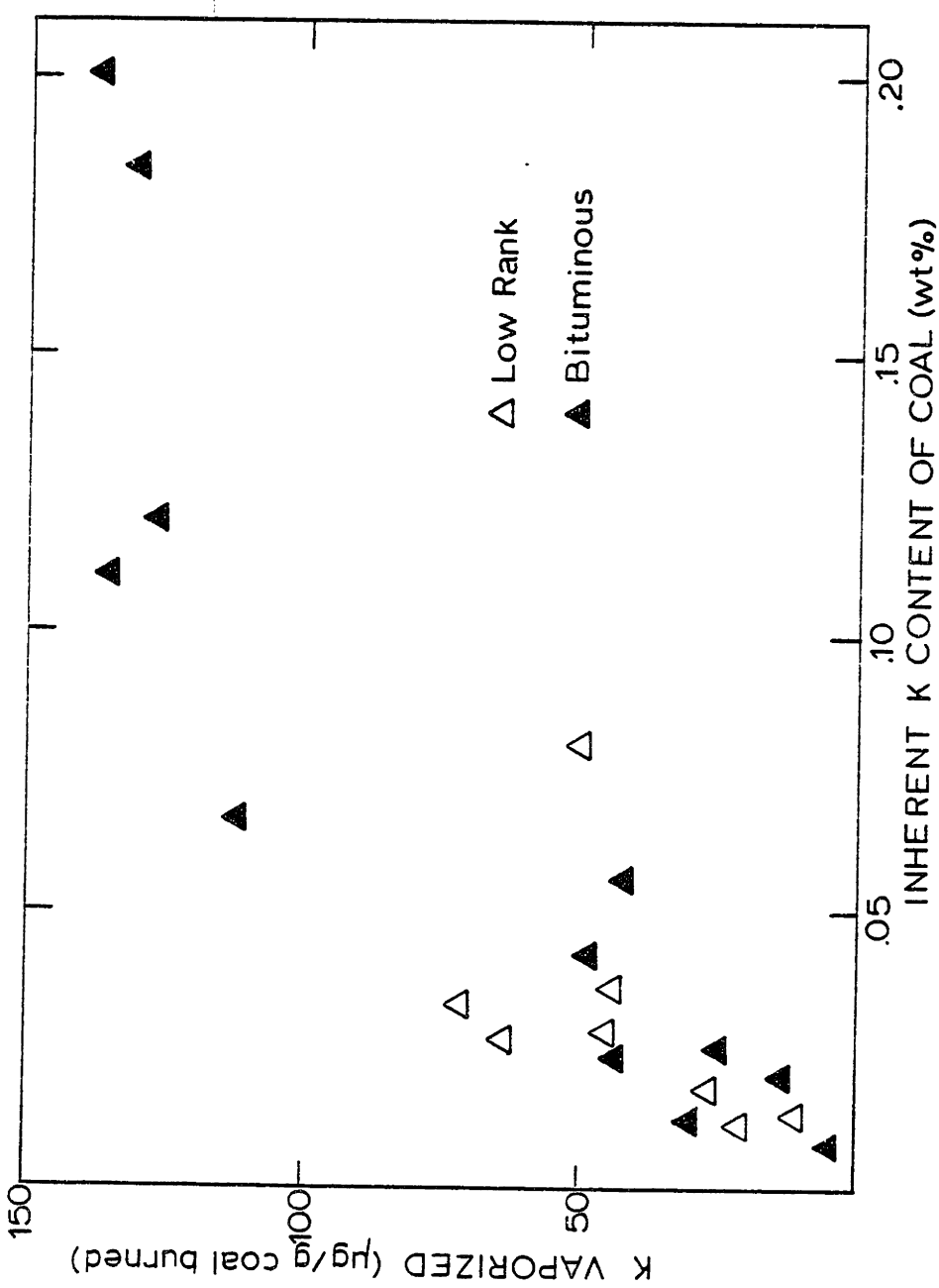

Figure 8.19 The Effect of the Potassium Content of the Coal on Potassium Vaporization. Furnace Temp. 1750 K, 20% Oxygen

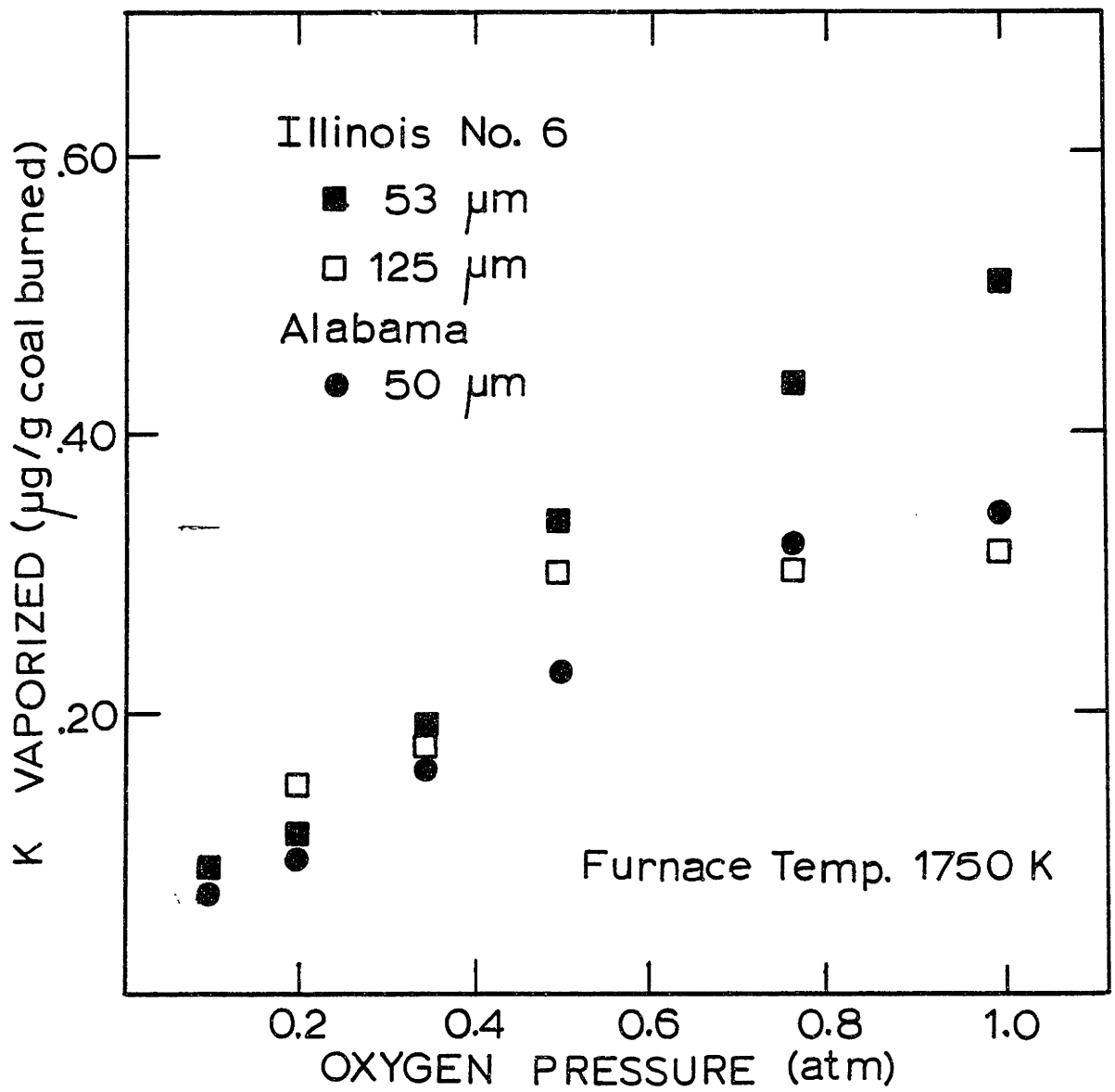

Figure 8.20 The Effect of Oxygen Pressure on Potassium Vaporization

vaporization of potassium under the present experimental conditions is similar to that of sodium insofar as it is relatively insensitive to combustions conditions. The potassium data reflect a minimum amount of vaporization due to possible condensation of vapors on the larger residual ash particulates.

8.8 The Effects of CO_2 on Ash Vaporization

Selected experiments using the Montana Savage lignite (138 micron) were performed to investigate the effects of CO_2 on the vaporization of the ash during combustion. In these experiments, the lignite was burned at 1750K in 20, 35 and 50 percent oxygen as in the experiments described previously. In this case, however, a partial pressure of 0.25 of CO_2 was maintained in the furnace. The submicron ash generated during combustion was collected and analyzed for elemental content. The results are shown in Table 8.7 with comparison to the results obtained when only mixtures of O_2-N_2 were metered into the furnace. The two-color optical pyrometry results (Chapter Six) indicated that 25% CO_2 in the main gas did not shorten the burning time of th coal or lower the combustion temperature for the case of 50 percent oxygen in the main gas. Hence, it was concluded that the presence of 0.25 atm. of CO_2 did not affect the temeprature history of the burning lignite at any of the conditions examined. It did, however, reduce the amount of ash vaporized as seen by the comparison of the results in Table 8.7. The effect of CO_2 in suppressing ash vaporization was more pronounced at the lower combustion temperature (20 percent oxygen).

TABLE 8.7

The Effects of CO_2 in the Furnace Gas on Elemental Vaporization for Combustion of the Montana Savage Lignite (138 μm). Furnace Temp. 1750K

Furnace Gas Composition (O_2-N_2-CO_2)	Amount Vaporized (μg/g coal burned) Si	Fe	Ca	Mg	Al
20 - 80 - 0	37	254	180	910	17
20 - 55 - 25	10	53	18.5	90	2
35 - 65 - 0	467	346	1140	2882	114
35 - 40 - 25	79	262	327	1276	23
50 - 50 - 0	1100	454	3220	3220	593
50 - 25 - 25	335	298	1805	1832	84

The model for ash vaporization, presented in Chapter [illegible] assumes that volatile suboxides or metal vapors (e.g. Si and Ca) are generated from condensed refractory oxides in the burning char particle as a result of chemical reduction by carbon monoxide:

$$MO_n(c) + CO = MO_{n-1}(v) + CO_2$$

The observed suppression of vaporization by the introduction of CO_2 in the main furnace gas qualitatively supports this mechanism. However, the partial pressure of CO_2 within the char particle may be somewhat less than in the bulk gas due to reaction and diffusion within the char. The level of CO_2 experienced by the ash will vary with position in the char particle.

8.9 Empirical Correlation of Ash Vaporization Kinetics

The results presented earlier in this Chapter showed that if the oxygen partial pressure in the furance main gas was increased, the amount of ash vaporized also increased due to the increase in the combustion temperature of the coal particles. However, as the pressure of oxygen in the main gas is increased, the burning time of the coal particles decreases as was shown in Chapter Six. We now wish to compensate for this decrease in experimental burning times to obtain an empirical correlation of ash vaporization kinetics. A more detail model taking into account proposed mechanisms, including the thermochemical aspects of ash vaporization reactions, is considered in Chapter Ten.

A phenomological expression for the rate of ash vaporiztion is obtained by dividing the fraction of ash vaporized by the burning time of the coal. The reasoning behind a correlation of this type is that the vaporization of ash is significant only during the char combustion process because of the locally reducing environment within the char particle and the particle temperature overshoot. The calculated fractional vaporization rates for the total ash (Figure 8.21) and for specific elements is shown in Figures 8.22 and 8.23 for the Montana Savage lignite and the Illinois No. 6, respectively, in an Arrhenius plot. For the calculations, the fraction vaporized was that for the inherent ash. The burning times correspond to the 61 micron diameter lignite and the 53 micron Illinois No. 6. This is therefore only an approximate correlation as it does not con-

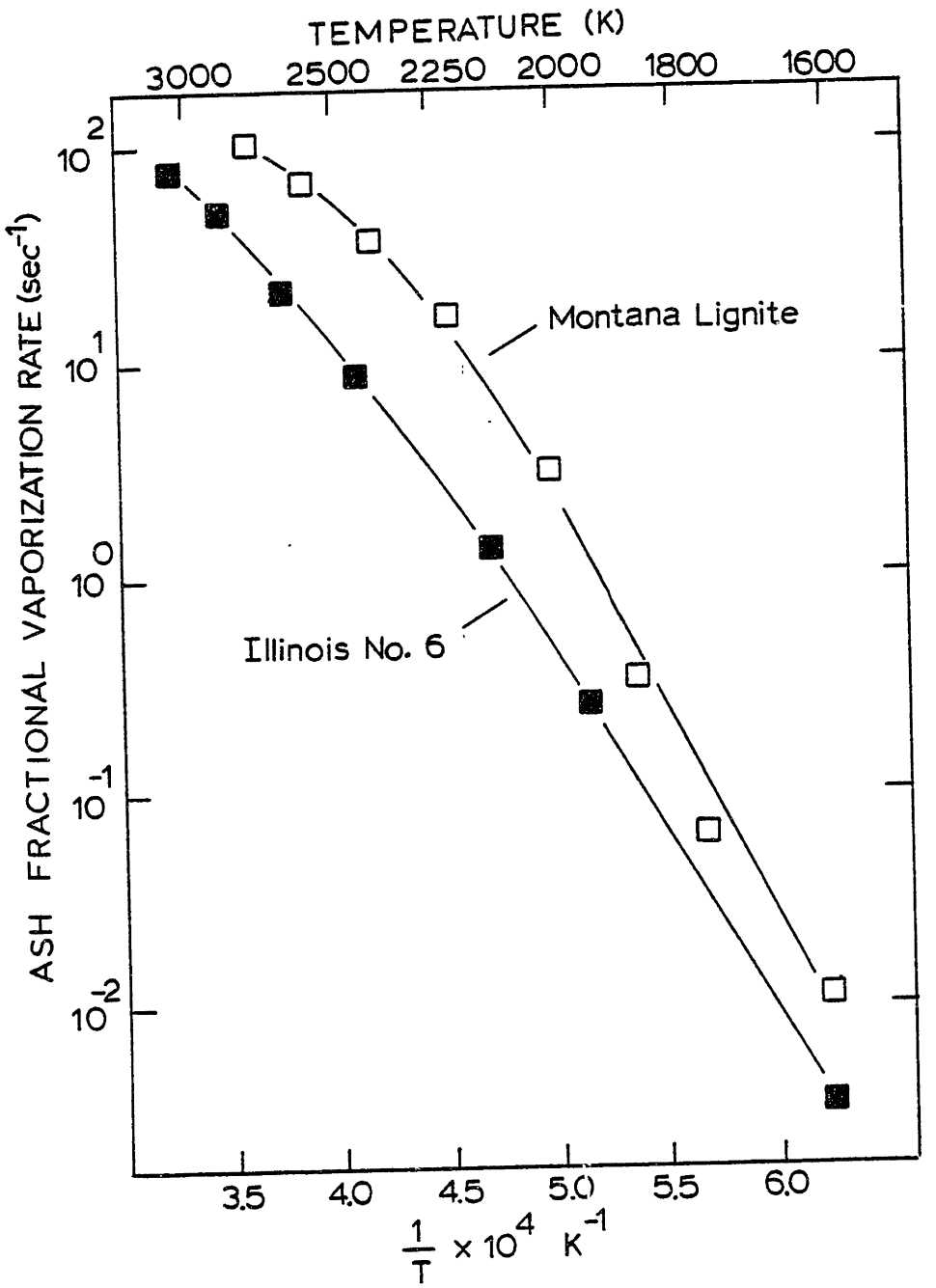

Figure 8.21 Fractional Vaporization Rate Correlation for Total Ash

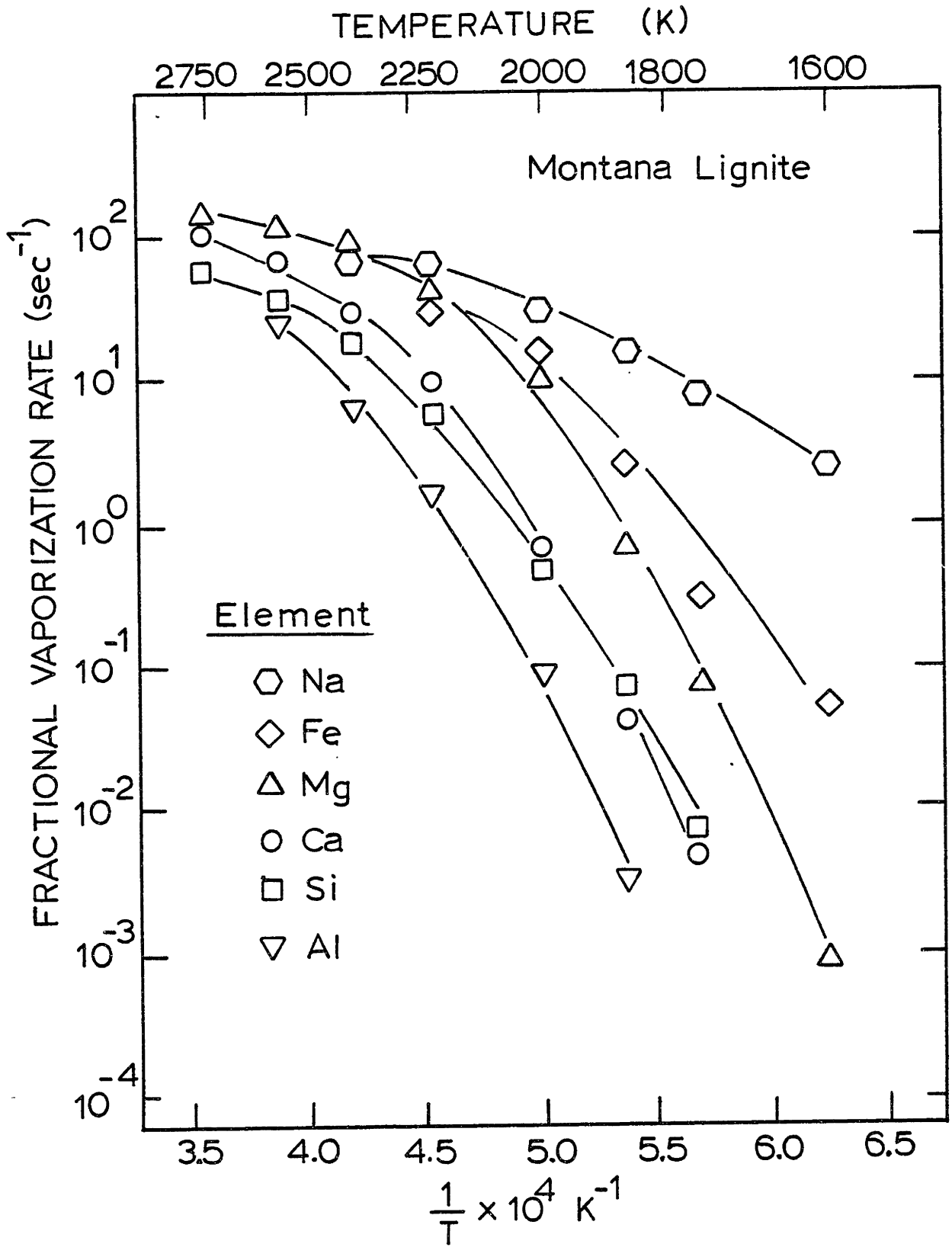

Figure 8.22 Elemental Fractional Vaporization Rates for Montana Lignite

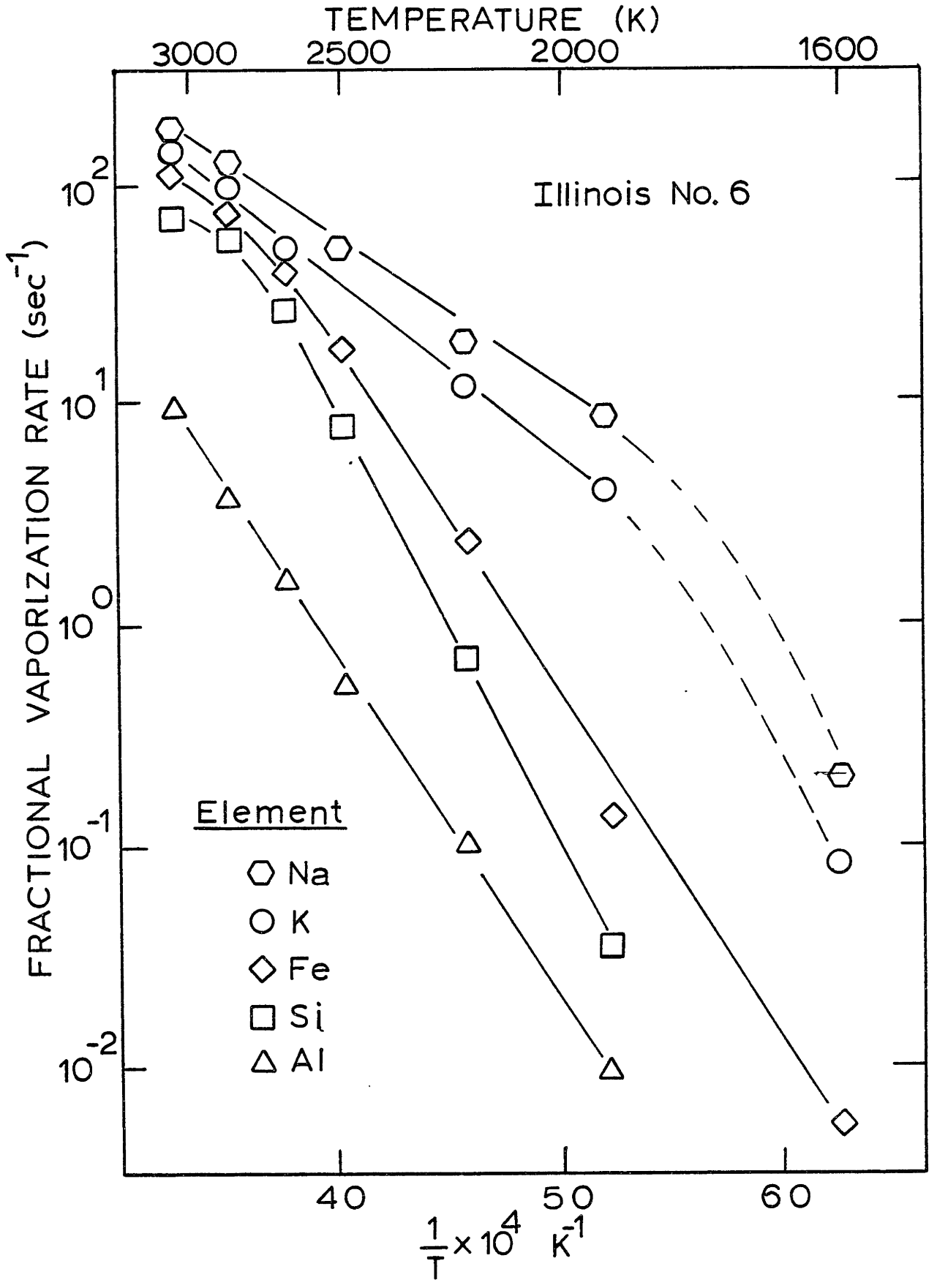

Figure 8.23 Elemental Fractional Vaporization Rates for Illinois No. 6

sider the effects of coal partical size on the burning time and the fraction of ash vaporized.

CHAPTER NINE

SCANNING ELECTRON MICROSCOPY OF THE CHEMICAL AND PHYSICAL EVOLUTION OF ASH DURING COAL COMBUSTION

9.1 Introduction

The total content and composition of mineral matter is widely variable in pulverized coals but generally found in the form of common minerals (e.g. quartz, clays, carbonates and pyrite), either embedded in the carbonaceous material as small (1-15 microns) descrete inclusions or as less common larger particles not associated with any appreciable organic matter (see Chapter Five). During the high temperature combustion of the coal, the minerals undergo physical and chemical transformations leading to the formation of fly-ash. Although the complex phenomena which govern the genesis of fly-ash are not completely understood, it is generally believed that the inclusions within the burning coal particles will fuse at the high temperatures (1700-2500 k) and coalesce on contact as the mass of the coal or char decreases during combustion (Padia, 1976, Flagan and Friedlander, 1978).

Not all of the so-called mineral matter occuring in coals is necessarily in the form of mineral phases. This is particularly true of low rank lignites and subbituminous coals where a major portion of the calcium, magnesium and sodium are chemically bound to the organic matter of coal as cations ion-exchanged on carboxylic and phenolic functional groups as discussed in Chapter 5. No detailed studies have been reported in which the fate during combustion organically bound inorganic

matter was investigated. There is interest, however, concerning what possible beneficial and adverse effects this highly dispersed inorganic matter might have on combustion processes. A possible benificial aspect is the utilization of the inherent calcium in low rank coals for the retention of sulphur as CaS during fuel rich combustion (Lyon and Freund, 1980). Possible adverse effects may include high volatization rates of these metals, accelerating corrosion in the case of sodium, and increased submicron particulate loading from the inorganic vapors. The results presented in the previous chapter demonstrated that the composition of inorganic vapors evolving from during combustion was strongly dependent upon the composition of the coal or the arrangement of the mineral matter. The effect of coal rank upon the composition and amount of submicron ash was particularly pronounced. Generally, more ash vaporized when low rank coals were burned compared to that measured for bituminous coals. Furthermore, the submicron ash generated from cobustion of low rank coals was composed primarily of the alkaline oxides or, in certain cases, Na_2O. In Section 9.2 of this chapter, the results of a detailed scanning electron microscopic examination of the transformations of organically bound mineral matter during combustion of the Montana Savage lignite are reported. In Section 9.3, microscopic observations of the physical changes of a bituminou coal during devolatilization and combustion are presented.

9.2 Transformations of Ion-Exchangable Mineral Matter During Lignite Combustion

The water-cooled collection probe was used to directly withdraw burning char particles from the combustion zone. At the probe inlet, gaseous and particulate products are instananeously quenched by a high volume flow of cold nitrogen gas. The position of the probe was adjusted with respect to the distance from the point of coal injection into the furnace to provide a means by which char particles at various extents of burnout could be collected for microscopic examination. The approximate extent of burnout at each probe position (or residence time) was determined by weight loss measurements. Laser velocimetry measurements indicate that particles velocities in the furnace are about 50 cm/sec. The thermal history of the burning lignite particles in the furnace were obtained directly by the two-color optical pyrometry method. The nominal diameter of the Montana lignite investigated here was about 138 microns. At a furnace temperature of 1750 K in 20 percent oxygen, the measured combustion temperature of the lignite particles was about 2000 K. The time elapsed from ignition to burnout was approximately 70 milliseconds.

The partially oxidized char samples were mounted on carbon discs and coated with copper to insure conductivity for scanning electron microscopy (SEM) examination. An AMR 1000, equipped with a KEVEX energy dispersive x-ray analyzer (EDXA) was used for examination of the chemical and morphological properties of char surfaces. The instrument has a point to point resolution of 50Å. The resolution of the EXDA

however, is on the order of 1 micron because of electron scattering within the sample.

Selected char samples were also examined by the powdered X-ray diffraction method to provide additional information on the nature of high temperature phases observed on the char surface by SEM/EDXA examination.

9.2.1 Montant Savage Lignite Combustion at 2000 K

The observations presented here are intended to demonstrate the evolution of organically held inorganic matter during the course of lignite combustion at a moderately high temperature. The chars examined were collected at 5.0, 5.7, 6.4 and 7.6 cm from the point of injection into the furnace, corresponding to residence times in the combustion zone of approximately 100, 115, 130 and 150 milliseconds, and dry ash free (DAF) weight losses of 46, 57, 72, and 82 percent respectively.

A scanning electron micrograph of the raw, size classified (138 μm) Montana lignite feed is shown in Figure 9.1. Char particles collected at 5.0 cm from injection into the furnace are shown in Figure 9.2A. In Figure 9.2B, the surface of a devolatized lignite particle obtained at this residence time is shown at high magnification, revealing the fissures or cracks in the structure resulting from the initial heat up and devolatilization. The EDXA of a one micron area (located by the arrows in Figure 2B) indicated the presence of organically bound Mg, Al, S and Ca, as shown in Figure 9.2C.

Figure 9.1 SEM of Raw Montana Lignite Particles

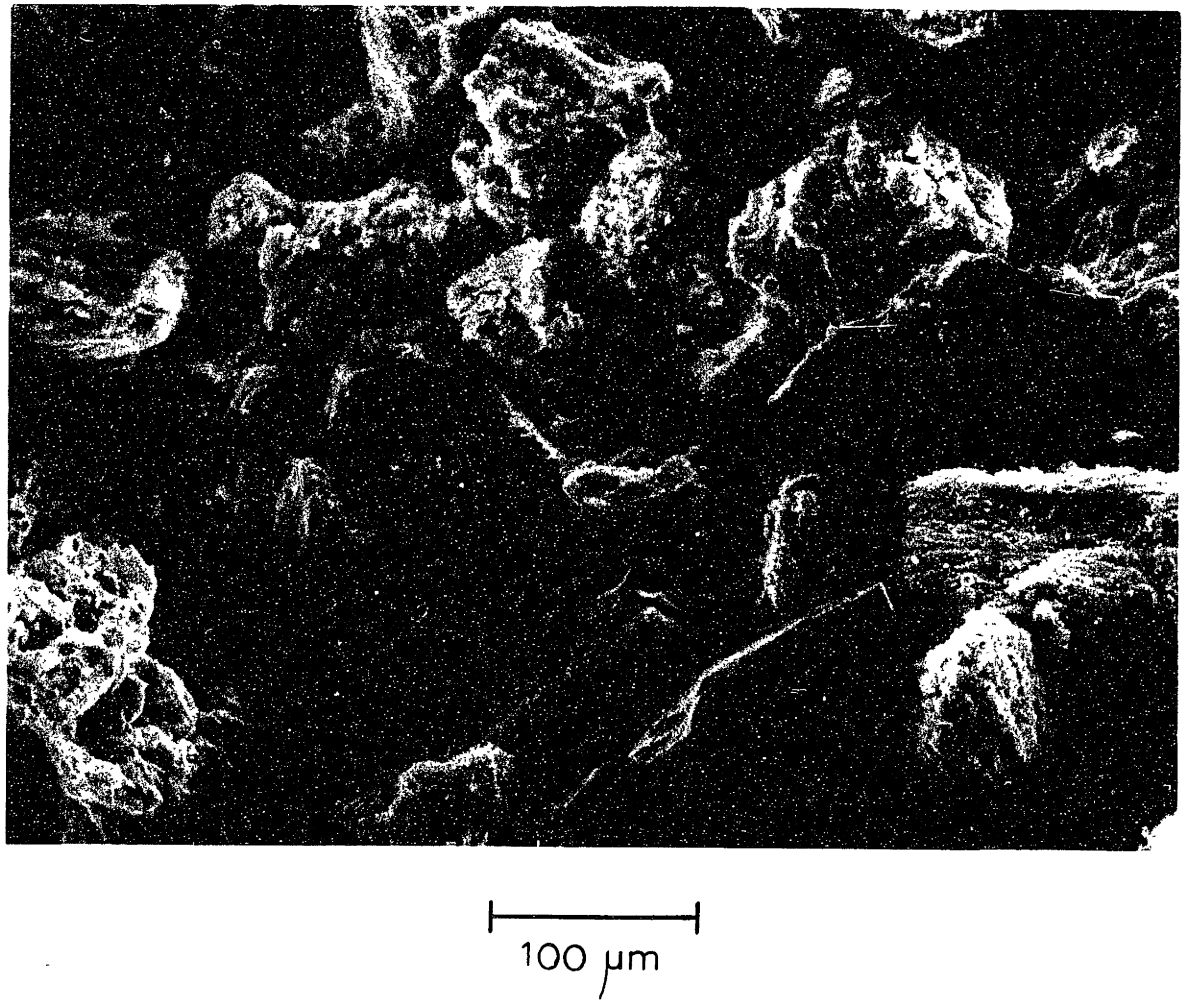

Figure 9.2A SEM of Devolatilized Montana Lignite Particles at 46% DAF Weight Loss. 1750K, 20% Oxygen

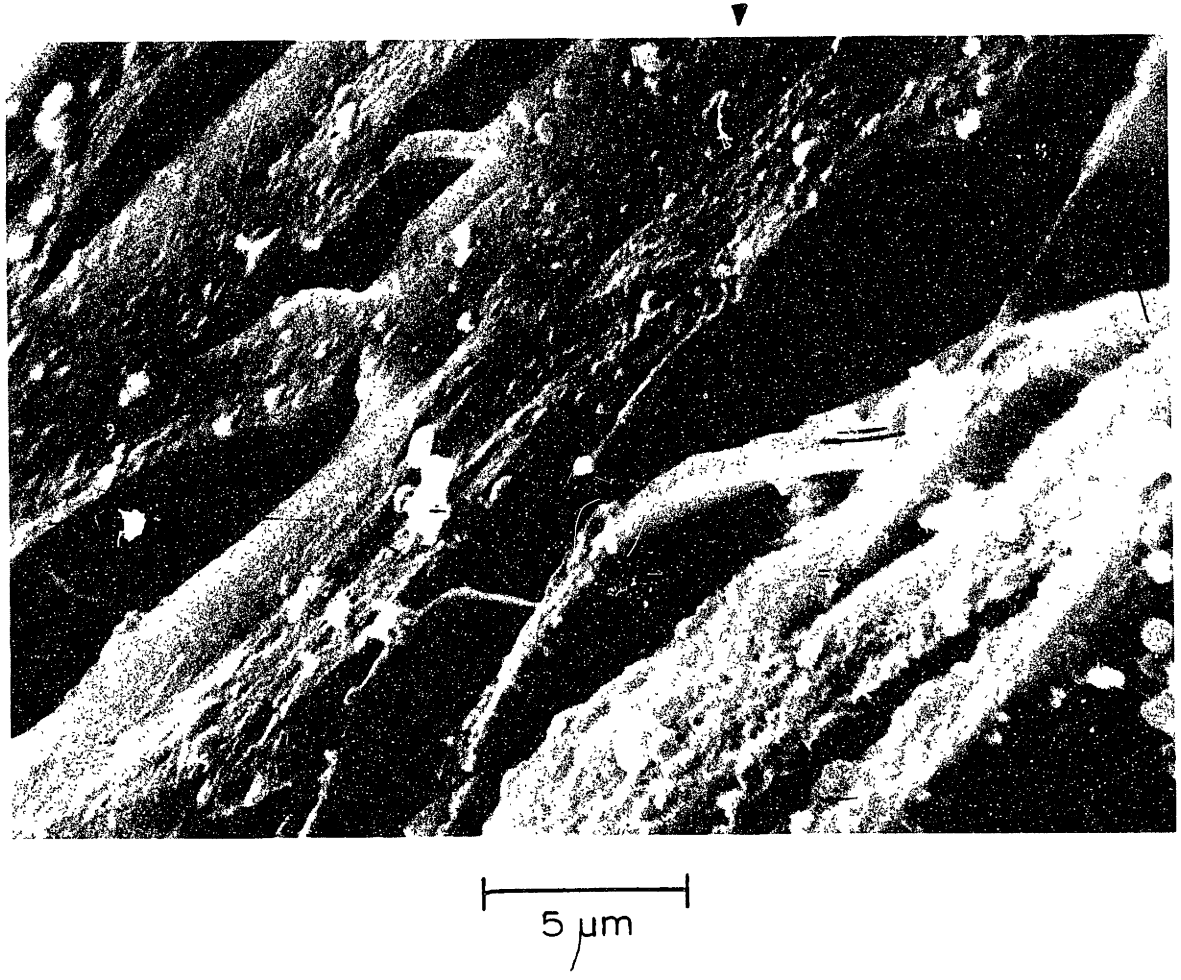

Figure 9.2B Surface of a Devolatilized Lignite Particle

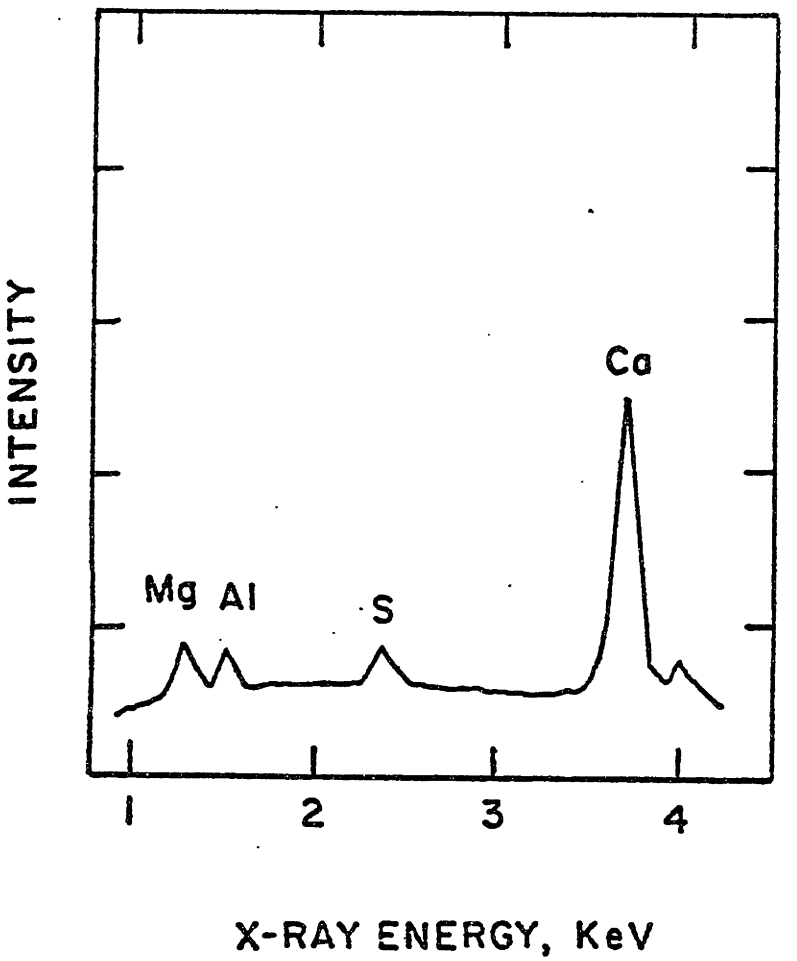

Figure 9.2C EDXA Spectra

Aluminum occurs primarily in clay minerals in coal. Other investigators, however, have also found by ion-exchange methods that some of the aluminum in lignites is organically bound (Miller and Given, 1978).

The char particle shown in Figure 9.3A was collected at 5.7 cm from injection and is representative of those at approximately 57 percent DAF weight loss. A region of its surface is shown at higher magnification in Figure 9.3B. Although the combustion rate of the char is expected to be controlled primarily by the external transport processes at this high temperature condition (Chapter Six), it is evident from the lacy structure of the surface and the development of large holes (1-5 microns) and pores, that oxygen is penetrating the chars outer layer to a certain extent. Also visible in Figure 9.3B are droplets of ash. At still higher magnification of the surface, the micrograph in Figure 9.3C clearly exhibits the characteristics of the char's surface structure. Close examination of the organic material reveals that it is entirely covered by submicron 'grains'. The EXDA of the ash droplet marked by (a) and the carbonaceous area (b) in Figure 9.3C are compared in Figure 9.3D. The nearly identical spectra with respect to relative intensities of elements provides evidence for the transformation of the organically bound material into ash droplets on the char surface as the organic matter is gasified. This process apparently first proceeds by the formation of minute grains of ash directly on the local faces of the carbonaceus matter,

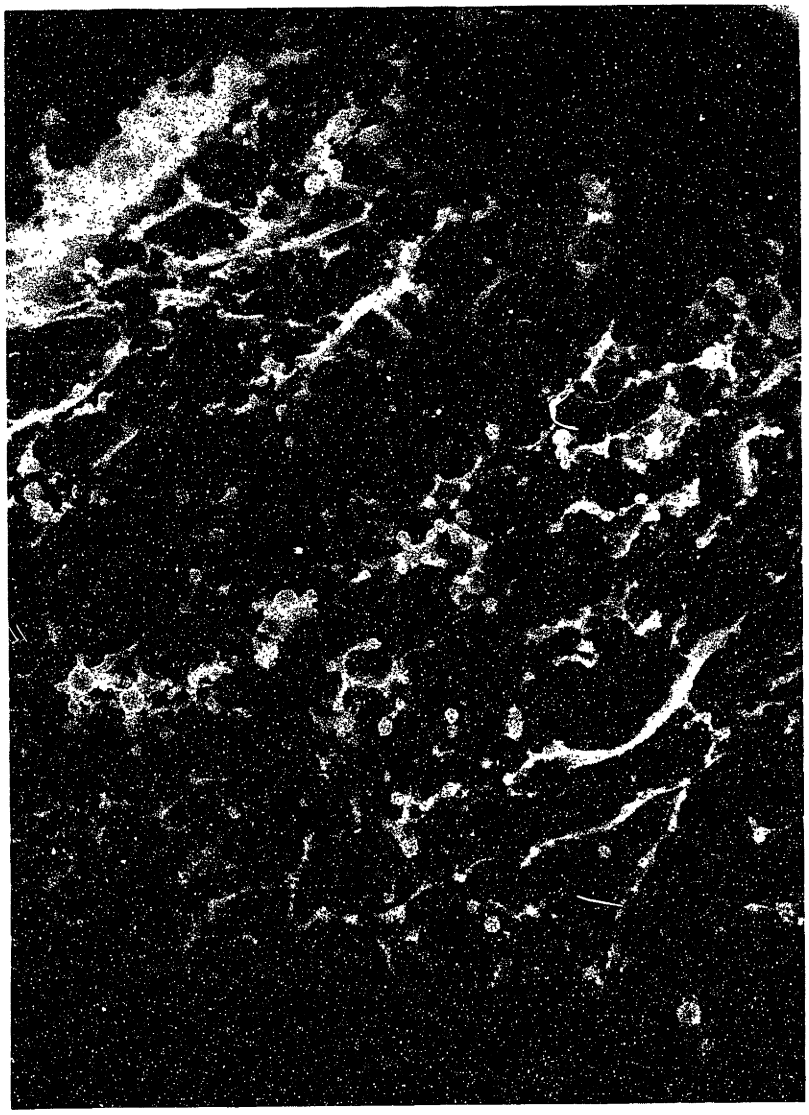

Figure 9.3A SEM of a Partially Oxidized Lignite Particle at 52% DAF Weight Loss. 1750K, 20% Oxygen

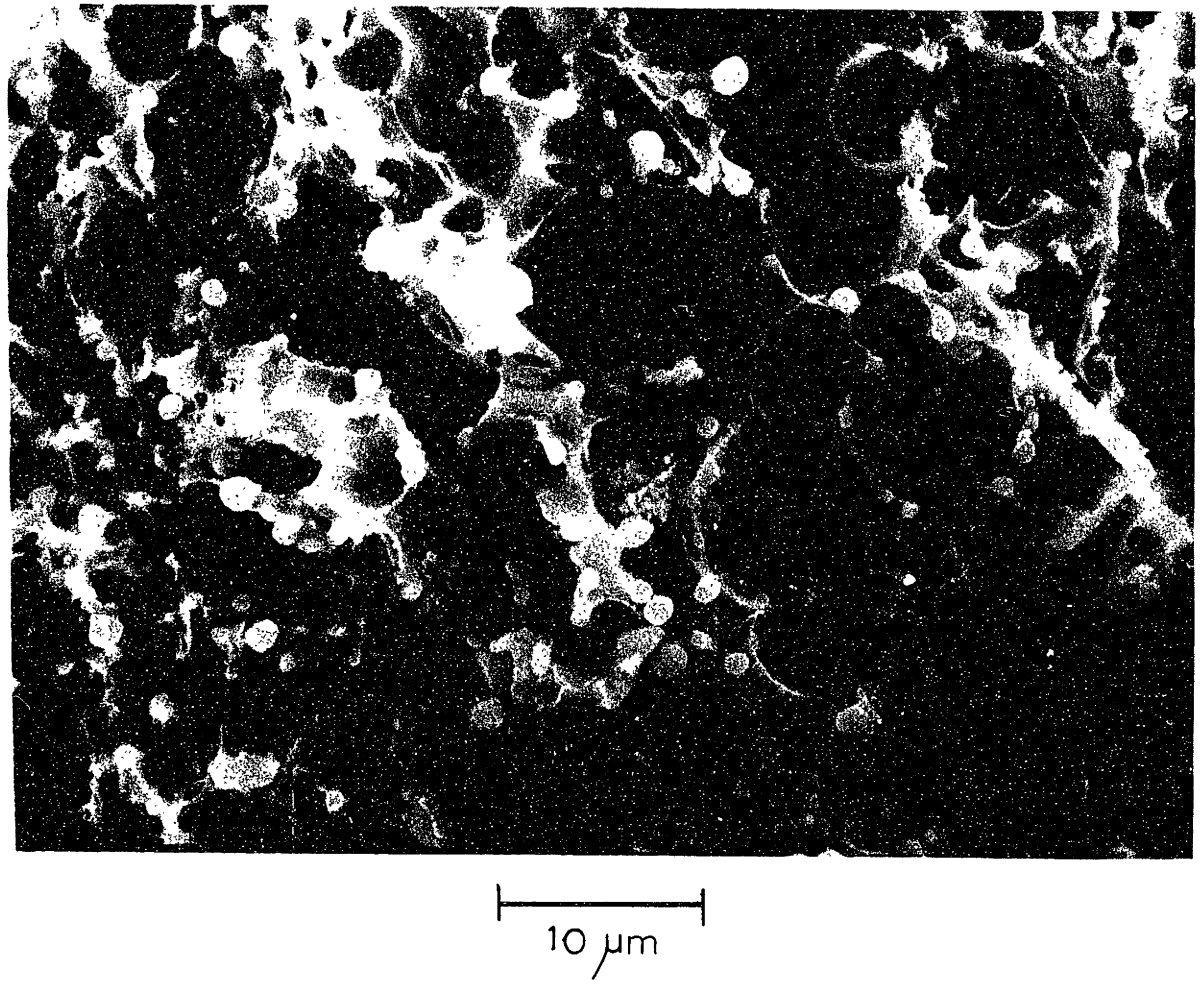

Figure 9.3B Surface of Partially Oxidized Lignite Particle

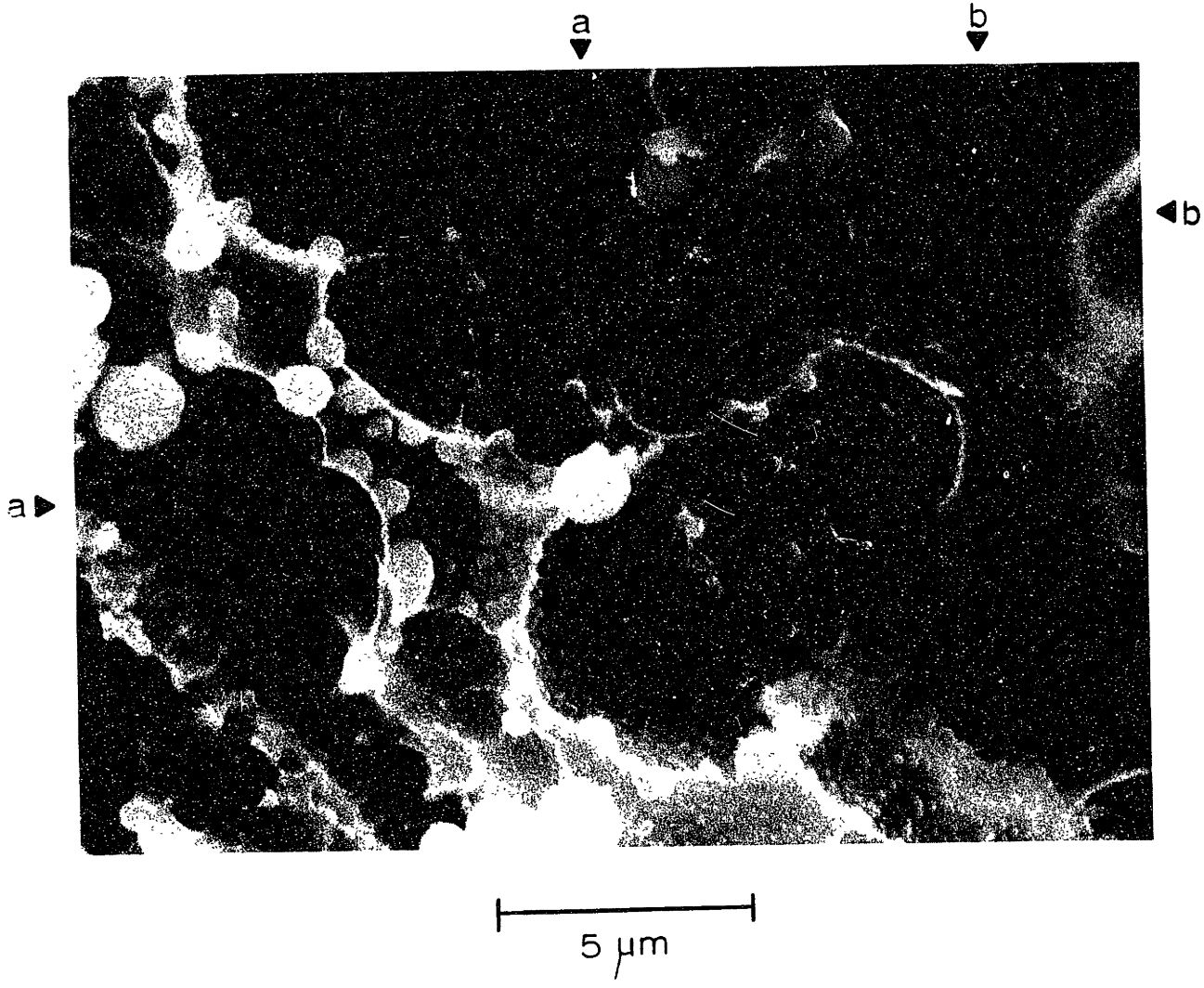

Figure 9.3C Surface of Lignite Char at High Magnification

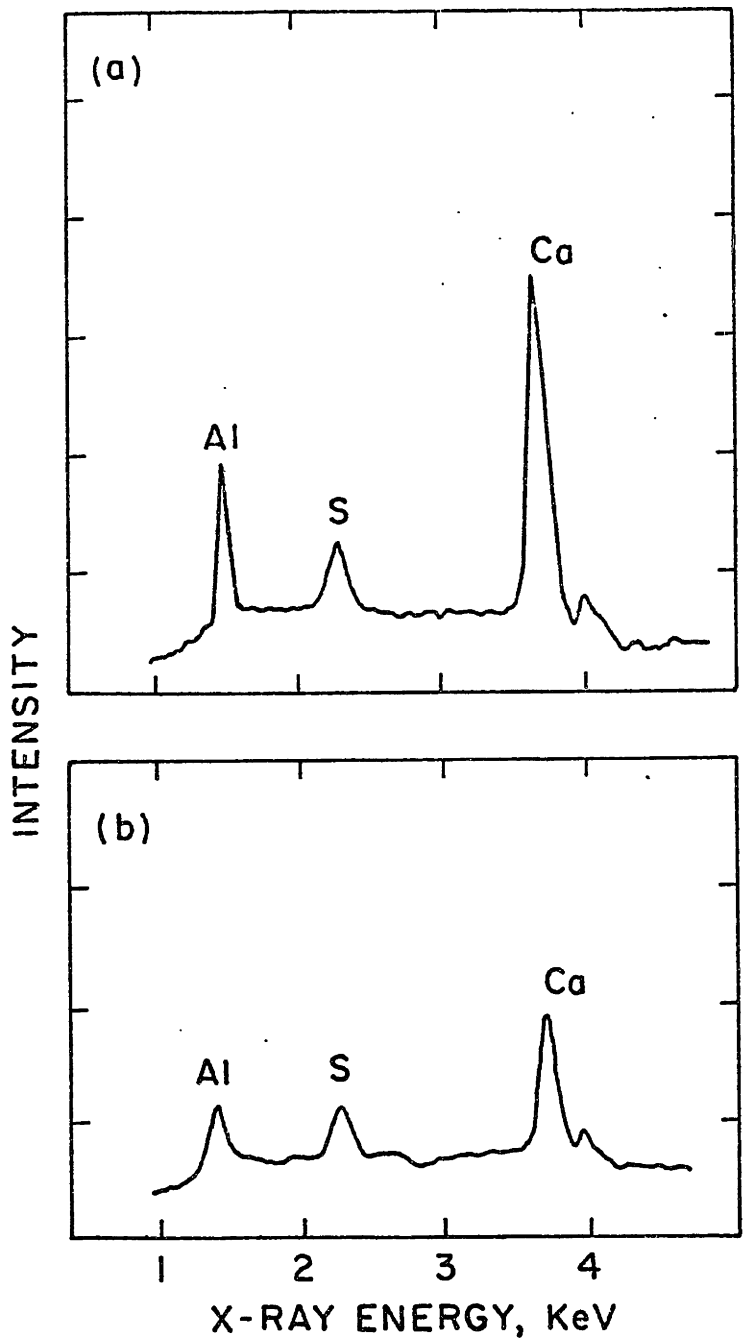

Figure 9.3D EDXA Spectra

which then continue to grow to dimensions greater than 1 micron along the ridges or edges created by the combustion process during the early stages of char burnout. The submicron grains and the growth process along the ridges are more clearly visible in the high magnification micrographs of carbonaceous surface material shown in Figures 9.4A and 9.5A. The EDXA of areas localized by the arrows in these micrographs are shown in Figures 9.4B and 9.5B, respectively.

An edge on view of the surface of another char particle obtain at the same degree of burnout, revealed that 1-3 micron ash droplets are attached to the char surface by thin filaments, as shown in Figure 9.6. It seems likely that further oxidation of the char may result in the direct release of droplets of this characteristic size during the early stages of char burnout.

The char particle shown in the micrograph of Figure 9.7 was collected at 6.4 cm from injection into the furnace, corresponding to approximately 50 percent burnout. It is typical of other char particles examined at this stage of burnout in that the surface ash has undergone considerable growth in terms of its characteristic dimensions and the degree to which it now covers the surface. Some significant differences are observed in the composition and morphology of the surface ash on different char particles examined at this stage of burnout. This is illustrated by comparison of the high magification micrographs of surfaces of different char particles and their EDXA shown in Figures 9.8 through 9.11. The arrows

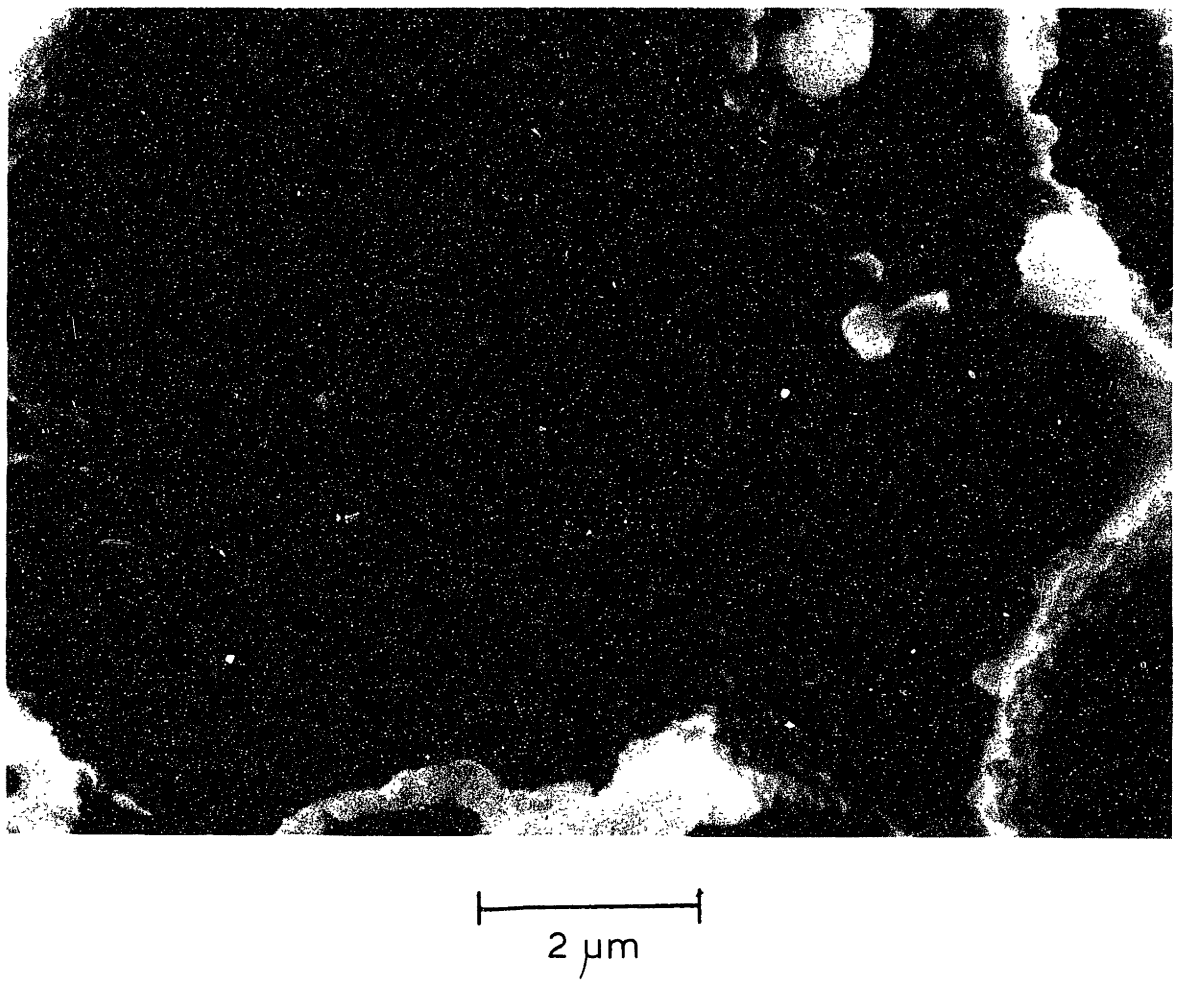

Figure 9.4A High Magnification SEM of the Surface of a Lignite Particle at 57% DAF Weight Loss. 1750K, 20% O_2

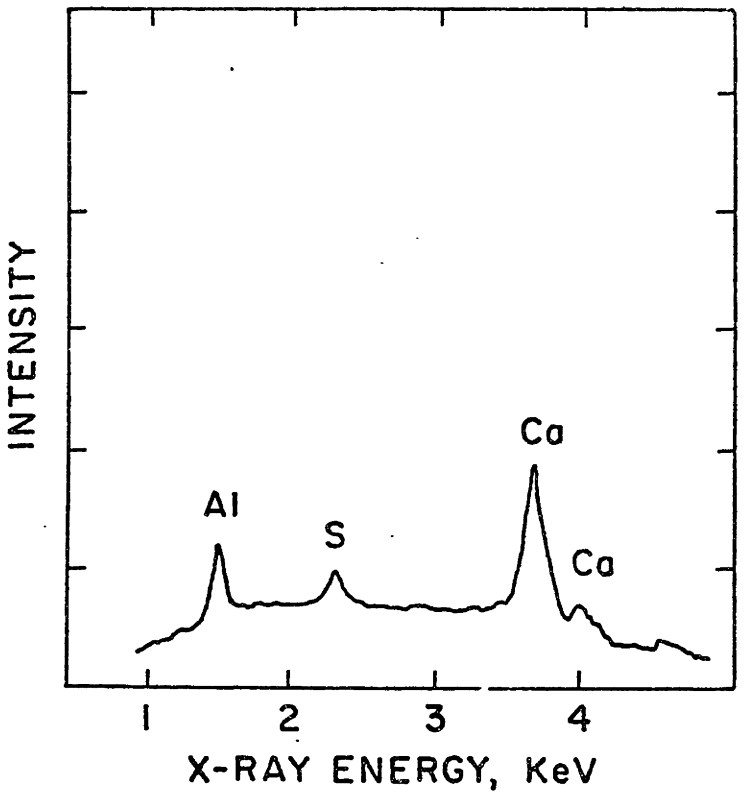

Figure 9.4B EDXA Spectra

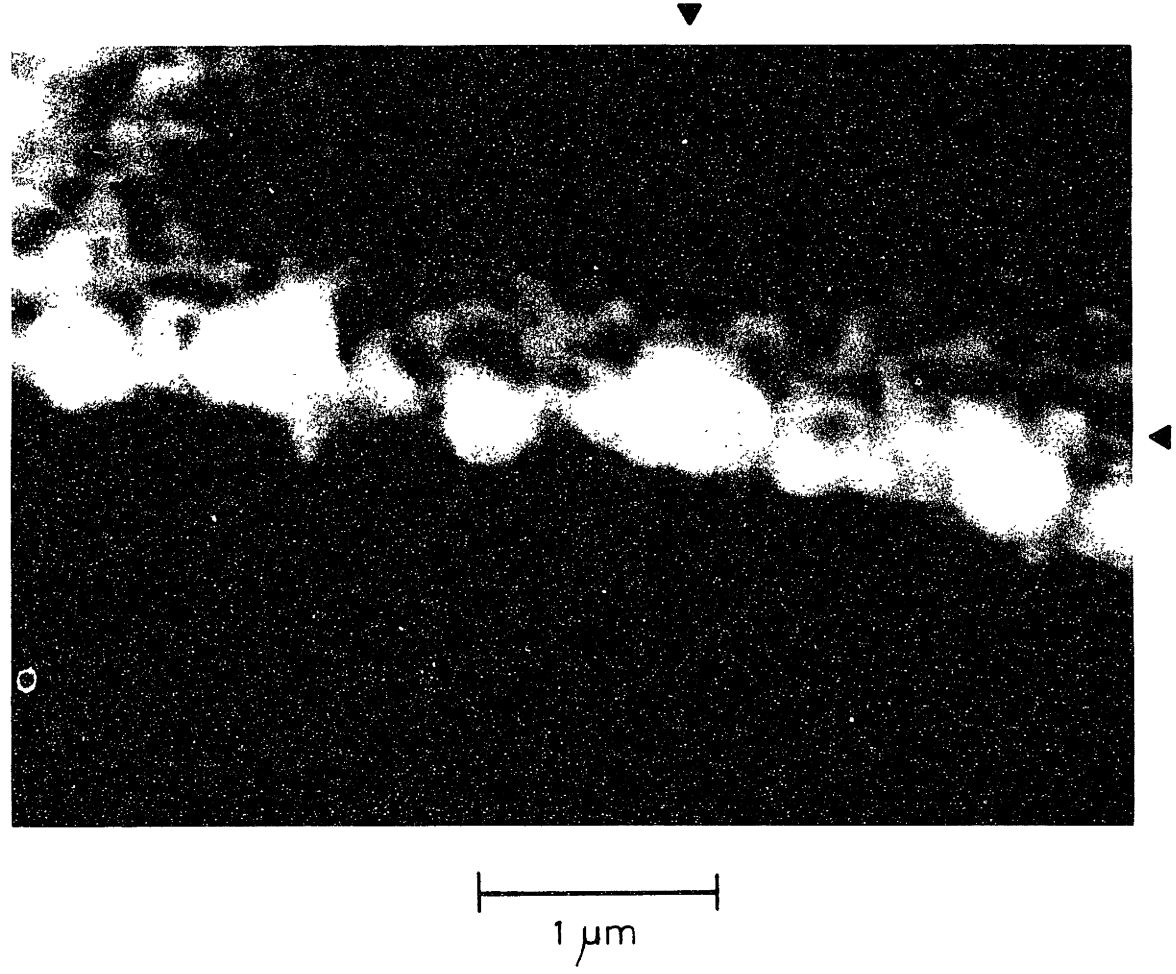

Figure 9.5A High Magnfication SEM of Lignite Particle at 57% DAF Weight Loss. 1750K, 20% Oxygen

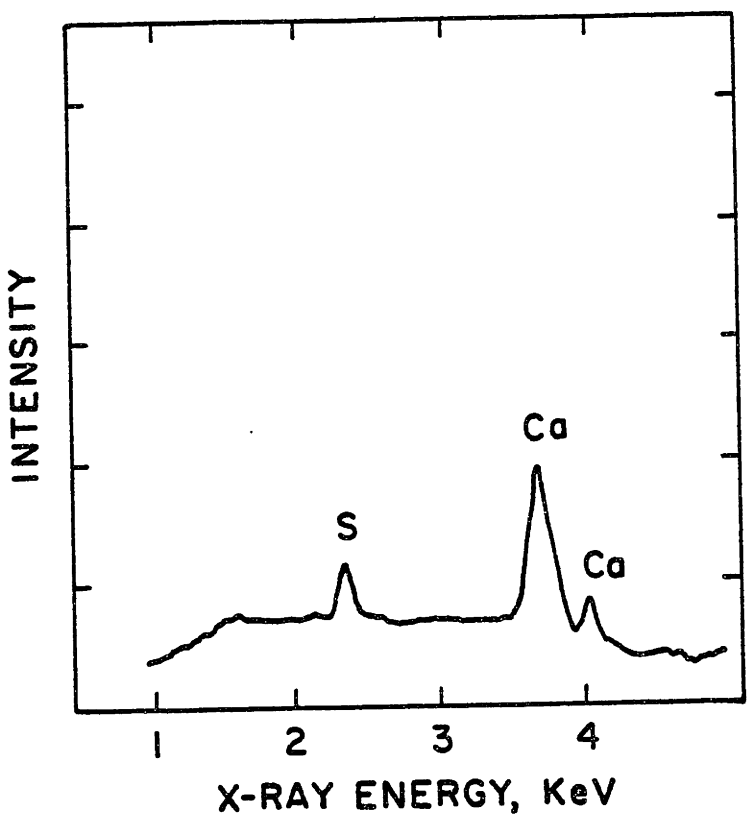

Figure 9.5B EDXA Spectra

Figure 9.6 Surface of Lignite Particle at 57% DAF Weight Loss. 1750K, 20% Oxygen

Figure 9.7 Partially Oxidized Lignite Particle at 72% DAF Weight Loss. 1750K, 20% Oxygen

again indicate the region analyzed by the EDXA. In Figure 9.8A, the ash droplets appear to be distinct and molten whereas, in Figure 9.9A, the ash appears to cover the surface as a crystalline mass with no descrete particles. The ash on the surface of the char shown in Figure 9.10A illustrates the intimate contact between ash and the carbon material for even the rather large droplets. The differences in morphology are undoubtedly due to differences in the composition of the has Although calcium is always present, there is some variability in magnesium, silicon and phosphorus content. Heterogeneity of magnesium distribution on the surface of a single char particle is shown in Figure 9.11A with the corresponding EDXA of regions analyzed given in Figure 9.11B.

The SEM micrographs of char particles, surface regions and corresponding EDXA shown in Figures 9.12 and 9.13 are representative of samples collected or 7.6 cm from injection into the combustion zone. Weight loss measurements indicated that at this distance, the char was nearly 80 percent burned. This is also clearly apparent from the decreased size of the char. At this late stage of char burnout, the average size of the surface and ash particles are considerably larger than at previous stages of burnout, reflecting agglomeration and growth of ash as the char mass and size diminish. The surface of the char particle shown in Figure 12.A is shown in Figure 12.B at higher magnification. The EDXA of the larger oblong ash droplet (a), the smaller spherical droplet, (b) and the organic region (c) are compared in Figure 12.C.

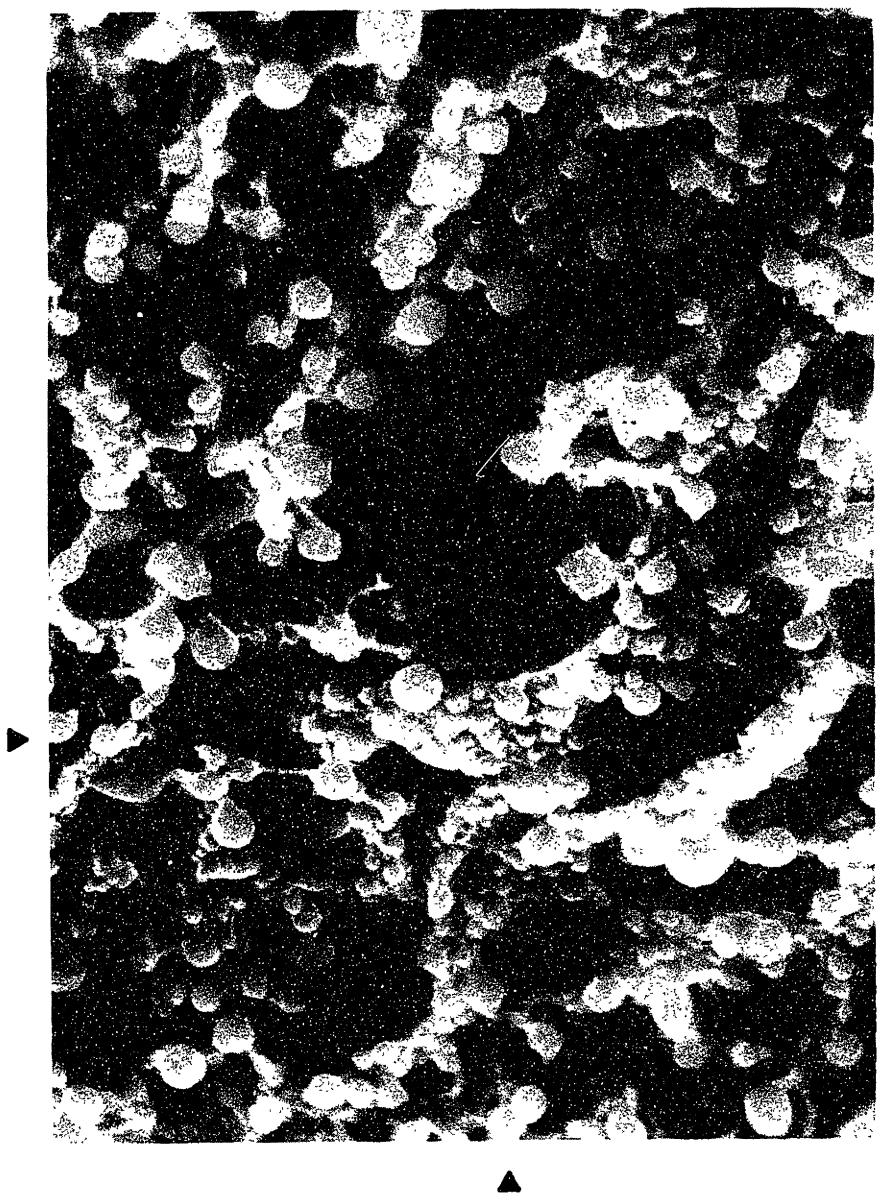

Figure 9.8A Surface of Lignite Char Particle at 72% DAF Weight Loss. 1750K, 20% Oxygen

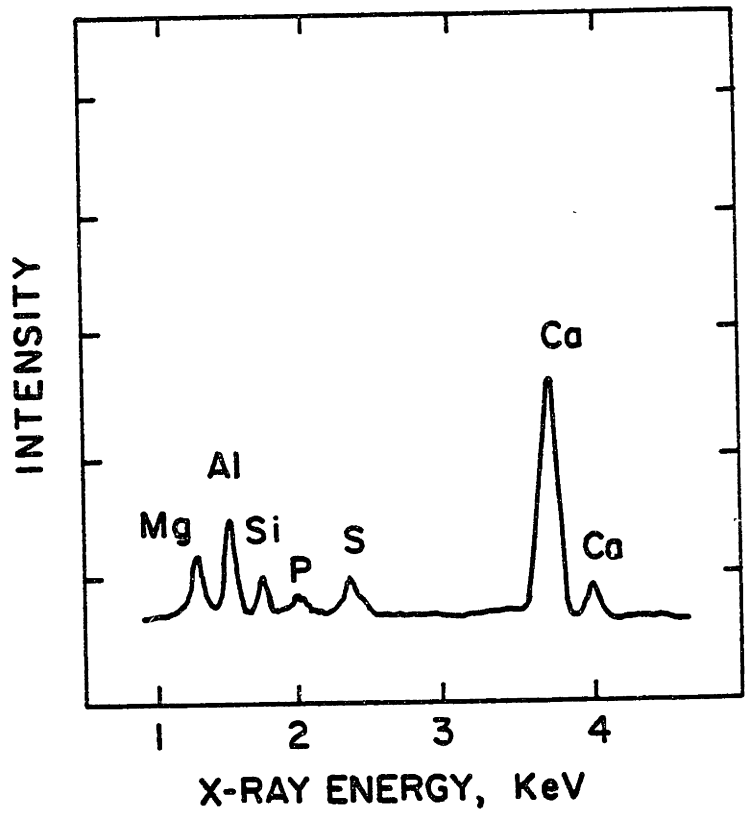

Figure 9.8B

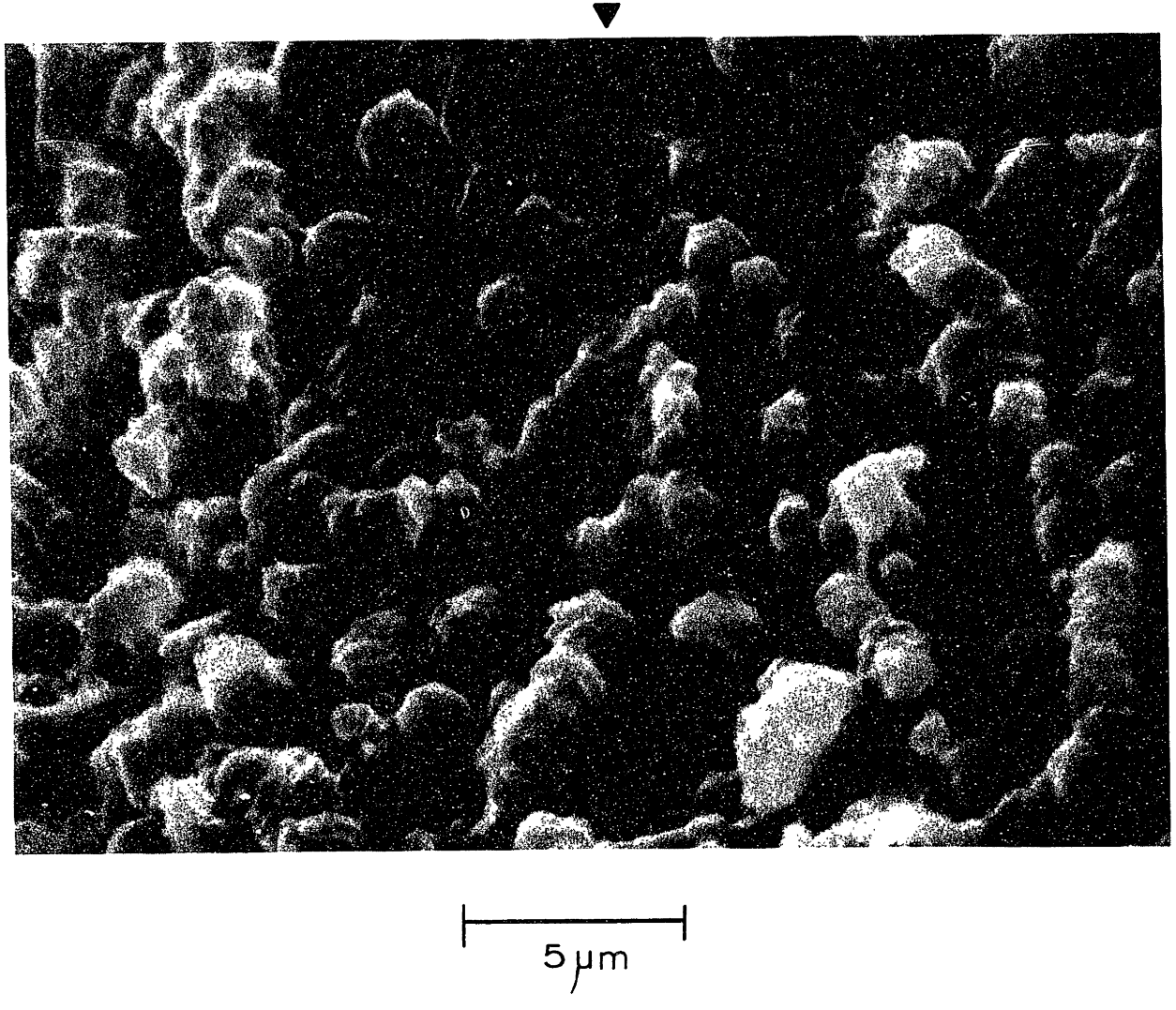

Figure 9.9A Surface of Lignite Char at 72% DAF Weight Loss. 1750K, 20% Oxygen

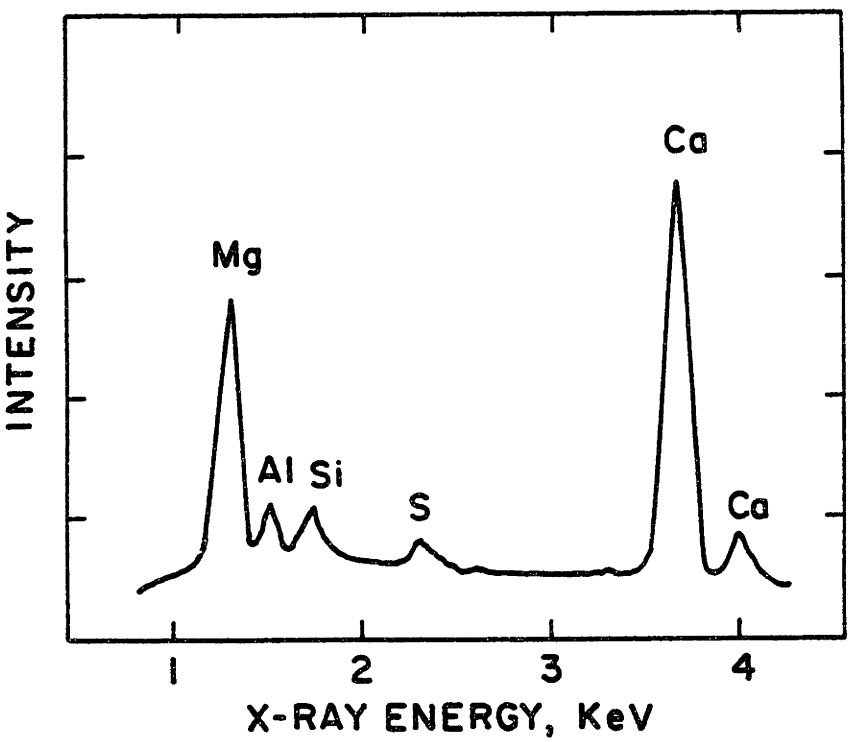

Figure 9.9B EDXA Spectra

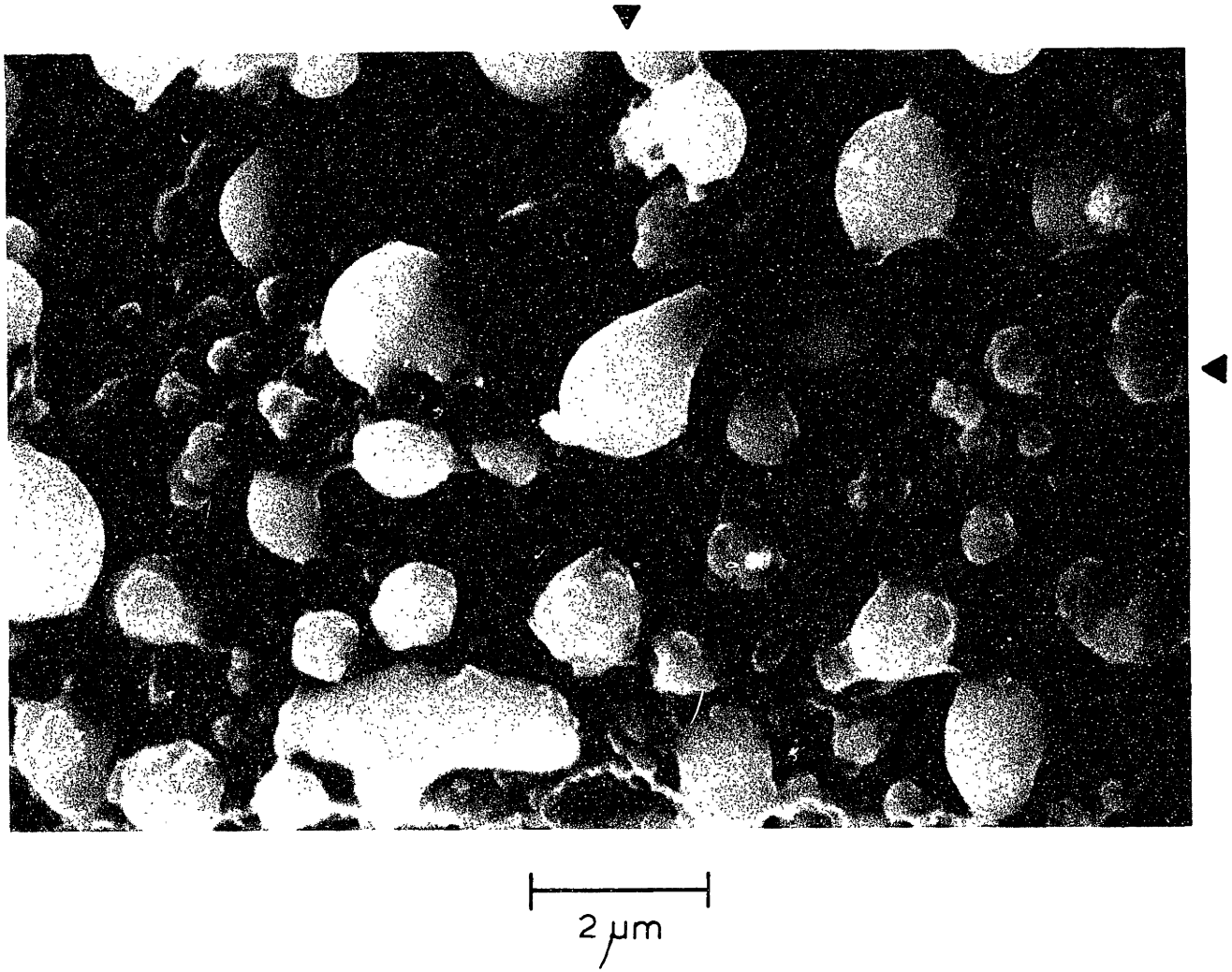

Figure 9.10A Surface of Lignite Char Particle at 72% DAF Weight Loss. 1750K, 20% Oxygen

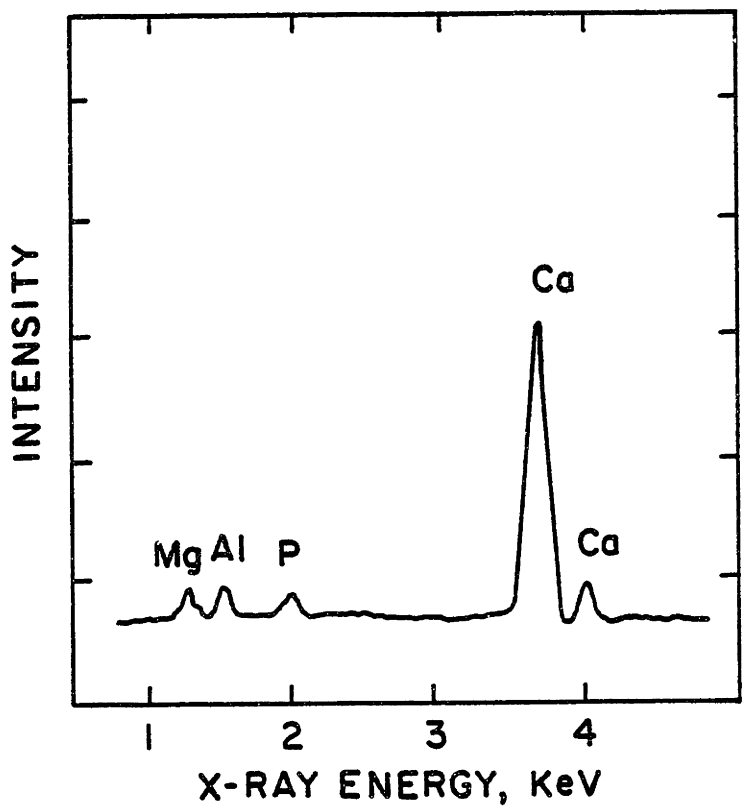

Figure 9.10B EDXA Spectra

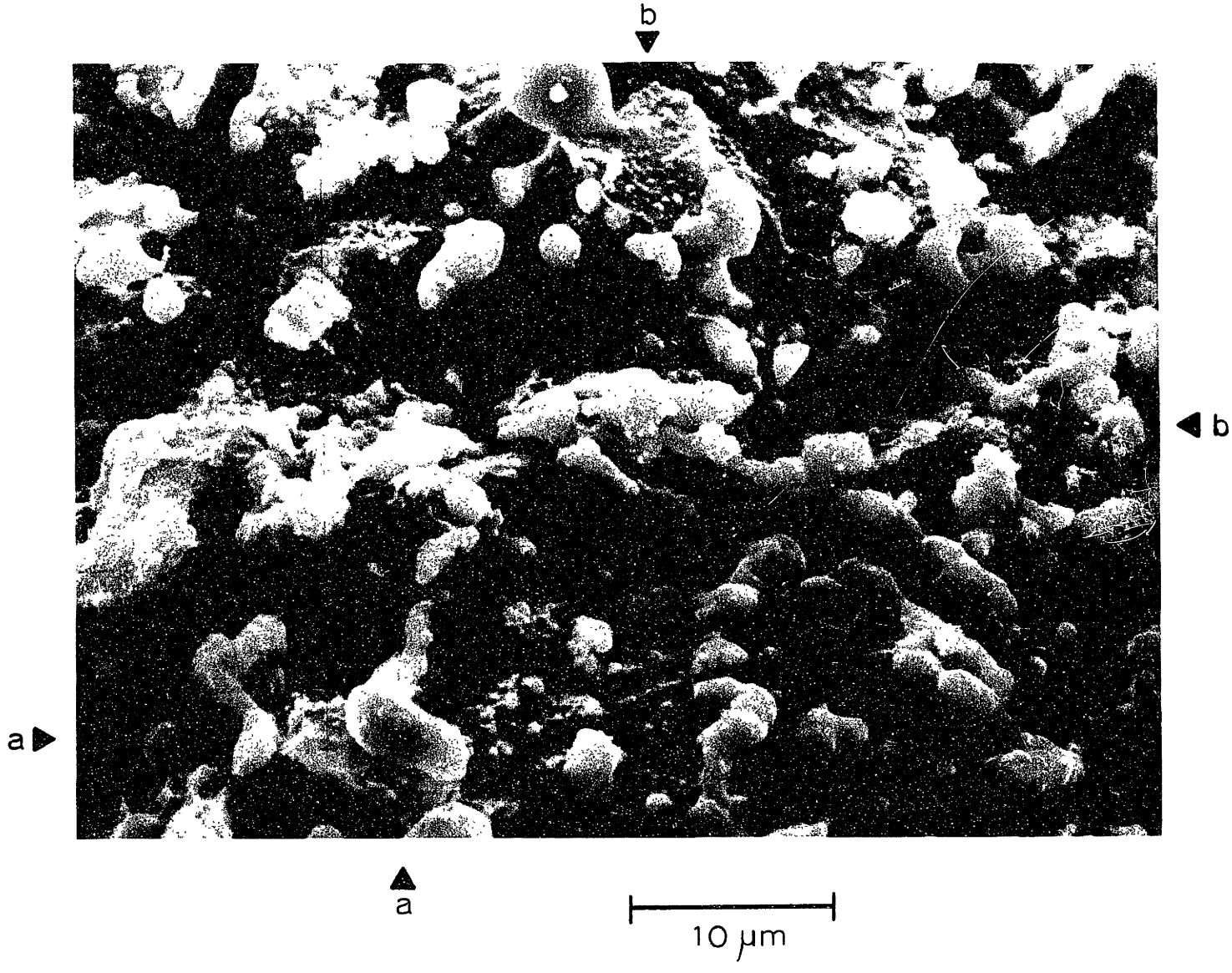

Figure 9.11A Surface of Lignite Char Particle at 72% DAF Weight Loss. 1750K 20% Oxygen

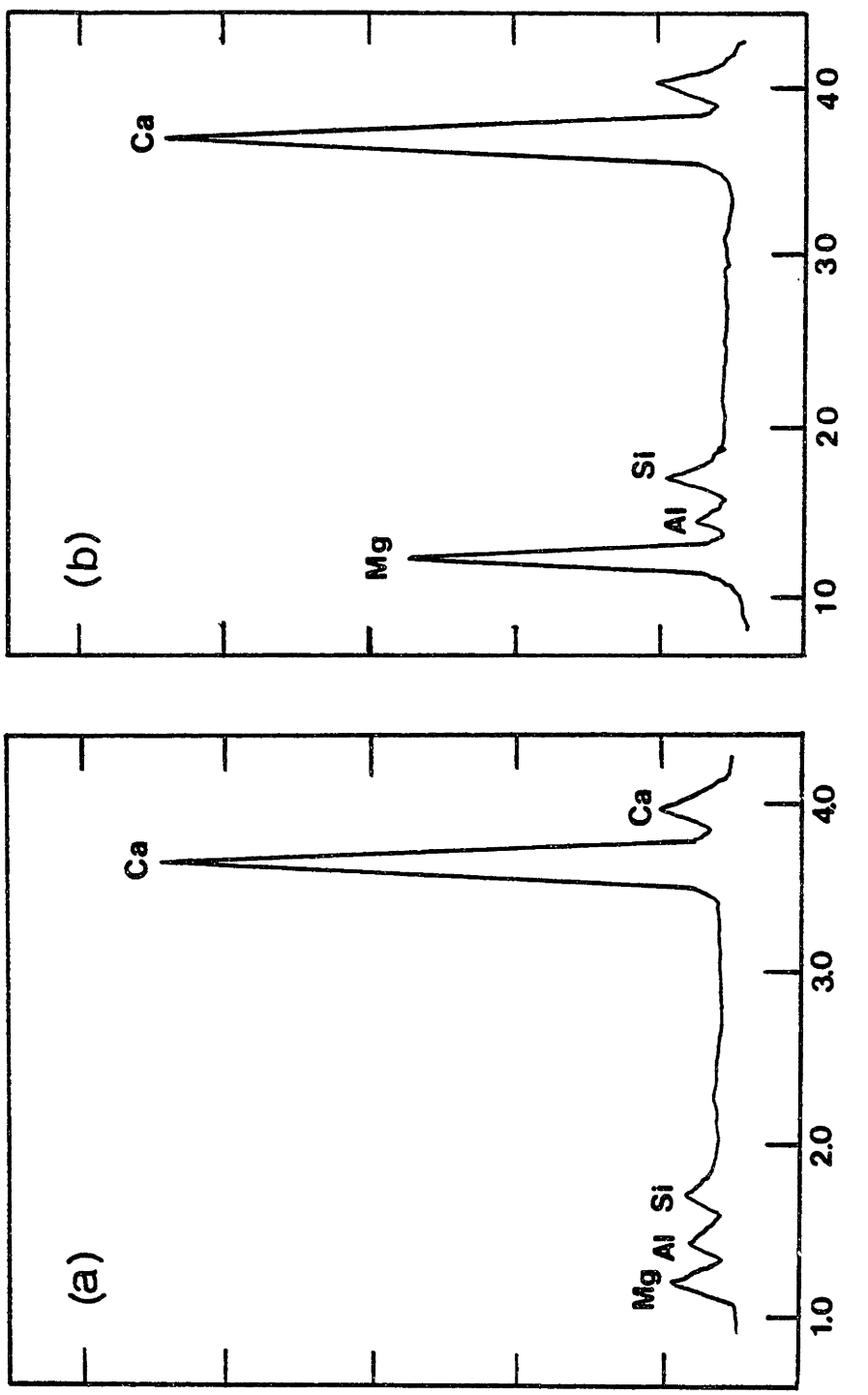

Figure 9.11B EDXA Spectra

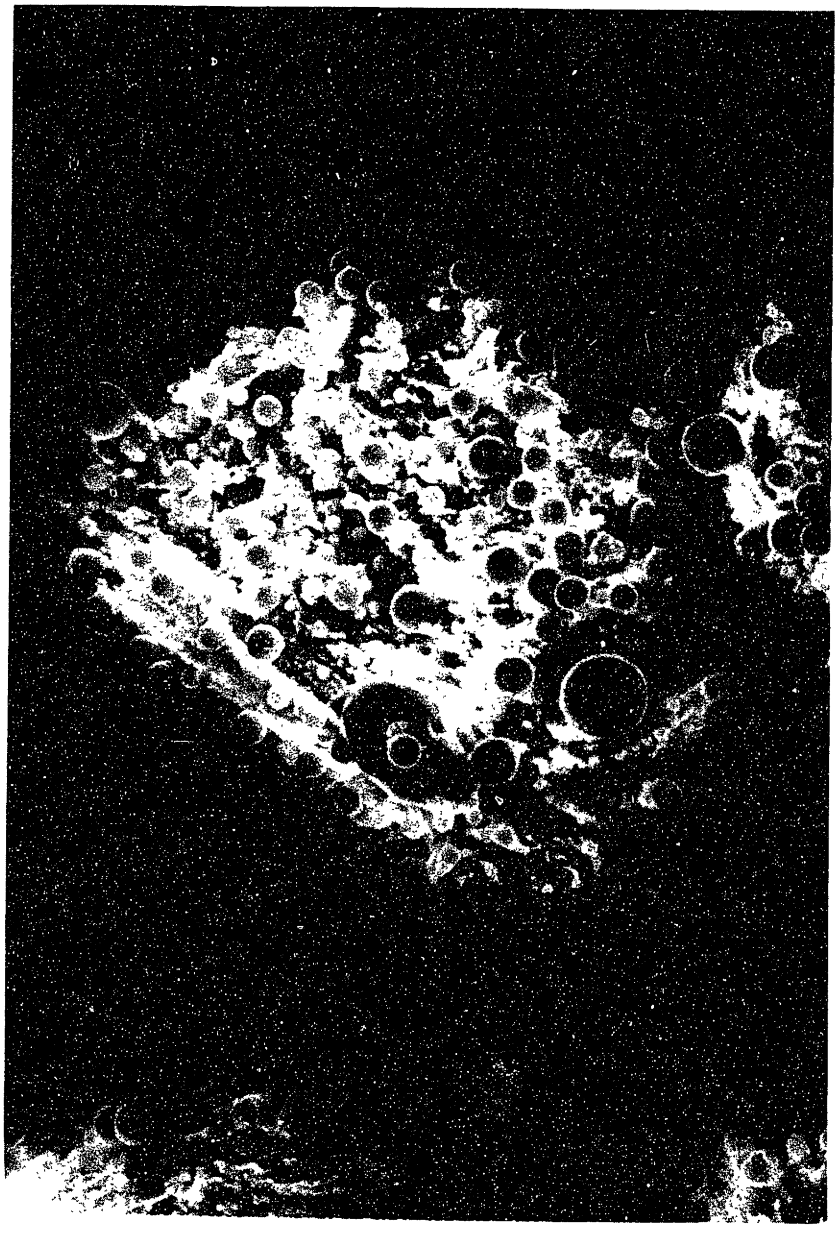

Figure 9.12A Lignite Char Particle at 82% DAF Weight Loss. 1750K, 20% Oxygen

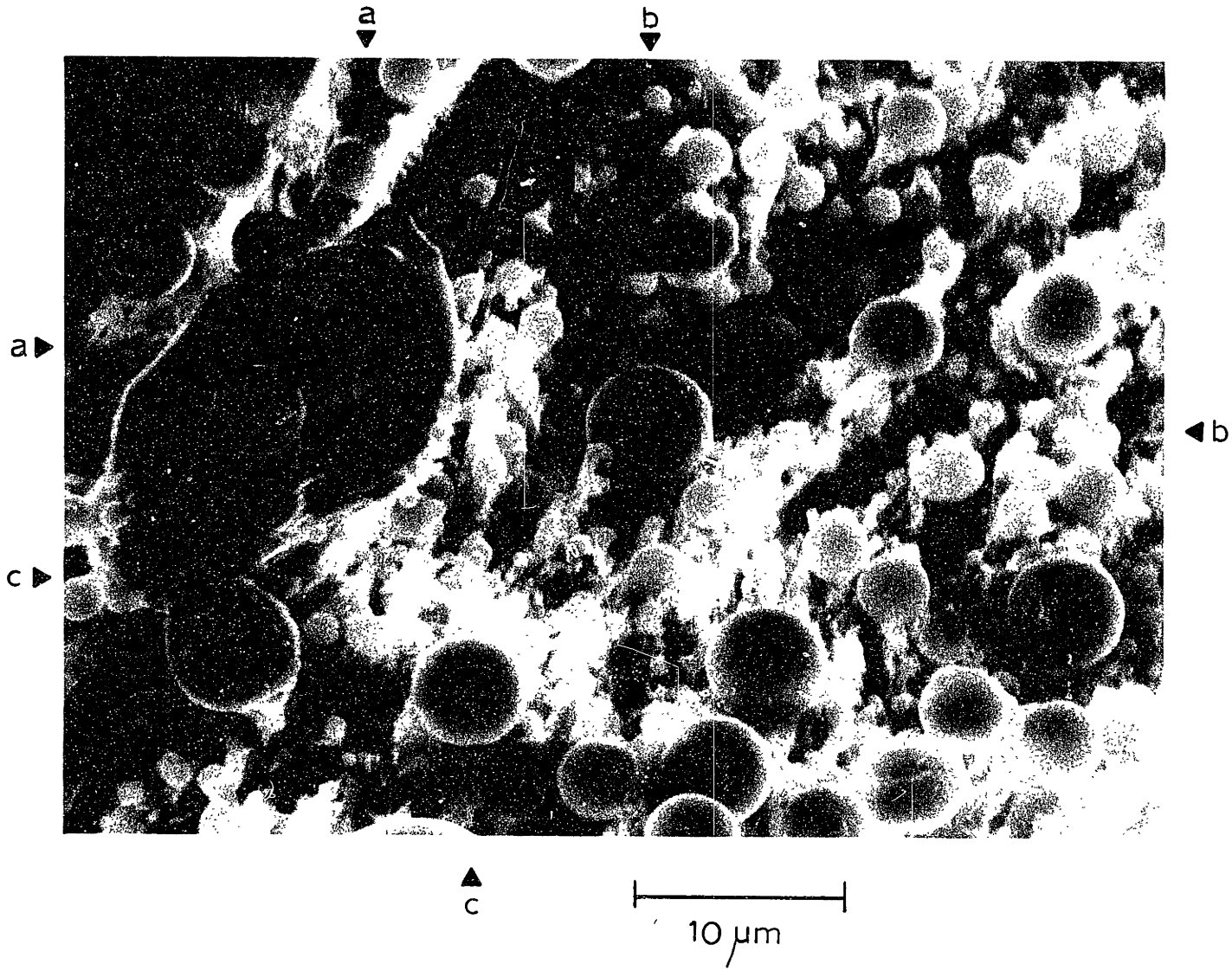

Figure 9.12B Surface of Lignite Char at 82% DAF Weight Loss. 1750K, 20% Oxygen

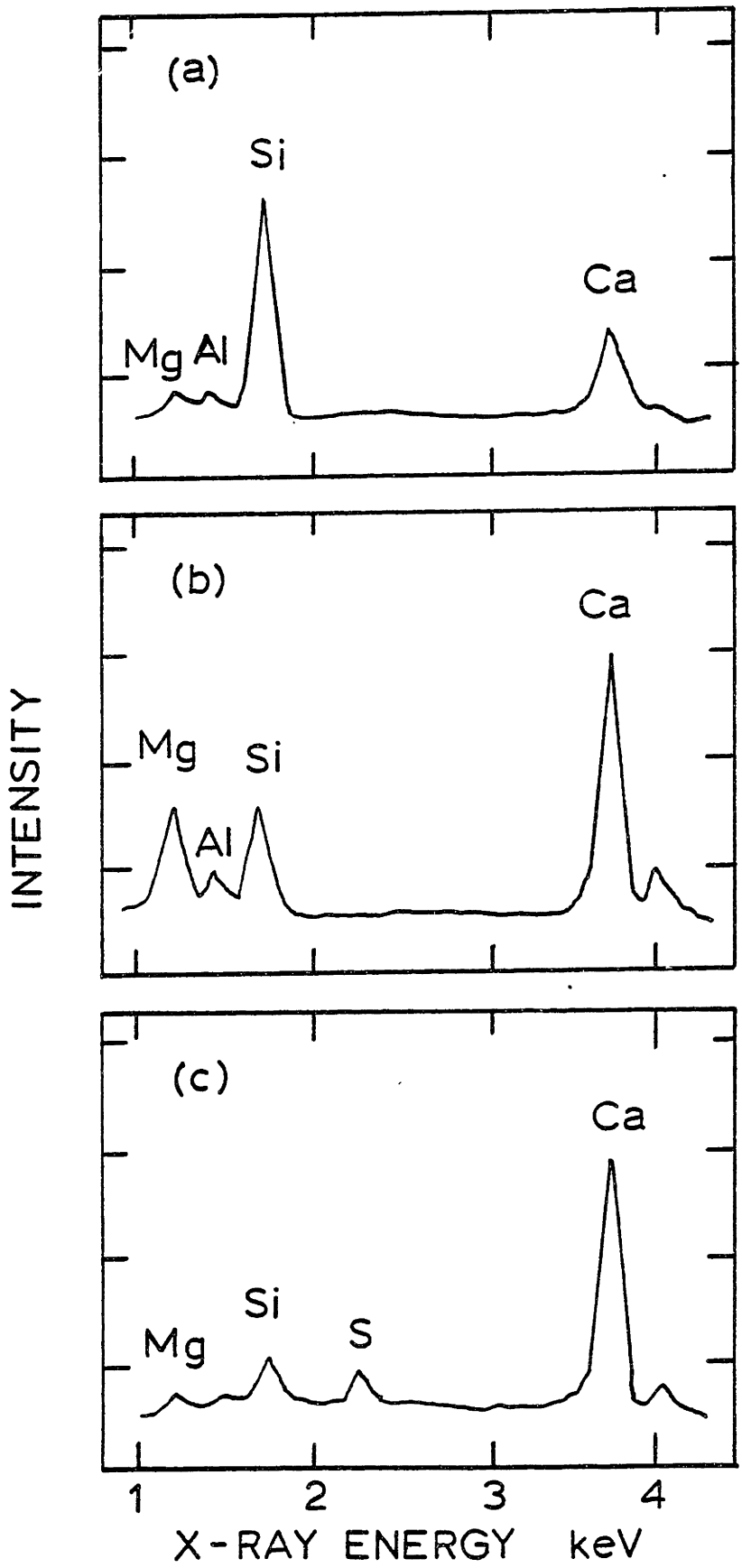

Figure 9.12C ECXA Spectra

The larger oblong droplet (a) is apparently a molten quartz particle that has appeared on the surface of the char at this latter stage of burnout, and during the course of burnout, reacted with the organic calcium to form a melt. The smaller spherical droplet (b) with high calcium and magnesium, apparently receive to the result of significant growth of the organically bound ash during the course of char oxidation. It is also seen to contain silicon. The EDXA of other smaller spherical particles showed similar composition. The region (1 micron area) located by the (c) arrows, corresponds to the ash forming from the organic matter as the last remains of the char is oxidized. It is of note that only the organic region (c) contains detectable sulpher. This char particle appears to contain relatively high silicon concentrations.

The surface of a different char particle (same combustion condition and residence time) is shown at high magnification in Figure 9.13A. The EDXA of the surface ash particles (a) and (b) are given in Figure 9.13B. The larger particle (a) protruding from the char surface is another molten alumino-silicate inclusion. Most of the ash on the surface of this char particle appears to have a similar crystalline morphology, contrasting that of the previous char particle in Figure 9.12A. From the EDXA of particle (b) in Figure 9.13A, it is evident that this material is mostly crystalling Ca0 and Mg0, both of which are expected to be in the solid phase at this combustion temperature. Apparently their is insufficient $Si0_2$ present to form a eutectic. It is of note that there is a

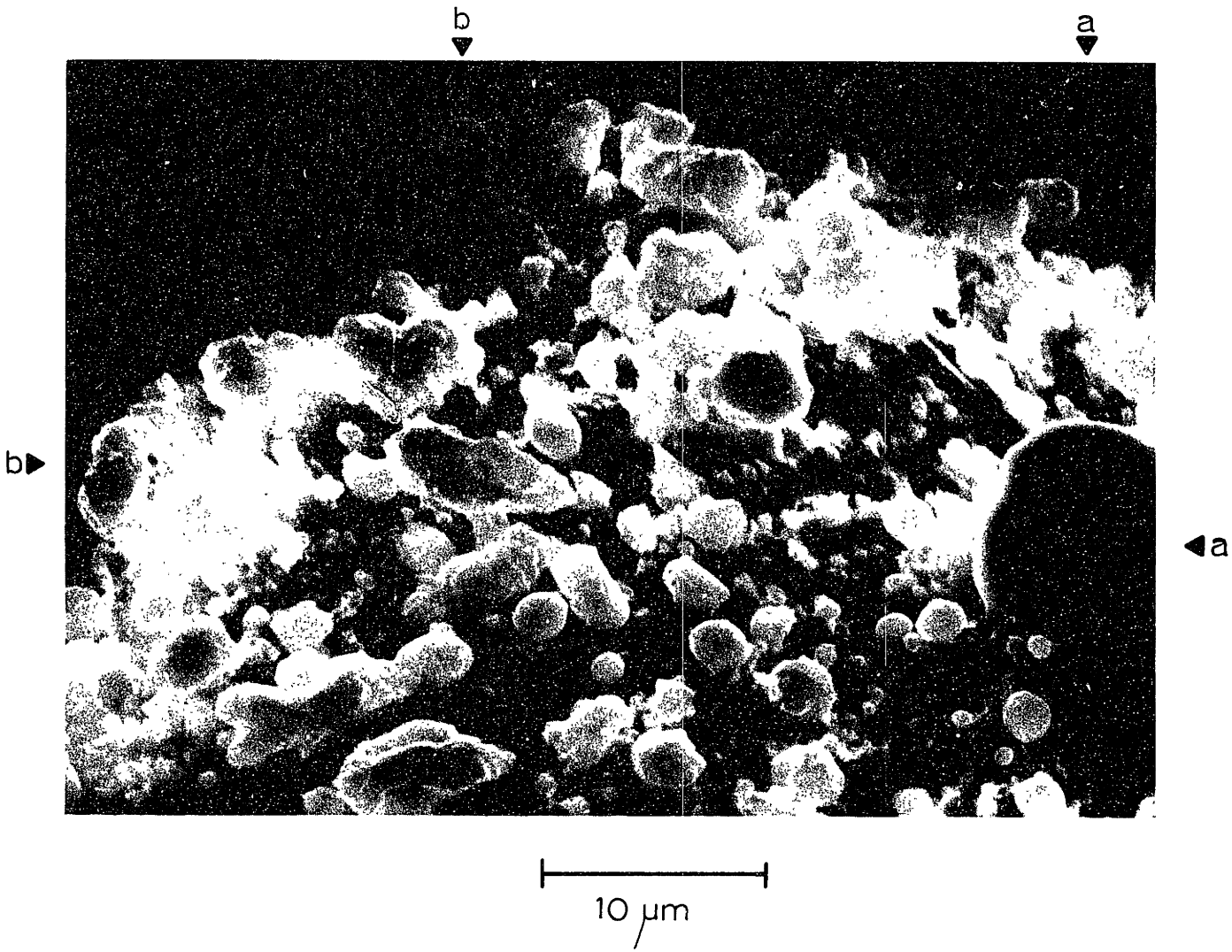

Figure 9.13A Surface of Lignite Char at 82% DAF Weight Loss. 1750K, 20% Oxygen

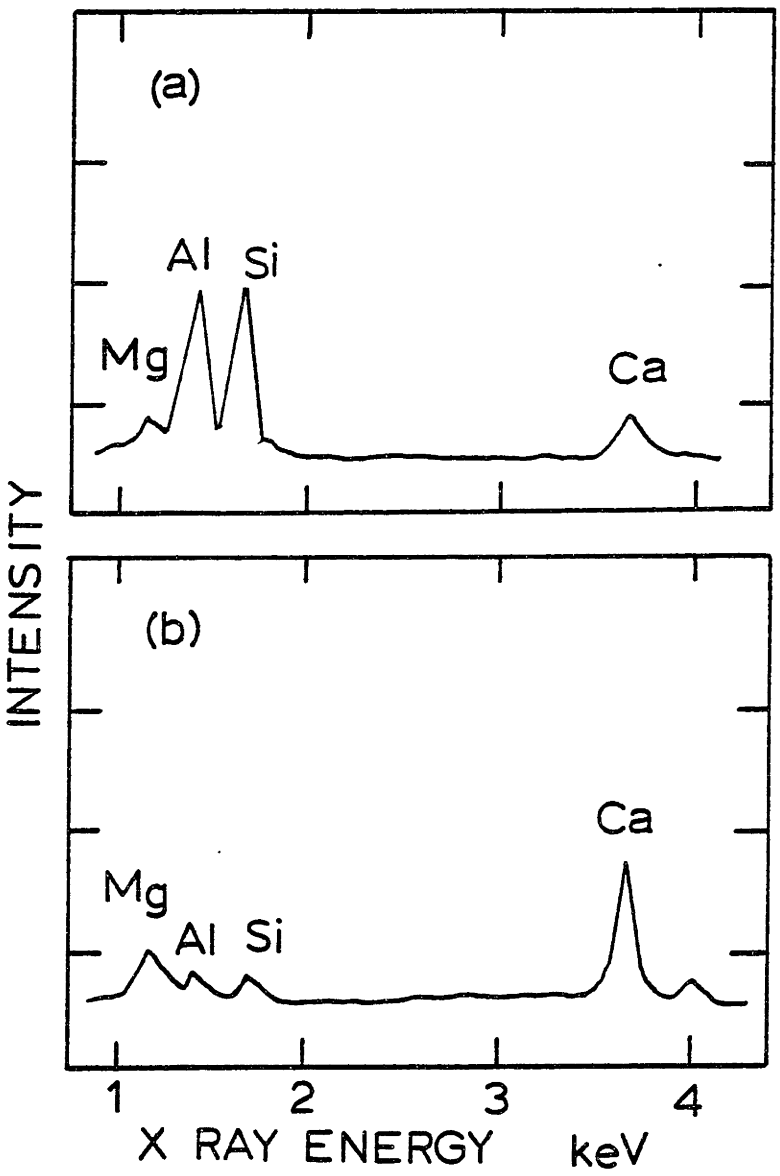

Figure 9.13B EDXA Spectra

trend of increasing crystallinity with increasing distance from the large alumino-silicate inclusion. This may reflect mass transport processes of silicon vapors.

Char particles obtained at each of the burnout stages described above were examined by X-ray diffraction (XRD). The combustion experiments were identical with the exception that the coal was first float in a medium of 1.5 specific gravity prior to combustion. The purpose of this was to remove all extraneous minerals (e.g. dolomite) so that only the transformations of the ion-exchangable mineral matter, and possibly that of quartz and clays occuring within coal particles, would be observed. XRD of char provides information on the nature of crystalline phases on the surface of the char. The high quenching rate of the sampling system made it possible to observe the crystalline phases that exist during high temperature combustion. The molten oxide material would form a glass under these circumstances.

At 46 and at 57 percent DAF weight loss, no descernable diffraction patterns were observed. However, at both 72 and 82 percent DAF weight loss, crystalline CaO and MgO were clearly observed. These results are presented in Figure 9.14.

9.2.2 Montana Savage Lignite Combustion at 2350 K

Particle combustion temperatures of about 2350 K were measured when the Montana Savage lignite was burned in 50 percent oxygen. However, the short burning times precluded the possibility of obtaining samples in which the char particles were of closely spaced stages of burnout. At this

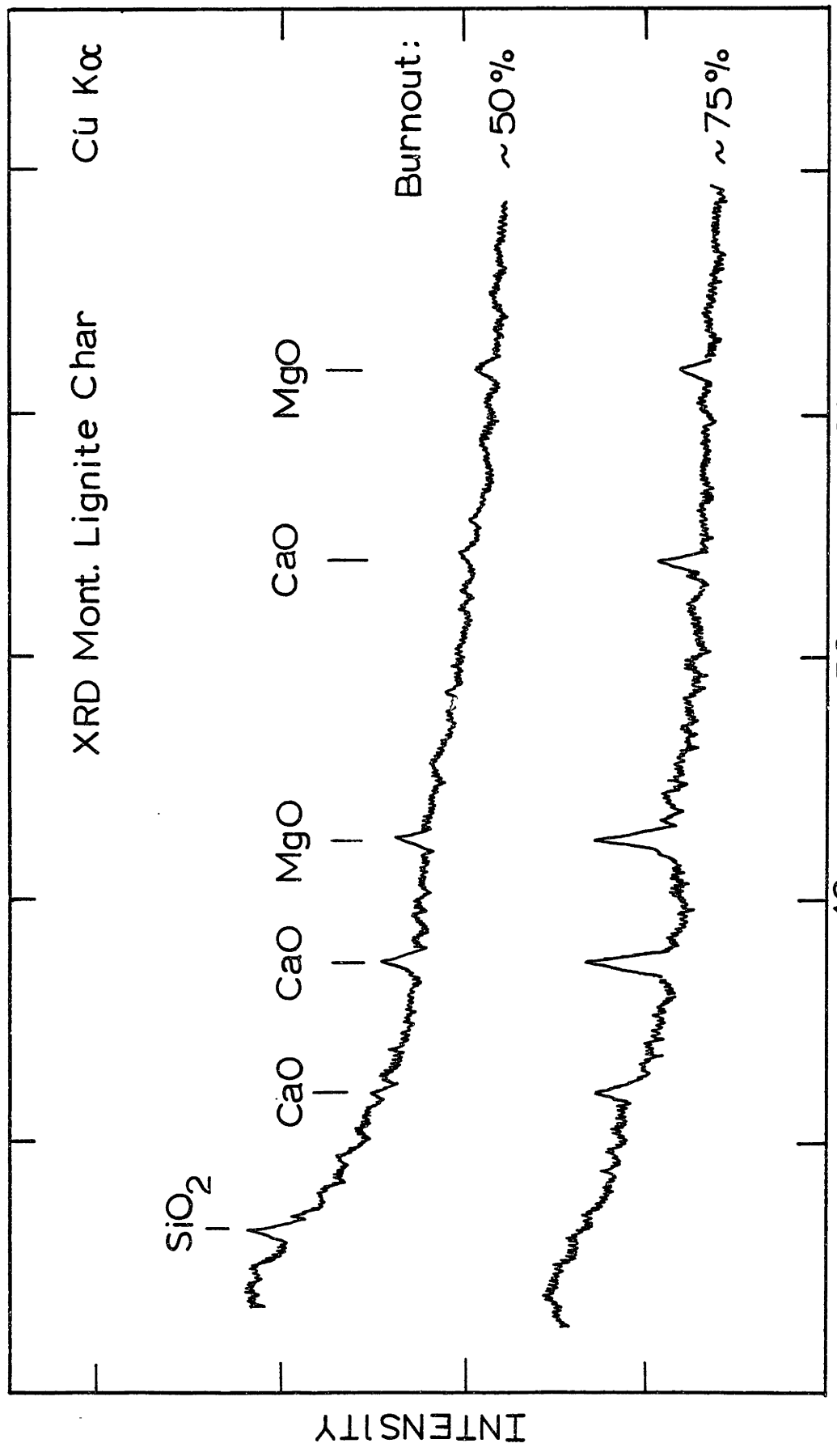

Figure 9.14 X-Ray Diffraction of Lignite Char

condition, the char samples were obtained at 5.7 cm from injection and were observed to have varying degrees of burnout. For this combustion condition, the extent of burnout was estimated by the size of the char particle, and the characteristic size and coverage of the ash on its surface. The SEM micrographs and EDXA shown in Figures 9.15 to 9.22 are of char particles obtained at this high temperature combustion conditions.

The exposure of the ion-exchangable material during the early stages of combustion at 2350 K was similar to that observed for the previously discussed lower temperature case. The only apparent difference was that the lacy structure of the char surface was not observed at this conditon.

The char particle shown in Figure 9.15A is, on the basis of its size, at a late stage of burnout. The ash on its surface was predominantly in the form of molten droplets during combustion. The larger droplet marked by the arrows was analyzed by EDXA and the results are given in Figure 9.15B. On the basis of high silicon content, this droplet was apparently a quartz inclusion which had fused and reacted with the organic Ca and Mg (as oxides) during the char burnout. Other smaller ash droplets in the general vicinity were also analyzed by EDXA. The micrograph shown in Figure 9.15C is of the same surface region at still higher magnification. The EDXA spectra of the droplets (a) and (b) are shown in Figure 9.15D. As seen, the smaller droplets are composed primarily of Ca (oxide), and less silica. Magnesium (oxide) was not

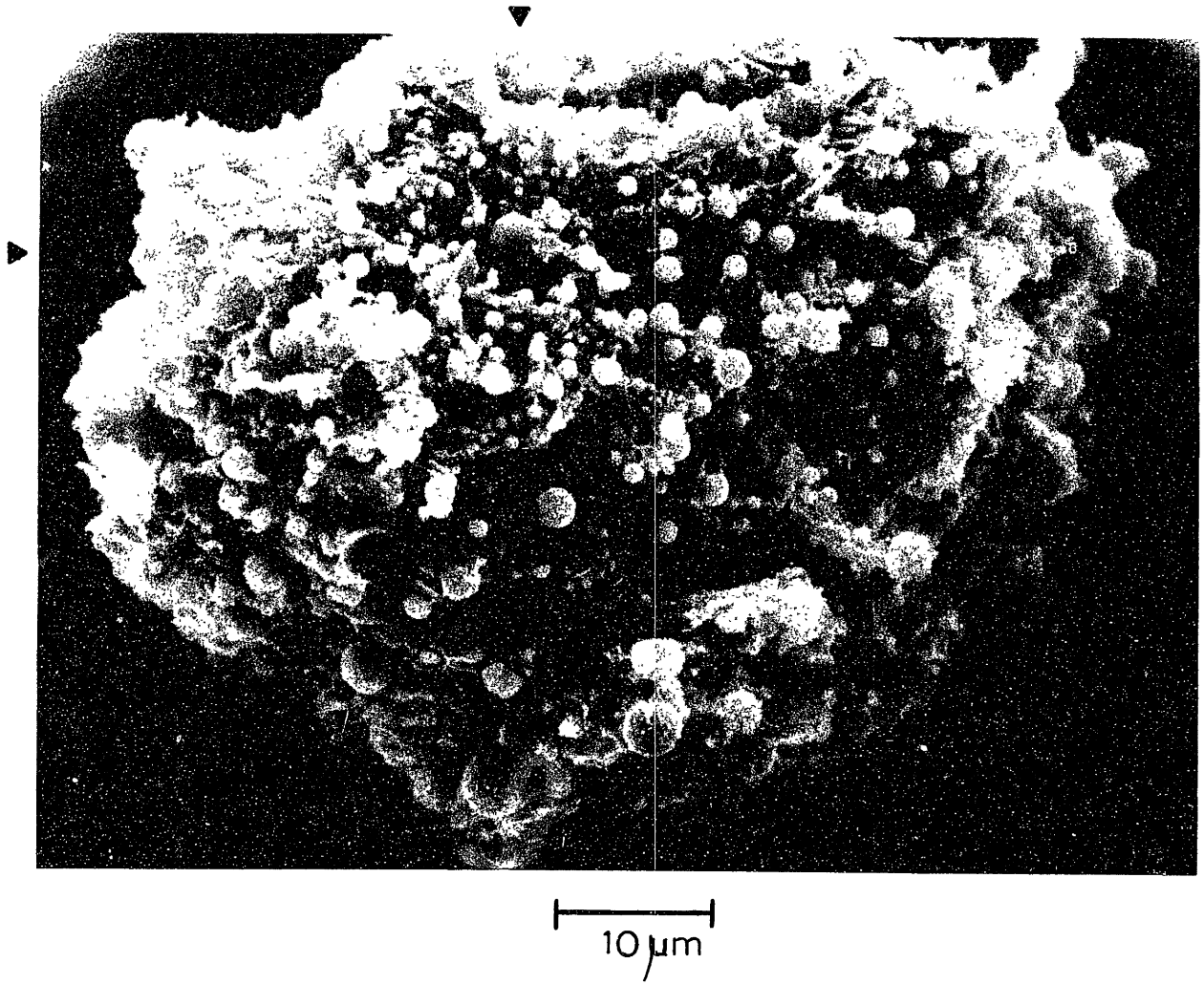

Figure 9.15A Partially Oxidized Lignite Particle
1750K, 50% Oxygen

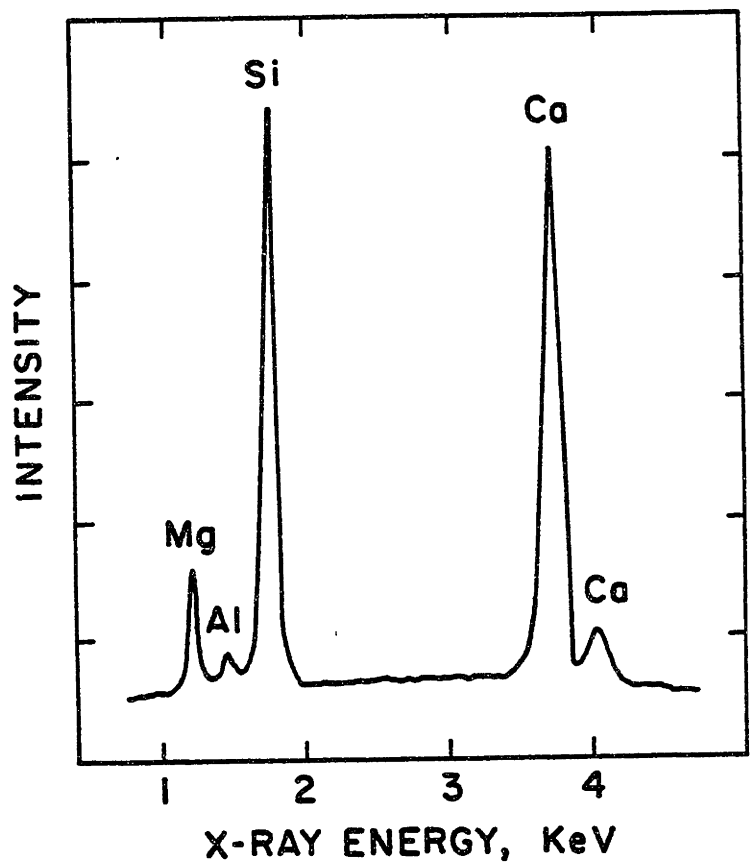

Figure 9.15B EDXA Spectra

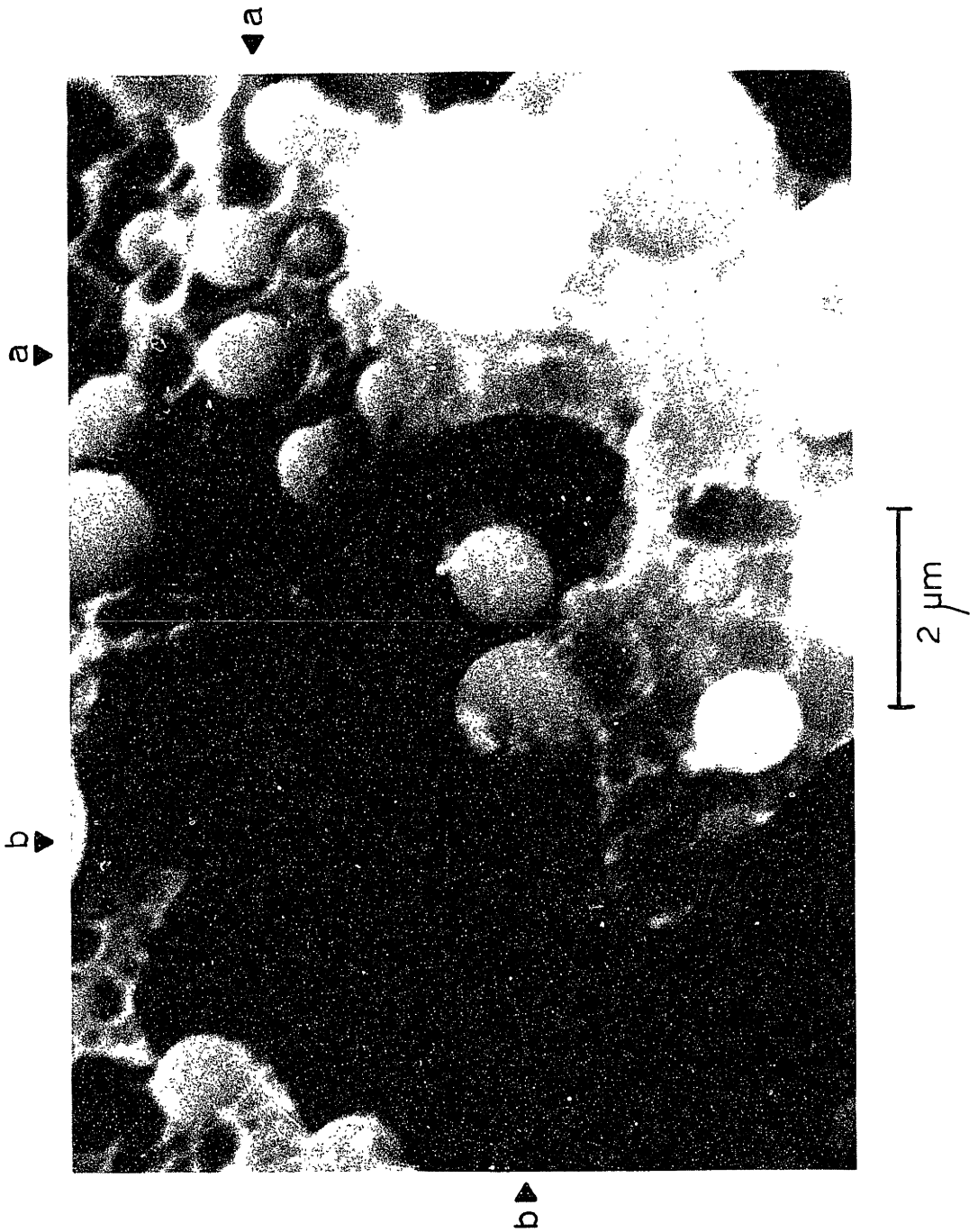

Figure 9.15C Surface of Lignite Char. 1750K, 50% Oxygen

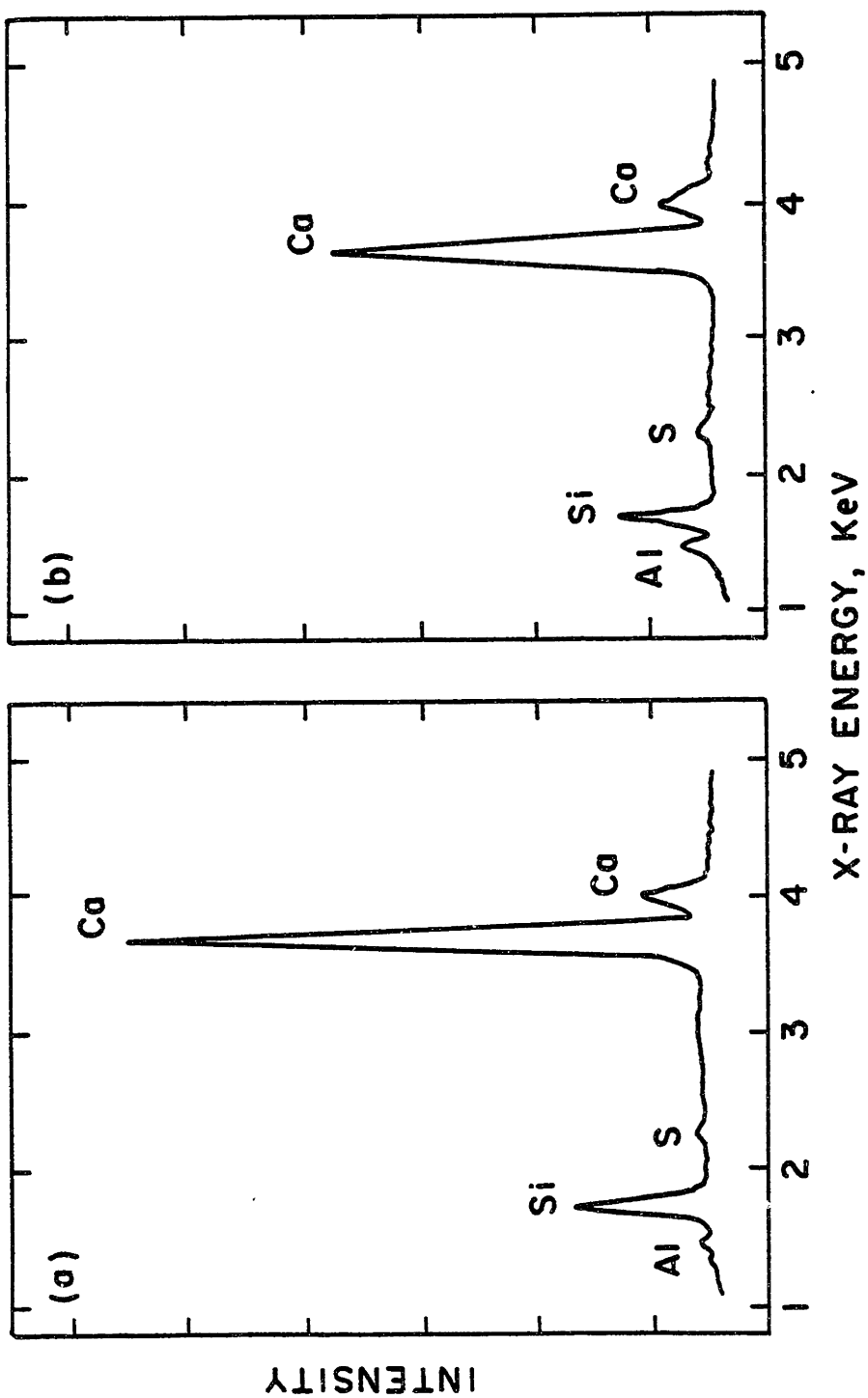

Figure 9.15D EDXA Spectra

observed here, although it was observed in the larger fused quartz particle. As it was shown in Chapter Eight, magnesium vaporized to a great extent at this condition. This may explain why it is not observed in the smaller droplets formed from the organically bound calcium. Its presence in the high silica containing droplet may reflect its low activity in an acidic silica melt (Rein and Chipman, 1965).

It is also seen in Figure 9.15C that a number of the ash droplets on the surface of the char are sitting in holes or pockets as if they have carved or etched the carbon material. This was a common observation for char particles containing molten ash droplets at this high temperature combustion conditions. Two plausible explanations of this phenomena include catalytic action by the ash on the heterogeneous oxidation process or, more likely, visual evidence of direct metal oxide reduction by the carbon leading to volatile inorganic vapors (e.g. SiO(g), Mg(g) and Ca(g) and gasification. The metal oxides (MO) are reduced by carbon monoxide:

$$MO + CO = M(g) + CO_2$$

The carbon dioxide is then cycled back to the carbon surface where it is reduced to carbon monoxide.

Another interesting phenomena that was occasionally observed at this combustion condition is shown in Figure 9.16A. This micrograph is of the surface of another partially burnt char particle. The EDXA of the ash droplets (a) and (b) are compated in Figure 9.16B. The ash droplet (b) is also shown at higher magnification in Figures 9.16C, where the presence

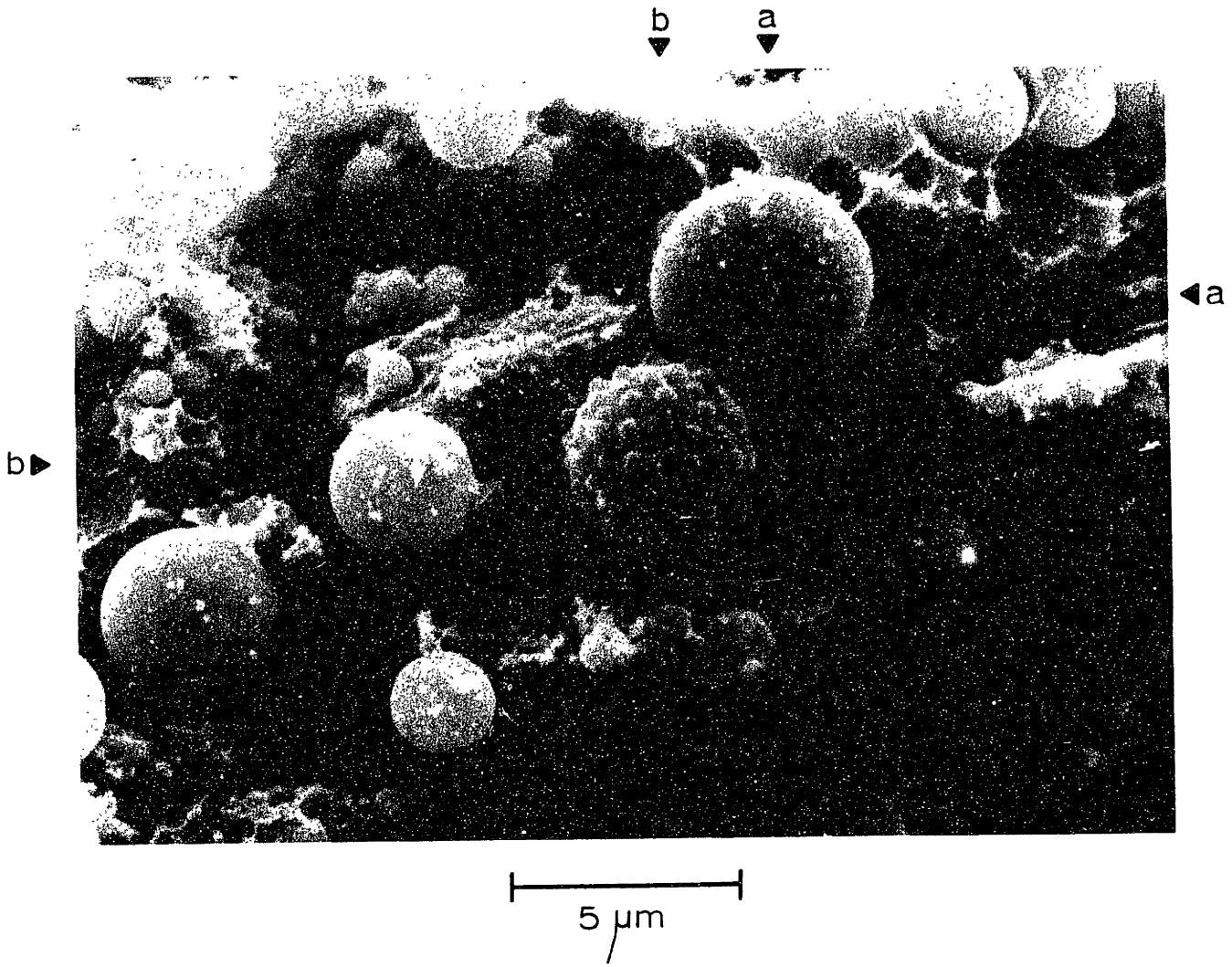

Figure 9.16A Surface of Lignite Char. 1750K, 50% Oxygen

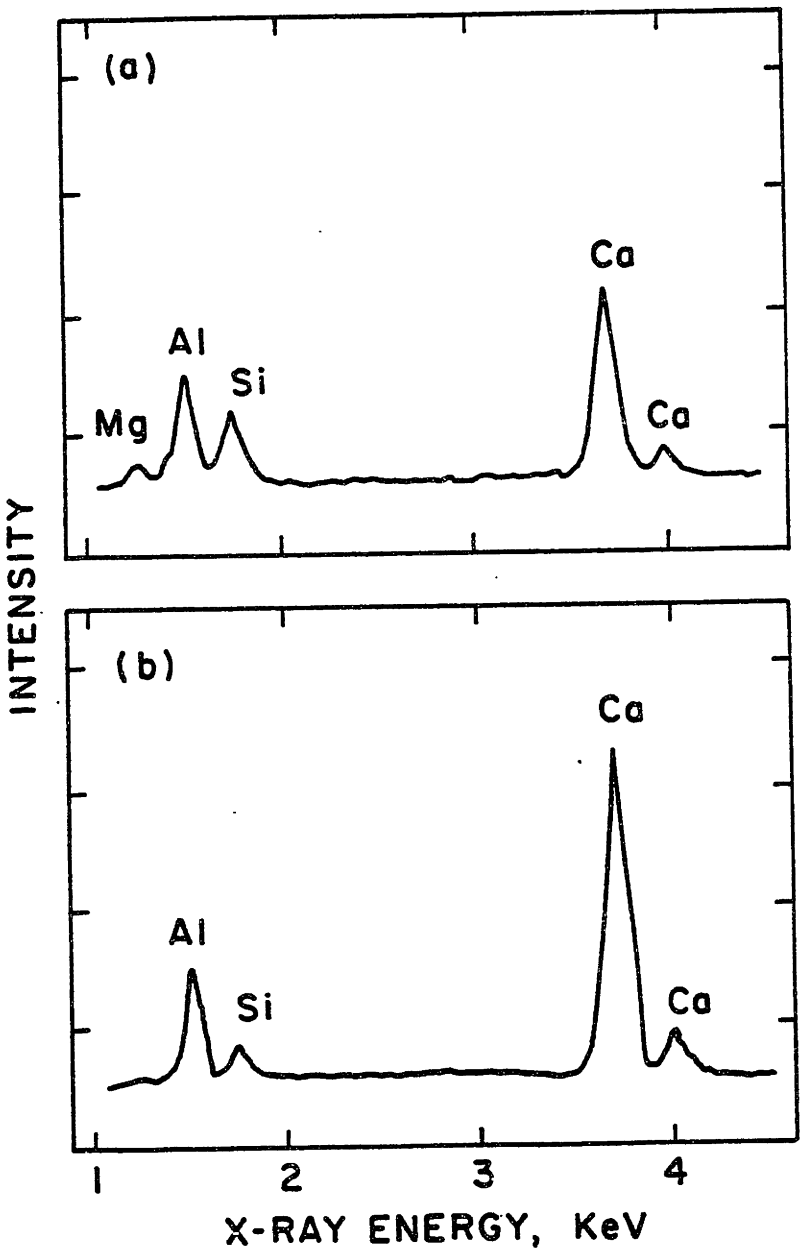

Figure 9.16B EDXA Spectra

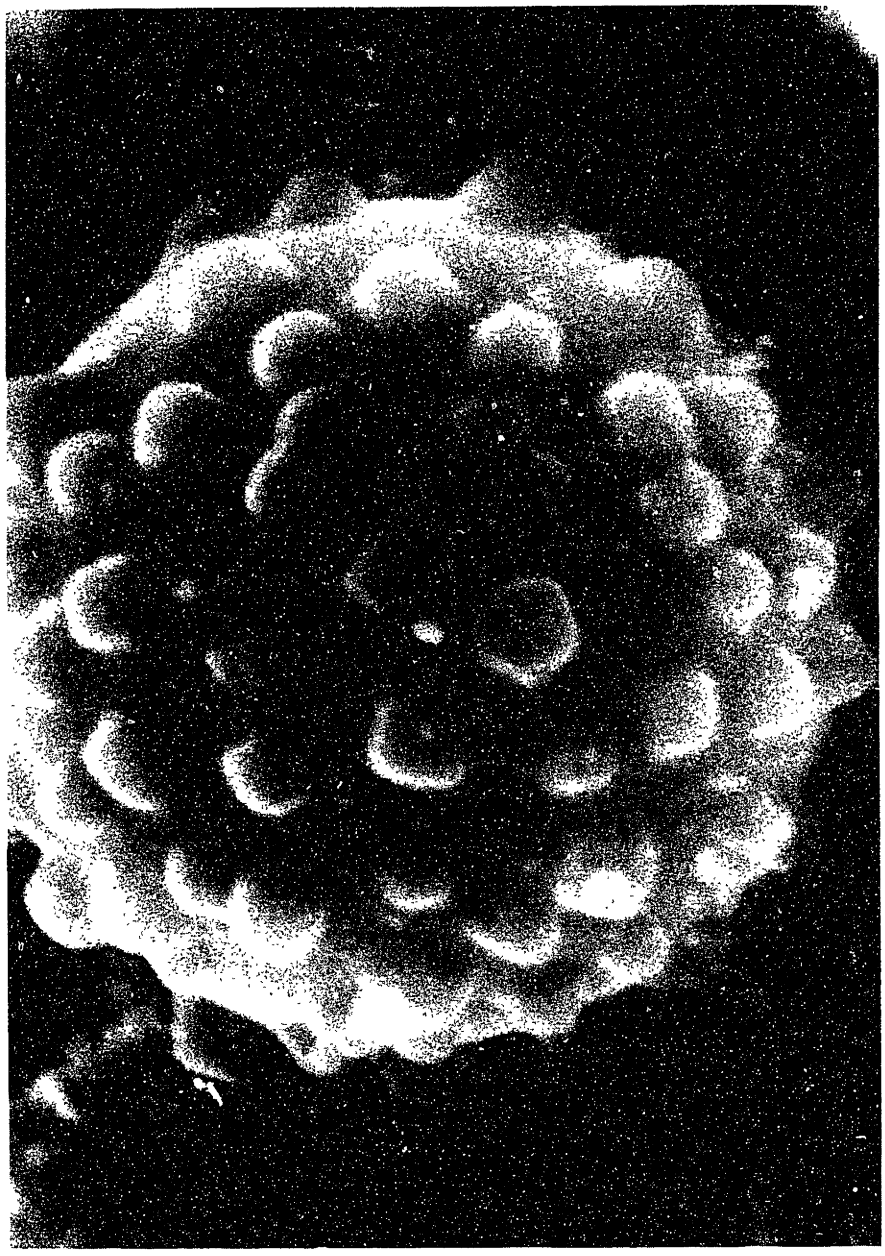

1 um

Figure 9.16C

of submicron crystals are clearly visable. The droplet (a) contains more MgO and SiO_2 than the crystal containing droplet (b). From the CaO - Al_2O_3 - SiO_2 phase diagram (Figure 9.21), it may be inferred that the crystals on the surface of ash droplet (b) are CaO(c), coexisting in phase equilibrium with the melt of somewhat lower Ca content than indicated by the EDXA spectra. For example, the melt of particle (b) may have a composition close to that of particle (a). Precipitation of crystals from a slag melt would not occur during the rapid quenching of combustion gases in the probe. Rather, a glass would form. It may be speculated that these crystals are formed from the melt as a result of changes in activity of the components brought about by the different vaporization rates. In this case, CaO in the melt may have reached its saturation value due to the higher vaporization or reduction rate of SiO_2.

The surface of another partially burnt char particle shown in Figure 9.17A was also obtained at this high temperature combustion condition. The morphological characteristics of the ash on its surface is dramatically different that that previously observed. At higher magnification, as shown, the crystalline nature of the ash is seen. Elemental analysis of the regions (a) and (b) are given in Figure 9.17B. It is likely that the ash is solid CaO, which does not melt until 3200 K. This char particle apparently contains insignificant amounts of SiO_2.

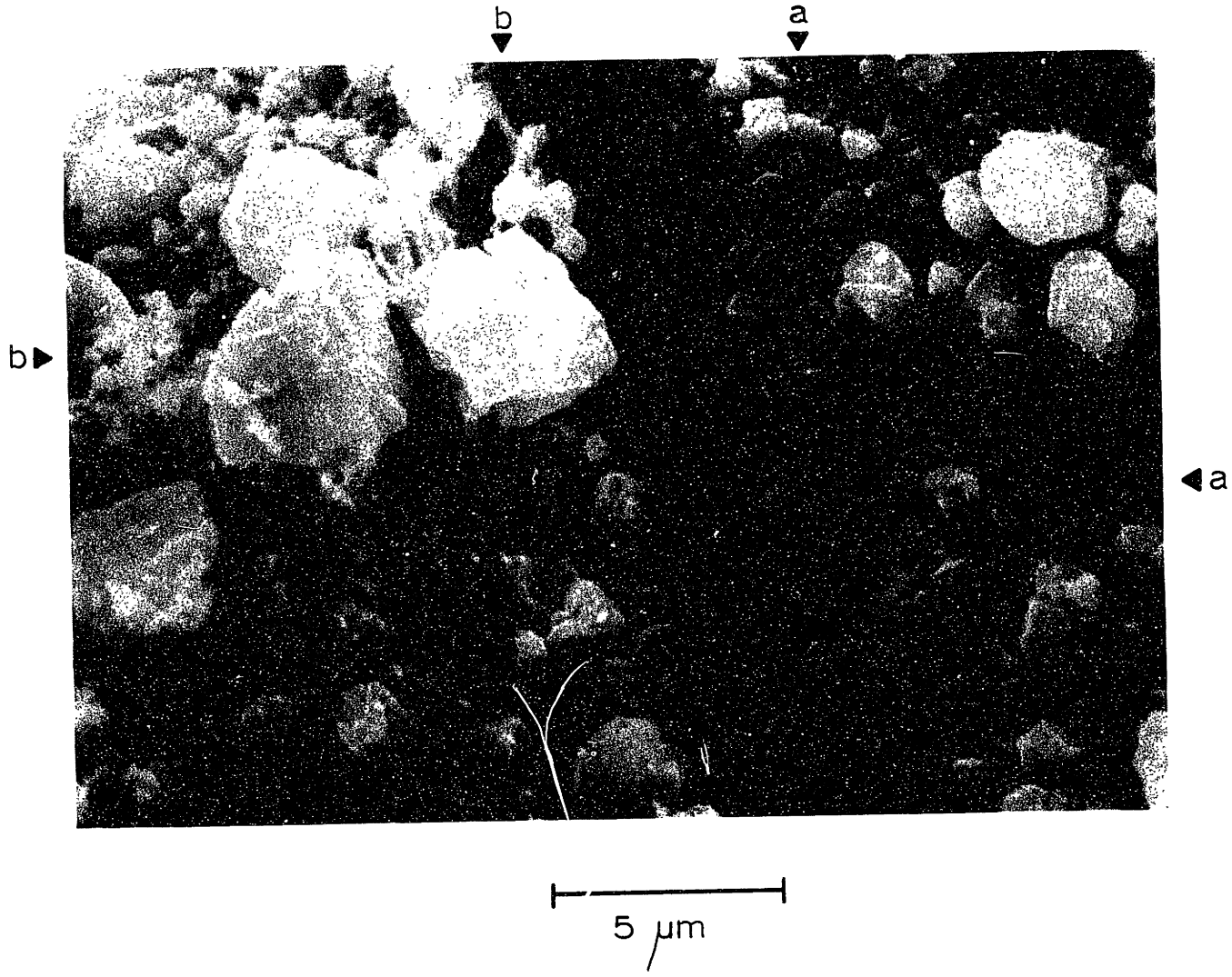

Figure 9.17A Surface of Lignite Char. 1750K, 50% Oxygen

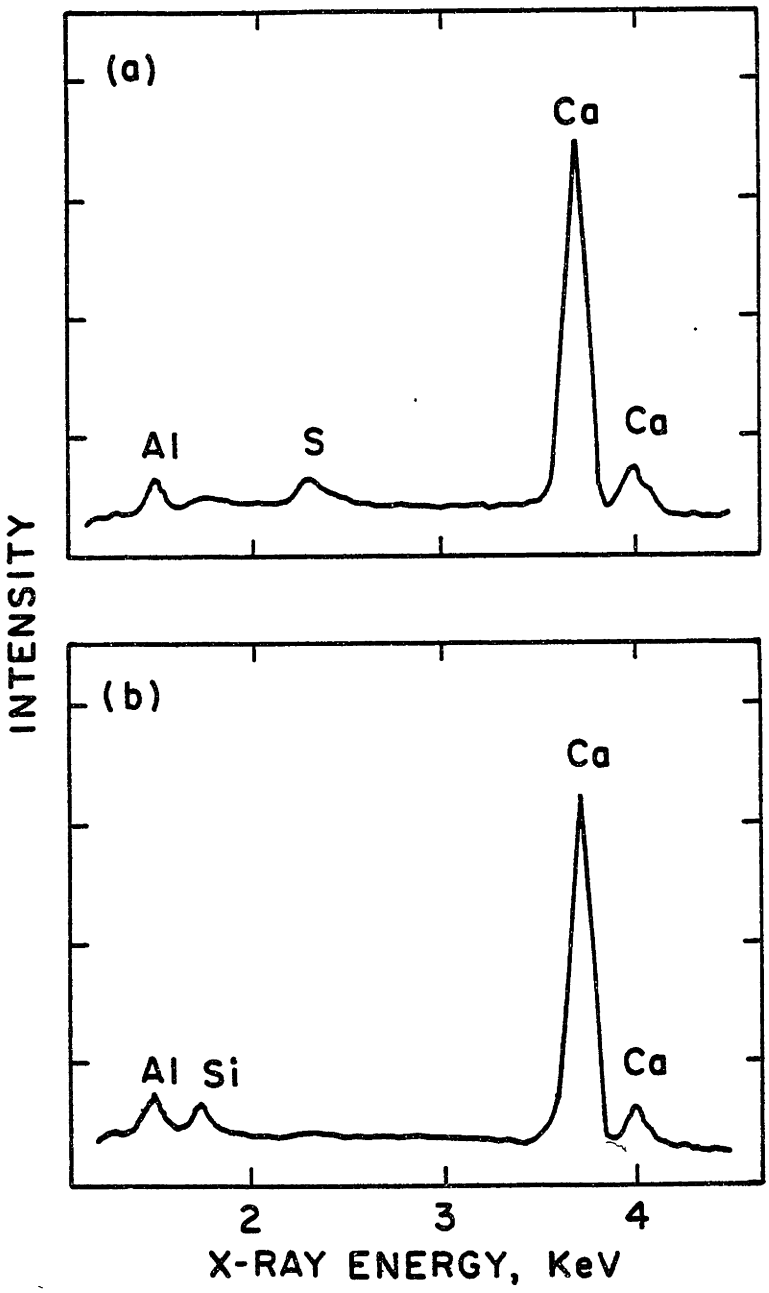

Figure 9.17B EDXA Spectra

9.2.3 X-Ray Diffraction of Combustion Ash

The ash obtained from the complete combustion of the Savage lignite was examined by XRD to determine the what crystalline compounds are formed. These results are presented in Figures 9.18 and 9.19 for combustion in 20 percent and 50 percent oxygen at a furnace wall temperature of 1750 K. Crystalline CaO, MgO and quartz were clearly observed at the lower temperature (20 percent oxygen). In 50 percent oxygen all of these phases, and particularly that of quartz, decreased relative to the background.

9.2.4 Discussion

The microscopic observation illustrate the complex phenomenology of mineral matter transformations during lignite combustion. The most important aspect in this regard is the evolution of calcium, magnesium and, to a lesser extent, aluminum from a high by dispersed-organically bound state in the coal to high temperature crystalline or oxide slag phases on the surface of oxidizing chars particles. The initial step is apparently the formation of submicron grains on the surface of the char after slight gasification of the carbonaceous material has occurred. These grains grow by further addition of 'released' inherent ash and possibly by sintering as the char is further oxidized. Silicate minerals contained within the char particles are affected by this process insofar as they appear to assimilate the alkaline material. Although it cannot be determined by these observations, vapor transport may play an important role in the redistribution or mixing of the metal oxides. For example, magnesium or calcium

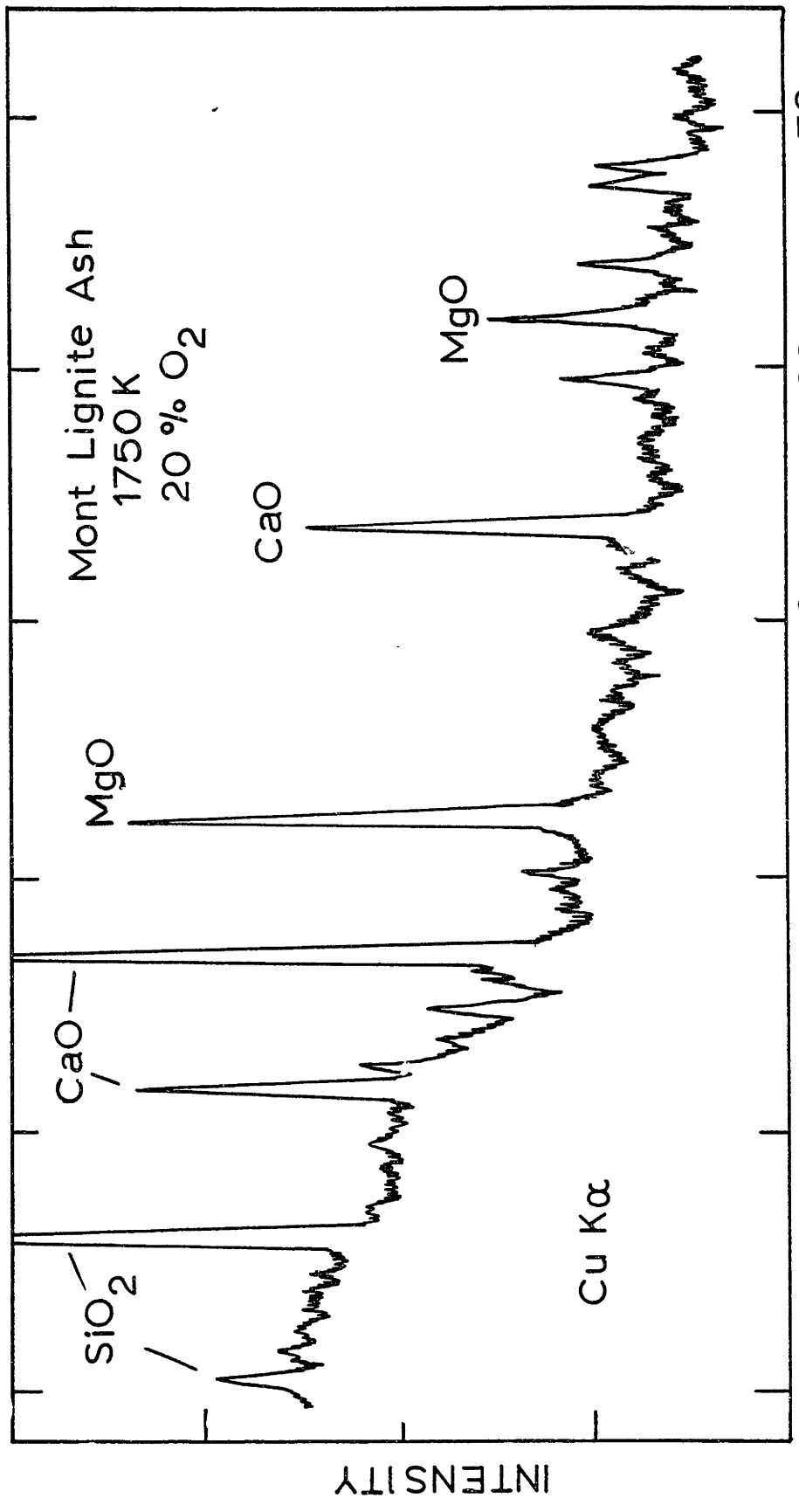

Figure 9.18 X-Ray Diffraction of Lignite Combustion Ash
1750 K, 20% Oxygen

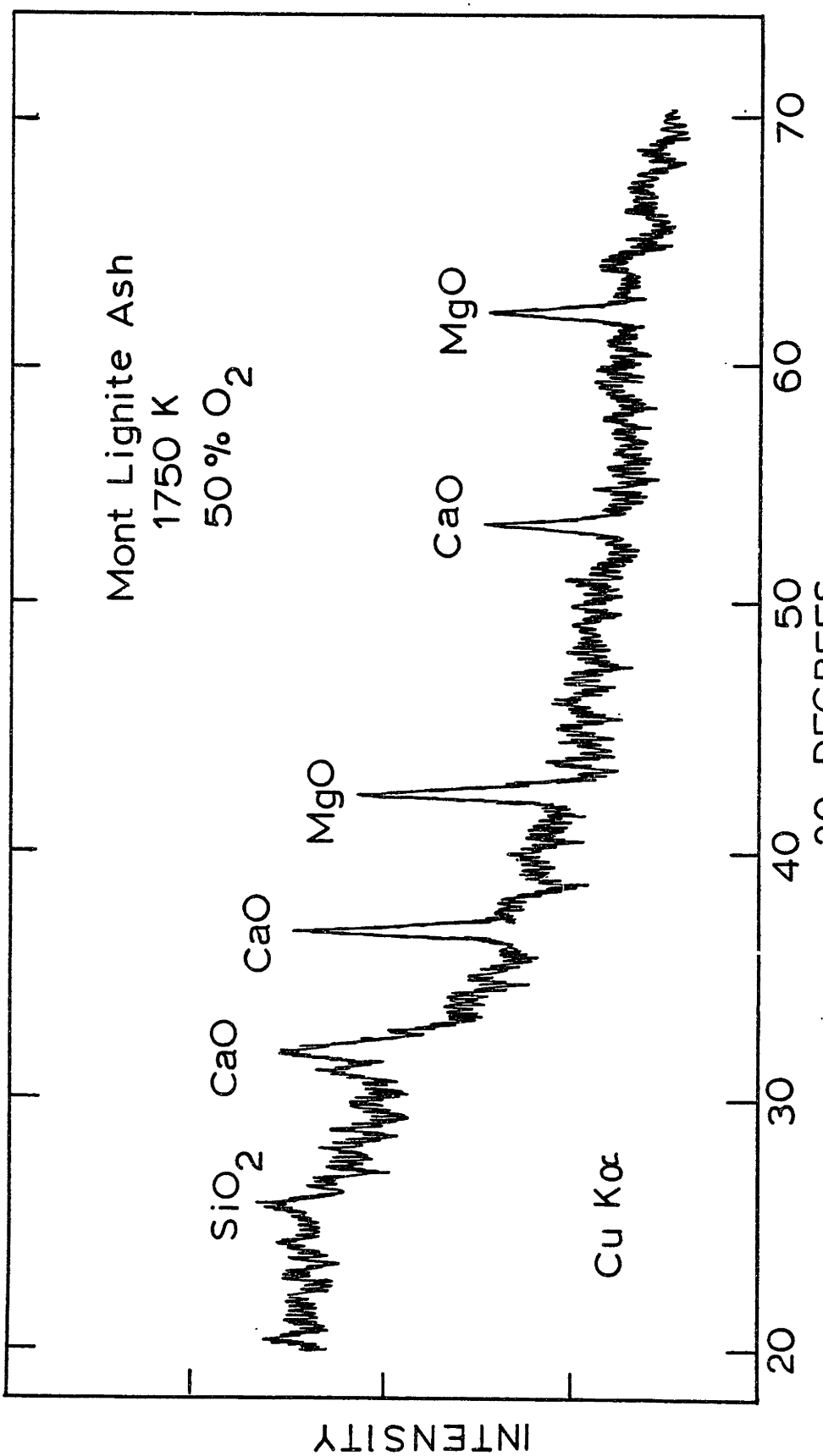

Figure 9.19 X-Ray Diffraction of Lignite Combustion Ash 1750 K, 50% Oxygen

metal vapors diffusing within the char may encounter and react with molten alumino-silicate or quartz inclusions and, similarily, SiO vapors may react with the alkaline oxide phases (Toguri and Pidgeon, 1961).

During the initial stages of char combustion, well-developed metal oxide phases were not observed by XRD. Schaefer (1978) has examined the effect of various metals ion-exchanged on carboxylic groups on the pyrolysis behavior of Brown coals in the 100 to 900°C temperature range. On the basis of an oxygen balance, he suggested that some of the calcium in the presence of carbon reacted with nitrogen yielding cyanides and cyanimides. Magnesium, on the other hand, appeared only to form the oxide. The time of exposure to the pyrolysis temperatures in his experiments was significantly longer (16 hours) than combustion time of coal particles. There have been several investigations on the soluability of nitrogen in $CaO-Al_2O_3$ and $CaO-Al_2O_3$ melts under reducing conditions in the presence of graphite at temperatures around 1600°C (Schwerdtfeger and Schubert, 1977; Chou et al., 1973). Generally the soluabilities of nitride N^{3-}, cyanide CN^{-1}, and barbide under reducing conditions are less than 1 percent. Under some of the experimental conditions of this present study (coal particle combustion temperatures above 2000 K) the formations of calcium, aluminum and silicon carbides are thermodynamically favored in the presence of excess carbide (Appendix D). The melting points of these carbides are all above 2500 K. EDXA of the submicron grains on the surface of the lignite char (Figures 9.3 through 9.5) did reveal

the presence of significant amounts of sulphur, probably in sulphide form. Some of the grains appeared to have irregular shapes. Although the above discussion mentions the possibilities as to what the composition of the initially evolved grains, it is probable that these grains are primarily oxides with dissolved sulphides and possibly carbide as well. From the $CaO-Al_2O_3$ phase diagram shown in Figure 9.20A, it is seen that CaO(S) will coexist with a melt of alumina at compositions approximating those of the EDXA of Figures 9.3D and 9.4B.

After further oxidation of the char, some mixing of the metal oxides has occurred and a variety of morphological forms of the surface ash are observed. In most cases, the observations can be matched with the oxide phase diagrams shown in Figures 9.20 through 9.22.

The XRD results of Figure 9.14 showed that both CaO(s) and MgO (s) were on the surface of the char for a particle combustions temperature of about 1910 K. If both of these components are initially homogeneously distributed throughout the organic matter of a char particle, it is expected that stable separate crystalline phases would develop as seen by the binary phase diagram of Figure 9.20B. In the ternary system of $CaO-Al_2O_3-SiO_2$ (Figure 9.26), stable liquid or solid phases may exist depending on composition and temperature. Examples of the variability of ash morphological characteristics with composition are evident in Figures 9.9 through 9.13.

A

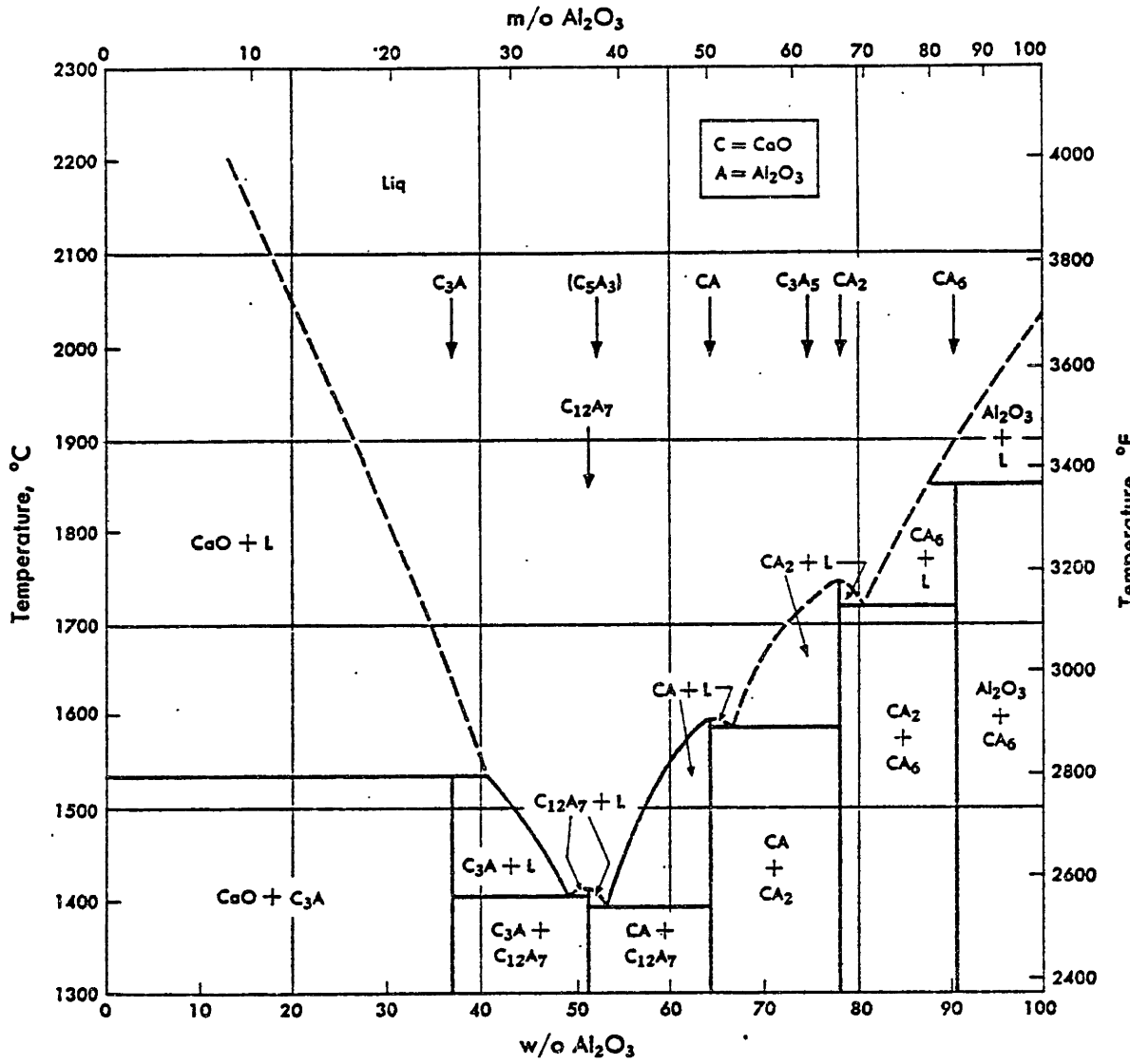

B

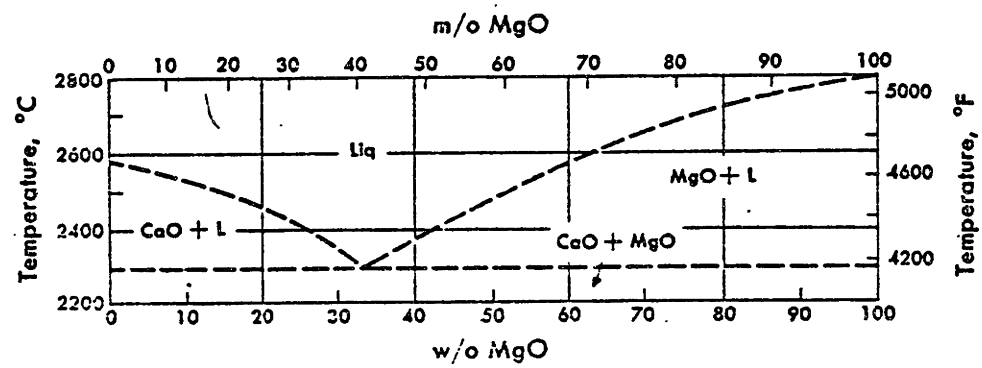

Figure 9.20 Phase Diagrams for $CaO-Al_2O_3$ and CaO-MgO Systems. (Elliot et al., 1963)

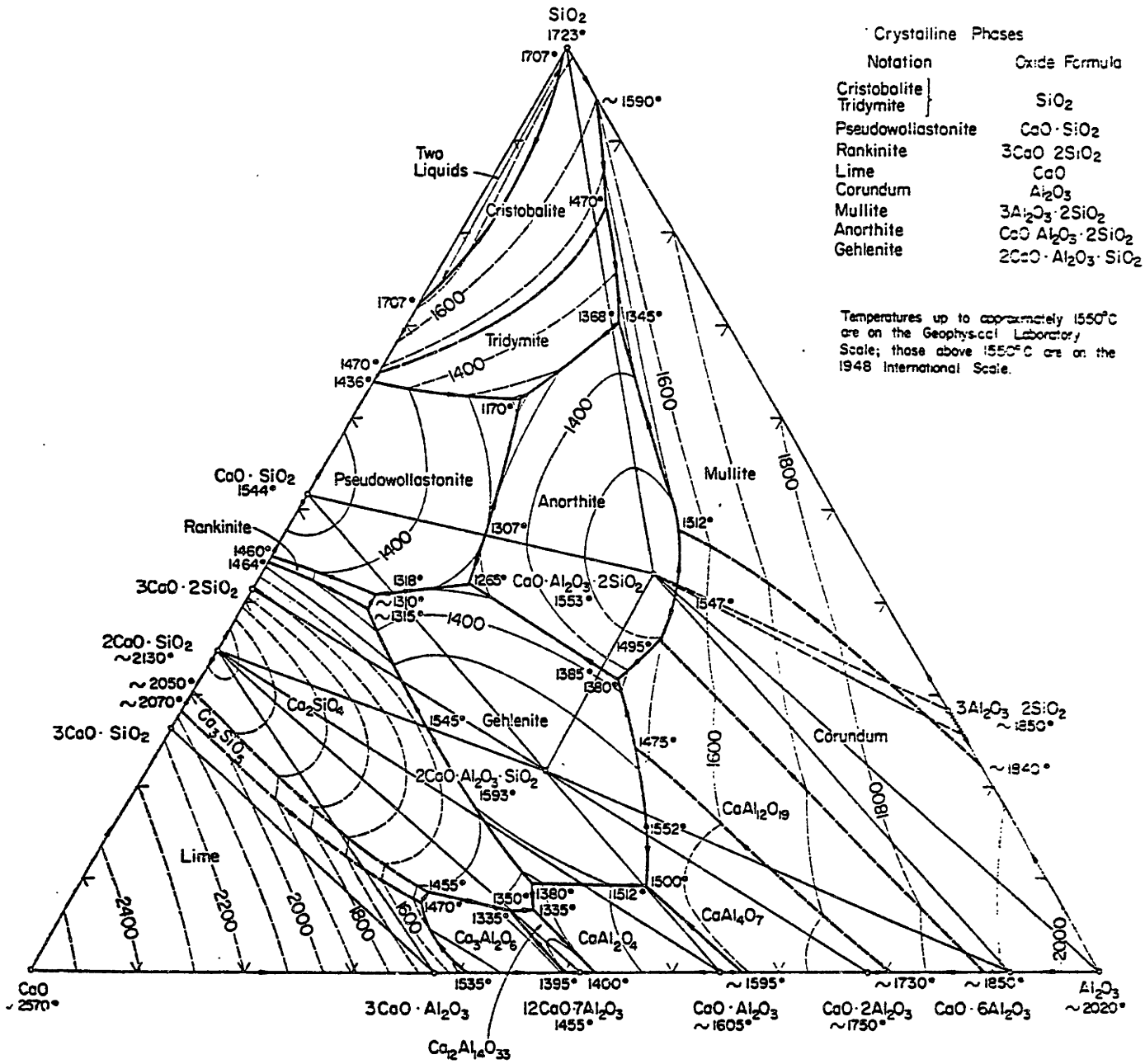

Figure 9.21 SiO_2 - Al_2O_3 - CaO Phase Diagram.
(Maun and Osborn, 1965)

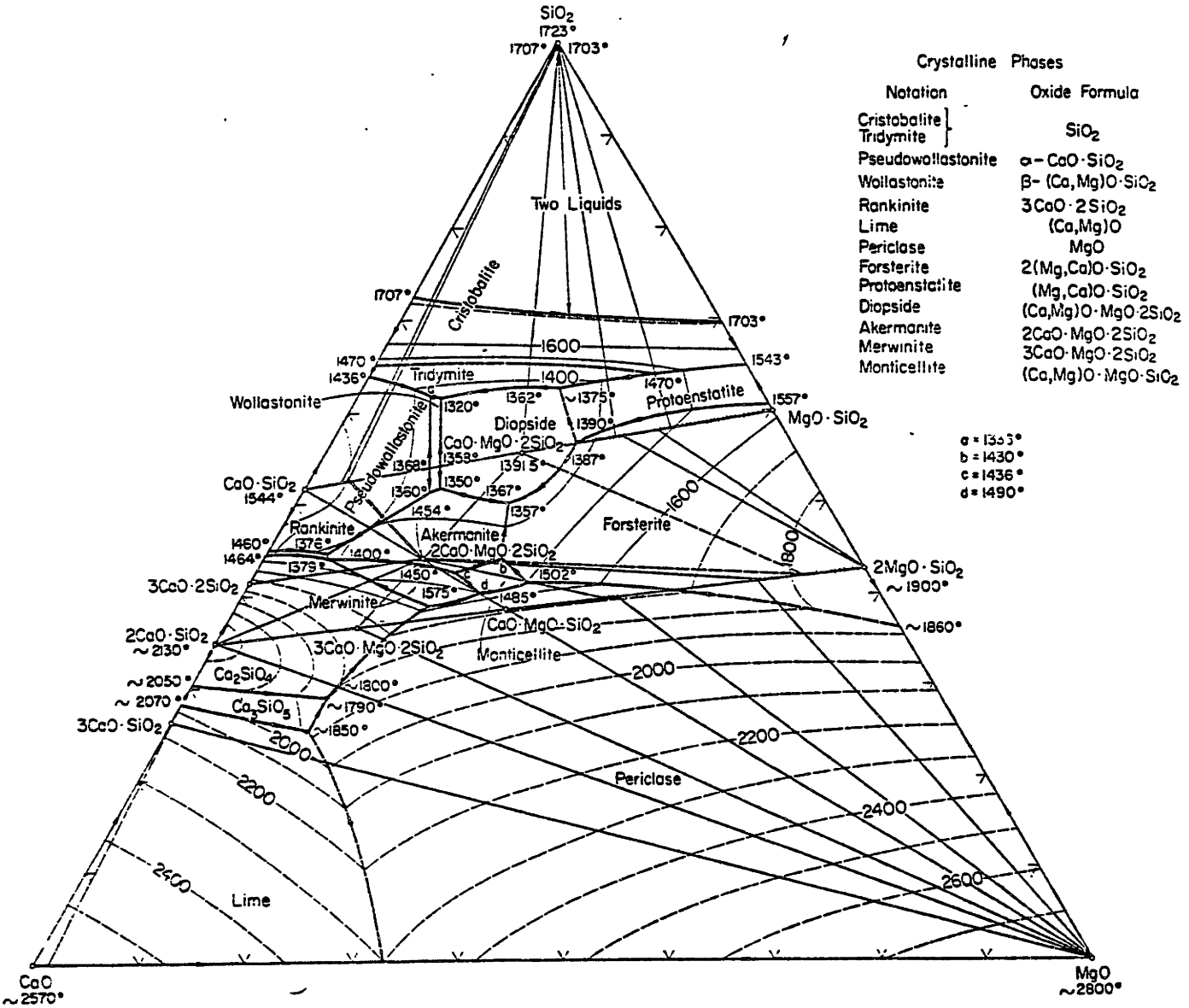

Figure 9.22 SiO_2 - MgO - CaO Phase Diagram.
(Maun and Osborn, 1965)

9.3 Microscopic Observations of the Physical Behavior of Bituminous Coals During Combustion

The Illinois No. 6 bituminous coal was also examined under the scanning electron microscope after exposure to the high temperature conditions of the furnace. This is a coal which exhibits thermoplastic behavior. Upon devolatization during initial hetaing, the coal softens and becomes a viscous fluid. Large scale voids are formed within the coal particles from the generation of the gaseous volatile matter. Often this volatile matter escapes the char particle by bubbling through the surface (Anthony and Howard, 1976). After a period of time, the char passes through the plastic state and resolidifies. Char particles formed in this manner are often cenospheres, having essentially hollow cores. In Chapter Six, the combustion model of cenospheres adopted for the bituminous coal was shown to be in good agreement with the measured particle burning times.

The Illinois No. 6 char particles in the scanning electron micrograph of Figure 9.23 were obtained by collection at 5.0 cm (~100 msec) from injection into the furnace. The furnace wall temperature was 1750 K and the gas was pure nitrogen. The transition to and from the plastic state is evident from their nearly spherical shape and relatively smooth surface morphology. The large scale voids within the particles are also visible. Apparently little swelling at this conditon has occurred.

The ash obtained from complete combustion of the Illinois No. 6 in 20 percent oxygen at a furnace wall temperature was

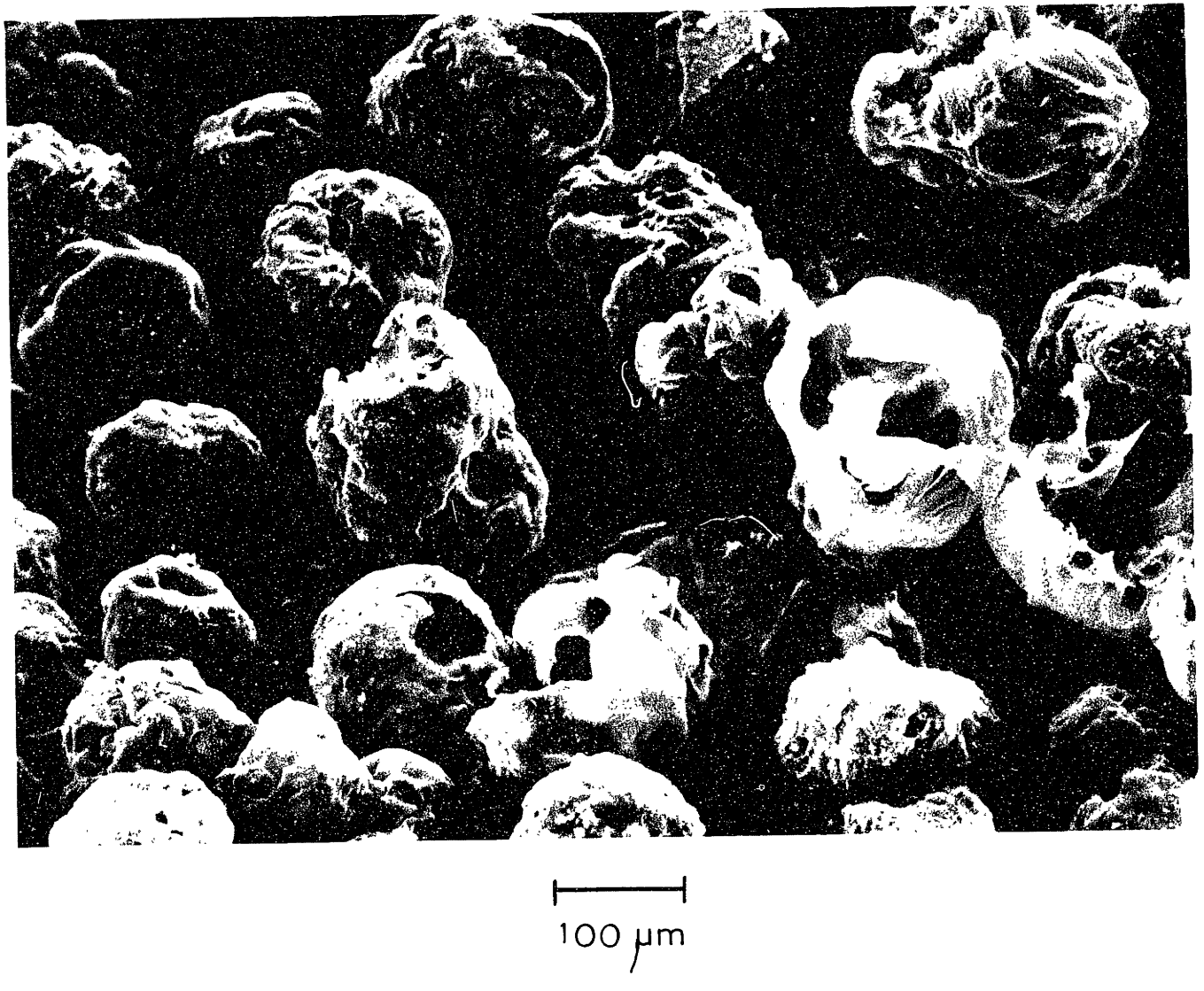

Figure 9.23 SEM of Illinois No. 6 Particles Devolatilized at 1750 K

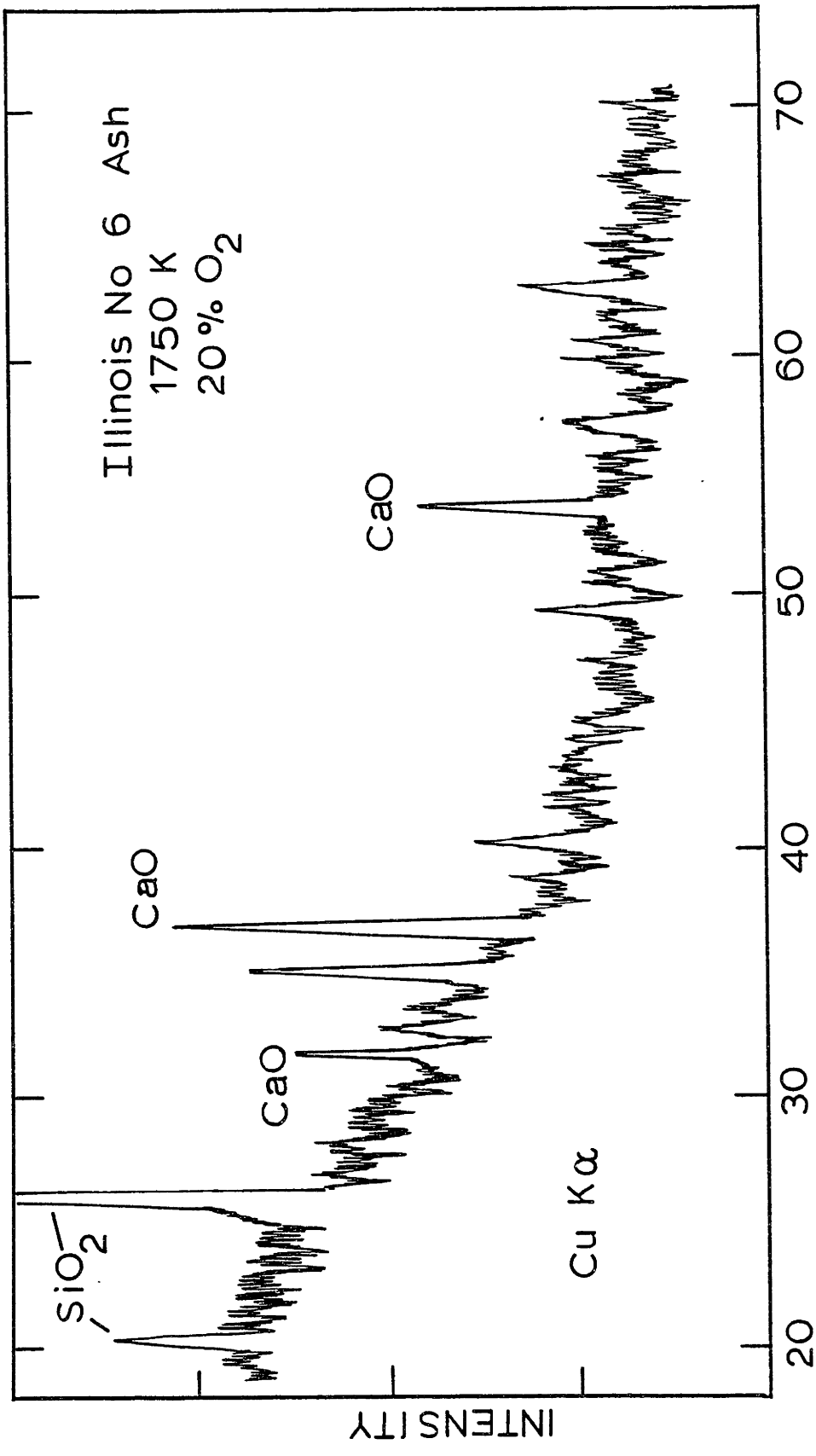

Figure 9.24 X-Ray Diffraction of Illinois No. 6 Combustion Ash. 1750K, 20% Oxygen

examined by XRD. The results are presented in Figure 9.24. The high background of low 2θ angles is due to the abundance of amorphous or glassy ash particles. Quartz has persisted at those temperatures as its transformations are kinetically controlled (Roberts, 1959). The lime peaks (CaO) probably reflect the abundance of extraneous calcite ($CaCO_3$) which has decomposed.

CHAPTER TEN

DISCUSSION AND MODELLING

10.1 Introduction

The results obtained in the experimental part of this investigation, which have been described in detail in the preceeding chapters, are briefly reviewed in the following. When pulverized coal particles are burned, the mineral matter contained within is decomposed, fused and, to a certain extent agglomerated to form ash droplets ranging in size from about 1 to over 20 microns. A fraction of the ash is evolved as vapor during the combustion process. By use of a laminar-flow, drop-tube combustion furnace with appropriate methods of product collection, the ash vaporized during combustion was recovered, isolated and analyzed as a submicron inorganic aerosol. The assumption that the submicron ash particulate arise from the vaporized ash by homogeneous condensation of the inorganic vapors evolving from burning char particles was examined and validated in Chapter Seven.

The extent of ash vaporization was measured for combustion of a number of coals under selected and controlled combustion conditions. These results were reported and discussed at length in Chapter Eight. The experimental results demonstrated that the amount and composition of vaporized ash is strongly dependent on both coal type and combustion condition.

When low rank coals were burned under an identical combustion condition (~2000K), the submicron ash was composed

primarily, in almost all cases, of the alkaline earth and alkali oxides (MgO and Na_2O), with iron oxide also being present at only minor levels. In contrast, silica was a major component of the submicron ash generated by the combustion of bituminous coals. For certain bituminous coals, the iron oxide content of the fume exceeded that of silica.

The composition of submicron ash reflects only the relative volatilization rates of the individual components. For example, the amount of magnesium are sodium vaporized during combustion was observed to correlate linearily with their respective concentrations in the coal. Hence, the levels of magnesium in the fume was low for bituminous coals and high for low rank coals. A simple linear correlation for silica vaproization with silicon content was not observed. Iron vaporization was found to be proportional to the inherent iron content of the coal, but that the proportionality was dependent on coal rank and the iron-bearing mineral forms.

The composition of the submicron ash was also found to be dependent on the combustion temperature. At low combustion temperatures (~1600K), the vaporized ash consisted mostly of the relatively volatile material (e.g. $Na_2O + K_2O$). At higher combustion temperatures (2000 - 3000K), the more refractory oxides (SiO_2, CaO, and MgO) being to appear as major species in the submicron ash depending on coal rank. These results reflect the activated nature of vaporization reactors. The fractional rate of total ash vaporization and of the individual components was correlated with reciprical

temperature.

The purpose of the present chapter is to examine and interpret the experimental results in terms of simplified models that consider both chemical and physical processes. This will include a treatment of vapor transport processes within porous char particles and in the char's external boundary layer, a consideration of the effects of mineral matter distribution patterns and forms within the original coal and in the higher temperature burning char particles, and a consideration of the ash thermochemistry involving vaporization reactions. With respect to this latter consideration, the ash vaporization thermochemistry is not independent of the particular of natures of the combustion process of small pulverized coal particles. Specifically, it will be shown in this chapter that the ash (e.g. SiO_2, MgO, CaO and FeO) vaporizes by reduction of refractory metal oxides to volatile sub-oxides or metals. Reduction will occur provided that the local oxygen potential within the char is sufficiently low. At high temperatures (>2000K), virtually all of the oxygen is consumed at or very near the char surface and the local oxygen potential is consequently low. With decreasing temperature, oxygen penetration into the porous char increases.

In the next section, mathematical models governing the transport processes of vapor species are developed to assist in interpreting the thermochemical aspects of volatization processes, which are then discussed in the subsequent section of this chapter.

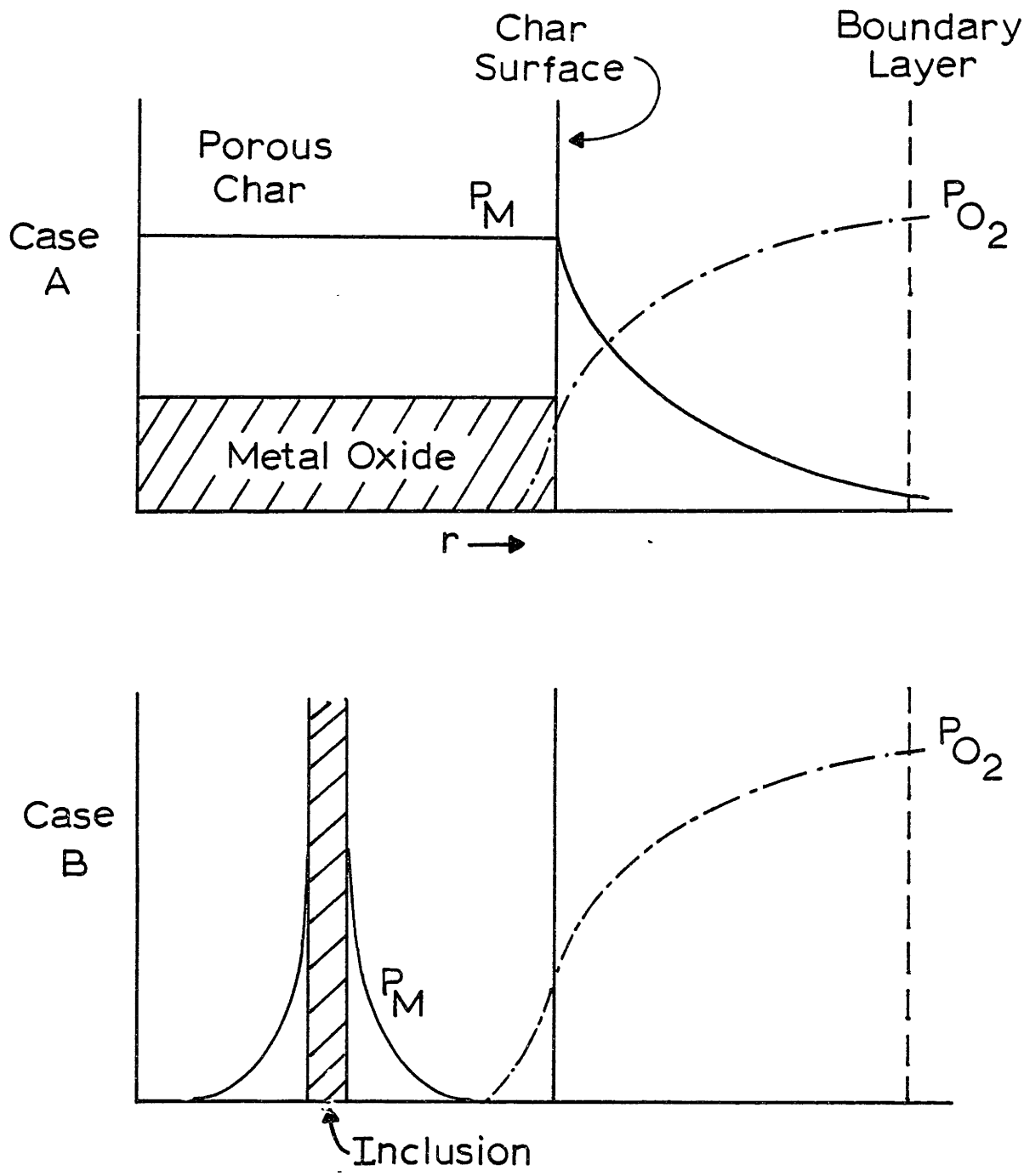

Figure 10.1 Schematic of Diffusion Controlled Vaporization (A) External Diffusion, (B) Internal Diffusion

10.2 Modelling of Vapor Transport Processes

The mineral matter in coal is distributed as either discrete mineral inclusions having dimensions ranging from less than one micron up to the size of the coal particles or as elements organically bound to the carbonaceous matter. Examples of the former category include quartz or alumino-silicat clay minerals and pyrite. The latter category includes the magnesium and calcium ion-exchanged on the carboxylic groups of low rank coals. During char combustion at high temperatures, the decomposed minerals are in the form of molten droplets of metal oxides. The evolution of the atomotically dispersed, organically bound alkaline earths in the Savage lignite has been discussed in Chapter Nine. It was shown by electron microscopy that on the surface of the char, the organically bound constituents form highly dispersed, submicron grains of ash.

Given the complexity in the distribution of mineral matter in coal or ash in chars, only models incorporating a number of simplifying assumptions can be usefully employed. Two simplistic models examining independently the effects of internal and external ash vapor transport processes are considered first. It will then be shown that these are limiting cases of a more general model. A schematic representation of the physical aspects of the two limiting rate controlling mechanisms are shown in Figure 10.1. A char particle is presumed to be burning under conditions in which the rate of combustion is controlled primarily by external diffussion of oxygen to the chars surface. Thus the oxygen concentration

is very low within the char. In this approach it is assumed that their exists and equilibrium partial pressure of gas phase mole fraction X_m^e that ascribes a maximum value of X_m. This value is determined by the thermochemical aspects of ash volatilization reactions. Specifically, under reducing conditions, X_m^e is the equilibrium gas phase mole fraction of some reduced form (M) of a metal oxide MO (Mg, Ca, Fe or SiO) that exists over the pure or multicomponent condensed metal oxide phase in the char. Further discussion of the factors that determine X_m^e are reserved for the next section of this chapter. In Case A of Figure 10.1, the ash is assumed to be so highly dispersed that X_m^e is the value of X_m throughout the char and at the chars surface. Teh vaporization rate of M from a char particle is then the rate of transport of M through the char's external boundary layer. In Case B, the metal oxide is assumed to be in the form of a discrete inclusion or droplet embedded within the porous char. In this case, an equilibrium X_m^e exists only at the surface of the inclusion (s). The rate of vaporization of M from a single inclusion is then controlled by Knudsen diffusion processes in the porous char.

For case A, the equation describing the external transport or flux N_m (moles/cm^2 sec) of vapor M with the inclusion of the Stefan flow contribution is

$$N_m = -cD_m \frac{dX_m}{dr} + X_m \sum N_i \qquad (10.1)$$

with D_m and X_m being, respectively, the metal (or suboxide)

diffusivity and gas phase mole fraction. From Chapter Six, equations 6.2, 6.3, 6.5 and 6.6, the net molar flux $\sum N_i$ is

$$\sum N_i = \frac{R_d}{8\pi r^2 w} = \frac{cDo_2 \ell_n (1+Xo_2^b)}{r_p}$$

where R_d is the gasification rate of the char (gm/sec) and w is the molecular weight of carbon. The (pseudo) steady-state vaporization rate V_m (moles/sec) of ash species m is

$$V_m = 4\pi r^2 N_m = 4\pi r_p^2 N_m \Big|_{r = r_p} \tag{10.2}$$

where r_p is again the char particle radius. Hence, by substitution, equation 10.1 becomes

$$\frac{1}{4\pi r^2}\left[V_m = \frac{X_m R_d}{2w}\right] = -cD_m \frac{dX_m}{dr} \tag{10.3}$$

The boundary conditions are specified as

$$r \to \infty \qquad x_m = 0$$

$$r = r_p \qquad x_m = x_m^S$$

where x_m^S is the partial pressure of vapor M at the char surface. Integration over the external coordinates and application of the boundary conditions leads to the result:

$$1 - \frac{X_m^s R_d}{2V_m w} = e^{-\frac{D_{O_2}}{D_m} \ell_n \left(1 + Xo_2^b\right)} = e^{-\alpha} \tag{10.4}$$

and

$$V_m = \frac{X_m^e R_d}{2w}\left[1 - e^{-\alpha}\right]^{-1} = 4\pi r_p c \alpha_1 D_{O_2} X_m^e \tag{10.5}$$

where

$$\alpha_1 = \frac{\ell_n\left(1+Xo_2^b\right)}{\left(1-e^{-\alpha}\right)} \tag{10.6}$$

For Case B of Figure 10.1, the vaporization rate, V_I, of M from a single inclusion is given by

$$V_I = 4\pi r_i C D_e X_m^e \tag{10.7}$$

where r_i is the radius of the inclusion, and on a microscopic scale, the value of X_m is taken to be zero far away from the inclusion. The total rate of vaporization of M is then obtained by the summation of equation 10.7 over all inclusions present in the char particle.

The two models presented above are limiting cases of a more general model that considers the existance of an assemblage of discrete inclusions within a given char particle. The physical distribution of inclusions is shown schematically in Figure 10.2. Padia (1976) has reported size distributions of mineral inclusions in pulverized coal. Typically, the volume mean diameter was found to be on the order of 2.4 microns for clay minerals. Ward (1977) has reported that the <2 micron fraction of mineral matter is composed primarily of alumino-silicate clays. To simplify the mathematics, the the present model assumes that all inclusions for a given mineral component are of uniform size and having a radius of r_i. As shown in the schematic, two types of inclusions are considered - those inside the char and those on the char's external surface. The initial number of inclusions N_I^o in an unburned char particle is given by

$$N_I = \theta_I \frac{r_o^3}{r_i^3} \tag{10.8}$$

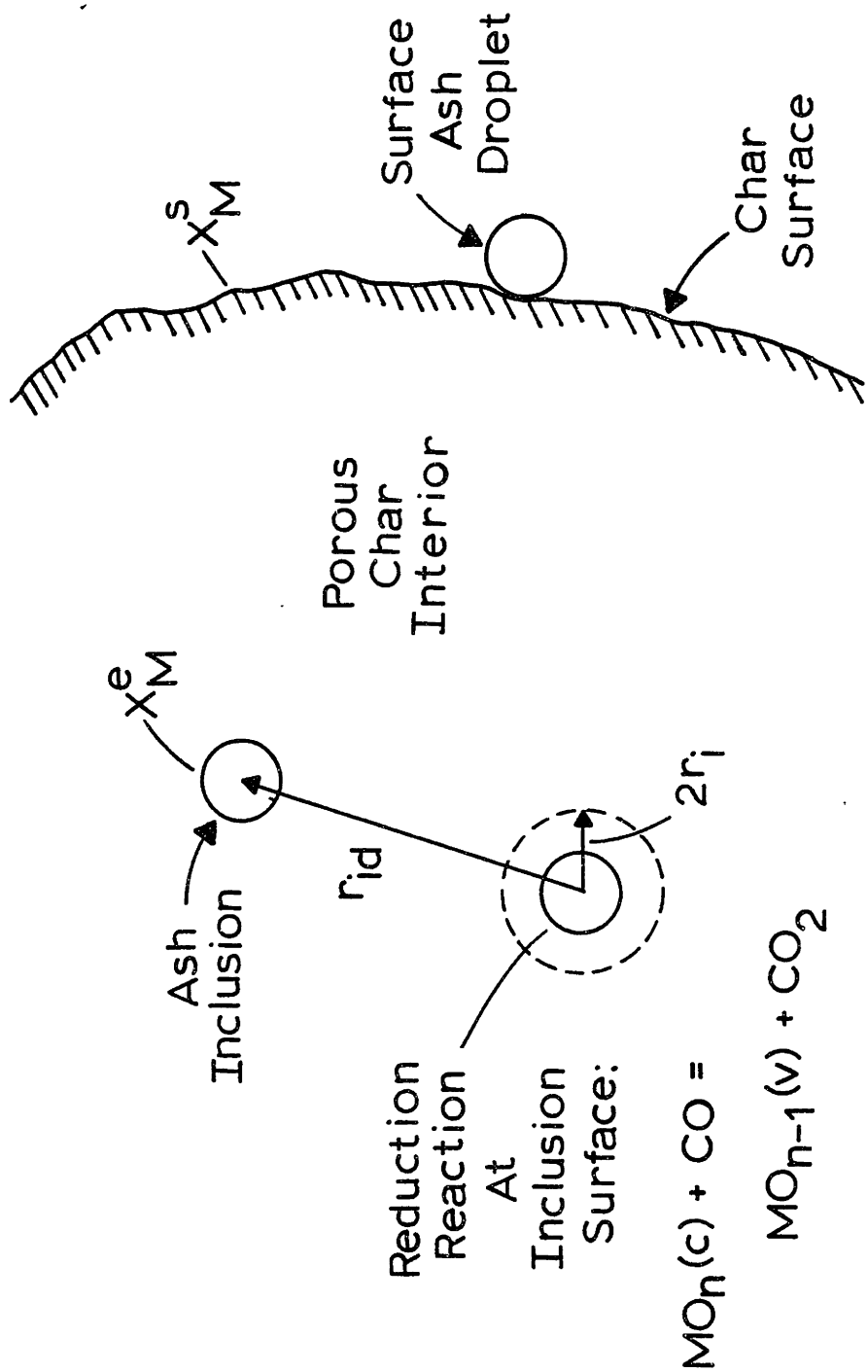

Figure 10.2 Schematic of the Physical Distributions of Inclusions in a Char Particle

where θ_I is the volume fraction of inclusions of component I and r_o is the initial char radius. As an example calculation, the volume fraction of silica in the coal, assuming it is in the form of quartz inclusions, is approximately .0036 for the Montana Savage lignite. If the quartz inclusion diameter is uniform at 1 micron, then for 50 micron diameter coal particle, the number of inclusions in the coal particle is 450. The number of inclusions drops off rapidly with increasing inclusion size. For a monodisperse inclusions size of 5 microns in diameter the number of inclusions in the char particle is on the average less than 4 for a 50 micron diameter coal particle. As combustion of the char begins, the chars surface recedes (for a shrinking sphere) and inclusions initially within the char will appear on the chars surface. The number of inclusions on the char surface $N_I^S(t)$ at time t is proportional to the chars volume change:

$$N_I^S(+) = N_I^o \left[1 - \frac{r_p^3(t)}{r_o^3}\right] \tag{10.9}$$

For a shrinking sphere, the char's radius $r_p(t)$ at time t is

$$r_p(t) = r_o \left(1 - \frac{t}{t_o}\right)^{1/2} \tag{10.10}$$

and

$$N_I^S(t) = N_I^o \left[1 - \left(1 - \frac{t}{t_b}\right)^{3/2}\right] \tag{10.11}$$

where t_b is the total burning time of the char. The number of inclusions remaining within the char, N_I^i, is given by

$$N_I^i = N_I^o\left[1 - \frac{t}{t_b}\right]^{3/2} \qquad (10.12)$$

where it has been assumed that the volume fraction θ_I within the char remains constant during burnout. For this inclusion population balance, it has been assumed that the surface inclusions adhere to the chars receeding surface (Raask, 1966). Sarofim et al. (1977) have modelled the agglomeration of inclusions on the char's surface using the classical equations of aerosol coagulation. From this purely physical model, it appears that significant agglomeration does not occur until the latter stages of burnout. Hence the present model is valid only up to a certain extent of char burnout.

The rate of vaporization for a single isolated inclusion within the char was given by equation 10.7:

$$V_I^{ni} = 4\pi c D_e r_i X_m^e \qquad \text{(moles/sec)} \qquad (10.13)$$

where again X_m^e is the equilibrium mole fraction of vapor M at the inclusions surface, the value of which is determined by the thermochemistry. The superscript ni designates that this rate is for an isolated (non-interacting) ash droplet. If the droplet density is sufficiently high, then the inclusions within the char will not be effectively isolated and will influence each other. An analogous problem is that of the drop interaction during the combustion or vaporization of sprays (Samson et.al, 1978; Deutch et.al., 1976; Labowsky and Rosner, 1978). In the immediate (microscopic) vicinity of an inclusion the gas phase mole fraction X_m will vary locally with position

particularly within $2r_i$ from an inclusions center. If, however, it is assumed that their exists an average value of X_m which is only a function of the chars radial (macroscopic) coordinate that does not vary significantly on the scale of the inclusion dimension, then the vaporization rate, V_I^i, of an inclusion is given by

$$V_I^i = 4\pi c D_e r_i \left(X_m^e - X_m\right) \tag{10.14}$$

where the superscript i denotes that this is the vaporization rate of interacting inclusions which is dependent on the inclusions position within the char. For this mean X_m approximation to be valid, it is required that the distance between inclusions r_{id} be (Labowsky and Rosner, 1976)

$$r_{id} = \left(\frac{\pi}{6}\right)^{1/3} \theta_I^{-1/3} r_i \gg \lambda_f \tag{10.15}$$

In this analysis, higher order effect due to closely spaced pairs (or triplets, etc.) are neglected (Felderhof and Deutch, 1976). This approximation is reasonable given the low volume fraction of ash within the char. Implicit in the rate equations is that characteristic inclusion size is assumed to be greater than that of the pore size and that the inclusions are isotropically distributed in an isotropic porous medium. Furthermore a quasi-steady x_m profile within the char is assumed because the characteristic time for combusiton is much greater than for diffusion. The time dependence in this analysis only arises as a result of changes in char particle radii during burnout and in the population balance of inclusions on the char's surface and within the char. The inclusion radius is assumed

constant, a valid approximation at low vaporization rates. In the analysis that immediately follows, the initial vaporization rate is examined. More specifically, the effects of surface inclusions are not considered as, initially, there are none. The time dependent problem, accounting for changes in char radii and in the effects of surface inclusions on the overall vaporization rate, will be examined later.

For the initial conditions, $r_p = r_o$ and $N_I^s = 0$, the equation describing the mean model fraction profile inside the char with respect to the chars internal radial coordinates is

$$cD_e \nabla^2 X_m + \frac{N_I^o}{\frac{4}{3}\pi r_o^3} V_I^i = 0 \tag{10.16}$$

or

$$\frac{1}{r^2}\frac{d}{dr} r^2 \frac{dX_m}{dr} + \frac{3\theta_I}{r_i}(X_m^e - X_m) = 0 \tag{10.17}$$

The boundary conditions are that:

$$\text{at } r = 0 : \quad \frac{dX_m}{dr} = 0 \tag{10.18}$$

$$\text{at } r = r_o \qquad -4\pi r_o^2 cD_e \frac{dx_m}{dr}\bigg|_{r=r_o} = 4\pi r_o c_{D02} \alpha_1 X_m^s \tag{10.19}$$

The second boundary conditions accounts for the external diffusion (with Stefan-flow) of the metal. Equation 10.17 can be cast into the form of the analagous problem of diffusion and reaction in a catalyst pellet (Satterfield, 1970):

$$\frac{1}{r^2}\frac{d}{dr}\,r^2\,\frac{dx_m}{dr} + \frac{\phi_I^{\,2}}{r_o^{\,2}}\left(X_m^{\,e} - X_m\right) = 0 \qquad (10.20)$$

where ϕ_I is a Thiele modulus:

$$\phi_I = \sqrt{3\theta_I}\,\frac{r_o}{r_i} \qquad (10.21)$$

The solution to equation 10.20 is

$$X_m = X_m^{\,e}\left[1 - \left(1 - \frac{X_m^{\,s}}{X_m^{\,e}}\right)\frac{r_o\,\sinh\left(\phi_I\,\frac{r}{r_o}\right)}{r\,\mathrm{Sinh}\,\phi_I}\right] \qquad (10.22)$$

and the mole fraction of M at the char surface $X_m^{\,s}$, is given by:

$$X_m^{\,s} = \left[\frac{\frac{D_e}{\alpha_1 Do_2}\left(\frac{\phi_I}{\tanh\,\phi_1} - 1\right)}{1 + \frac{D_e}{\alpha_1 Do_2}\left(\frac{\phi_I}{\tanh\,\phi_I} - 1\right)}\right] X_m^{\,e} \qquad (10.23)$$

The total (initial) rate of vaporization or loss of M from a char, $V_c^{\,o}$ (moles/sec), of radius r_o is determined from

$$V_c^{\,o} = 4\pi r_o^{\,2} c D_e \left.\frac{\partial X_m}{\partial r}\right|_{r=r_o} = 4\pi r_o c D_{o_2} \alpha_1 X_m^{\,s} \qquad (10.24)$$

For non-interacting inclusions, the total (initial) vaporization rate from the char $V_c^{\,ni,o}$ would be

$$V_c^{\,ni,o} = N_I^{\,o}\,4\pi r_i c D_e X_m^{\,e} \qquad (10.25)$$

An effectiveness factor η,

$$\eta = \frac{3}{\phi_I}\left[\frac{1}{\tanh\,\phi_I} - \frac{1}{\phi_I}\right]\left[1 + \frac{D_e}{\alpha_1 Do_2}\left(\frac{\phi_V}{\tanh\,\phi_V} - 1\right)\right]^{-1} \qquad (10.26)$$

gives the ratio of the total vaporization rate of M with particles interacting and with external diffusion control over that of the rate of N_I^o isolated ash droplets in the char. Thus

$$V_c^o = \eta N_I^o V_I^{ni} \tag{10.27}$$

This expression for V_c^o has several limiting cases. When ϕ_I approaches zero because the volume fraction of M in the char approaches zero, then η approaches unity and the total vaporization rate from the char is just that of the summation of individual rates, V_I^{ni}, of N_I^o non-interacting inclusions. Thus for this limit

$$V_c^o = N_I^o V_I^{ni} = \theta_I \frac{r_o^3}{r_i^2} 4\pi c \mathcal{D}_e X_m^e \tag{10.28}$$

and the total vaporization rate of M from the char is proportional to the volume fraction of M (as a metal oxide) and the volume of the char. When ϕ_I gets large (i.e. > 5) but with

$$1 >> \frac{D_e \phi_I}{\alpha_1 D_{o_2}}$$

because of the low effective diffusivity (small pores), then

$$\eta \to \frac{3}{\phi_I}$$

and

$$V_c^o = \sqrt{3\theta_I} \frac{r_o^2}{r_i} 4\pi c \mathcal{D}_e X_m^e \tag{10.29}$$

Under this circumstance, the total vaporization rate of M is proportional to the square root of the volume fraction and to the external surface area of the char. In the limit when

the Thiele modulus is very large, a situation that might arise from extremely small inclusion size, then

$$1 << \frac{D_e \phi_I}{\alpha_1 D_{o_2}}$$

and

$$\eta \rightarrow \frac{3\alpha_1 D_{o_2}}{D_e \phi_I^2}$$

In this limiting case, the total vaporization rate of M from a char particle of radius r_o is then

$$V_c^o = 4\pi c \alpha_1 D_{o_2} r_e X_m^e \qquad (10.30)$$

This is equivalent to the problem of total external diffusion control and the surface mole fraction X_m^s is equivalent to that of the equibibrium mole fraction X_m^e which is determined by thermochemical factors. The total vaporization rate under these circumstances is independent of the volume fraction of ash in the char. With the formalism employed here, there is a limit to how large ϕ_I can become. It is assumed, of course, that the volume fraction of ash is realistically small. The value of ϕ_I in the present context then depends on r_i. For equation 10.14 to be valid, r_i must be significantly greater than the pore size. Rather if the size of the inclusion is on the order of the pore size (25Å), then local Fickian diffusion controlled evaporation from an inclusion is not applicable. Intuitively, this is expected to be the case for the highly dispersed or atomically dispersed ion-exchangable calcium and magnesium in the lignite. If these molecules* mobilize and collide by surface diffusion phenomena to form extremely

*Assuming the carboxylic groups yield alkaline oxides upon pyrolysis.

small inclusions within the char in virtually oxidized free regions of the char, then the inclusions must be less than the characteristic pore size. The theory of molecular evaporization would be more applicable. Thus,

$$V_I^{\,i} = \frac{\pi r_i^{\,2}(X_m^{\,e} - X_m)p}{(2\pi mkT)^{1/2}} \qquad (10.31)$$

The Thiele modulus for equation 10.20 would then be

pyrolysis.

$$\phi_I = r_o \left[\frac{3\theta P}{4c\mathcal{D}_e r_i (2\pi mKT)^{1/2}}\right]^{1/2} \qquad (10.32)$$

where P is total pressure and m is the mass of the metal vapor or molecule. The Thiele modulus would be exceedingly large and

$$\eta \rightarrow \frac{3\alpha_1 Do_2}{D_e \phi_I^{\,2}}$$

The result is that $V_c^{\,o}$ is again given by equation 10.30. In effect, when ϕ_I is extremely large, it does not matter whether molecular or Fickian diffusion processes govern the rate of evaporation of a metal from an inclusion in this analysis. In this limit, external diffusion processes govern the rate of vaporization.

In summary, as the Thiele modulus is increased from either increased volume fraction of ash or decreased inclusion size, the effectiveness factor η decreases due to inclusion interaction. The net effect, however, is that as ϕ_I increases,

and η decreases due to interaction the total vaporization rate of M from the char increases.

The time-dependent problem is now considered simultaneously with the effects of the evolution of surface inclusions on the total vaporization rate of ash species M. The time dependent variables include the chars radius r_p:

$$r_p = r_o \left(1 - \frac{t}{t_b}\right)^{1/2}$$

the Thiele modulus ϕ_I;

$$\phi_I(t) = \sqrt{3\theta_I}\, \frac{r_o}{r_i} \left(1 - \frac{t}{t_b}\right)^{1/2} \qquad (10.33)$$

and the population of inclusions within the char, $N_I^{\,i}$, and the surface of the char, $N_I^{\,s}$, as given by equations 10.11 and 10.12, respectively. The starting point is to consider what effects surface inclusions may have on the volatilization rate, as depicted in Figure 10.3. The trivial case is where the partial pressure or mole fraction of M at the char's surface $X_m^{\,s}$, is equivalent to that at the surface ash droplet's surface, $X_m^{\,es}$. Hence, there is no net vaporization effect caused by their presence. If $X_m^{\,s}$ is greater than the surface ash droplets equilibrium partial pressure, $X_m^{\,es}$, then the surface inclusions act as vapor sinks. Conversely, if $X_m^{\,es}$ is greater than $X_m^{\,s}$, then the surface inclusions are additional source terms. There is no apriori method to ascertain which one of these possibilities is likely. However, on considering the nature of the combustion process, it is likely that $X_m^{\,es}$ is less than or, at most, equal to $X_m^{\,e}$.

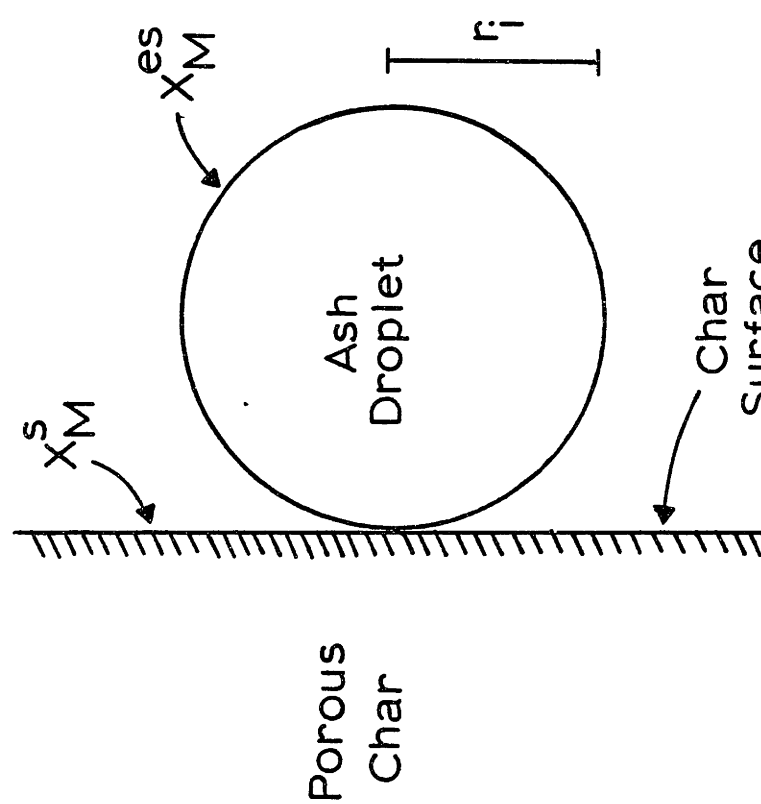

Figure 10.3 Schematic of Ash Droplet on Char Surface

This is expected because the local oxygen potential about a surface inclusion is necessarily greater than that about an inclusion within the char. Thus if vaporization of metal oxides proceeds via a reduction reaction (e.g. $SiO_2 \rightarrow SiO$ or $MgO \rightarrow Mg$), then X_m^{es} may be less than X_m^{e}. Whether X_m^{s} is less than or greater than X_m^{es} then depends on the oxygen potential, the Theiele modulus (e.g. the limiting cases) and the pore structure. Each of the possibilities will be considered below for the limiting cases of the Thiele modulus. The assumption of a single ash component system is continued for the present. It is further assumed that condensation of vapors does not occur on the char's porous structure. That is, the penetration of oxygen into the pores near the chars surface does not perturb X_m^{s}. This assumption is valid for small pores where gas phase reactions (between M and O_2) leading to condensible oxide vapors cannot occur. The effect of oxygen is, therefore, to influence the value of X_m^{es}, so that if condensation of metal vapors occurs, it occurs on the surface inclusions as a result of $X_m^{s} < X_m^{es}$.

The case of $X_m^{s} = X_m^{es}$ is considered first. Under this condition, there is no net loss or gain of material from the surface inclusions. Only the vaporization from internal inclusions. The time dependent rate of vaporization of M from a single char particle is given by (in moles/seconds)

$$V_c(t) = \eta(t) N_I^{i}(t) V_I^{ni} \qquad (10.34)$$

and the total moles vaporized N_{tb} from a single char particle is obtained by integrating over the live time of the char particle:

$$N_{tb} = \int_{o}^{t_b} V_c(t)\,dt \tag{10.35}$$

For the limiting case of ϕ_I approaching zero and, hence, η approaching unity, then

$$N_{tb} = \int_{o}^{tb} N_I{}^{o}\left[1 - \frac{t}{t_b}\right]^{3/2} 4\pi r_i c D_e X_m{}^{e}\,dt \tag{10.36}$$

which yields

$$N_{tb} = \frac{8\theta r_o{}^{3}\pi c D e X_m{}^{e}}{5 r_i{}^{2}} tb \tag{10.37}$$

The moles of metal M vaporized per gram of coal burned, N_g, is obtained by

$$N_g = N_c N_{tb} \tag{10.38}$$

where N_c is the total number of coal particles per gram of coal. Thus

$$N_g = \frac{3\rho_c r_o{}^{2}\theta D_e X_m^{e}}{10 w \rho_o r_i{}^{2} Do_2 \ln(1+Xo_2{}^{b})} \tag{10.39}$$

where the expressio or the burning time t_b (equation 6.9) has been substituted. Thus for non-interacting inclusions within the char, and for

$$X_m{}^{s} = X_m{}^{es} = 0$$

the moles vaporized per gram of coal burned is proportional to the square of the initial radius of the coal and to the volume fraction of the mineral component in the coal. This is equivalent to a volumetric reaction problem.

For the case when $X_m^s = X_m^{es}$, with ϕ_I large but

$$\frac{D_e \phi_I}{D_{c_2} \alpha_1} << 1$$

then

$$V_c(t) = \frac{3}{\phi_I(t)} N_I^i(t) \; V_I^{ni} \tag{10.40}$$

or

$$V_c(+) = \frac{3N_I^o 4\pi c r_i^2 x_m^e D_e}{\sqrt{3\theta}\; r_o} \left(1 - \frac{t}{tb}\right)^{1/6} \tag{10.41}$$

and

$$N_{tb} = \int_o^{t_b} V_c(t)dt = \frac{18N_I^o 4\pi c r_i^2 D_e X_m^e t_b}{7\sqrt{3\theta}\; r_o} \tag{10.42}$$

The moles of M vaporized per gram of coal burned is then

$$N_g = \frac{9\sqrt{3\theta}\rho_p D_e X_m^e r_o}{14 r_i \rho_o w D o_2 \ell_n (1+Xo_2^b)} \tag{10.43}$$

In this limiting case, the moles vaporized per gram of coal burned is proportional to the initial radius of the coal and to the square root of the volume fraction.

In the limit where ϕ_I is very large and

$$1 << \frac{D_e \phi_I}{\alpha_1 D_{o_2}}$$

and necessarily with

$$X_m^e = X_m^s = X_m^{es}$$

then

$$V_c(t) = 4\pi c\alpha_1 D_{o_2} r_o \left(1 - \frac{t}{t_b}\right)^{1/2} X_m^e \qquad (10.44)$$

and

$$N_{tb} = \frac{8}{3}\pi c\alpha_1 D_{o_2} X_m^e t_b r_o \qquad (10.45)$$

The moles of M vaporized per gram of coal burned is given by

$$N_g = \frac{\rho_p \alpha_1 X_m^e}{2\rho_o w \ln\left(1+Xo_2^b\right)} \qquad (10.46)$$

and is seen to be independent of the initial coal size and the volume fraction θ_I. This is simply the external diffusion control problem.

If $X_m^s > X_m^{es}$, then the external inclusions or droplets on the char's surface are sinks for metal vapor species. To account for this effect, the boundary condition at the chars surface must be modified (neglecting external Stefan flow):

$$-cD_e\, 4\pi r_p^2 \left.\frac{\partial X_m}{\partial r}\right|_{r=r_p} = 4\pi r_p D_m X_m^s + N_I^s\, 8\pi r_i c D_m \left(X_m^s - X_m^{es}\right) \qquad (10.47)$$

The second term on the right hand side of this equation is the rate of vapor transport from the char surface to the surface droplet of radius r. D_m is the bulk gas diffusivity for vapor M. This rate of expression for the transfer of vapor from a flat surface to a sphere was adopted from an analogous heat transfer problem (Grober, Erk and Grigull,

1961). The total rate of vaporization of the metal (or loss of metal from the char is again

$$V_c(t) = \eta_s(t)\ N_S^{\,i}(t)\ V_I^{\,ni} \tag{10.48}$$

with the effectiveness factor now being

$$\eta_s = \frac{3}{\phi_I}\left[\frac{\left(\frac{1}{\tanh\ \phi_I} - \frac{1}{\phi_I}\right) + \frac{2}{3}\ \phi_I f(t)\ \frac{X_m^{\,es} D_m}{X_m^{\,c} D_e}}{1 + \frac{D_e}{D_m}\left[\frac{\phi_I}{\tanh\phi_I} - 1\right] + \frac{2}{3}\ \phi_I^{\,2} f(t)}\right] \tag{10.49}$$

with

$$f(t) = \left[\left(1 - \frac{t}{t_b}\right)^{-3/2} - 1\right] \tag{10.50}$$

Since $f(t) \to \infty$ as $t \to t_b$, this analysis is not valid near the end of char burnout. Physically, this fialing arises because the number of inclusions on the surface of the char exceeds surface area availability as the char size decreases.

For the limit of $\phi_I \to 0$, then

$$X_s > X_m^{\,es} \to 0$$

and the effectiveness factor again becomes unity. Thus where internal diffusion controls the vaporization rate, surface inclusions have no effect on the total vaporization rate of M from the char.

For large values of ϕ_I, the last term in the denominator of equation 10.49 is expected to dominate during most of the char burnout as

$$\frac{D_e \phi_I}{D_m} << \phi_I^2$$

The effectiveness factor becomes

$$\eta_s = \frac{3}{\phi_I}\left[\frac{D_m X_m^{es}}{D_e X_m^{e} \phi_I}\right] \tag{10.51}$$

This problem then reduces to one of external diffusion control with X_m^{es} being the apparent mole fraction of M at the chars surface:

$$V_c = 4\pi r_p D_m c X_m^{es} \tag{10.52}$$

The problem of surface inclusions acting as sources because

$$X_m^{s} < X_m^{es}$$

is now considered. To estimate the maximum magnitude of the effect it is assumed for convenience that the vaporization of the metal from surface icnlusions has no significant effect on the vaporization rate of internal inclusions. This is rigourously true for the case where ϕ_I approaches zero. It is also true when ϕ_I is large with $X_m^{s} << X_m^{es}$. A further assumption employed is that the surface inclusions are non-interacting among themselves. This approximation fails, of course, at the latter stage of burnout when inclusions contact each other.

Provided $X_m^{s} << X_m^{es}$, then the vaporization rate of a surface inclusion can be approximated as (neglecting Stefan-flow from the char surface)

$$V_I^{s} = 4\pi r_i c D_m X_m^{es} \tag{10.53}$$

The total vaporization rate (moles/sec) from a single

char particle is given by

$$V_c(t) = \eta N_I^{\,i} V_I^{\,ni} + N_I^{\,s} V_I^{\,s} \tag{10.54}$$

For the limiting case of ϕ_I approaching zero

$$\eta \rightarrow 1$$

so that

$$V_c(t) = N_I^{\,0}\, 4\pi c r_i \left[D_e X_m^{\,e} \left(1 - \frac{t}{t_b}\right)^{3/2} + D_m X_m^{\,es} \left\{ 1 - \left(1 - \frac{t}{t_b}\right)^{3/2} \right\} \right] \tag{10.55}$$

Integrating over the life time of the char particle yields:

$$N_{tb} = N_I^{\,o} 4\pi c r_i t_b \left[\frac{2}{5} D_e X_m^{\,e} + \frac{3}{5} D_m X_m^{\,es} \right] \tag{10.56}$$

The moles of M vaporized per gram of coal burned is then obtained as

$$N_{tb} = \frac{3\theta \rho_p r_o^{\,2} \left[D_e X_m^{\,e} + \frac{3}{2} D_m X_m^{\,es} \right]}{10 r_i^{\,2} w D o_2 \ln\left(1 + X o_2^{\,b}\right)} \tag{10.57}$$

The relative importance of contribution of vaporization from surface inclusions depends on the magnitude of the terms $D_e X_m^{\,e}$ and $D_m X_m^{\,es}$. For example if $X_m^{\,e} \approx X_m^{\,es}$, then the principle source of vapors would be the surface inclusions as

$$D_e << D_m$$

for most chars. On the basis of the combustion behavior of coals, intuitively it might be expected that $X_m^{\,e} >> X_m^{\,es}$ because the local oxygen potential will be greater at the chars surface than within the char - assuming that metals vaporize by reduction of their oxides. In any case the

relative contribution of surface inclusions to the total vaporization rate cannot be determined from experimental variables (e.g. r_o).

For the limiting case where ϕ_I is large but

$$\frac{D_e \phi_I}{\alpha_1 Do_2} << 1$$

then

$$V_c(t) = \frac{3}{\phi_I(t)} N_I{}^i V_I{}^{ni} + N_I{}^s V_I{}^s \qquad (10.58)$$

Integrating over time and multiplying by N_c, the number of coal aprticles per gram of coal, the total moles of M vaporized per gram of coal burned is

$$N_g = \frac{9\theta_I \rho_p}{4wDo_2 \ln\left(1+Xo_2{}^b\right)}\left[\frac{r_i D_e r_o X_m{}^e}{2\sqrt{3\theta_I}} + \frac{D_m r_o{}^2 X_m{}^{es}}{5}\right] \qquad (10.59)$$

Thus if vaporization from surface inclusions was dominant, i.e.

$$\frac{r_i D_e X_m{}^e}{2\sqrt{3\theta_I}} << \frac{D_m r_o X_m{}^{es}}{5}$$

then

$$N_g \alpha {}_I r_o{}^2$$

Conversely, if

$$\frac{r_i D_e X_m{}^e}{2\sqrt{3\theta_I}} >> \frac{D_m r_o X_m{}^{es}}{5}$$

then

$$N_g \alpha \sqrt{\theta_I}\, r_o$$

Experimentally, this can be, and was tested. Although all of the metals under consideration showed some dependence of

vaporization on their concentration (θ) in the coal, none of the elements for a given coal (Illinois No. 6 or Montana Savage lignite) had an r_o^2 dependence on the amount vaporized per gram of coal burned.

For the limiting case where ϕ_I is very large and also that

$$1 << \frac{D_{e\,I}}{\alpha_1 Do_2}$$

then

$$X_m^s \simeq X_m^e$$

Since X_m^{es}, cannot exceed the maximum value of X_m^e, then in this limit, the problem of surface inclusions acting as individual sources, i.e.

$$X_m^{es} > X_m^e$$

cannot be formulated.

In the analysis presented above, it has been assumed that the coal was a one-component system with respect to an ash species, or equivalently, that the presence of other ash components has no effect on the vaporization of metal M. A two component system can be considered where one component strongly absorbes the inorganic vapors of another component present in the same char particle. A specific example would be the strongly interacting system of SiO_2 - CaO leading to the formation of stable silicates or solutions in which one component, in dilute concentration, has extremely low activity (Elliot, 1955).

If metal M is vaporizing from its oxide inclusions within

the char an N_s absorbing inclusions are also present in the same char particle as effective sinks for the vapor M, then

$$cD_e \nabla^2 X_m + N_I{}^i V_I{}^i + N_s V_s{}^i = 0 \qquad (10.60)$$

where $N_I{}^i$ and $V_I{}^i$ are given by equations 10.8 and 10.14, and $V_s{}^i$ is the net rate of loss of vapor M to a single absorbing inlcusion of the other ash component. $V_S{}^i$ is expressed as

$$V_s{}^i = 4\pi r_s c D_e (X_s - X_m) \qquad (10.61)$$

where r_s is the radius of the absorbing or sink inclusion and X_s is the mole fraction of vapor M at the surface of the absorbing inclusion. In the limit of strong absorption X_s = 0), equation 10.60 becomes:

$$\nabla^2 X_m + \frac{\bar{\phi}^2}{r_p{}^2} - \frac{\phi_e{}^2}{r_p{}^2} X_m = 0 \qquad (10.61)$$

where

$$\bar{\phi}^2 = \phi_I{}^2 X_m{}^e + \phi_s{}^2 X_s \qquad (10.62)$$

$$\phi_e{}^2 = \phi_I{}^2 + \phi_s{}^2 \qquad (10.63)$$

The term ϕ_I is the Thiele modulus for the vaporizing inclusions (for M), as defined before, and the term ϕ_s is the Thiele modulus for the absorbing or sink inclusions of the other ash component:

$$\phi_s = \sqrt{3\theta_s}\ \frac{r_p}{r_s} \qquad (10.64)$$

The solution of equation is

$$X_m = \left[\frac{\bar{\phi}^2}{\phi_e{}^2} - \left(\frac{\phi^2}{\phi_e{}^2} - X_m{}^s \right) \frac{r_p \sinh \left(\phi_e \frac{r}{r_p} \right)}{r \sinh \phi_e} \right] \qquad (10.65)$$

and the mole fraction of vapor M at the chars surface is

$$X_m^s = \frac{\bar{\phi}^2}{\phi_e^2} \left\{ \frac{\left[\frac{\phi_e}{\tanh \phi_e} - 1\right]}{\frac{Do_2 \alpha_1}{D_e} + \left[\frac{\phi_e}{\tanh \phi_e} - 1\right]} \right\} \qquad (10.66)$$

where the same boundary conditoins applied before have been applied here. The effects of surface inclusions have been neglected here.

An effectiveness factor for the two component problem, η_b, is defined as the rate of vaporization of M from the char with interacting inclusions, sink inclusions, and external diffusion resistance contributions over the rate of N_I non-interacting inclusions in the absence of sinks. The effectiveness factor obtained is:

$$\eta_b = \frac{3}{\phi_e}\left[\frac{1}{\tanh \phi_e} - \frac{1}{\phi_e}\right]\left[\frac{1}{1 + \frac{D_e}{\alpha_1 Do_2}\left[\frac{\phi_e}{\tanh \phi_e} - 1\right]}\right]\left[1 + \frac{\phi_s^2}{\phi_I^2}\frac{X_s}{X_m^e}\right] \qquad (10.67)$$

and the total rate of vaporization of M from the char is

$$V_c = \eta_b N_I V_I^{ni} \qquad (10.68)$$

This effectiveness factor is now used to examine several cases in which the presence of sinks influences the total vaporization rate, V_c, of M from a char particle.

In the limit where the sinks are highly disperses, in comparison to the sources to the effect that

$$\phi_I << \phi_S$$

then

$$\eta_b = \frac{3\ {}_1Do_2X_s}{D_e\phi_I{}^2X_m{}^e}$$

and

$$V_c = 4\pi r_p\alpha_1 cD_{o_2}X_s$$

This is, again, simply an external diffusion control problem where X_s is now the mole fraction of M at the surface of the char particle. It was assumed above that X_s was finite and that

$$1 << \frac{\phi_s{}^2X_S}{\phi_I{}^2X_m{}^e}$$

If the reverse were the case, i.e.

$$1 >> \frac{\phi_s{}^2X_s}{\phi_I{}^2X_m{}^e}$$

because

$$X_s \simeq 0$$

for complete absorption of the metal M vapors by the sink inclusions, then

$$\eta_b = \frac{3\alpha_1 Do_2}{D_e\phi_s{}^2}$$

and

$$V_c = 4\ r_p c\alpha_1 D_{o_2}\frac{\phi_I{}^2}{\phi_s{}^2}\ X_m{}^e$$

This rate is again that of external diffusion control with the mole fraction of M at the surface of the char being:

$$X_m^s = \frac{\phi_I^2}{\phi_s^2} X_m^e$$

If the case of strongly absorbing sinks is again considered ($X_s \tilde{} 0$) but now the dispersion of sinks and sources are equivalent so that

$$\phi_s = \phi_I$$

then for a large modulus ϕ_I, but with

$$\frac{D_e \sqrt{2} \phi_I}{\alpha_1 Do_2} << 1$$

the effectiveness factor becomes:

$$\eta_b = \frac{3}{\sqrt{2}\phi_I}$$

In this case, the vaporization rate of M is given by equations 10.29 times a factor of $(2)^{-\frac{1}{2}}$. If $\phi_s = \phi_I$ but with

$$\frac{D_e \sqrt{2} \phi_I}{\alpha_1 Do_2} >> 1$$

then

$$\eta_b = \frac{3}{2} \frac{\alpha_1 Do_2}{\phi_I^2}$$

and the rate of V_c is given by equation 10.30 multiplied by a factor of $\frac{1}{2}$. In summary, other ash components in the char will not significantly influence the vaporization behavior of the metal M unless the sinks are more highly dispersed than the sources, i.e. $\phi_I << \phi_s$.

Before examining the experimental data in light of the combined aspects of ash vapor transport processes and ash vaporization thermochemistry, it is worth considering how chemical kinetics may influence the vaporization of ash. If

it is assumed that chemical kinetics controls the rate of ash vaporization, then the concentration of ash in the char C_a is determined by

$$-\frac{dC_a}{dt} = k_v C_a$$

where k_v is the vaporization or reaction rate constant. Intergrating over the burning time of the char particle yields

$$\ell_n(1 - f_v) = -k_v t_b$$

where f_v is the fraction of ash vaporized. At low conversions, the fraction of ash vaporized is proportional to the burning time of the char particle or the square of the initial char diameter:

$$f_v = k_v t_b \propto d_o^2$$

This volumetric production rate of ash vapor from a burning char particle is experimentally indistinguishable from the internal diffusion controlled vaporization rate for the case where the individual inclusions act independently ($\phi_I \to 0$). However, none of the data for the elements (Chapter Eight) suggest a r_o^2 dependence for the amount of ash vaporized per gram of coal burned.

10.3 Thermochemical Modelling and Discussion

The model described in the preceeding section is essentially a two parameter model, with the inclusion modulus ϕ_I (or inclusion size, r_i) and the effective diffusivity D_e being adjustable, but with a temperature dependence of vaporization (accounting for the effects of temperature on effective and bulk diffusivities) explicitly given by the thermochemical equilibria at the surface of each inclusion within the char particle. Values of ϕ_I and D_e, however, can be estimated within reason given the present knowledge of the occurance of mineral matter in coal and the structure of coal char. Rather than directly compare the experimental fraction vaporization rates with model predictions for assumed values of ϕ_I and D_e, the approach taken in this discussion is to compare predicted partial pressures (or mole fraction x_m^s) of inorganic vapor species at the char's surface with that calculated from the experimental vaporization rates. It will become apparent that this approach provides an easier comparison of the experimental data.

The key to the thermochemical aspect of ash volatilization is that, although the coal particles are burning in oxygen rich environments, the atmosphere experienced by the inherent mineral matter within the char particle is of low oxygen potential or reducing. Under this high temperature locally reducing environment, created by the coal particle combustion process the refractory metal oxides of the inherent ash may undergo chemical reduction to more volatile forms. The

overall chemistry in the presence of excess carbon may be expressed as

$$MO_n(c) + C = MO_{n-1}(v) + CO \qquad (a)$$

where MO_n is the stable condensed metal oxide (i.e. SiO_2, MgO or CaO) and MO_{n-1} is the volatile suboxide (SiO) or metal vapor (Mg or Ca). Silicon monoxide (SiO) is only stable as a gas and the boiling points of Mg and Ca are below the combustion temperatures examined here. Reaction (a) as written is an inherently show processes requiring the contacting of three phases. Under the time scales of combustion (< 1 second) it is unlikely that reaction (a) reaches equilibrium. It is more likely that chemical reduction proceeds through gaseous intermediates (Szekely et al., 1976) via the heterogeneous reactions

$$MO_n(c) + CO = MO_{n-1}(v) + CO_2 \qquad (b)$$

$$CO_2 + C = 2CO \qquad (c)$$

An analagous reaction system that has been investigated extensively is the high temperature reduction of iron oxide pellets by coke (Rao, 1971; Fruehan, 1977; Sasaki and Tanekazu, 1977) where it has been found that reaction (c) is rate controlling. Reaction (b) probably involves a number of elementary steps (absorption, surface reaction, desoption) characteristic of heterogeneous reactions. Precise information on the physical chemistry is unknown at present nor is it likely that it would be useful in an enviornment as ill-defined and

complex as coal combustion. Other gaseous species including H_2 and radicals may act as reducing agents. In the present analysis, these are neglected as they are expected to be at much lower concentrations in this experimental system.

The arguments presented above force the assumption within the framework of the model that reaction (b) is occuring and is at equilibrium at the surface of each inclusion within the char. The equilibrium partial pressure of the metal or suboxide vapor, P_m^e, at the surface of each inclusion is then determined from the equilibrium constant K_e for reaction (b)

$$K_e = \frac{P_m^e P_{CO_2}}{a_{MO_n} P_{CO}}$$

The inclusions may be pure components such as molten silica from quartz or CaO (s) from decomposed calcite minerals, or as a multicomponent system resulting from, for example, the rapid high temperature decomposition of alumino-silicate clays. For the present, the coal is assumed to be a single system with respect to a metal oxide. The presence of other ash components in the char or in solution may influence the volatilization of a specific component in several ways and a qualitative consideration of these effects is reserved for the last section of this chapter. For a single component system, and assuming there is no other source of carbon dioxide to influence the equilibria at the surface of each inclusion, the partial pressure of the inorganic vapor at an inclusion surface is simply expressed as

$$P_m^e = P_{CO_2} = (K_e P_{CO})^{1/2}$$

The partial pressure of CO in the char particle is obtained by assuming that the oxygen diffusing to the surface of the char is completely consumed at the surface and that CO is the only product of combustion.

According to the model as evident in equation 10.23, the partial pressures of metal containing vapors at the char surface will, in general, be less than the equilibrium value at the inclusion surface due to internal diffusion resistance, as shown in Figure 10.4, and vary during the course of char burnout for shrinking sphere combustion behavior. This time dependence arises as a result of the function dependence of ϕ_I on char radius r_p. Since the experimental measurements are taken for complete combustion of the coal particles, a theoretical or model time average value of X_m^s is needed and can be calculated as

$$\bar{X}_m^s = \frac{1}{t_b} \int_o^{t_b} X_m^s \, dt$$

using the time dependent modulus

$$\phi_I(t) = \phi_I^o \left(1 - \frac{t}{t_b}\right)^{1/2}$$

with ϕ_I^o defined as the initial modulus:

$$\phi_I^o = \sqrt{3\theta} \, \frac{r_o}{r_i}$$

Thus, a predicted value of $\bar{X}_m^s$ or average partial pressure of metal vapor at the char particle surface can be obtained

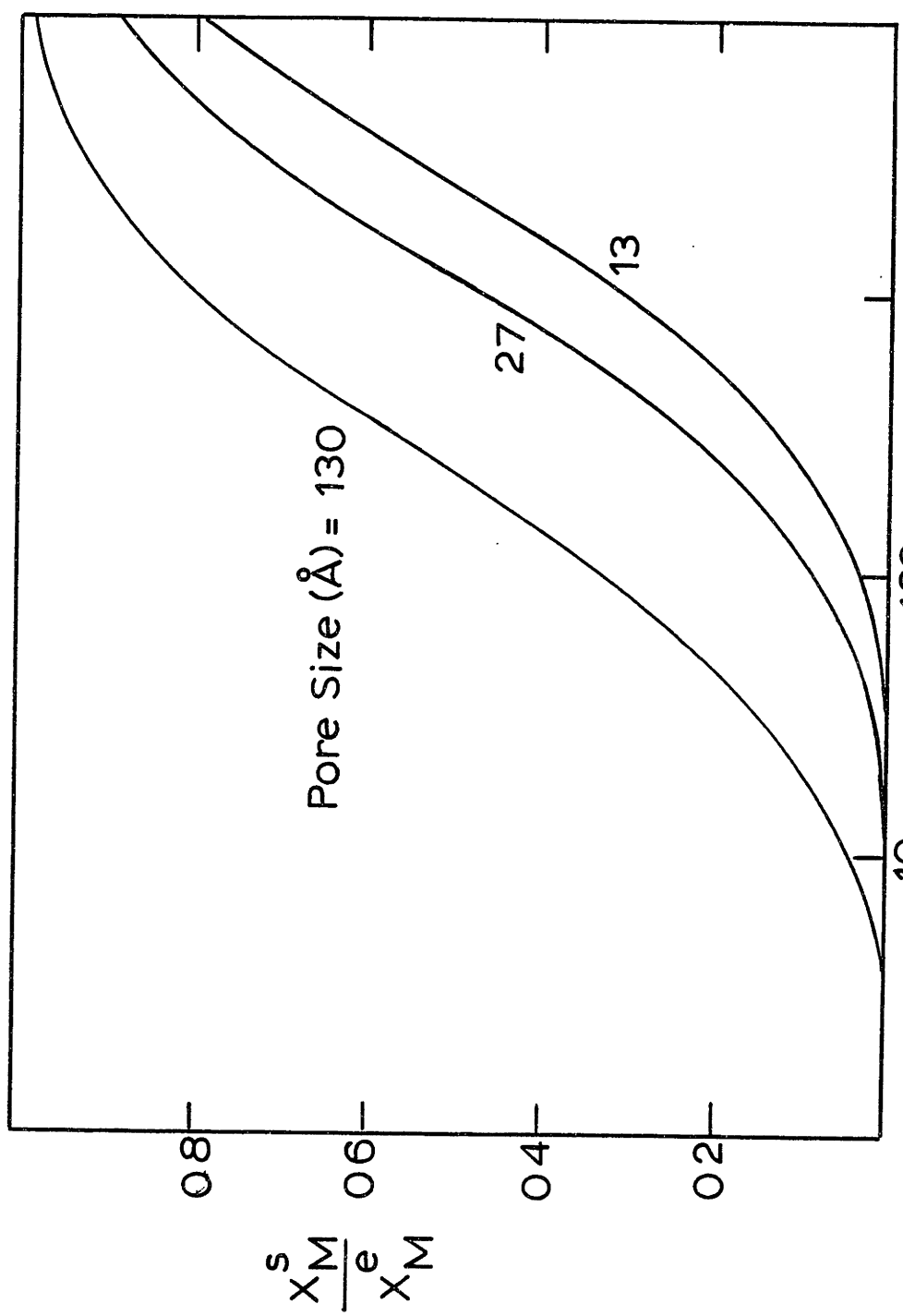

Figure 10.4 The Dependence of the Gas Phase Mole Fraction of Metal Vapor $\left(\frac{x_M^m}{x_M^s}\right)$ at the Char Surface on the Modulus ϕ_I and Pore Size

from the thermochemical equilibria at the inclusion(s) surface and assumed values of ϕ_I^o and D_e.

The instantaneous vaporization rate of the metal from a single burning char particle is directly proportional to the partial pressure of the metal containing vapor at the char surface, as seen in equation 10.24, since internal and external diffusion resistances are in series. An experimentally determined (average) metal partial pressure may be unambiguously calculated from the vaporization data using the external transport rate equation. In the following, experimentally determined partial pressures at the char particle surface are compared with model predictions for each element under consideration. Although the coal is a multicomponent system, the comparisons are made assuming a single component system for each metal. A final discussion will consider, in qualitative terms, multicomponent effects.

10.3.1 Silicon

Silicon is distributed as silica (SiO_2) in either quartz or finely deseminated micron sized clay minerals in the pulverized coal particles. For an inclusion diameters of about 0.5 to 2 microns, and an initial coal size of 55 microns, the Thiele modulus ϕ_I^o is on the order of 5 to 20 for the coals examined in this study. Thus, if the effective diffusivity is small due to small pores such that

$$\frac{D_e \phi_I}{\alpha_1 DO_2} << 1$$

then $\bar{X}_m^s$ is significantly less than X_m^e and is approximated by

$$\bar{X}_m^s = \frac{2D_e\phi_{I^o}}{3\alpha_1 Do_2} X_m^e$$

The term $D_e/\alpha_1 Do_2$ is on the order of 10^{-3} for chars having an average pore radius of about 25 Å and porousity of about 0.5. It is quite obvious that in this case the rate of vaporization is highly dependent on the structural characters of the char, which are likely to be changing during burnout, and the size of the inclusions.

From the experimental vaporization rate data, average gas phase mole fractions of various species were calculated from the external diffusion rate. The results of these calculations for Si (presumed SiO) are shown by the data points in Figure 10.5 for several coals. For comparison the vapor pressure of SiO_2 and Si metal are also included. As evident, experimentally determined partial pressures of Si containing vapors at the char's surface far exceed the oxide vapor pressure at most combustion temperatures.

The solid lines corresponding to different values of ϕ_I in Figure 10.5 are the predicted partial pressures of SiO at the char's surface for the given value of ϕ_I, the equilibrium value of X_m^e at each inclusion's surface within the char, and a porosity of 0.5 and pore radius of 25Å for the calculation of D_e (Satterfield, 1970). The equilibrium mole fraction of SiO vapor at each inclusions surface (X_m^e) is calculated for the reaction

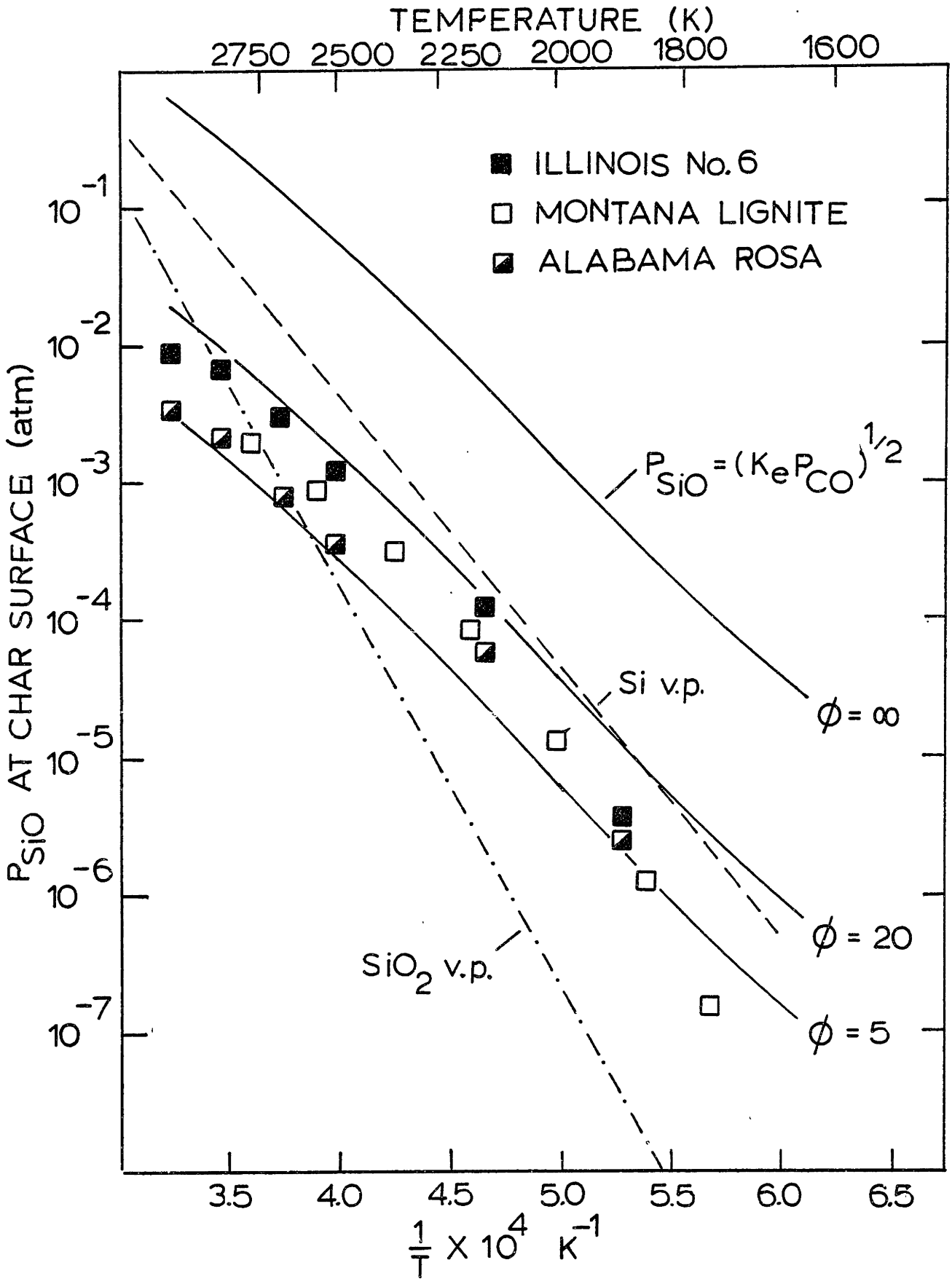

Figure 10.5 Comaprison of Experimentally Determine Partial Pressures of SiO at Char Surface with Model Predictions

$$SiO_2\ (c) + CO = SiO\ (v) + CO_2$$

assuming a single component system, i.e.

$$X_m{}^e P = P^e_{SiO} = P^e_{CO_2} = (K_e P_{CO})^{1/2}$$

The solid line corresponding to $\phi_I = \infty$ is this calculated partial pressure of SiO vapor at an inclusion's surface. This rotation is used, because according to the model, at a value of ϕ_I that approaches infinity, the partial pressure of SiO at the char particles outer surface becomes equivalent to that at each inclusions surface. This is a special limiting case which will be re-examined in the discussion of the vaporization behavior of calcium and magnesium. The significant point here is that, for typical volume fractions of ash in the coal and characteristic mineral inclusion dimensions on the order of a micron, internal diffusion resistance significantly suppresses the SiO partial pressure at the char surface.

The transport model considering internal/external diffusion resistance in series and a thermochemical equilibria at the inclusion surfaces for reduction of SiO_2 by CO predicts with reasonable agreement the average partial pressure of SiO at the char surface or, equivalently, the rate of vaporization and, quite accurately, its temperature dependence over nearly the entire range of combustion conditions. The observed suppression of the vaporization of Si by CO_2, and other elements as well (Table 8.7) qualitatively supports the proposed thermochemical mechanism.

The hypothesis that inclusions within a single char particle can be further examined in terms of the size

dependence of the fractional volatilization rate correlation, used in Chapter Eight, on the initial size of the coal. For values of ϕ_I expected for silica and with

$$\frac{D_e \phi_I}{\alpha_1 Do_2} << 1$$

then the effectiveness factor is approximated by

$$\eta = \frac{3}{\phi_I}$$

indicating strong interaction. The instantaneous vaporization rate from a single char particle is then

$$V_c = \sqrt{3\theta_I} \frac{r_p^2}{r_i} 4\pi_e D_e X_m^e$$

Integrating over the burning time, the fractional volatilization rate obtained is

$$\frac{f_v}{t_b} = \frac{54 w \rho_a c D_e X_m^e}{7\sqrt{3\theta_I}\, r_i\, r_o} \alpha \frac{1}{r_o}$$

where f_v is the fraction vaporized for complete combusiton. This inverse dependence on the initial coal particle radius is observed for Si as shown in Figure 10.6. Had the vaporization been model assuming no interaction the f_v/t_b predicted would have been independent of coal size, as is also predicted by a purely chemical kinetic model.

The value of the modulus ϕ_I^o may be evaluated experimentally for the purpose fo comparing the different coals. This comparison for Si is shown in Figure 10.7 for combustion at 1750K in twenty percent oxygen. The same porosity (0.5) and pore size (25Å) was used for all coals in the calculation,

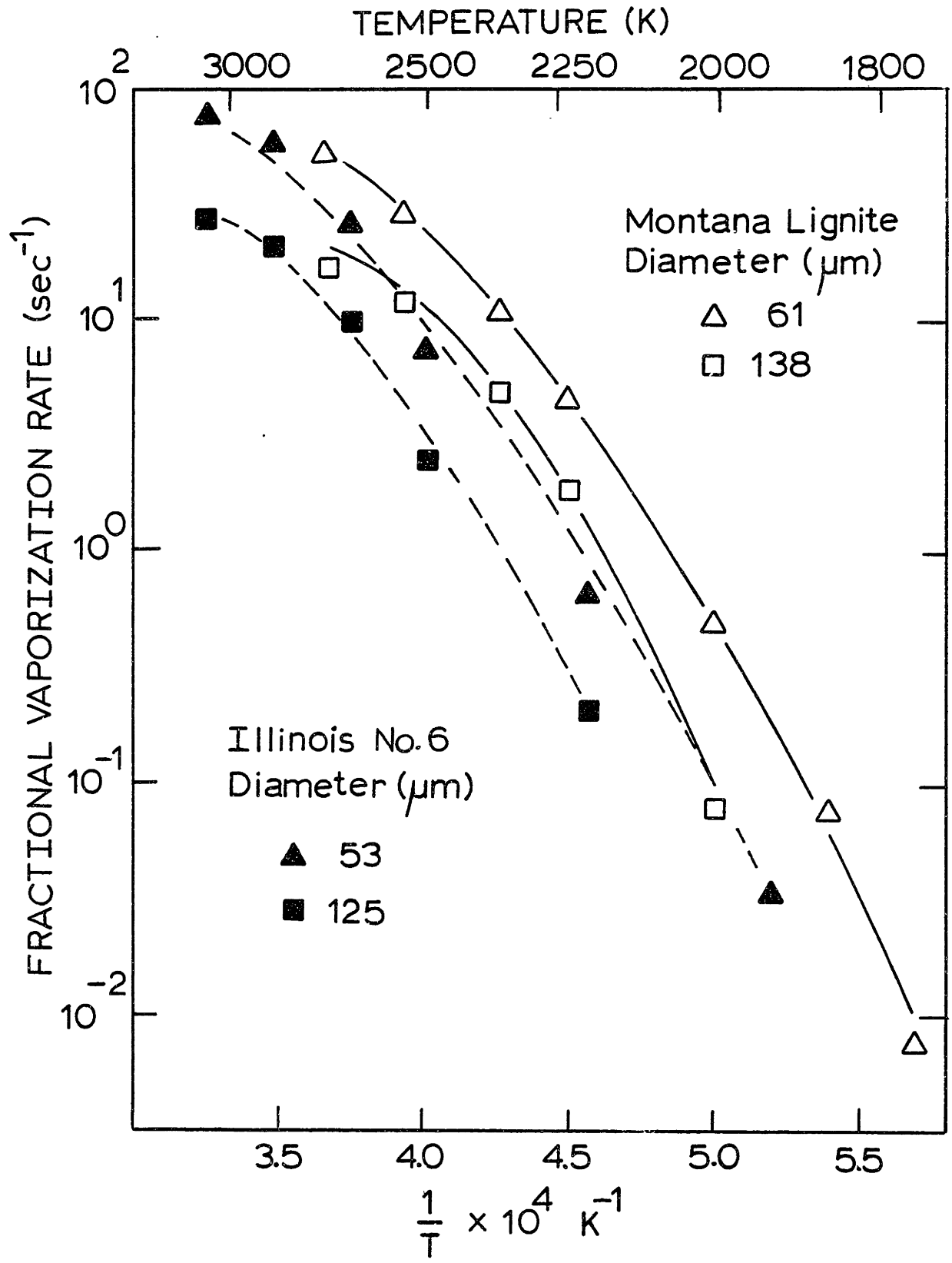

Figure 10.6 The Effect of Coal Size on the Fractional Vaporization Rate of Silicon

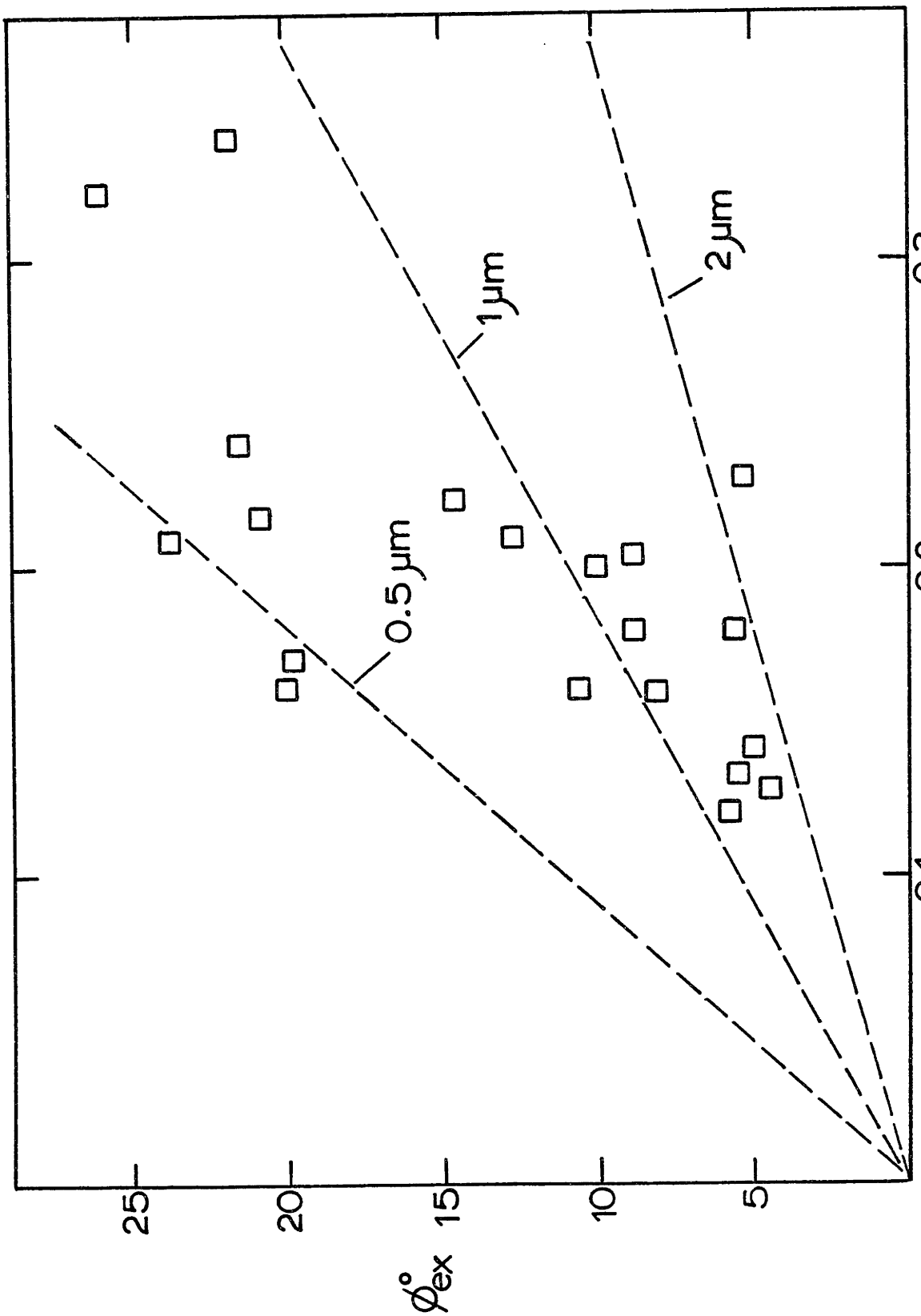

Figure 10.7 Comparison of Experimentally Determined ϕ_I^o for Different Coals

although these properties may vary considerably among coals. Teh volume fraction of silica (θ) was calculated by assuming it exists as pure SiO_2. The trend and the values of ϕ_I calculated are reasonable considering that mineral matter is not distributed uniformly (Chapter Five) among all coal particles, (b) inclusion sizes are not monodispersed or necessarily the same for all coals; (c) that much of the silica is distributed in alumino-silicate clay minerals and therefore of non-unit activity in the high tempeature inclusion melts; and (d) chars from different coals do not have the same structural characteristics and the use of a monodisperse pore model is a great oversimplification of the internal transport phenomena.

10.3.2 Iron

Iron is another element occuring as mineral inclusions in pulverized coal. However, its thermochemistry is significantly more difficult to deduce than silica as it occurs primarily in the disulfied pyrite [FeS_2].

Under the rapid heating conditions and locally reducing environment characteristic of the combustion process, the decomposition of pyrite to FeS or a non stoichiometric FeS melt can be assumed instantaneous (Halstead and Raask, 1969). The FeS melt may undergo further but slower decomposition to liquid iron metal or be oxidized by oxygen bearing gases (Halstead and Raask, 1969; Attar, 1978). The Fe-S-O system and its melt at these temperatures is complex and its composition or the activity of Fe(ℓ) or FeO(ℓ) will depend strongly

on the gaseous environment (Nagamori and Mitsuo, 1965) with respect to oxygen and sulpher bearing gases (O_2, Co_2, CO, H_2O, H_2, H_2S, SO_2, COS and S_2). The pronounced effect of coal type and iron-bearing mineral forms on the volatilization of Fe (Figure 8.11) may reflect the complicated nature of this system.

The experimentally determined partial pressures of Fe at the chars surface are compared in Figure 10.8 with predictions assuming a unit activity of Fe (ℓ) and the vapor pressure of Fe at the inclusion surface. Fair agreement is obtained for values of ϕ_I between 10 and 100, corresponding to inclusion sizes of less than a micron.

10.3.3 Calcium and Magnesium

Inherent calcium and magnesium in Bituminous coals are physically distributed in a manner similar to that of silicon. Calcium occurs primarily in the calcite mineral but may also occur in alumino-silicate clay minerals. The mineral dolomite was rarely observed so it is likely that magnesium occurs, for the most part, in the alumino-silicate clays of bituminous coals. Hence, the modulus ϕ_I is expected to be close to that for silicon and on the order of 10 for these elements. In the calculation of ϕ_I, the volume fraction θ for the clays bearing magnesium would be used rather than the metal oxide volume fraction in the coal.

The calculated partial pressures of Ca and Mg at the char's surface are shown for several coals in Figures 10.9 and 10.10. Again the solid lines corresponding to different

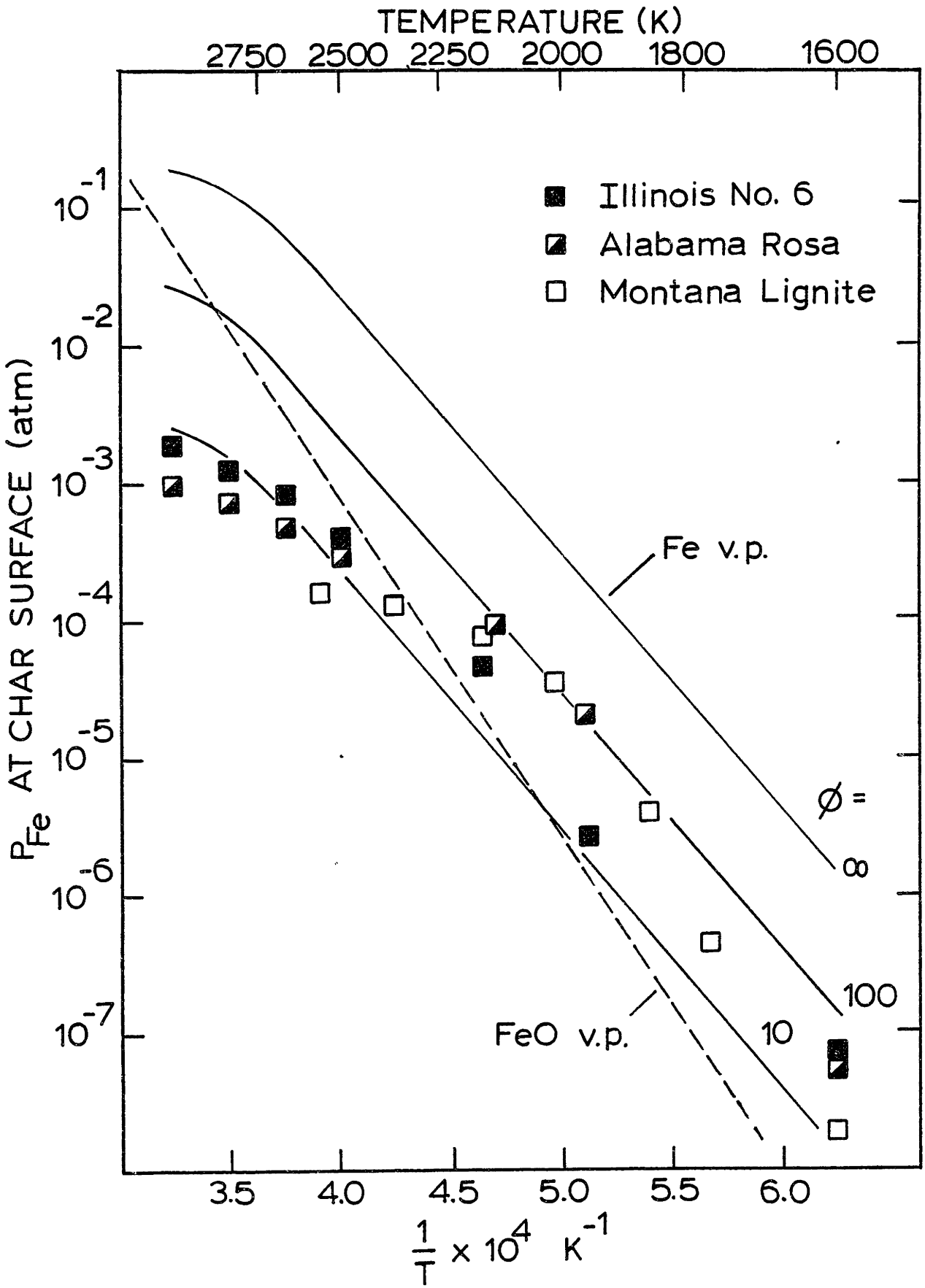

Figure 10.8 Comparison of Experimentall Determined Pressures of Fe Vapor at Char Surface with Model Predictions

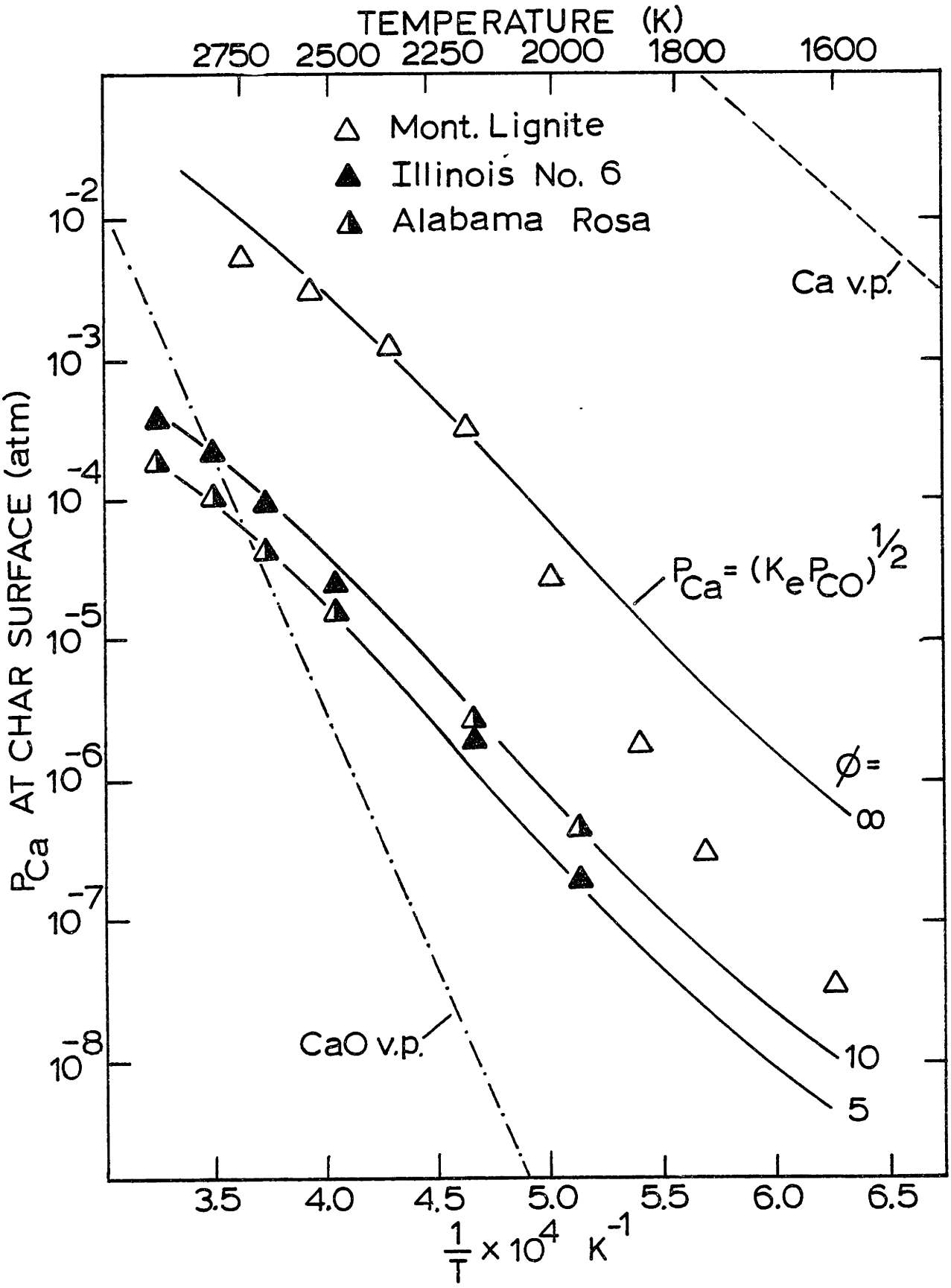

Figure 10.9 Comparison of Experimentally Determined Partial Pressures of Calcium at the Char Surface with Model Predictions

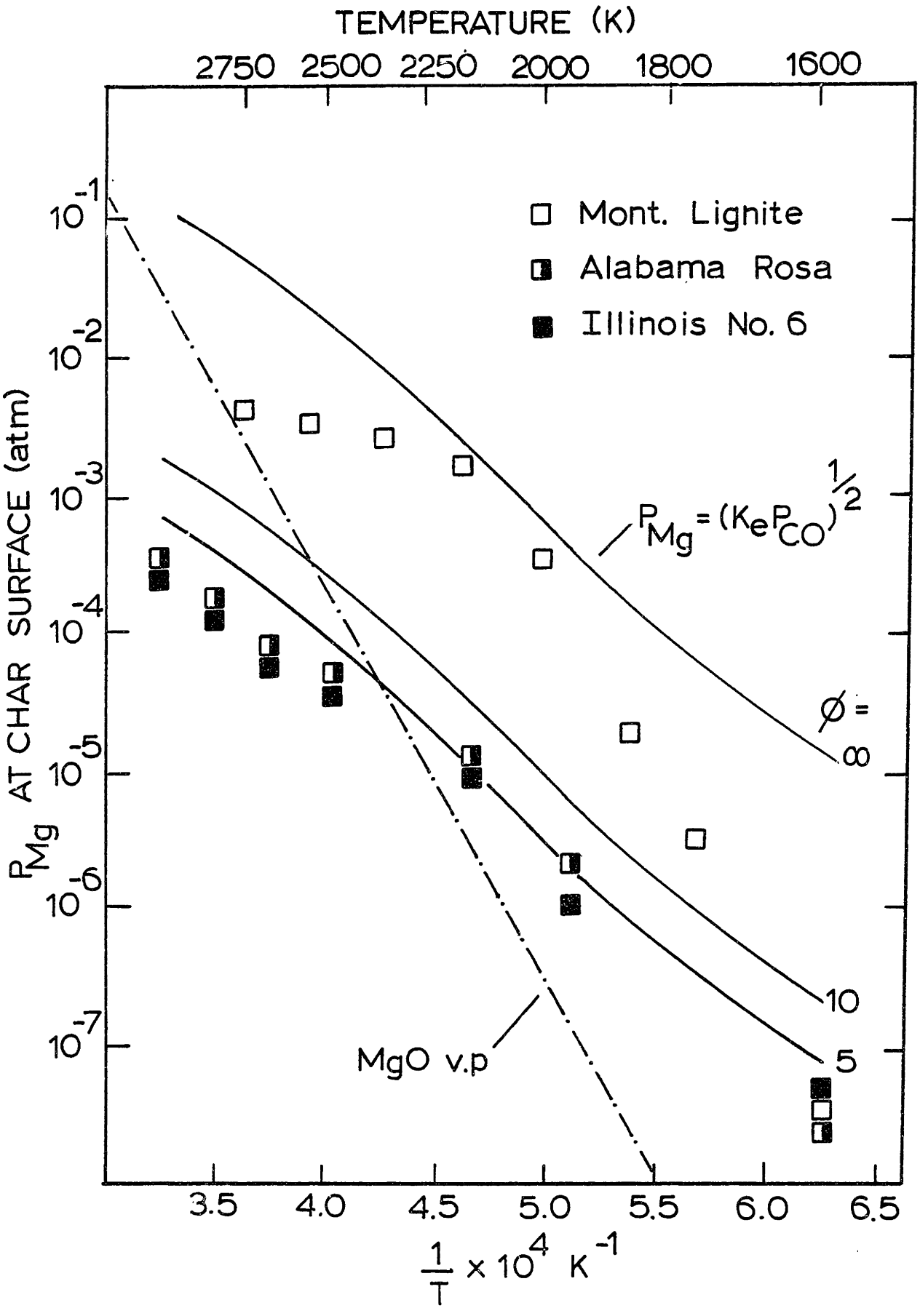

Figure 10.10 Comparison of Experimentally Determined Partial Pressures of Magnesium at the Char Surface with Model Predictions

values of ϕ_I are predicted partial pressures at the char surface assuming the following reactions are at equilibrium at inclusion surfaces for pure component condensed phases:

$$CaO(s) + CO = Ca(g) + CO_2$$

$$MgO(s) + CO = Mg(g) + CO_2$$

For the bituminous (Illinois No. 6 and Alabama Rosa) coals, it is observed that the temperature dependence and the magnitude of the surface partial pressure for reasonable values of ϕ_I are in close agreement with values calculated from experimental rate data. For the lignite, however, partial pressures of Mg and Ca calculated from the data approach predicted values for $\phi = \infty$. This is undoubtedly a consequence of the atomic dispersion of elements throughout the organic matter of the original coal. The scanning electron microscopy study (Chapter Nine) revealed that these metals form minute grains fo ash on the chars surface during oxidation. Although it cannot be experimentally ascertained what their chemical or physical state is within the burning char, it appears that the parameter ϕ_I is exceedingly large due to this original atomic dispersion in the raw coal and the effectiveness factor would be

$$\eta \rightarrow \frac{3\alpha_1 Do_2}{D_e \phi_I^{\,2}}$$

The instantaneous rate of vaporization would, in this limit of ϕ_I approaching infinity as a result of extremely small

inclusion size, be

$$V_c = 4\pi c\alpha_1 \, Do_2 \, r_p \, X_m^e$$

Thus the rate of vaporization is controlled by diffusion through the char's external boundary layer and it is not necessary to specify the exact mechanism of local vaporization in the char. The surface gas phase mole fraction X_m^s of the metal is close to the equilibrium mole fraction X_m^e, as is observed experimentally for calcium and magnesium during lignite combustion.

The fraction vaporization rate f_v/t_b for calcium and magnesium in the case of the bituminous coals is given by the same expression obtained for silicon. As shown in Figure 10.11, inverse dependence on coal size, as predicted, was observed for the fractional rate of magnesium vaporization for combustion of the Illinois No. 6. For the lignite however, where the working limit is $\phi_I \rightarrow \infty$ for the organically bound metals, the fractional vaporization rate for external diffusion controlled vaporization is

$$\frac{f_v}{t_b} = \frac{2c\alpha_1 Do_2 w\rho_a X_m^e}{\theta r_o^2} \alpha \frac{1}{r_o^2}$$

This inverse square dependence on the initial coal diameter was observed experimentally for the magnesium fractional vaporization rate in the case of lignite combustion as shown in Figure 10.11.

It is also observed that the partial pressure of Mg and Ca at the surface of the burning lignite particles drops off systematically from predicted values at lower temperatures.

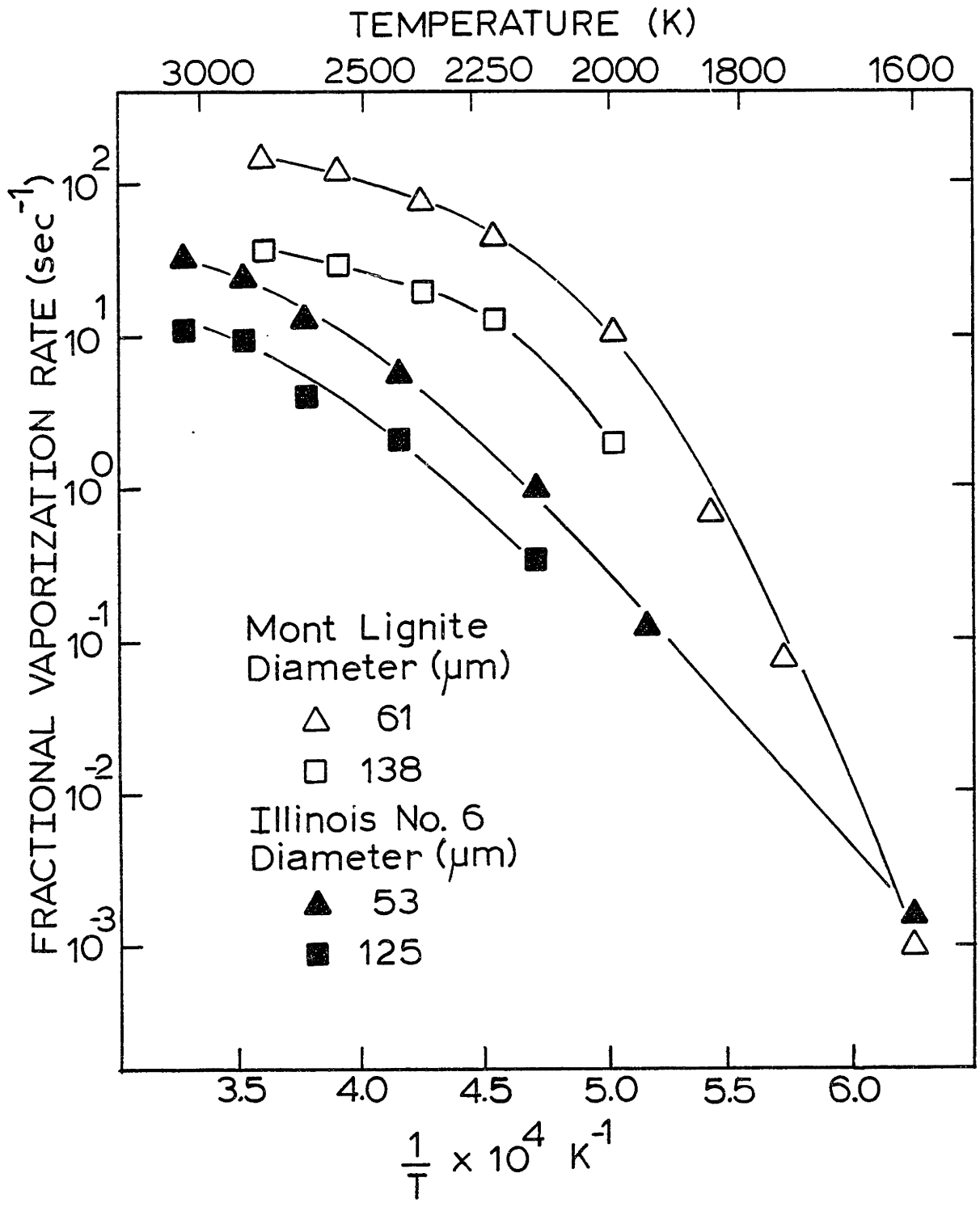

Figure 10.11 The Effect of Coal Size on the Fractional Vaporization Rate of Magnesium

It is believed that this is a consequence of the increasing degree to which oxygen penetrates the char with decreasing combustion temperature, resulting in a suppression of the mole fraction of metal vapors near the surface of the char.

10.3.4 Multicomponent Effects

The preceeding thermochemical analysis assumed that the metal oxides (SiO_2, MgO and CaO) exist within the char as pure and physically isolated phases. This was implicit in th assumption of unit oxide activities and independent reaction equilibria. The only pure phases existing within the coal are quartz [SiO_2], calcite [$CaCO_3$] and pyrite [FeS_2] if it completely decomposes to iron metal. Silica, as well as Ca, Mg and Fe (for iron-bearing clay coals) may occur in alumino-silicate melts arising from the high temperature decomposition of the clays. If it is presumed that an inclusion is a mixture of oxides, then the simultaneous multicomponent reaction equilibria would be

$$P_{CO}^{\Sigma K_i a_i} = P_{CO_2}^{2}$$

where K_i and a_i are the equilibrium constant and the activity of oxide i in the inclusion. The partial pressure of metal or suboxide i at an inclusion surface is

$$P_i = K_i a_i \frac{P_{CO}}{P_{CO_2}}$$

and P_{CO_2} is not necessarily equivalent to P_i as in the pure component case. As an example, magnesium may occur as a minor

component in the clays of bituminous coals and as a consequence its oxide activity in the melt may be quite low (Elliot 1955). However, the values of Ki for silica and magnesia reduction are fairly close over the entire temperature range. It would therefore be difficult to determine from the temperature dependence of vaporization if X^{e}_{Mg} (or X^{s}_{Mg}) is strongly affected by the equilibration of P_{CO_2} by all components, and particularly silica, at the inclusion surface. Furthermore, given the fact that the properties of chars are different, that inclusion sizes may vary from coal to coal, and that the elements may occur in a multiple of mineral forms, it would be equally difficult to determine the role of activity from a comparison of coals and their compositions.

The volatilization of specific ash components in a coal particle may be influenced by the presence of other physcially isolated volatilizing ash components through the CO_2 product generated by the reduction reactions if the CO_2 does not react sufficiently fast with the carbon within the char particle. If, for the sake of argument, it is assumed that CaO, MgO and SiO_2 exist as pure and physically isolated inclusions throughout the matrix of char, the CO_2 profile (in the absence of further reaction with carbon) would have the most significant effect on the vaporization of CaO by reduction with CO at inclusion surfaces. The equilibrium constant for the reduction of CaO by CO is about an order of magnitude less (over the whole temperature range) than the corresponding equilibrium constants for SiO_2 and MgO reduction. The expected values of ϕ_I for CaO are in the range of 5 to 10 for bituminous

coals if calcium is distributed as calcite minerals with inclusion dimensions of about 1 micron. Apparent ϕ_I's would have been an order of magnitude less. This was not observed experimentally. Similar considerations apply to the lignite where $\phi_I \rightarrow \infty$ for calcium and magnesium. There is apparently sufficient CaO free of local association with MgO to the end that the pure component calculation for CaO reduction is in agreement with the experimental data.

The effects of condensed phase activity may be reflected in the Mg vaporization data for low rank coals. As shown in Figure 8.13, the amount of magnesium vaporized is well correlated with the magnesium content of low rank coals. The model predicts that for the limiting case of $\phi_I \rightarrow \infty$, the amount (μg) of magnesium vaporized should have been independent of the magnesium content of the coal. It is likely that a CaO-MgO melt with additional impurities (e.g. Na_2O, Al_2O_3, P_2O_5) is formed from the ion-exchangable material in the coal during combustion (see Section 1.4.4). The data in Figure 8.14 may then reflect the non-unit activity of MgO in the melt.

It was initially suspected that the highly dispersed calcium and magnesium in the lignite would suppress the volatilization of silica, as the activity of silica in highly basic slags is quite low (Elliot, 1955) by the reaction of SiO vapors diffusing through the char with the alkaline earth oxides via the formation of low silica activity slags or stable ortho-silicates:

$$SiO(v) + 3CaO(c) = Ca_2SiO_4(c) + Ca(v)$$

This was investigated experimentally by measuring silicon vaporization during lignite combustion for lignite samples that had been acid washed to remove the ion-exchangable alkaline metals. There was no significant difference in the amount of silicon vaporized between acid washed and raw lignite samples (8.10). It was concluded, therefore, that if such reactions between different components are occurring, their rates are not significant enough to influence the volatilization of silicon.

CHAPTER ELEVEN

CONCLUSIONS AND RECOMMENDATIONS

Conclusions

The volatilization behavior of mineral matter during pulverized coal combustion was studied under the controlled experimental conditions of a laboratory laminar flow furnace. The mineral matter which volatilizes during combustion of the coal forms a submicron aerosol. Collection and isolation of this aerosol provided a means by which accurate measurement of vaporization could be obtained. The major experimental findings are summarized in the following:

(a) Time resolve measurements of ash vaporization indicate that significant vaporization of inorganics occurs only after the coal has ignited but ceases after the char has been completely burned. This is also consistance with the fact that that the fractional vaporization rate of ash and specific components is well correlated with the temperature and time of combustion of the coal particles. These results reflect the higher particle burning temperature over the gas temperature, the locally reducing environment is burning particles which facilitates chemical reduction of the refractory metal oxides, and the activated nature (equilibrium constant) of such reactions. The vaporization rate for refractories (SiO_2, CaO, and MgO) spanned over four orders of magnitude in the temperature range of 1600 - 2750K.

(b) Coal type and particularly rank has a pronounced effect on the amount of ash vaporized and the composition of submicron ahs generated during combustion. Low rank subbituminous coals and lignites containing organically bound calcium and magnesium yield submicron particles composed primarily of these components (as oxides). Bituminous coals, however, vaporize mostly silica. For the bituminous coals, the amount of ash vaporized increased with increasing inherent ash content of the coal. This trend was also observed for specific elements. Low rank coals produce considerably more submicron material during combustion than bituminous coals and this is solely due to the occurance and volatilization of the organically held metals in the low rank coals.

A single coal particle model for mineral matter vaporization during combustion was developed. The model predicts in excellent agreement with the experimental data the temperature dependence of volatilization, the magnitude of volatilization and the effect of coal size on the volatilization rate for mineral matter in the form of micron sized minclusions or organically held metals. The model assumptions are:

(a) Mineral inclusions of uniform radius are distributed homomeneously through a coal particle and that each of these inclusions act as point vapor sources contributing to the overall vaporization of a metal from a burning coal or char particle. Organically held metals correspond to a liminting case of extremely small inclusion size.

(b) Inorganic vapors are produced at the surface of each inclusion in the coal particle via the reduction reaction:

$$MO_n\ (c) + CO = MO_{n-1}\ (v) + CO_2$$

where MO_n (c) is the refractory oxide (SiO_2, MgO or CaO). This reaction is at equilibrium at the surface of each inclusion.

(c) The rate of vaporization of a metal is governed by internal and external diffusion resistances in series. Knudsen diffusion processes through the char's pores describe the rate of vaporization from a single inclusion. However, the inclusions within a single char particle do not act independently but are rather interacting due to a macroscopic potential field of the vapor throughout the porous char.

The rate of vaporization of a metal from a single char particle, according to the model, is dependent on the equilibria for reduction, the structure of the char in so far as an effective diffusivity in the char is needed, and the size and number of inclusions in the char particle.

Recommendations

(a) A scanning electron microscopy investigation of the low temperature ash obtained from a fixed array of isolated coal particles to determine the sizes of mineral inclusions and the coal particle to particle heterogeneity. The number and size distribution of mineral inclusions are important parameters in the vaporization model. It would

be particularly interesting to determine the variability among coals.

(b) Further measurement of vaporization behavior under conditions containing levels of CO_2 and H_2C representative of gasifiers and combustors. Both CO_2 and H_2O could suppress reduction (as was experimentally observed for CO_2), but under certain conditions, their reaction with carbon in the char particle could produce reducing agents (H_2) and shift the reaction equilibria for metal oxide reduction.

(c) A comparison of the char characteristics different coals to obtain and compare volatilization data with more representative effective diffusivities which are used in the model to evaluate internal vapor transport processes.

(d) The Mössbauer spectroscopy method was used to determine the iron-bearing mineral forms in raw coals. This method could be extended to determine the state of Fe in chars obtained during combustion at high temperature and representative of the complex and reducing environments occuring within burning particles. This may be particularly fruitful as iron was always a major component of the submicron ash and its volatilization behavior was found to be dependent on coal rank and mineral forms.

(e) Examine the volatilization process in greater detail by use of model experimental systems such as single component inorganics deposited in pure carbons or prescribed multicomponent systems.

APPENDIX A

COAL DATA BASE

Table A.1 Composition of Bituminous Coal 1.8 Floats (WT%)

Coal	Si	Al	Fe	Ca	Mg	K	Na
Illinois No. 6	1.97	0.848	.618	.180	.088	.150	.045
Western Kentucky	1.41	0.629	.890	.031	.035	.110	.010
West Virginia	3.38	1.77	.540	.198	.078	.183	.039
Pittsburgh No. 8	1.31	0.765	.520	.340	.065	.067	.061
Alabama Rosa No. 18	0.756	0.4270	.258	.054	.031	.057	.021
Utah	1.35	0.6800	.0940	.152	.030	.024	.034
Utah Price No. 1	1.40	0.732	.106	.110	.030	.025	.035
PSOC-3	0.937	0.44	.089	.049	.017	<.001	.017
PSOC-26	1.51	0.701	.710	.078	.056	.120	.014
PSOC-130	0.802	0.580	.320	.335	.087	.020	.026
PSOC-136	.505	.414	.120	.030	.001	.012	.014
PSOC-997	1.12	.655	.150	.104	.036	.043	.031

Table A.2 Composition of Low Rank Coal 1.8 Floats (WT%)

Coal	Si	Al	Fe	Ca	Mg	K	Na
Montana Savage	0.552	0.495	.088	1.38	.552	.0172	.0186
North Dakota	0.499	0.338	.350	1.08	.453	.028	.650
Texas	4.55	1.35	.740	.434	.180	.080	.027
Montana Rosebud	0.840	0.460	.330	.920	.210	.029	.023
Montana Hardin	0.740	0.540	.109	1.02	.189	.026	.250
Montana Powder River	1.75	0.861	.178	.988	.330	.037	.023
Wyoming Commanche	0.535	0.355	.230	.901	.290	.012	.062
Wyoming Rawhide	0.770	0.430	.250	1.05	.270	.013	.043

Table A.3 Raw Coal Ash Composition-Bituminous Coals (WT%)

Coal	SiO_2	Al_2O_3	FeO	CaO	MgO	Na_2O	K_2O
Illinois No. 6	50.09	18.58	18.50	9.17	1.38	0.52	1.78
Western Kentucky	43.72	21.71	29.97	1.20	0.91	0.22	2.27
West Virginia	46.97	26.31	19.78	3.56	1.09	0.42	1.89
Pittsburgh No. 8	42.26	25.51	15.70	11.83	1.95	1.28	1.48
Alabama Rosa	51.17	19.13	10.44	14.20	1.45	0.64	2.97
Utah	54.00	30.07	4.98	8.37	1.11	0.88	0.58
Utah Price No. 1	68.05	24.42	2.86	2.73	0.69	0.70	0.61
PSOC-3	68.42	23.38	4.18	2.44	0.86	0.57	0.15
PSOC-26	38.90	19.68	35.89	1.62	1.09	0.23	2.59
PSOC-130	38.14	26.46	11.48	18.25	4.22	0.84	0.60
PSOC-136	44.69	37.31	13.94	1.72	1.11	0.66	0.57
PSOC-997	50.32	28.68	13.32	4.33	1.42	0.81	1.11

Table A.4 Composition of Inherent Ash for Bituminous Coals (WT%)

Coals	SiO_2	Al_2O_3	FeO	CaO	MgO	K_2O	Na_2O
Illinois No. 6	58.10	22.09	10.99	3.47	2.03	2.49	0.84
Western Kentucky	53.80	21.20	20.49	0.77	1.04	2.37	0.24
West Virginia	60.37	28.07	5.85	2.33	1.09	1.85	0.44
Pittsburgh No. 8	49.47	25.50	11.84	8.04	1.92	1.42	1.45
Alabama Rosa	54.25	27.05	11.07	2.54	1.74	2.30	0.95
Utah	62.37	27.73	2.62	4.59	1.08	0.62	0.99
Utah Price No. 1	62.45	28.83	2.85	3.21	1.04	0.63	0.99
PSOC-3	65.25	27.05	3.74	2.23	0.94	0.04	0.75
PSOC-26	55.35	22.68	15.69	1.87	1.60	2.48	0.32
PSOC-130	44.02	28.11	10.59	12.03	3.73	0.02	0.90
PSOC-136	51.19	37.04	7.33	2.00	0.87	0.69	0.90
PSOC-997	58.08	29.97	4.69	3.53	1.46	1.26	1.02

Table A.5 Raw Coal Ash Composition-Low Rank Coals (WT%)

Coal	$Si0_2$	Al_20_3	Fe0	Ca0	Mg0	K_20	Na_20
Montana Savage	28.48	18.63	5.96	31.10	14.93	0.55	0.33
North Dakota	19.52	12.12	13.23	25.47	14.34	0.60	14.72
Texas	77.26	11.28	5.24	3.48	1.66	0.93	0.16
Montana Rosebud	35.88	19.32	22.49	17.17	4.05	0.75	0.35
Montana Hardin	35.94	20.43	9.35	24.34	4.36	0.54	5.04
Montana Powder River	44.16	20.03	12.82	16.82	5.19	0.68	0.32
Wyoming Commanche	28.77	20.55	9.36	29.54	9.59	0.36	1.83
Wyoming Rawhide	44.09	17.73	7.23	23.33	6.36	0.27	0.98

Table A.6 Composition of Inherent Ash-Low Rank Coals

Coal	SiO_2	Al_2O_3	FeO	CaO	MgO	K_2O	Na_2O
Montana Savage	23.03	18.24	2.21	37.66	17.97	0.40	0.49
North Dakota	20.01	11.97	8.46	28.33	14.17	0.63	16.44
Texas	68.17	17.86	6.69	4.25	2.10	0.67	0.26
Montana Rosebud	37.47	18.12	8.87	26.85	7.31	0.73	0.65
Montana Hardin	32.60	21.01	2.90	29.40	6.50	0.64	6.95
Montana Powder River	49.20	21.38	3.02	18.17	7.24	0.59	0.41
Wyoming Commanche	28.94	16.96	7.50	31.88	12.24	0.37	2.12
Wyoming Rawhide	34.49	17.01	6.75	30.77	9.44	0.33	1.22

APPENDIX B

X-RAY DIFFRACTION PATTERNS OF COAL LOW TEMPERATURE ASH

Table B.1 Minerals Identified by X-Ray Diffraction of Coal Low Temperature Ash

Mineral		Symbol
Quartz	SiO_2	Q
Kaolinite	$Al_2Di_2O_5(OH)_4$	K
Illite	$[(Al, Mg, Fe)_2(OH)_2\ (Si,Al)_4(O,OH)_{10}[K,H_3O]$	I
Calcite	$CaCO_3$	C
Pyrite	FeS_2	P
Dolomite	$CaMg(CO_3)_2$	D
Siderite	$FeCO_3$	S
Bassanite	$CaSO_4 \cdot \frac{1}{2}H_2O$	B
Gypsum	$CaSO_4 \cdot 2H_2O$	G

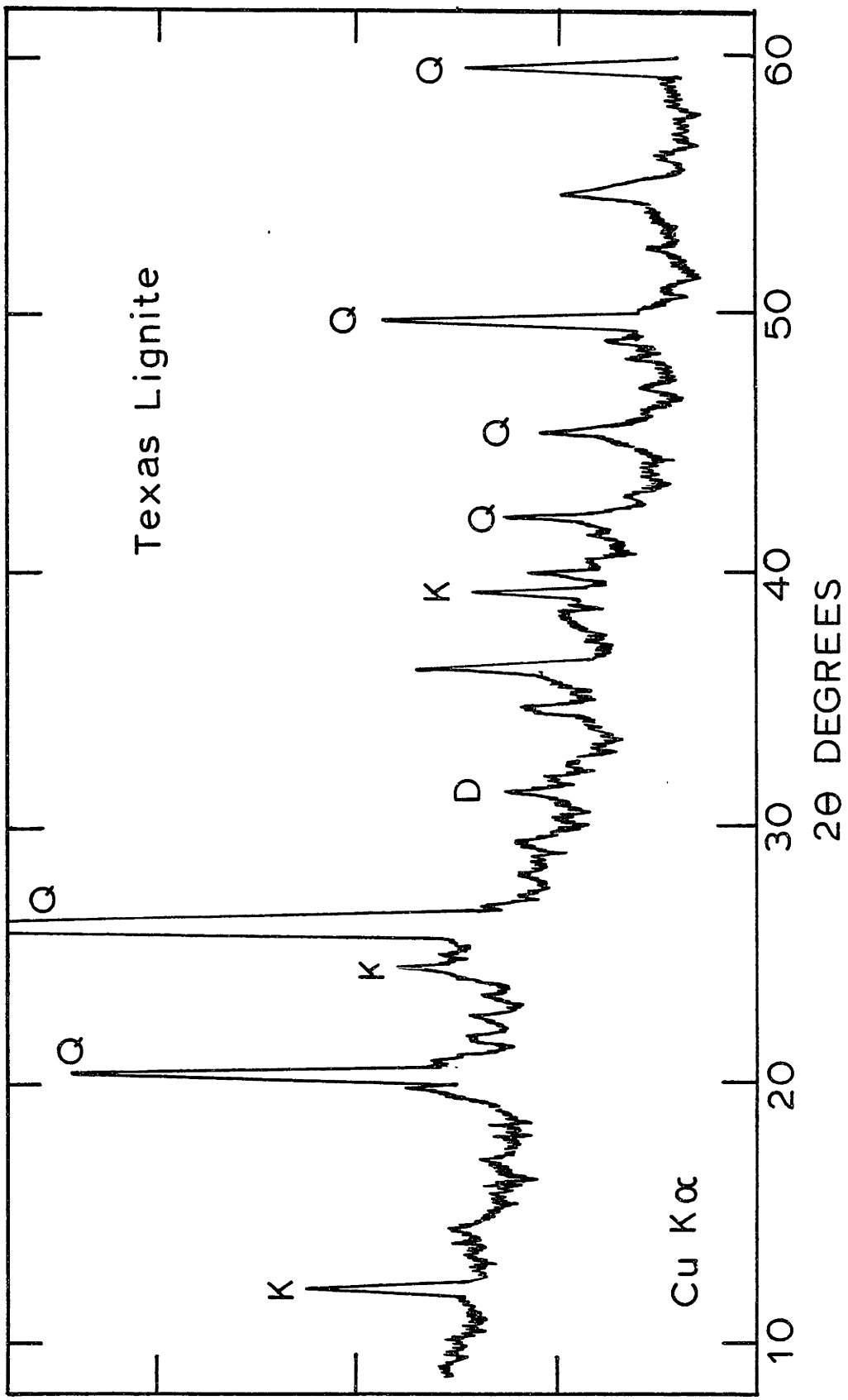
Texas Lignite
Cu Kα
Q
K
Q
K
Q
D
K
Q
Q
Q
10
20
30
40
50
60
2θ DEGREES

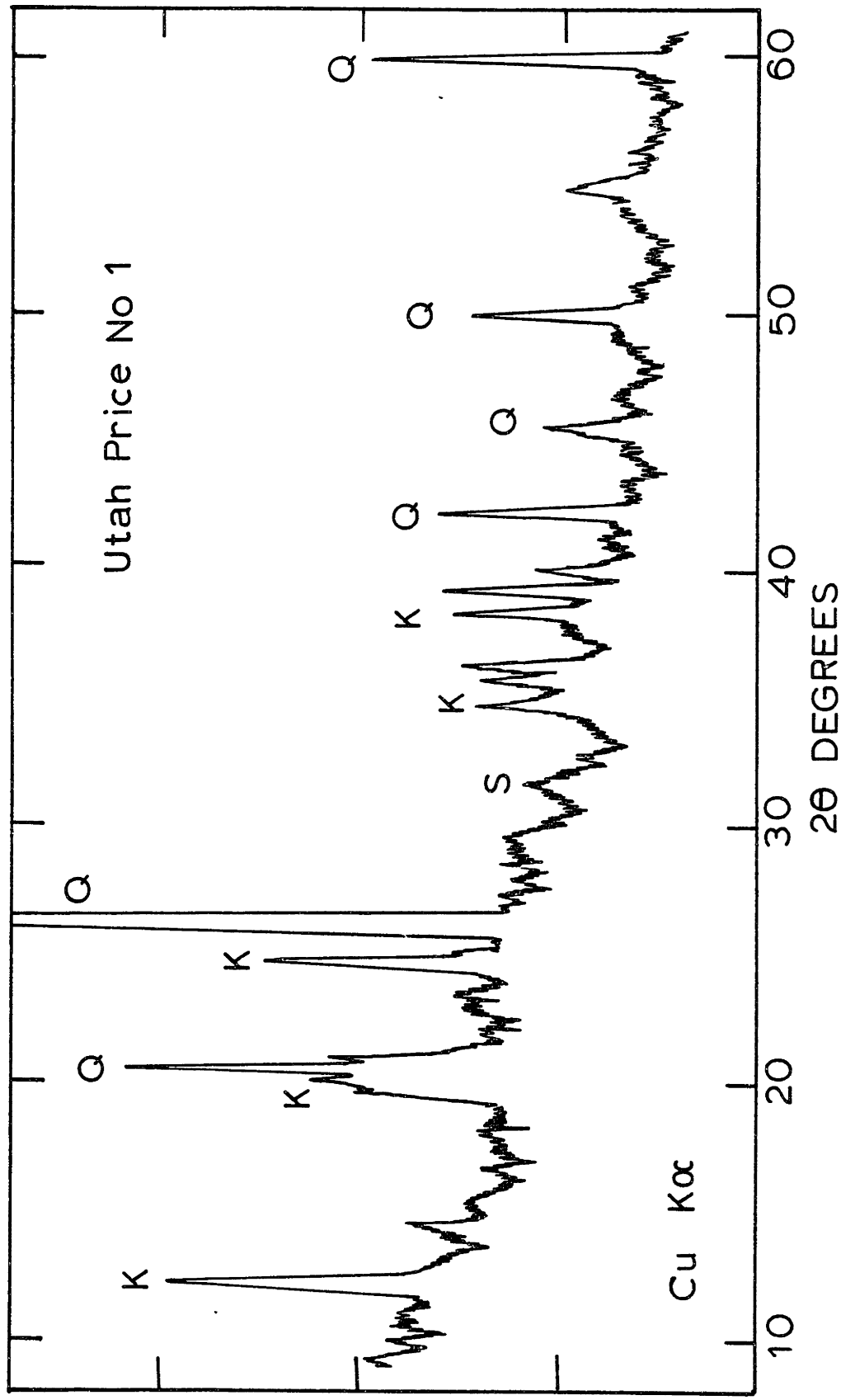
Utah Price No 1
Cu Kα
K
Q
K
K
Q
S
K
K
Q
Q
Q
10
20
30
40
50
60
2θ DEGREES

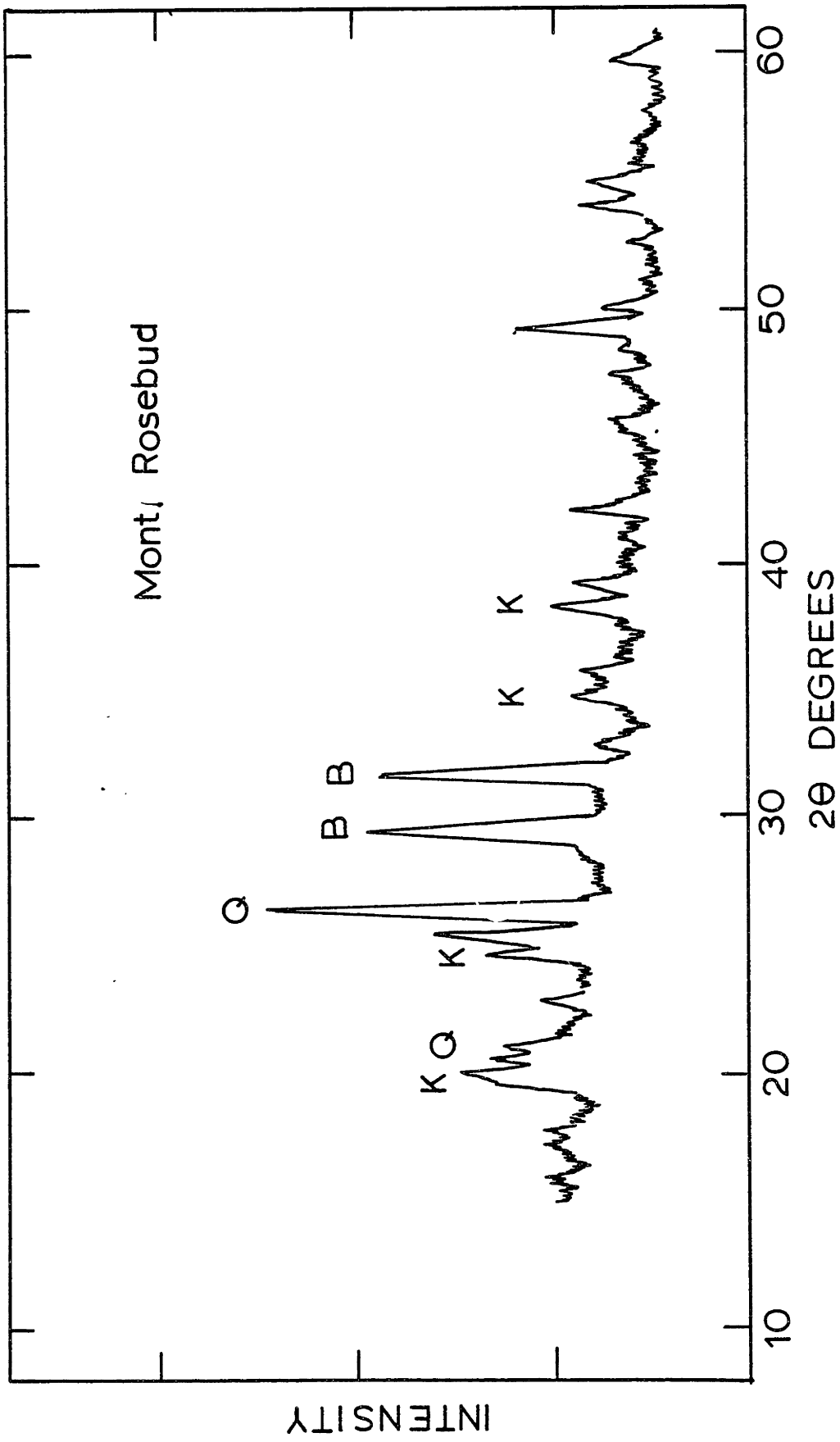
Monti Rosebud
INTENSITY
10
20
30
40
50
60
2θ DEGREES
K Q
K
Q
B B
K K

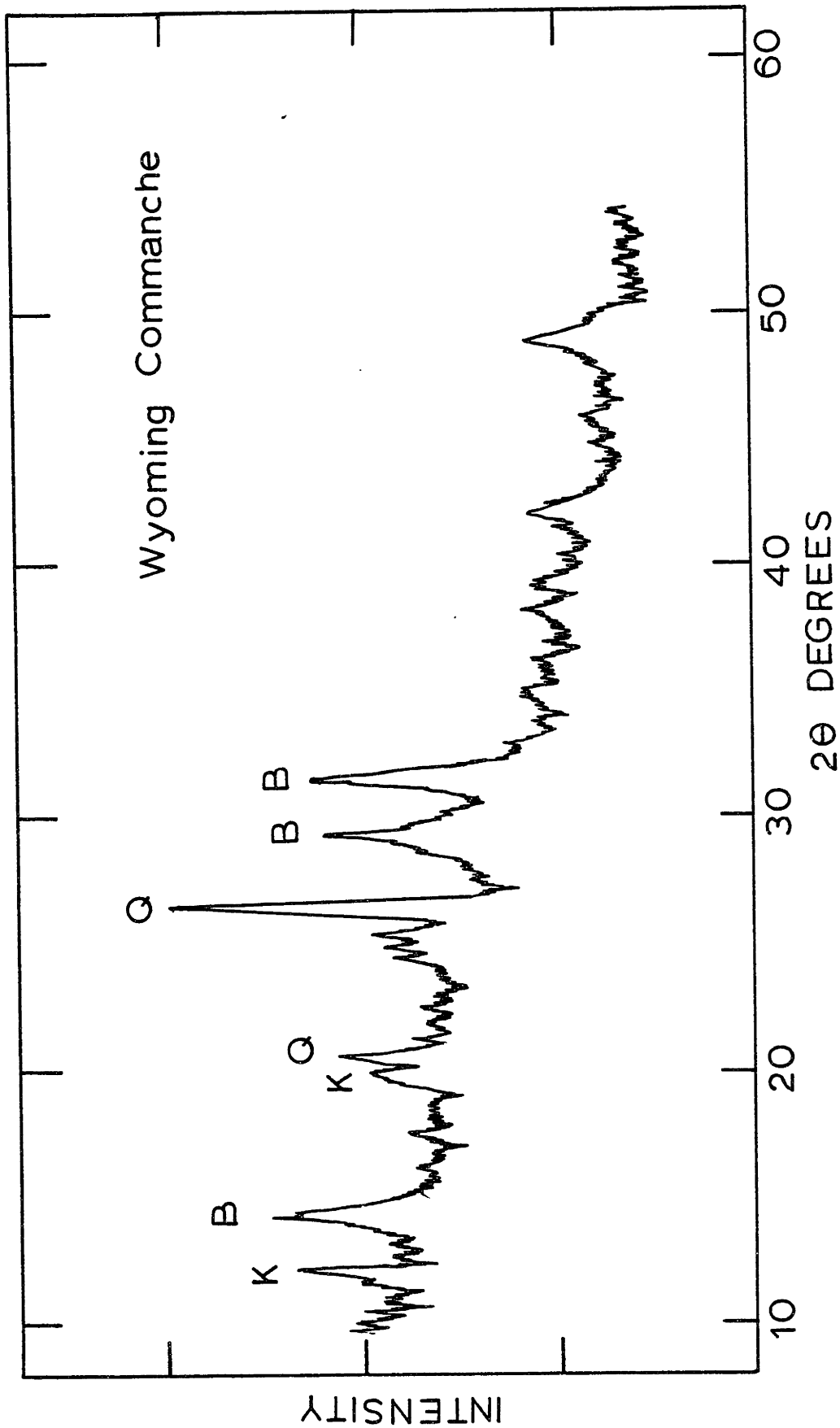
Wyoming Commanche
INTENSITY
2θ DEGREES
10
20
30
40
50
60
K
B
Q
K
Q
B
B

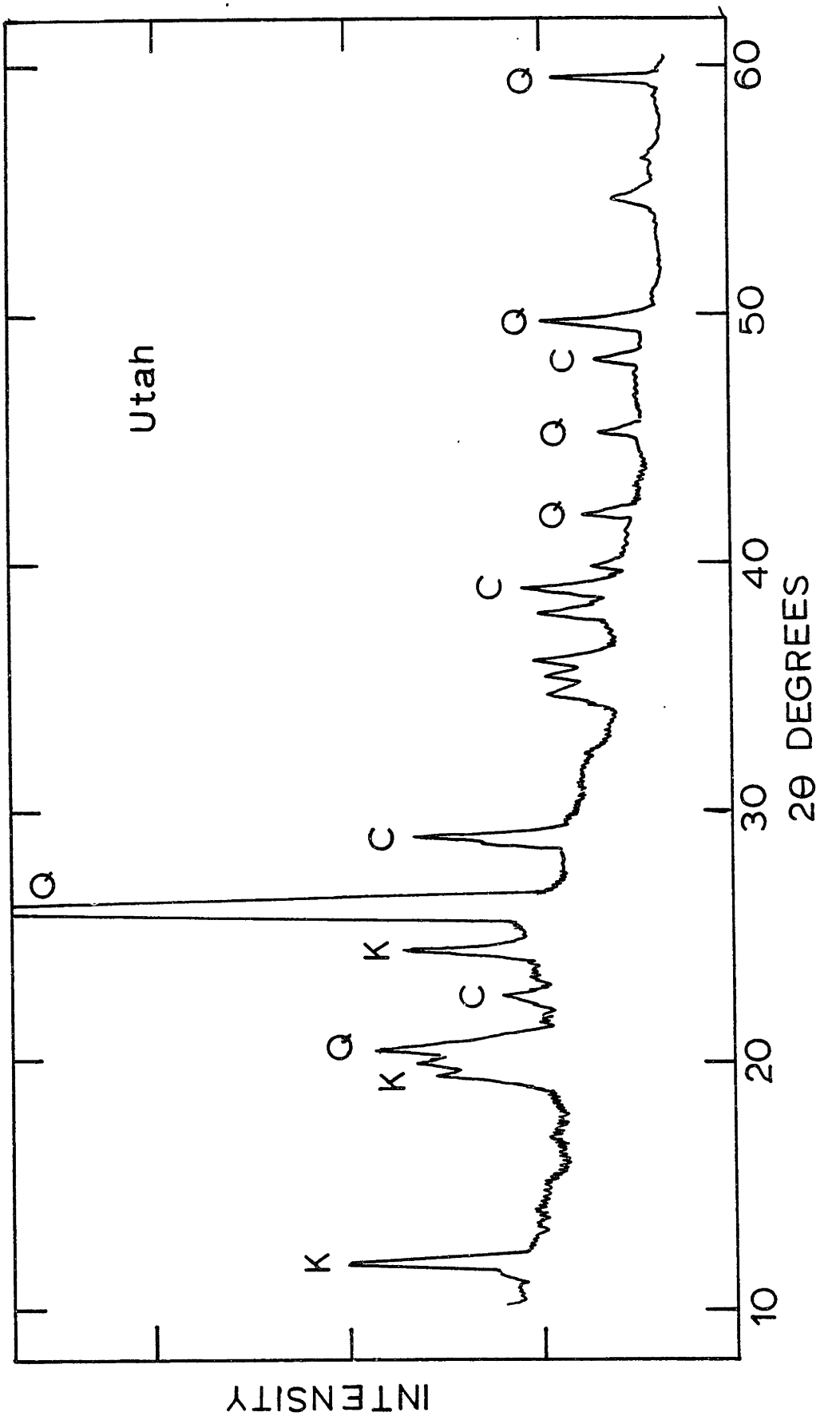
Utah
INTENSITY
2θ DEGREES
10
20
30
40
50
60
K
Q
K
C
K
Q
C
Q
Q
C
Q
Q

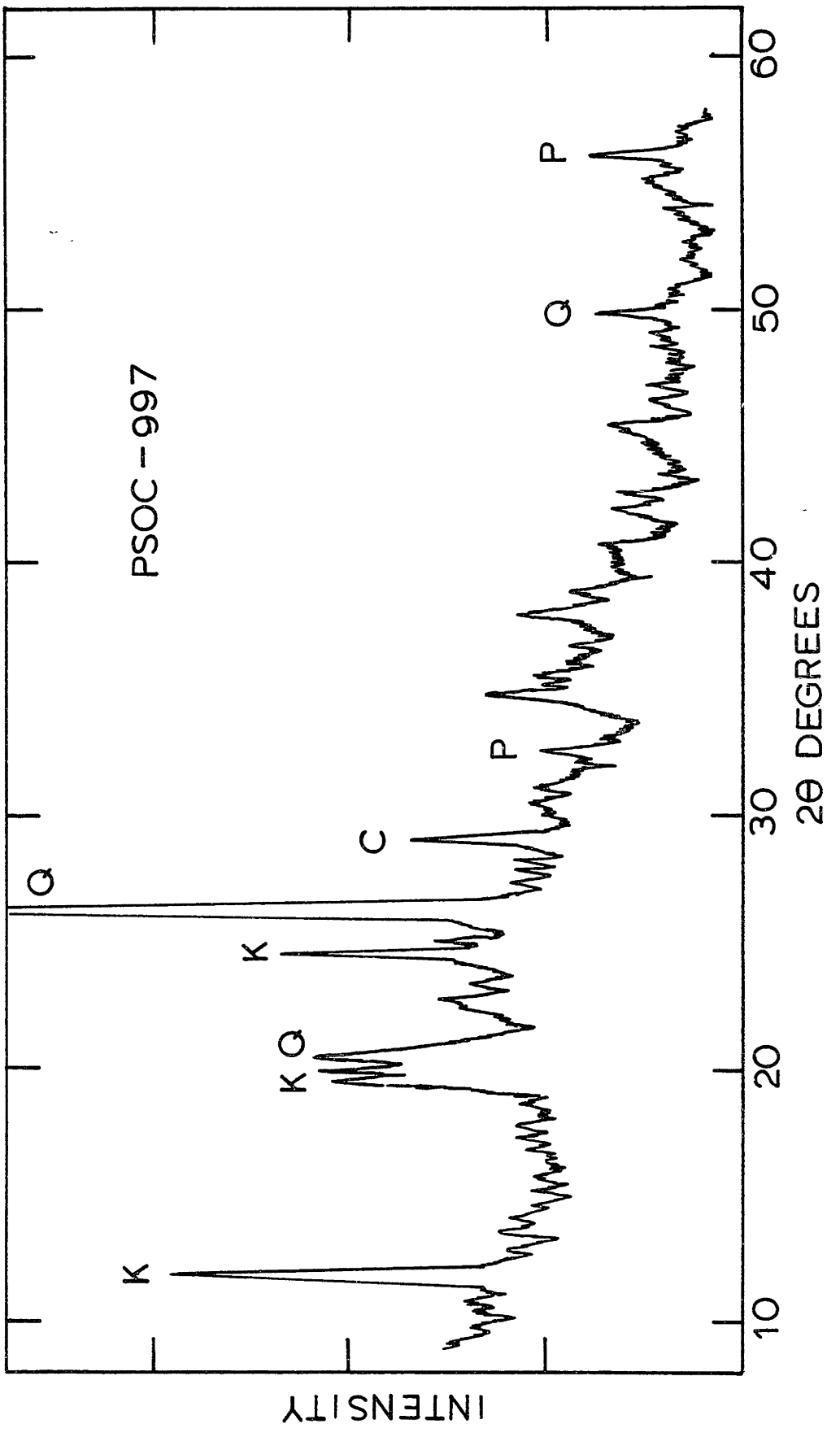
PSOC-997
INTENSITY
2θ DEGREES
10
20
30
40
50
60
K
K Q
K
Q
C
P
Q
P

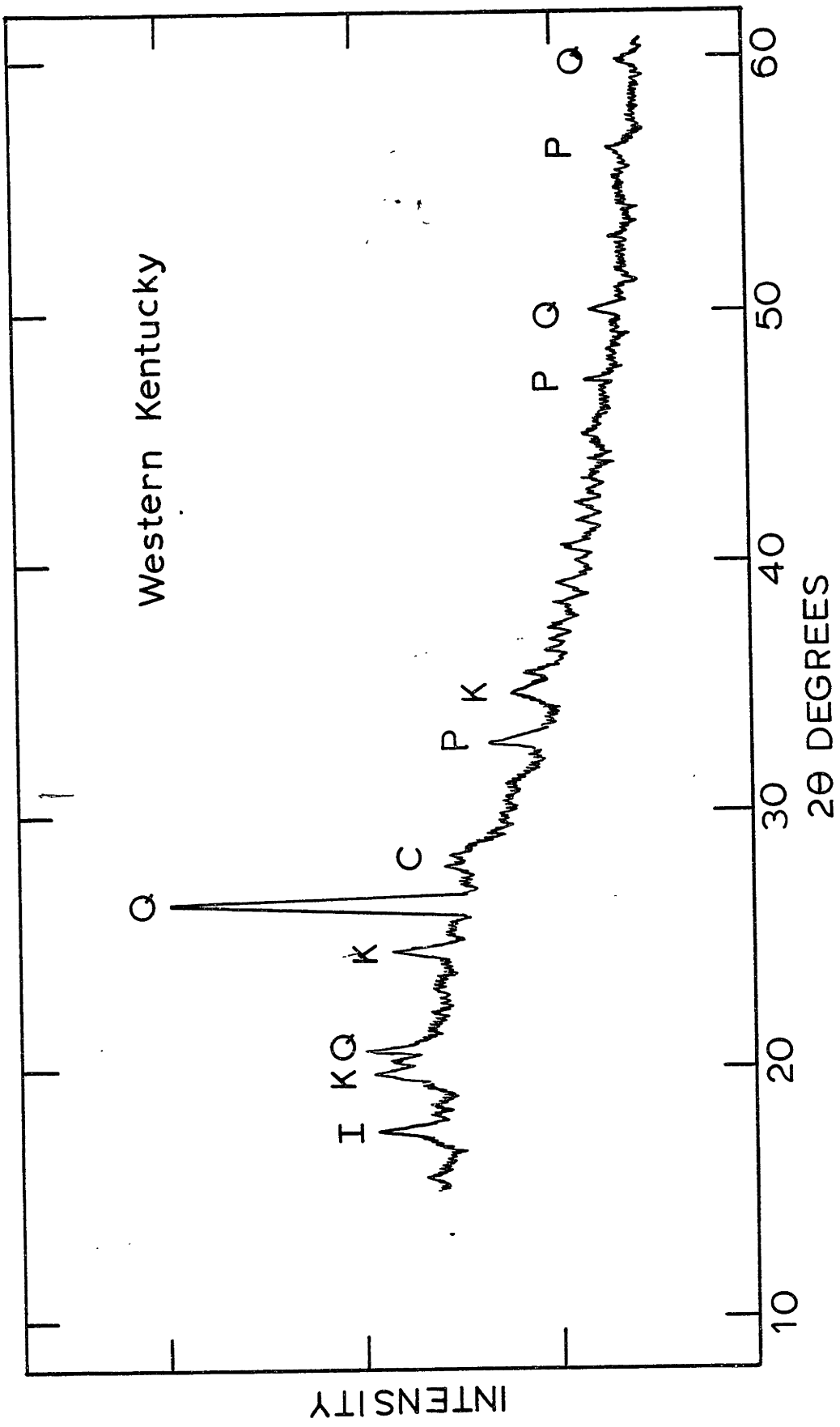
Western Kentucky
INTENSITY
2θ DEGREES
10
20
30
40
50
60
I
K
Q
K
Q
C
P
K
P
Q
P
Q

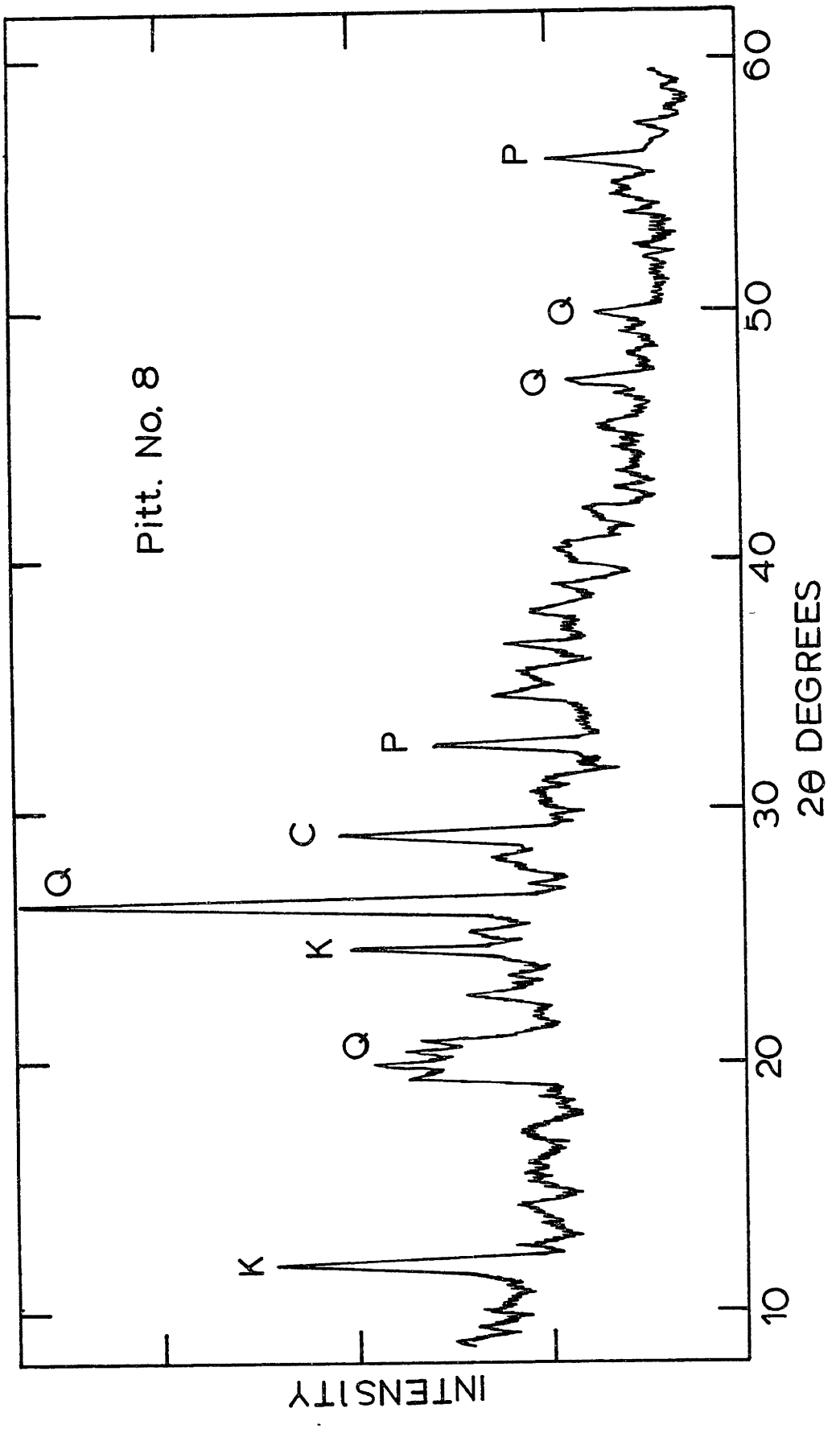
Pitt. No. 8
INTENSITY
2θ DEGREES
10
20
30
40
50
60
K
Q
K
Q
C
P
Q
Q
P

APPENDIX C

MÖSSBAUER SPECTRA OF COALS

The Mössbauer effect is essentially the recoilles resonant absorption and emission of V-rays by nuclei. Not all of the elements (or isotopes) exhibit a Mössbauer effect. Of the major elements occurring in coal, only the isotope ^{57}Fe of iron is suitable for Mössbauer spectroscopy analysis.

For iron analysis, the ^{57}Fe V-rays are generated by the radioactive decay of ^{57}Co by electron capture to an excited ^{57}Fe state. ^{57}Fe then decays by the emission of a 123 keV V-ray followed by another emission of 14.4 keV V-ray. The 14.4 KeV V-rays so emitted from the Co source are used to scan the energy levels of the ^{57}Fe isotope in a target sample such as coal. Resonant emission and absorption of the 14.4 KeV V-rays will occur provided that the excited state energy levels of the ^{57}Fe nucleus in the sample coincides that of the source. The energy levels of the ^{57}Fe nucleus, however, depend on the chemical environment of iron in a solid matrix. Furthermore, the energy levels of the ground and excited states of the ^{57}Fe nuclei may be split into a multiple of levels by hyperfine interactions that can be characterized by three Mössbauer parameters; the isomer shift, the quadrapole splitting and magnetic hyperfine splittings. The reader is referred to Huggins and Huffman (1979) and references therein for a more detailed discussion of these interactions and the method. In order to scan the multiple energy levels by the resonant emission and absorption, the V-ray source is oscillated

over a velocity range (~1 cm/sec) by electrochemical methods to induce a Doppler shift in the energy of the 14.4 KeV V-ray. Resonance occurs when the energy of the doppler shifted V-ray precisely matches that for a transition between a ground and excited state of the ^{57}Fe nuclei in the sample. The transition energies depend on the chemical environment. Huggins and Huffman (1979) have tabulated the Mössbauer parameters for a number of iron-bearing coal minerals. Their reported values were used to identify the various iron-bearing mineral forms in the coals used in the present study. The Mössbauer spectra were obtained using a Co in rhodium source. The Mössbauer facility was located at the Francis Bitter Magnet Laboratory at M.I.T. This work was performed under the direction and assistance of R.B. Frankel and G.C. Papaefthymiou.

Table C.1

Iron-Bearing Minerals in Coal
Identified by Mössbauer Spectroscopy

Mineral	Formula	Symbol
Pyrite	FeS_2	P
Jarosite	$xFe_3(SO_r)_3(OH)_6$	J
Szomolnokite	$F_eSO_4 \cdot H_2O$	S_z
Marcasite	FeS_2	M_r
Siderite	$FeCO_3$	S
Illite	(Alumino-silicate clay)	I

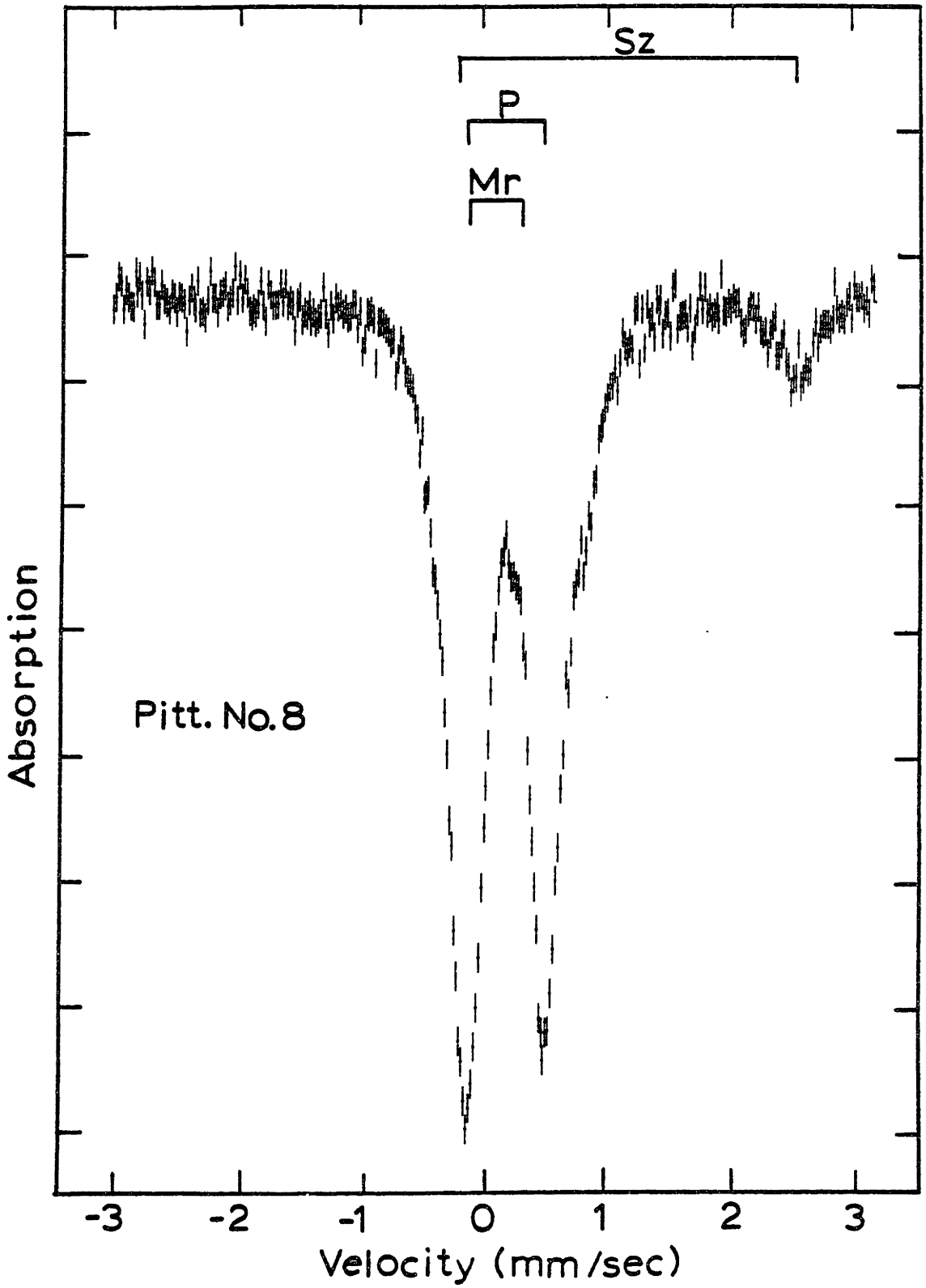
Sz
P
Mr
Absorption
Pitt. No. 8
-3
-2
-1
0
1
2
3
Velocity (mm/sec)

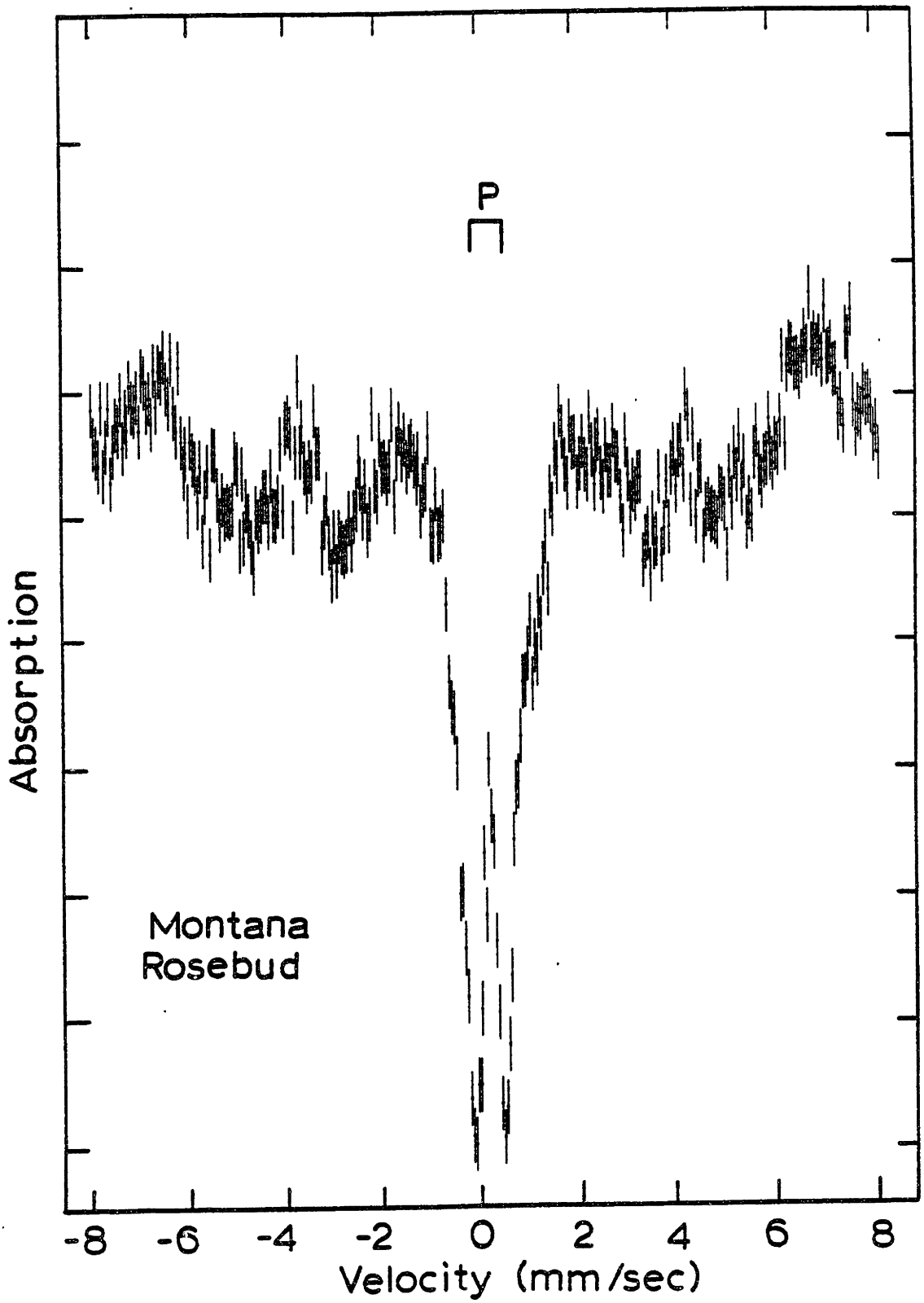
P
Absorption
Montana
Rosebud
-8
-6
-4
-2
0
2
4
6
8
Velocity (mm/sec)

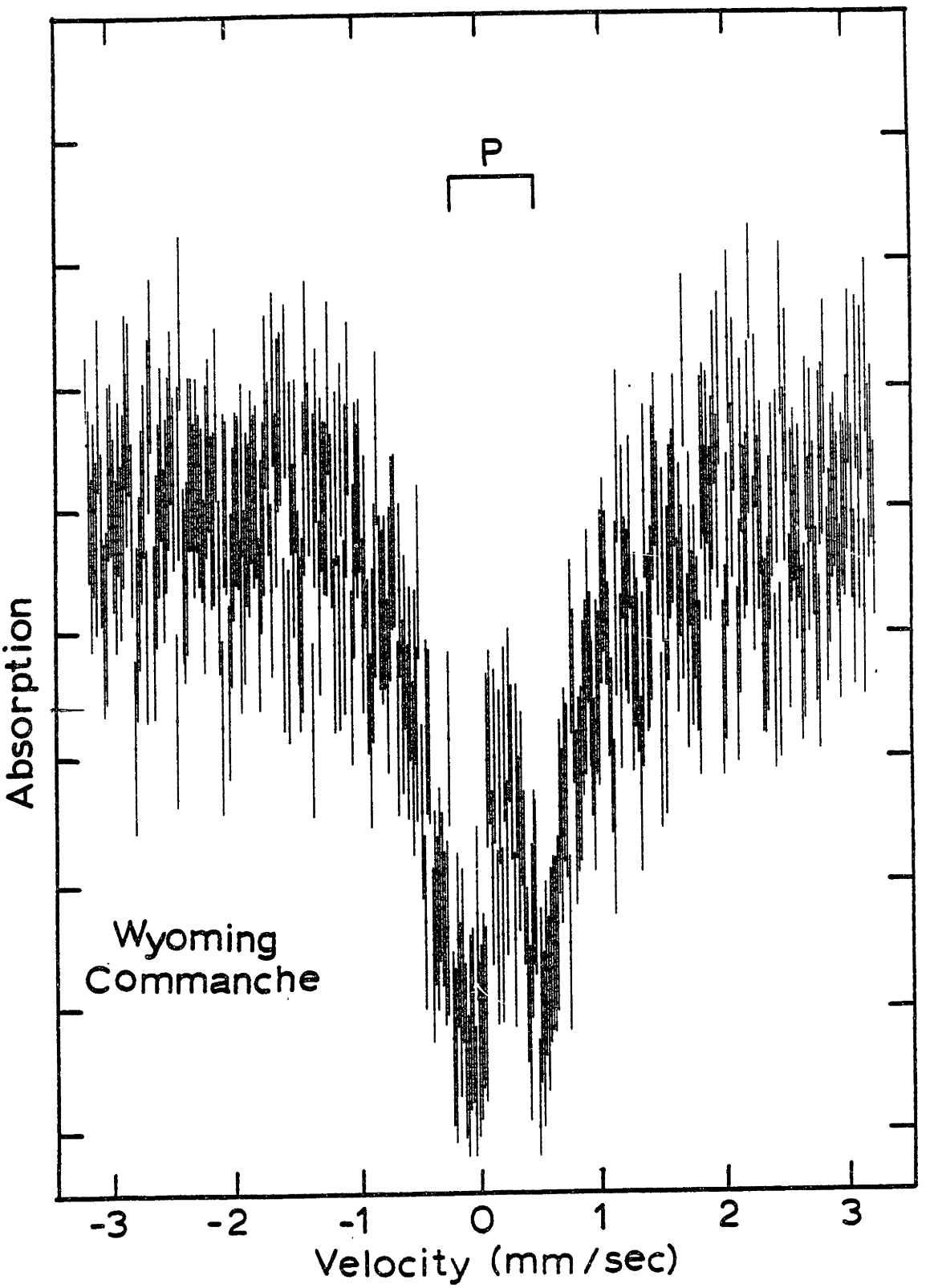
P
Absorption
Wyoming
Commanche
-3
-2
-1
0
1
2
3
Velocity (mm/sec)

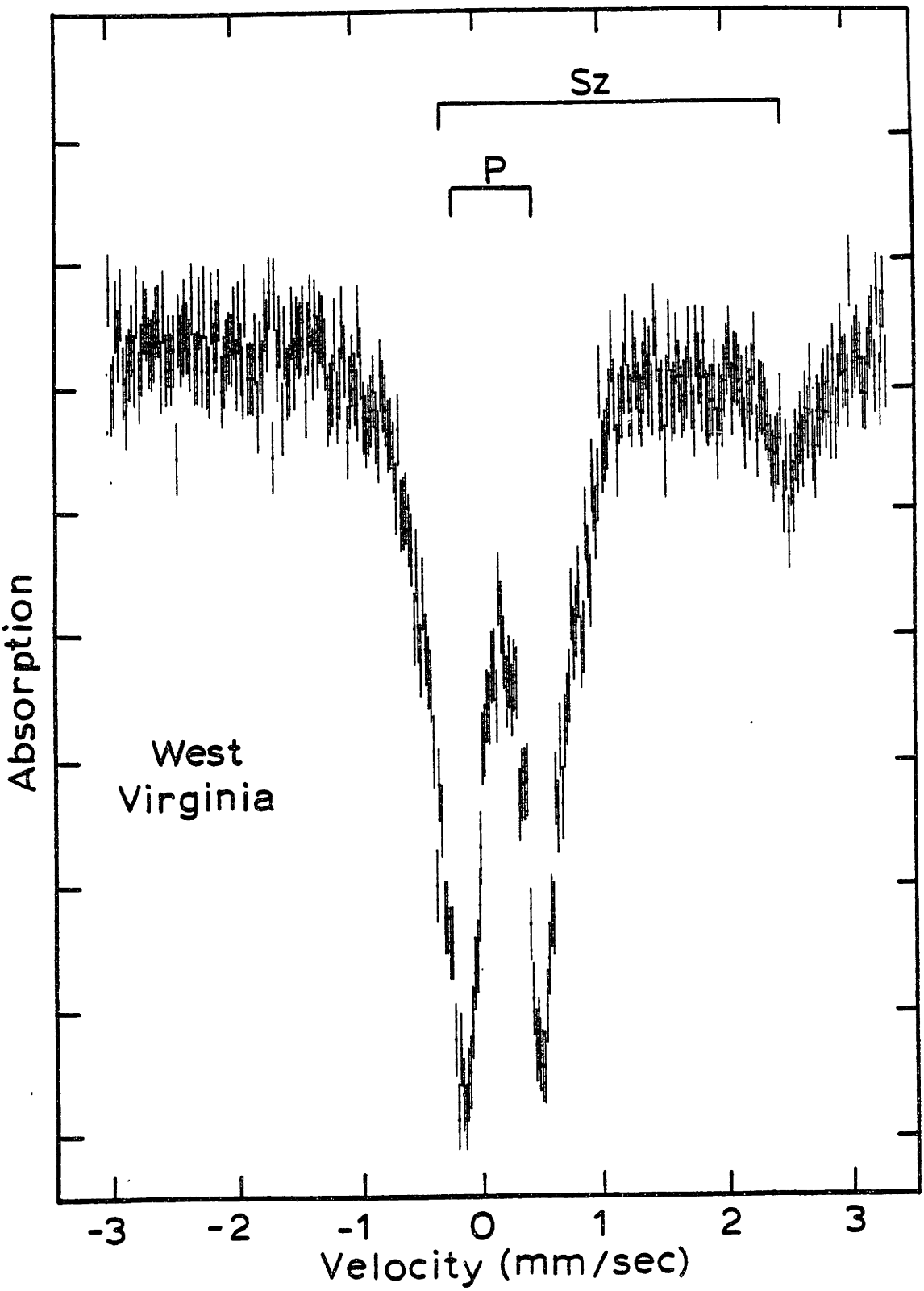
Sz
P
Absorption
West
Virginia
-3
-2
-1
0
1
2
3
Velocity (mm/sec)

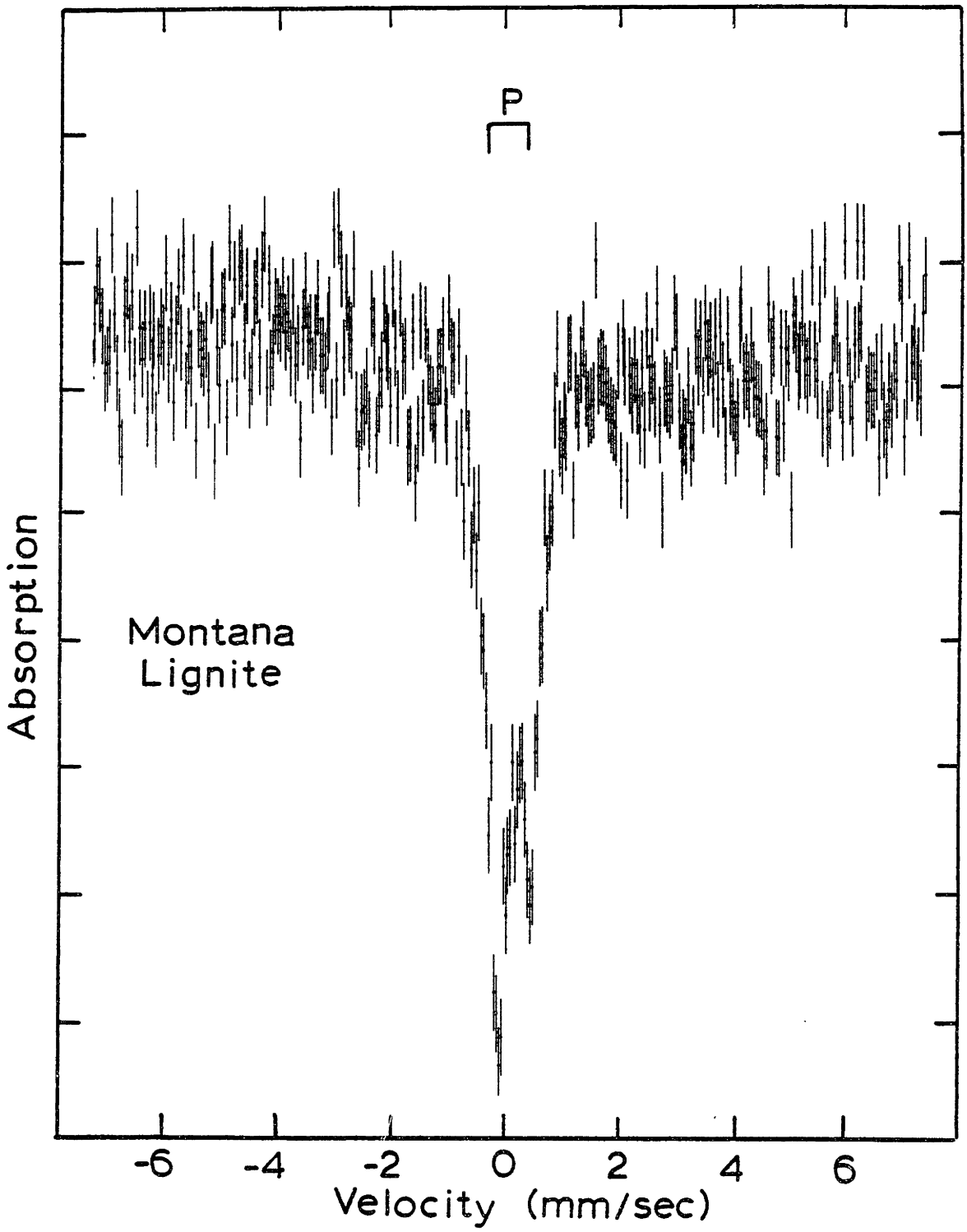
P
Absorption
Montana
Lignite
-6
-4
-2
0
2
4
6
Velocity (mm/sec)

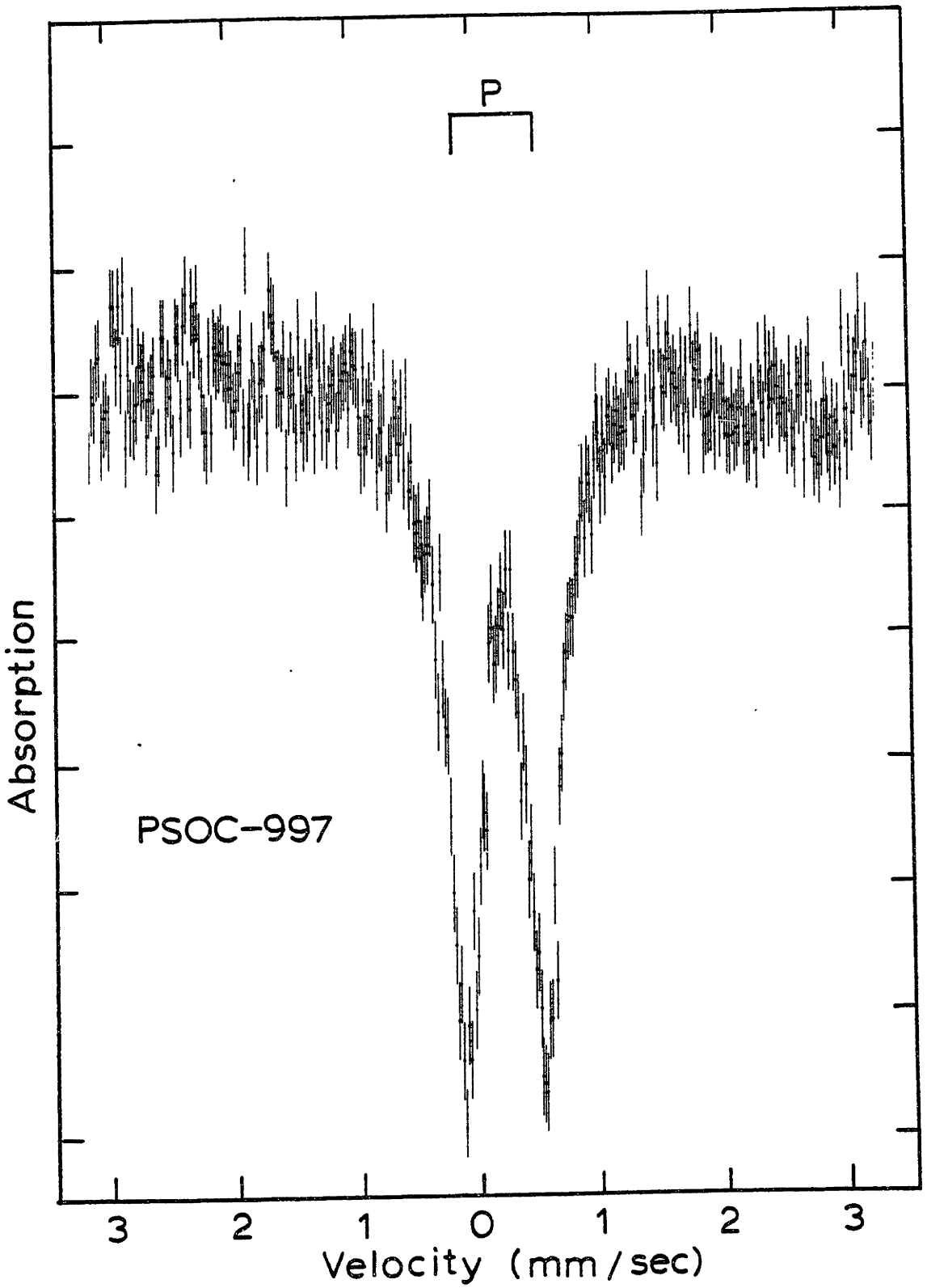
P
Absorption
PSOC-997
3
2
1
0
1
2
3
Velocity (mm/sec)

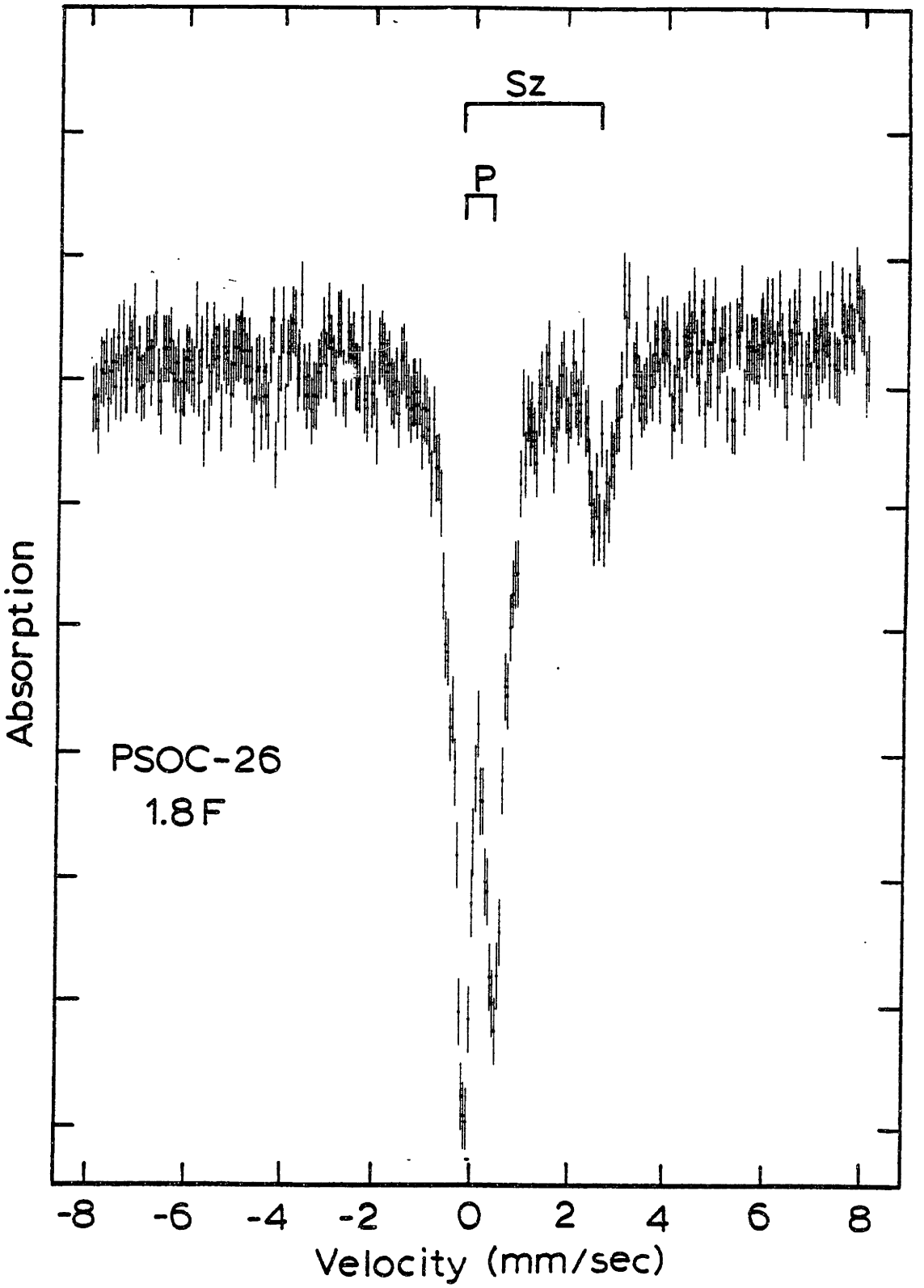
Sz
P
Absorption
PSOC-26
1.8 F
-8
-6
-4
-2
0
2
4
6
8
Velocity (mm/sec)

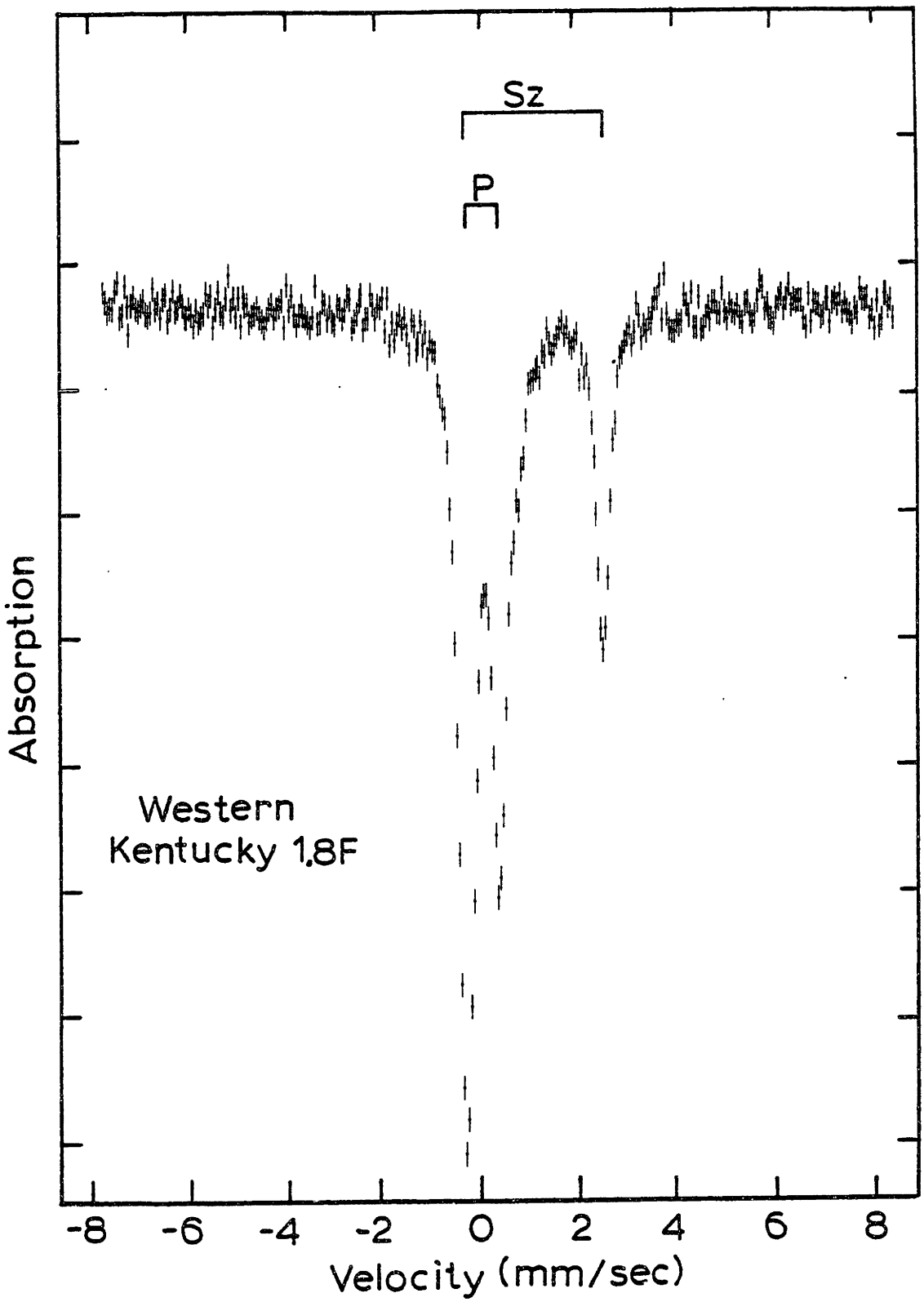
Sz
P
Absorption
Western
Kentucky 1.8F
-8
-6
-4
-2
0
2
4
6
8
Velocity (mm/sec)

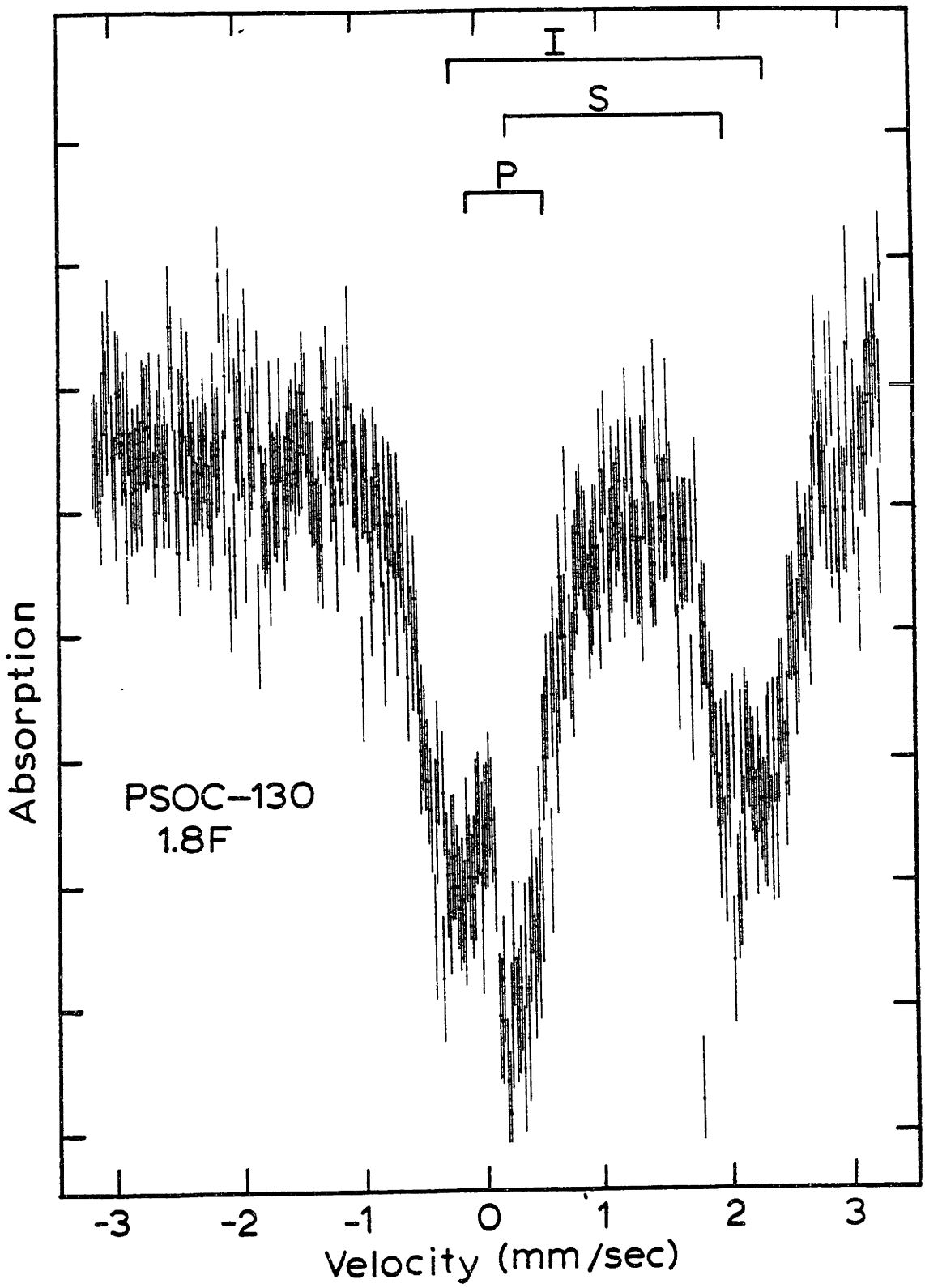
I
S
P
PSOC-130
1.8F
Absorption
-3
-2
-1
0
1
2
3
Velocity (mm/sec)

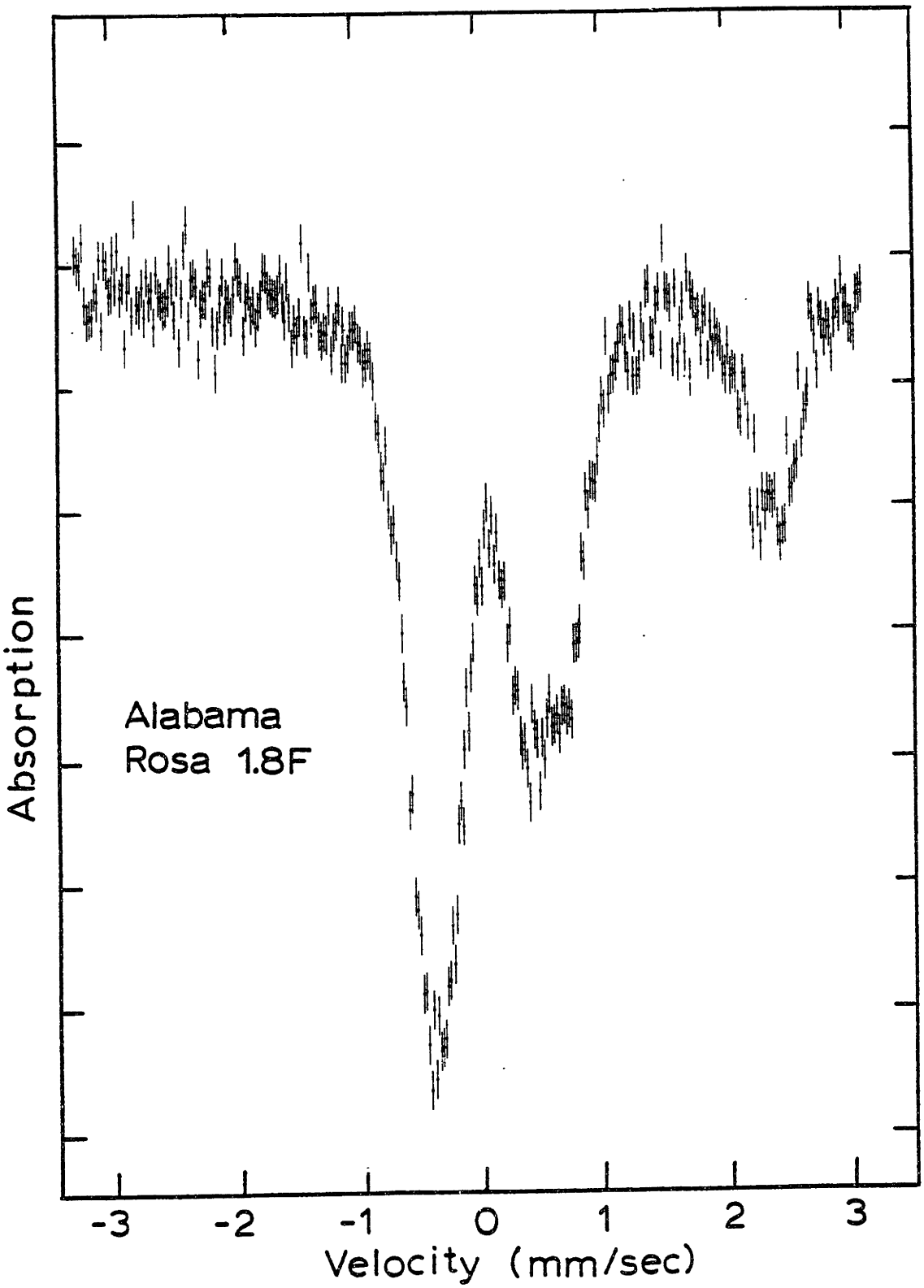
Absorption
Alabama
Rosa 1.8F
-3
-2
-1
0
1
2
3
Velocity (mm/sec)

APPENDIX D

EQUILIBRIUM CONSTANTS FOR ASH-CARBON REACTIONS

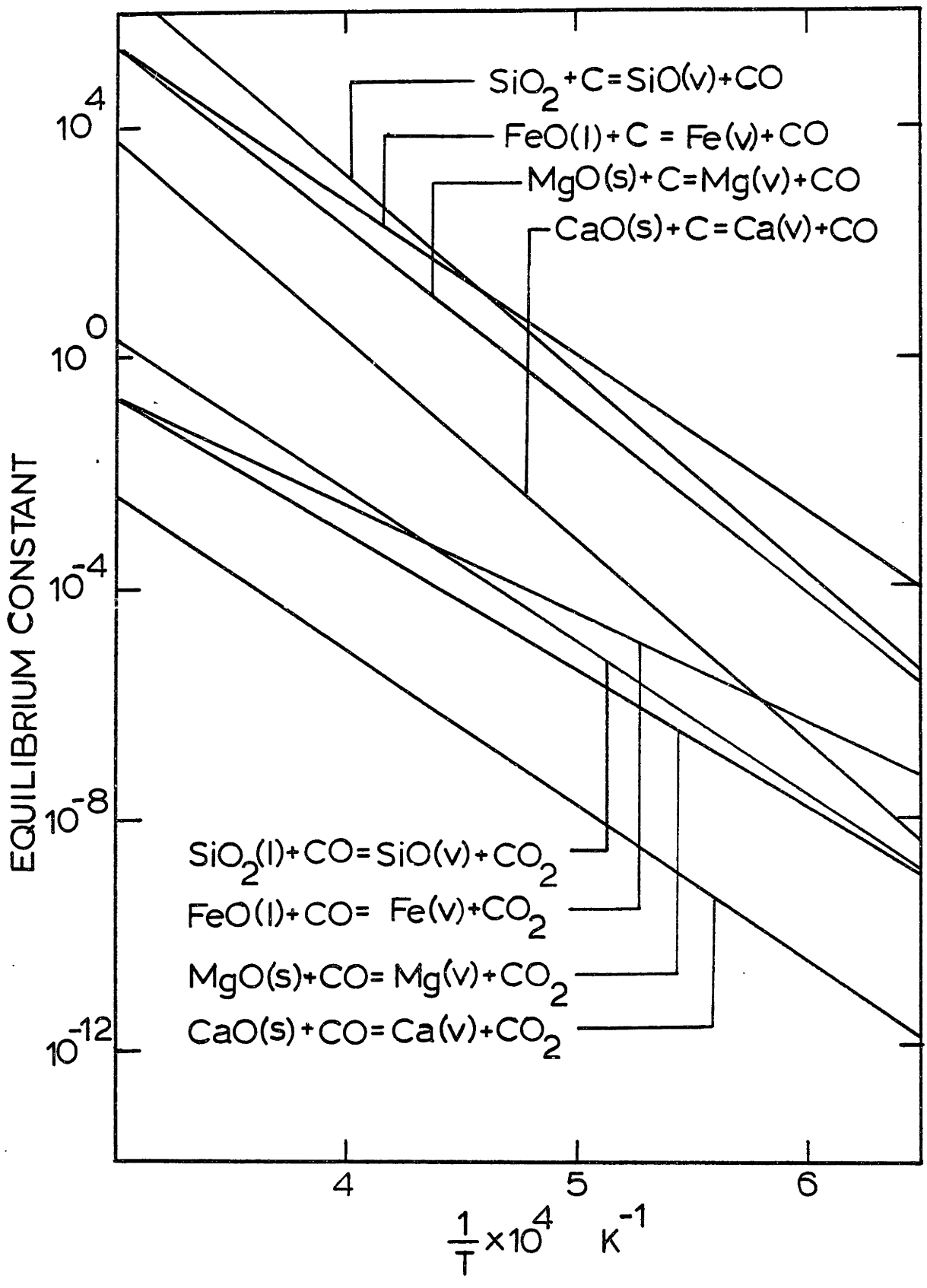
SiO2+C=SiO(v)+CO
FeO(l)+C = Fe(v)+CO
MgO(s)+C=Mg(v)+CO
CaO(s)+C=Ca(v)+CO
SiO2(l)+CO=SiO(v)+CO2
FeO(l)+CO= Fe(v)+CO2
MgO(s)+CO= Mg(v)+CO2
CaO(s)+CO=Ca(v)+CO2
EQUILIBRIUM CONSTANT
10^4
10^0
10^-4
10^-8
10^-12
4
5
6
1/T x10^4 K^-1

REFERENCES

1. Altricher, D.A., M.S. Thesis, "Optical Determination of Time Temperature Profiles for Single Particle Combustion", M.I.T., Cambridge, Mass., 1980.

2. Anthony, D.B. and Howard, J.B., A.I.Ch.E. Journal 22, (4), (1976).

3. Attar, A., Fuel, Vol. 57, p. 201, (1978).

4. Bird, R.B., Stewart, W.E. and Lightfoot, E.N., Transport Phenomena, John Wiley and Sons, Inc. (1960).

5. Borio, R.W. and Narciso, Jr., R.R., ASME Paper No. 78-WA/CD-3, (1979).

6. Bryers, R.W., ASME Paper No. 78-WA/CD-4, (1979).

7. Choh, T., Hanaki, Y., Kato, T., Inouye, M., Transactions IS/J, 13 (1973).

8. Coles, D.G., Ragaini, R.C., Ondov, J.M., Fisher, G.L., Silberman, D., Prentice, A., Env. Sci. Tech., 13, 455-459, 1979.

9. Cullis, C.F. and Mulcahy, M.F.R., Comb. Flame, 18, p. 225 (1972).

10. Darken, L.S. and Gurry, R.W., J. Am. Ceram. Soc., Vol. 68, p. 798, (1946).

11. Davison, R.L., Natusch, D.R.S., Wallace, J.R., and Evans, C.A., Environmental Science and Tech., 8, 1107 (1974).

12. Desrosiers, R.F., Riehl, J.W., Ulrich, G.D., and Chiu, A.S., Seventeenth Symposium (International) on Combustion, p. 1395, The Combustion Institute, 1979.

13. Deutch, J.M., Felderhof, B.U., Saxton, M.J., J. Chem. Phys. 64 (11), p. 4559, (1976).

14. Dunderdale, J. And Durie, R.A. J. Inst. Fuel, 37, 493, (1964).

15. Dzubay, T.G., Hines, E.E., and Stevens, R.K., Atmos. Env., 10, 229 (1976).

16. Elliot, J.F., J. Metals, p. 485, March (1955).

17. Elliot, J.R., Gleiser, M., Ramakrishna, V., Thermochemistry for Steelmaking, Vol. II., (Addison-Wesley, 1963).

18. Ensor, D.S., Cowen, S., Hooper, R. and Markowski, G., "Evaluation of the George Neal No. 3 Electrostatic Precipitator", Final Report, EPRI, 1979.

19. Felderhof, B.U. and Deutch, J.M., J. Chem. Phys. 64 (11), p. 4551, (1976).

20. Field, M.A., Combustion and Flame, 13 (3), 237-252 (1969).

21. Field, M.A., Gill, D.W., Morgan, B.B., and Hawksley, P.G.W., Combustion of Pulverized Coal, BCVRA, (1967).

22. Fisher, G.L., Prentice, B.A., Silberman, D., Ordov, J.M., Biermann, A.H., Ragaini, R.C., McFarland, A.R., Env. Sci. Tech., 12 (4), (1978).

23. Flagan, R.C., Seventeenth Symposium (International) on Combustion, p. 97, The Combustion Institute, 1979.

24. Flagan, R.C. and Friedlander, S.K., Recent Developments in Aerosol Science, (J. Davis, ed.), John Wiley and Sons, N.Y. (1978).

25. Flament, G., "Direct Sulpher Capture in Flames through the Injection of Sorbents", Int. Flame Res. Foundation, Report, November 1980.

26. Friedlander, S.K., Smoke, Dust and Haze, John Wiley and Sons, N.Y. (1977).

27. Gluskoter, H.J., Fuel (London), 44, 285 (1965).

28. Fruehan, R.J. Met. Trans., 8B, 279, (1977).

29. Gluskoter, H.J., Jour. Sed. Petrology, 37, 205 (1967).

30. Gluskoter, H.J. and Mitchell, R.S., Fuel, 55, 2, (1976).

31. Gluskoter, H.J, Ruch, R.R., Miller, W.G., Cahill, R.A., Dreher, G.B. and Kuhn, J.K., "Trace Elements in Coal: Occurance and Distribution", Ill. State Geo. Surv. 499, (1977).

32. Gordon, G.E., Gladney, E.S., Ondov, J.M., Conry, T.J. and Zoller, W.H., Intercomparison of Several Types of Cascade Impactors. Presented before Am. Chem. Soc. Div. Env. Chem., Los Angeles, CA, March 1974.

33. Gröber, H., Erk, S., and Grigull, U., Fundementals of Heat Transfer, McGraw-Hill, (1961).

34. Halstead, W.D. and Raask, E., J. Inot. Fuel, 42, 344 (1969).

35. Hidy, G.M., and Brock, J.R., "The Dynamics of Aerocolloidal Systems, Pegamon, Elmsford, N.Y. (1970).

36. Howard, J.B. and Essenhigh, R.H., Eleventh Symposium (Int.) on Combustion, The Combustion Institute (1967).

37. Huffman, G.P. and Huggins, F.E., Fuel, 57, 592, (1978).

38. Jackson, P.J., in "Pulverized Coal Firing - Mineral Matter and Its Effects" (ed. I. McC. Stwart, T.F. Wall), U. of Newcastle, (August, 1979).

39. Kaakinen, J.W. Jordan, R.M., Lawasani, M.H., and West, R.E., Env. Sci. Tech., 9, 862 (1975).

40. Kemezys, M. and Taylor, G.H., J. Inot. Fuel, 369, Sept. 1964.

41. Labowsky, M. and Rosner, D.E., "Group Combustion of Droplets in Fuel Clouds. I. Quasi-steady Predictions" in Advances in Chemistry Series 166, ACS, (1978).

42. Lai, F.S., Friedlander, S.K., Pich, J., Hidy, G.M., J. of Colloid and Interface Science, 39, No. 2, (1972).

43. Levin, E.M., Robbins, C.R., McMurdie, H.F., Phase Diagrams for Cermists, Am. Ceram. Soc., 1964.

44. Littlejohn, R.F., J. Inot. Fuel, 59, (Feburary 1966).

45. Lyon, R.K. and Freund, H., "The Sulfur Retention of Calcium-Containing Coal During Fuel Rich Combustion" paper presented at Fall Meeting, Western States Section of the Combustion Insitute, 1980.

46. Mackowsky, M. Th., Proc. Int. Comm. for Caol Petrology, No. 2, p. 31, (1956).

47. Martinez-Sanchez, M., Kolb, C.E., and Kerrebrock, J.L., J. Energy, A.I.A.A., February 1978.

48. McCain, J.C., Gooch, J.P., Smith, W.B., J. Air. Poll. Control Assoc., 25, 117-121 (1975).

49. McElroy, M.W., and Carr, R.C., in "Proc. of the Joint Symp. on Stationary Combustion NO_x Control", Vol. V, Addendum, 1980.

50. McNallen, M.J., Yurek, G.J., Elliot, J.F., Comb. Flame, (1981).

51. Miller, R.N., Ph.D. Thesis, "A Geochemical Study of the Inorganic Constituents in Some Low-Rank Coals", Penn. State Univ., (1978).

52. Miller, R.N. and Given, P.H., "A Geochemical Study of the Inorganic Constituents in Some Low Rank Coals", Penn State University, PSU-TR-IL, (1978).

53. Muan, A., Osborn, E.F., Phase Equilibria Among Oxides in Steelmaking, (Addison-Wesley, 1965).

54. Mulcahy, M.F.R., "The Combustion of Carbon", First Priestly Conf., The Chemical Society, London, p. 178, (1978).

55. Mulcahy, M.F.R. and Smith, I.W., Rev. Pure and Appl. Chem., 19, 81, (1969).

56. Nagamori, M. and Kameda, M., Trans, J.I.M., Vol. 6, p. 21, (1965).

57. Neville, M., Sc.D. Thesis, in preperation, 1981.

58. O'Gorman, J.V. and P.L. Walker, Jr., Fuel (London) 50, (1971).

59. O'Gorman, J.V. and Walker, P.L., "Mineral Matter and Trace Elements in Coal", Research and Development Report No. 61, Interim Rept. No. 2, Office of Coal Research, U.S. Dept of Interior, (1972).

60. Ondov, J.M., Ragaini, R.C., and Biermann, A.H., Env. Sci. Tech., 946 (1979).

61. Ondov, J.M., Zoller, W.H., Olmez, K., Aras, N.K., Gordon, G.E., Ranticelli, L.A., Albe, K.H., Filby, R.H., Shah, K.R., Ragaini, R.C., Anal. Chem., 47, 1102-9 (1975).

62. Padia, A., Sc.D. Thesis "The Behavior of Ash in Pulverized Coal under Simulated Combustion Conditions", M.I.T., 1976.

63. Paulson, C.A.J. and A.R. Ramoden, Atmospheric Environment, 4, 175 (1970).

64. Raask, E. and Wilkins, D.M., J. Inst. Fuel, 38, 255 (June 1965).

65. Ramoden, A.R., Fuel (London) 48, 121 (1969).

66. Ramoden, A.R. and Smith, I.W., Fuel, 47, 253 (1968).

67. Rancitelli, L.A., Cooper, J.A. and Perkins, R.W., Multi-element Characterization of Atmospheric Aerosols by Instrumental Neutron Activation Analysis and X-Ray Fluorescence Analysis, p. 152 in Environmental Quality and Safety, Vol. 5 (Academic Press, 1976).

68. Rao, C.P. and Gluskoter, H.J., Ill. State Geo. Surv. Circ. 476 (1973).

69. Rao, Y.K., Met. Trans., Vol. 2, 1439, (1971).

70. Rein, R.H. and Chipman, J., Trans. A.I.M.E. 233, p. 415, (1965).

71. Roberts, A.L., Kinetics of High Temperature Processes, p. 222, John Wiley and Sons, (1959).

72. Samson, R., Bedeaux, S., Saxton, M.J., Deutch, J.M., Comb. Flame, 31, 215-221 (1978).

73. Sarofim, A.F., Howard, J.B. and Padia, A.S., Combust. Sci. Tech., 16, 187 (1977).

74. Sasaki, H. and Tanekazu, S., Met. Trans., 8B, 189, (1977).

75. Satterfield, C.N., Mass Transfer in Heterogeneous Catalysis, M.I.T. Press, (1970).

76. Schaefer, H.N.S., Fuel, 57, pp. 686-692, (1978).

77. Schwerdtfeger, K., Trans, A.I.M.E., Wol. 236, 1152, (1966).

78. Schwerdtfeger, K. and Schubert, G., Met. Trans. B, 8B, p. 535, (1977).

79. Selvig, W.A. and Gibson, F.N., Bulletin U.S. Bureau of Mines, No. 567 (1956).

80. Simons, G.A., Comb. Sci. and Tech., Vol. 20, pp. 107-116 (1979a).

81. Simons, G.A. and Lewis, P.F., Comb. Sci. and Tech., Vol. 20, pp. 117-124, (1979b).

82. Smith, I.W., Fuel, 57, 1978.

83. Smith, R.D., Prog. Energy. Comb. Sci. 6, (1), (1980).

84. Smith, R.D., Cambell, J.A. and Nielson, K.K., Env. Sci. Tech. 13, 553 (1979).

85. Song, H.Y., Sc.D. Thesis "Fate of Fuel Nitrogen During Pulverized Coal Combustion", M.I.T., (1978).

86. Street, P.J., Weight, R.P. and P. Lightman, Fuel (London) 48, 343 (1969).

87. Szekely, J., Evans, J.W. and Sohn, H.Y., Gas-Solid Reactions, Academic Press, 1976.

88. Toguri, J.M. and Pidgeon, L.M., Can. J. Chem., Vol. 39 (1961).

89. Timothy, L., Sc.D. Thesis, in preparation, 1980.

90. Ulrich, G.D., Riehl, J.W., French, B.R. and Desrosiers, R.E., ASME Symposium on Corrosion and Deposits from Combustion Gases, Henniker, N.H., 1977.

91. Ward, C.R., "Mineral Matter in the Springfield-Harrisburgh (No. 5) Coal Member of the Illinois Basin, Ill. State Geo. Surv., Circular 498, (1977).

92. Watt, J.D., and Fereday, F., J. of the Inst. of Fuel, Vol. 42, No. 338, p. 99, (1969).

93. Wriedt, H.A. and Darken, Trans, SME-AIME, Vol. 254, p. 1, (1973).

94. Wibberley, L.I., Ph.D. Thesis, "Alkali Ash Reactions and Deposit Formation in Pulverized Coal Boilers," University of Newcastle, 1980.